MICROCOPY RESOLUTION TEST CHART

NATIONAL BUREAU OF STANDARDS-1963-A

PAPERS SELECTED
for
PRESENTATION
at the
SIXTEENTH
INTERNATIONAL SYMPOSIUM
ON REMOTE SENSING
OF ENVIRONMENT

Volume II

2-9 JUNE 1982

Buenos Aires, Argentina

$\sum$ E N V I R O N M E N T A L
RESEARCH INSTITUTE
OF MICHIGAN
Ann Arbor, Michigan

DTIC
ELECTE
OCT 1 1 1983
S
D

83 10   002

NOTICES

COMPONENT PART NOTICE

THIS PAPER IS A COMPONENT PART OF THE FOLLOWING COMPILATION REPORT:

(TITLE): Papers Selected for Presentation at the International Symposium on Remote

Sensing of Environment (16th) Held at Buenos Aires, Argentina on 2-9 June

1982. Volume 2.

(SOURCE): Environmental Research Inst. of Michigan, Ann Arbor.

To ORDER THE COMPLETE COMPILATION REPORT USE __AD-A134 720__ .

THE COMPONENT PART IS PROVIDED HERE TO ALLOW USERS ACCESS TO INDIVIDUALLY AUTHORED SECTIONS OF PROCEEDINGS, ANNALS, SYMPOSIA, ETC. HOWEVER, THE COMPONENT SHOULD BE CONSIDERED WITHIN THE CONTEXT OF THE OVERALL COMPILATION REPORT AND NOT AS A STAND-ALONE TECHNICAL REPORT.

THE FOLLOWING COMPONENT PART NUMBERS COMPRISE THE COMPILATION REPORT:

COMPONENT PART NOTICE (CON'T)

Accession For

NTIS GRA&I ☑
DTIC TAB ☐
Unannounced ☐
Justification

By
Distribution/

Availability Codes

Dist | Avail and/or Special

A-1

DTIC
SELECTED
JUL 1 1 1983

A

CONTENTS

Page

ix

x

LAND USE STRATIFICATION IN THE PAMPA HUMEDA THROUGH
LANDSAT IMAGES--ITS USE IN AGRICULTURAL ESTIMATES

Claudio Fonda
Eduardo Lucesole

Secretaria de Agricultura y Ganaderia de la Nacion
Buenos Aires, Argentina

Claudia Gargantini
Francisco Redondo

Comision Nacional de Investigaciones Espaciales
Buenos Aires, Argentina

SUMMARY

As the Secretaria de Agricultura y Ganaderia de la Nacion needs more accurate estimates about agriculture and livestock production, a new sampling design was formed.

Present land-use strata were delimited as the base of that design. This will decrease the values of total variance of estimates grouping farms in homogeneous conglomerates according to equal features.

Satellite false color images were analyzed through visual interpretation. These images belong to the province of Buenos Aires, Cordoba, Entre Rios and Santa Fe, were given by the Comision Nacional de Investigaciones Espaciales. The work scale was generally 1:500,000 though some images were 1:1,000,000.

Field size, color and tones shown by the image were the main features taking into account to estimate present land use.

To support the work, many soil maps, soil capacity maps, statistics and census data, were consulted. Besides the staff of the Secretaria assigned in the named provinces did their best in order to help us.

The corresponding legend of each strata was focused under an agricultural point of view, so this land use map cannot be considered as a standard one.

In this way, six strata of different agricultural levels were determined, four to livestock and three miscellaneous.

After finishing office work, several testing trips on the ground were needed to modify or to confirm the boundaries delimited during the interpretation work.

MICROWAVE RADIOMETRIC MAPPING OF OCEANOGRAPHIC AND ATMOSPHERE PARAMETERS BASED ON SATELLITE MONITORING

N.A.Armand, V.F.Krapivin, B.G.Kutuza,

F.A.Mkrtchyan, B.L.Petrenko

Institute of Radioengineering and Electronics
USSR Academy of Sciences, Moscow, USSR

ABSTRACT

The problems of processing of satellite radiophysical measurement and mapping of ocean surface and atmospheric characteristics in a monitoring regime are discussed. The principles of two-dimensional processing of multiparametric and multichannel measurements with regard to the requirements of operativeness and reliability of the monitoring system, accuracy of solution of identification and detection problems are considered. The structural solutions on organization of a real-time data processing are suggested. The importance of the development of operative methods of geophysical parameter determination in a monitoring system technology is noted. As an example of microwave radiometric data processing, we describe the computer technique used on the satellite Cosmos-1151 for measuring the atmospheric and oceanographic parameters. The estimations of accuracy of geophysical parameter determination are given.

The study of environment in global scales requires the organization of global monitoring systems. Such systems may have a complex hierarchy structure involving a satellite, earth-based receiving and data processing complexes, aeroplanes, ships etc. The operative detection and identification of anomalies (pollutions, fires, typhoons, hurricanes, tropical cyclones on the Earth's surface etc.) are regard to be one of the principle purposes of such systems.

The problem of detecting anomalies on the Earth's surface requires for its solution the application of up-to-date automatic decision machines for processing the large arrays of satellite measurements. This problem involves

the organization of in-line data processing at all detection system levels under time conditions ensuring an uninterrupted matching of operation of all cybernetic devices of the system taking into account their functional limitations (computer speed, memory capacity, etc.)

The search for anomalies on the Earth's surface involves, on the whole, the following main stages: the in-line data enters the computer in the form of m-dimensional vector T, where the number m is determined by the number of information channels and by the number of measured parameters. Then according to the computer program, statistical analysis of this information is realized by making the following two decisions: 1) storage of the landscape element features in the computer memory for accumulation of a large amount of information ("candidate"); 2) decision-making on the presence of anomaly and transmission of the anomaly information to the ground facilities.

The effectivity of the search system operation will depend, in particular, on how we construct the selection algorithm for the "suspected" landscape elements: on the one hand, the storage of these elements in the computer memory decreases its capacity for preserving current in-line data, on the other hand, roughening of the criteria of selection of suspected elements deminishes the detection probability. The solution of this contradiction lies in applying the procedure of time exhaustive search for values of separate T components as suggested in [1] . Let us consider the peculiarities of applying this procedure in problems of global detection of anomalies on the Earth's surface under monitoring conditions.

Let the entry of the monitoring system have the information going through the m channels in the form of vector $T=(t_1,\ldots,t_m)$. In this case, the parallel successive procedure for estimation of value $T=T^*$ based on the successive fixation of signal values of components with the help of m successive computers is used. The simultaneous operation of all m selection devices is achieved by matching the influxes of variants of T component values. While the accepted variants are transferred from F_{i-1} to F_i the last has time to process the previous information. After F_m, the computer makes a final estimation for T with the speed V op/sec. Taking into account the computer speed V of the monitoring system at given period of time τ for estimation of T signal value we can express the condition of information influx matching in terms of the following formula:

$$V\tau = n_1 N_1 = \alpha_1 n_2 N_1 N_2 = \ldots = \alpha_1 \cdots \alpha_m n_m N_1 \ldots N_m \frac{V}{v} \qquad (1)$$

586

where N_i is possible number of different values of t_i, n_i is sample volume; α_i is probability of classificating t_i as a signal one.

The presence of random deviations from matching conditions in T in flux requires the buffer memory for storage of variants delaying from F_{i-1} in each device.

Two types of memory characterized by different forms of the information transfer from F_{i-1} to F are given:
1) preserving the constant variant number;
2) preserving variants for given delay time.

In work [2] were obtained the estimate of probability of an error system and wanted memory capacity with constant waiting time as well as an error system and wanted delay memory capacity with constant number of memory sells. The principle scheme considered above makes possible a complex using the different wave ranges (optical, infrared and radiorange) for the Earth's surface sensing. However, the problem concerning the realization of such scheme requires the more comprehensive consideration.

The criteria of estimation of the monitoring system effectivity lies in probability of solving of a global problem of detection and classification of phenomena on the Earth's surface. This probability depends on all complexes of parameters of a system and, in particular, on distribution of anomal signals and noises (phone).

One of the possible models of the monitoring system may be founded on the conception of "spotness" of space. As usual, the moving anomaly reserves a trace for itself which may change the spot structures and sizes. The immovable anomaly may also cause the similar local changes and be the smaller size The character of these changes depends on the relation between spot and anomaly sizes. In order to solve the problem of detecting the anomalies based on using "spots", it is necessary to have their distribution which, obviously, may be obtained only by empirical way.

Under real conditions, the study of "spots", acquisition of statistical data on them and the use of this data in a detector present difficulties. The conventional method of detecting spots is the cut-off selection method. Because of this, the spot is considered as a part of space for which the parameter of environment for given channel exceeds or does not exceed a cut-off value. The development of algorithm of spot contour description and creation of the computer program for calculating their statistic parameters

587

wait for further consideration.

The problems of detecting the anomalies are included into the general problem of mapping according to data on microwave sensing the Earth's surface The recognition of homogeneous formation contours and the determination of geophysical characteristics may be carried out by microwave radiometry. Therefore the development of new methods of automatic data processing from satellite and fixing the measurements on the surface are required.

After satellite K flights, we obtain the sample from K - ζ processes for two-dimensional processing. Here ζ flights are excluded from studing as no having useful information. The knowledge of each flight course using the two-dimensional correlation analysis and interpolation method permit us to make and print a map of radiobrightness temperature which may be used directly when observing different phenomena on the Earth's surface. The simpliest algorithm of making such map by a computer is determined in the following way.

Let $W^{(i)} = \{ \varphi^{(i)}, W_1^{(i)}, W_2^{(i)}, \ldots, W_{\omega-1}^{(i)}, W_\omega^{*(i)}, t_\omega^{(i)}, W_{\omega+1}^{(i)}, \ldots, W_\mu^{(i)} \}$ be a vector of registration data of i flight, where $W_\omega^{*(i)}$ is reper object response; $t_\omega^{(i)}$ is flight time moment over reper object; $\varphi^{(i)}$ is angle between course and given constant direction; $W^{(i)}$ are measurement results

After K flights, the computer obtains matrix $\| W \|$ the lines of which are vectors $W^{(i)}$ and reduces it by removing ζ lines as no having the response from reper object or useful information.

It should be noted that for further operation $\| W \|$ lines are recorded so that the $W^{(i)}$ corresponds to $\varphi^{(i)}$ in one direction. Then on placing $\| W \|$ lines in increasing order of $\varphi^{(i)}$, the brightness temperature at the arbitrary point $M(\tau, \varphi)$ of the region being studied may be calculated according to the formula

$$W(\tau, \varphi) = W^{(i+1)} + (\varphi - \varphi^{(i+1)}) \frac{W^{(i)} - W^{(i+1)}}{\varphi^{(i)} - \varphi^{(i+1)}} \tag{2}$$

where $\varphi^{(i+1)}$ and $\varphi^{(i)}$ are the closest to φ.

There are also other algorithms of interpolation.

The development of operative methods for determining the atmosphere and underlying surface geophysical characteristics is considered to be the important aspect for construction of the monitoring system. The automatization of satellite measurement processing involves the increase of quality of mathematical methods applied. The filtration of errors on registration the telemetric signal and the estimation of accuracy of geophysical parameter measurements

588

are of great importance. The highest accuracy of geophysical parameter determination may be achieved by joint using the information containing in remote measurements and a priori information which may be obtained by other ways.

Some formalization possibilities of remote sensing inverse problem will be demonstrated by way of example, by processing microwave radiometric measurements from the oceanographic satellite Cosmos-1151 [5,6] . In January 1980 this satellite was launched into a circular orbit at the altitude of 650 km and a slope angle of 82,5° to equator plane. Fourchannel microwave radiometer mounted on the satellite, recorded nadir radiothermal radiation at the wavelengths of 0,8; 1,35; 3,2; 8,5 cm. In the course of present experiment there was developed the statistic method for determination of atmospheric water vapor abundance ς, liquid water content of clouds W, ocean surface temperature T_s and wind speed V at the oceans surface from microwave measurements in above mentioned channels. The method takes into account statistic properties of errors in absolute microwave measurements and available a priori information on the sought parameters.

A block diagram for automatic processing of satellite measurements is given in Fig.1. At the primary processing stage the file of telemetric readouts of the output signal in operating channels of the microwave radiometer is into a computer. The values of the signal normalized to internal calibration are determined. These normalized values are transferred to the scale of absolute brightness temperatures T_{br}. For this purpose the homogeneous earth surface regions in cloudness conditions are used as standard radiators. In parallel to T_{br} determination, the covariance matrix C of absolute measurement errors in various microwave channels is estimated by the proceedings presented in [6] . The obtained brightness temperatures are averaged according to the given space resolution, which partly makes up for the difference in antenna patterns in various channels.

At the secondary processing stage n geophysical parameters along the satellite orbit projection are determined from the obtained spectra of T_{br}. The parameters are estimated by solving the set of equations which presents the relation between geophysical parameters and T_{br} in m microwave radiometric channels:

$$\Psi(\Theta) = T + \delta T \qquad (3)$$

where $\Psi(\Theta)$ is m – dimensional vector function of n – dimensional vector of geophysical parameters ; T is m – dimensional vector of the measured value T_{br}; T is m – dimensional vector of measurement errors. In solution of the inverse problem are used additional limitations to determinable parameters taking into account a priori information on permissible variation boundaries of these parameters. This makes it possible to avoid senseless values,

589

involved with application of, for example, the "quasistical method" (negative values of the cloud liquid water content in Fig.1,2 [7]).

As a result, the optimal value Θ^* is determined by solving the extremum problem

$$\Theta^* = \arg\min_{\Theta \in F} \mathcal{P}(\Theta, T) \qquad (4)$$

where F is the set singled out in n - space of parameters by a priori limitations. The objective function $\mathcal{P}(\Theta, T)$ is constructed by the least-squares technique. In this case the value of the covariance error matrix, obtained at the primary processing stage, is used:

$$\mathcal{P}(\Theta, T) = [\Psi(\Theta) - T]^T C^{-1} [\Psi(\Theta) - T] \qquad (5)$$

This approach enables the information provided by remote measurements and a priori data on the sought parameters to be optimally considered in the solution. The least-squares technique makes it possible to estimate the accuracy of geophysical parameter determination with due regard for noise and calibration measurement errors. The extremum problem (4) is solved by gradient methods. It does not take much machine time due to small dimension of the problem. When processing every following point of measurements, the solution obtained for the preceding point is used as zero-order approximation. This saves machine time because the values of geophysical parameters in neighbouring geographic points stand close together.

The present method has the advantage of single-valued relation between the function of $\mathcal{P}(\Theta, T)$ and the density of posterior parameter distribution according to the problem (4). The value of $\mathcal{P}(\Theta, T)$ at its local minimum point at F may serve as a quality criterion for the obtained solution in automatic processing. A very large value of $\mathcal{P}(\Theta, T)$ indicates either a hardwave error or inadequacy of the accepted model (3). The condition may serve as a solution quality criterion [8] .

The meansquare errors in geophysical parameter determination for the present experiment are the following: Q-0,3 g/cm^2; W-0,07+0,1 cg/m^2; V-3+4 m/sec. The values of Ts may be determined with reasonable accuracy from measurements in radiometer nadir channels of satellite Cosmos-1151 only in the absense of foaming caused by storm. Under these conditions the mean-square error of Ts determination constitites 2-3K.

In Fig.2 is shown a latitudal distribution of Q, W, ΔV and Ts determined from measurements with satellite Cosmos-1151 over the northern part of the

590

Atlantic Ocean on January 25, 1980. In conformity with available models, the value of ΔV stands here for the difference between V and the critical wind speed of $V_o (V_o \approx 7 + 10$ m/sec) which induces foaming. At the background of latitudal humidity distribution one can clearly see anomalous regions of Q increase caused by cloudv systems of the intertropical convergence zone (2-6 S,L) and powerful atmospheric front at 35-50 S,L. Marked anticorrelation of W and ΔV values in this front zone is due to incomplete distinction between these parameter variations in remote measurements.

For comparison, in Fig.3 are given the processing results of the sance measurements neglecting a priori limitations to parameters. It can be seen that measurement errors in this case result in the negative values of W and ΔV parameters which present difficulties for interpretation. The negative values of ΔV obtained at 2°-4°S,L and 6°-10°S,L most probably indicate the absence of foaming in these regions. In Fig.2 are given the values of Ts obtained with regard for $\Delta V=0$ limitations. These values are in good agreement with climatic data for these regions.

References

1. Fleishman,B.S. "Elements of potential efficiency theories for comples systems", Moscow, Sovetskoe Radio, 1971.

2. Fleishman,B.S., Krapivin,V.F. Izvestiya AN SSSR, Tehn.Kibernetika, 1965, N°2, pp.25-34.

3. Basharinov,A.E., Gurvich,A.S., Egorov,S.T. "Radio emission of Earth as a planet", Moscow, Nauka, 1974.

4. Gurvich,A.S., Egorov,S.T., Kutuza,B.G. "Earth investigation from space", 1981, N°1, pp.63-70.

5. Akvilonova,A.B., Armand,N.A. et al., "Determination of temperature of Oceanic surface and other geophysical parameters using the results of microwave radiometric measurements from satellite Cosmos 1151", Ocean investigation by remote methods, MGI, Sevastopol, 1981, pp.131-138

6. Akvilonova, A.B., Egorov,S.T. et al., "Instruments and methods for processing microwave radiometric measurements performed from satellite Cosmos 1151, Ocean investigation by remote methods, MGI, Sevastopol, 1981, pp.123-130.

7. Chang,A.T., Wilheit,T.T., "Remote sensing of atmospheric water vapor, liquid water and wind speed at the ocean surface by passive microwave techniques from the Nimbus 5 satellite", Radio Science, v.14, N°5,1979.

8. Bard,Y., "Nonlinear parameter estimation", Academic Press, 1974, New York, San Francisko, London.

```
┌─────────────────────────┐
│ PRIMARY PROCESSING      │ ◄────────  parameters of the
│ Determination of        │            standard regions
│ T_BR and C              │
└─────────────────────────┘
            │
            ▼
┌─────────────────────────┐
│ SPATIAL AVERAGING       │            model
│                         │            parameters
└─────────────────────────┘
            │
            ▼
┌─────────────────────────┐
│ SECONDARY PROCESSING    │ ◄────────  a priori
│ Determination of the    │            limitations
│ geophysical parameters  │
└─────────────────────────┘
```
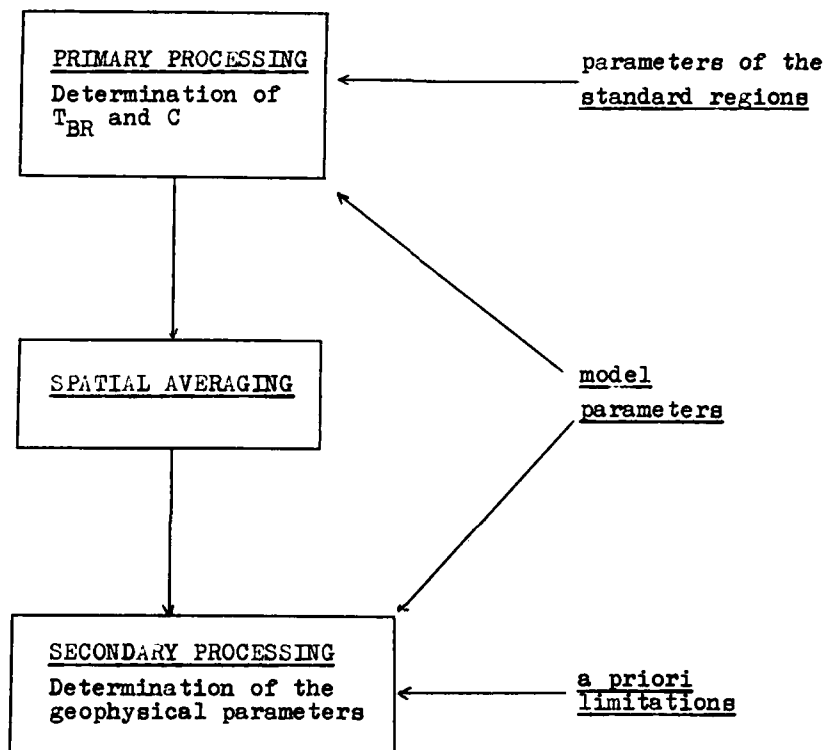
Fig.1. Automatic processing block diagram for
microwave radiometric measurements from
Cosmos-1151.
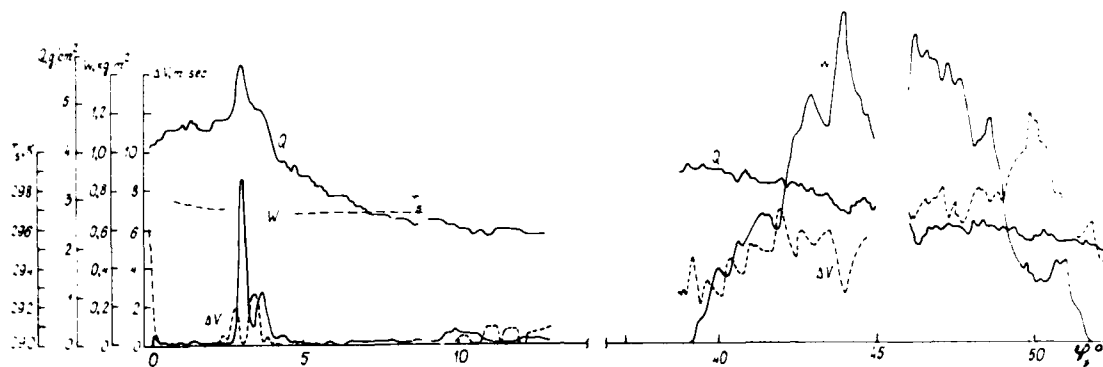
Fig.2. Latitudal distributions of Q,W, V and Ts
obtained by processing satellite measurements
over northern part of Atlantic Ocean on
January 25, 1980.
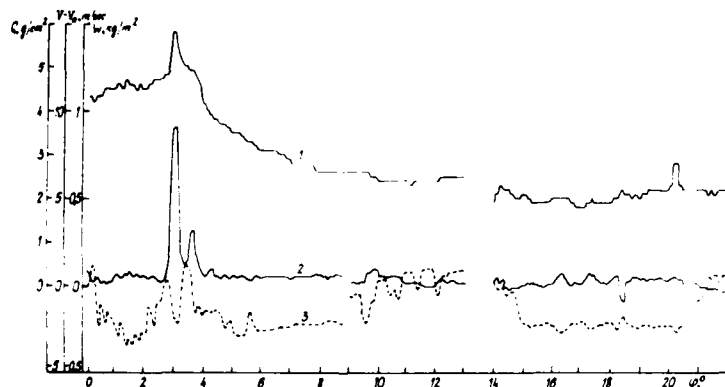
Fig.3. Latitudal distributions of Q,W, V obtained by
processing the same measurements neglecting a
priori information.

STUDY OF SEDIMENTARY FLOW AND DISPERSION
FROM THE RIO BERMEJO BASIN THROUGH SATELLITE INFORMATION

Ernesto E. Portalet
Aurora Quinteros
Osvaldo Bonanatta
Gloria Pujol

Comisión Nacional de Investigaciones Espaciales
Buenos Aires, Argentina

SUMMARY

Here, a synthesis of the geomorphologic, physiographic and hydrologic characteristics of the three basins is given. Likewise, the methods used for information processing and analysis are described.

With the results obtained through this work the importance and scope of satellite images is stressed with respect to the possibility of a better knowledge and utilization of the rivers since the sedimentary flow directly falls into great economic activities like the construction of a hydroelectric complex.

Besides, since Landsat satellites allow to obtain sequential information the method may be used to control periodically sedimentary changes and river volumes which are produced seasonally.

MAPPING OF PHYTOECOLOGICAL UNITS OF THE "CERRADOS" OF THE CENTRAL PLATEAUS OF BRAZIL

Yara Simas Eneas *

SUPERINTENDÊNCIA DE RECURSOS NATURAIS E MEIO AMBIENTE-SUPREN/IBGE
Rua Equador, 558/2º andar - Santo Cristo
20220 - Rio de Janeiro - RJ
BRAZIL

ABSTRACT

The mapping of phytoecological units in the Region of Cerrado, of Brazil, has the purpose of giving a global view of the result obtained through the mapping of a big extension of the country's vegetation cover, where predominates the "cerrado". The phytoecological units represent the close links between the vegetation physiognomy and other environmental elements. Thus, its overall goal is to provide elements which will serve as a basis for the setting uf of a rational settlement and development policy of a still not well known area because of its complexity.

On the Cuiabá Sheet (Lat. 12^0S - 16^0S - Long. 54^0W - 60^0W), which constitutes the main subject of this paper, there were identified 13 (thirteen) different units in which, besides several "cerrado" physiognomies, some forests were found. On the north of the area it occurs the contact between the dominium of the "cerrado" and the Amazonian dominium. Right now in this transition zone takes place a new, different, phase of territorial occupation, operated by large enterprises implanting agricultural and cattle raising projects. Considering the outmost vulnerability of the ecosystem of the transitional areas, particularly concerning the soils, we believe that this study could be useful for further detailed research viewing programing purposes.

Due to the big extension of the "cerrados" continuous area, the IBGE applied the remote sensing technique to realize such important task in a relatively short time with a small staff.

INTRODUCTION

The "cerrado" itself constitutes the typical vegetation physiognomy of the Central Plateau of Brazil. It covers an area of more than 2 000 000 km^2 stretching out either to the North - towards the Amazonian Region - or to the south, reahcing the State of São Paulo.

The "cerrado" not so only depends on climate conditions - warm and semi-humid climate with 4 to 5 dry months - but also it is influenced by other environmental factors, such as topography, lithology and soils, not to mention the man's action by fire.

The denomination "cerrado" actually includes a variety of physiognomies placed in a sequence which stretches from the "campo limpo" (grassland) to the "cerradão" (xeromorphical forest)

---

*The author is responsible for the Cuiabá sheet and took part in a group which worked in the project as a whole, whose participantes are: Japiassú, A.M.; Mello Fernandes, A.L.; Kuhlmann, E.; Balassiano, H.M.M.; Bulhões, M.G. and Silva, Z.L.

passing through other types whose characteristics are the greater or smaller density of woody plants and scrub.

In the last years, government agencies, concerned with the possible expansion of the agricultural frontiers, developed several researches about tne Region of Cerrado whose topographical characteristics are propitious for mechanization. Some researchs and studies have been carried out by IBGE with the aim of obtaining the environmental characterization of the this region. Those studies served as a basis for synthesis maps, such as that of the phytoecological units of the area subject of this study.

METHOD

The map of phytoecological units was elaborated based on the vegetation cover map and making use of elements provided by geomorphological mapping, as well as informations about the climate and other available data refering to soils, geology and land use. Through the mapping there were identified 52 (fifty two) different units in the whole area under study.

For the basic vegetation map, was exclusively taken into consideration the degree of ecological perception, according to the concept of Long (1974). This method is the most suitable for the scale corresponding to ghe ecological region and is made evident by types of vegetation. The physiognomical aspect of the present-day vegetation, which reveals to a certain extent the man's intervention, was taken into consideration as well.

28 types of vegetation were classified in the area which is represented by 12 sheets 1:1.000.000.

The methodology employed in this mapping included the following procerues:

a) Selection of the images according to favorable periods concerning to the differentiation of the vegetation types;

b) Visual interpretation of the images - LANDSAT channels 5 and 7 (1:1.000.000) and RADAR (1:1.000.000 and 1.250.000).

c) Preliminary mapping in accordance with established patterns based on both interpretation and refering to the documentation.

d) Field check (ground and aerial);

e) Re-examination of the established patterns;

f) Setting up of legend;

g) Final mapping.

RESULTS

The mapping of the Cuiabá sheet led to the identification of 13 (thirteen) phytocological units: 1) Parecis Plateau; 2) Parecis Platform; 3) High Teles Pires; 4) Xingu Depression; 5) High Gua poré Pediplan; 6) High Paraguai Pediplan; 7) Cuiabá Pediplan; 8) Araras Mountain Ridge; 9) Paranatinga Depression; 10) High Garças Pediplan; 11) Rondonópolis Depression; 12) Guimarães Plateau; 13) Pantanal Plain.

It follows the summary description of the units considered more significant:

1. Parecis Plateau: A sedimentary plateau with uplifted meridional edge ending in "cuestas" with southward front. The biggest altitudes reach roughly 700m. It consists of cretaceous sandstones containing detrital cover ("Cachoeirinha" Formation) which is typical of the South-American Surface in the central plateaus of Brazil. This surface gives origin to high acidity

598
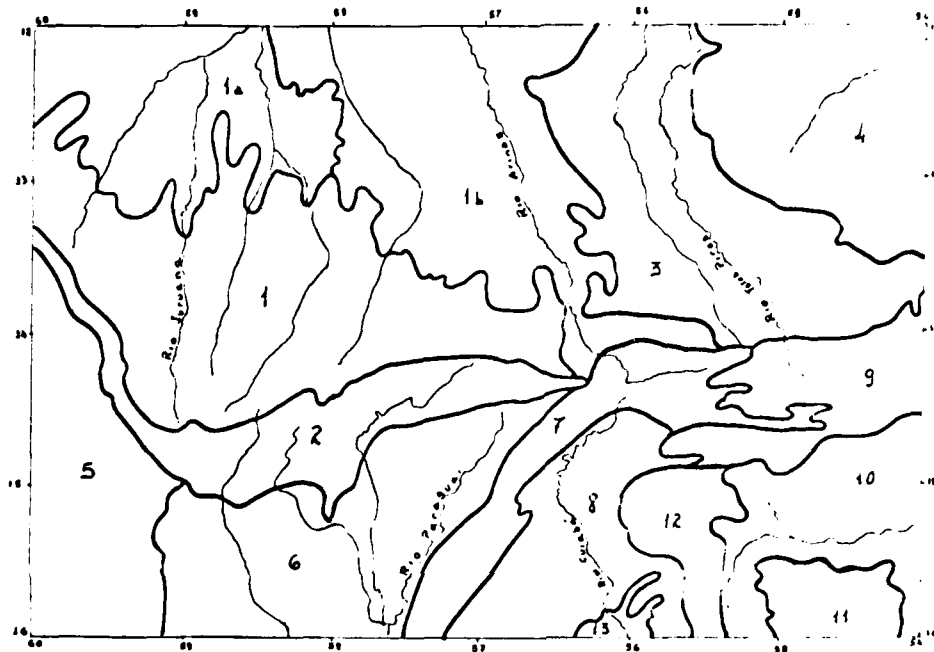
Fig. 1   Scale 1:4.500.000
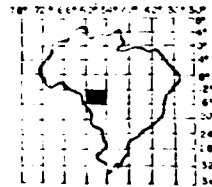
Phytoecological Units:

1. Planalto dos Parecis (Parecis Plateau): 1ª Bacia do Juruena (Juruena Basin); 1b. Bacia do Arinos (Arinos Basin); 2. Patamares dos Parecis (Parecis Platform); 3. Alto Teles Pires (High Teles Pires); 4. Depressão do Xingu (Xingu Depression); 5. Alto Guaporé (High Guaporé); 6. Alto Paraguai (High Paraguai); 7. Serra das Araras (Araras Mountain Ridge); 8. Pediplano Cuiabano (Cuiaba Pediplain); 9. Depressão do Paranatinga (Paranatinga Depression); 10. Alto Garças (High Garças); 11. Depressão de Rondonópolis (Rondonópolis Depression); 12. Chapada dos Guimarães (Guimarães Plateau); 13. Pantanal (Pantanal Plain).

soils, poor in exchangeable bases and with low water retention. It is responsible   for   the predominantly flat topography of the plateau's southern part. The vegetation is "cerrado" with poor physiognomies of "cerrado ralo" (xeromorphic well open woodland)   and   "campo   sujo" (xeromorphic very open scrub).

The annual precipitation is 1.300 - 2.200mm, with low values of potential evapotranspiration, reaching 1.282 over the year. The hydric surplus is high (400-1.200mm) and my extend to a   7 months period. On the contrary, there are low hydric defficiencies which occur with a duration of 5 months.

The climate varies from humid to super-humid; concerning the thermic efficiency is classified from mesothermic to megathermic.

The plateau bends northward where two depressed sectors, whith undulating topography,   are located:

a) Jurema Basin, with "cerrado denso" (xeromorphic low arboreal woodland). Valley forest range along the main rivers constituting the penetrations of the evergreeen forest farther North, characteristic of the amazonian dominium.

b) Arinos Basin. Characterized by evergreen forest which alternates with big spots of "cerradão" (xeromorphic forest).

2. Alto Guaporé: (Higher Course of Guaporé River). A pediplan elaborated by denudational processes developed at the Parecis plateau periphery, predominating the surface of Paraguaçu Cycle.

Its topography varies from undulating to flat, the latter one where detrital deposits   were formed. It features large residual reliefs, consisting by crests and mountain ranges, made up on the metasediments of Aguaperí Series. Remmantes of the South American Surface are found   at the top of these reliefs.

Tle climate varies from the sub-humid and negathermic - the predominant - to the humid   and mesothermic. The annual precipitation varies between 1.200 to 2.000 mm, from the South to the North. The hydric defficiencies (100/200mm) are inferior to the hydric surplus (300/400 mm) and occur whithin a 6 months period.

The vegetation cover physiognomies are strictly related to this climate variation and to   the landforms.

The forest is found on the very pediplan area varying South-North, from the semideciduous type whith "babaçu" (Orbignya martiana) to the evergreen, dense, rich in species, similar to   the amazonian forest.

"Cerradões" appear in the pediments located on the periphery of residual reliefs. The "cerrados", in turn, are found on tops of them. Some seasonal flooded grassland and   "capões de   matas" (forest spots), appear on the low levels of the Guaporé sedimentary   plain   beside   some physiognomies of cerrado,

In the whole forest area, big farms, mainly for cattle raising, are taking the place of   the original vegetation.

3. Alto Garças: It is a high pediplain (800-900m for the highest altitudes)   formed   by sedimentary Paleozoic and mesozoic rocks, with some basalt outcrops. Contains large detritical lateritic cover, formed during the Sul Americano Cycle, being responsible for the poor quality of the soils. Where this cover was removed, better soils, originated by sandstones,   shalles or basalt, are to be found.

The flat to slightly undulating topography is predominating, although existing some dissected areas.

Concerning its climate the annual precipitation is 1.200-2.000 mm, potential evapotranspiration varying from 997-1.140mm. The period November to April is characterized   by hydric surplus
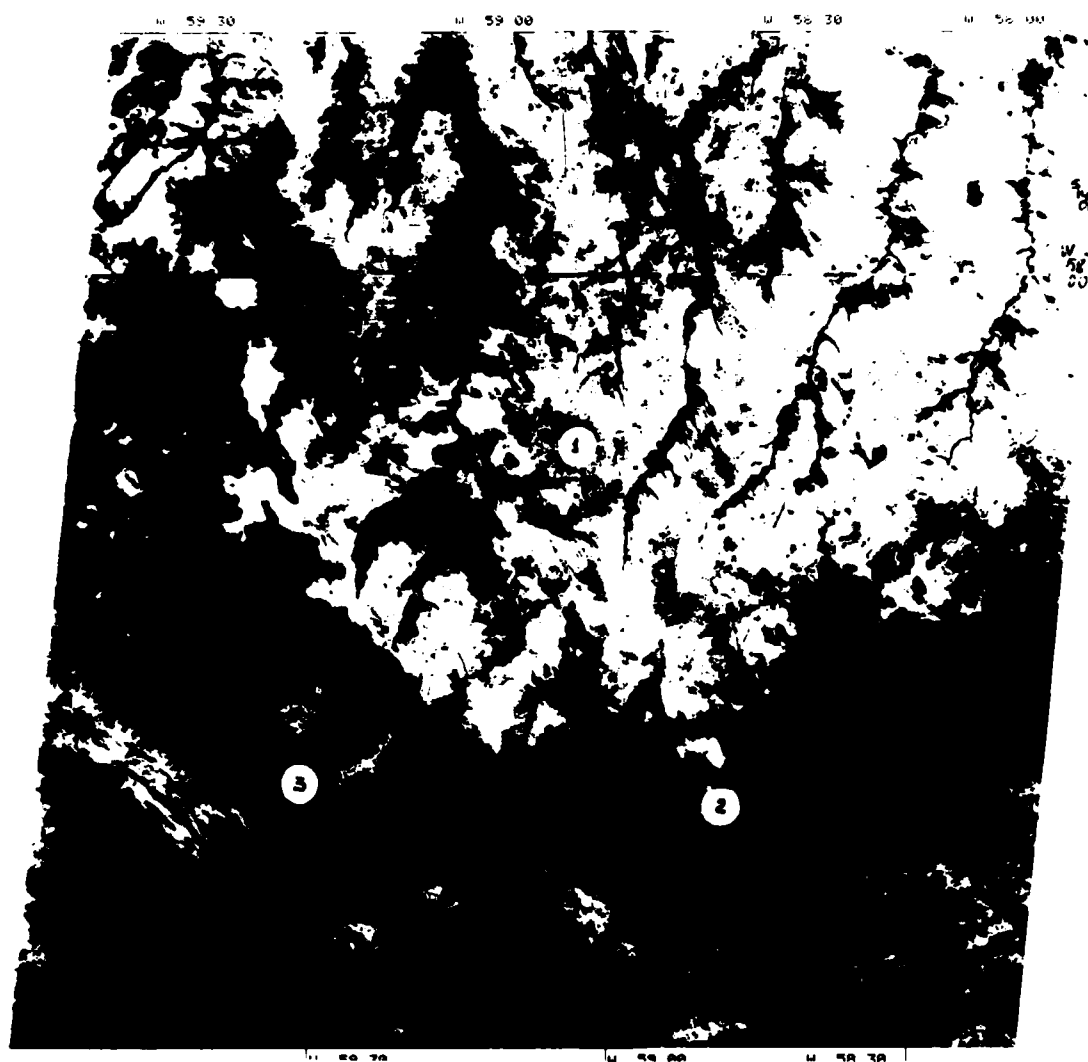
24JUL76 ORB 384 PT 22 C: S14-26/W058-56 MSS 5   SOL: EL29 AZ056 B 189 LC 20384 INPE/LANDSAT 176206-124018-5
                        N: S14-26/W058-51   RO1 N   =BRASIL= 19JAN77 CENA 010

Fig. 2 - Some phytoecological units in W Cuiabá Sheet:
       1. Parecis Plateau, 2. Parecis Platform, 3. Alto Guaporé Pediplain

24JUL76 ORB 384 PT 22 C: S14-26/W058-56 MSS   7 SOL: EL29 A2056 B 189 LL 20384 INPE/LANDSAT 176286-124018-7
NI S14-26/W058-51   R81 N   =BRASIL= 19JAN77 CENA 810

Fig. 3 - The same units as shown in channel 7.

602

(400-800mm), while in the May to September period there are deficits from 100 to 200mm. So, it is a humid and megathermic climate, going over mesothermic in the more elevated areas.

The vegetation cover is the "cerrado", mainly "cerrado denso" (xeromorphic low arboreal woodland). In the dissected areas predominates the "cerradão" (xeromorphic forest), also occuring some semideciduous forests.

4. Cuiabá Pediplain: It is a surface formed through erosive processes developed on the periphery of sedimentary plateaus lying to the north and to the east of the area.

The pediplanation connected to the Velhas Cycle occurred during the low Pleistocen. The process originated lateritic concretionary crusts, which cover the rocks of the Cuiabá Serie, specially quatzites and phyllites. There are many residual reliefs, as the crests in the western part of the unit, constituted by folded structures facing northeast. The soils of this unit are poor, thin, excepted those developed on the alluvial deposits related to the Paraguaçu Cycle. There are also some richer soils where coluvial deposits, originated from limestone, are located.

The climate varies from sub-humid to first-humid; fourth-mesothermic to third-mesothermic, concerning the thermic efficiency. The annual precipitations range from 1.400 to 1.800mm, the potential evapotranspiration from 1.140 to 1.425mm. The hydric defficiencies range from 200 to 300mm, within a six months period (Apr.-Oct); the hydric surpluses from 100 to 800mm (Jan. - Apr.).

The vegetation cover is "cerrado". The north is dominated by "cerrado ralo", alternated with "campos sujos", with a well open herbaceous layer, leaving the soil pratically uncovered. Here and there appear "campos limpos" (xeromorphic grassland).

GENERAL CONCLUSION

The remote sensing technique provides an excellent working tool for the identification of broad phytoecological units in small scale. Even so, many additional informations have to be used, including those obtained through field survey, to achieve reliable results.

The use of different types of remote sensing data, in various scales, is advisable to facilitate the task of the mapping.

Radar mosaics and Landsat imagery (channels 5 and 7) were enough to accoomplish this study.

Special cares were taken concerning Landsat scenes, such as the selection of optimum date of the year, considering the purpose of the mapping and the photographical process of the imagery. For instance, for the "cerrado", the optimum dates are during the dry season, because the small differences among the various physiognomies are best enhanced so, it will be easier to distinguish the different types of "cerrado". The same occurs for separating "cerrado" from "caatinga" (xerofitic forest), as the species of the "caatinga" become leafless in the dry season, while the trees of the "cerrado" remain practicially unchanged. But to distinguish the different levels in the alluvial plains, and its types of vegetation, it is imperative the utilization of multiemporal data along the rainy season.

Concerning the field checking of large areas, it is advisable the use of underflights (100-200m from ground level), still at the begining of the task, since the preliminary interpretation of a significant area is finished. This procedure, not only allows the final mapping of this first area, but will make easier the interpretation of the following parts, througn the already established patterns. Still, the underflights might decide the necessity of eventual ground field checks. The radar mosaics are very efficient as a support of this aerial operations, specially in areas with few marks of land se (villages, hamlets, roads etc.) which might be used as references for the flight lines. In such areas, the use or radar (side-looking type) is more helpfull because it outlines the landforms better than the Landsat, specially in forest areas. The most adequate scale for this purpose is 1:250.000, because it suits well to the moderate velocity of the flight, possibiliting good observation conditions for the interpreter.

At last, we may say that the method used made possible the accomplishment of the mapping in   a relatively short time with a small staff.

For detailed surveys we advise the use of additional remote sensing informations,   such   as conventional and multispectral aerial photos.

REFERENCES

Ab'Saber, A.N. 1954. O Planalto dos Parecis na Região de Diamantino (M.Grosso) - Notas Prévias e fotografias. Bol. Paulista de Geografia, São Paulo.

_____. 1971. A Organização natural das paisagens inter e subtropicais brasileiras. Simpo- sio sobre o Cerrado, São Paulo.

Departamento Nacional da Produção Mineral (M.M.E.). 1974, 1975. Carta Geológica do Brasil   ao Milionésimo, Brasília.

Domingues, A.P. et alii. 1980. Cartas de Geomorfologia   da   área do Cerrado. Projeto   Cerrado IBGE. EMBRAPA (Inédito), Rio de Janeiro

Ferri, M.G. 1944. Ecologia dos cerrados. Simpósio sobre o cerrado, 4. Brasília.

Kuhlmann, E. et alii. 1980. Região do Cerrado, uma caracterização ambiental (cobertura vegetal), Projeto Cerrado IBGE/EMBRAPA (relatório inédito) Rio de Janeiro.

Moraes. E.M.L.; Leite, M.A. 1975. Mapeamento fotogeomorfológico através de imagens do Landsat 1. INPE (CNPq) S. José dos Campos.

Moraes, E.M.L.; Santos, A.P. 1978. Deforestation Planning for cattle graizing in Amazon Basing using Landsat data, INPE (CNPq).

Morai, S.A. 1974. Interpretation and mapping of natural vegetation In: Estes, J.E.;   Singer, L.W. Remote Sensing Techniques for environmental analysis. Santa Barbara, Califorinia.

Nimer, E. et alii. 1980. Balanço Hídrico e Clima da Região dos Cerrados, Projeto Cerrado - IBGE EMBRAPA (relatório inédito), Rio de Janeiro.

Ramalho, R. 1980. Pantanal Matogrossense: Compartimentação Morfológica. C.P.R.M. Rio de Janei- ro.

Varela, S. 1977. El uso de las imagenes de satelite en la direcion del inventário   nacional florestal. Seminário International sobre el uso da los sensores remotos en el   desarrolo de los países. México.

Veloso, H.P. 1972. Aspectos fitoecológicos da Bacia do Alto Paraguai. Biogeografia, U.S.P.,São Paulo.

THE USE OF LANDSAT IMAGERIES FOR MAPPING OF
FISHPONDS IN THE PHILIPPINES

Ernesto N. Lorenzo
Cesar E. Magno

Natural Resources Management Center
Quezon City, Philippines

SUMMARY

The value of Landsat for resource inventory and monitoring is well known. Several studies conducted by the NRMC have shown its applicability as a tool for resource management and planning. The Philippines has extensive fishpond areas, an important resource which contributes about 8% of the total annual fish production. The formulation of an effective management scheme for full utilization of this resource requires several types of information. At present, however, there is a lack of information on fishponds in most parts of the country especially data on their geographic distributions. It is for this reason that this study is carried out to determine its value as cost and time-efficient survey method for inland fisheries. The primary objective of this study is to determine the usefulness of Landsat imageries for determining the fishpond areal extent and geographic distributions.

Preliminary results showed that because of their distinct coloration and unique patterns on false color composite imageries, separation of fishponds is possible. However, it was also shown that in certain areas, and especially in areas adjacent to rice fields, accurate delineation may be unlikely to be achieved during certain times of the year. To find solutions to this problem, a detailed analysis was carried out using Landsat imageries collected from 1972 to 1978 (representing the two distinct seasons in the country). Landsat imagery interpretation confirmed that not all imageries are useful for mapping but through proper selection of Landsat date of coverages fishponds can be easily separated on false color composite imageries. This study was also extended to fishponds areas located adjacent to irrigated fields. The results obtained from this study now serve as the basis in the conduct of nationwide Landsat-based fishpond mapping project. The procedures used and the results obtained including diagrams and tables will be presented.

AD P002038

EVALUATION AND DEVELOPMENT OF TECHNIQUES FOR CROP INVENTORY IN THE WHEATBELT OF WESTERN AUSTRALIA USING SATELLITE DATA

N.A. Campbell[1], F.R. Honey[2], P.T. Hick[2] and M.D.W. Carlton[2]

[1] CSIRO, Division of Mathematics and Statistics
Perth, WA, Australia
[2] CSIRO, Division of Land Resources Management
Perth, WA, Australia

ABSTRACT

Progress results from an ongoing collaborative project between the Commonwealth Scientific and Industrial Research Organization (CSIRO) and Cooperative Bulk Handling (CBH) to evaluate the role of remotely-sensed data in crop production forecasting in Western Australia are outlined.

The project has three distinct phases: i) discrimination of grain crops from pasture, and determination of the area planted to crop; ii) discrimination between grain types; and iii) estimation of yield.

Estimation of the area planted to crop has received most attention to date. The analysis of data from several overpasses improves the discrimination of crops from pasture and hence the estimation of the area planted to crops. Variations in planting practice and the effect of this variation on the identification of areas planted to crop are discussed.

INTRODUCTION

The Western Australian wheatbelt is situated in the south-west corner of Australia (Figure 1). It covers an area slightly in excess of 6 million hectares. Yearly rainfall ranges between 300 and 600 mm. Wheat accounts for approximately 85% of the area planted to crop. The crop is planted after early winter rains, usually in May and June, and the harvest is gathered between October and December. Total yield varies between 3.5 and 6 million tonnes. To enable planning for regional and central storage, transport and marketing, considerable effort is expended in obtaining early estimates of area planted to crop, of crop type and of potential yield.

Projects such as LACIE (Large Area Crop Inventory Experiment) in the United States have used satellite data from different times in the growing season to monitor crops and have produced impressive results. A collaborative project by the New South Wales Department of Agriculture and IBM Australia (Dawbin and Beach, 1981) has reported encouraging results.

607

Large variations in soil type occur across the whole wheatbelt of Western Australia; this variability is even observed within paddocks. There is a nonuniform distribution of rainfall in space and time and also in intensity. Farm management practices such as planting time and planting technique, and fertilizer levels applied, differ between farms and between districts.

In 1978, CSIRO began a pilot project to assess the role of Landsat data for crop discrimination in the wheatbelt of Western Australia. Unfortunately only two cloud-free images were acquired. While results held some promise for the identification of wheat and barley, differences between and within paddocks of the same crop were sometimes as great as differences between paddocks of different crops. The lack of temporal data resulted in a postponement of further work until the Australian Landsat Station commenced operation, in 1980. Data from the Landsat satellites are now recorded for the whole of Australia every eighteen days. Since these data can be acquired by a user within ten days of an overpass, the potential now exists to use Landsat data as a practical and timely method for crop assessment.

THE CURRENT PROJECT

The current project commenced in 1981 and involves collaboration between the remote sensing group in the Division of Land Resources Management, CSIRO, the Perth group of the Division of Mathematics and Statistics, CSIRO, and Co-operative Bulk Handling [CBH are responsible for the collection, storage and transport of the wheat harvest in Western Australia.] The project is designed to evaluate the capability of Landsat data to determine areas planted to crops, to discriminate between crops, and ultimately to estimate yield in the wheatbelt of Western Australia. The effect of variation in soil type, the spatial and temporal pattern of rainfall, and the individual management practices of farmers on this capability is to be examined.

The proposed project is divided into three distinct phases:

   i) the discrimination of grain crops from pasture and the determination of the area planted to crop;

   ii) discrimination between grain crops of different types; and

   iii) estimation of yield.

The project is designed to use the Landsat data for several overpasses during each growing season, with the scenes being registered to the Australian map grid. Ultimately the Landsat data will be integrated with data on soils and the climatic and management variables.

This paper reports some preliminary results related to the first objective.

Figure 1 illustrates the areas chosen for the study. Sites within each of seventeen locations have been included in the study. Each site consists of 3-5 farms distributed throughout the locality. The sites were chosen by CBH district superintendents, to provide a representative sample of soil types and management practices.

Six Landsat scenes cover the study area (Figure 1). Twenty-six Landsat tapes were purchased during 1981; these cover the period 18 June to 1° November. Area H had seven cloud-free images, areas F and I had six, and area G had five cloud-free images.

608

GROUND-TRUTH DATA

CBH district superintendents collected detailed ground-truth data in consultation with the farmers involved in the study. Three sets of cards provide detailed records of each paddock on each farm in the study. Details of the site, including the name of the farmer, the Landsat scene, local government area and the nearest rail siding for delivery of grain are contained on a master record card. This card also records the availability of historic records of rainfall, fertilizer and cropping details, together with details of the area planted or quantity of grain to be retained on the property.

Detailed information on crop development for each paddock in the study is recorded on crop phenology cards. The farmer keeps one set of cards and the CBH district staff keep another set. The name of the farmer and the paddock name and number, and the grain crop, including variety and number of hectares planted, is recorded. A pictorial record of the development of the crop: for wheat - planting; emergence; 3-6 leaf stage; 6-8 leaf stage; fully tillered; jointing; flowering; and maturity, is then given. The date at which the illustrated growth stage is reached, together with details of weed growth (type, density, patchy or uniform cover, etc) and crop health (including insect damage, fungus or other disease), is entered by the farmer. The CBH district staff visit each farm in the study fortnightly, with details of growth stage, weed growth and crop health for each paddock being recorded at the time of the visit.

Paddock details are recorded on soil type and paddock history cards. The name of the farmer; paddock name, number and description; area in hectares; landscape position; terrain and microrelief; elevation; and aspect are recorded. The soils within each paddock were grouped according to their principal profile form (Northcote, 1971), a system based upon depth of soil horizons, colour, texture, gravels, mottling and consistence and pH. The Atlas of Australian Soils (Northcote et al, 1967), the pre-release soils and landform mapping prepared by the Western Australian Department of Lands and Surveys, air photo interpretation and ground inspection were used to map the soils. The date of clearing for each paddock, and the paddock history for the period 1970-1981 are recorded. The paddock history includes use (crop type, pasture, fallow); fertilizer applied; yield; rainfall; and specific comments.

The ground-truth data are used to identify training paddocks for crop and for pasture. The data will also be used to assist in the interpretation of differences in spectral signatures between crop paddocks where these are shown to exist.

DATA ANALYSIS

In the first stage of the analysis, an overall description of the separation between the training paddocks is provided. This is used to assess whether differences between paddocks sown to crop and paddocks sown to pasture are greater than those between paddocks sown to the same crop. The term group will refer to the pixels for a training paddock, while the term variables will refer to the Landsat bands for all the overpasses, or for a subset of them. The approach adopted here is to provide an ordination of the group means based on the first few canonical variates. Since the canonical vectors are chosen to maximize the variation between the training groups relative to the variation within groups over all possible linear combinations of the variables, the description provided by the first few canonical variates will usually contain most of the relevant information. The associated canonical roots - the ratios of the between-groups sum of squares to the within-groups sum of squares for the resulting canonical variate scores for each pixel - indicate the degree of group separation. Subsets of the variables may also be examined; the canon-

609

ical roots are then compared with those based on all variables to determine whether most of the important information has been retained. The ordination based on the resulting adequate subset of variables may be used to determine the effective number of training or reference groups required.

Once the training groups have been established, the second stage involves allocation of the pixels from each of the training groups, and allocation of pixels from additional groups if available. Because additional groups were not available at the time of writing, the approach adopted here uses leave-one-out calculations for the pixels for the training groups. Posterior probabilities are estimated using multivariate Student densities rather than multivariate Gaussian densities (Anderson, 1958, Section 6.3; Aitchison and Dunsmore, 1975; Aitchison, et al., 1977; Murray, 1977). There is also the question of whether equal or unequal covariance matrices should be assumed for the calculations. An index of typicality is also calculated for each pixel (see Aitchison, et al., 1977, for a formal definition). This index reduces to the probability associated with the individual squared Mahalanobis distance for the pixel. For leave-one-out calculations or for pixels from additional testing paddocks, the probability is calculated by referring the squared Mahalanobis distance to the F distribution.

<div align="center">SOME RESULTS</div>

Since seven cloud-free overpasses are available for area H, and six cloud-free overpasses are available for area F (only four for part of F), this paper will concentrate on analyses of data from these areas.

Results from Analyses of Area H

Seven cloud-free overpasses are available for ten paddocks from study farms in area H. Dates of overpasses are: 19 June, 25 July, 12 August, 30 August, 5 October, 22 October and 9 November, 1981.

A plot of the group means for area H for the first two canonical variates based on the four bands for the seven overpasses shows clear separation of the pasture groups from the crop groups (Figure 2). There is also substantial separation between crop paddocks along the second canonical variate. This appears to be related to date of sowing, with those sown early in the season (W4, W5, W6 on 3 June) showing some separation from those sown later (W1, W2, W3 on or about 15 June). The barley paddock shows some separation from the wheat paddocks.

The first two canonical roots based on the four bands for the seven overpasses are 21.81 and 7.11, accounting for 91% of the overall between-groups variation. The relationships between the groups are little changed when either band 4 and band 6 or band 4 and band 7 for the seven overpasses are eliminated from the analysis (first two canonical roots of 18.47 and 6.59 versus 19.18 and 5.79 respectively); analyses based on either band 5 and band 7 or on band 5 and band 6 give similar ordinations.

CBH is interested in being able to estimate accurately the area sown to crop by the end of August. To this end, an analysis has been carried out on the data for overpasses on 25 July and 12 August; the data for 19 June have not been included since not all areas were sown by this date (see, e.g., the results for area F below). The separation of crops from pasture is reduced considerably, the first two canonical roots for the four bands for the two overpasses being 10.15 and 1.24.

Even with this reduced separation, the results from the allocation of individual pixels are encouraging (Table I). Group membership probabilities are pooled for all wheat paddocks and for all pasture paddocks.

<div align="center">610</div>

Table I.   Results of Allocation of Each Pixel for Each of the
Training Paddocks - Leave-One-Out Calculations are Used.   W denotes
wheat; B - barley; O - oats; P - pasture.

number of pixels
allocated to:

training paddock	no of pixels	W1+...+W6	B1	O1	P1+P2
W1	119	118[#]	0	1	0
W2	123	121	0	2	0
W3	47	47	0	0	0
W4	53	47	0	6	0
W5	58	48	0	10	0
W6	169	158	5	3	3
B1	47	0	46	0	1
O1	23	23	0	0	0
P1	269	7	5	0	257
P2	199	4	18	0	177

[#] for W1, 118 of the 119 pixels are allocated to one of
the wheat groups W1-W6 if a forced allocation is adopted,
while 1 pixel is allocated to the oats group.

In Table I, pixels are allocated to the group or set of groups with the
highest group membership probability though, ideally, regions of doubt should
also be incorporated. Most of the pixels are correctly allocated, with very
little overlap between crops and pasture. Approximately half the pixels for
the oats paddock are more likely to belong to oats than to any particular
wheat paddock, though collectively one or other of the wheat paddocks is more
likely.

An example of pixels that are wrongly allocated or are found to be
atypical is summarized in Table II. In each case, distinct clusterings of
pixels are evident. One of the priorities this year will be to visit the
pasture sites to identify the reasons for the anomalies.

Table II.   Representation of (a) Pixels Wrongly Allocated Using a Forced
Allocation Approach and (b) Pixels Found to be Atypical (at the 0.05 level)
for the Pasture Paddock P2. Paddock dimension is 12 lines by 13 pixels.
Row and column refer to the pixel position relative to the N-W corner of the
paddock.

a) misallocated pixels   b) pixels allocated as pasture
                                               but atypical

column

row	8	9	10	11	12	13
2	x	x	x			
3		x	x			
4				x		x
5					x	
6		x				

column

row	1	2	3	4	5
6	x	x	x	x	
7	x	x		x	
8	x	x	x	x	x
9			x	x	
10			x		

In view of the promising results obtained for the separation of crops
from pasture, some additional data were extracted. This was done by selecting
what appeared to be homogeneous areas on a three-band colour display of the
data. A tentative labelling, as crop or pasture, was made on the basis of the

611

visual similarity with areas known to be crop or pasture from the ground-truth data.

A canonical variate analysis of the amended data set based on the four bands for the seven overpasses shows clear and marked separation between all paddocks tentatively labelled as pasture and those labelled as crop (or known to be crop) (Figure 3). The first two canonical roots for all bands for all seven overpasses are 11.91 and 3.28, while those for the analysis based on band 5 and on band 7 are 10.93 and 3.02. Clearly most of the information for discrimination is contained in these two bands. An analysis based only on the linear combination (band 7-band 5) gives corresponding canonical roots of 8.56 and 2.46, with marked separation between crops and pasture still evident.

Results for Analyses of Area F

Six cloud-free overpasses are available for eight paddocks from study farms in area F (12 August was cloud-covered). A canonical variate analysis based on the four bands for the six overpasses again shows marked separation between crops and pasture (Figure 4(a)), with first three canonical roots of 6.72, 5.34 and 2.26. There is also an obvious difference between crops planted before 19 June and the wheat planted on 20 June. Excluding the data for 19 June gives first three canonical roots of 6.00, 3.21 and 2.00, with marked separation between crops and pasture still evident (Figure 4(b)). The second canonical variate separates the crop paddocks by date of planting.

Four cloud-free overpasses are available for fifteen paddocks from study farms in area F (25 July, 12 August and 23 October were cloud-covered). A canonical variate analysis based on the four bands for the four overpasses shows less obvious separation (Figure 5). However, even with this separation, the allocation results are encouraging (Table III).

Table III. Results of Allocation of Pixels for 15 Paddocks from Area F for Overpasses on 19 June, 30 August, 5 October and 9 November – Leave-One-Out Calculations are Used.

paddock	number of pixels	Equal Covariance Matrices			Unequal Covariance Matrices		
		W1-W10	B1-B3	P1-P2	W1-W10	B1-B3	P1-P2
W1	245	210[#]	30	5	240	5	0
W2	219	199	16	4	206	13	0
W3	85	83	2	0	84	1	0
W4	179	172	7	0	166	13	0
W5	230	288	2	0	224	6	0
W6	135	90	33	12	103	29	3
W7	210	197	13	0	201	9	0
W8	275	275	31	1	254	20	1
W9	434	423	11	0	429	5	0
W10	104	104	0	0	104	0	0
B1	48	18	30	0	13	35	0
B2	98	30	64	4	25	72	1
B3	39	11	28	0	11	28	0
P1	99	1	1	97	0	0	99
P2	224	21	3	200	11	4	209

[#] 210 of the 245 pixels are allocated to one of the wheat groups W1-W10 if a forced allocation is adopted, while 30 pixels are allocated to one of the barley groups B1-B3, and 5 pixels are allocated to one of the pasture groups P1 or P2.

DISCUSSION

A temporal analysis of the Landsat data shows significant separation between paddocks sown to pasture and those sown to crop. Successful allocation of individual pixels to either crop or to pasture has been achieved, even for only two overpasses, and without incorporating spatial information.

Differences between wheat paddocks sown at different times and/or on different soils exist. Fieldwork is underway to collect detailed paddock histories for farms falling within areas H, F and I, to allow a more extensive examination of this aspect.

REFERENCES

Aitchison, J. and Dunsmore, I.R. (1975). Statistical Prediction Analysis. Cambridge University Press.

Aitchison, J., Habbema, J.D.F. and Kay, J.W. (1977). A critical comparison of two methods of statistical discrimination. Appl. Statist., 26, 15-25.

Anderson, T.W. (1958). An Introduction to Multivariate Statistical Analysis. Wiley.

Dawbin, K.W. and Beach, D.W. (1981). Crop monitoring in Australia using digital analysis of Landsat data. Seventh International Symposium on Machine Processing of Remotely Sensed Data, LARS/Purdue University.

Murray, G.D. (1977). A note on the estimation of probability density functions. Biometrika, 64, 150-152.

Northcote, K.H. (1971). A Factual Key for Recognition of Australian soils. Rellim Technical Publications.

Northcote, K.H., Bettenay, E., Churchward, H.M. and McArthur, W.M. (1967). Atlas of Australian Soils Sheet 5. Melbourne University Press.

ACKNOWLEDGEMENTS
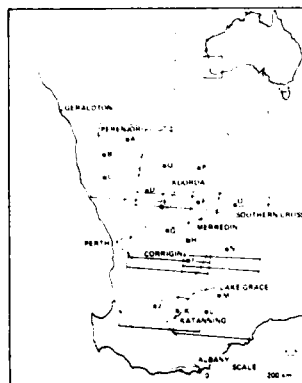
Figure 1. Location of Wheatbelt and Distribution of Study Areas. Approximate coverage of six Landsat scenes is shown.

Figure 2. Means for Paddocks from Area H for First Two Canonical Variates based on all Bands for all Dates. The canonical vectors are scaled to unit standard deviation within groups.
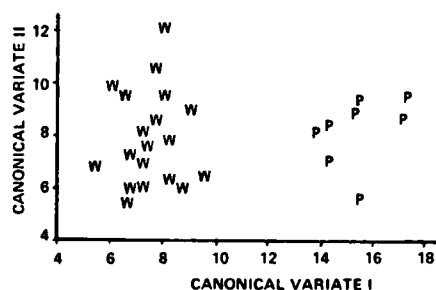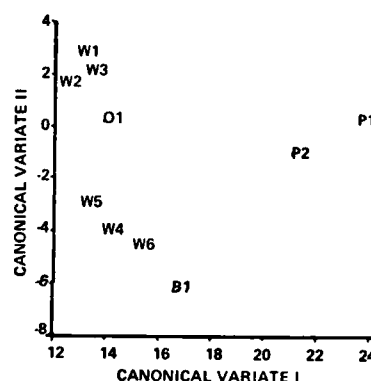
Figure 3. Means for Paddocks from Area H for First Two Canonical Variates based on Amended Data for all Bands for all Dates. The canonical vectors are scaled to unit standard deviation within groups.

614
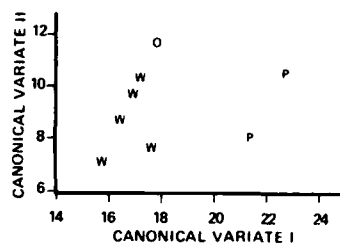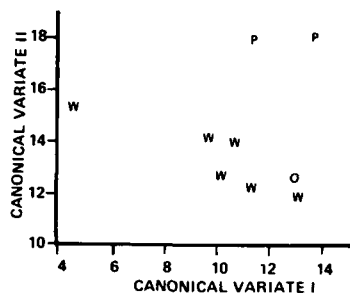
Figure 4. Means for Paddocks from Area F for First Two Canonical Variates based on Data for all Bands for (a) all Dates except 12 August and (b) all Dates except 19 June, 12 August. The canonical vectors are scaled to unit standard deviation within groups.
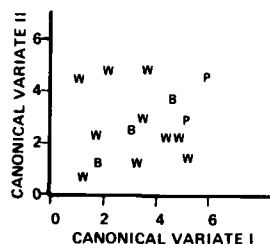
Figure 5. Means for Paddocks from Area F for First Two Canonical Variates based on Data for all Bands for 19 June, 30 August, 5 October and 9 November. The canonical vectors are scaled to unit standard deviation within groups.

615
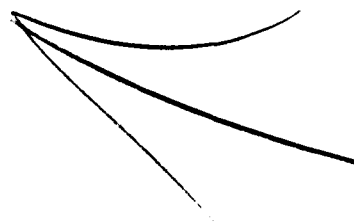
EVALUATION OF SPATIAL FILTERING ON THE ACCURACY OF WHEAT AREA ESTIMATE

M.A. Moreira, S.C. Chen and A.M. de Lima

Instituto de Pesquisas Espaciais - INPE
Conselho Nacional de Desenvolvimento Científico e Tecnológico - CNPq
C.P. 515 - São José dos Campos - SP - Brazil

ABSTRACT

The objetive of this study was to select the optimal combination of threshold values for the 3x3 pixel spatial filtering for post-classification implanted in Image-100 system of INPE and to evaluate the effects of this procedure on the accuracy of wheat area which was estimated by Image-100 system using a hybrid classifier and LANDSAT digital data obtained from a single pass. An area of 800 km² in Cruz Alta which is one of the most important municipals for wheat production in southern Brazil, was selected for this study. Different threshold combinations: (1,2), (2,1), (2,2), (2,3), (3,2), (3,4) and (3,5) were employed in the spatial class filtering for the whole study area after wheat was classified. Alphanumeric theme prints of classification results with and without employing spatial filtering were compared using aerial photographic mosaic as "ground information". The combination of (2,2) was then selected as the best threshold values in spatial filtering and was applied to five test sites (≤ 40 km² each) with different wheat densities for a quantitative evaluation of the accuracies of wheat area estimates. T tests showed that filtering with threshold values (2,2) significantly decreased errors of commission and omission, also, the accuracy in area estimate was improved from the over estimate of 4.5% to 2.7% and the root-mean-square error decreased from 126.18 ha to 107.02 ha. Extrapolating the same procedure of automatic classification using spatial filtering for post-classification to the whole study area, the accuracy in area estimate was improved from the overestimate of 10.9% to 9.7%. This study concludes that when a single pass LANDSAT data is used for crop identification and area estimation the post-classification procedure using a spatial filter provides a more accurate area estimate by reducing classification errors.

1. INTRODUCTION

The ideal LANDSAT pass for wheat identification and area estimate is in the late September or in the beginning of October when this crop is at yellow-ripe stage in southern Brazil. However, these months coincide with the initial of the rainy season, thus, cloud-cover is a serious problem for image analysis. LANDSAT data prior to the yellowing stage may also be used for area estimation purpose; nevertheless , a less accurate estimate is obtained, since a large commission error is expected due to the similar spectral responses among wheat, pastureland and fallow fields. The objective of this study was to verify whether improved classification results and a more accurate estimate of crop area might be obtained through post-classification using spatial class filtering when only LANDSAT digital data of a single pass were available for analysis.

2. STUDY AREA AND DATA ACQUISITION

Cruz Alta is one of the major municipals for wheat production in Rio Grande do Sul State, Brazil. The geographic location of this municipal is around 28°35'S and 53°45'W. An area in Cruz Alta (approximately 20 x 40 km²), which represents the wheat plantation of the state, was selected for this study (Figure 1). In this region, depending on climatic conditions, wheat may be planted in April or May and be harvested in October or November.

Aircraft data acquisition

On September 2, 1979, INPE's (Instituto de Pesquisas Espaciais) aircraft Bandeirante was flown over the study area using a RC-10 photogrammetric camera and color infrared (CIR) aerial photographs of medium scale (1:20,000) with 30% sidelapping and overlapping were taken. Aerial photographs were later interpreted visually according to a predetermined legend. The photointerpretation results were then used as "ground information" to assess the computer-aided classification performance of Image-100 system.

LANDSAT data acquisition

The ideal LANDSAT pass for wheat identification and area estimation is in the late of September or in the beginning of October when wheat is matured and presents a golden-yellowish color, different from the surrounding crops (predominantly pastureland) which are still green (Chen et al, 1981). However, LANDSAT data on September 22, 1979 was with 100% cloud cover, thus LANDSAT CCT's on September 4th when most of wheat plantations were at heading/flowering stage, were used for this study.

3. METHODS

For wheat classification, the unsupervised clustering algorithm (K-means) was first employed to separate homogeneous spectral classes; these spectral classes were then transformed to informational classes and training areas for each informational class were located on the image monitor of Image-100 system using the electronic cursor. The spectral information of these training areas were used to derive training statistics required by MAXVER which is a supervised classifier based on the Gaussian maximum-likelihood decision rule (Velasco et al, 1978). This hybrid procedure of using clustering to assist the selection of training areas which were later used in a supervised classification was called M-2 procedure (Lima et al, 1982). For *homogeneization* of classification results, a post-classification procedure named UNITOT was used.

UNITOT is a three-by-three pixel spatial class filter implanted in INPE's Image-100 system (Dutra, 1982). There are two threshold values which should be predetermined by the analyst. The first threshold value, T_1, is the number of times the analyst wants the central pixel to be considered in calculation of class frequency. After calculation of the frequency for all the classes in the 3x3 pixel matrix the highest class frequency will compared to a second threshold value T_2 which is arbitrarily assigned by the analyst. If the T_2 value is smaller than the highest class frequency then the class of the central pixel will be substituted by the class which has the highest class frequency. If the T_2 value is larger than the highest frequency then the class of the central pixel remains unchanged. The best combination of T_1 and T_2 to be used in spatial filtering should improve classification performance by diminishing classification errors. To select the optimal threshold values for this study the following combinations of (T_1, T_2) were tested, they were (1,2), (2,1), (2,2), (2,3), (3,2), (3,4) and (3,5).

Analysis procedure

In order to work at the scale of 1:100,000 on the image monitor the study area was divided into two square subareas (A and B) of approx. 20x20 km² each. Analysis procedure was carried out similarly for both areas. Once the subarea was delimited, wheat was classified using the M-2 procedure as mentioned above, afterwards, spatial filtering (UNITOT) using different combinations of threshold values were applied and alphanumeric print out (1:20,000) of the classified wheat, with and without using spatial filtering, were obtained. Each alphanumeric printout was overlaid on the aerial photographic mosaic; on

a light table, and a visual comparison was made observing the commission and
omission errors presented on the print-out. After comparing all the print-outs
with aerial photographic mosaic the best combination of threshold value was
selected.

In order to evaluate quantitatively the effects of spatial class
filtering using the best threshold values on the classification results, five
test sites ($\cong$ 40 km^2 each) with different wheat densities were selected from the
study area. A point-by-point comparison of alphanumeric print-out of each test
site to its corresponding aerial photographic mosaic provided data for
statistical analyses. Paired t-tests were applied to the percentages of
correct classification (CC), error of commission (EC) and the estimated wheat
areas obtained by using and without using the spatial filtering. Correct
classification, commission error, omission error and relative difference are
defined as below:

$$\text{correct classification (CC \%)} = \frac{\text{n}^{\underline{o}} \text{ of wheat pixels which were classified correctly}}{\text{area-transformed pixel n}^{\underline{o}} \text{ of wheat from aerial photographs.}} \times 100\%$$

$$\text{commission error (CE \%)} = \frac{\text{n}^{\underline{o}} \text{ of non-wheat pixels which were erroneously classified as wheat}}{\text{n}^{\underline{o}} \text{ of wheat pixels classified by Image-100 system}} \times 100\%$$

$$\text{omission error (OE \%)} = 1 - \text{CC\%}$$

$$\text{relative difference (RD \%)} = \left(\frac{\text{estimated wheat area by Image-100 system}}{\text{estimated wheat area from aerial photographs}} - 1\right) \times 100\%$$

4. RESULTS AND DISCUSSION

Figure 2 shows the classification results of subarea A using procedure
M-2. Even though M-2 was selected as the best procedure for wheat
classification (Lima et al, 1982) there were some confusion among the classes
of wheat, pastureland and sparse arboreal vegetation. This might be explained
by the fact the LANDSAT data were gathered at the time when wheat was in
heading/flowering stage, consequently perfect separation could not be obtained
due to the similarity between spectral responses of wheat and pastureland. It
was noted that in most of the cases the sparse arboreal vegetation which was
misclassified as wheat possessed a understore of vigorous grass which might
contribute to the spectral similarity to wheat.

Quantitative comparisons of alphanumeric print outs to aerial photographic
mosaic showed that the application of spatial class filtering with the
combination of threshold values (2,2) gave better classification results. This
improvement can be observed by comparing Figure 2 and 3. Quantitative
comparisons were performed using data of Table 1 and 2 which were obtained
after classification with and whithout the application of UNITOT, combination
(2,2), for five test areas. T tests showed that the application of UNITOT
(2,2) increased significantly (α = 0.05) the percentage of correct
classification and decreased significantly (α = 0.01) the error of commission.
Comparing area estimates obtained by using of without using UNITOT to that of
the aerial photographs no statistical difference was found. However, with the
applying of UNITOT after classification the root-mean-square error of area
estimates for these five areas decreased from 126.18 ha to 107.02 ha. The relative
difference in area of these five test sites decreased from an overestimate of

619

4.5%, when no spatial class filtering was used, to +2.7% when UNITOT with threshold values (2,2) was applied in analysis procedure. Applying UNITOT (2,2) to the whole study area an improvement in area estimation was observed, i.e. RD of +10.9% obtained by classification whithout the application of spatial class filtering was decreased to +9.7%. Even though the improvements in area estimate were not pronounced the better classification accuracy caused by a higher correct classification and a smaller error of commission when spatial class filtering was employed made this post-classification worthwhile.

5. CONCLUSIONS

When multitemporal LANDSAT digital data are not available for crop identification studies the classification errors caused by the similarities of spectral responses among classes on a single-pass LANDSAT data may be diminished by the application of spatial class filtering with optimal threshold values in post-classification. The improvements in crop classification results using spatial class filtering for post-classification are contributed by a higher percentage of correct classification, a smaller error of commission and a more accurate estimate in area.
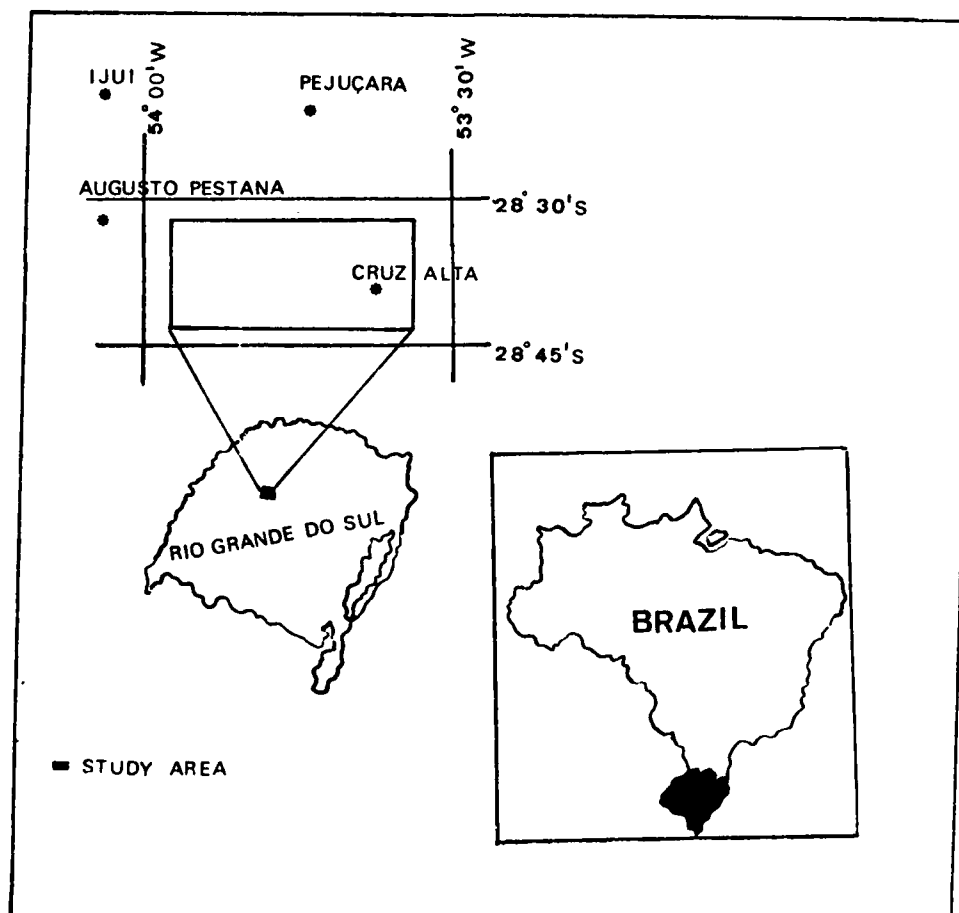
Fig. 1 - Location of study area.

620
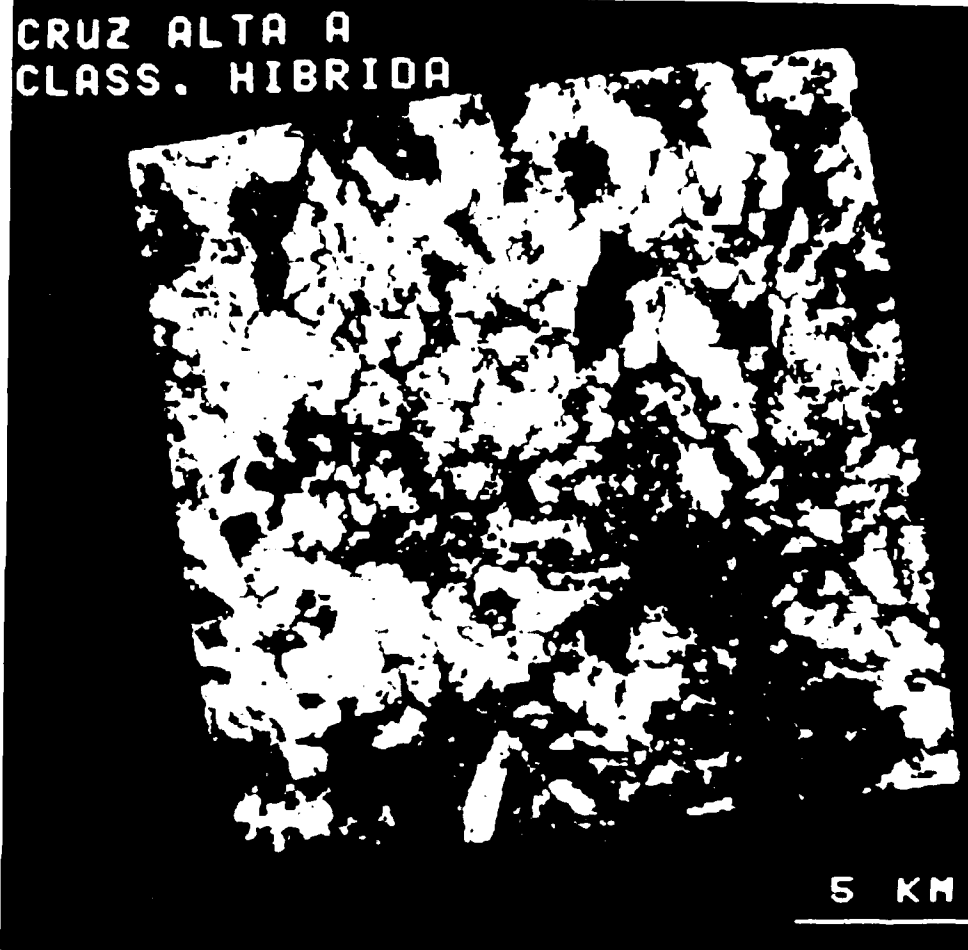
Fig. 2 - Result of wheat classification without using UNITOT (2,2) in subarea A.

Fig. 3 - Result of wheat classification using UNITOT (2,2) in subarea A.

Table I. Estimated wheat area based on aircraft and LANDSAT data for five test sites

TEST SITE	WHEAT DENSITY (%)	ESTIMATED WHEAT AREA (ha)		
		AERIAL PHOTOGRAPHS	LANDSAT CCTs	
			WITHOUT SPATIAL FILTERING	SPATIAL FILTERING WITH UNITOT (2,2)
1	56.69	2531.77	2290.26 (-1.78)*	2286.98 (-1.92)
2	46.13	1897.60	1906.26 (+0.45)	1852.51 (-2.38)
3	39.28	1615.72	1999.77 (+0.51)	1600.79 (-0.92)
4	22.87	971.05	1481.95 (+23.55)	1137.96 (+17.18)
5	31.15	1322.50	8502.32 (+12.05)	1481.06 (+11.99)
TOTAL	-	8138.64	8502.32 (+4.46)	8359.30 (+2.7)
RMSE	-	-	126.18	107.02

* Percentage of relative difference (RD%)

Table II. Wheat classification accuracies resulted by using and without using UNITOT (2,2) in five test sites

TEST SITE	CORRECT CLASSIFICATION (CC%)		COMMISSION ERROR (CE%)	
	WITHOUT SPATIAL FILTERING	SPATIAL FILTERING WITH UNITOT (2,2)	WITHOUT SPATIAL FILTERING	SPATIAL FILTERING WITH UNITOT (2,2)
1	83.75	86.05	14.73	12.26
2	82.83	83.93	17.54	14.67
3	77.51	78.93	22.89	20.33
4	88.41	89.08	28.45	23.98
5	87.85	88.30	21.60	21.15

6. REFERENCES

CHEN, S.C., M.A. Moreira, and A.M. LIMA. (1981). "Comparison of wheat classification accuracy using different classifiers of the Image-100 system" INPE-2125-RPE/349. São José dos Campos. S.P.

DUTRA, L.V. 1982. *Desenvolvimento de alguns métodos de pós-processamento apli cados a imagens digitais multiespectrais.* (Técnicas de uniformização de te mas). São José dos Campos, INPE, (in processing).

LIMA, A.M., S.C. CHEN, and M.A. MOREIRA. (1982). Avaliação de dois métodos de aquisição de estatísticas de treinamento para classificação automática INPE (in processing).

VELASCO, F.R.D., L.O.C. PRADO, and R.C.M. SOUZA. 1978. Sistema MAXVER: Manual do usuário. INPE-1315-NTI/110. São José dos Campos. S.P.

ACQUISITION OF SPECTRAL SIGNATURES OF CROP FEATURES
IN THE TRENQUE LAUNQUEN AREA

Mirta A. Raed

Comisión Nacional de Investigaciones Espaciales
Buenos Aires, Argentina

SUMMARY

Multispectral measurements acquired from satellite data increase knowledge
and understanding of the spectral properties of crops and soils in relation to
their physical, biological and agronomic characteristics.

The spectral response of the crop represents the integrated effect of all
cultural, soil and meteorological factors affecting crop growth and development.

The area we studied, named Trenque Launquen, is situated west from Buenos
Aires Province and its surface comprehends 550,000 hectares.

Multispectral data can take advantages from spectral signature character-
istics. Analysis can be successful in delinating several land vegetative
classes and it can aid in differentiating areas of contrasting densities.

Most of the computerized image processing methods are based exclusively on
spectral signatures recorded by the multispectral systems.

We are interested in spectral signatures of crop species and their changes
as a function of the site conditions, and the phenological stage of species.
This knowledge is very important to select the spectral bands that yield the
maximum differentiation between particular crops.

It must be taken into account that the IR aerial photography and the sup-
porting ground truth information will help the classification of the spectral
signatures into classes.

The effects of different soil type are evident, early in the season, when
the plots containing lighter colored soils have higher reflectance. These
differences diminish as the ground cover increases until the soil in the field
of view of the radiometer is predominately shaded.

It must be taken into account to determine spectral characteristics and
separability of crops as a function of growth stage.

Crop development stage is an important variable because knowledge of the
temporal-spectral response of crops is probably the most important factor
required for accurate spectral signature features.

Factors such as planting date, plan population, row width, different kind
of soils, soil moisture, nutrient supply and varietal response are important
determinants of crop growth and development.

Spectral data includes reflectance factors in the four Landsat MSS bands
and in infrared/red ratio bands for plots of wheat, corn, sunflower, soybean
and sorghum with varying agronomic practices.

The acquisition of spectral signatures of land features is done by locating "training fields" of these features of MSS data and computing their statistics using a maximum likelihood classifier which assigns to training classes, which means land feature on which training field statistics are available.

It is necessary to select very small training fields from over a number of each individual, such that there will result a sufficient number of elements to produce reliable statistics.

The most effective qualitative analysis can be made by plotting the spectral signatures of all the crop features. Besides we shall compare all the training fields of each class just to settle down homogeneity of each field and the differences among them due to development stage and environmental factors.

A spectral signature plot means the graph of the statistical mean data value versus spectral channel. The mean values are obtained from analysing the training fields of each crop. Identifications of cover types in all fields were recorded on site maps. Detailed agronomic observations, on ground, were made on 10 fields of each kind of crop above mentioned.

626

CARTOGRAPHIC DIGITAL ENHANCEMENT OF
REMOTELY SENSED URBAN IMAGES

Jonathan Friedman

New Jersey Institute of Technology
Newark, New Jersey

SUMMARY

Any image system generalizes the optical detail of its physical source at the limit of its resolution. A low cost method to selectively enhance the resolution of parts of the image through hybrid digital-optical means is proposed and developed. The method involves identifying pattern and structure candidates for enhancement in detail, searching a library of previously digitized larger scale detail sources, and inserting the data for detail at appropriate addresses in the original image. The results are cost-effective because they do not require complete magnification of the original image. Such interpolation yields composite, multiplexed, and hybrid images which can generate a new order of information otherwise unobtainable from the two or more segregated source images. Interpolated detail may not be visible at the low-resolution broad coverage scale, but as the image is magnified to high-resolution narrow coverage scale, detailed features of these smaller structures become apparent. Most important for study, however, is the intermediate scale, where evidence of broad pattern may be combined with the precise complexity of substructures, and their interactions may be documented and modeled.

One application of such enhancement to parts of an image occurs in the use of remote sensing in urban studies. Typically, Landsat products to date resolve ground features on the order of 60 meters. This resolution permits statistical mapping of broad land use and geophysical features such as farmland, forests, and fault zones, but fails to distinguish urban features such as roads and individual buildings, which require a resolution on the order of 10 or 15 meters. Landsat imagery can show housing density in urban regions through analysis of albedo values and the like, but the image of city form reveals little if any information about the city's operational structure. It is as if our model of human anatomy still did not include veins and arteries, and we postulated that blood flowed in undifferentiated pools and seas throughout our bodies.

Although the European SPOT system promises resolution of this higher order when it becomes operational, our method shall continue to be useful, since higher resolution at low cost in selected areas of an image always remains desirable. Further applications in such fields as microbiology, surgery, and astronomy seem likely.

Our work in both urban and rural states shows that it is possible to map entire states using Landsat imagery and include precise data on the order of 10 meter resolution from other aerial photographic and cartographic sources in such a manner that the homes of more than half the statewide population and every road (including rural routes and urban grid patterns) can be depicted for little more than twice the cost of processing the original Landsat images themselves. This kind of digital cartographic interpolation has already produced striking images of urban form in its terrestrial and vegetative context.

High resolution digitized data for urban regions and their environs permit a new delicacy in modeling for urban planning. For instance, changes in

transportation demands as the result of variously proposed demographic and housing locations may be displayed as animated sequences that carry meaning even for individual elements in the system. Drainage and percolation hydrology can be plotted throughout the watershed as a function of ground coverage for different housing development plans. A powerful new tool for planners which combines the range of vision of remote sensing with the urban surgical delicacy of community action groups is able to model existing conditions and proposed changes in a manner and scale visible to all.

628

CONSTRUCTION OF A DYNAMIC MODEL OF LAND USE/LAND COVER FROM SEQUENTIAL REMOTE SENSING DATA

Mostafa K. Nosseir

SUPERINTENDÊNCIA DE RECURSOS NATURAIS E MEIO AMBIENTE-SUPREN/IBGE
Rua Equador, 558/2º andar - Santo Cristo
20220 - Rio de Janeiro - RJ
BRAZIL

ABSTRACT

The present paper, demonstrates a methodology for constructing a dynamic model of Land use/Land cover from sequential aerial photographs, over a period of 1938 - 1976, in the south eastern region of the state of Ohio, USA. The USGS Land use/Land cover legend was adapted to identify the classes, starting from the one suffering highly rejection mechanism (Water) to that of climax (Mixed mesophytic forest). A discretization procedure was applied to divide the site into 56 equal size cells (1 km by 1 km). Photogrammetry techniques were applied to transfer the ground coordinates of the cell corners (nodes) into photo coordinates. The central projective equations were the main tools in this transformation. Photo coordinates were plotted on the most recent aerial photographs (1976). Zoom transfer-scope was used in transformation of these coordinates to the 1938, 1951, 1958, 1966 and 1976 aerial photographs. Land use/Land cover classes were mapped for each cell for each set of photographs. Acreage was computed at a one hectare resolutation.

Cluster analysis was used to group cells of similar Land use/Land cover composition of the 1976 aerial photographs. Cells each cluster were traced through time to determine the pathway through which they passed and to determine their initial stage in 1938. A proposed Land use/Land cover model was constructed indicating the pathways and the most responsible mechanisms.

It is believed that the future space remote sensing technology, such as Thematic Mappers (TM), will permit the construction of more efficient models for Land use/Land cover changes.

INTRODUCTION

The importance of monitoring Land use changes for better, management of natural resources was demonestrated by different authers (Anderson, 1977). The objectives of this paper are: to develop a quantitative method for monitoring land use changes from sequential aerial photographs and to construct a dynamic model of these changes.

METHODS AND MATERIALS

The investigated site is a 14 km by 4 km area located east of the glacial boundary in the Applachian plateau, Kanamha section of Hocking county, south-eastern Ohio. The natural vegetation pattern of the region can be divided into three major communities: Upland forest composed of Oak-Hickory, Oak-Chesnut, Mixed-Oak. The roling uplands composed of Oak-Chesnut-

Tuliptree. The low relief areas are covered with mixed mesophytic (Beatley 1959). Soil series of Alfisol order dominate the landscape positions from the summit to the footslopes (terrace). Toeslopes positions (floodplanis) are dominated by Inceptisol. Soils of mining sites belong to Entisol order (Nosseir 1980).

Two bed rock series have been mapped in the studied area: pottasville, dominating the western part and allegheny bedrock, dominating the eastern part (Hall 1951). Both series belong to the Pensylvanian system. Very limited areas of recent alluvium were mapped along West branch Raccoon Creek and Honey Fork (Hall 1951).

Grid Construction

Aerial photographs of USDA were used in this investigation for the period of 1938-1976 in five sets: 1938, 1952, 1958. 1966 and 1976.

To satisfy the requirements for a quantitative monitoring of the Land use/Land cover classes from multisources data, a especial approach was required in order to develop a data colection system. Treatment of the areas as a closed system, on a detailed level, is not desirable because there is possible energy input and mass movement everywhere. The alternative approach was a combination of the finite element approach (Segerlind 1976) and Hugget's approach (1975). A well defined point was chosen as the origin point. In this case it was the southeastern corner (longitude 82^0 20' and latitude 39^0 24' 03"). The site was divided into 14 by 4 equal size cell of 1 km, independent of the scale of the source. Each cell was coded by its northeastern corner (node). The coordinates of the nodes of the origin point was digitized and transformed to obtain the equivalent Universal Transverse Mercator (UTM). Coordinates of all the nodes were computed by adding 1 000 meters intervals in X and Y directions.

Map coordinates were transfered int photo coordinates using the most recent set of aerial photographs (1976). The interior orientation of the photographs was obtained using the camera calibration certificate. The exterior orientation of each photograph was performed using control points from 1: 24 000 topo-maps. Correction for atmospheric refraction was made using the subroutine "REFRAX" of the Geodetic Science Dept., at the Ohio State University. Ground control coordinates were treated as observations with a standard deviation of 5 m. in X and Y directions and with 0.3m. in elevation (Z) (Wright 1980).

Block adjustment was performed for conducting the analytical triangulation computation. The central projection equation were used in conducting a three dimensional transformation. A computer program from the above mentioned department was available. It conducts a simultaneous lesast square solution based on the collinearity condution (first order theory) (Merchant 1974 and 1978). Computed photo coordinates, from each photograph, were plotted by computer on overlay paper then transfered to the coresponding photographs. Additional control points, on the photographs, were needed for the manual rectification of the stereo-model. Posto Block Aerial Survey (PBAS) (Merchant 1973) was performed to obtain the ground coordinates of these points. The 1976 aerial photographs were used as a data base for the previous flights. Transformation of the nodes locations to the other flights was conducted using a Zoom Transfer Scope.

Monitoring Land use/Land cover

The USGS Land use/Land cover legend (Anderson et-al 1976), was adapted in order to include the different classes of land use in addition to indicate the different stages of secondary succession. Succession was consider the mechanism forcing the system to reach its climax, which is Oak-Hichory (Gilbert 1979). On the other hand, the rejection mechanism acts in a reverse direction avoiding the system from reaching its climax. The legend (Figure 1) was constructed having water as one extreme on the scale and it progresses to mixed forest on the other extreme.

A description sheet was designed to evaluate Land use/Land cover changes from the aerial photographs. One sheet was filled for each cell to cover the monitored period (1938-1976). The objectives of these sheets are to obtain qualitative information about each cell; to evaluate the relationships between land use and landscape; to sumarize the dynamics of land use whithin the 1938-1976 period; and to be used as supporting documents in analysis and interpretation of the quantitative land use data. The Land use/Land cover description sheets

630

contain: county and township names; cell identification number; the topographic map name and scale where the cell is located; photo number and dates; location, a description of how to reach the cell, physiography including the values and locations of the maximum elevation, a brief description of topography, streams, and surface drainage; bedrock includes the dominant bedrock series; Soil Association; cultural features; changes in Land use/Land cover including description of the Land use/Land cover classes for each time period, the spatial distribution of each class, in relation to landscape position is described, using Ruhe's hillslope components system (Ruhe, 1975), indicates the changes in land use patterns over time, which are not included in the quantitative analysis; and Remarks or observations.

Mapping Land use/Land cover

A Zeiss stereotope was used to rectify the cells due to any local relief effect. Mapping was conducted at the cell level. The measuring marks were used as the pointer to trace the boundaries of each land use class.

Due to the seasonal difference of the aerial photos, a calendar for field operations was established to indicate the expected field operation and land cover during the time of the flights. A photo interpretation key was constructed using photo elements: tone, texture and geometric patterns as tools in identification of land use classes (Nosseir 1980). Acreage of each class was estimated by dividing each cell into 100 divisions, which is equal to one hectare (each division is 100 x 100 m.).

Spectral analysis procedures were applied as a statistical tool, to each Land use/Land cover class, to evaluate their pattern and periodicity, in two steps: the quantitative values of each variable per cell were plotted against their location, then the spectrum procedure was used to determine the frequency and periodicity of the distribution (Harris 1967, Jenkins and Watts 1968, Bartlett, 1966 and SAS 1979).

Cluster analysis was used to group the cells of similar Land use/Land cover composition. It was applied using the 1976 data to classify the cells according to their most recent land use. This was considered the latest stage in the succession. Cells of each cluster were traced through time to determine the pathway through which they passed and to determine their initial stage in 1938. Description sheets were used for the purpose of tracing the cells/pathways.

Description sheets were classified base on the clusters of 1976. The qualitative information recorded on these sheets covering the period of 1938-1967 was used to follow the Land use/Land cover changes and the relation between these changes and the landscape.

RESULTS AND DISCUSSION

Changes in Land use/Land cover

The sixteen land use classes are grouped, in this paper, into five categories: forests, grassland, agricultural land, mines and others. In general, the process of natural vegetation succession, during the period of 1938 to 1976 proceded from the later categories to forest. Table 1 demonstrates the continuous increase in the acreage of forest land during the period studied. As a result of the succession process, the forest boundaries advanced into the grassland. The period of 1958 to 1966 showed the lowest rate of increase in forest, which coincided with the lowest rate of decrease in the grassland. This lower rate of change was a result of a temporary steady state in the system when the amount of farm land stabilized the introduction of mechanization practices in the fifties. The relatively small difference between the loss in the grassland and the gain in the forest may be due to the increase in mining activities during the same period. In 1938 grassland aes the dominant land cover category.

In fact grass land had a unique changing pattern. It gained acreage from abandoned farm land but lost acreage to mining during the 1958-1966 period. During the period of 1966 to 1976, grassland registered its seconds largest loss in acreage while mining registred its highest increase and forest registred its second highest increase (Table 1). These facts prove that generally the two dominant process affecting land cover during the period of 1938 to 1976 were

631

secondary succession and mining (which is a rejection mechanism).

Agricultural land showed signficant change in acreage and in its spatial distribution. In 1938 it represented 11,4% of the site and dominated the summits and shoulders of the hillslopes. By 1951, as a result of the introduction of mechanization, agricultural land gained 0.9% but became restricted to the flootslope and toeslope positions.

Mining activities were always associated with the Allegheny bed rocck which dominates the eastern part of the site and contains a surface strata of coal (Hall 1951). Limited areas of mines in individual cells were observed in the western part of the site where Allegheny bed rock dominates the hilltops.

Land use/Land cover Dynamic Model

In 1976 the general pattern of Land use/Land cover included forest, mines, or a combination of these categories. Changes in cells cover of each 1976 cluster were followed quantitatively then qualitatively, from the discription sheets, in order to build up the model stages, (Figure 2). Secondary succession and rejection mechanism are the two major driving forces in the site. The model shows that clearing of land, farming, harvesting and coal mining exploration were the rejection mechanisms introducing energy into the system. This avoided or retarded the system from reaching a steady state, leading to its Climax.

Land or mines abondonment or reclamation, conservation and lake sedimentation were the main mechanisms favorating the secondary succession. It was observed that rate of rejection mechanism was high in the initial classes such as going from mining sites to herbaceous grassland. The reverse was true with the rate of the succession mechanism. It was slow in the begining then its rate increased. Encroachment was the observed process in changing from exposed land to herbaceous grassland where infiltration was observed in changing from shrubby grassland to evergreen and mixed forests.

Mixed forest is the climax of this region (Beatley, 1959, Gilbert, 1979) and all land use classes are undergoing secondary succession leading to mixed forest. However, *there are* rejection mechanisms which tend to counteract this process. Most of these rejection mechanisms were in the form of external energy introduced by man for the purpose of food and energy production. In the case of crop production, energy input was in the form of machinery, labor, fertilizers, insecticides and herbicides. In addition, natural forms of energy such as solar radiation and precipitation were also received. The expected output of the land system was crops but, in addition, there was mass and particulate movement of soil material in order to release excess energy. A similar analogy can be applied to mining activities where energy input caused a great disturbance in the land system and resulted in the output of coal and the mass movement of the eroded spoiled materials (Nosseir 1980).

Conclusions

Sequential black and white aerial photographs provided quantitative data for monitoring Land use/Land cover changes. The discretization procedure and the analytical photogrammetric techniques, permited accurate transformation of the ground coordinates of the nodal points into photographic coordinates.

A dynamic model can be constructed from the quantitative data by applying clustering and spectral analysis. Quantitative data with shorter time interval can improve the model construction. This will permit better definition of the model stages and permit quantitative evaluation of the changing rates through the pathways.

Therefore, it is expected that future remote sensing vehicles such as Landsat D and D' and SPOT will offer high resolution data at a shorter intervales. These data can improve the monitoring of Land use/Land cover.

References

Anderson, J.; E.E. Hardy, J.T. Roach and R.E. Witmer. 1976. Land use/Land cover classification system for use with remote sensing data. Geological survey professional paper 964. US Government Printing Office. Washington, DC.

Anderson, J. 1977. Land use and Land cover changes - a ɪʀame - work for monitoring J. Res. USGS. 5: 143 - 153.

Barlett, M.S. 1966. An introduction to stochastic processes. 2nd Edition. Cambridge. Cambridge University Press.

Beatley, J.C. 1959. The primeval forest of periglacial area in the Allegheny Plateau. Ohio Biological Survey, Bulletin Vol. 1, 1.

Gilbert, G.E. 1979. Personal communication. Department of Botany. Ohio State University.

Hall, J.F. 1951. The geology of southern Hocking County, Ohio. Ph. D. dissertation Geology Department. Ohio State University.

Harris, B. (Editor). 1967. Spectral analysis of time series. John Wiley and Sons Inc.

Huggett, R.J. 1975. Soil landscape system. A model of soil genesis, Geoderma 13: 1-22.

Jenkins, G.M. and D.G. Watts (Editor). 1968. Spectral analysis and its applications. Hol day-day.

Merchant, D.C. 1973. Photo Block Aerial Survey Proceeding of the American Society of Photogrammetry, Fall convention.

_____. 1974. Calibration of the air photo system. Photogrammetric Engineering. 40: 605-614.

_____. 1979. Analytical photogrammetry theory and practice. Part I Department of Geodetic Science. Ohio State University.

Nosseir, M.N. 1980. Monitoring erosion features affected by land use from remotely sensed data (1938-1979). Ph.D. dissertation. Department of Agronomy. Ohio State University.

Segerlind, M.L. 1976. Applied finite element analysis. John Wiley and son, Inc.

Wright, E.J. 1980. An application of analytical photogrammetry in support of land use research. Internal report of Department of Geodetic Science. Ohio State University.

LEGEND

1. WATER
    11. LAKES

2. BARREN LANDS
    21. EXPOSED
    22. MINES
    23. RECLAIMED MINES

3. BUILT ON

4. AGRICULTURE LANDS
    41. FARMLANDS
        411. STRIP FARMING
        412. CONTINUOUS FARMING
    42. ORCHARD

5. GRASSLAND
    51. HERBACEUOUS
        511. ERODED
    52. SHRUBS AND BUSH
        521. ERODED
    53. MIXED

6. FOREST LAND
    61. EVERGREEN
        611. SUCCESSION
        612. AFFORESTATION
    62. MIXED

SECONDARY SUCCESSION INCREASES

REJECTION MECHANISM INCREASES

LAND USE/LAND COVER LEGEND   FIG. 1

634
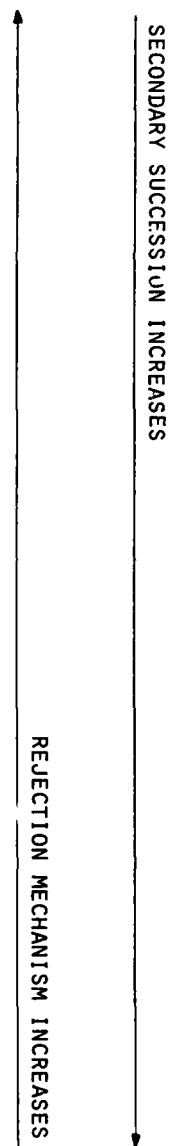
Table 1   Changes in Land Use/Land Cover Classes (1938-1976)

Class	Area					Changes in Area			
	1938	1951	1958	1966	1976	1951-38	58-51	66-58	76-66
Water	0	0	1	10	5.5	0	1	9	-4.5
Built On	45.5	57	45.5	36	15.5	11.5	-11.5	-°.5	-20.5
Exposed	1114	19	10	20	42	-95	-9	10	22
MINE	7	102	162	168.5	278.5	95	60	6.5	111
RECSTMIN	0	0	0	56	79.5	0	0	56	23.5
STRFAR	3	182	130	89	81.5	179	-52	-41	-75
CONFAR	610	493.5	391.5	442.5	194.5	-116.5	-102	51	-24.8
ORCHARD	39	39	34	25	26	0	-5	-9	1
HERGR	2042	1224.5	957.0	821.5	748.5	-816.5	-268.5	-135.5	-73
EHERGR	175	53	46	10	35	-122	-7	-36	25
SHRGR	1110	1354.5	1011	949.5	528	244.5	-343.5	-615	-421.5
ESHRGR	39	43	11	3	0	4	-32	-8	-3
MIXGR	641.5	508.5	583	555	361.5	-133	74.5	-28	-203.5
FOREST	776	1524	2208	2419.5	3133	748	684	211.5	313.5

Note: Area is in hectares

Source: Aerial photographs, USDA

RECSTMIN = Reclaimed Mines
STRFAR   = Strip Farming
CONFAR   = Continuous Farming
HERGR   = Herbaceous Grassland
EHERGR   = Eroded Herbaceous Grassland
SHRGR   = Shrub Grassland
ESHRGR   = Eroded Shrub Grassland
MIXGR   = Mixed Grassland

635

Increasing successional rate

Increasing rejection mechanism

Land Use/Land Cover classes

1. Lakes
2. Mines
3. Built on
4. Exposed Land
5. Eroded Herbaceous Grassland
6. Continuous Farming
7. Orchard
8. Strip Farming
9. Herbaceous Grassland
10. Mixed Grassland
11. Shrub Grassland
12. Evergreen Forest
13. Mixed Forest

Mechanism:

I   Succession/reclamation or abandonment
II Succession/sedimentation
III Removal or abandonment
IV Rejection/exploring
V   Sucession
VI Conservation
VII Rejection/clearing
VIII Rejection/farming
IX Afforestation
X   Rejection/harvesting

Proposed Land Use/Land Cover Dynamic Model of Southeastern Hocking County,
Based on Photo Interpretation.

FIG. 2

636

AD P002041

APPLICATION OF REMOTE SENSING TECHNIQUES IN GEOLOGICAL MAPPING - A CASE STUDY

OF A PRECAMBRIAN TERRAIN

G.SRINIVAS & C.NAGANNA

School of Earth Science, Bangalore University,
Bangalore, India.

ABSTRACT

The paper presents the results of MSS data
processing for the specific purpose of geological
mapping. The data has been collected over a
Precambrian terrain in South India in an area
locally known as Chitradurga schist belt.

The investigations have been carried out
at three levels by collecting field, aerial MSS
and satellite MSS data over the same area.
The characteristic reflectance patterns of some
of the commonly occurring rock types have been
determined. The lithological units in general
have a limited range of reflectances. The
interfering effects of soil, vegetation and
moisture content in identifying lithological
types on aerial MSS imageries are pointed out.

Reflectances measured from aerial MSS data
cannot be directly correlated with those
measured from satellite MSS data, mainly because
of the scale difference of the two imageries and
the accompanying constraints. Landsat
imageries can be conveniently used for structural
and lithological mapping of an area. More
geological information can be extracted from
the MSS data by using simple image enhancement
techniques like colour combinations and Band
ratioing.

1. INTRODUCTION AND OBJECTIVES

The present work examines the use of MSS data in geological mapping. MSS
data is likely to be more informative than conventional aerial photography as
more number of variables are available in terms of reflectances over
different bands. Information that can be extracted from the MSS data
naturally depends upon the scale at which the data has been collected. The
present investigations have been carried out by collecting data at three
levels, viz., ground, aerial MSS and satellite MSS surveys. The investiga-
tions have been carried over a Precambrian terrain in South India locally
known as the Chitradurga schist belt.

The specific objectives of the present work are to find:

a. Characteristic reflectance combinations of different lithological types;
b. whether lithological mapping is possible without a prior knowledge of the lithological types in a given area;
c. the extent soil and vegetative cover interferes in data interpretation, particularly, in marking the lithological contacts;
d. the relative merits of MSS vis-a-vis conventional aerial photography in geological interpretations;
e. the extent to which the study can be used in the interpretation of satellite imageries;
f. the relative importance of different MSS bands of satellite imageries in lithological and structural mapping;
g. the possibility of extracting more information by carrying out standard image enhancement techniques.

2. AREA OF INVESTIGATION

The Chitradurga schist belt in Karnataka State in India is roughly bordered by Lat. 13° and 14°45'N and Long. 76° and 77°E (Fig.1). A test area of about 400 sq.kms. was chosen in the schist belt for collection of aerial MSS data. MSS data has been collected on a scale of 1:50,000 and over 5 bands viz., MSS 1:0.5-0.6 μm; MSS 2:0.6-0.7 μm; MSS 3:0.7-0.8 μm; MSS 4:0.8-1.1 μm; MSS 5:8.0-12.0 μm. A detailed field mapping was carried out on a scale of 1:16,667 (6 cm.= 1 km.) over an area of about 800 sq.kms. in the test area and surrounding regions. The entire schist belt and neighbouring areas extending over an area of about 20,000 sq.kms. was studied through landsat imageries followed by extensive field checks.

3. METHODOLOGY

The aerial MSS data was examined frame by frame (positive prints) and correlated with the corresponding area on the map. The field map was reduced to a scale of 1:50,000 (Fig.2) to facilitate an easy correlation with the MSS imageries. The reflectance of different lithological types was determined in terms of grey level steps provided by a step wedge. The values are given as 1 for darkest and 16 for the lightest. The frequency distributions of the grey levels were studied and the modal values were chosen as the characteristic reflectance values of the lithological types. These values are plotted on a graph (Fig.3).

The landsat enlargement to a scale of 1:250,000 was used for lithological and structural interpretation of the schist belt. All the MSS bands 4,5,6 and 7 were used. The different lithological units were separated by tonal differences and were identified based on (a) information collected from test area (b) field checks in different places and (c) other existing data on the area in the form of reports and maps. Information from one area of known lithologies were extended to other areas having the same reflectance pattern. The structural map was prepared by picking up trends of lithologies and formation contacts.

For extracting more information from MSS data, two image enhancement techniques have been tried. In the first method, colour composites were prepared by using different possible combinations by means of a colour additive viewer. The second method is an optical image enhancement technique. This is some what similar to the band ratioing method without the accompanying stretching.

4. BRIEF GEOLOGY OF THE AREA

The Chitradurga schist belt is made up of members of Javanahalli Formation, Chitradurga Formation and G.R. Formation (Sampath Iyengar, 1905). This three-fold classification is retained for convenience in the present discussion, although there have been several modifications in recent times (Radhakrishna, 1968; Sreenivasan and Srinivas, 1972; Mukhyopadyaya et al, 1981) based on evidence not relevant for the present paper. The Javanahalli Formation is represented by hornblende schists and quartzites. The Chitradurga Formation is represented by chlorite schists, traps, hematite quartzites and conglomerates. The youngest G.R. Formation consists of clays, phyllites, jaspery hematite quartzites, ferruginous sandstones and conglomerates. Number of dyke intrusions have been noticed in addition to major granite emplacements.

The major structure in the area is a syncline with the axial-trace running north-south along the east-central portion of the map and curving to NNW in the northern portion (Fig.5). The main evidence for the synclinal axis are the dips of ferruginous quartzites and associated rocks, and the disposition of the chlorite schist whose cleavage pattern indicates a synclinal nature. The synclinal axis is refolded into an anticlinal cross-fold trending nearly SSE with the Chitradurga granite occupying the core of this crossfold. The crossfold axis can be traced southwards from the granite through the arcuate ridges of ferruginous quartzites and the axis dies out further south. The traps in-between the ferruginous quartzite ridges also appear to have been crossfolded although no mesoscopic structural features are apparent in them. The ferruginous quartzite ridges normally occupy synclinal axes. The minor folds within these ridges follow this regional structural pattern. The area is subjected to repeated tectonic activity accompanied by polymetallic mineral deposition. Sulphide mineralisation has been noticed along fracture zones. Copper is being extracted at Ingaldhal, about 6 kms. SE of Chitradurga.

The lithological sequence in the area commences with the basic flows, which, after metamorphism have resulted in the formation of the present hornblende schists. This is the earliest recognisable distinct rock unit belonging to the Javanahalli Formation. The chlorite schists are meta-sediments and clearly overlie hornblende schists. The contact between hornblende schist and chlorite schist is sharp and the contrast in meta-morphism also suggests a stratigraphic gap between the two. The chlorite schists of the Chitragurga Formation have limestone intercalations and are underlained by conglomerates. The traps are later and clearly overlie both hornblende schist and chlorite schist, and appear to have been emplaced along linear fissures. This stage appears to have been followed by folding and metamorphism. The main synclinal fold was developed during this stage. This was accompanied and followed by intrusion of dykes. The clays and ferruginous quartzites of G.R. Formations were next deposited. The G.R. Formation commences with the deposition of a bed of conglomerate followed by clays and ferruginous cherts. The deposition of G.R.Formation is followed by tectonism and development of crossfolds. The Chitradurga granite was emplaced in the core of a major crossfold probably contemporaneous with the folding episode.

5. CORRELATION OF AERIAL MSS DATA WITH FIELD DATA FROM THE TEST AREA

There are seven major lithological types in the test area. They are chlorite schists, traps, granites, hornblende schists, clays, banded ferruginous quartzites/cherts and conglomerates. The other rock types like quart reefs, dykes and ferruginous sandstones have too small an areal extent to sh

any recognisable pattern on the imageries at the available resolution.

The following observations are made on the MSS imageries in relation to field mapping:

a. The MSS bands 1,2 & 3 are useful in geological mapping. The tonal boundaries in these bands generally coincide with the boundaries of the lithological types. The tones in the bands 4 & 5 appear to be controlled by factors other than the reflectances of the lithological types.

b. The general range of grey levels of most of the lithological types even over different bands in between 4 & 10 in the step wedge scale (Fig.3). This variation is too limited for an effective identification. In practice, however, the reflectance of the rock types is often characterised by an uniformity in grey values - a sort of photo texture.

c. Only in a few cases are the reflectances measured directly from the lithological types. This is so in case of hard rocks devoid of soil cover and vegetation and which frequently occur as ridges. In many cases the rock types are either partly or completely covered with soil and vegetation. In these cases the reflectance measured is a function of the relative areas exposed of lithology, soil and vegetation. The combined reflectance of these appear to be characteristic of rock types and this may be due to a complex interrelation between lithology, soil, slope and vegetation. If the rock type is covered by a transported soil as is often in the case of low lying areas, the reflectances measured may be neither directly nor indirectly related to lithologies.

d. There is a further difficulty in identifying rock types in low lying areas. These areas are very often cultivated, and the moisture content significantly varies from place to place. The tonal variations in such cases are very much greater than those due to any lithological variations. The presence of soil cover and moisture often causes difficulties in demarcating the boundaries on the imageries. This defect may possibly be reduced by choosing a proper season for MSS data collection.

e. The contrast in reflectance is an important factor in distinguishing a particular feature. If there is a prior knowledge of the existence of a particular unit in an area, it is often possible to locate it on the imagery, although, such location may not be possible without this knowledge. This is due to subjectivity.

f. The variation in reflectance of the different lithological types over different bands is shown on the graph (Fig.3). The reflectances vary widely and the values plotted are the modal values. Variation within a given frame is limited, while from frame to frame reflectances vary very widely. This may be due to unfaithful data recording and/or poor image reproduction. The variations are particularly severe in bands 4 & 5. Certain features of the graph are particularly striking. Hornblende schist has uniformly a lighter tone than chlorite schist in all the bands. Clay has a higher reflectance than either chlorite schist or hornblende schist. Trap can be separated from chlorite schist and hornblende schist in bands 1 and 2. In granites and granitic soils the reflectance decreases from band 1 to 5. The granitic soil generally shows a lot of tonal variation due to landuse and associated moisture change in the soil. This fact could be used in its identification although a chlorite schist might show a similar characteristic and raise difficulties. The ferruginous quartzite has the darkest tone than any other rock type studied in band 3. The conglomerates have generally a lighter tone.

g. Geological interpretation in conventional aerial photography is very much based on landform pattern. The main advantage of the aerial photography is that the photographs can be observed stereoscopically. In geological mapping they are more useful than aerial MSS data. MSS data can supplement the aerial photographic information in cases where lithologies form similar landforms but may have different reflectances.

6. STUDIES BASED ON LANDSAT IMAGERIES

An attempt was made to use the aerial MSS data as correlated with ground truth, to identify lithological types on the landsat imageries in an endeavour to geologically map the entire schist belt and the surroundings extending over an area of about 20,000 sq.kms. It was however found that reflectance patterns in the two imageries were difficult to be compared. This was mainly due to the scale differences of the two imageries and the accompanying constraints. A unit in the aerial MSS imagery may be made up of a single lithological unit. A unit in satellite imagery on the other hand is often made up of several lithological types. So it was decided to study the landsat imageries independently in terms of tonal changes and trend lines without comparing with the aerial MSS results.

6.1 GEOLOGY OF THE SCHIST BELT

The different lithological units on the landsat imageries have been separated in terms of tonal differences (Fig.4). Landsat MSS 4 is particularly useful in lithological mapping followed by MSS 5. MSS 5 is also useful for marking the drainage pattern. It has been possible to identify hornblende schist, chlorite schist, traps, ferruginous quartzites, granites/gneisses. These units apparently contain intercalation of other lithological types. In the test area, for example, only the major lithological types can be made out. The boundaries of the units can be marked with a fair degree of sharpness. The hornblende schist is found fringing the schist belt every where. The chlorite schist forms the main mass of the schist belt and is found to continue in the southern extension of the schist belt. The traps occur as pockets and lenses and follow the general trend of the other lithological types. Only the major ferruginous quartzite ridges can be made out. But their borders are not sharp. The granites and gneisses have a characteristic light tone and can be very easily identified. The tone of a granite depends on whether it is a hilly terrain or plain country and whether it is covered with soil and vegetation or not. This could be made out by studying the different granite masses in the area.

The geological map shows a striking similarity with the geological map of Mysore published in 1915. The overall disposition of the schist belt and granitic rocks is similar. The marking of chlorite schist and traps is also fairly accurate. There are a number of features in that map like minor ferruginous quartzite ridges, conglomerates etc., which cannot be made out on the landsat imageries. No distinction between granites and gneisses can be made.

The schist belt is mainly drained by rivers Vedavathi, Cauvery, Shimsha and Hemavathi. The density of stream network is concentrated in the gneissic area and is very less within the schist belt. The three main reservoirs in the area are Vanivilasa Sagara, Borana Kanive and Marconahally. Some of the major river courses are controlled by the lineaments in the area. The drainage pattern around the major folds within the schist belt are structure controlled. Northerly direction of drainages appears to be controlled by the general Dharwarian trends. The region south-west of location 10 in Fig.5 has a peculiar drainage pattern. The drainage appears to be radial and

641

cannot be correlated with any particular lithological feature or any structural trend. This might represent a basement high as suggested by Krishnamurthy et al (1979).

6.2 STRUCTURE OF THE SCHIST BELT

Landsat imageries are more useful for structural than for lithological mapping. MSS 6 is particularly useful followed by MSS 5. It is fairly easy to mark the trend lines, formation contacts, and lineaments. But interpretation of these trends often become ambiguous and will need confirmation with field checks. The lineaments may have different significance at different places in the tectonic setup of the area.

The main structure of the area is a syncline with the axis running in a near-NNWly direction (Fig.5). There are two major anticlines, one in the western region (loc.4) and the other in the northwestern region occupied by Chitradurga granite (loc.1). An anticline (loc.2) and a syncline (loc.8) can be traced in the eastern region. These two folds are cut off by faults and their eastern limbs are not sharp probably due to the granitisation effects during emplacement of peninsular gneiss. There are two other anticlinal folds trending in the same general direction (loc.3,5) whose cores are occupied by granites/gneisses. There are other minor folds sympathetically folded along with these major folds. Few minor faults are noticed.

A tentative tectonic succession can be made out. There is a very important trend relation in the southern portion of the map (loc.12) where the Chitradurga trend lines clearly truncate the earlier trend lines. The anticlinal fold at loc.1 is plunging SSEly and is distinctly later than the main syncline and appears to be a crossfold. The crossfolded nature can be made out by the trends of lithologies and that of synclinal fold axes in this region. The anticline at loc.4 has the same plunge direction as that of the Chitradurga cross fold. But its exact nature is not clear on the landsat imagery, and even after careful field check, the structure could not be confirmed due to paucity of exposures. The Dodguni anticline at loc.9 has a NNWly plunge and its two limbs are abruptly terminated. The eastern limb is highly disturbed and some isoclinal folds appear to be present in this region. The folds at loc.2 & 8 in the eastern part also have northerly plunges and appear to have been highly disturbed tectonically. They are probably remnants of an early tectonic event. The anticlines at loc.3 & 5 and their associated folds appear to be contemporaneous with the main syncline. Some folds in the southern region show complex interference patterns.

The lineaments in the area have two prominent directions. One set is parallel to the trend of the schist belt. The second is nearly perpendicular to this direction. The lineaments are a late feature and can be seen cutting through the different members of the schist belt. They have developed after folding and the main metamorphic event and even later than the younger granites of the area. There is a prominent lineament in the east parallel to the Closepet granite body and probably related to it. Many of the lineaments are deep seated fractures. Such fractures are weak planes and they often control the river courses locally. There is a higher frequency of lineaments in the north compared to the southern region around loc.12. This indicates that the deformation is of a deep-seated nature in the region around loc.12, where the material has flown without fracturing. On the other hand the deformation in the rest of the area is of a shallow type with fracturing playing a more prominent role.

Although the NNWly lineaments are post-mineralization, they are controlled by the folding pattern in the area and may have an indirect significance. The

642

near-east-west fractures are of release-type and are unimportant from the mineralization point of view. They may have importance in hydrological studies as they can transmit water from the high rainfall areas in the west to low rainfall areas in the east.

The trend lines from north to south show an arcuate pattern suggesting a major thrust in the eastern direction. This has also affected the lineament pattern in the area. This may also explain the disturbed eastern contact of the schist belt south of loc.2.

Polymetallic sulphide mineralization with the predominance of primary copper sulphides is known to occur in the area. Besides this, associated with cherts and quartzites, manganese and iron ores which have a stratigraphic control are also known to be present in the area. Neither aerial MSS data nor the landsat imageries were directly helpful in locating areas of ore mineralization. However, since all the known ore deposits of the area are either structure controlled or stratigraphy controlled, the MSS study has an indirect bearing in location of ore deposits.

7. RESULTS FROM ENHANCED DATA PRODUCTS

More information can be extracted from the MSS data by using standard image enhancement techniques. Number of methods are available like linear range stretching, gaussian stretching and band ratioing, all these methods requiring computer processing (ISRO, 1978; Gillespie and Billingsley, 1975; Rovan et al 1977). In the present study two techniques have been attempted. In the first method colour composites were prepared using different bands. By using an additive colour viewer, different combinations were tried for getting the best possible results. The lithological variations and structural details are more clearly broughtout in the colour composites than in the imageries of individual bands. A second method attempted was an optical method somewhat akin to the band ratioing technique. In this method the positive transperency of one band is superimposed over a negative transperency of another band to get the ratioing effect. However, no stretching is involved. The bands chosen for the study depend on slopes of the refletance spectra. The technique was attempted both over aerial MSS data and landsat MSS data. In the following discussion the results from landsat are presented. The four bands 4,5,6 and 7 of landsat yield 6 possible ratios. Using each combination a separate map was prepared. Information from all these maps and from the colour composites was consolidated and presented as Figs. 4 and 5. The striking feature of this exercise is the development of sharp contacts between the lithological types. For example, some of the ferruginous quartzite ridges appear with very sharp contacts with the surrounding lithology; so also the contact between chlorite schist and hornblende schist. The trend lines are also much sharper.

REFERENCES

1. Gillespie,A.R. and Billingsley,F.C.: Digital processing of ERTS images.
   Technical report No.32-1597, Jet Propulsion Laboratory, Pasadena,
   California, 1975.

2. Indian Space Research Organisation: Workshop on Digital processing of
   Remotely sensed data, Ahmedabad, 1978.

3. Krishnamurthy,J.G., Gopalakrishnan,K.P., & Ramachandran,T.V.: Geological
   groundtruths and Landsat imagery interpretation for parts of Karnataka
   State, India, Workshop on "Remote sensing & Mineral exploration".
   COSPAR meetings, Bangalore, 1979.

4. Mukhyopadyaya,D., Baral,M.C. & Ghosh,D: A tectonostratigraphic model of
   the Chitradurga schist belt, Karnataka, India. Jour.Geol.Soc.Ind.,
   Vol.22, 1981.

5. Radhakrishna,B.P.: Reconsideration of some problems in the Archaean
   complex of Mysore. Jour.Geol.Soc.Ind., Vol.8, 1968.

6. Rowan,L.C. et al: Discrimination of hydrothermally altered and unaltered
   rocks in visible and near infrared multispectral images. Jour. Geophysics,
   Vol.42, No.3, 1977.

7. Sampath Iyengar,P: Report on the survey work in the Chitradurga district.
   M.G.D. record, Vol.6, 1905.

8. Sreenivasan,R. & Sreenivas, B.L.: Dharwar stratigraphy. Jour.Geol.Soc.
   Ind., Vol.13, 1972.
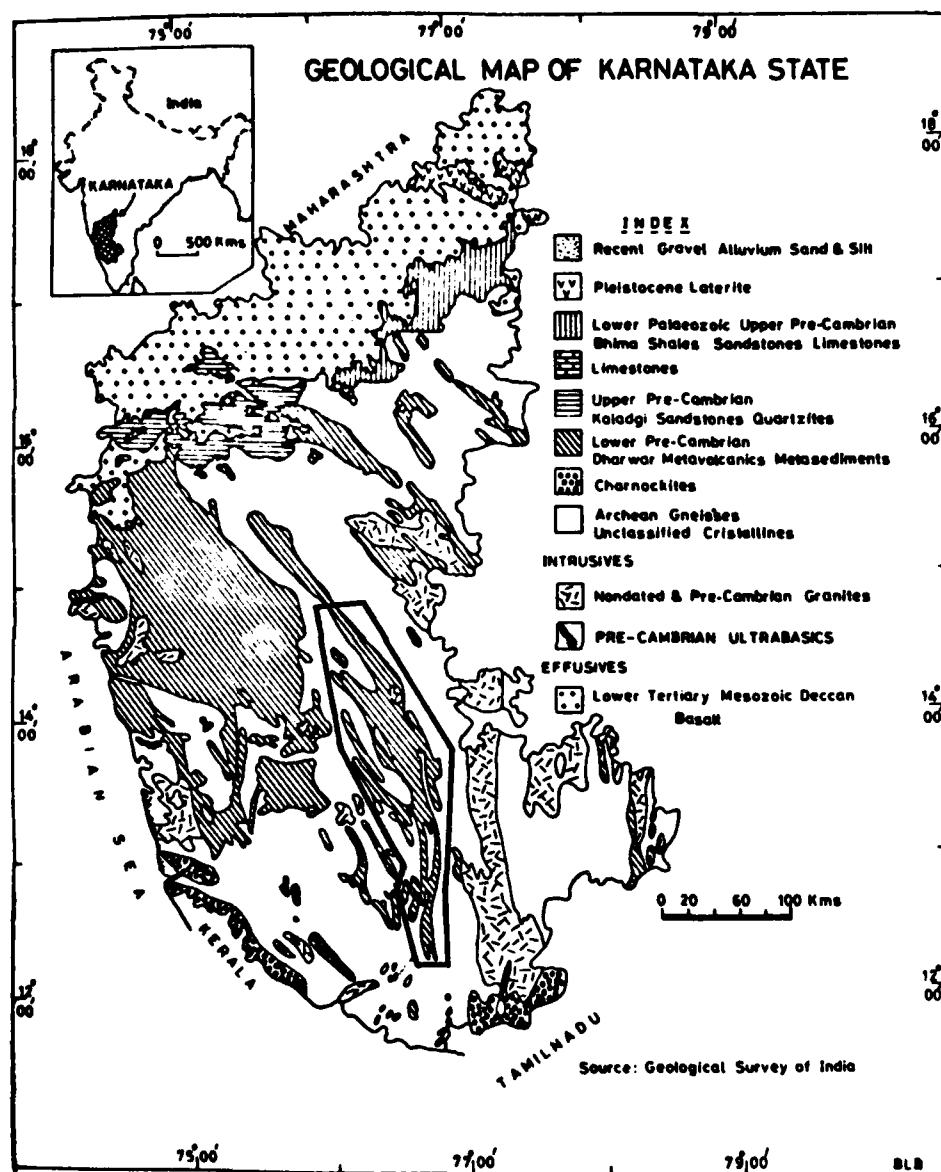
Figure 1: Geological map of Karnataka showing the location of the study area.

MSS Bands

Figure 3: Graph showing the
reflectance spectra
of different lithologies.

Figure 2: Geological map of the test area.
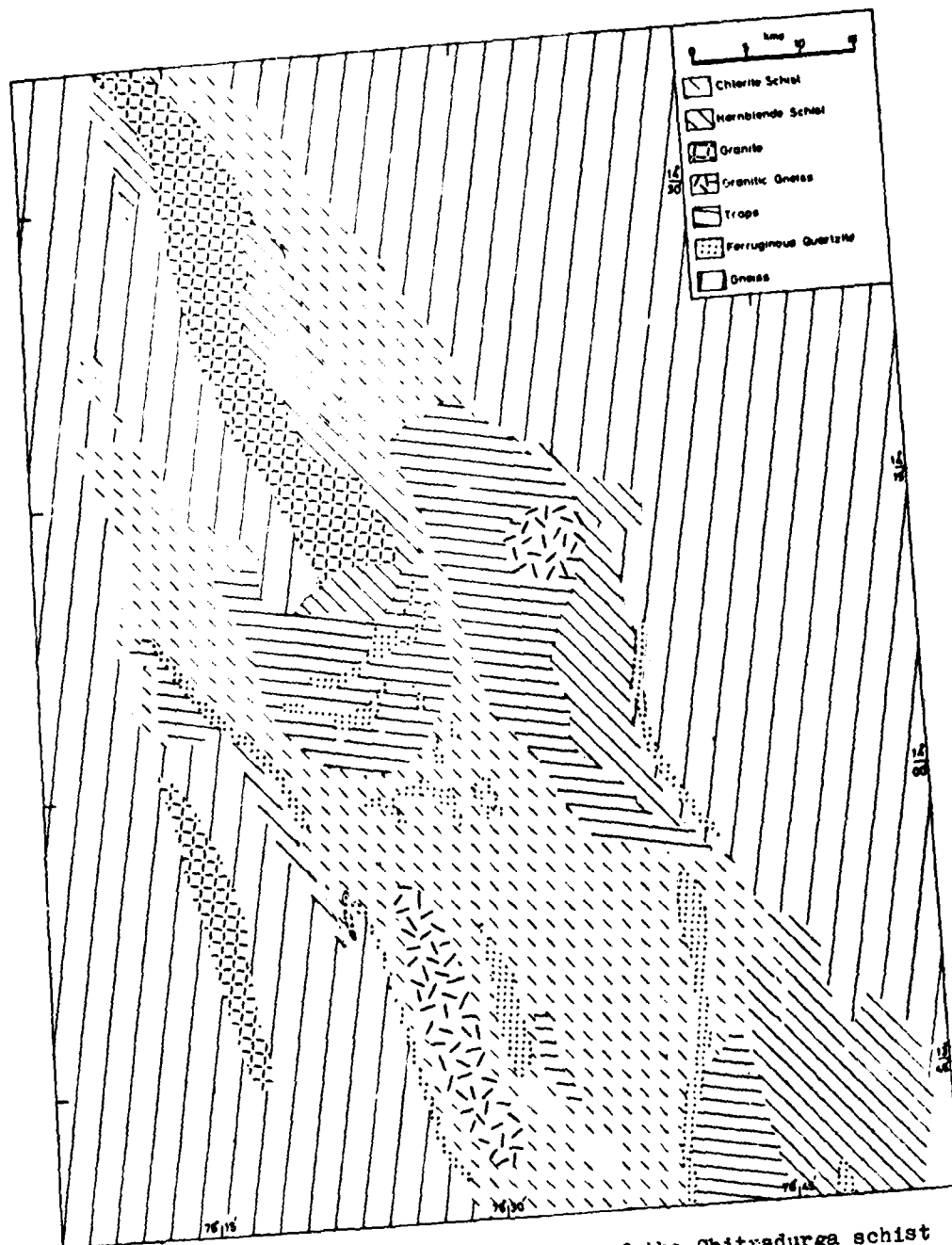
Figure 4: Geological map of central part of the Chitradurga schist belt based on image enhancement studies.
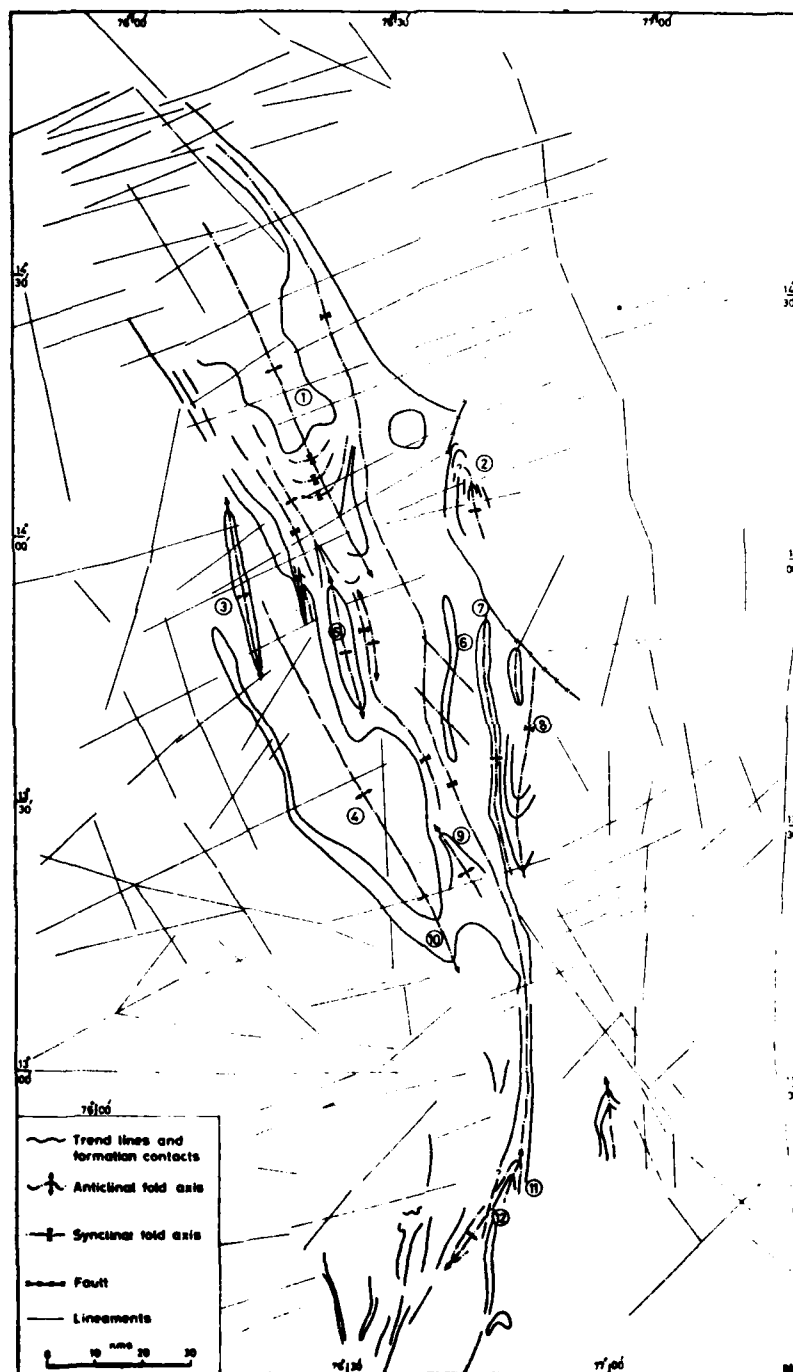
Figure 5: Structural map of the Chitradurga schist belt based on image enhancement studies.

648

DEVELOPMENT OF THE TIROS-N DATA PROCESSING SYSTEM FOR VERTICAL SOUNDINGS

TADAO AOKI, SHINOBU NAKAJIMA AND KAZUYASU KATO
Meteorological Satellite Center, Kiyose, Tokyo, Japan

ABSTRACT

In Meteorological Satellite Center(MSC), the vertical sounding of temperature, moisture and other atmospheric parameters from TIROS-N satellite series is now operational beginning from January 1981. The products from the vertical sounding system involve the vertical temperature profile, vertical precipitable water profile, total ozone amount, sea or ground surface temperature, cloud top height, cloud emissivity and cloud amount.

This article briefly summarizes the theoretical background of the data processing system of MSC for the retrieval of these atmospheric parameters. The accuracies of some of these products are also described.

1. RETRIEVAL OF THE CLOUD PARAMETERS AND CLEAR RADIANCES

The most outstanding point of the vertical sounding system of MSC is the cloud parameter determination and clear radiance retrieval. About 300-450 pixels of AVHRR(Advanced Very High Resolution Radiometer) are contained within a HIRS(High Resolution Infrared Radiometer Sounder) spot. In MSC system the cloud amount in each HIRS spot is calculated by counting the number of the AVHRR pixels of cloudy radiance. Here, the cloudy radiance is defined as the radiance that is smaller than a critical value. The critical value of the AVHRR radiance is given by reducing, by some amount, the initial guess value of the AVHRR clear radiance given for every 1x1° latitude/longitude area.

The AVHRR clear radiance is calculated from the initial guess field of the surface temperature and atmospheric temperature and moisture. The surface temperature is given for every 1x1° latitude/longitude area, which has been compiled by the objective analysis method using the surface temperature data obtained from the last soundings.

The atmospheric temperature and moisture fields are given for every 5x5° latitude/longitude area, compiled from the NMC(National Meteorological Center of America) data acquired through GTS(Global Telecommunication System) and/or the climatological data compiled by MSC. In future the temperature and moisture profiles obtained by the vertical sounding system of MSC may also be used. At present such a module has not yet been developed.

The field of the surface temperature and atmospheric temperature and moisture are updated twice a day. The initial guess field of AVHRR clear radiance is also calculated twice a day. At the same time the clear radiance of all HIRS channels are also calculated for 5x5° latitude/longitude areas. This latter data is used in the next step as the initial values for the clear radiance retrieval.

In the process of the cloud amount determination, we also obtain the maximum and minimum AVHRR radiances and two kinds of average of the AVHRR radiance; the average over all pixels and over only cloudy pixels of AVHRR contained within each HIRS spot. These data are used for the clear radiance retrieval. (For the details see Aoki, 1980a, 1982.) Also used are these data for the estimation of the cloud top height and cloud emissivity as described later.

In the navigation of the AVHRR radiance data within each HIRS spot for the calculation of the cloud amount and others described above, it is necessary to know what pixel of AVHRR belongs to a HIRS spot. For the details of the determination of the relative position of the AVHRR pixels and HIRS spots see Aoki(1980b) and Aoki and Nakajima(1981). Since the relative position of the AVHRR and HIRS pictures are unchanged through the operation of a satellite, it is determined only once for each satellite of TIROS-N satellite series.

2. RETRIEVALS OF ATMOSPHERIC PARAMETERS

Denoting the atmospheric temperature at the j-th level or the precipitable water from the top of the atmosphere to the j-th level, by X_j, we calculate it by the following equation:

$$X_j = \sum_i C_{ji}(\mu) R_i(\mu), \tag{1}$$

where C_{ji} is the regression coefficient and R_i the clear radiance of the i-th channel except for i=0, where $R_0(\mu)=1$. The regression coefficient is determined from many coincident data of radiosonde data, X, and satellite data, R. μ is the inverse of the cosine of the zenith angle θ'($\mu=1/\cos\theta'$) of line of sight from scan spot on the surface to the satellite. θ' is a function of the scan angle θ. θ and θ' are not equal because the earth surface is not flat.

Observations by HIRS are made at 56 scan spots in the scan angle range of ±49.5 degrees. As the μ changes with scan step we have to prepare many number of the value of the coefficient C depending on the scan step, i.e., μ. However, considering the fact that according to the theoretical study of these aurthors(unpublished) the clear radiances vary only a very small range of less than 10 percent, we can expect that μ-dependence of C is also weak so that it can be parameterized with a simple function of μ. One of the simplest form of C may be given by

$$C_{ji} = K_{ji} + C_{ji}' \Delta\mu, \tag{2}$$

$$\Delta\mu = \mu - \mu_r, \tag{3}$$

where μ_r is the μ at a reference step angle, K_{ji} is the $C_{ji}(\mu)$ at $\mu= \mu_r$,

650

being independent of μ:

$$K_{ji} = C_{ji}(\mu_r). \tag{4}$$

Now, the number of the parameters of C_{ji} that must be determined for each value of j has been reduced to $2(L+1)$; that is, they are the K_{ji} and C_{ji}' (i = 0, ..., L), where L is the total number of the channels used. To obtain the stable solution C_{ji} we must have sufficiently large number of the coincident data of X and R, and they, at the same time, should evenly be distributed over various values of the step angle. Considering this fact it is desired to reduce further the number of the parameters in the coefficient to be determined.

According to the so-called Minimum Information Method(see, e.g., Smith et al., 1972), the calculation of the atmospheric temperature or moisture profiles are made by the same functional form as the Eq.(1) except that the coefficient C is now determined theoretically from the weighting function. The weighting function, in turn, obtained from the transmission function τ, given in the form:

$$\tau = \exp[-\int_0^p k\mu dp], \tag{5}$$

where p is the pressure and k is the absorption coefficient. If we plott against the vertical axis

$$z = \ln(p), \tag{6}$$

the vertical profile of τ for a slant path is roughly represented by shifting, by amount $\ln(\mu)$, the profile of τ for the vertical path toward the direction of z. Accordingly, it is expected that the function C for a slant path can also be obtained from the C for the reference step angle.

From this consideration we approximate the curve of $C_{ji}(\mu)$ by K_{ji} with slightly shifting toward the direction of z as follows:

$$C_{ji}(z_j, \mu) = K_{ji}(z_j + \delta_i), \tag{7}$$

where δ_i is the amount of the shift, which is assumed to be proportional to $\Delta\mu$:

$$\delta_i = \eta_i \Delta\mu, \tag{8}$$

where η_i is the constant depending only on the channel number.

Now the number of the parameters that must be determined reduced from $2(L+1)$ to L+3: They are K_{ji}(i = 1, ..., L), η_i, $C_{j0}(\mu_r)$ and C_{j0}', and the Eq.(1) is rewritten in the form:

$$X_j = C_{j0} + C_{j0}'\Delta\mu + \sum_i K_{ji}(z_j+\delta_i)R_i(\mu). \tag{9}$$

651

For the case of the surface temperature(SST) and total ozone amount the η-technique described above can not be used so that the Eq.(2) was adopted. The field of the retrieved SST is further optimized by the procedure of the objective analysis recently developed by Aoki(1982b) and Aoki et al.(1982).

The cloud top height is determined by the method of Smith and Platt (1978). According to the method of Smith and Platt(1978) the cloud top height is determined by finding the value of the pressure p_c that satisfies the following equation:

$$\frac{R(\nu_1) - I(\nu_1)}{R(\nu_2) - I(\nu_2)} = \frac{\int_{p_c}^{p_s} \tau(\nu_1,p)\frac{\partial B(\nu_1,p)}{\partial p}\,dp}{\int_{p_c}^{p_s} \tau(\nu_2,p)\frac{\partial B(\nu_2,p)}{\partial p}\,dp}, \qquad (10)$$

where I is the observed radiance, B is the Planck function and p_s is the surface pressure. ν_1 and ν_2 denote the different two channels of HIRS; in the present system of MSC they are the 7 and 8th channels.

Another information of the cloud top height is obtained from the minimum radiance of AVHRR: As has been described in Aoki(1982a) the minimum radiance of AVHRR upwells from the cloud whose emissivity is likely unity. Thus the cloud top height is obtained from the apparent blackbody temperature of AVHRR minimum radiance with the use of the retrieved temperature profile. The results of these two kind of the cloud top height calculation are both archived in the magnetic tape.

The cloud emissivity is calculated by

$$\varepsilon_c = \frac{R - I_c}{R - I_c{}^*}, \qquad (11)$$

where R is the clear radiance of AVHRR, which is determined by

$$R = \frac{\sum\limits_i^M (1 - n_i)I_i(max)}{\sum\limits_i^M (1 - n_i)}, \qquad (12)$$

where M is the number of the HIRS spot used for the retrieval of the clear radiance of HIRS channels, n_i the partial cloud amount in the i-th spot of HIRS and I_i(max) the maximum of clear radiances of AVHRR, which are larger than the critical radiance. $I_c{}^*$ is the minimum radiance of AVHRR in the most cloudy HIRS spot. I_c is the mean cloudy radiance of AVHRR averaged over cloudy pixels of AVHRR within the most cloudy spot of HIRS.

Table 1 is the lists of the products from the vertical sounding system of MSC. The details of this section is described in Aoki(1982c).

3. EVALUATION OF THE PRODUCTS

Fig.1 shows the rms difference between soundings of the temperature profile and precipitable water profile by NOAA-6 satellite and radiosonde, where the precipitable water is defined by that contained in the column from the top of the atmosphere to the pressure level concerned. The results in Fig.1 are those for the so-called 'clear' cases, where the 'clear' and 'cloudy' are defined by the following parameter:

$$\gamma = (1 - \bar{n})^2 + n_{max} - n_{min},\tag{13}$$

where $\bar{n}$ is the mean cloud amount averaged over M of HIRS spots and n_{max} and n_{min} are the maximum and minimum cloud amount, respectively. If γ is greater than the critical value(at present it is 0.3) it is 'clear' and if not it is 'cloudy'. Roughly speaking, if $\bar{n}$ is smaller than about 0.93, it is 'clear'. As a comparison, the result of rms error in NESS/NOAA system for temperature profile is also shown in Fig.2. It is found that our result is slightly better especially in lower atmospheric layers. This will be because in our system the AVHRR 4th channel is used in the clear radiance retrieval and in vertical profile retrieval.

Figs.3 and 4 are comparisons between the satellite derived SST, analyzed ship reports of SST made by Marine Department of Japan Meteorological Agency and the so-called GOSSTCOMP made by NESS/NOAA. The general agreement of the SST pattern between ours and Marine Department is excellent.

REFERENCES

Aoki, T., 1980a: A statistical method to retrieve the clear radiance from cloud-contaminated radiances. J. Meteor. Soc. Japan, 58, 58-66.

_____, 1980b: A method for matching the HIRS/2 and AVHRR pictures of TIROS-N satellites. Meteor. Satellite Center Tech. Note, No. 2, 15-26.

_____, 1982a: An improved method to retrieve the clear radiance from partially cloudy spots of radiometer on board satellite. J. Meteor. Soc. Japan, 60(to be published).

_____, 1982b: Development of a generalized objective analysis and its relationship to the current methods. Meteor. Satellite Center Tech. Note(to be published).

_____, 1982c: Theoretical background of the vertical sounding from TIROS-N satellite series. Meteor. Satellite Center Tech. Note, No. 5, 25-32.

_____ and S. Nakajima, 1981: On misalignment between HIRS and AVHRR pictures of NOAA-6 meteorological satellite. Meteor. Satellite Center Tech. Note, No. 4, 63-67.

_____, S. Nakajima and K. Kato, 1982: Remote Measurements of the sea surface temperature by multichannel observation and its objective analysis. (to be published).

Smith, W. L. , H. M. Woolf and H. F. Fleming, 1972: Retrieval of atmospheric temperature profiles from satellite measurements for dynamical forecasting. J. Appl. Meteor., 11, 113-122.

_____ and C. M. R. Platt, 1978: Comparison of satellite-deduced cloud heights with indications from radiosonde and ground-based laser measurements. J. Appl. Meteor., 17, 1976-1802.

_____, F. W. Nagle, C. M. Haydon and H. M. Woolf, 1981: Vertical mass and moisture structure from TIROS-N. Bull. Am. Meteor. Soc., 62, 388-393.
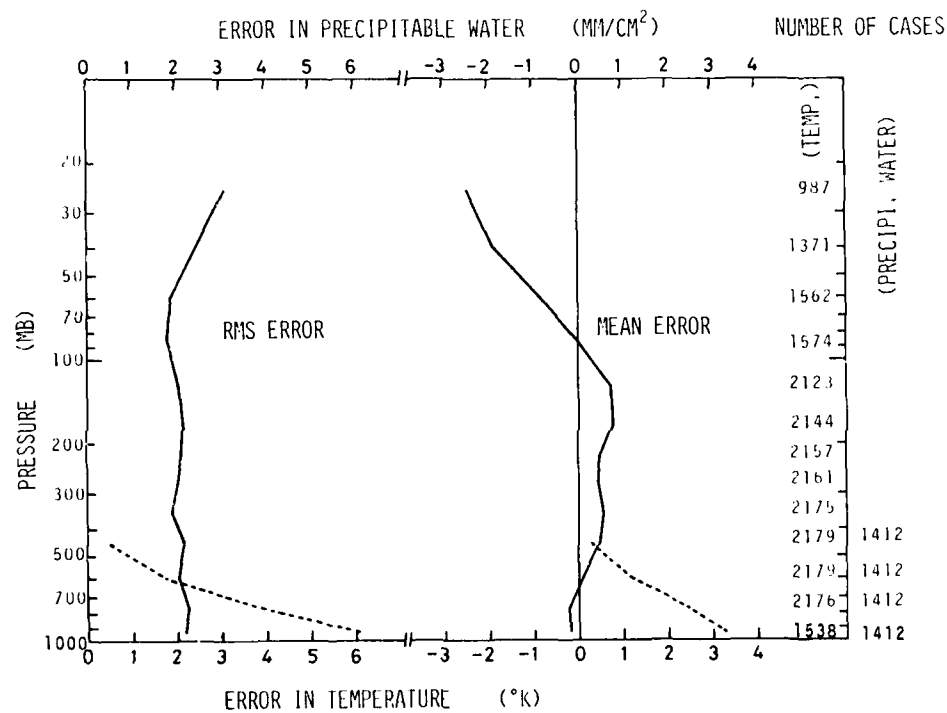
Fig.1 RMS and mean differences in atmospheric temperature (solid lines) and precipitable water dashed lines) between radiosonde and satellite soundings by MSC sytem, averaged over about 90 days of three months, January, April and July 1981.

654

Table 1   The data in archive magnetic tape

1. TOVS DATA
    Calibrated radiances of HIRS, SSU and MSU.

2. CIL DATA
    (For every HIRS spot)   Location on earth surface. Cloud amount.
    Averaged AVHRR radiance over whole area. Average AVHRR radiance
    over cloudy area. Maximum AVHRR radiance. Minimum AVHRR radiance.
    Initial guess of AVHRR clear radiance.

3. APRET DATA
    Clear column radiances of HIRS and AVHRR. Temperatures at
    1000, 850, 700, 500, 400, 300, 250, 200, 150, 100, 70, 50, 30, 20,
    10 mb. Precipitable waters from the top of the atmosphere to 400,
    500, 700, 850, 1000 mb. Sea or ground surface temperature. Total
    ozone amount. Mean cloud amount. Cloud top height by the method
    of Smith and Platt. Cloud top height from the minimum radiance
    of AVHRR radiance. Cloud emissivity.
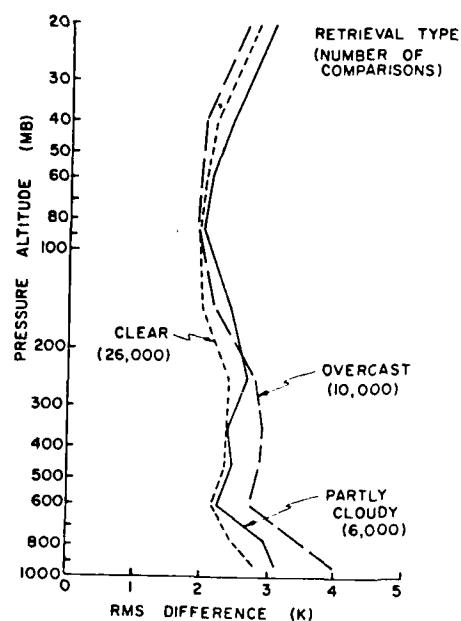
Fig.2;
RMS differences between
radiosonde and satellite
soundings of the atmos-
pheric temperature by
NESS for April 1980.
(by Smith et al., 1981).

655
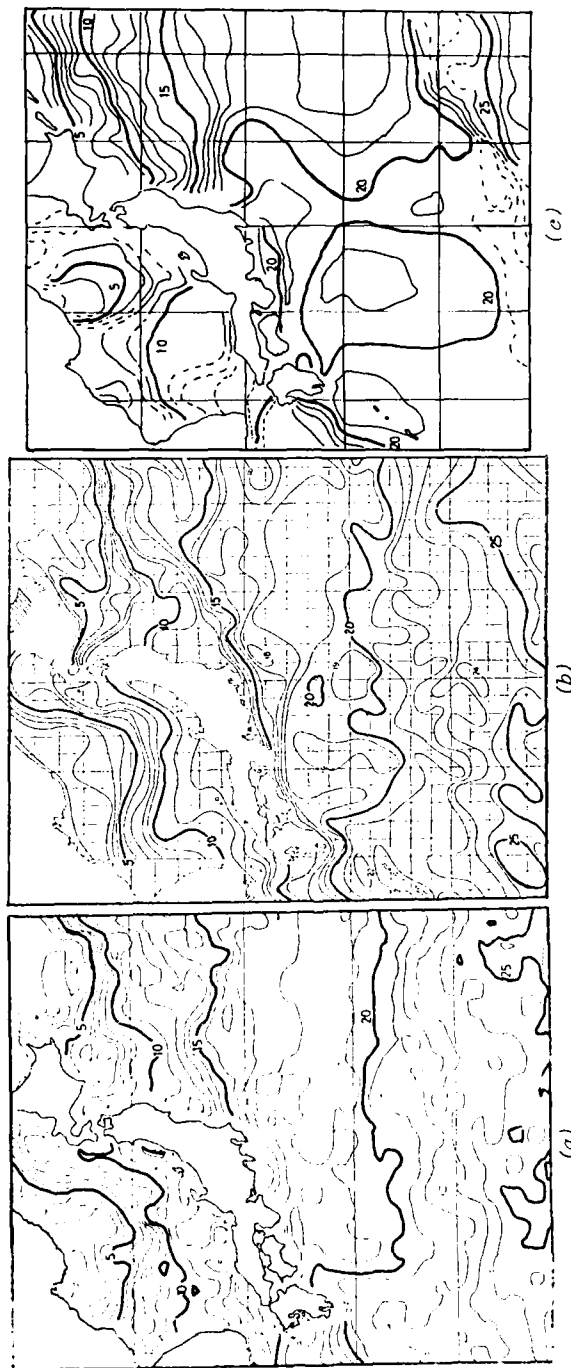
Fig.3 Comparison of the analyzed mean SST fields, by MSC(a) and Marine Department using ship reports(b) averaged over 11 - 20 January 1981, and GOSSTCOMP by NESS/NOAA(c) averaged over 13 - 20 January 1981.

656
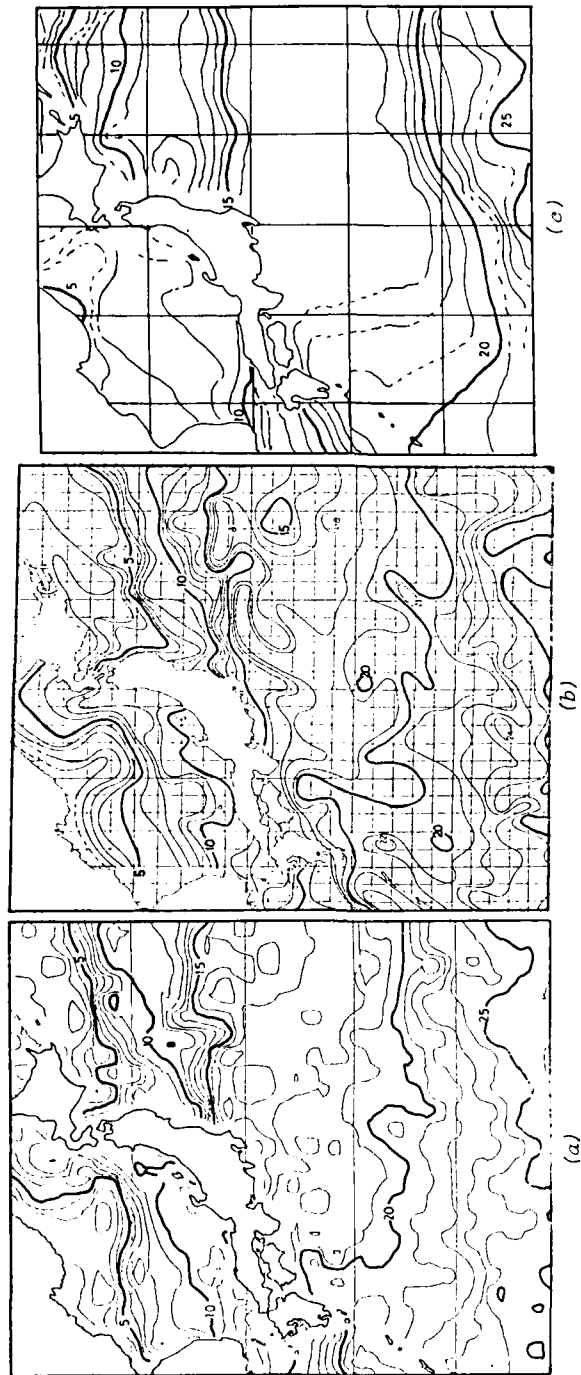
Fig.4 Same as Fig.3 except for the period 11 – 20 February 1981 for MSC(a) and Marine Department(b), and 10 – 17 February 1981 for GOSSTCOMP(c).

AD P002043

COASTAL ZONE MAPPING OF GUYANA
USING DIGITAL LANDSAT DATA *

V. Singhroy

Ontario Centre for Remote Sensing
Toronto, Ontario, Canada

B. Bruce

Canada Centre for Remote Sensing
Ottawa, Ontario, Canada

ABSTRACT

Four major types of development projects in the
coastal zone of Guyana require that a detailed mapping
of resources be performed for the region. First,
projects have begun, and others are planned, to
increase the land area which can support agriculture
through irrigation and defence against flooding by
seawater. Second, a program to develop a data base
for crop acreage estimation and forecasting has begun.
This program requires a reliable means of monitoring
the major rice and sugar-producing areas year-round.
Third, access roads are being constructed to farms
and logging areas near the coast. This development
requires detailed information on engineering construc-
tion materials, terrain and land cover. Finally,
the development of offshore fisheries has made it
essential to collect oceanographic data for forecasting
fish population and distribution. To manage the
fisheries, it is vital to obtain an understanding of
conditions in coastal waters and the processes which
produce them.

Existing information on land and water resources
in the coastal zone is partial or outdated. It would
be extremely costly to obtain new, complete data by
conventional means.

This pilot study demonstrates that LANDSAT imagery,
supported by information from 1:10,000-scale black and
white aerial photographs, can provide a cost-effective
and efficient source of baseline information on agricul-
tural crops, forest cover types, and engineering
materials.

An October LANDSAT image of a study area in Guyana's
coastal zone was digitally analyzed to distinguish spectral
classes corresponding reliably to known crop types, forest
cover types, inland "pegasse" wetlands, mangrove swamps

---

and tidal flats. Several coastal water colour zones
were also identified. The boundaries between these
zones represent the temporary fronts of local current
movement, and were found to correspond to known areas
of the best commercial fishing in the study area.

The digital analysis was carried out on the image
analysis system of the Ontario Centre for Remote Sensing
(OCRS). This system includes a computerized colour
plotter with OCRS-developed software, for the production
of full-colour, hard-copy maps of digital analysis
results.

A series of 1:50,000-scale colour-coded thematic
maps of land use and land cover were prepared for a
4000 km^2 area between the Demerara and Berbice Rivers.
In addition, data from existing sources on the regional
distribution of surficial sediments, terrain types,
lineaments and engineering construction materials were
combined with the LANDSAT and airphoto interpretation
to produce a multipurpose geotechnical map. The results
demonstrate that the LANDSAT-based method is a
practical means of obtaining comprehensive information
on coastal zone resources.

INTRODUCTION

Accelerating development in the coastal zone of Guyana has made it
necessary for the resources of the region to be mapped in detail. The
following four major types of development are underway:

(i) Drainage, Irrigation and Sea Defence
     Current and planned drainage, irrigation and sea defence projects
     aimed at improving the agricultural land base for increased production.
     Many coastal areas are below sea level; thus, flood control is a
     serious problem. Since 1978, major irrigation projects have extended
     water control to nearly 300,000 acres of agricultural land.

(ii) Feeder Road Construction
     The construction of feeder roads to farms and near-coastal logging
     areas has created the need for detailed information on engineering
     construction materials, terrain types and land cover.

(iii) Agricultural Productivity
     The establishment of a data base of crop production and forecast
     information has created a need for a reliable and sequential crop
     inventory system to monitor the year-round activities of the major
     rice and sugar production areas. This would make possible a more
     efficient marketing and distribution system.

(iv) Offshore Fisheries Development
     The recent development of offshore fisheries has focused attention on
     various techniques for the collection of oceanographic data aimed at
     forecasting the quantity and distribution of the fish population for
     improved fisheries management.

Of the wide variety of data required for these major projects, little
is currently available. Systematic collection by traditional methods
is prohibitively expensive. The combination of digital LANDSAT data and

existing aerial photography offer much potential to help provide vital agricultural, engineering, geological and oceanographic data. The production of integrated LANDSAT and airphoto preliminary maps seems a logical step in the planning and execution of various detailed field programs. This paper demonstrates the potential contribution of LANDSAT to coastal zone management in data-scarce environments.

STUDY AREA

The study area in Guyana includes the flat coastal plain and offshore area between the Demerara and the Berbice Rivers (Figure 5). This area occupies approximately 4000 km^2, fifty percent of which is offshore. The narrow coastal strip, approximately 20 km wide, is below sea level.

The surficial sediments include mud flats, fluvio-littoral sand ridges and aprons, alluvial silt and clay, and pegasse (organic) accumulations. These deposits are underlain by recent soft marine fossiliferous clay of the Demerara Formation. Further inland, interbedded Pleistocene silty clay and sand of the Coropina Formation are found, as well as Pliocene coarse sand, and clays with lignite beds which form the White Sand Series (Bleackley, 1957).

The region is drained by the Demerara, Berbice, Abary, Mahaica and Mahaicony Rivers. With an average of eighty inches of annual rainfall coupled with the tidal influences, the major Demerara and Berbice rivers frequently overflow their banks, creating extensive natural levees.

The original vegetation was mixed tropical forest, most of which has been cleared for agriculture and urban development. The Wallaba forest occupies the inland White Sand plateau. Mangrove swamps are found on the tidal flats, and pegasse swamps occupy the inland depressions. The major agricultural crops include sugar, rice and coconuts, while the growing of tropical fruits and market vegetables and the raising of livestock are secondary agricultural activities.

METHODOLOGY

A combination of visual and machine-assisted analysis techniques has been established for image interpretation. This procedure involves three steps:

1. Stereoscopic interpretation of 1:10,000-scale black and white aerial photos for selected areas along the coast. The sample areas were selected to represent different land cover types and served as verification areas for the digital LANDSAT analysis. Figures 1 to 4 show annotated examples of four of these test sites. The other test sites represent typical land cover of the hinterland, and were selected from 1:30,000-scale black and white stereograms (Welch, 1972). Included were examples of mixed forests on steep high hills, and Manni-Dalli forest (Welch, 1972) on flat, swampy pegasse soils; mangrove forest on tidal flats and the Wallaba forest on the flat well-drained white sand plateau.

2. Visual analysis of a 1:100,000 LANDSAT colour composite combining Band 4 (blue), Band 5 (green) and Band 7 (red) was performed on 500 x 500 pixel grid units for the entire study area. The interpretation of pattern and tone variations of the LANDSAT colour composite, the stereoscopic interpretation of the airphotos, integrated with existing soils, geomorphological, and forestry maps (Bleackley, 1957; Welch, 1972) all contributed to the production of a series of interpretative keys (Table 1). These keys represent the various types of terrain and land cover of the coastal areas and provide the basis of digital

661

land classification. The synoptic coverage of the LANDSAT colour composite provided regional structural drainage trends and assisted in the revision of a number of lithologic-vegetation boundaries. Similar association of vegetation and lithologic units occurs in the Amazon forest (Disperati, 1978). The discrimination of geologic materials in these tropical forested environments is based on geobotanical characteristics such as major indicator flora and vegetation density.

Digital analysis of LANDSAT MSS data was performed on the image analysis system of the Ontario Centre for Remote Sensing (OCRS). This system is based on PDP 11/34 and 11/44 computers with four separate image display terminals - one Norpak 3050 and three Dipix LCT-11 workstations. Supervised and unsupervised classifications using the maximum-likelihood algorithm (Goodenough, 1974; Singhroy, 1976) were performed on a scene recorded on October 1977 (SRB:346/07). Airphotos at a scale of 1:10,000 were used to select training statistics for the supervised signature classification. The characteristics of surface cover (Table 1) provided the basis for automatic classification.

Thematic maps were produced by the OCRS Applicon Colour Plotting System. The method of map production is described by Pala, 1981, and Jano, 1981. The flexibility of producing colour thematic maps at any selected scales permitted easy registration and overlaying with existing resource maps, thereby facilitating the interpretation process.

LANDSAT DATA FORMAT AND ACQUISITION

The computer-compatible tape of the October 1977 scene was obtained from the Instituto de Pesquisas Espaciais (INPE) in Brazil. This data is recorded in the BIP2 format (band interleaved by pixel pairs). To permit the data to be read by the OCRS image analysis system, this format was converted to the JSC universal CCT format at the Canada Centre for Remote Sensing. A detailed account of the JSC universal CCT format is documented by Murphy (1979).

The acquisition of usable LANDSAT MSS data in tropical areas is difficult. The EROS computer search for LANDSAT images with less than 30% cloud cover over the period 1972 to 1981 revealed that the scene of October 1977 was the only image acceptable for analysis. The continuous cloud cover over tropical areas greatly limits the usefulness of LANDSAT data in these regions (Hsu, 1978; Pacheco, 1980). The interpreter must, therefore, be prepared to work with sub-optimal LANDSAT data in a flexible methodology.

CLASSIFICATION OF COASTAL WATER CHARACTERISTICS BY SPECTRAL REFLECTANCE

Remote sensing techniques were researched to assess their potential to contribute to the study of Guyana's coastal waters in two important contexts:

1. To provide a compilation of synoptic fish distribution charts;

2. To provide an understanding of the coastal processes, particularly the mobility and behaviour of offshore bars and shoals and their effect on drainage and irrigation projects along the coast.

Fisheries Modelling

To assess the value of remote sensing information to the survey of fisheries resources, an understanding of the principles of fish distribution chart compilation is necessary. Commercial fishing operators use synoptic fish distribution charts along with real-time acoustic methods (echo sounders

662

and sonars) to find fish. The quantity of fish in an area (in weight and number) is given by:

$$T = \int_A P_{1A}\, dA + \int_A P_{2A}\, dA + \ldots\ldots + \int_A P_{nA}\, dA$$

where $_A P_{1\ldots}\, dA$ is the density of fish per unit area, and 1, 2 ....n refer to different species within the area. In order to obtain estimates of T by integration, it is essential to discriminate between species and to make synoptic distribution charts of $_A P_{2A}\, dA$ for each species through out the area. Suspended sediment, phytoplankton (chlorophyll) and other substances in the upper layers determine, in part, the species and distribution of fish. Moreover, the colour of sea water varies according to the concentration of these elements with it.

The optical properties of coastal waters are affected by the physical, chemical and biological processes occurring within them. Some of these properties - water colour, sediments and chlorophyll - were mapped from spectral reflectance techniques by Klemas (1980), Egan (1980) and others. Holley (1980) and Tassan (1980) discussed the relationship of these properties to fish distribution, and Amos (1979) and McCluney (1976) considered the influences of atmospheric and bio-optical effects on the classification of coastal waters. Spectral reflectance was used to classify the coastal waters and to determine fisheries and oceanographic processes.

Figure 6 is a LANDSAT thematic map showing spectral classification of the coastal waters of the study area. This automatic classification was based on the unsupervised approach using the maximum-likelihood algorithm. Four significant water colour/suspended sediment zones were identified. Each spectral zone corresponds to a known water colour (Hines, 1978). The interrelationships among depth, bottom sediment, mean suspended sediment concentrations and fishing zones are shown in Figure 7. Existing known boundaries were refined and two additional zones were delineated from the remote sensing analysis. The accuracy with which the boundaries of the various water colour zones can be defined is significant, since current fishing records indicate that the most productive trawl areas exist within them.

T'ese boundaries represent temporary fronts of local current movement. Their significance to fisheries is documented by Laevastu (1980). They are associated with local anti-cyclonic eddies which cause the retention and accumulation of plankton fish eggs and fry. It is believed that aggregation might also be connected with adult fish in current eddies. Therefore, knowledge of local current movements, boundaries and eddies are important in the search for commercial fishing grounds. To understand their behaviour and seasonal variability, sequential LANDSAT data (Thomas, 1980) and the Nimbus 7 Coastal zone scanner data (Hovis, 1979; Mehl, 1980) are recommended.

Coastal Processes

Kranenburg (1972) and the Guyana Hydraulics Division (1968-1972) have collected limited oceanographic data in their attempt to understand the peculiar behaviour pattern of the sea bed adjacent to the coastlands. The mobility of mud shoals and the significance of these shoals to near-shore erosion and sedimentation processes is not fully understood. Their potential effects on future and current water control and reclamation projects must be studied. The Guyana Hydraulics Division, therefore, requires annual surveys and offshore mapping of a region 20 km in width along the entire coastline, where these mobile shoals occur. Current surveys using echo-soundings, distance-measuring equipment, and level rods are

663

sometimes inadequate in the deeper zones. In addition, the lack of offshore airborne data makes satellite remote sensing a vital means of investigation, thereby increasing the efficiency and reliability of the poorly equipped surface surveys.

The following is a summary of significant hydrological information interpreted from the LANDSAT colour composite and digital classification of the near-shore zone:

1. The delineation and the calculation of the areal extent of the mud flat zone and mangrove swamps between the Demerara and Berbice rivers is information essential to the management of fish farms and to the planned construction of sea dams for land reclamation. Coastal deposition along mud flat zones must be carefully monitored to prevent sediment clogging at the mouths of drainage canals.

2. The mapping of zones of erosion at several areas along the coast focused attention on stability assessment of existing dyke structures, and confirmed the need for regular monitoring.

3. The mapping of isolated clear-water basins in predominantly shallow zones are significant to the fisheries. To determine whether these pockets are temporary or permanent would require sequential LANDSAT analysis and verification.

4. The delineation of water colour zones from digital LANDSAT classification is particularly significant for surface survey planning. Water colour zones are influenced by the concentration of suspended sediments, chlorophyll, sea bed composition and location current movements.

AGRICULTURAL LAND USE AND LAND COVER MAPPING

Aerial photographs and LANDSAT MSS data have the potential to provide a useful means of land use/land cover mapping, particularly because of extensive coverage, timeless and relatively low cost per unit area. The particular techniques used are determined by the level of classification required. Aerial photographs are generally used where cover type units are complex and small. Digital classification of LANDSAT data was used for regional categorization (Meijerink, 1978; Ryerson, 1980; Pala, 1981; and Jano, 1981).

The lack of land cover maps requires that a multi-level classification be produced for comprehensive land use planning, tax assessment and water supply management. Local planning districts rely on such data to plan construction projects and to calculate area estimates of various crops. In this study, levels I and II classification (Anderson, 1976) were produced from the digital classification of LANDSAT data and aerial photographs at scales of 1:10,000 and 1:30,000 provided a more detailed level II and IV classification.

VISUAL INTERPRETATION KEYS

Table 1 summarizes the visual keys developed for recognition of the major land cover types which occur on airphotos and LANDSAT data. These keys are a prerequisite for the production of resource inventory maps based on digital LANDSAT data. The LANDSAT component of this series of keys provides a synoptic dimension to the limited documentation usually available for similar tropical environments (Miller, 1960; Philipson, 1975, 1982). These interpretative keys do not include crop development or crop calendars, since this would require sequential aerial photography. The cropping patterns, textures, management practices and characteristic appearance of the major vegetation cover types are described. Considerable

664

familiarity with the environment being studied is thus an important element in the methodology.

DIGITAL CLASSIFICATION

The supervised approach (Goodenough, 1974) was used for the land cover classification. Training sites on the LANDSAT data were selected from interpretation of 1:10,000-scale panchromatic black and white photographs. The fact that each major crop (sugar cane, rice and coconut palms) has extensive coverage and a distinctive tonal and textural appearance enhances classification accuracy (Figures 1-4). The fact that rice paddies were being harvested at the time of the October LANDSAT scene also aided in the spectral separation of the major crops. The mean spectral intensities (Table 2) and the autocorrelation distances (Table 3) demonstrate the different spectral responses and the resultant classification accuracy to the major agricultural land use types. Since atmospheric correction was not performed on the data, the spectral intensity values are relative and cannot be extrapolated beyond this one scene. Figure 8 shows an example of a colour-coded thematic output of the West Berbice area. Similar maps at scales of 1:50,000 and 1:250,000 were produced for the entire study region.

Market gardening and the associated cultivation of fruits such as mangoes, bananas and oranges, etc. were difficult to identify from the aerial photographs; hence digital LANDSAT classification of these land use types was not attempted. The difficulty is compounded by the fact that mixed farming plots are relatively small and are blended in with the more spectrally dominant coconut palms.

The time of year (Mendonça, 1981), the size of the plots, and the nature of local farming practices have a particularly important influence on the classification accuracy of tropical crops.

FOREST COVER

The advantages and limitations of using aerial photography for forest inventory in tropical rain forests have been documented by Nyyssönen (1961), Heinsdijk (1952), Howard (1975), Neilsen (1976), Aldred (1968, 1976), Sayn-Wittgenstein (1978) and others. The complex canopy structures and species composition make the recognition of tropical species difficult, even from airphotos. As an example, Jenns (1980) noted that, within the mixed forest region of Guyana, the two major commercial species - greenheart (Ocotea rodiaei) and mora (Mora excelsa) occurred only rarely in highly pure sands making airphoto identification a difficult task.

LANDSAT data can, therefore, only be expected to be useful in regional forest typing. Heavy reliance must be placed on the distribution of spectral reflectances of vegetation types according to geomorphologic and physiographic regions (Hsu, 1978). Welch (1972) noted a close association between major forest types, drainage and physiography. Swellengrebell (1959) documented the association of vegetation types and soils. The Wallaba forest, for instance, occurs on white sand, mixed forest on brown sand, and mora forest on alluvium within creek valleys. Digital LANDSAT classification permitted five major forest types to be distinguished within the study region (Table 4). Mean spectral intensity values and autocorrelation distances (Table 3) show the degree of spectral separation provided by the October scene. Different spectral values are recorded in all bands for the mixed Wallaba and swamp (pegasse) forest. However, the close association shown between the forest cutover and the pegasse wetland is typical only of the Georgetown clay belt region. In this region forest cutovers are small and isolated. Rapid regeneration of the understory create signatures similar to those of the wetland species. In the white sand district, cutovers

within the Wallaba forest are easily separated from other land cover classes.

GEOTECHNICAL MAPPING

Several engineering projects planned for the coastal zone of Guyana require that detailed geotechnical mapping be completed to provide necessary base-line data for various construction programs. The geotechnical mapping includes the delineation of various types of surficial materials and terrain, thus providing information on their engineering properties. Such maps contain information required for the design of foundations and drainage networks. The integrated LANDSAT airphoto technique provided an economical means of obtaining new information on engineering terrain, surficial material and geological structure. Such data are not available on current geotechnical maps produced by Bleackley (1957) and the Directorate Overseas Survey (1967). The resulting regional geotechnical compilation (Figure 5) has the following advantages:

1. All existing data bases are integrated to produce a regional multi-purpose map. Descriptions of landforms, the texture of materials, topographic variability, and surface drainage (Figure 5) are basic considerations for many current engineering geology projects.

2. The compilation can be used as a special-purpose map for:

   (a) the investigating of the suitability of sites for the construction of foundations;
   (b) the investigating of the suitability of sites for waste disposal;
   (c) selecting of routes for agricultural drainage, irrigation networks and roads.

   Factors affecting foundation construction such as wetness, risk of flooding, ease of excavation and soil texture can be obtained from such compilations. Solid waste disposal sites include well-drained areas provided by the sand ridges and deltaic aprons along the coastline; areas of high water table and areas susceptible to flooding are unsuitable. Periodic wet and dry seasons make soil texture and the rate of water movement into and through the soil important considerations for the construction of drainage and irrigation canals. In addition, soil and terrain properties hich affect the design construction and performance of highways and access roads can be deduced from the compilation. Any checklist for engineering-suitability mapping must include topography, surface soils, drainage patterns, surface water, ground water, erosion, land use and land cover. Information on these subjects is included in the map legend (Table 5).

   The close association of land cover with surficial materials (Swellengrebell, 1959; Welch, 1972) facilitates the use of remote sensing information to map surficial geology. The appearance of land cover types on 1:10,000-scale air photographs and 1:100,000-scale LANDSAT colour composites and their association with surficial materials are summarized in Tables 1 and 5. The digital classification of LANDSAT data permitted the delineation of vegetation boundaries and corresponding engineering soils. Hence, in coastal Guyana, LANDSAT based vegetation cover maps can be considered quasi-surficial materials maps. When this is integrated with patterns interpreted from the airphoto and colour composites, which indicate drainage and lineaments, and with existing suitability maps, a regional geotechnical compilation can be made. The structural trend interpreted from the LANDSAT colour composite (Figure 5) not only has implications in the location of reservoir dam sites, but does provide vital information on possible exploration targets for current offshore and onshore oil and gas exploration.

666

SUMMARY AND CONCLUSIONS

In this operational pilot study, LANDSAT imagery made a significant contribution to the data bases required for the major types of development projects being undertaken in the coastal zone of Guyana. The environmental conditions and the scarcity of existing data are typical of much of the Caribbean, as is the urgent need for comprehensive coastal zone information generated by development programs. Within the constraints of LANDSAT data availability, similar results could be obtained anywhere in the region.

The methodology is dependent upon the following four critical factors:

1. The availability of LANDSAT imagery of usable quality;

2. Access to a small representative sample of recent aerial photography;

3. Access to digital image analysis facilities capable of performing basic classification operations;

4. The availability of experienced interpreters who are familiar with the region.

When applied to the study of the offshore zone, the methodology yields the following information:

(a) The location and extent of water colour zones, which have been identified with known levels of fish productivity;

(b) Data required to plan and supplement costly surface surveys of current and sediment movement which are required for fisheries development and coastal engineering.

When applied to the study of the tidal z⁄   the integration of LANDSAT data, airphotos and existing mapped data rmits

(a) The delineation of mud flats and mangrove swamps important for fisheries management, sea dam engineering, and migratory bird. habitat protection;

(b) The mapping of erosion and deposition critical to the protection of coastlines.

In rapidly-developing coastal regions, the multi-purpose mapping concept provides

(a) low-cost mapping of agricultural land use, forests and other land cover types, for development planning and production monitoring;

(b) Geotechnical information required for the construction of local and regional transportation and drainage networks.

The remote sensing methodology demonstrated in the present study is appropriate for Caribbean countries, for the following reasons:

1. On-site access to image analysis equipment is not required, as all mapping operations could be performed by a remote organization, in consultation with users but without their actual presence;

2. The maps which are the end product of this methodology can be produced rapidly and economically on an operational basis;

667

3. The visual interpretation keys developed as the first stage of this methodology provide local interpreters with the means of conducting subsequent, more detailed airphoto interpretation on their own;

4. The skills and technology available locally are sufficient to produce the final, integrated map, when the airphoto interpretation keys, LANDSAT-derived maps and final map legend have been provided.

More extensive applications of the methodology in the Caribbean region are anticipated, and a similar study is presently underway in West Africa. It is also expected that studies may be launched in Mexico and Southeast Asia in the near future to adapt the integrated remote sensing methodology to conditions present in those regions.

REFERENCES

Aldred, A.H., 1976. Measurement of Tropical Trees on Large Scale Aerial Photographs. Canadian Forest Service, Department Environment, Forestry Management Institute Information Report FMR-X-86, p. 38

Amos, C.L. and T.T. Alfoldi, 1979. The Determination of Suspended Sediment Concentration in a Macrotidal System Using LANDSAT Data. Journal of Sed. Pet., Vol. 49, #1, pp. 159-17'.

Anderson, J.R. et al, 1976. A Land Use Land Cover Classification System for Use with Remote Sensor Data. Geological Survey Professional Paper 964. U.S. Government Printing Office, Washington, D.C., p. 28.

Bleackley, D., 1957. Observations of the Geomorphology and Geological History of the Coastal Plain of British Guyana. Geological Survey of Guyana, Georgetown, 21 pp.

Disperati, A.A. and M.A. Keech, 1978. The Value of Using SLAR, Satellite Imagery and Aerial Photography for a Forest Survey in the Amazon Basin in Remote Sensing Applications in Developing Countries. Remote Sensing Society, University of Aston, Birmingham, England. pp. 49-55.

Directorate Overseas Surveys, 1967. Engineering Soils on Part of the Coastal Plain of Guyana. 1:250,000 map. Ministry of Agriculture, Forest and Lands, Georgetown, Guyana.

Egan, W.G., 1980. Optical Remote Sensing of the Sea - A Caribbean Example. Proc. 14th International Symposium on Remote Sensing of Environment, ERIM, Ann Arbor, Michigan. pp. 563-586.

Goodenough, D. and S. Shlein, 1974. Automatic Classification Methodology. Canada Centre for Remote Sensing Research Report 74-1, 20 pp.

Guyana Hydraulics Division: Sea Defence Programme. 1968-1972. Ministry of Works and Hydraulics Internal Report, Georgetown, Guyana.

Heinsdijk, Dammes, 1952. Forest Photo-Interpretation in Surinam. Photo Eng., Volume 18, #1, pp. 158-162.

Hinds, L., 1978. By Catch Project CIDA International Document, Ottawa, Canada.

Holley, H.J., and K.J. Savastano, 1980. Remote Sensing for Coastal Fisheries Resources. Proc. 14th International Symposium on Remote Sensing of Environment, ERIM, Ann Arbor, Michigan, pp. 587-595.
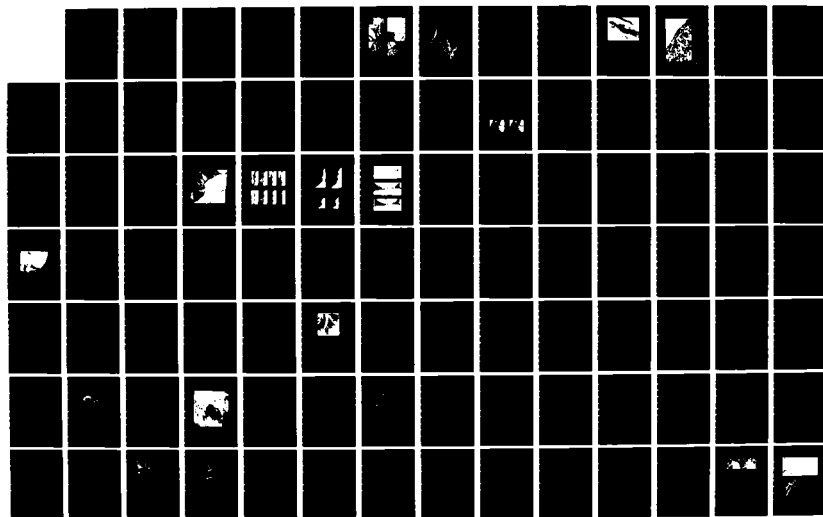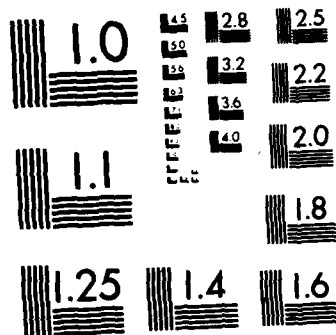
MICROCOPY RESOLUTION TEST CHART

NATIONAL BUREAU OF STANDARDS-1963-A

Hovis, W.A., and D.K. Clark, 1979. Remote Sensing of Chlorophyll and
     Derived Pigments. Proc. 13th International Symposium on Remote Sensing
     of Environment. ERIM, Ann Arbor, Michigan. p. 711.

Howard, J.A., and J.P. Lanly, 1975. Remote Sensing for Tropical Forest
     Surveys, Unasylva, 27 (108): pp. 32-37.

Hsu, Kou-Shih, 1978. The Evaluation of LANDSAT Data and Analysis Techniques
     for Mapping Tropical Forest Areas. Unpublished Ph.D. Thesis, Purdue
     University, 176 pp.

Jano, A., and S. Pala, 1981. LANDSAT-Based Forest Mapping in Ontario, North
     of Latitude 52°North. Proc. 7th Canadian Symposium on Remote Sensing,
     Winnipeg, Manitoba, pp. 228-232.

Jenns, W.E., 1980. Forest Inventory Manual. CIDA Forest Technical Assistance
     Project 440/00605: Guyana Forestry Commission: 33 pp.

Klemas, V.E., and D.S. Bartlett, 1980. Remote Sensing of Coastal Environmen-
     tal and Resources. Proc. 14th Intern. Symp. on Remote Sensing of
     Environment. ERIM, Ann Arbor, Michigan. pp. 543-562.

Kranenburg, P.L., 1972. The Limitations of Present Coastal Mapping Programme
     in Guyana, and the Need for Its Expansion. Proc. Coastal Mapping
     Symposium, Am. Soc. Photogrammetry. pp. 175-190.

Laevastu, T., and I. Hela, 1970. Fisheries Oceanography Fishing News
     (Books) Ltd., London, England. p. 238.

Mahl, W., and B. Sturm, 1980. Analysis of Coastal Zone Colour Scanner
     Imagery over Mediterranean Coastal Waters. Proc. 14th International
     Symposium on Remote Sensing of Environment. ERIM, Ann Arbor,
     Michigan, p. 10.

McCluney, W.R., 1976. Remote Measurement of Water Colour. Remote Sensing
     of the Environment, Vol. 5, #1, pp. 3-34.

Meijerink, A.H., and H.W. Donker, 1978. The ITC Approach to Digital
     Processing Applied to Land Use Mapping in the Himalayas and Central
     Java; in Remote Sensing Applications in Developing Countries. Remote
     Sensing Society, Univ. of Aston, Birmingham, England. pp. 75-83.

Mendoça, F.J., 1981. Use of LANDSAT data for automatic classification and
     area estimate of sugar cane plantation in São Paulo State, Brazil.
     International Journal Remote Sensing, Vol. 2, #4, pp. 361-368.

Miller, R.C., 1960. Interpretation of Tropical Vegetation and Crops on
     Aerial Photographs. Photogrammetria #16, pp. 232-240.

Murphy, J., 1979. Format Specification for Canada's MSS System Corrected
     Computer Compatible Tape. CCRS Research Report 79-2, Ottawa, p. 69

Neilsen, U.E., and A.H. Aldred, 1976. Canadian Tropical Forest Inventories
     Benefit from Recent Developments in Aerial Photography. Presented at
     XVI IUFRO World Congress, Oslo, Norway, June 20-July 1, p. 16.

Nyyssönen, A., 1961. Survey Methods of Tropical Forests. FAO Report, 71 pp.

Pacheco, R.A., 1980. Applications of Remote Sensing to Agriculture Develop-
     ment in Tropical Countries. Proc. Remote Sensing Applications in
     Agriculture and Hydrology, ISPRA (Varese), Italy, pp. 299-308.

Pala, S, T.J. Ellis and D.B. White, 1981. Operational Land Cover Type
    Mapping in Ontario by LANDSAT-based Digital Analysis and Map.
    Proc. 7th Canadian Symposium on Remote Sensing, pp. 42-50.

Philipson, W.R., and T. Liang, 1975. Airphoto Analysis in the Tropics:
    Crop Identification. Proc. 10th International Symposium on Remote
    Sensing of Environment, ERIM, Ann Arbor, Michigan, Vol. II,
    pp. 1079-1092.

Ryerson, R.A., 1980. Land Use Information from Remotely Sensed Data.
    Users Manual 80-1, Canada Centre for Remote Sensing, Ottawa, Canada,
    30 pp.

Sayn-Wittgenstein, L. et al, 1978. Identification of Tropical Trees on
    Aerial Photographs. Canadian Forest Service, Information Report
    FMR-X-11, p. 33.

Singhroy, V., and B. Bruce, 1976. Surficial Geology of The Pas Area of
    Manitoba: An Application of Digital LANDSAT Data. Proc. 4th Cana-
    dian Symp. on Remote Sensing, Quebec City, pp. 57-66.

Swellengrebel, E.J., 1959. On the Value of Large Scale Photographs in
    British Guyana Forestry. Emp. For. Rev. 38(1), 95: pp 54-64.

Tassan, S., 1980. Application of Global Sensitivity Analysis Model to
    the Retrieval of Chlorophyll Concentrations in Water from Remotely
    Measured Radiances. Proc. 14th International Symposium of Remote
    Sensing of Environment, ERIM, Ann Arbor, Michigan, pp. 807-818.

Thomas, I.L., 1980. Suspended Sediment Dynamics from Repetitive LANDSAT
    Data. International Journal of Remote Sensing. Vol. 1, #3,
    pp. 285-292.

Welch, I.A., O.R. Sampson and G.S. Bell, 1972. Photo Interpretation Key
    Vegetation Types of Guyana. Forestry Bulletin #4, 59 pp.

TABLE I   AIR PHOTO AND LANDSAT IDENTIFICATION KEYS FOR LAND USE/LAND COVER FOR COASTAL GUYANA

Image Date   Oct 14??

LAND USE - LAND COVER	PANCHROMATIC AIR PHOTO SCALE 1:10,???	LANDSAT COLOUR COMPOSITE Band 4 (Blue), Band 5 (Green), Band 7 (Red) SCALE 1:1?,???
1. SUGAR CANE		
Terrain & Soils	- Low, flat, moist to wet clayey soils	Large rectangular uniform purple red fields represent
Tone & Texture	- Medium grey tone & medium to fine texture in growing season. Dark grey tone, and uniform texture during periods when field is flooded.	unharvested sugar cane plantations. Large greenish-blue to dark blue represents fallowed and flooded fields.
Farming Practices	- Large rectangular fields (>100 acres), bordered by drainage and irrigation canals. Parallel "beds" and rows are visible, particularly in early growing periods. Dark parallel lines on "beds" represent piles of harvested cane, awaiting transportation to refineries.	
2. RICE		
Terrain & Soils	- Low, flat, moist to wet clayey soils.	Small rectangular and longi-tudinal fields. Harvested fields appear as whitish
Tone & Texture	- Rice generally appears dark grey. The smooth texture indicates recently plowed fields or flooded fields. Medium grey tone & smooth texture often represent growing rice paddies. Light grey tone with mottled appearance and smooth texture represent mature and harvested crops.	blue in colour. Fields plowed immediately after harvest appear a dark bluish grey because of visible soil moisture.
Farming Practices	- Linen pattern, representing cutting rows on rectangular fields, along with subdued mottling, are typical patterns in the harvesting season.	
3. COCONUTS		
Terrain & Soils	- Flat to undulating sand ridges, loose well drained and aerated sand to clay loam soils.	Appears as characteristic uniform bright red on sandy beach ridges along
Tone & Texture	- Medium grey tone, rough to granular texture, small opening in canopy.	coastline. No visible sign of field pattern as in rice and sugar cane
Farming Practices	- Generally grown in rows on large plantations. Trees have characteristic star-shaped crowns with heights varying from 10 to 25 m. Parallel drains are easily identifiable where growth is sparse. Coconuts on sand ridges are usually dense (dominant crown), with other fruit trees (mangoes, bananas, guava, etc.) having billowy crown.	Coconut plantations should not be confused with the Ite (Eta) palm which also appears bright red. Ite palm prefers wet inland depressions and wet alluvium along river valleys, and coconuts prefer well drained sand ridges which are easily identified along the coastline.
4. MIXED FARMING		
Terrain & Soils	- Low sand ridges, well drained sandy soils to moist to wet, clay to clay loam soils.	Cannot be identified from LANDSAT because garden plots are less
Tone & Texture	- Medium grey to dark grey tones, coarse texture.	than an acre and are often associated with large stands of coconuts.
Farming Practices	- Coconuts, star-shaped crowns of coconuts are dominant. Rounded to multiple crowns representing fruits and vegetables are codominant: fruits and vegetables - mangoes, guava, bananas, citrus, cassava, tomatoes, etc. - produce multistoried vegetation, sometimes dichotomous branching, particularly mangoes.	
5. PASTURE		
Terrain & Soils	- Low, flat areas, moist to wet clayey soils.	Because abandoned fields are sometimes used as pasture,
Tone & Texture	- Mottled light grey to dark grey tone; light grey spots represent dried grass and over-grazed areas. Dark grey spots represent low wet areas. Pasture has a generally smooth texture, though where clumps of trees exist, the texture is coarse.	it is difficult to separate rice paddies from pasture. However, in the upper Abary River where large areas are used as pasture, these areas appear as mottled bluish purple. There are no visible signs of regular field pattern.
Farming Practices	- Some animal tracks are visible. Pastures usually occupy abandoned rice fields. Extensive pastures in the upper Berbice and Abary Rivers demonstrate a mottling pattern due to large open savanna areas with isolated clusters of trees and wet depressions.	

671

Table I: cont'd.   PANCHROMATIC AIR PHOTO   SCALE   1:10,000   LANDSAT COLOUR COMPOSITE
                                                                  SCALE   1:100,000

6. MANGROVE FOREST

Terrain — Tidal mud flats, sometimes submerged.
Easily identified as bluish green and bluish purple along the coastline.

Appearance — Young dense black mangrove or courida occurs next to shoreline. Appears as light toned medium to fine textured, with small crown surface, and no openings. Older courida are more coarsely textured, with larger crowns and darker tones. Height varies from 5-15 metres. Sparse mangrove and occasional depressions (mudflats) produce a speckled appearance. Dark areas indicate sea water in depressions. Small drainage streams are sometimes present. The sparse courida has a small to medium crown.
Bluish green along the water edge represents tidal flats. Bluish purple along mud flats represents courida trees and vines of the mangrove swamp.

7. SWAMP FOREST

Terrain — Low wet poorly drained pegasse soils in depressions, and along river banks.
Dark greenish blue represents low wet inland depressions and ponding.

Appearance — Light toned to dark tone, medium textured, occupied by clumps of Ite (20-40 feet high) palm, razor-grass and small bushes.
Clumps of bright red areas amidst wet depressions (dark blue) represent Ite palm and razor-grass

8. MIXED FOREST

Terrain — Low flat sometimes sloping terrain with moist to well drained clay loam to sandy loam soils.
Generally uniform red with medium to coarse texture. Small areas of greenish hue represent wet openings in the forest. Mixed forest zone is wedged between pegasse wetlands in the north, and white sand plateau, with wallaba-forest, in the south.

Appearance — Generally coarse textured, produced by single and rounded interlocking crowns (small to large) multistoried vegetation with dichotomous branching. Tone varies from light to medium grey. Openings and tracks suggest some cutting for firewood and timber. Species are of different types and difficult to identify on air photos.

9. WALLABA FOREST

Terrain — Well drained flat and dissected areas of white sand. This area is dotted with hills varying from 30-100 metres in height.
Characteristic greyish blue with white spots giving area a speckled appearance. White spots represent exposed sand along river valley and hillsides.

Appearance — Light grey tone, grainy to uniform textured, small rounded crowns are characteristic of the wallaba forest. Indentations along borders of wallaba forest are caused by dissection of creeks in the easily eroded white sand. Exposed white sand appears as highly reflective white spots in the forest.

10. 'SALT GRASS'

Terrain — Low, flat, wet, sometimes submerged by sea water.
Bluish green in areas of exposed wet soils and mottled yellowish red in areas where short grass and shrubs are present.

Appearance — These areas are smooth, fine textured, and have a mottled appearance with light to dark grey tone. Drainage ditches are sometimes seen. Mainly occupies areas behind mangrove swamp. Dark grey spots represent low wet areas on marine clay flats.

11. TOWNS, RURAL SETTLEMENTS & TRANSPORTATION NETWORKS

Terrain — Flat, well drained areas on sand ridges.
Whitish yellow lines and medium to coarse textured grids along dry sites on beach ridges and river banks.

Appearance — Rural linear settlements are located along major routes predominantly on sand ridges. Individual houses and sometimes fruit and vegetable gardens (1-5 acres) are identified. In small towns, buildings, playgrounds and rectangular street patterns are clearly visible. Industrial buildings such as sugar refineries, rice mills and bauxite processing plants, etc. are also recognized. In larger urban centres, commercial, industrial, residential and recreational areas are also identified

LOCATION: EAST BANK
BERBICE, EVERTON

SCALE 1:9,600

1 BERBICE RIVER
2 SETTLEMENTS
3 SUGARCANE
4 WOODLAND
5 BAUXITE REFINING PLANT

Figure 2

LOCATION: WOODLY PARK,
WEST COAST BERBICE

SCALE 1:12,000

1 ATLANTIC OCEAN
2 GEORGETOWN - ROSIGNAL HIGHWAY
3 RAILWAY
4 RURAL SETTLEMENTS
5 COCONUT PLANTATIONS
6 SHALLOW MUDFLATS
7 MANGROVE SWAMP
8 DRAINAGE CANALS
9 SEA DAM (DYKE)
10 PARALLEL BEACH RIDGES

Figure 4

LOCATION: WEST BANK OF DEMERARA
RIVER AT VREED-EN-HOOP STELLING

SCALE 1:9,600

1 DEMERARA RIVER (SILT LADEN)
2 VREED-EN-HOOP - PARIKA HIGHWAY
3 VREED-EN-HOOP STELLING
4 RURAL SETTLEMENTS &
MARKET GARDENING
5 COCONUTS & MARKET GARDENING
6 RICE FIELDS
7 SUGARCANE PLANTATIONS
8 MUDFLATS
9 MANGROVE SWAMP

Figure 1

LOCATION:
EAST COAST DEMERARA

SCALE 1:9,600

1 MAHAICA RIVER
2 GEORGETOWN - ROSIGNAL HIGHWAY
3 RAILWAY
4 SETTLEMENTS, COCONUTS, &
MARKET GARDENING
5 COCONUT PLANTATION
6 RICE FIELDS
7 RICE MILL

Figure 3

673

PRELIMINARY COMPILATION
OF COASTAL ZONE
OF GUYANA
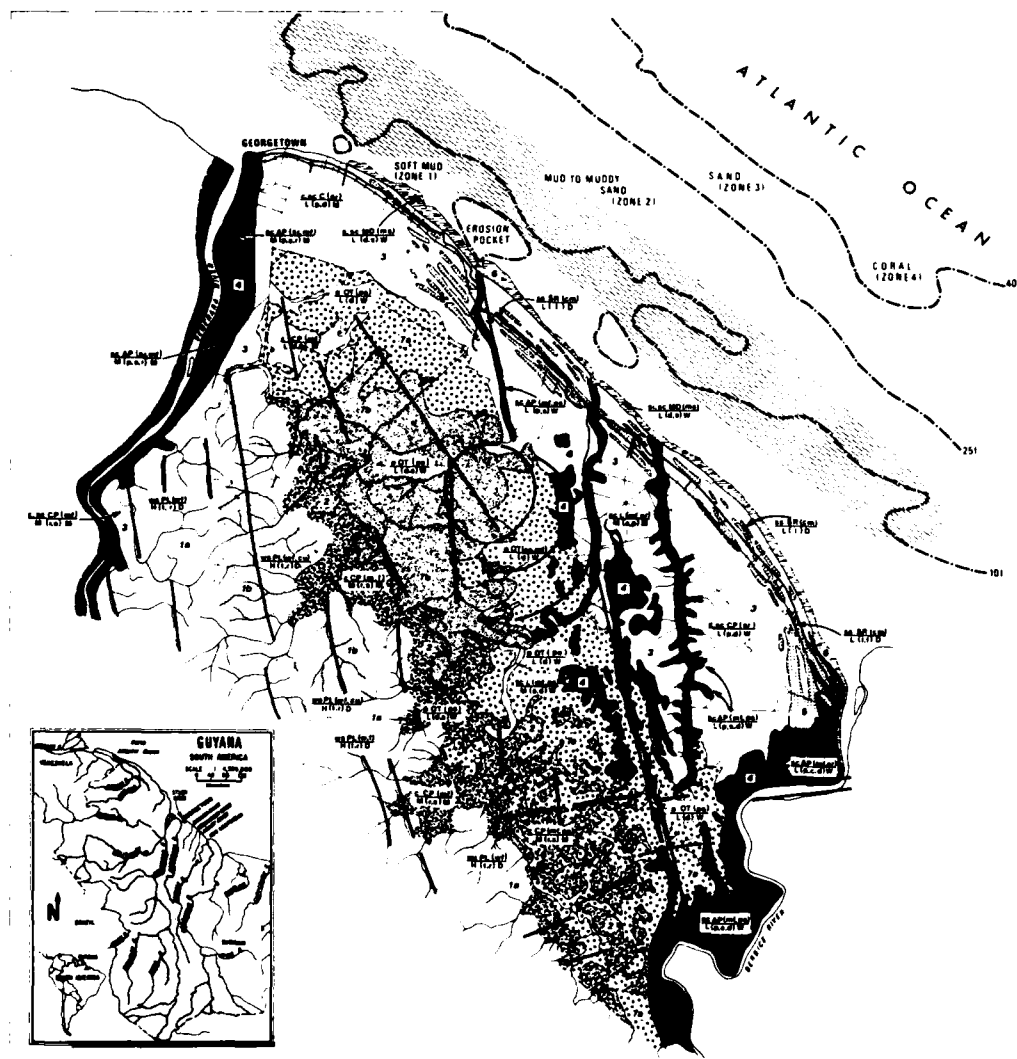
A ENGINEERING AND SURFICIAL GEOLOGY.

B DISTRIBUTION OF OFF SHORE SEDIMENTS AND RELATED FISHING ZONES.

Figure: 5

GEOLOGICAL, GEOTECHNICAL AND RELATED REMOTE SENSING ∘ LAND COVER NOTES OF COASTAL SEDIMENTS IN GUYANA

Table 1

		GEOLOGICAL					GEOTECHNICAL			REMOTE SENSING		
STRATIGRAPHIC COLUMN & THICKNESS	MAP UNIT	SURFICIAL MATERIALS	DEPOSITIONAL SEDIMENTARY ENVIRONMENT	LANDFORM DESCRIPTION TOPOGRAPHY, % Slope (m/100m)	DRAINAGE *	WORK-ABILITY **	CONSTRUCTION PROBLEMS	SUITABILITY FOR FOUNDATION CONSTRUCTION (COMPRESSION INDEX) Cc. (approx.)	IDENTIFICATION ON 1:10,000 AIRPHOTO AND 1:100,000 LANDSAT COLOUR COMPOSITE BAND 4 (BLUE), BAND 5 (GREEN), BAND 7 (RED)		LAND COVER AND LAND USE
RECENT 0 - 1m	7b	muck and pegasse peat	organic	low wet depression swamps (0 to 0.5)	very poorly drained	poor	high water table (seasonal to permanen)	low	AIRPHOTO:	Low wet depressions, dark grey uniform tone, surrounded by medium textured light tone representing its palm	bunduri rite palm & sedges in wet depresso*
									LANDSAT:	Dark greenish blue to dark grey within inland areas	
5 - 3m	7a	deep pegasse and forest peat	-	-	-	-	permanent surface water	low			mainly mangrove swamp
2 - 15 m	6	soft mud to muddy sand and sand, mud, pebbles and peats. Magnoconnos, shells & megaripple bedding are common	tidal flats	channel, mud-flat, sand flat subtidal sand bars, shoals, with intertidal ripple systems (0 to 0.9)	very poorly drained	poor	high erosion and flooding	medium (0.1 - 0.3)	AIRPHOTO:	Courida occurs adjacent to the shoreline. Light tone, medium textured with small crown surface	mainly mangrove swamp
									LANDSAT:	Bluish green and bluish puple along coastline	
3 - 10m	5	alternating layers of sand & shells, and sand pockets	fluvio-marine	sand ridges, distinct, some and washover fans (0.5 to 2)	well drained	good	medium to low erosion (high erosion in case of unprotected sand	low (0.05 - 1)	AIRPHOTO:	Parallel ridges along shoreline occupied by coconut plantation settlements and roads	mainly coconut palm, market gardening settlements & transportation routes
									LANDSAT:	Bright red elongated ridges parallel to the shoreline	
3 - 6m	4	silty clay	channel alluvium & flood plain deposits	elongated to fan shaped lenses in flood plain and along river banks (1 to 5)	moderately to well drained	fair	medium to high erosion and seasonal flooding	medium (0.2 - 0.3)	AIRPHOTO:	Coarse textured medium grey along river valleys	Low forest rte palm & lowiang grass along cultivated
									LANDSAT:	Bright red along river valley	river banks rice sugar cane & pasture

Table 2

		GEOLOGICAL					GEOTECHNICAL			REMOTE SENSING		
STRATIGRAPHIC COLUMN & THICKNESS	MAP UNIT	SURFICIAL MATERIALS	DEPOSITIONAL SEDIMENTARY ENVIRONMENT	LANDFORM DESCRIPTION TOPOGRAPHY, % Slope (m/100m)	DRAINAGE *	WORK-ABILITY **	CONSTRUCTION PROBLEMS	SUITABILITY FOR FOUNDATION CONSTRUCTION (COMPRESSION INDEX) Cc. (approx.)	IDENTIFICATION ON 1:10,000 AIRPHOTO AND 1:100,000 LANDSAT COLOUR COMPOSITE BAND 4 (BLUE), BAND 5 (GREEN), BAND 7 (RED)		LAND COVER AND LAND USE
PLEISTOCENE Demerara Clay 20 - 80 m	3	soft marine fossils from clay	marine and deltaic	flat to gently sloping clay plain (1 - to 5)	poorly drained	fair	differential settlement, high water table and seasonal flooding	medium (0.1 - 0.2)	AIRPHOTO:	A combination of tones and pattern representing variable landuse	mixed forest pegasse swamps & cultivated rice sugar cane & savannah
									LANDSAT:	A combination of red, and greenish blue and yellow representing mainly agricultural areas	
Coropina Formation 20 - 50m	2	stiff plastic clay and interbedded sand & silt	marine littoral and deltaic	rolling hills & sloping sandy loam plan to sandy loam plan (5 - to 10)	moderately to well drained	fair	medium erosion and seasonal flooding	high (0.5 - 1)	AIRPHOTO:	Coarse textured medium to light grey tone	dense mixed forest
									LANDSAT:	Uniform bright red areas wedged between pegasse wetland and white sand plateau	
PLIOCENE White Sand Series 100 - 1600m	1a/1b	poorly sorted subangular coarse white quartz-sand & clay lenses	marine littoral and deltaic	(1a) dissected plateau to steep hills (5 - to 20), (1b) highly dissected steep white sand hills (deforested & burned areas) (5 - to 10)	well drained	good	high erosion for unprotected sands	low (0.05 - 15)	AIRPHOTO:	Even textured dark velvety appearance highly dissected with white sand exposed on river banks	Wallaba Forest
									LANDSAT:	Characteristic grey-blue whitish spots, giving area a speckled appearance. White spots represent exposed white quartz sand on surface and along river valleys. Easily eroded white sand produced in high degree of dissection	

Table: 5
to accompany Figure: 5

*
Drainage: Refers to ponding of water in poorly drained closed depression and along streams subject to over bank flooding. It also includes the likelihood of a high water table, commonly following removal of excess surface waters and the need to provide adequate drainage control during construction

**
Workability: Refer to how quickly soils dry out and become workable following wet weather, the tendency of equipment to become bogged down in soils that lose strength and become soft and unworkable under traffic, and near surface variability

675

ENGINEERING TERRAIN LEGEND

LAND COVER

MATERIAL	LANDFORM
TOPOGRAPHY	DRAINAGE

EXAMPLE

$$\frac{c\ CP\ (cm)}{L\ c\ W}$$

MATERIAL → LANDFORM → LAND COVER
LOCAL RELIEF → TOPOGRAPHIC VARIETY → DRAINAGE

SYMBOLS

GEOLOGIC BOUNDARY (APPROXIMATE)

LINEAMENT FROM LANDSAT (IMAGERY)

BEACH RIDGE.

BOUNDARY OF SUSPENDED SEDIMENT CONCENTRATION.

MOST PRODUCTIVE TRAWL AREAS.

DRAINAGE AND IRRIGATION CANALS.

LETTER SYMBOLS

MATERIAL

c - HIGHLY PLASTIC CLAY ss - FINE SAND & SEA SHELLS
k - SILTY CLAY ws - COARSE WHITE SAND
g - SILT p - PEGASSE PEAT

TOPOGRAPHY

H - MAINLY HIGH LOCAL RELIEF L - MAINLY LOW LOCAL RELIEF
M - MAINLY MODERATE LOCAL RELIEF

VARIETY

f - DISSECTED m - SUBMERGED d - DEPRESSIONAL
p - PLAIN l - PARALLEL c - CHANNELLED
r - ROLLING f - FANLIKE s - SLOPING

LANDFORMS

CP - CLAY PLAIN OT - ORGANIC TERRAIN
AP - ALLUVIAL FLOOD PLAIN SR - SAND RIDGES
L - LEVEES MD - MUDFLAT
PL - PLATEAU

DRAINAGE

W - WET
D - DRY
M - MOIST

LAND COVER

cs - COCONUTS AND MARKET GARDENING ps - INLAND PEGASSE SWAMP
sr - SUGAR RICE PASTURE ms - MANGROVE SWAMP
wf - WALLABA FOREST ef - MIXED EVERGREEN FOREST
cb - CUT OVER / BURN

SOURCES

Bleackley D 1957 Observation of the geomorphology and geological history of the coastal plain of British Guyana Geol Survey of Guyana Summary #1 Geological Survey of Guyana. Georgetown 21 pp

Engineering Soils on part of the coastal plan of Guyana (1967) 1 250 000 map. accompanies Road Research Technical Paper 81 Road making materials in the Caribbean Directorate of Overseas Surveys Misc 441 and Ministry of Agriculture Forest and Lands Georgetown Guyana

Hines L O 1981 Guyana Fishing Grounds C I D A Internal Report

Kranenburg P L 1972 The limitations of present coastal mapping programme in Guyana and the need for its expansion Proc Coastal Mapping Symp ASP Falls Church Virginia p 175-190

Singhroy V 1982 Digital Landsat land cover map and Landsat colo-r composite scale 1 250 000 Ontario Centre for Remote Sensing

Welch I A et al 1972 Photointerpretation key vegetation types of Guyana Forestry Bulletin #4 Ministry of Mines and Forest Georgetown Guyana 59 pp

To accompany Figure : 5

676

DIGITAL LANDSAT CLASSIFICATION OF COASTAL ZONE.

Figure: 6

Figure: 7

SCHEMATIC DIAGRAM SHOWING RELATIONSHIPS BETWEEN SEDIMENT DISTRIBUTION, DEPTH AND FISHING ZONES
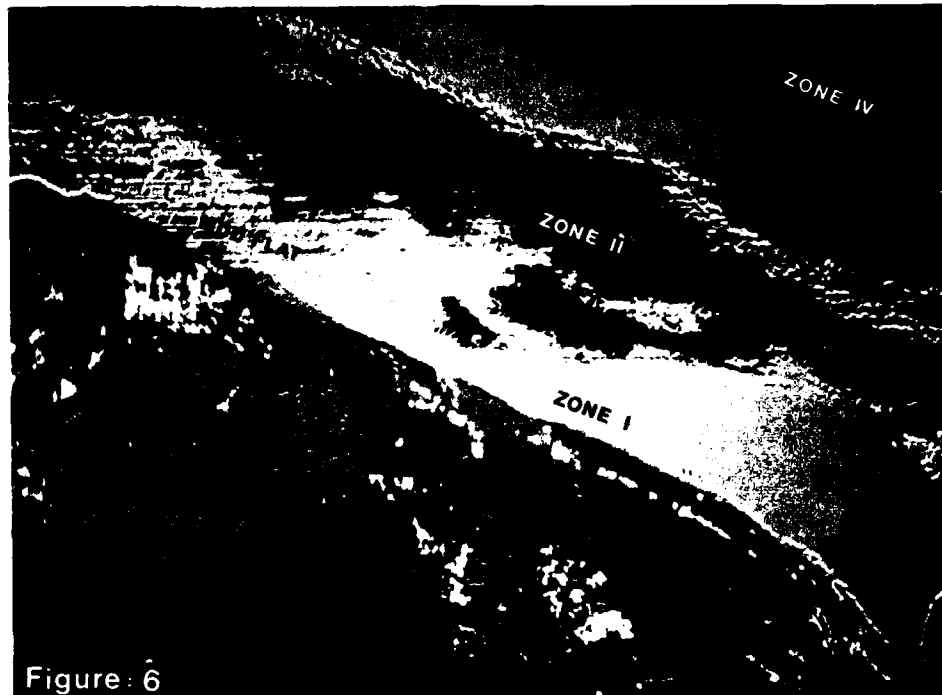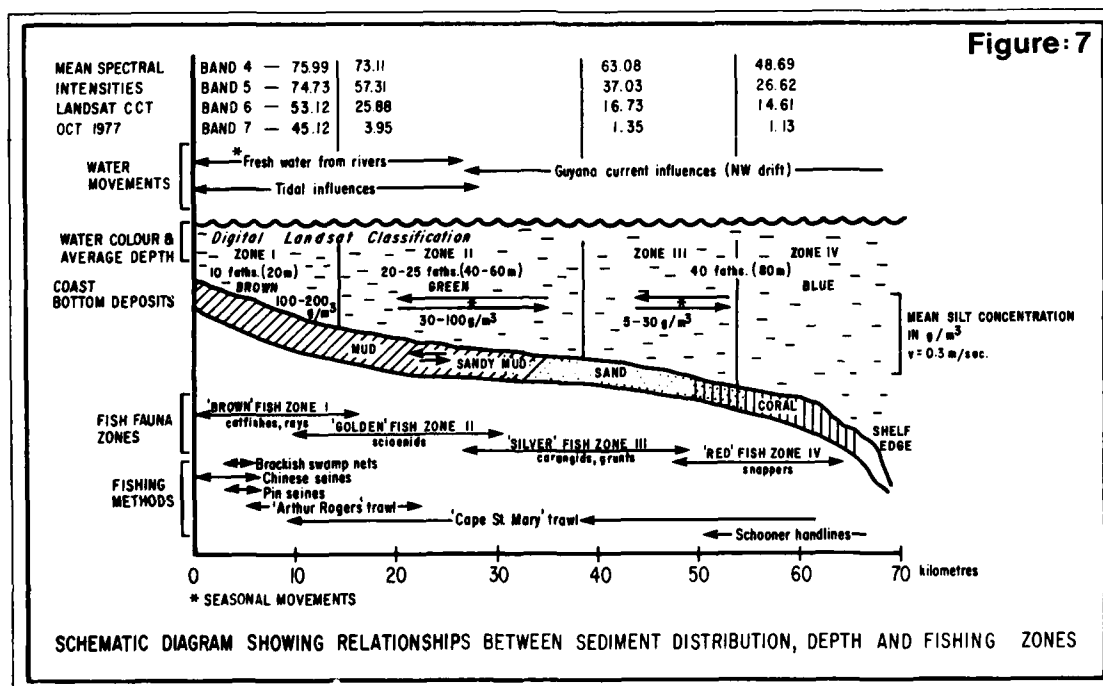
WEST BERBICE, GUYANA

LAND USE-LAND COVER CLASSIFICATION FROM DIGITAL LANDSAT DATA
PRODUCE AT O.C.R.S WITH 10KM GRID AUG. 82/IMAGE DATE OCT.77.

SCALE 1:1000000

COCONUT PLANTATIONS
MARKET GARDENING
BUNDARI-ITE PALM

WATER

TIDAL MUDFLAT
MANGROVE SWAMP
SCRUB FOREST

PEGASSE WET-LAND
FLOODED FIELDS

SUGAR CANE
MATURE RICE PADDIES
HARVESTED RICE

PASTURE
ABANDON RICE FIELDS

FALLOW FIELDS

MULTICLASSIFIED   UNCLASSIFIED

Figure 8

678

TABLE 2: Mean Spectral Intensities* of Land Cover
LANDSAT Overpass Date Oct. 11, 1977

Class	MSS 4 0.5-0.6nm	MSS 5 0.6-0.7nm	MSS 6 0.7-0.8nm	MSS 7 0.8-1.1nm
Coconut Palm	63.60	60.81	75.56	59.34
Rice Paddy	60.06	67.09	70.61	58.52
Sugar Cane	48.68	38.79	92.00	95.67
Pasture	75.62	78.81	59.67	28.90
Mixed Forest	38.48	33.57	74.66	76.79
Wallaba Forest	34.49	28.49	61.68	58.28
Pegasse Wetland	36.72	28.23	77.20	80.77
Fallow Fields	59.22	63.20	65.91	50.47
Tidal Mudflat	57.96	54.56	45.12	22.00

*No atmospheric correction.

TABLE 4: Forest Type Mapped from Digital LANDSAT Techniques

Forest Type	Major Species (after Welch, 1972)
Lowdakawa (Scrub savanna)	Dakama - Dimorphandra conjugata Sandw. Yaruru - Aspidosperma spp. Manabodin - Emmotum fagifolium Desv. Muri - Humiria floribunda Mart.
Wallaba	Wallaba - Eperua spp. Clump Wallaba (fine leaf) - Dicymbe altsoni Sandw. Clump Wallaba (broad leaf) - Dicymbe corymbosa Bth. Wamara - Swartzia leiocalycina Bth.
Mixed	Greenheart - Ocotea rodiaei (Schomb.) Mez. Mora - Mora excelsa Bth. Kakaralli (black) - Eschweilera sagotiana Miers Baromalli - Catostemma spp. Kabukalli - Goupia glabra Aubl. Bulletwood - Manilkara bidentata (ADC) Chev. Purpleheart - Peltogyne venosa Bth
Manni-Dalli (Pegasse swamp vegetation)	Corkwood - Pterocarpus Jacq. Manicole palm - Euterpe edulis Mart. Ite palm - Mauritia flexuosa L. Kirikaua - Iryanthera lancifolia Ducke Manni - Symphonia globulifera L.f. Razor grass - Scleria sp. Dalli - Virola surinamensis (Rol.) Warb.
Mangrove	Courida (black mangrove) Avicennia marina (Forsk) Kaili (White mangrove) - Laguncularia racemosa (L) Gaertn.

679

TABLE 3: Autocorrelation Distances Between Maximum-Likelihood Signatures - Land Cover Georgetown Region - LANDSAT Image Date Oct. 1977

	Settlements	Water	Tidal Flat	Fallow Fields	Pegasse Wetland	Scrub Savanna	Mixed Forest	Forest Cutover	Young Sugar Cane	Young Sugar Cane
Settlements	0,000	6,052	7,093	1,133	9,049	7,762	12,156	3,087	5,679	9,877
Water	6,052	0,000	7,913	9,579	78,066	80,722	117,963	26,516	48,691	75,268
Tidal Flat	7,093	7,913	0,000	5,074	17,283	28,321	60,296	9,416	27,588	38,835
Fallow Fields	1,133	9,579	5,074	0,000	12,610	13,880	25,727	3,795	12,708	20,368
Pegasse Wetland	9,049	78,066	17,283	12,610	0,000	1,936	9,496	892	6,148	7,633
Scrub Savanna	7,762	80,722	28,321	13,880	1,936	0,000	3,960	2,305	3,835	3,400
Mixed Forest	12,156	117,963	60,296	25,727	9,496	3,960	0,000	9,707	4,202	1,370
Forest Cutover	3,087	26,516	9,416	3,795	892	2,305	9,707	0,000	5,770	8,742
Young Sugar Cane	5,679	48,691	27,588	12,708	6,148	3,835	4,202	5,770	0,000	2,137
Mature Sugar Cane	9,877	75,268	38,835	20,368	7,633	3,400	1,370	8,742	2,137	0,000

A FUNDAMENTAL APPROACH TO TEMPORAL DATA ANALYSIS*

Y. Kawata, T. Kusaka and S. Ueno

Kanazawa Institute of Technology, P.O. Kanazawa-South,
Ishikawa 921 , Japan

ABSTRACT

In the present study we describe a
method to estimate the optical thickness of
the atmospheric haze from a Landsat data set
itself. Then we give a conversion method from
the original CCT level data to the true ground
albedo data with an aid of the Atmospheric
Effect Correction System developed at the
Kanazawa Institute of Technology. We also show
that the signature extension become possible
by correcting the original Landsat data for
the atmospheric effects and this approach will
be a powerful tool in temporal data analysis.
Finally, a processing system implementing the
signature extension of the remotely sensed
data is described. As for such a signature
extension system, we introduce a new and power-
ful table look-up method in classification and
a data base containing the statistical infor-
mation on albedos for various ground classes
with time. ←

1. INTRODUCTION

It has been known that the contrast of the surface images obtained by the
Landsat's MSS is frequently degraded by atmospheric haze. This atmospheric haze
causes a significant decrease in classification accuracy. In the temporal analysis
of one particular geographyical location it is very unfortunate that we can not
compare a Landsat data set quantitatively with another Landsat data set taken at
different time (because of different haze conditions). If the optical thickness
of haze is known, the true spectral response by ground, namely the ground albedo,
can be computed from the observed data set. This problem has been studied by
Odell and Weinman (Ref.1) and more intensively by us (Ref.2 and 3). Since it is
not always possible to get the optical thickness of the haze by direct measurement,
a method to determine the value of the optical thickness of the haze is highly
desirable. In addition to the foregoing discussion, it is imperative to increase
performance in data processing as the remote sensing of the Earth surface becomes
operational and the volume of data increases. These are major motivations by which
we begin to work on the present study.

Here we first describe a method to estimate the value of the optical thickness
of the haze from the remotely sensed data itself. Then we convert a relative CCT
level data set into a absolute ground albedo data set using the Atmospheric Effect
Correction System. Finally, we give a signature extension system consisting of the
data base phase and table look-up phase.

---

2. COMPUTATIONS FOR ATMOSPHERIC SCATTERING

Hansen (Ref.4) developed programs for computing atmospheric reflection and transmission, assuming a plane-parallel atmosphere containing the standard atmospheric gases, and arbitrary vertical distribution of ozone and aerosol by adding and doubling method. In the computation the reflected intensity and the scattering phase function are expanded into Fourier series in the azimuthal angle. As the result, the reflected total intensity I_T (unit of $mw/cm^2 sr$ μm) is a function of the optical thickness τ, the solar elevation angle, the view angle, the single scattering albedo of atmospheric particle, and the ground albedo A. Since the range of view angle by the Landsat is small, we may consider only the upward normal intensity here.

In this paper we use the programs similar to Hansen's to compute the atmospheric effect on the Landsat data. The model atmosphere is bounded by the underlying surface with Lambertian characteristics. The scattering aerosols are assumed to be spherical particles with refractive index n=1.33. The scattering pattern for a aerosol is computed according to Mie theory. The haze model used here is a water haze M defined by Deirmendjian (Ref.5). Assuming the standard atmosphere of Elterman (Ref.6) as a model atmosphere, we compute the relationship between the reflected upward normal intensity and the ground albedo in the case of band 7 and the result is shown in Figure 1. Almost linear relationship between I_T and A is found. This linearity holds also in other bands. The reflected intensity and the direct radiance I_D may be expressed in quadratic form with respect to the ground albedo A. The direct radiance consists of photons which are reflected by a target on the ground and then directly transmitted by the free atmosphere.

$$I_T = P A^2 + Q A + R \qquad (1),$$

$$I_D = A (S A + T) \qquad (2).$$

These coefficients P,Q,R,S and T are determinded by applying the least square method to the computed intensities for a given atmospheric model.

3. ATMOSPHERIC EFFECT CORRECTION SYSTEM

We have implemented a system of computer software program called the ATMOSPHERIC EFFECT CORRECTION SYSTEM (AECS) which corrects the atmospheric effect for both the Landsat and aircraft data. Since we described this system in detail in our previous paper presented at 12th international symposium on remote sensing of environment (Ref.3),we will give only a brief summary here. The overall flow of the AECS is shown in Figure 2. The AECS consists of two subsystems, that is, the inter-extrapolation subsystem and the correction subsystem. The parameterized radiance coefficients P,Q,R,S and T for typical atmospheric models are stored in the radiance file in the inter-extrapolation subsystem. To make this file we computed the theoretical radiances for many combinations of wavelengths, flight altitudes,view angles, solar elevation angles, ground albedos and atmospheric models. Although considerable amount of computer time is required for such computations, it is well worth doing. Once the radiance file is made, then the intensity is computed very fast for any wavelength, flight altitude ,solar elevation angle and the optical thickness value with an aid of inter-extrapolation program.

In the correction subsystem we assume that the underlying surface is characterized by an albedo for the target A_t and by a mean background albedo $\bar{A}$ of the area whose horizontal scale is about 300m. From equations (1) and (2), the reflected upward normal intensity above a target site is given by equation (3).

682

$$I_t = A_t (S \bar{A} + T) + (P - S) \bar{A}^2 + (Q - T) \bar{A} + R \qquad (3).$$

From equations (1) and (3) we can find a ground albedo value for a pixel in the Landsat image in the following.

$$\bar{A} = (-Q + \sqrt{Q^2 - 4 P (R - \bar{I}_{obs})}) / 2 P \qquad (4),$$

$$A_t = (I_{obs} - (P - S) \bar{A}^2 - (Q - P) \bar{A} - R) / (S \bar{A} + T) \qquad (5),$$

where I_{obs} is the observed intensity for a target and $\bar{I}_{obs}$ is the observed average intensity around a target. These two quantities are computed from the observed CCT level with known gain and offset values of the Landsat MSS. A ground albedo data set is, thus, obtained by applying the above procedure to every pixel and every band. Since wavelength, flight altitude, and solar elevation angle are known quantities, the AECS is a system which converts a observed Landsat data set (given in a relative scale) into a ground albedo data set in a absolute unit if the optical thickness of the haze at the time of observation is provided.

4. ESTIMATION OF OPTICAL THICKNESS OF HAZE

In order to use the AECS effectively we need to know the value of the optical thickness of the haze at the time of observation. The value of the optical thickness τ can be found by using the relationship between the theoretical CCT level and the ground albedo. In Figure 3 we show such theoretical mean CCT level curves as a function of mean ground albedo for several different values of τ. Curves in Figure 3 are valid only in the case of solar elevation angle 58° and band 4 of Landsat II. For given values of solar elevation angle, the optical thickness τ, and the mean ground albedo $\bar{A}$, the mean theoretical intensity is given by equation (1). The theoretical mean CCT level $\bar{X}$ is given by

$$\bar{X} = 127 (\bar{I} - R_{min}) / (R_{max} - R_{min}) \qquad (6),$$

where $\bar{I}$ is the mean theoretical intensity, R_{max} and R_{min} is a gain and offset factor, respectively. These factors are known quantities, namely, $R_{max}=2.63$ and $R_{min}=0.08$ for band 4 of Landsat II.

We apply these curves in Figure 3 to the band 4 data covering the Kanazawa area taken on May 23, 1979 by the Landsat II. The solar elevation was 58° at the time of the observation. We need also to have information on ground albedos for a few uniformly extended areas. For such test areas, we choose the sea and coastal sand dune in the image. The observed average CCT levels and the measured mean albedo values for these two test areas are tabulated in Table 1 at the wavelength λ =0.55 μm. We may find a curve with an appropriate value of τ which passes through the points ($\bar{X}$, $\bar{A}$) having both the observed CCT level and the measured albedo value of test areas. It is found from Figure 3 that a curve with τ = 0.4 passes through such two points, more specifically, a point of ($\bar{X}_{sea}$= 19.24, $\bar{A}_{sea}$=0.06) and that of ($\bar{X}_{sand}$=41.3, $\bar{A}_{sand}$=0.17). Similarly, we can

683

estimate the value of τ for other band by making another curves of $\bar{X}$ and $\bar{A}$.

Once the value of τ at the time of the observation is obtained, then the AECS can give a ground albedo data set. In Figure 4 we show the 6 class-classification map of the Kanazawa area (256x256 pixels) computed from the original CCT level data set taken by the Landsat II on May 23,1979. We also show the same classification map in Figure 5, except that the ground albedo data set made from the May 23,1979 Landsat II data set is used in the computation. In both cases the classification is performed by a maximum likelihood decision rule and a supervised method choosing the same test sites in four band space. We can recognize that the quality of the image based on the ground albedo data set is much improved, compared with that in Figure 4. For example, the river systems, the water way connecting the port to the lake and several valleys entering the mountain regions are more visible in Figure 5 than in Figure 4. This example shows clearly the importance of the correction for the atmospheric effect in the remote sensing data.

5. TEMPORAL CHANGES IN CLASS STATISTICS

Let us consider the temporal changes in the CCT level between two Landsat data sets covering one particular geographical location, namely, the Kanazawa area, taken at different time. The statistical regions for four typical pattern classes are plotted in the feature space of band 5 and 6 in Figure 6. The solid line elipses represent the reliability range of certain pattern classes based on the May 23,1979 Landsat data set. The broken line elipses are the similar pattern class ranges, except that they are based on the Oct.23,1979 Landsat data set. The center of a elipse is given by the mean vector point of a certain pattern class and its boundary is drawn with 95 % reliability limit. The pattern class numbers in Figure 6 represent the specific ground covers. The number 430 and 520 represents the shallow water and the sand,respectively. The number 210 and 320 corresponds to the rice field and the forest, respectively.

We recognize immediately from Figure 6 that the temporal changes of the same pattern class in CCT level between May and October are too great. Although some temporal changes of the biological system are expected due to its natural variations with season, the temporal changes for the water or sand should be small. The result in Figure 6 show the opposite of what we expect. We believe that the discrepancy between the above result and the expectation is basically caused by the atmospheric effects, such as, the different haze thicknesses and solar elevations. Figure 6 indicate that it is difficult for us to make a quantitative comparison among the data sets taken at different time.

On the other hand, we can expect that the temporal changes in spectral response become small if we use the ground albedo data sets because data are express in the same absolute unit. Dynamic range of the relative CCT level data depends on time (specifically,the solar elevation angle or τ), wheras that of the absolute unit data is expected to be constant. In Figure 7 we plot the statistical regions for the same pattern classes based on the May albedo and the October albedo data sets. They are made from the May and Oct. ,1979 Landsat data sets. Figure 7 shows that the temporal changes for the water and sand in albedo become very small, while those for the forest and rice field still exist, but they are not large. It can be said that the location of the elipse for a certain class in May is generally close to that in October, compared with the result in Figure 6. The spectral characteristics of the forest and rice field vary in the time interval between May and October. If we use two albedo data sets at the same season in different years, instead of using the May and Oct. data sets, the temporal changes for all classes are expected to be very small. This suggests that one Landsat data set could be

684

classified according to the class statistics based on another Landsat data set taken at different time if these data set are converted in albedo unit. Such a signature extension method would be a powerful tool in the temporal data analysis. In the next section we describe a processing system implementing the signature extension of the remote sensing data.

6. STRUCTURE OF SIGNATURE EXTENSION SYSTEM

We show the overall data flow in signature extension system in Figure 8. There are two phases, i.e., the data base phase and the table look-up phase in a signature extension system. The data base phase consists of three program steps, that is, the AECS step, the classification step and the updating step. In the AECS step the original CCT level Landsat data set is converted into the absolute albedo data set. Then the classification step produces both classification map and the statistical quantities for certain classes of land cover. The updating step updates the statistical quantities for new classes if necessary. The accumulated statistics on pattern classes are stored in the form of Table of Reflectance Pattern Class (TRPC) in computer disk. In the TRPC each class is expressed in terms of three digits. The first digit gives a basic land cover such as the forest, sea, urban and so on. The next two digits specify more detailed category such as evergreen forest, deciduous forest and so on. The correspondence between this three digits class and the actual land cover should be done throgh the ground truth. The TRPC should contain the following information: three digits class number, its mean albedo values in bands 4,5,6 and 7, its covariance matrix elements, its scene iD number, the date of exposure and the reliability bound. The reliability bound gives the seasonal reliability of class statistics.

The table look-up phase consists of three steps, other than the AECS step. In the extraction step an appropriate part of the large data base TRPC is extracted according to the date when the Landsat data set to be classified was taken. If all patterns are normally distributed, it is said that the Mahalanobis distance $D^2(i)$ between a point beloning to a class with class number i and its class center has a chi-square distribution. In the table look-up and link-index step we construct confidence regions for classes in a two dimensional band space using the extracted class statistics. If a sample point satisfying the equation (7), we can expect that a sample point belongs to a class with class number i, with $100 \times (1-\alpha)$ % confidence.

$$D^2(i) \le \chi^2(2\alpha) \qquad (7).$$

In our study $\alpha = 0.05$ is used. When the overlap domains appear as are shown in Figure 9, they are sequentially numbered as 1001, 1002, .. and so on. Such numbers are called index number. The linked list structure is useful to determine which classes are involved in the overlap domain. We use two tables here, i.e., a index table INDEX and a link list LINK shown in Figure 10. Column 1 of INDEX contains nonnegative integers,called pointers, the value of which is the row of the array LINK. LINK has the class numbers in column 1 and the pointers in column 2. The values of the pointers in column 2 of LINK is the row of its array containing the next class number. When the value of the pointer becomes zero, it indicates the end of the list. For example, we can find the classes with class number 210 and 110 by which the overlap domain 1001 is made from the tables in Figure 10.

The confidence regions for pattern classes in a two dimensional band space

685

are tabulated and stored in a look-up table LUT. More specifically, row number
m and column number n of the table LUT corresponds to the integer part of 100x
albedo value in band I and in band J, respectively. We have that $0 \leq m \leq 100$,
and $0 \leq n \leq 100$: m , n are positive integer. Values of I and J could be chosen
from 4,5,6 and 7, but I $\neq$ J. In a disrete two dimensional I-J space a point
(m,n) fallen in the confidence region of a certain pattern class is assigned to
have a corresponding class number and each element of LUT(m,n) is, thus, deter-
mined to have a corresponding class number. When a point (m,n) can not belong
to any confidence region, then class number 0 is assigned. The sample array of
a look-up table LUT is shown in Figure 11.

Consultation of the LUT is done in the table look-up step. If an unknown
albedo pattern having p = (15, 10) in a I-J space, the LUT assigns immediately
to a class with class number 440 for such a pattern in the case of Figure 11.
Suppose an assigned class number k > 1000, then a pattern falls in an overlap
domain. In this case tables of INDEX and LINK are referred to identify classes
involved in the overlap. Then, the Mahalanobis distances from a pattern to each
class center of involved are computed and a pattern is assigned to a class which
gives the minimum $D^2(i)$. We can obtain a classification result by applying the
foregoing table look-up approach to evry point in a new albedo data set. As for
computer times, the time required to classify 256x256 pixels into 11 classes by
our table look-up approach was about 50 seconds of IBM 3031 CPU time, whereas
8 minutes were needed to do the same classification by a convensional method based
on a maximum likelihood decision rule.

7. DISCUSSIONS

One of the most important results in this paper is that the values of ground
albedos can be found from the observed relative CCT level data using the Atmosphe-
ric Effect Correction System. The quality of the classification map based on such
an absolute albedo data set is improved, compared that based on a relative CCT data
set. In addition to that, the use of absolut albedo data sets makes possible to
design a signature extension system in the temporal analysis of the remote sensing
data. In designing a signature extension system an idea of the data base, TRPC
(Table of Reflectance Pattern Class), is essential. Statistical Quantities for
classes obtained from one data set are of value to another data set. In the past
such statistical quantities are only valid in one data set, and of no use in
another data set. As the result, we can expect the increase of performance in
temporal data processing. Our signature extension system remains still in the
very beginning stage and much work should be done before the completion of a solid
and workable signature extension system.

REFERENCES

1. Odell, A. P. and Weinman, J. A., " The effect of atmospheric haze on images of the Earth's surface", J. Geophys. Res., Vol. 80, pp.5035-5040(1975).

2. Kawata, Y., Haba,Y.,Kusaka,T.,Terashita,Y.,and Ueno,S.," Atmospheric effects and their correction in airborne sensor and Landsat MSS data", Proc. of the 12th Intl. Symp. on Remote Sensing of Environment, ERIM, pp. 1241-1257(1978)

3. Haba, Y., Kawata, Y., Kusaka, T., and Ueno, S., " The system of correcting remotely sensed Earth imagery for atmospheric effects ", Proc. of 13 th Intl. Symp. on Remote Sensing of Environment, ERIM, pp. 1883-1894(1979).

4. Hansen, J. E., " Radiative transfer by doubling very thin layers ", Astrophys. J., Vol 155, pp. 566-573 (1969).

5. Deirmendijian, D.," Electromagnetic scattering on spherical polydispersions ", American Elsevier, New York (1969).

6. Elterman, L., " UV, Visible and IR attenuation for altitude to 50 km ", Rept. AFCRL -68 -0153., AFCRL, Bedford, Mass. (1968).
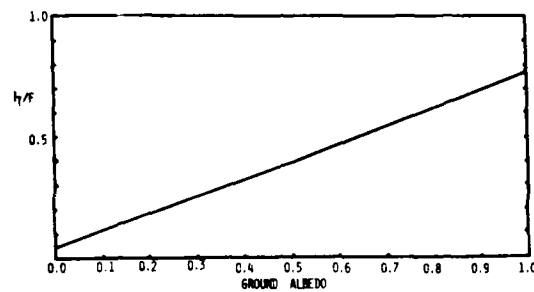
Figure 1. The theoretical upward normal intensity in band 7 against ground albedo. Incident solar flux is normalized to ΠF. Solar elevation angle is assumed to be 48°.

Figure 2. The block diagram of the AECS.
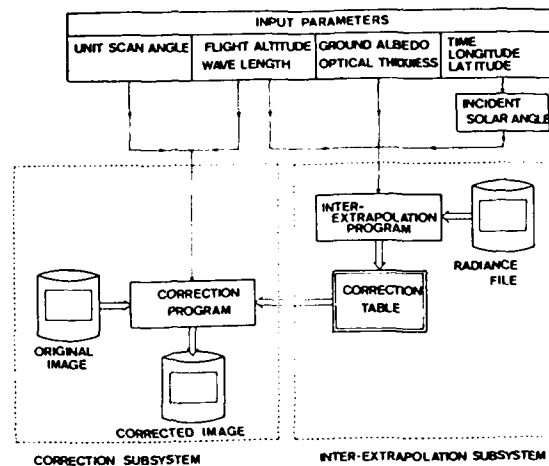
Observed CCT level	measured albedo
$\bar{X}_{sea}$ = 19.24	$\bar{A}_{sea}$ = 0.06
$\bar{X}_{sand}$ = 41.30	$\bar{A}_{sand}$ = 0.17

Table 1. The observed mean CCT levels for the sea and sand area are given from the May 23, 1979 Landsat II in band 4. The mean albedo values for the same areas are measured in Oct., 1978.

688

Figure 3. The theoretical mean CCT level curves with different values of τ are plotted as a function of mean ground albedo.
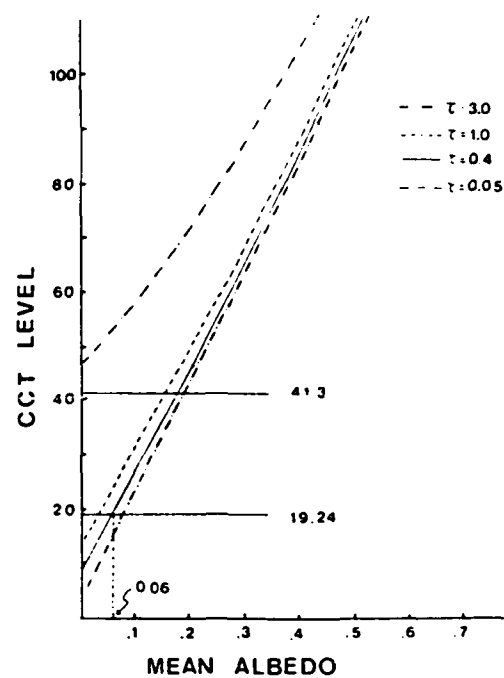
Figure 4. Six class classification map based on the relative CCT level Landsat data set.

Figure 5. Six class classification map based on the absolute albedo data set.
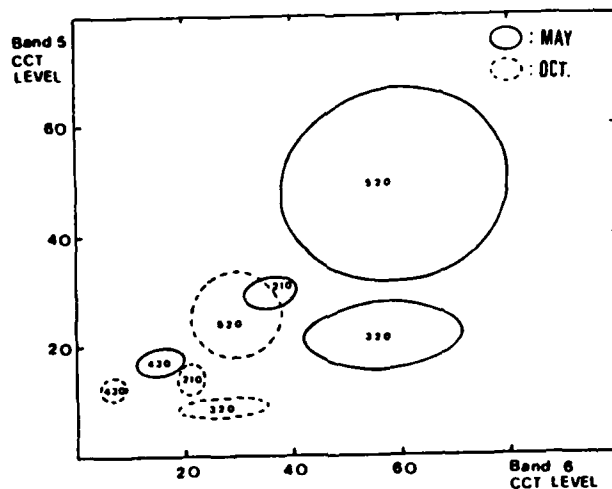
Figure 6. Temporal changes for several
pattern classes in CCT level between
May and October. Class number 430- the
shallow water , 210- the rice field,
520- the sand, and 320- the forest
area.
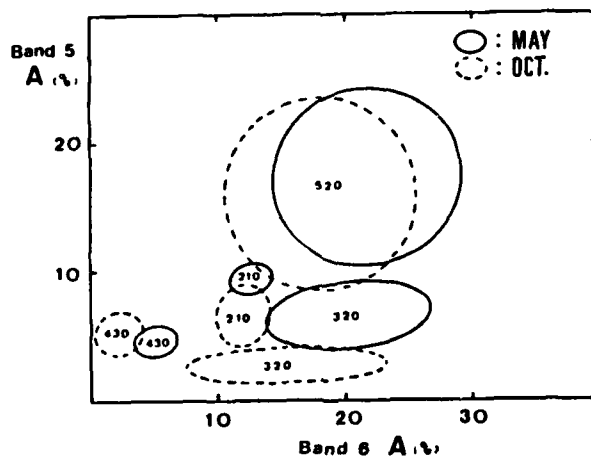
Figure 7. The same temporal changes as
in Fig. 6., except that they are expressed
in absolute albedo unit.

Figure 9. Confidence regions for classes in a two dimensional space.

Figure 8. The overall flow of the Signature Extension System.

Figure 10. Tables of INDEX and LINK.
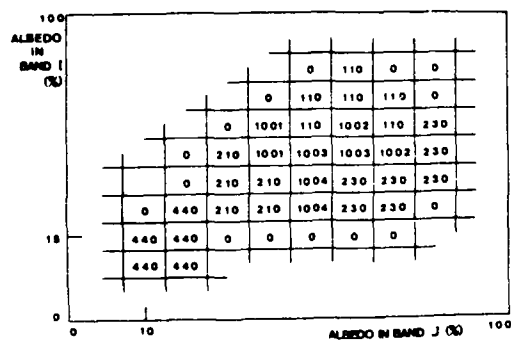
Figure 11. Sample array of look-up table LUT.

691

SATELLITE SENSING OF TUTICORIN PORT AND
ENVIRONS ON THE EAST COAST OF INDIA

S. THIRUVENGADACHARI, P. SUBBA RAO AND K.R. RAO
National Remote Sensing Agency, Hyderabad, India.

ABSTRACT

Landsat has emerged in rec ent years as a versatile surveying tool for synoptic large area mapping and monitoring of coastal features and processes. The demonstrated capability of satellite sensors coupled with the need for current coastal zone information in the southeast coast of India led to this study to evaluate the use of remotely sensed data from space for this purpose. Though practical constraints such as nonavailability of suitable Landsat data and inadequate ground (sea) truth information limited the study to a qualitative appraisal, the results are promising and justify a concerted effort to a cquire updated information in this stretch of coast in the Gulf of Manaar. Landsat in particular has the definite potential to study the impact of the recently commissioned major port of New Tuticorin which could have an influence over several kilometers of coastline on either side, not easily emanable to ground surveys.

1. INTRODUCTION

Remote sensing observations from aircraft and spacecraft and their application in coastal zone studies are relatively new survey tools. Significant progress has been made in recent years in demonstrating the use of remote sensing techniques to derive information about the character and conditions of coastal water. Although airborne surveys, using camera and scanner systems, can provide more detailed information about coastal processes, satellite data is superior in its synoptic large area coverage. Landsat data, in particular, has been useful in surveying and mapping regional coastal features as well as in mapping and monitoring subsurface bathymetry, location and measurement of pollutants, surface circulation and current patterns, and identification of navigation hazards such as shoals.

2. PREVIOUS STUDIES

Using high gain Landsat band 4 and 5 data depths upto 22 metres were reliably verified at accuracies with 10 percent (rms) of measured values near Barry Islands, where water transparencies of 0.05 m^{-1} and 26 percent bottom reflections were encountered. Computer compatible tape (CCT) signals 2 digital counts above deep water signals were identified to be caused by high reflected

from about 40 meters depths. Depths upto 10 metres were verified at the Flori-
da site where water was less transparent with attenuation of $0.11m^{-1}$ and bot-
tom reflection equal to 20 percent (Polcyn, 1976). Detection of the presence
of 18.5 m depth was feasible in the area. For these values to be generally
realisable the bottom reflectance should typically be between 20 to 26 percent
in the green band. Another experiment with normal gain Landsat-1 data used
two channel processing and gave results upto 9 metres with band 4 data and 3
metres with band 5 data (Polcyn and Lyzenga, 1975). The results of the study
with high gain data indicate that better digitation of signal range was provided
with a wide range of signal spread over more digital values and a finer depth
resolution is achieved. This means that greater depths can be measured, that
depth estimation is more accurate and that smaller range of depths can be esti-
mated.

The use of Landsat data has helped considerably in expanding the knowledge
of nearshore water circulation, and in some respect, by inference, the movement
of littoral materials. Sequential Landsat imagery of suspended sediment plu-
mes in coastal waters was used to define the seasonal variation of current di-
rection in nearshore waters (Carlson and Harden, 1973). Hunter (1973) identi-
fied turbid water masses off the Texas coast on Landsat imagery to d lineate
the complex current patterns of the area. Landsat-1 and 2 multispectral scan-
ner data could be caliberated for accurate measurement of suspended sediment
concentration and used to determine the spatial distribution of suspended sedi-
ments in the macrotidal coastal embodyment of Mines basin, NOAA Scotia (Amos
and Alfold; 1979). It was suggested that multidate thematic maps showing sur-
face sediment distributions can be used qualitatively to determine circulation
patterns, sources of material, and volume of suspended sediment for the low
countries (Cracknell et al, 1980). Muralikrishna (1979) evaluated the flow
directions of the nearshore surface currents along certain reaches of east
coast of India, using suspended sediment patterns in MSS 5 imagery. Nath and
Rao (1979) were able to d lineate various turbidity levels in the Gulf of Cam-
bay on the West coast of India.

3. STUDY AREA

The eastern coast of India, extending from Kanyakumari to the mouth of
Hooghly river, has an approximate length of 2800 km, with most of the sediment
laden major central and southern Indian rivers such as Ganga, Mahanadi, Krishna
Godavari and Cauvery, flowing eastwards into the Bay of Bengal. The sea bed
slope is relatively steep compared to the western coast. The large amounts of
sediment discharged by the rivers into the sea travels back and forth along
the coast. The littoral drift is from south to north during the southwest
monsoon and from north to south during the northeast monsoon. The net drift
from south to north is approximately of the order of 1 milli n tonnes/year
through the actual quantity would vary along the coast. The east coast recei-
ves its rainfall mainly during the northeast monsoon period, but the littoral
drift being large during the southwest monsoon, the inlets along the east coast
tend to get choked up during the southwest monsoon period. The construction of
harbours and other coastal structures could affect the movement of such large
quantities of sediment in comparitively shallow depths along the coast. The
east coast is also subject to cyclonic activity with attendant effects on the
nearshore coastal environment.

The stretch of east coast between Rameswaram island at the north and
Kanyakumari at the southern most tip of India was selected for this study
(Fig.1). This coastline includes the recently operational major port of New
Tuticorin. This is an artificial harbour constructed in a fairly sheltered
area with two long breakwaters, north and south, including an eastern arm,
enclosing 960 acres of tranquil sea area. Extending 4103 metres, the north-
ern breakwater is considered to be the world's longest breakwater.

4. BASIC DATA

Temporal Landsat data acquired over ten different dates, one in February 1977 and the rest in the period between December 1979 to March 1981 were considered in this study. Both return beam vidicon (RBV) and MSS data were utilised. Though the major portion of the study involved visual interpretation of RBV imagery, digital analysis was also attempted using MSS data in CCT format. Since the Indian earth Station near Hyderabad does not generally record RBV data on High Density Digital Tapes, only the quick look products were available in the case of recent RBV data. Ground truth in regard to underwater bottom contours was obtained from the existing hydrographic charts. Soundings taken by the Tuticorin Port Trust every year is restricted to the area immediately around the harbour, and hence could not be used in the study. Very little data was available on the coastal circulation and sediment transport patterns.

5. WATER QUALITY AND SPECTRAL RESPONSE

The detectable spectral differences in the nearshore coastal environment may be a result of turbidity and/or depth. Turbidity may be a result of pollutant influx and dispersion or due to littoral drift. The backscattered energy increases with increasing turbidity as also with decreasing depth and both are restricted to shallower waters. Hence it may be difficult to separate the spectral responses due to the causative factors of turbidity and bottom reflectance when both are present. Discrimination of the two may call for multidate Landsat as well as sea truth information. Conclusions arrived at on the basis of single date data have to be confirmed through a study of temporal data to descriminate seasonal dynamic fluctation from long-term and permanent effects.

Remote bathymetry is restricted to relatively clearer waters, and takes advantage of two spectral characteristics. Water selectively absorbs different wave lengths of light, and energy at each wave length is strongly absorbed as a function of the depth of water. The strength of bottom reflected signal gives an indication of the depth of water through which it has traversed.

6. DISCUSSION OF RESULTS

The high land/water contrast in the band 7 imagery aids in accurate delineation of the coastline and to monitor its changes if any, with time. However the resolution of the Landsat imagery does not allow recognition of shoreline changes of less than about 100m, and generally the changes may be less than this value. Thus, the usefulness of the Landsat imagery lies in providing clues to the Hydrodynamics of the system causing erosion and to the frequency with which certain patterns of water flow and associated erosion occur (Welby, 1978). Further, future satellite systems with improved spatial resolution may permit detection of smaller coastline changes than currently possible. The potential for coastline mapping and monitoring seems exciting an view of the possible effect due to the major part of Tuticorin extending over long stretches of the coastline on either side, not amenable to conventional ground surveys.

The satellite data acquired on 26th February 1973 and in its original format was studied for extraction of bathymetry information. Satellite data in black and white band imagery, false colour composite and density sliced format were studied. But since the reflected radiation from water, with its characteristically high absorption of incident energy, is recorded by the satellite sensor typically in the lower one-third of the total brightness range limited water quality detection capability was offered in the original format. Hence the data was contrast stretched to provide images with higher brightness and contrast in the lower digital range, but saturating in the higher brightness area (Fig.2). Contrast stretching was preceded by Histogram analysis for a

test site within the study area, which indicated the distribution of pixels over the total dynamic range. Original data in the 20 to 50 digital count range in band 4, 9 to 10 in band 5, 5 to 15 in band 6, and 1 to 8 in band 7 were linearly stretched over the total range of 0 to 127 counts. A comparision of original and contrast stretched imagery indicates improvement in the detection of underwater phenomena in the latter.

The bathymetry information from existing hydrographic charts was overlaid on the Landsat data. The highest tidal range in this area is 1.07 m and the tidal range 26th Feb. 1973 was only 0.55m, and hence has been neglected in this study.

A study of contrast stretched imagery indicates that saturation of different bands occur at different depths. Though definite depth limits for saturation could not be established in this preliminary study, it could be observed that the 2m depth which could be identified on the band 6 imagery cannot be so clearly seen, in band 5 imagery and the 5m depth identifiable on band 5 is not that distinguishable from lesser depths on band 4, indicating that saturation occurs below different depths, in different bands. The incident radiation obviously penetrates to different depths in the four bands. While the radiation is almost completely absorbed in the surface strata in band 7, there is greater penetration in band 6. While the original unstretched band 6 imagery snows almost no underwater details, in the contrast stretched imagery can be seen the 2m and 5m contours. However it should not be construed that depth estimation could be attempted upto 5m in this band. These depths are much greater than those reported in literature so far using band 6 data, and hence observed spectral response should be considered as deep water signals coming from these depths, perhaps with high bottom reflectance and high water transparancy, and may only indicate the maximum penetrability and not the range in which spectral response could be correlated with depth. The 2m and 5m contours could be identified on the stretched band 5 imagery, while upto about 10m depth could be penetrated in band 4.

Use of the multivariable categorisation algorithm implemented on the multispectral data analysis system (MDAS) at NRSA resulted in unsatisfactory classification of water depths. Sequential density slicing of the three bands 4, 5 and 6 over different depth ranges, taking into account the different penetrating capabilities in the 4, 5 and 6 bands and saturation of the first two bands at smaller depths, yielded better results. A comparision of the false colour composite of contrast stretched band 4, 5, 6 data as well as the density sliced band imagery with the hydrographic chart demonstrated the feasibility of conducting, bathymetric studies using satellite data in the area. However, absence of ground truth on bottom reflectance and water transparency precluded further quantification of the spectral signal-water depth relationship.

Results obtained on the basis of this single date were confirmed and supplemented through a study of temporal data on 9 more dates in the period Dec. 1979 to Mar 1981, some of which were affected by cloud cover and haze.

The multidate study indicated change in bottom contours. The 2 metre contour as suggested by Landsat data conforms to hydrographic chart position while the 5m and 10 m contours have changed (Fig.2). A significant landward shift in the 5m contour and hence deepening of the sea could be identified in the vicinity of Van Tivu and Kosvari Tivu islands north of the Tuticorin harbour, while further north it generally con orms to hydrographic chart positions. The 10m contour shows a general landward shift all along the coast north of the harbour. Again, south of the harbour, between Tiruchendur and Manapad, the 5m contour has shifted leading to widening of shallow areas. The 10m contour has smoothened out within the narrow necked loop shown in the hydrographic

chart. The 5m contour has moved seawards leading to shallower coastal waters at the mouth of Tamrparani river.

Satellite imagery acquired in December 1979 indicates significant north to south littoral drift, contrary to the general impression of little or no long-shore sediment transport (Fig. 3). The sediment transport patter during the southwest monsoon could not be studied due to the constant cloud cover during the monsoon months of June to September. During the nonmonsoon months of January to May satellite data do not indicate any significant sediment transport activity. Spiral patterns are seen along the coast south of Tiruchendur point in the September RBV imagery (Fig. 4).

The accretion south of the eastern arm of the southern breakwater seems to be a dynamic feature, appearing and disappearing with seasons. For instance, it is noticed in the satellite data acquired in February and March while it is absent in the December imagery. Seasonal accretion and erosion of sea bed is also noticed along the coast at the mouth of Gundar river.

Exposed and submerged coral formations could be identified, as for instance in the Ramnad coast south of Rameswaram island (Fig. 5). Identification of such shoals indicate great promise in ensuring safer coastal maritime traffic.

7. CONCLUSIONS

Though the results presented in this paper are preliminary in nature, in the context of limited sea truth data available, they serve to establish the feasibility of using satellite sensed data for studying coastal features and processes over the large coastline that might be affected by the newly functioning Tuticorin harbour. The limited historic coastal data base also calls for such remote sensing surveys to gain a better understanding of this stretch of coast.

Though the spectral range and resolution and spatial resolution of current Landsat sensors are not ideal for such survey efforts, future satellite systems such as Landsat D, SPOT and Indian Remote Sensing satellite (IRS) hold significant promise for the use of space-borne data for studying coastal features and processes.

REFERENCES

Amos, C.L., and Alfoldi, T.T., 1979, "The Determination of Suspended Sdeiment Concentration in a Macrotidal System Using Landsat Data", Journal of Seminentary Petrology, Vol. 49, No.1, p 159-174.

Carlson, P.R., and Harden, D.R., 1973, "Princi al Sources and Dispersal Patterns of Suspended Particulate Matter in Nearshore surface Waters of the Northeast Pacific Ocean", Type I Progress Report to NASA, Period 1 June - 15 Aug. 1973, U.S. Dept. Commerce Natl. Tech. Inf. Service, E 73-11099/WR, 14 p.

Cracknell, A.P., Singn, S.M., and Macfarlane, N., 1980, "Remote Sensing of the North Sea Using Landsat-2 MSS and Nimbus-7 CZCS Data", Fourteenth International Symposium on Remote Sensing of Environment, San Jose, Cost Rica, April 23-30, p 1643-1651.

Hunter, R.E., 1973, "Distribution and Movement of Suspended Sediment in the Gulf of Mexico Off Texas Coast", Symposium on Significant Results obtained from the Earth Resources Technology Satellite-1, Maryland, USA, March, Vol. 1, Sec. B, p 1341-1348.

Muralikrishna, I.V., 1979, "Landsat Application to the Study of Coastal Processes", COSPAR Symposium series, The contribution of Space Observations to Water Resources Management, Pergamon Press, Oxford, U.K.

Nath, A.N. and Rao, K.R., 1979, "A study of Coastal Morphology and Evaluation of Depths, Turbidity and Current Pattern in Gulf of Cambay and Kutch using Landsat Data", Technical Report, National Remote Sensing Agency, Hyderabad, India.

Polcyn, F.C., 1976, "NASA/COUSTEAU Ocean Bathymetry Experiment", Final Report NASA CR-ERIM 118500-1-F, July 197 p.

Polcyn, F.C., and Lyzenga, D.R., 1975, "Remote Bathymetry and Shoal Detection with ERTS", Report No.193300 - 51-F, Environmental Research Institute of Michigan, Ann Arbor, U.S.A.

Welby, C.W., 1978, "Application of Landsat Imagery to Shoreline Erosion", Photogrammetric Engineering and Remote Sensing , Vol. 44, No.9, p. 1173-1177.
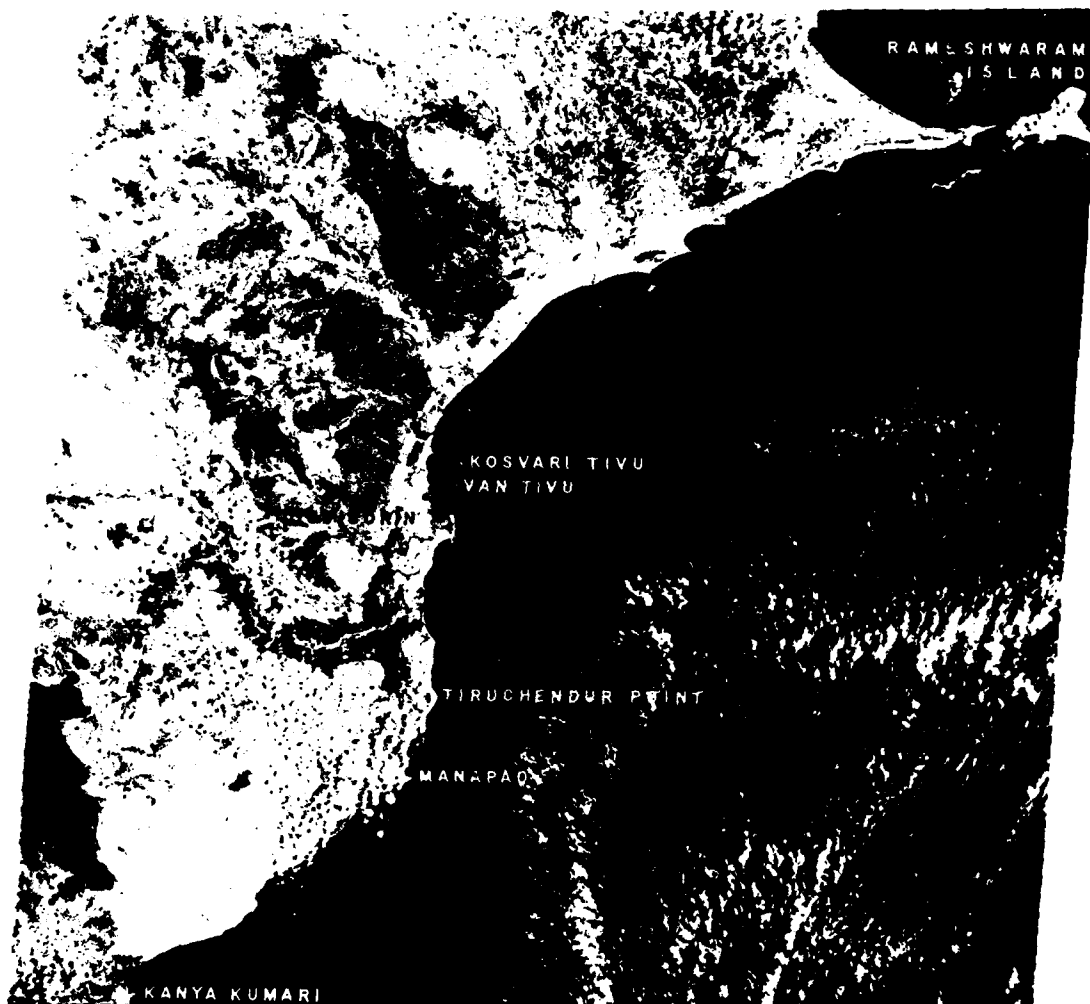
Fig. 1. Landsat imagery covering the Tuticorin coast in the Gulf of Manaar

ORIGINAL DATA

BAND 4   BAND 5   BAND 6   BAND 7
0.5 - 0.6 Mm   0.6 - 0.7 Mm   0.7 - 0.8 Mm   0.8 - 1.1 Mm

CONTRAST STRETCHED FOR WATER
Scale 1:10^6

Fig. 2. Original and contrast stretched band imagery of part of Tuticorin
coast

700

Band – 4   Band – 5

Fig.3. Landsat MSS imagery acquired on 16th December 1979
(north east monsoon period)

11.9.80   29.9.80

Fig. 4. Landsat RBV imagery of southwest monsoon period indicating
circulation patterns below Tiruchendur point

701
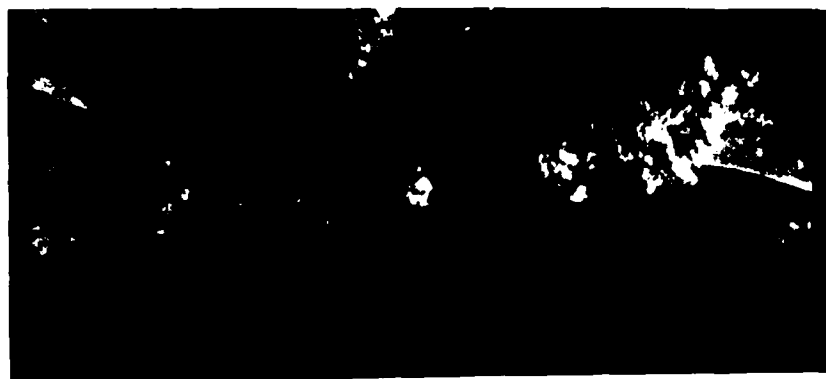
Band - 4

Band - 5

Band - 6

Fig. 5. Explosed and submerged islands off Ramnad coast

702

AD P002046

A SYNOPTIC APPROACH TO STUDYING CHANGES IN SEA SURFACE TEMPERATURE USING GEOSTATIONARY SATELLITE DATA*

M.R. Stevenson

Instituto de Pesquisas Espaciais - INPE
Conselho Nacional de Desenvolvimento Cientifico e Tecnologico - CNPq
C.P. 515 - São Jose dos Campos - SP - Brasil

ABSTRACT

Data from radiometers aboard meteorological satellites provide a unique method to study surface thermal features of the ocean on a large scale, synoptic basis. The ultility of such a data base, however, depends upon both thermal and spatial resolution of the sensors. Because the geostationary SMS and GOES satellites provide essentially the same geometric perspective each time the earth is scanned, this type of orbital platform was selected for use in this study. Three computer programs are used in sequence to process and convert the data into a machine contoured map of surface temperature. Each chart covers a 15° X 15° area and uses a map scale of 8 million to 1. The contour interval is set at $2^\circ C$. When the software becomes operational, the contoured maps of temperature will be of considerable use for diverse regional studies such as marine climatology and marine resource development.

1. INTRODUCTION

The natural variability in the ocean has a synopticity that varies from a few days to several months, has spatial scales of about 50-100 km and horizontal velocities of about 10 cm/sec. Information on synoptic variability of the surface temperature of the ocean is of broad scientific interest because many of the dynamic processes occurring in the upper ocean provide a thermal signal at the sea surface. Successful studies in marine climatology for example, require synoptic coverage of the surface temperature. In addition to physical processes, information on the surface temperature field can be related to important economic factors such as fishing potential and success e.g., Stevenson and Miller (1974), Monin et al 1977, etc. The relation of water temperature to fishing success is readily seen in Figure 1. Once the surface temperature field is available, it is possible to derive a thermal gradient field ∇_h ($\partial T/\partial x + \partial T/\partial y$) and also to relate this field to fishing success (Monin et al 1977).

To properly observe synoptic variations in the surface temperature field then, we need to consider data series to extend over a range of months and a spatial scale to stretch over hundreds of kilometers. To achieve this level of data sampling from conventional data platforms would require large numbers of research vessels and/or a network of buoys. In either case, the costs involved in maintaining such a monitoring system would be extremely high. An alternate method to observe synoptic changes in the sea surface temperature is to utilize data from satellite platforms.

The polar orbiting meteorological satellites e.g., NOAA-7, offer the advantage of 1 km spatial resolution with the Advanced Very High Resolution

Radiometer (AVHRR) system but orbital constraints prevent more than 1 good pass on alternate days over low latitude areas. The geometric perspective from the AVHRR sensor varies each time depending upon the equatorial crossing points of the satellite. The geometric distortion increases relatively quickly with increased distance from the nadir point of the sensor due to the relatively low orbital altitude.

The Visible and Infrared Spin Scan Radiometer (VISSR) system aboard geostationary satellites, however, provides essentially the same viewing angle and can readily provide multiple earth images each day. The principal disadvantage of using the VISSR data is that the infrared channel has a data footprint that varies from 8 km at the equator to about 12 km near the southern limits of Brazil, about 1/100 as good as the AVHRR data. The VISSR infrared resolution of 0.5°C is about the same as for the thermal infrared channel of the AVHRR system. For the purpose of providing synoptic coverage it was considered that the advantages of constant perspective and flexibility of data acquisition outweighed the disadvantages of using the geostationary data and VISSR data from the SMS-2 were therefore used to develop the software described in this report.

2. METHODOLOGY

VISSR infrared data, the data base for this report, are obtained from a telemetry station located on the São Jose dos Campos (State of São Paulo) campus of INPE. The station presently receives daily visual and thermal imagery and produces film products which are available to the different departments for research purposes. Digital tapes of the infrared channel are generated upon request.

The synoptic approach consists of passing the desired digital images through a set of 3 computer programs in order to obtain machine contoured maps of sea surface temperature for the ocean off Brazil. The first program is written in Algol while the second and third programs are written in Fortran-4. All programs are presently run on a Burroughs 6800 computer system. The data processing procedures are shown schematically in Figure 2. The first program (SATDAT) reads a digital tape containing a full earth image at a tape density of 800 BPI. Due to present computer core limitations, the user specifies a set of 210 scanlines through the use of control cards. These scanlines represent a particular latitudinal band and correspond to 1 of 4 contiguous map locations. A full earth image contains 1,821 infrared scanlines where each scanline consists of 3,821 16 bit words. The program decodes the 16 bit words into two corresponding 8 bit words. Only the 8 bit words containing information on the radiometric brightness is retained at the present time. The entire 210 scanlines are then stored onto both a disk and an archival tape for further processing.

The second program (PRSCR) reads in the disk information or the archival tape generated from the SATDAT program. From this large array the user specifies the longitudinal area of interest by control cards and extracts a block of 200 pixels from the 210 scanlines. It is this smaller block of data that is subsequently screened for clouds, land and converted into temperature values. This array is then subjected to a cloud screening procedure to detect and eliminate those pixels containing radiometric energy from clouds present within the pixels. Maul (1981) has shown that the best cloud screening results when both the visible and infrared channels are used together. Present telemetry capabilities at INPE do not permit the digital acquisition of the higher resolution visible channel, so the visible channel data could not be incorporated at this time. The screening technique used in the second program requires that the 210 scanlines by 200 pixels (42,000 total pixels) be subdivided into 20 X 21 subarrays (each containing 100 pixels). Mean and standard deviation parameters are then computed sequentially for each subarray as shown in Figure 2. Those subarrays containing mean temperatures warmer

than a preset value and a σ ≤ 2 are retained. If the mean values are cooler than the preset value, the subarray is zeroed out. If the mean value is within the temperature criteria but σ > 2, a secondary retrieval is used to determine which pixels in the subarray are most likely contaminated by cooler cloud radiation (see Figure 2). In this screening procedure a Gaussian equivalent function is computed using the warm side of the histogram associated with a particular subarray. Pixels cooler than the values indicated on the cool side of the Gaussian curve are eliminated and a new mean and standard deviation are computed from the remaining pixels of the subarray. If the remaining pixels still show a σ' > 2, the subarray is zeroed out. If the σ' ≤ 2 and the number of pixels retained are at least 60% of the subarray total, then the partial subarray is retained for further use. This procedure is performed for each of the 420 subarrays in a given image field of 42,000 pixels. This method generally follows that proposed by Bristor (1975), but with several modifications. Following the screening of all subarrays, those pixels with nonzero values are converted to radiometric brightness temperatures using the NOAA/NESS algorithm

$$T(^{O}K) = \frac{(C + 406)}{2} \qquad\qquad 1.$$

where C is the count associated with an individual pixel. The output consisting of an array of temperatures (in ^{O}C) and zeroed values is then written onto disk storage and also onto an archival tape for further processing.

The third program (TESTGRID) either reads from disk storage or the archival data tape. The user specifies which of the 4 predetermined geographic areas are to be used with the data to generate a contoured map of sea surface temperature. The program, containing a number of subroutines first generates the margins of a 15° X 15° modified Mercator map, using a scale of 8 million to 1. A digitized version of the Brazilian coast is next read into the program and the appropriate part of the coastline corresponding to the particular map (1, 2, 3 or 4) area is extracted and the coastline drawn onto the map. The program then uses the digitalized coastline to zero out those pixels west of the coastline that correspond to land. The program next moves to another subroutine where the whole array is scanned to determine the warmest and coolest temperature values. These values form the limits of the contoured thermal field. The program normally is set for a contour interval of 1 or $2^{O}C$. The subroutine begins with the coolest contour value and starts a search routine in one corner of the array. The program surveys the entire array for the same contour level before proceding to the next higher value. Some subroutines follow Miller and Bliss (1972). The program detects the presence of clouds from the zeroed pixels and terminates isotherms when zero values are encountered. After all line segments of a particular isotherm are computed, a 2-dimensional smoothing function is used to make the contoured lines more realistic. Following the smoothing of the segments, the segments are plotted, after which the program resets to the next higher contour level and the whole process is repeated. An example of the sea surface temperature maps produced from a VISSR infrared image field (Figure 3) is shown and discussed in the next section.

3. RESULTS

Contoured charts of sea surface temperature are seen in Figures 4 to 7. Isotherms frequently terminate without closure, a condition caused by the program TESTGRID detecting the presence of zeroed pixels due to the presence of clouds/land. In locations possessing relatively heavy cloud cover, some cloud contamination of pixels is inevitable as may be seen by slightly lower isotherms adjacent to cloudy areas. The availability and incorporation of visible channel data in the second program will greatly reduce this screening problem.

705

The surface temperatures shown in the charts do not contain corrections for atmospheric moisture. These temperatures therefore are typically 2 - 6°C cooler than actual surface measurements, although Maul (1981) has observed that the temperature difference between measured and actual surface temperatures may approach 10°C. The temperature field may be adjusted by incorporating a least squares fit of sea truth measurements and applying this correction to the data array before contouring the field (Stevenson et al 1977).

A number of small scale features are apparent in all of the charts. If only larger synoptic features are of interest, the third program can be modified to use a heavier smoothing function, or as is done in the NOAA/NESS GOSSTCOMP charts, the individual pixels are averaged into mean values centered on a (1/2)° X (1/2)° grid and those values are then used to construct the isotherms. Although the averaging of many pixels into such a grid gives a much smoother field, many small scale and some mesoscale features are either eliminated or greatly diminished in detail. Our present plan for evaluation of synoptic surface temperature variations off Brazil is to use the smoothed field of individual pixels and to smooth them prior to generating a contoured field. With our present data array size and incorporating a 2-dimensional smoothing function we are able to retain thermal wavelike features whose wavelength is 70 km or longer, based on a 50% transmittance response of the filter. The smoothing reduces the significance of individual extreme values but will allow initial thermal gradients of 2°C/10 km or larger to remain as long as the feature does not cause the standard deviation of the subarray to exceed ± 2 digital counts. This thermal response sensitivity of the data array and filter is separate from but inherently dependent upon the basic 0.5°C temperature change between adjacent digital levels in the range of ocean temperatures.

The amount of CPU time on the B6800 computer that is required to generate 1 of the 4 contoured charts, including tape read and write times is shown below.

Table I. Time and costs to produce temperature charts

PROGRAM	CPU TIME (sec)	COST ($Cr.)	COST ($US)
SATDAT	49	1,825.00	12.20
PRSCR	24	1,440.00	9.60
TESTGRID	71	1,735.00	11.50
TOTAL	144	5,000.00	33.30

To produce the set of 4 charts the above totals are multiplied by 4. The time and cost per program presently reflects the developmental phase of the study. It is recognized that an appreciable reduction in CPU time will result when the programs are integrated into an operational mode. The time required from the first tape read to the finished map would also be considerably reduced. The feasibility of running the programs with larger arrays during times of minimum usage of the B6800, as well as the possibility of using a PDP11/45 computer with large disk capability are both presently being explored.

The present sea surface temperature charts generated from geostationary VISSR infrared data appears to be satisfactory for synoptic observation of sea surface temperature variations in the ocean off Brazil. As the software becomes operational, the charts are expected to be of interest to a large group of users in Brazil, particularly those persons whose activities involve the development of commercial fisheries.

706

4. ACKNOWLEDGMENTS

5. REFERENCES

Bristor, C.L. 1975. Central processing and analysis of geostationary satellite data. National Oceanic and Atmospheric Admin. Washington, D.C. NOAA Techn. Memo. NESS 64. 155 p.

Maul George. 1981 Application of GOES visible-infrared data to quantifying mesoscale ocean surface temperatures. Jour. Geophys. Res. Vol86(C9): 8007-8021.

Miller, Forrest R. and Kenneth A. Bliss. 1972. Processing EASTROPAC STD data and the construction of vertical temperature and salinity sections by computer. National Marine Fisheries Service, Seattle, WA. NOAA Techn. Rep. NMFS CIRC-365. 17 p.

Monin, Andrey S., Vladimir M. Kamenkovich and Vladimir G. Kort. 1977. Variability of the oceans. John Wiley & Sons, Inc. New York, NY. Translated from Russian. 241 p.

Stevenson, Merritt R. and Forrest R. Miller. 1974. Application of satellite data to study oceanic fronts in the Eastern Pacific. Inter-Amer. Trop. Tuna Comm. La Jolla, CA. Final Rep. Grant Nº 04-3-158-59. 111 p.

Stevenson, Merritt R., Robert G. Kirkham and Bruce J. Madsen. 1977. Development and testing of a cloud screening technique for use with satellite-borne scanning radiometers. Inter-Amer. Trop. Tuna Comm. La Jolla, CA. Naval Environ. Predict. Res. Fac. Final Rep. Nº 0228-76-C--3163. 95 p.
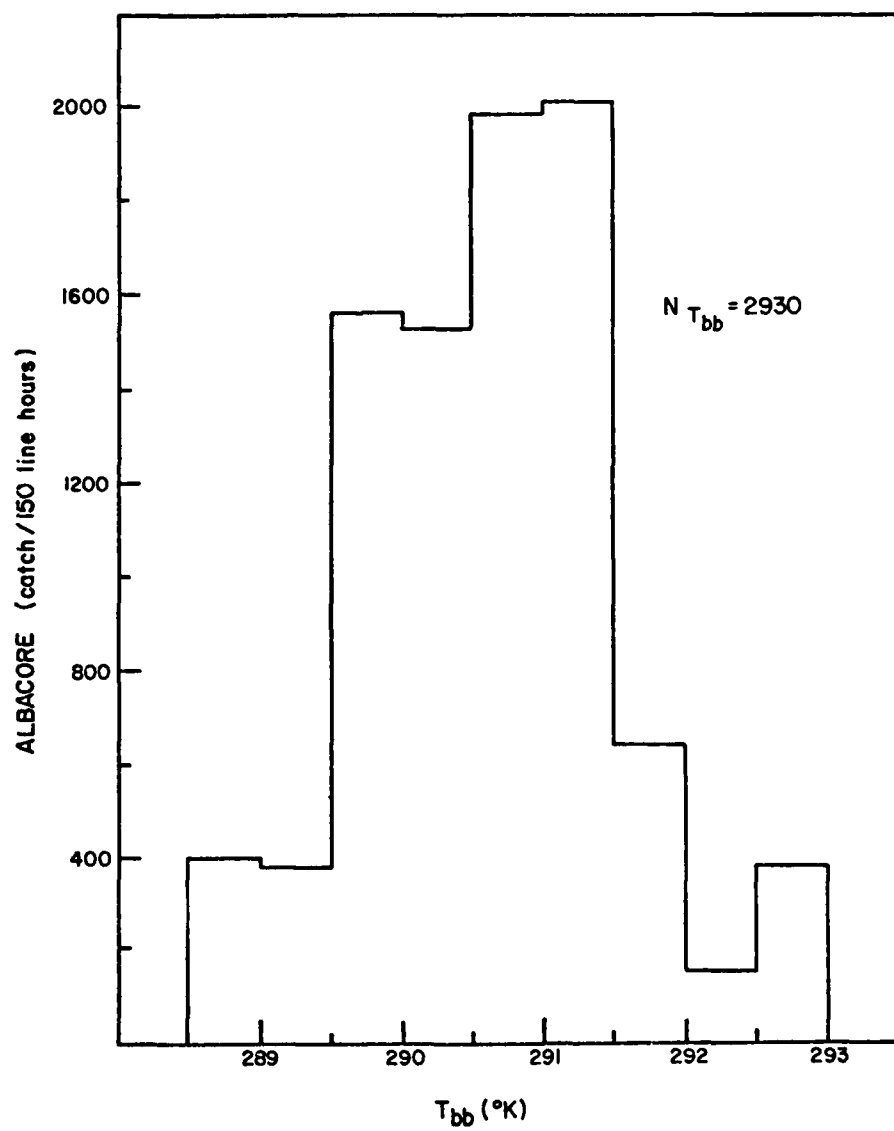
Figure 1. Relation between albacore tuna catch and satellite derived surface temperature (from Stevenson and Miller 1974).
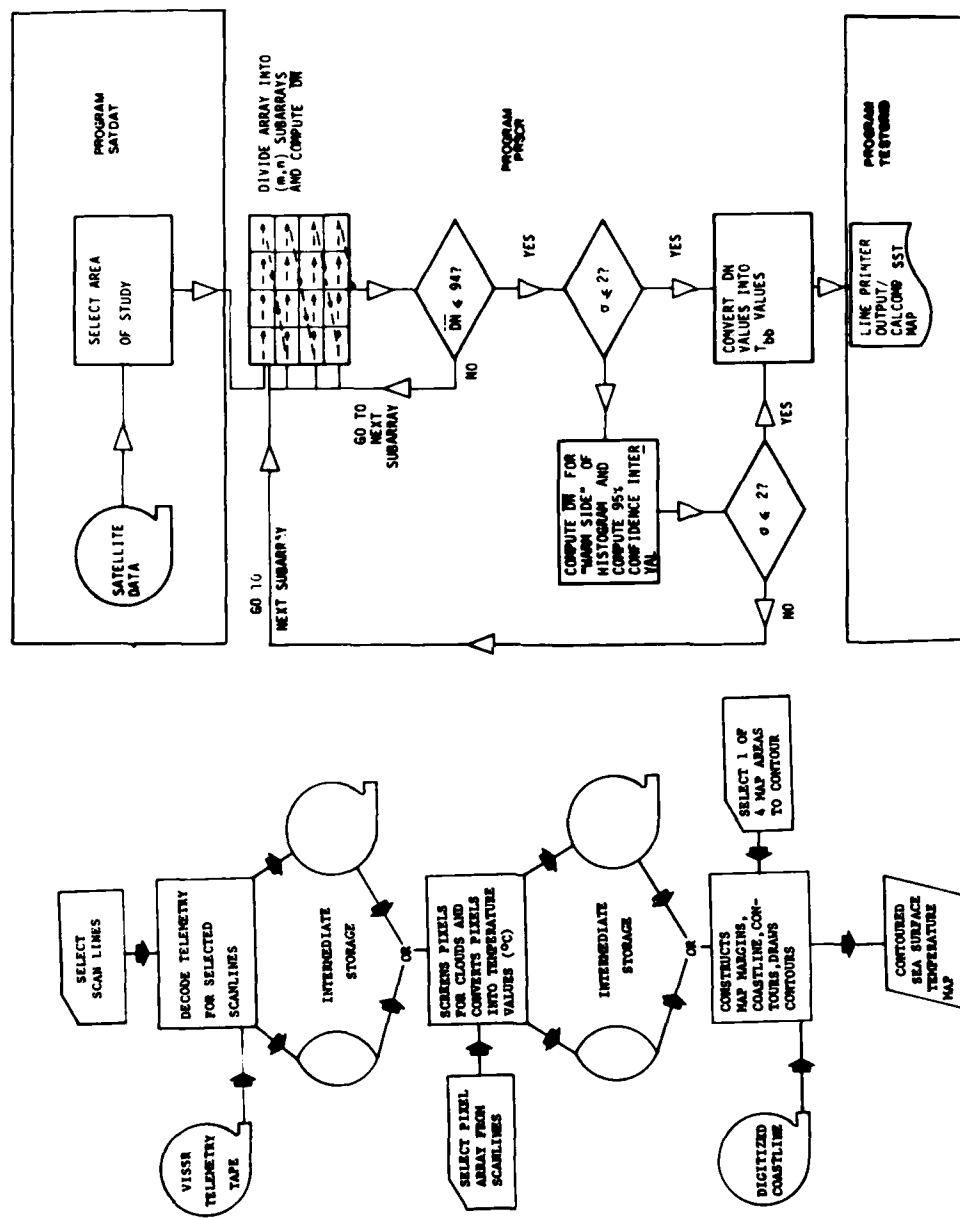
Figure 2. Flow and logic diagrams of three programs used to produce contoured sea surface temperature charts.

Figure 3.   Infrared VISSR image for August 2, 1979. Data
            from image used to generate temperature fields
            shown in Figures 4-7.
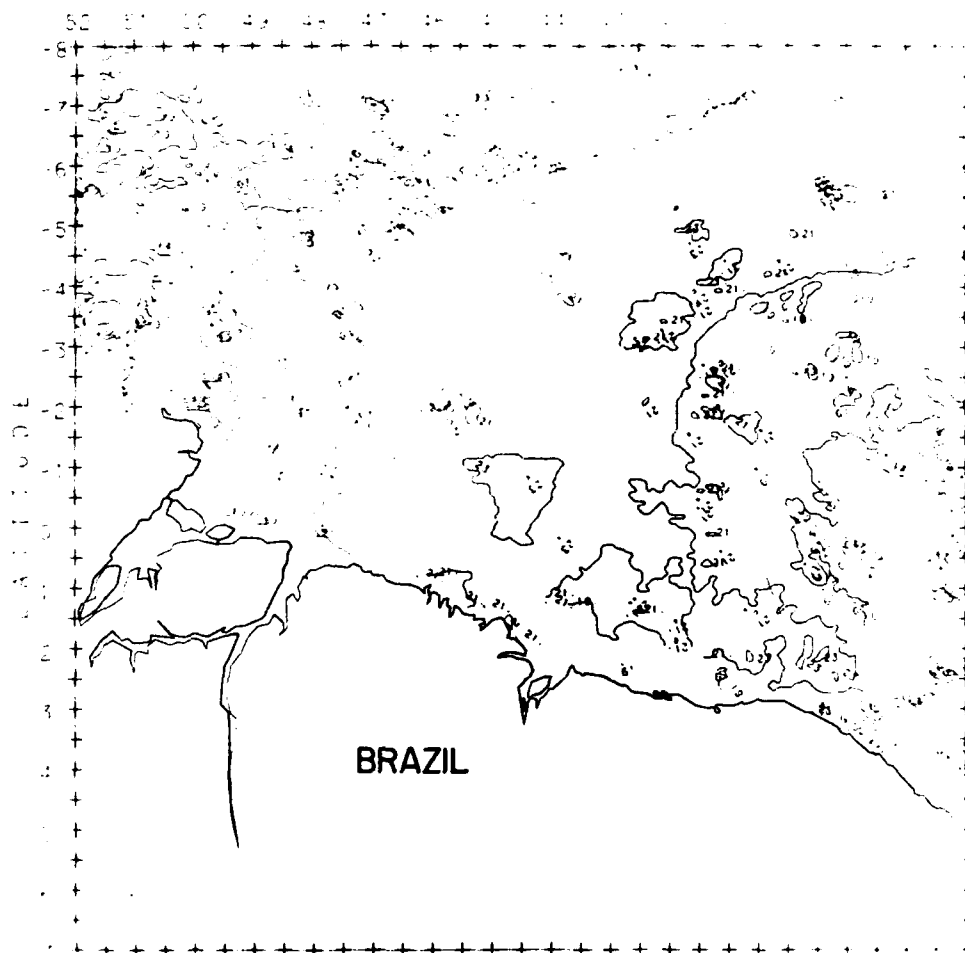
Figure 4. Sea surface temperature chart for northernmost area of
Brazil for August 2, 1979.
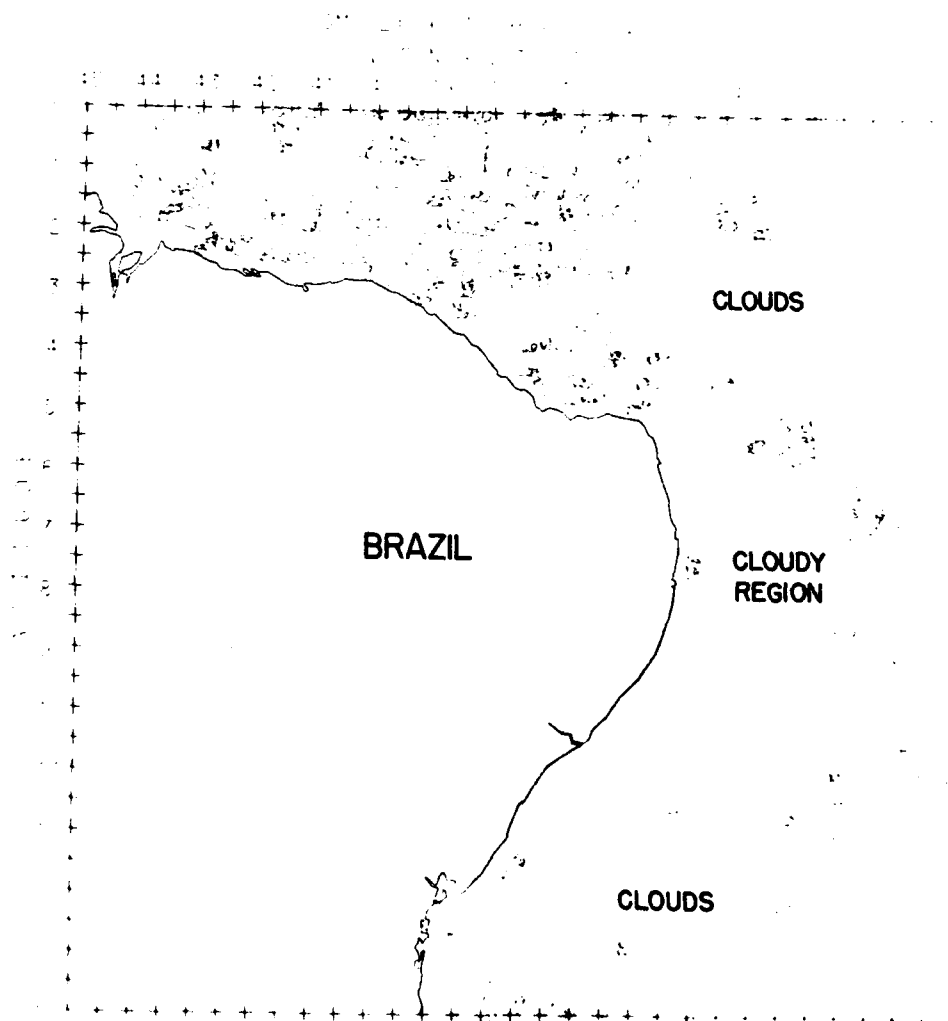
Figure 5. Sea surface temperature chart for northern area of Brazil for August 2, 1979.
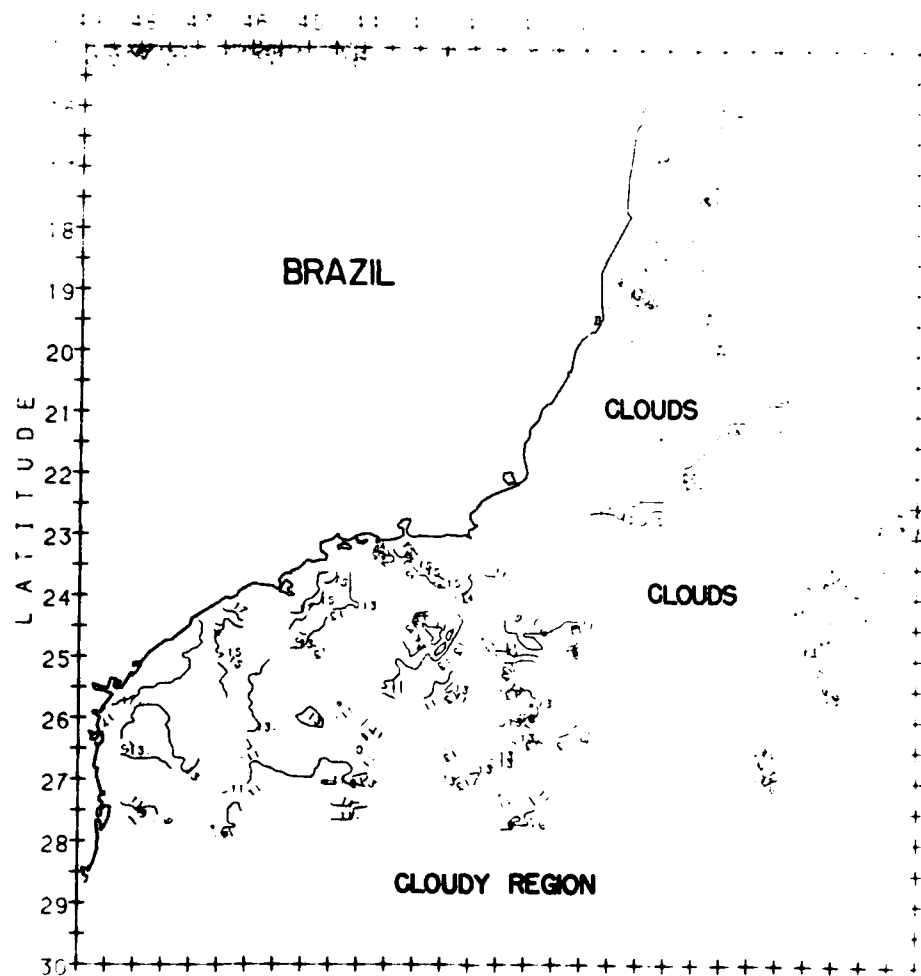
Figure 6. Sea surface temperature chart for southcentral area of Brazil for August 2, 1979.

713
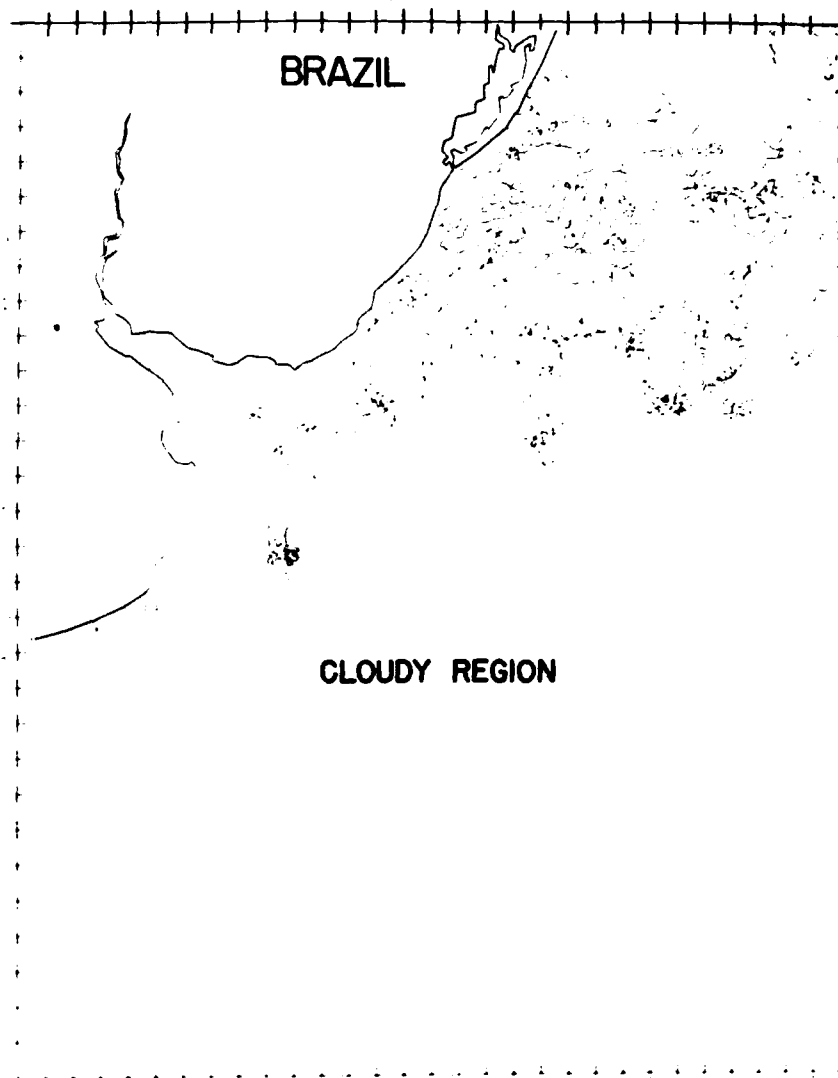
Figure 7. Sea surface temperature chart for southernmost area of
Brazil for January 7, 1981.

714

DEVELOPMENT OF A METHODOLOGY TO LOCATE
AND EVALUATE SUPERFICIAL THERMAL ANOMALIES
USING AIRCRAFTBORNE MULTISPECTRAL SCANNERS

J.A. Espejo and
M.C. Fernández-Luanco

Empresa Nacional ADARO de Investigaciones
Mineras, S.A.

J.L. Díez

Universidad Complutense de Madrid

M. Kindelan and
A. García

IBM Scientific Center

Madrid, Spain

ABSTRACT

_? A methodology is presented capable of suppling in a semi-auto
matic manner information regarding the location, shape, dimensions
and absolute and relative surface temperatures in areas with   geo
thermal anomalies.

The data acquisition system used has been an aircraft borne M
2S Multispectral Scanner form Bendix, mounted on a CASA 212   air
craft. This sensor collects data in 11 wavelength bands   including
a thermal infrared one at wavelengths between 8 and 14 μm.

The region selected as a test site has been the west half of
the Lanzarote Island which possesses interesting geothermal charac
teristics and of which there exist a large amount of data.

The results obtained form the scanner data make it possible -
the detection and study of surface anomalies and the elaboration -
of a map of thermal anomalies. ←

1.- INTRODUCTION

The objective of this work is to develop a methodology capable of   sup
plying in a semi-automatic manner information regarding the location, shape,
dimensions and absolute and relative surface temperatures in areas with geo
thermal anomalies. This information is used to detect areas of potential geo
thermal interest to be investigated in greater detail.

The region selected for this study corresponds approximately to   the
west half of the Lanzarote Island, which possesses interesting geothermal   -
characteristics. Furthermore, there are a large amount of existing data   re

garding this area, so that its selection as test site appears to be well jus
tified.

The data acquisition system has been an aircraft borne M2S   Multispec
tral Scanner from Bendix, which collects data at 11 wavelength bands,   inclu
ding a thermal infrared band between 8 and 14 μm.

The results obtained from the data supplied by the multispectral   scan
ner, after correction of the environmental and geological thermal   effects,
make it possible the detection and study of surface anomalies which may   be
related with more important thermal sources located deep in the ground.   The
proposed methodology is applicable to any geothermally anomalous.

2.- METHODOLOGY

The prospection of regions of geothermal interest, using aircraft borne
remote sensors active in the thermal infrared region of the spectrum, is   a
well established technique in constant development, which takes advantage of
the benefits derived from the digital storage and processing of the informa-
tion.

Digital processing of the data gathered provides great flexibility in -
the visualization, filtering, smoothing, enhancement and other techniques   -
used to facilitate the investigation of an image from different points   of
view matched to some particular interest.

Furthermore, using digital processing it is possible to use   mathemati
cal and physical models to correct the distortions introduced by the   effect
of the environment, using data measured directly in the zone under study.

3.- PROCEDURE

3.1.- IN SITU DATA GATHERING

3.1.1.- Radiometric Data

Data regarding the thermal infrared radiation emitted by the terrain we
re obtained using an M2S multispectral scanner form Bendix, owned by the   Na
tional Institute of Aerospace Technique (I.N.T.A.), and mounted on a CASA   -
212 aircraft from the Spanish Air Force.

The area was from during the night, with approximate direction SO-NE, -
and covering the area between 13° 35' west longitude and 13° 50' west longi-
tude over Lanzarote Island.

I.N.T.A. processed the HDDT obtained by the M2S and provided the corres
ponding computer compatible tapes (CCT).

3.1.2.- Air Photography

Simultaneously with the flight, a complete photographic coverage of the
area was obtained during the day, using a metric camera and flying in appro-
ximately the same direction. As a result 260 photographs were obtained,which
represent the area under study at a scale of approximately 1:6000.

3.1.3.- Surface Temperatures

Monitoring of the surface temperature history and assistance with ther-
modynamic matters, has been carried out by the Department of Mechanics   and
Thermodynamics of the School of Physics in the Universidad Autónoma in   Ma
drid.

During the time of the flight, the surface temperature was measured   -
with the following two objectives:

- To determine the time at which the surface temperature variations be
  come small. This condition is necessary in order to relate surface -
  temperature and ground thermal flux.

- To obtain in situ the surface temperature distribution (ground truth)
  in order to adjust the data provided by the M2S.

The data obtained in Lanzarote may be classified in the following items:

- Sea surface temperature: due to its large thermal inertia, these data
  provide a common reference for the whole flight, and may be used   to
  check the accuracy of the M2S calibration.

- Surface temperature in similar lithologies: these data obtained at di
  fferent topographic altitudes, are used to correct the effect of the
  atmosphere.

- Surface temperature in different lithologies: these data obtained at
  approximately the same topographic altitude, are used to analyze the
  data in relationship to the lithologic characteristics.

- Surface temperature in previously known geothermically anomalous   -
  areas: these data are used for an a priori evaluation of the   anoma
  lies.

- Surface temperature evolution in a certain point: these data are used
  to check the thermal stability of the ground during the time of the
  flight.

- Wind induced surface temperature cooling: these data were used to eva
  luate the effect of forced convection in different lithologies, in or
  der to analyze the thermal response of the ground.

- Temperature in a certain point: these data were used as a global refe
  rence for the whole flight.

The temperature measurements were obtained with platinum thermistors Pt
-100 provided by the Department of Mechanics and Thermodynamics, and were ca
librated using standard resistances. The calibration was performed before -
and after each measurement to eliminate any systematic errors. In this way -
the estimated errors are smaller than $0.2°$ K.

3.1.4.- Surface Geology

Before the flight, a survey of the surface geology was carried out in -
order to know the main lithologies present in the area under study. In parti
cular the differences in emissivity and thermal characteristics of the mate-
rials were analyzed.

717

In general, it may be concluded that the present morfology in Lanzarote is determined by the surface distribution of volcanic origin materials, covered in some areas by other materials of sedimentary or chemical origin, particularly "caliches". The surface geology may be roughly summarized as follows:

- Tabular succession of basalts with different ages but with similar thermal responsivities. These materials posses an intermidiate conductivity and emissivity.

- Lavas resulting from different eruptions, which constitute what is generally called "Malpaís". These materials posses a low emissivity and conductivity.

- Pyroclastic products with fine granulometry which posses a conductivity and emissivity larger than those of lavas and basalts.

3.1.5.- Meteorological Data

Meteorological data gathering was carried out by the Geophysics Department of the Universidad Complutense in Madrid, using a moveable station. These data, obtained simultaneously with the flight, provide information on the meteorological parameters up to 600 m. above the observation point. These parameters include:

- Air temperatures used to correct the effect of the atmosphere on the surface temperature, and to deduce the location of the inversion layer with respect to the topography.

- Relative humidity to correct the effect of water vapor absorption on the infrared region of the spectrum.

The observation sites chosen were the Arrecife airport and the town of Tinajo, located in the extremes of the region under study.

Data gathering was performed at two o'clock in Tinajo and at 3 o'clock in Arrecife, since it was necessary to leave the airspace free during the flight.

In addition, the average humidity of the atmosphere was obtained at 12 o'clock using an absorption photometer, in order to calibrate the meteorological data.

3.2.- DATA PROCESSING

The data obtained by the M2S were stored in CCT's of 6250 BPI. All the data of one flight are contained in ten files, which are stored in a total of 3 and 1/3 tapes.

These data are processed at the UAM/IBM Scientific Center using an interactive image processing system made up of a RAMTEK image display terminal, and an IBM 3277 display station linked to an IBM 370-158 computer system. The software used has been developed in this Center and among other possibilities includes image enhancement, color density slicing, line pixel plot, statistics and histograms of selected areas, ...

3.2.1.- Visualization

As a first step, the data provided by the sensor are visualized in the image display terminal in order to topographically locate the different - flight paths. This visualization is carried out using sub-images of 1024 x 1024 pixels at a time, and since each file contains approximately 20,000 li nes, it is necessary to visualize 200 subimages in order to locate completely the flight.

The information of the M2S is coded in 256 gray levels (8 bits), which can be transformed to a temperature scale in degrees, whose extreme values - are determined by the black body temperatures are adjusted before each - flight in relationship with the expected temperatures of the terrain.

3.2.2.- Identification of Topographic References

In each sub-image a set of topographic references (roads, towns, coast-line, ...) are established in order to determine exactly on the map the di rection and width of each path of the sensor.

3.2.3.- Geometric Correction

The M2S images contain important geometric distortions associated to - the panoramic effect and to the movements of the aircraft. As a first step - the panoramic effect is corrected in all the images thus obtaining data with geometric characteristics similar to those of a map. To carry out a more pre cise correction capable of partly removing the geometric distortions associa ted to the movement of the aircraft, a set of ground control points are loca ted on the panoramically corrected images, and a polynomial fit is performed. This polynomial is then used to geometrically correct the image using the - nearest neighbour technique.

3.2.4.- Location of Thermal Anomalies

The M2S data are then analyzed in order to locate points, lines and re-gions which exhibit a thermal contrast with the surrounding region. Using a temperature difference of 1° C with respect to the surrounding area, a rough catalog of anomalous areas is obtained. From this catalog, those anomalies - which are of a human activity origin (roads, houses, factories, ...) are - eliminated.

3.2.5.- Elaboration of a Catalog of Anomalies

The catalog of anomalies previously obtained has been used as a basis - for an in situ survey. This survey was performed to confirm the origin of - each detected relative anomaly, neglecting those due to differences in ther-mal emissivities of similar materials (see map).

The resulting catalog of anomalies includes its coordinates, its tempe-rature and the temperature of its surrounding area. Therefore, it is possi ble to infer the thermal characteristics of the materials present.

3.3.- DATA CHECKING

3.3.1.- Comparison of the Temperature Data Obtained in the Ground Simultaneously with the Flight, with those Obtained with the M2S

This checking was necessary in order to calibrate the M2S sensor, and - in order to evaluate the possible effect of the atmosphere on the resulting measurements.

3.3.2.- Study of the Geological Characteristics of the Area and Comparison with the Data Obtained by the Sensor

It appears from the thermal infrared emission measured, that differen ces in lithology with its corresponding differences in thermal emissivities may have produced differences in observed temperatures. Therefore, it is ne cessary to consider the lithologic characteristics of the area under study , in order to correctly interpret the data provided by the M2S.

3.3.3.- In Situ Geothermal Prospection

As a final check, the anomalies found in the previous steps were analy-zed in situ, in order to classify them according to its etiology. This check was carried out using the appropriate instrumentation to identify all the thermal effects responsible for the observed behaviour.

4.- RESULTS AND CONCLUSIONS

. Different lithologies result in different thermal responses, due to the differences in thermal inertia of the materials. It is interes ting to observe the apparent anomaly produced by small basalt areas - surrounded by pyroclastic products. These areas are easily identified on the images.

. It is important to point out the behaviour of the regions which show a temperature 2° C above that of its surrounding area, which may be identified as a specific behaviour of that material with respect to infrared radiation.

. Industrial, human and biologic activity produce a local increase in - energy which shows an atypical thermal behaviour frequently coupled - to an important increase in noise level.

. The sea is a very stable thermal system with very small temperature - variations.

. The anomalies whose existence was previously known in Parque del Ti manfaya and other sites of the island have been confirmed and their - structure better understood. These anomalies are highly contrasted - with the background and show clearly the general structure of the su perficial geothermal field.

. Using the catalog of anomalies a map of thermal anomalies has been - drawn.

At the present time we are working on the following items to complete this work:

. Geometric and topographic correction of all the images using ground - control points.

720

. Elaboration of a global map of isothermal lines to be superposed   to
  the topographic map. To this end we are completing a mosaic of all   -
  the images obtained.

. Correction of the atmospheric effects using atmospheric models deter-
  mined from the meteorological and thermal data obtained simultaneous-
  ly with the flight.

REMOTE-SENSING OBSERVATION OF GLACIERS

TOWARDS THEIR MONITORING

A. Della Ventura

I.F.C. - C.N.R.
Milano, Italia

R. Rabagliati

IBM Italia
Mestre, Venezia, Italia

A. Rampini

I.F.C. - C.N.R.
Milano, Italia

R. Serandrei Barbero

I.S.D.G.M. - C.N.R.
Venezia, Italia

ABSTRACT

The knowledge of glaciers dynamics
has a great social impact for energy
production, so that a continuous monitoring
is desirable.

The object of this work is to show how
the application of pattern description and
recognition techniques to remote-sensed data
may help in overcoming the difficulties
related to the present surveying methodolo-
gies, integrating traditional measurements.

The data investigated are images from
Landsat MSS concerning the Disgrazia group
(Central Alps) at the end of ablation period
in three different years.

The radiance values of the four bands
were compared with data from the Istituto
Geografico Militare (IGM) maps at scale
1:25,000 and stereo aereal photographs.

The analysis of different glaciers
exposed to the sun, glacier borders and
shaded areas allows the definition of the
glacier identification program.

The second step was the automatic
description of the contours of the
interesting objects in a specialized lan-
guage (a subset of english language).

The analysis carried out on the images recorded in three different years has produced descriptions in which some invariant structures, such as the glacier limit with rocky walls can be observed.

The invariant subset of glacier descriptions is the base for the construction of a ground control point table for the automatic registration of different images.

The multitemporal comparison allows the observation of surface variations and the recognition of transient snow line positions.

1. INTRODUCTION

Alpine glaciers act as hydrologic resources and as climatic indicators on a regional scale. In spite of their importance, only a hundred of the 837 Italian glaciers, are directly checked. Measurement campaigns are made by the Comitato Glaciologico Italiano at the end of each ablation season.

During this campaign, the height of the transient snow line is recorded and front fluctuations measured. Moreover on two Alpine glaciers (1.Zanon, 1976) researches are being carried out on the mass balance.

The transient snow line, delimiting the area with snow cover against the area free of snow, at the end of the ablation period is identical with the equilibrium line and closely related to the mass balance. Data concerning both equilibrium line and frontal positions are related to the knowledge of annual and perennial ice and snow masses and to the estimate of hydrologic power on a short and long term. In view of this it is desirable to extend the knowledge of these parameters to larger areas.

The glaciers variations may be monitored by satellite remote sensing, if the variations exceed satellite resolution. With the present resolution the annual surface fluctuations of the majority of Italian glaciers are detectable (2.Rabagliati and Serandrei Barbero 1979).

The multispectral image of the Ventina glacier (Disgrazia group, Central Alps, Italy) recorded on September 13, 1975 was compared with the August 14, 1977 image using its fixed structures, represented by the borders versus rocky walls of the accumulation basin in the sunny area (3.Della Ventura et al.,1981).

In the present study, besides the Ventina glacier, adjacent formations belonging to the Disgrazia group are investigated. A comparison between September 13, 1975, August 28, 1978 and September 4, 1980 is made to verify their surface variations due to the expansion stage still in progress, and to recognize the transient snow line.

To this purpose, software instruments have been implemented which allow the identification of the interesting areas in the multispectral images. The subsequent integration of these images with the topographic and altitude data allows the estimate of glacial surfaces and the association to the identified structures of the corresponding glaciological terms.

2. INVESTIGATED GLACIERS

Investigated glaciers extend from 46° 16' 40" and 46° 15' 19" N and 2° 42' 45" and 2° 4o' 20" W. They pertain to the Disgrazia group, which lies

724

in the Central Alps, about 100 km NNE of Milan (Fig.1). The chosen area extends from Mount Disgrazia peak (3678 m a.s.l.) towards the south and the east. The highest glacier in the studied area is the Cassandra whose accumulation basin reaches 3500 m a.s.l.; the lowest one is the Ventina glacier whose front, exposed to the north, flows down to 2200 m a.s.l..

All the studied glaciers pertain to the 2nd order hydrological basin of the Adda River, tributary of the Po River. Some data about the investigated glaciers, as described in the Catasto dei Ghiacciai Italiani (C.G.I. 1959-1962), are reported in Table I. The highest heights of glaciers were deduced from the topographic map; the lowest ones were accorded to heights measured during the glaciological campaigns.

3. ANALYZED DATA

Invariant structures of investigated glaciers were recognized using the Istituto Geografico Militare map at a scale 1:25,000 compiled in 1935. On this map the positions of advancing or retreating fronts in examined years, provided by the Comitato Glaciologico campaigns, were added and the projected shade cones on glaciers surfaces of neighboring mountain ridges drawn.

Stereo aereal photographic coverage of September 1962 was also available for the whole area. The flight altitude was 5,000 m providing photographs with an approximate scale of 1:12,000, useful in recognizing detailed topographic features and shaded areas. (Fig.4)

With the purpose of comparing cartographic images and Landsat data, a grid was manually superimposed on the map, using the angle between Landsat orbits and the meridians and, as a reference point, borders versus rocky walls of the glaciers facing the sun (3.Della Ventura et al.,1981).

Three Landsat MSS scenes from September 13, 1975, August 28, 1978 and September 4, 1980, near the end of the ablation season, were selected: the images were first processed to correct the 6-line stripings due to the non-linearities of the brighteness transfer characteristics and non-matching of the sensors. The applied method consists in identifying a homogeneous area large enough to find systematic repetition of the six sensors saturation radiance. These values were normalized to the maximum by computing the multiplicative coefficients, one for each line and the whole image was corrected by mutiplying each line by its corresponding coefficient.

It was observed that in the image taken in 1975, the sensors were saturated in all four bands corresponding to the ice surfaces facing the sun, and the systematic repetitions are easily identified; in 1978 and 1980 images, the radiance values are much lower and the systematic repetitions are un-identifiable in all the bands. In this case we left the radiance values unchanged. No other destriping algorithm was applied so as not to reduce those radiance discontinuities which allow the identification of glaciers and of their internal structures.

Histograms for the years 1975, 1978 and 1980 of the Disgrazia glaciers window are shown in Fig.2. The reduction of high radiance values (225-255 range) on glaciers is evident from 1978 and 1980 histograms. This is partly due to high atmospheric absorption in 1978 and 1980 and partly to the sensors characteristic variation.

725

4.   IDENTIFICATION OF GLACIAL SURFACE AREAS

The following analysis has been carried out using band 5 and band 7 containing the informations on external boundaries and internal structures of glaciers according with (3.Della Ventura et al.,1981),(4.Haefner,1979),(5.Pagliari and Rossi,1980).

To obtain a better discrimination of the glaciers areas with respect to the background, band 5 was multiplied by band 7 and normalized to the maximum value of band 5 in order to facilitate the multitemporal comparison of images. In Fig.3 are reproduced the Ventina glacier radiance cross-sections of bands 5 and 7 and their product. The product line shows a greater resolution in the glacier radiance range. This technique, even if magnifying the radiance errors can be utilized, as in our case, if it is sufficient the discrimination of radiance variations in the more significant radiance digits which are independent of the introduced error.

The obtained image is then subdivided in strips for which statistical parameters (mean and median) were computed. On the basis of the value of these parameters, different threshold functions combined among themselves through logical operators were identified (6.Brambilla et al.,1980) and applied to the various image strips.

The comparison of the images of 1975, 1978, 1980 is shown in Figures 5, 6, 7. All the glaciers reported in Table I are identified in three years images. In the 1975 the high radiance values recorded on the glaciers bodies exposed to the sun (histograms of Fig.2) made uncertain the identification of the Disgrazia glacier n.419. This is due to its exposition (north) in nearly grazing light and to the large number of crevasses which highly reduce the radiance.

The transient snow line is localized in the maps of Figures 5, 6, 7 as the boundary between the two pixel classes used for the glaciers identification. The transient snow line from 1975 to 1980 maps appears to move towards higher altitudes in good agreement with experimental observations carried out during the glaciological campaigns. The computed surfaces are reported in Table II: the computation is carried out only to obtain qualitative check of the glacier identification procedure. The computed figures are obtained using the mean inclination of the glaciers included in Table I and are in good agreement with the glacier surfaces there reported.

5.   STRUCTURAL DESCRIPTION OF GLACIERS

In the maps of Figures 5, 6, 7 the identified glaciers are objects (blobs) in which it is possible to recognize morphological structures such as ramifications from a central body, inlets, rectilinear or indented margins. The definition and the recognition of these structures are effected by linguistic pattern recognition methods through devices implemented as production systems (7.Bianchi et al.,1981).

The description of the Ventina glacier oserved in 1975 is obtained assigning to the recognized structures the corresponding glaciological terms in accordance with the altitude data furnished to the system with the digital data. (Fig. 8)

The search for fixed structures for the ground control point table construction is made comparing the descriptions obtained in different years. For example, in the descriptions referring to two years of the Ventina glacier, of which only the part covered with snow has been considered, because less subjected to variations, the fixed structures are the inner rocky outcrop and

726

the boundary of the accumulation basin with the rocky wall (Fig.8b and 8c).
With these reference points it is possible then to compare the moving struc-
tures for the extraction of information such as the advance or retreat of the
fronts and the equilibrium line positions.

6. CONCLUSIONS

The Disgrazia glaciers have been identified in the Landsat images of
September 13, 1975, August 28, 1978 and September 4, 1980.

The identification algorithm defines the glacier contours and the tran-
sient snow line positions on the glaciers. The identified transient snow line
positions seem agree with their higher heights observed during the glaciologi-
cal campaigns of 1975, 1978 and 1980. The automatic glacier description allows
the identification of invariant structures to be used for Landsat images reg-
istration. The glaciers surface has beeen computed with the pixels belonging
to the different identified objects using the mean glacier inclination
according to the Catasto dei Ghiacciai Italiani. This approximate surface
evaluation allows a preliminary test of the identification algorithm. The
computed surfaces agree with the present advancing front phase, even if snow
covering may yeld larger surfaces.

The Landsat images registration obtained by the invariant glaciers struc-
tures will allow the computation of the glaciers surface variations in the
ablation area. These yearly computed surface variations and identified tran-
sient snow line positions will help in a better forecast of the long and short
term hydrological resources.

7. REFERENCES

1.Zanon G.,1976,"Fluctuations of the Italian glaciers and some remarks on
      their recent trends" Italian Contributions to the 23th International
      Geographical Congress, CNR, Roma.
2.Rabagliati R.,Serandrei Barbero R.,1979,"Possibilità d'impiego del remote
      sensing da satellite per il controllo annuale dei ghiacciai" Geografia
      Fisica e Dinamica Quaternaria 2, 35-40 9 ff, Torino.
3.Della Ventura A.,Mussio P.,Rabagliati R.,Rampini A.,Serandrei Barbero R.,
      1981,"Determination of the spectral signatures of a glacier" Internatio-
      nal Cclloquium on spectral signatures of objects in remote sensing,
      Avignon,INRA vol.5 pp.477-485.
4.Haefner H.,1979,"Digital mapping of mountain snowcover under european
      conditions" Operational applications of satellite snowcover observations,
      NASA Conference Publication n.2116 pp.73-92.
5.Pagliari M.,Rossi G.,1980,"Considerations sur les rapports entre le climat
      et les variations volumetriques des glaciers: Marmolada et Careser
      (Alpes Orientales)" Atti XVI Congrés International Méthéorologie Alpine.
6.Brambilla P.,Della Ventura A.,Mussio P.,Rampini A.,1980,"Classificazione
      esplorativa di dati da telerilevamento" XX Convegno sullo Spazio, Roma.
7.Bianchi S.,Della Ventura A.,Dell'Oca M.,Mussio P.,Rampini A.,1981,"An APL
      pattern-directed module for bidimensional data analysis" APL 81 Conference
      Proceedings, APL Quote Quad vol.12 n.1 pp.54-61.
8.UNESCO IASH,1970,"Perennial Ice and Snow Masses. A guide for compilation and
      assemblage of data for a world inventory" Techn.Pap.in Hydrology 1,Paris.
9.Comitato Glaciologico Italiano,1959-1962,"Catasto dei Ghiacciai Italiani"
      1-4, Torino.
10.Comitato Glaciologico Italiano,1976,"Relazione della campagna glaciologica
      1975" Bollettino del C.G.I. n.24.
11.Comitato Glaciologico Italiano,1979,"Relazioni della campagna glaciologica
      1978" Rivista di Geografia Fisica e Dinamica Quaternaria n.2 (2).
12.Comitato Glaciologico Italiano,1981,"Relazioni della campagna glaciologica
      1980" Rivista di Geografia Fisica e Dinamica Quaternaria n.4 (2).

8. FIGURES AND TABLES
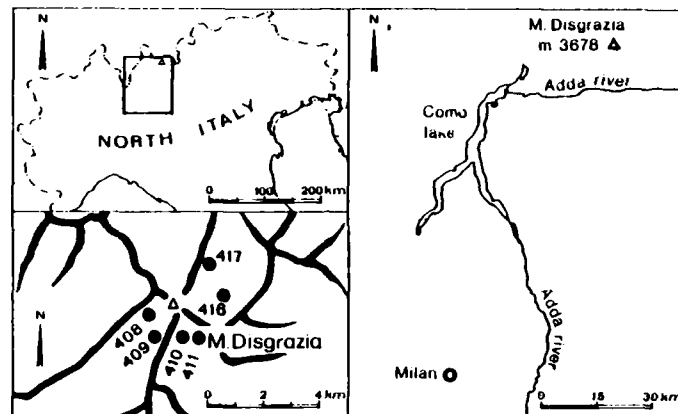
Figure 1. Location of investigated glaciers (see Table I)
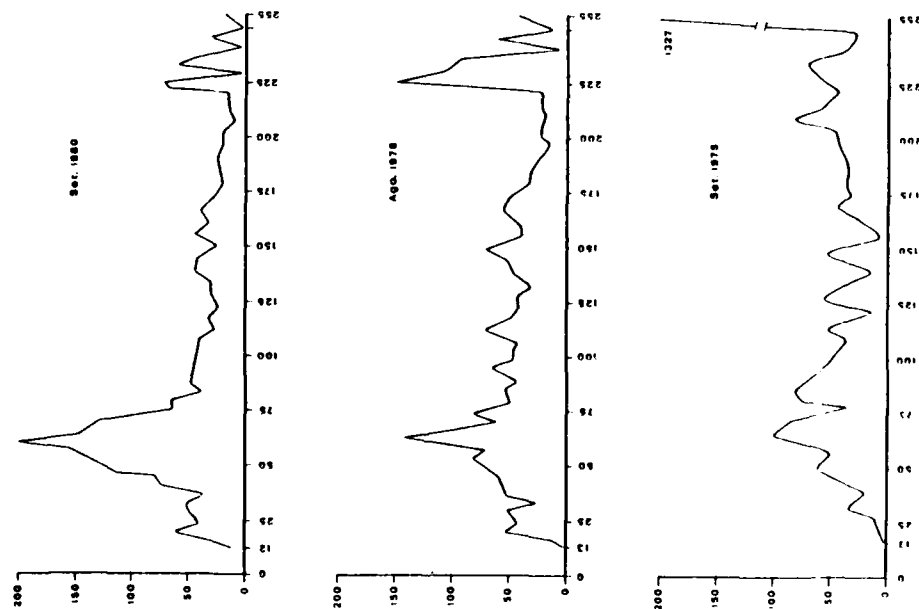
Figure 2. Radiance histograms of a Disgrazia glaciers window showing
the reduction of high radiance response in 1978 and 1980

728
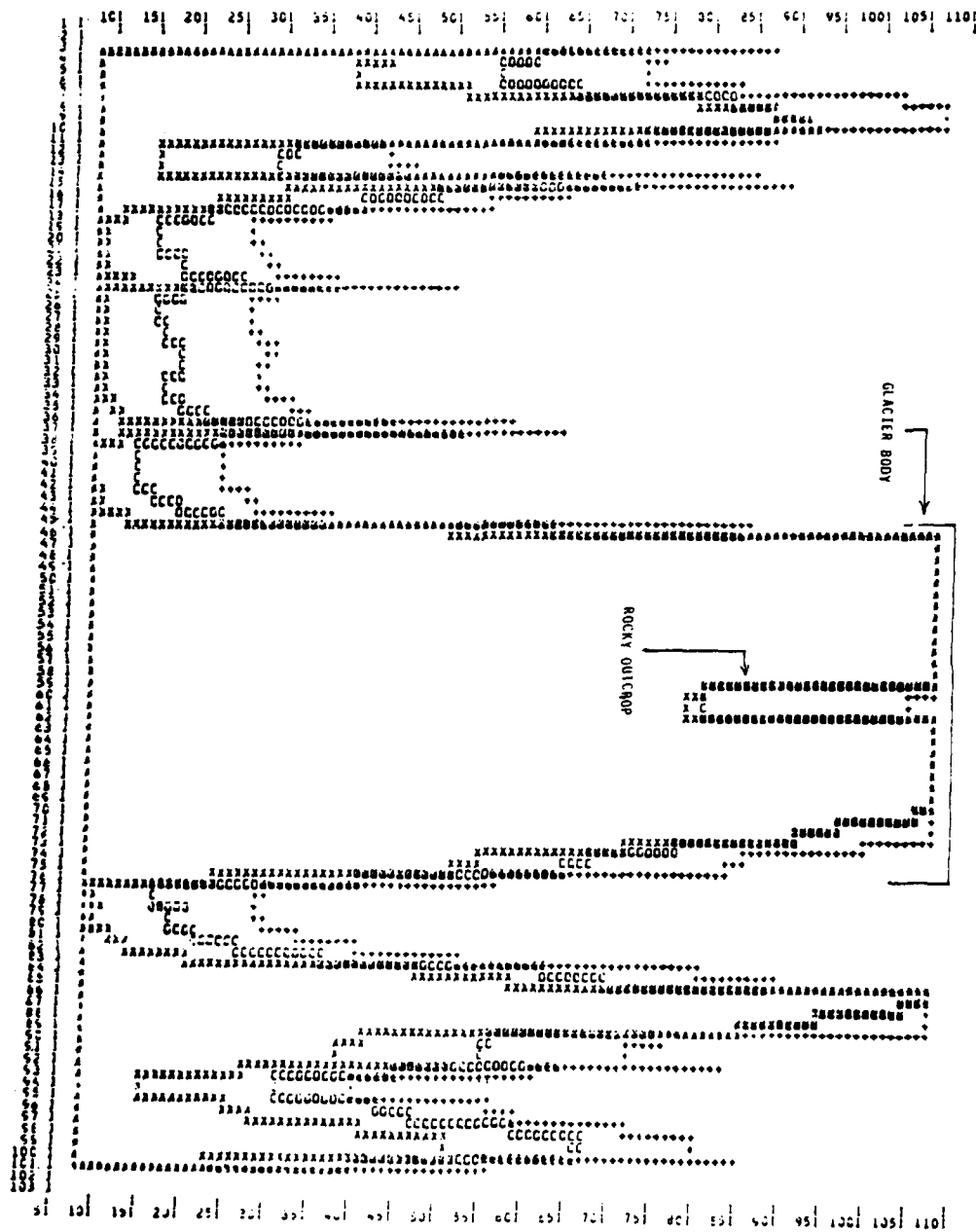
Figure 3. Radiance cross-sections along a horizontal line through
the Ventina glacier

(· :band 5   o :band 7   x :(band 5 x band 7)/band 5)

729
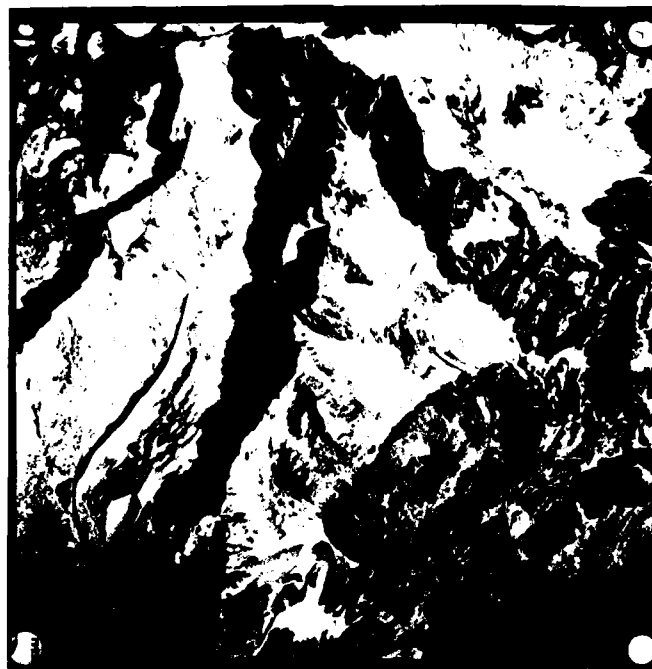
Figure 4.   Stereo aereal photography of the southern glaciers
in the Disgrazia group
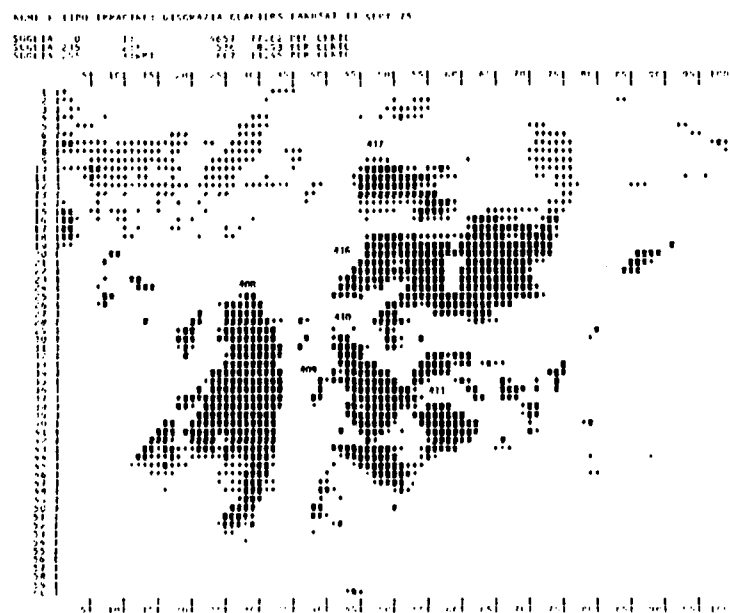
Figure 5.   Grey level map of the processed multispectral image
recorded on September 13, 1975

Figure 6.   Grey level map of the processed multispectral image
recorded on August 28, 1978

Figure 7.   Grey level map of the processed multispectral image
recorded on September 4, 1980

731
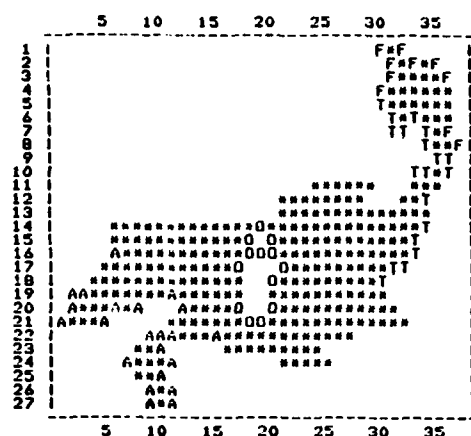
8a

DESCRIBE X75MAX

INTERNAL ROCKY OUTCROP WITH CENTER   IN 18 19
TONGUE FROM 10 33 TO 18 30
FRONT FROM 4 30 TO 8 37
ACCUMULATION BASIN RAMIFICATION FROM 20 8 TO 16 6
ACCUMULATION BASIN RAMIFICATION FROM 22 15 TO 19 11
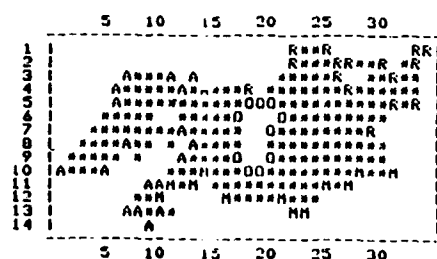
DESCRIBE X75RID   8b

INTERNAL ROCKY OUTCROP WITH CENTER   IN 7 19
RAMIFICATION FROM 4 18 TO 4 27
RAMIFICATION FROM 2 30 TO 7 29
INDENTED MARGIN FROM 10 31 TO 12 10
ACCUMULATION BASIN RAMIFICATION FROM 13 10 TO 7 12
ACCUMULATION BASIN RAMIFICATION FROM 8 7 TO 4 14
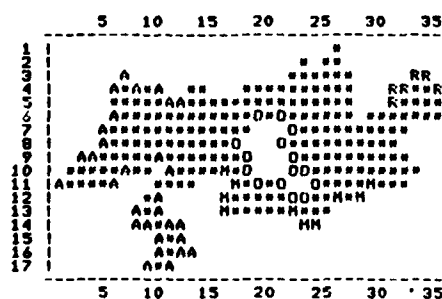
8c

DESCRIBE X78

INTERNAL ROCKY OUTCROP WITH CENTER   IN 9 20
RAMIFICATION FROM 3 31 TO 4 35
INDENTED MARGIN FROM 11 29 TO 10 16
ACCUMULATION BASIN RAMIFICATION FROM 12 10 TO 9 10
ACCUMULATION BASIN RAMIFICATION FROM 10 7 TO 8 5
ACCUMULATION BASIN RAMIFICATION FROM 7 5 TO 5 12

Figure 8.   Structural descriptions of the Ventina glacier

(8a : whole image in the 1975; 8b : glacier snowcover
in the 1975; 8c : glacier snowcover in the 1978.
The contour vertices belonging to recognized structures
are marked with the corresponding initial letters.
In the descriptions the couples of numbers are the
pixel coordinates in the beside window.)

8.2 TABLES

Table I. Data about the investigated glaciers

Glacier number C.G.I.	Glacier name	Type(1)	Highest glacier elevation m a.s.l.(2)	Lowest glacier elevation m a.s.l.(3)	Surface area(4) Km^2	Inclination °C	Orientation (4)
408	di Predarossa	valley	3400	2560 (1974)	0.88	19°	SW
409	di Corna Rossa	mountain	3250	3000	0.035	30°	W
410	Cassandra Occidentale	mountain	3150	2760 (1974)	0.22	27°	SSE
411	Cassandra Orientale	mountain	3500	2680 (1974)	0.40	13°-30°	SSE
416	della Ventina	valley	3450	2200 (1977)	2.1	17°	N
417	del Canalone della Vergine	mountain	3250	2900 (1977)	0.25	27°	ENE

(1) after the classification in "Perennial Ice and Snow Masses"(UNESCO-IAHS, 1970)
(2) the highest glaciers elevations are obtained from the topographic map
(3) the lowest glaciers elevations are accorded with the data measured during the glaciological campaign in the years 1974, 1977
(4) from "Catasto dei Ghiacciai Italiani" (C.G.I., 1959-1962)

Table II. Computed surface areas

Glacier number C.G.I.	Glacier name	Surface area Km^2 Sept. 1975	Surface area Km^2 Aug. 1978	Surface area Km^2 Sept. 1980
408	di Predarossa	1.081	0.985	1.052
409	di Corna Rossa	0.046	0.051	0.036
410	Cassandra Occ.	0.293	0.313	0.368
411	Cassandra Orient.	0.492	0.516	0.641
416	della Ventina	1.854	1.940	2.024
417	del Canalone della Vergine	0.470	0.515	0.566

SATELLITE STUDIES OF FRONTAL INTERACTIONS
AT THE MOUTH OF THE LA PLATA RIVER

D.A. Gagliardini*
H. Karszenbaum*

Centro Argentino de Estudios de Radiocomunicaciones
y Compatibilidad Electromagnetica
Buenos Aires, Argentina

R. Legeckis

NOAA-NESS
Washington, DC

V. Klemas

College of Marine Studies
University of Delaware
Newark, Delaware

SUMMARY

Estuaries serve as spawning and nursery grounds for many important species of fish and shellfish as well as being the conduits through which nutrients pass into productive coastal waters. Also, estuaries and coastal waters become subject to a number of sources of environmental stress: industrial thermal and waste discharges, sewage imputs from the great and small coastal cities, and spills of oil and other materials associated with maritime transport. At the same time all these phenomena depend on the dynamics of estuaries and the dynamics are strongly dependent on frontal systems. Therefore, no serious effort to model circulation dynamics and pollutants transport in most bays and estuaries can be done without the knowledge of previous studies of frontal systems.

The La Plata River is a large shallow estuary found at 35° south on the coast of South America. It covers 35000 sq km and is 270 km long. Its width varies from 32 km in the upper region to a maximum of 230 km in the lower region which are considered the theoretical river boundaries. The water mass is formed by the junction of Parana and Uruguay Rivers which drain the rain off the second largest hydrographic basin in South America after the Amazonas River. The frontal system formed by the interaction of these water masses and the ocean water vary with tides, currents and winds. Tides produce marine water movements in the estuary, and the saline water penetrates much more at the northern shore than in the south. The incoming tide is deflected toward the south coast producing there the greatest tidal amplitude. The main currents are dominated by tides and river flow which are strongly interrelated. Tidal currents follow the astronomical tide with some retardation due to friction and river flow influence. Wind systems, particularly from west to south, have relevant importance in the dynamics of the estuary; they modify the predicted tides, retarding or advancing them. These forces also produce changes in currents and salinity. Therefore, it

is evident that the frontal system is strongly variable with time and metereo-logical conditions and to study it, it is convenient to get a synoptic view in real-time. Remote sensing from satellites gives the possibility of doing this type of measurement. The objective of this work was to study this front and its variability using remote sensing techniques.

The water masses of the La Plata River differ from those of the South Atlantic Ocean from an optical and thermal point of view. These properties have been analyzed for this study. Information from Landsat and NOAA satellites has been used, the first one for the optical bands and the second for the 10.5 - 12.5 µm thermal infrared band. Of particular interest was the information corresponding to the 10/31/75 and 01/29/76 overpass dates, since for these dates there exists data from both satellites.

Thermal and turbidity maps were obtained showing that differences in color and temperature can be observed between the ocean and the river water masses. In this way the fronts between these two water masses and their variability have been studied. It is also shown that this type of work can be of considerable value in studies of tidal currents, suspended sediments and pollution plumes in the river.

AD P002049

HYDROGEOLOGICAL EVALUATION OF QATAR
PENINSULA USING LANDSAT IMAGERY AND GEOPHYSICAL DAT.

MOHAMED A. YEHIA
University of Qatar, Doha, Qatar

I.E. HARHASH
Agricultural and Water Research Department
Ministry of Industry and Agriculture, Qatar

ABSTRACT

The application of image processing techniques to landsat
satellite images proved to be of major significance in the
evaluation of the hydrogeological situation in Qatar peninsula.
The images are correlatable with the geophysical resistivity
maps of the peninsula. The latter reveal the presence of two
major hydrogeological provinces of different character. The
landsat images showed the structural lineation patterns and
geomorphological features which are important in the hydrogeo-
logical studies. This implies that such images are useful in
updating the Qatar hydrographic charts.

1. INTRODUCTION

The present consumption of water for all purposes in Qatar amounts to
102 million cubic meters per annum made up of 70 MCM of groundwater and 32 MCM
of distilled sea water. Due to the rapid economic growth of the country and
its consequent demands on freshwater supplies, we are forced towards elaborate
investigation using every up-to-data sophisticated tool to help us in solving
our water resources problems. The remote sensing technology is one of these
tools which we tried.

The present work deals with the hydrogeological evaluation of Qatar
peninsula (Fig. 1) using landsat imagery *and geophysical data **. The images
in this work, were produced by digitally processing magnetic tapes recorded
over Qatar peninsula using the MDAS Systems in the remote sensing center in
Cairo, Egypt. Electronic color density slicing image was prepared using the

---

*   Processed and analyzed by Qatar University

**   Carried out by Agriculture and Water Research Department
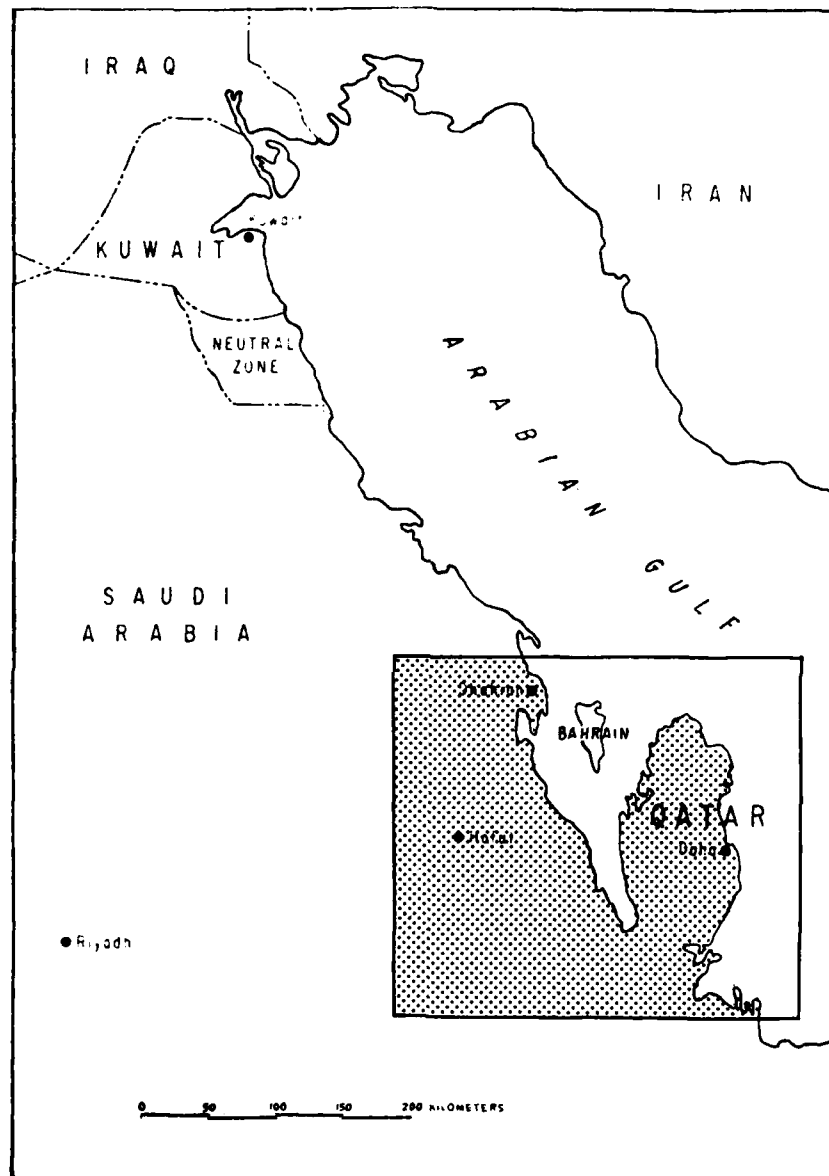
FIG (1) LOCATION MAP

equidensitometer procedure adopted by Steiner et al (1975). In this procedure, the density range is subdivided into a number of intervals and a distinct gray level is assigned to each interval, that is, the density of each image point is replaced by the value of the level into which it falls. The slicing procedure can be expanded to include color enhancement. In this case, each density level is assigned a particular color. Furthermore, color component densities (i.e. blue, green, red densities) can be extracted from color imagery and translated into full spectral range of colors.

Groundwater possibilities in Qatar have been explored since 1959 using different geophysical techniques. These techniques were summarized by the FAO* (1981). Seismic and gravity surveys did not give much information about the regional and national hydrogeology of the peninsula. The electric resistivity method, on the other hand, gave valuable information, it showed that the Qatar peninsula can be subdivided into a northern and southern hydrogeological provinces (Fig. 2). The uppermost part of the succession in the northern province is represented from top to bottom, by : (i) dry surface rock; (ii) limestone containing fresh water, and (iii) conductive medium made up of limestone with a saline water. The uppermost part of the succession in the southern province, on the other hand is made up of : (i) dry surface rock; (ii) an aquifer zone include the Rus Formation and the upper part of Umm er Radhuma Formation, and (iii) compact dry rock of low resistivity.

Isoresistivity map (Fig. 3) constructed by Seltrust**(1980) revealed a zone of highly conductive material ($<$ 6 ohm.m) surrounds Qatar, generally between 5 and 15 km wide; forming the coastal belt. This belt is narrow in the northern and northeastern parts of Qatar, it is wider at the western coast, the areas of the Dukhan Sabkhas, north and west of Doha and along the southeastern coast, and much wider at the southern border. In large part, this depicts the major sabkhas and low lying saline, coastal flats. However, salt flats do not represent a geomorphic feature in the north. The irregular shape of the northern part of the higher resistivity, along a line between Al Khour and Al Zubarah, is also indicative of breakdown in the otherwise regular progression of the isoresistivity contours inwards from the coastline. The center of the zone of highest resistivity also shows a shift westwards from the axis of the peninsula due to the greater development of agriculture in the east than in the west causing a decline in the fresh water reserves and their displacement by more saline groundwater. In the southern province, the apparent resistivity map shows a complex pattern of isolated resistivity areas.

739

FIG(3) NEAR-SURFACE APPARENT RESISTIVITY
(from Airborne Survey by Geoterrex Ltd)
(IDTC;1980)
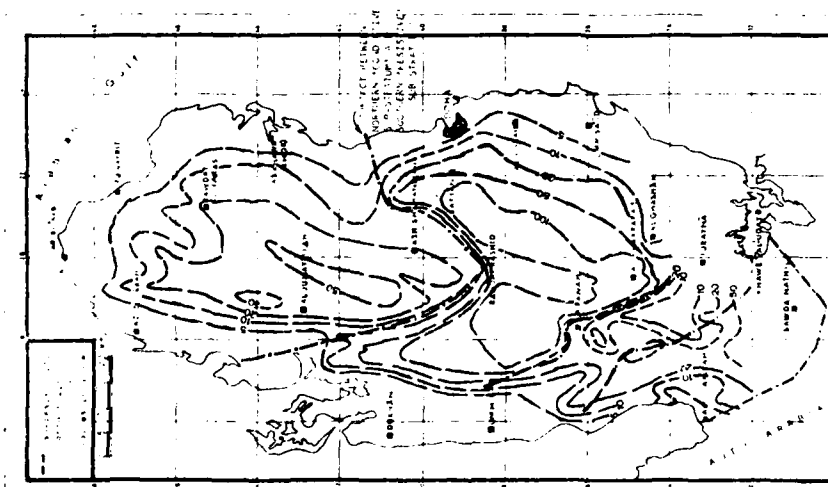
FIG(2) RESISTIVITY MAP
(FAO; 1981)

740
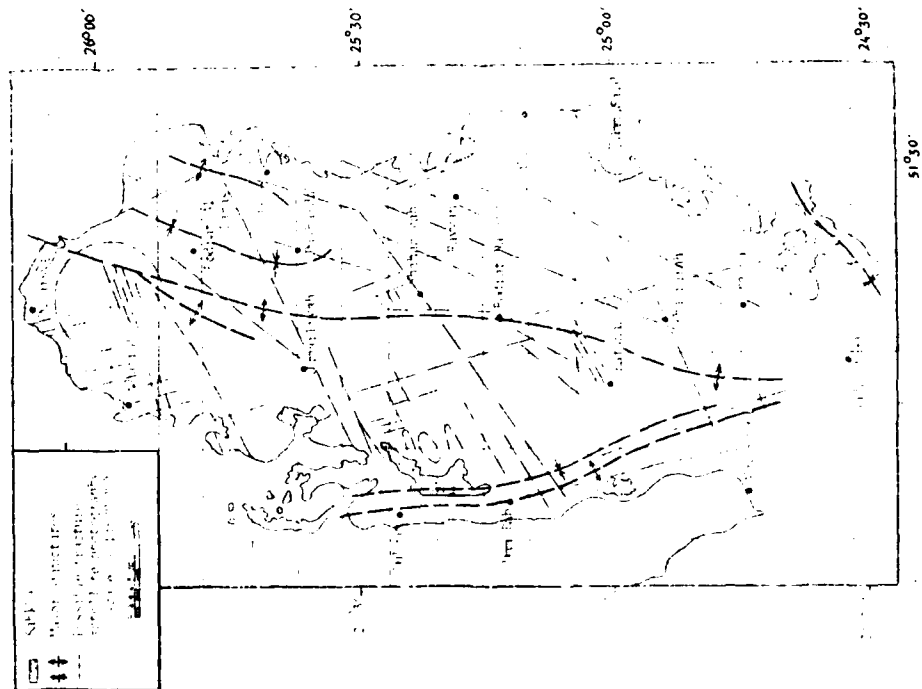
FIG (4) TOPOGRAPHIC MAP

Depressions & Wadies | | Sabhhas

Hammdas [ ] Sand accumulation

Jebel & Ridges

FIG(5) GEOLOGICAL STRUCTURES

Morpho-geological Characteristics of the Peninsula

Analysis of the landsat images provides geomorphological and geological information which are important not only for the understanding of the relation between structural aspects and aquifer occurrences but also for the recognition of the changes in the interaction factors. The analysis revealed that the surface of Qatar peninsula is of low to moderate relief with a highest evalu-ation of 103 m above sea level, where mesa type hills and large barchan type sand dunes serve to break the monotony of an otherwise flat eroded landscape. The lowest part of the peninsula is at a level of 6 m below sea level (15 km south-east of Dukhan). The following is a summary of the main landforms (Fig. 4) which can be recognized in Qatar (Yehia, et.al.,1982) :

(A)	Low-lands	:	A.1 Depressions
			A.2 Wadies
			A.3 Sabkhas
(B)	Up-lands	:	B.1 Hammadas
			B.2 Ridges and Jabels
			B.3 Sand accumulation

The surface stratigraphical succession in Qatar is composed of Tertiary limestones and dolomites with interbedded clays, marls and shales covered in places by a series of Quaternary and Recent surfacial deposits. The oldest rocks exposed in the peninsula are the limestones of the Rus Formation (lower Eocene), although the most widespread outcrops are the dolomites and crystalline chalky limestone of the upper Dammam Formation (middle Eocene). The Dam Forma-tion which was deposited during the middle and late Miocene, consists of marls and sandy limestones in its lower part and limestone with minor clay and sand intercalated with evaporites in its upper part. The Mio-Oligocene Hofuf Formation is conglometric with a calcareous cement. Quaternary and surfacial deposits in Qatar are very widely distributed. They consist mainly of beach conglomerates, pseudo-oolitic and conglomeratic limestones and sands. Silts are present as internal drainage deposits in differently-shaped depressions. Eolian sands in the form of sheets and dunes cover the southern part of Qatar and extend to the south-eastern coastal plain.

Structurally, the peninsula is a broad anticline. This anticline is accompanied with two major structural lineation patterns trending NE-SW and NNW-SSE. These were originated as tension fractures during uplift of the Qatar arch (Fig. 5).

2. RESULTS

The obtained landsat data were analysed electronically and visually. Fig. 6 shows a color slice image of the northern and central parts of Qatar produced by the processing of bands 4 and 5 electronically. The image reveals two major color zones; a yellow one in the north and a red one in the south. Less significant light and dark green spots and patches are also observed especially in the yellow zone. The yellow and red color zones reflect the morpho-geological characteristics of the peninsula. The yellow zone (province I) is correlatable with the table Eocene limestone with its chara-

Fig. 1 Electronic color slice image over the northern and central parts of the State of Qatar. Color variations are mainly due to the morpho-geological features. This image demonstrates the value of color slicing for increasing data yield; the V-shape boundary between the red and yellow colors is mainly due to the intersection between the main NE – SW and NNW – SSE fracture patterns.

cteristic karst topography, (the latter is represented by the light green patches and spots). The red zone (province II), on the other hand, represents the surfacial and unconsolidated sediments covering the Eocene limestone. The dark green patches represent the sabkha deposits.

Combined visual investigation and field studies were used to construct a geomorphological map of scale 1:200,000 (Fig. 4) of Qatar. The visual analysis was carried out on bands 5 and 7, together with color composits. The analysis depended mainly on two factors, (i) water features (drainage, seepage ....etc.) and (ii) character and areal distribution of rocks (types of rocks, stratigraphy and structures, relation of rock units to surface water bodies ...... etc.).

Based on the above-mentioned investigations, it was possible to evaluate the hydrogeological aspects of the main rock units in the peninsula. The following is a summary of this evaluation :

1. **Soil and Surfacial Deposits**

   The soil cover which overlies the bedrock is mainly thin and even lacking in many places; thus it is not important as a reservoir.

2. **Carbonate Rocks**

   The carbonate rocks cover about 80% of the surface of the peninsula. They are important reservoir rocks. The main characteristics of these rocks are given below :

   2a. **Karst Topography**

   Collapse and dolinas sinkholes are dominant in the limestones. These are characterized by internal drainage system which is important for the water accumulation. Karst topography was formed during the Pleistocene pluvial period; thus it is considered to be Fossil karst.

   2b. **Table Rocks (Hammadas)**

   These cover most of the surface of the peninsula. Sink holes occupy a considerable part of the northern region of the peninsula, while largely diminishes to the south. They are characterized by fine external dendritic drainage.

   Fractures, solution openings and dolomitization are more abundant in the limestones of the northern part of Qatar. This makes these lime-stones more attractive for underground water investigations.

3. **Unconsolidated Sediments**

   These are dominant in the Qatar peninsula. The most characteristic water feature of these unconsolidated sediments is the lack of external drainage systems. These sediments are represented by :

   3a. **Sand Dunes**

   These are well-sorted barchan sand dunes having north-east trend. They have rapid internal drainage. The fact that sand dunes are important as water reservoirs, in case of presence of an obstruction to the free drainage (Picard, 1953), makes further detailed investigation on the sand dunes of Qatar a very urgent objective.

744

3b. Sabkhas

These are arid lake deposits of fine sand, silt, clay and salts
accumulated in depressions or lowlands. The distribution of such
deposits is shown in Fig. 4. These deposits are not so attractive
for hydrogeological investigations.

4. Coastal Plains

These are characterized by intense fracturing which makes it good areas for
water accumulation. However, the presence of saline drainage reduces its
importance.

3. DISCUSSIONS

Comparison between resistivity maps and the map constructed in the present
work based on the landsat image (electronic color slicing) reveals considerable
matching (Fig. 7). Both maps show the presence of two main hydrogeological
provinces; the northern and southern provinces. However, the color slice image
reveals more details which are not obvious in the resistivity maps. The
northern province, for instance, includes some areas having characters resembl-
ing these of the southern province (e.g. Fwairat and El-Arish), due to simila-
rity in their morpho-geological features. Moveover, scattered light and dark
green spots and patches in the northern province representing the karst topo-
graphy and sabkhas are clearly seen in Fig. 6. The high moisture content of
these areas results in the absorption of some of the electromagnetic spectrum
resulting in different signatures. This explains the yellow zones surrounding
the green patches present in parts of the southern province.

The previous geophysical investigations (FAO, 1981) revealed that the
V-shaped facies boundary divided Qatar peninsula into two hydrogeological
provinces may be due to deep faulting. A V-shaped boundary separates a condu-
ctive zone from resistive one. This V-shaped boundary coincides with a major
facies division in the Rus Formation (lower Eocene). The same boundary has
been easily detected in the color slice image. It is thought to be a result of
intersection between two fracture systems trending NE and NNW-SSE. It is
worth-mentioning that similar, but more faint, V-shaped boundaries have been
recognized in the image (color slice) in other locations of the peninsula.
This may support the view that these boundaries signify structural features
rather than changes in the facies characteristics.

The above discussion clearly shows that the landsat images can be of much
benefit in detecting and evaluating the different hydrogeological aspects of
Qatar especially during the preliminary stages of investigation. Moreover,
they provide useful tool for the monitoring of the hydrographic changes.

The Present Work,1982

The Northern Province(I)

The Southern Province (II)

Depressions & Wadies

Sabkhas

Rus Formation Facies and Province Delineation

(FAO 1981)
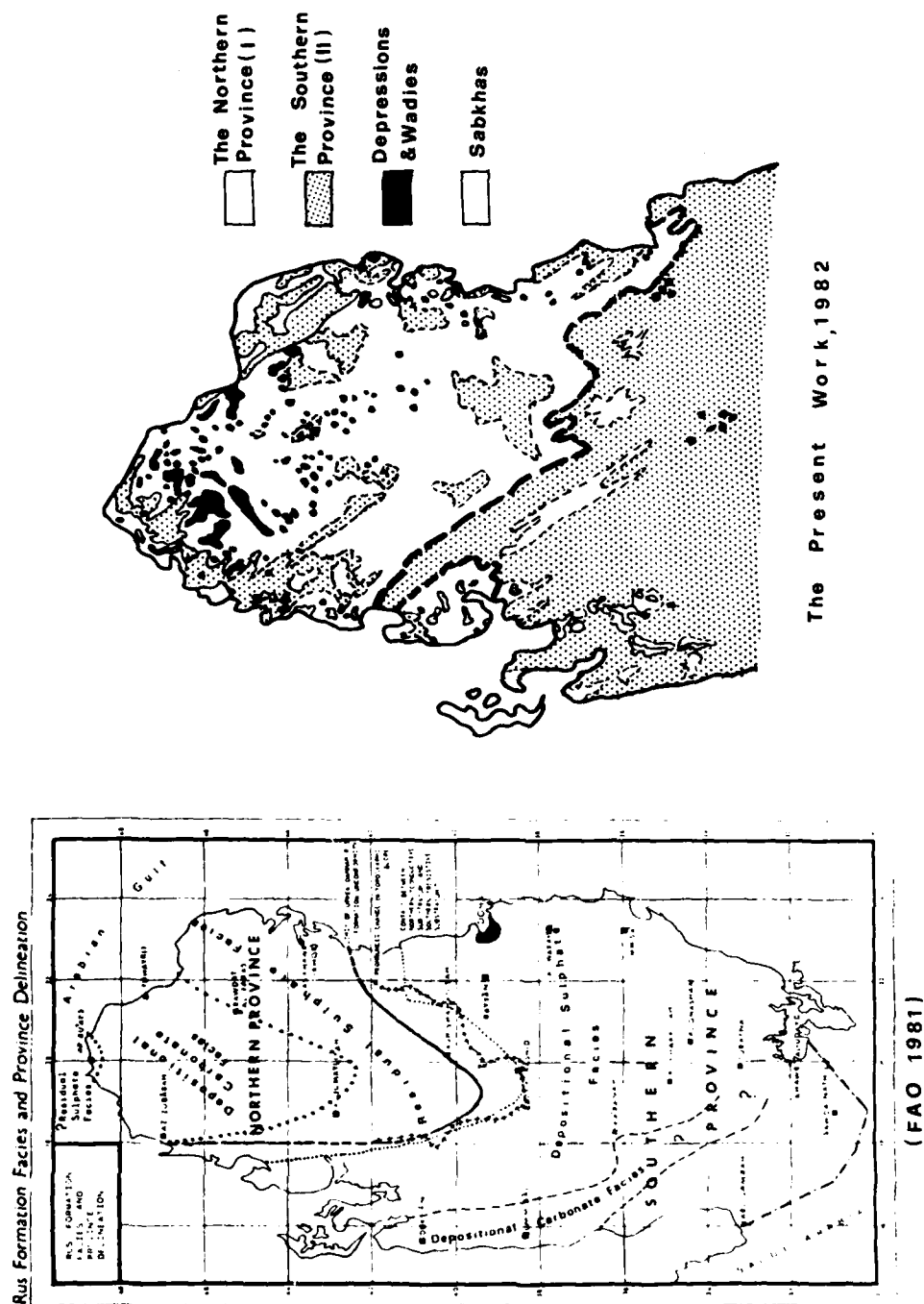
Fig. 7   Correlation chart between the electrical resistivity zones and the map constructed in the present work based on the color slicing image.

4. REFERENCES

Eccleston, B.L.; Pike, J.G. and Harhash, I.; 1981 - The Water Resources of Qatar and their development, Vol. I, FAO, Doha, Qatar.

IDTC, 1980 - Qatar Geological Map and Exploratory Booklet, Seltrust Eng. Ltd. Govt. of Qatar.

Picard, 1953, Outline of Groundwater Geology in Arid Regions, Ankara Symposium Unesco.

Steiner, D.; Salerno, A. 1975, Manual of Remote Sensing, Vol. 1, Am. Soc. of Photogrammetry.

Yahia, M.A., Harhash, I. and El Harouni, M., 1982. Landsat Image Investigation of major Surface Structures, Topography and Hydrology in Qatar - 1st Thematic Conference "Remote Sensing of Arid and Semi Arid Lands, Cairo, Egypt.

AD P002050

DEVELOPMENT OF A REMOTE SENSING-AIDED DIGITAL

DATABANK FOR LARGE SCALE LAND USE PLANNING*

Siamak Khorram**

North Carolina State University
Raleigh, NC 27650 USA

ABSTRACT

The primary objective of this investiga-
tion was to combine remotely-sensed data with
ground-acquired data in development of a pro-
cedure specifically for selection of a site for
urban development and generally for large scale
land use planning. The performance of this
investigation was aided with direct participa-
tion and close cooperation of the resource
managers of the U.S. Forest Service at Plumas
National Forest and Plumas County Planning
Department. The study area, jointly selected
by the resource managers and researchers, is
approximately 500 km² in size and covers the
Frenchman Reservoir basin in northeastern
part of the Sierra Nevada Mountains in Cali-
fornia.

The approach involved a spatially-refer-
enced databank based on both remotely-sensed
and ground acquired data. The remotely-sensed
data included Landsat Multispectral Scanner
(MSS) data, NOAA-5 satellite Very High Reso-
lution Radiometer (VHRR) data, and U-2 color
infrared photography. The ground-acquired data
included USGS topographic maps, Defense Mapping
Agency (DMA)/USGS digital terrain data, soils
maps, vegetation data, and accessibility maps.

A series of mathematical models were
developed to generate: 1) net radiation
based on total incoming solar radiation, tem-
perature, vegetation, slope, aspect, and
cloud cover; 2) potential evapotranspiration
based on a model using temperature and radia-
tion; 3) potential timber growth rate; 4) de-
velopability based on potential timber growth
rate and accessibility; and 5) potential
residential suitability based on developability
and slope.

The results included a series of color-coded maps of the same coordinate system for the final outputs as well as the intermediate products. The final outputs were developability and potential residential suitability (with individual septic tank systems) maps. The intermediate products were useful in the assessment of resource conditions and resource management when overlayed or combined with other data types such as geologic maps, political and geographic maps (e.g., ownership, zoning, general plan), and water resources-related maps. These intermediate products included a series of maps with respect to net radiation, elevation, slope, aspect, vegetation, potential evapotranspiration, and potential timber growth rate.

Based on our findings, it was concluded that: 1) spatially-referenced databank proved to be very useful in combining the data of various kinds, viz., satellites, aircraft, conventional maps, and ground truth to achieve the desired results; 2) Landsat MSS data were very useful in vegetation mapping; 3) DMA/USGS digital terrain data provided adequate database for topographic analysis; 4) NOAA-5 satellite data provided a good means of mapping surface termperature; and 5) remote sensing proved to be very useful in providing the required data for large scale land use planning.

1. INTRODUCTION

With the increase in population and economic growth, the pressure on the existing resources of the State of California continues to increase, thus requiring accurate and current information on land use and land cover. The accurate maps of resource-related parameters such as soils, elevation, slope, aspect, and vegetation are essential for a well-developed land use planned for the identifying and regulating of criitical areas. The data on timber production capacity of land in wildland areas play an important role in the urban development planning. Timely, repetitive and cost-effective remotely-sensed data combined with conventional tabulated and map form data can provide the required information for large scale land use planning.

The officials of the Plumas County Planning Department in northern California were considering to select an area that would be highly suitable for urban development as well as being located within the commuting distance from the city of Reno, Nevada. Besides the available maps and data with respect to soils type and permeability, availability of water, and ownership, there was a need for additional data (in map form) on the capacity of land for timber production, the accessibility, and the slope of the entire study area for selection of an area for urban development.

The research discussed in this paper, funded by a NASA Grant NGL-05-003-400 describes the procedures that were used for the development and utilization of a spatially-referenced digital databank to provide the required spatial data for selection of urban development site(s) by the Plumas County Planning Department. These maps included intermediate maps such as slope, ownership, soils type, and potential timber growth capacity as well as final maps of land developability and potential residential suitability. All of these maps were of the scale of 1:62,500 in color-coded transparency forms and of the same registration (coordinate system).

Objective:

The objective of this investigation was to combine remotely-sensed data with conventional tabulated and map form data in development and utilization of a procedure for providing the spatial data to be used in large scale land use planning. The performance of this investigation was aided by the direct participation and close cooperation of the resource managers of the U.S. Forest Service at Plumas National Forest and the personnel of the Plumas County Planning Department. The results of this study was designed to be used by the County Planning Department primarily for selection of an area for urban development and generally for land use planning. The urban development was aimed at providing a bedroom community for the city of Reno, Nevada.

Study Area:

The study area, selected jointly by the resource managers and the investigators, covers approximately 500 km^2 extending from latitude 39° 45' to 40° 30' North and 120° 00' to 120° 35' West. This area, located in the upper part of the Middle Fork of the Feather River Watershed along the northeastern edge of the Sierra Nevada Mountains in California, is within the commuting distance (approximately 40 ± 12 miles) of the city of Reno.

2. MATERIALS AND METHODS

The approach involved the development and utilization of a spatially-referenced digital databank based on both remotely-sensed data and conventional tabulated and map form data. Types of remotely-sensed data included: 1) Landsat Multispectral Scanner (MSS) data; 2) NOAA-5 Satellite Very High Resolution Radiometer (VHRR) data; and 3) U-2 color infrared photography. The conventional

ground-acquired data included: 1) U.S. Geological Survey (USGS) topographic maps; 2) Defense Mapping Agency (DMA)/USGS digital terrain data; 3) "ground truth" data composed of land cover, vegetation type and density, timber-producing capacity based on tree age and height; 4) soil plant available water; and 5) ownership and accessibility maps.

The final products were defined as a Land Developability map and a Potential Residential Suitability map of the study area. Both land developability and potential residential suitability maps, produced to the scale of 1:62,500, were designed to be visually overlayed onto the ownership map and soils permeability map of the same scale and the same registration for planning purposes. In this section, the spatially-referenced databank, the models for generation of both land developability and potential residential suitability maps, and the preparation of the required input parameters for these mathematical models are discussed.

I. Spatially-Referenced Digital Databank

The databank used in this study was a storage and retrieval system, known as MAPIT, developed by personnel of Remote Sensing Research Program. In this system, remotely-sensed data, map-based data, and ground-acquired data for a given geographic area may be stored as "profiles." "A profile represents a relationship between a point and some attribute or condition of that point. The point is described by an X, Y coordinate pair and the attributes belonging to that point are usually referred to as its Z values." (Remote Sensing Research Program's E.D.P. Unit Info. Note 73-4,1974). Typically, MAPIT may handle any number of profiles for an area.

Structurally, MAPIT consists of a number of distinct programs controlled by the user to accomplish a number of tasks related to manipulating, interpolating and displaying area data. Mathematical models, such as those used for preparation of some of the input parameters as well as the final products in this study, that require a variety of areal inputs reside in and use MAPIT data storage and organizing capabilities.

II. Model for Generation of Land Developability Map

The criteria for land developability models were based on Table I as recommended by the Plumas County Planning Department.

A four-class accessibility map of the study area was combined digitally with a map of potential growth rate, as an indicator of timber-producing capacity based on tree age and height, of the study area to generate a six-class land developability map. The form classes used ranged from Class I (representing the most developable) to Class VI (representing the least developable) areas. The procedures used for preparation of accessibility map and potential growth rate map are discussed later in this paper.

III. Model for Generation of Potential Residential Suitability Map

The criteria for potential residential suitability model were based on Table II as also recommended by the Plumas County Planning Department.

The land developability map, discussed earlier in this paper, was combined digitally with a four-class slope map to produce a potential residential suitability map of the study area (assuming that the residents would need to be equipped with septic tank systems). In this way, a potential residential suitability map composed of 8 classes was produced. The form of classes used ranged from Class 1 (representing potentially the most suitable land for residential development with individual septic tank systems) to Class 9 (representing potentially the least suitable land for residential development with

752

individual septic tank systems) areas. The procedure used for preparation of slope map is discussed later in this paper.

IV. Preparation of Required Input Parameters for Land Developability and
     Potential Residential Suitability Models

The required input data were accessibility, slope, and timber producing capacity based on potential growth rate.

(a) Accessibility

The four-class accessibility map of the study area, prepared by the Plumas County Planning Department, was digitized in terms of the geographic coordinates and corresponding accessibility, transferred to the Landsat-based coordinate system and stored in MAPIT. The accessibility classes were: Class 1 = accessible during all times of the year; Class 2 = accessible during the summertime with paved roads; Class 3 = accessible during the summer with dirt roads; and Class 4 = not accessible.

(b) Slope

The slope map was computed from the elevation data of study area generated from the DMA/USGS digital terrain data. See U.S. Department of the Interior (1978) for description of digital terrain tapes. The technique for generation of elevation databank included reformatting of the digital terrain tapes into a format compatible with our computer system, determining the boundaries of the study area, selecting the control points, and transferring the data into the Landsat-based coordinate system. To determine the slope, the normal vectors were defined to represent the elevational gradients between each pixel and the four pixels surrounding it. The slope data were then grouped into the slope classes and stored in MAPIT. The detailed procedure for slope mapping used in this study is discussed by Khorram and Smith (1979a).

(c) Timber Producing Capacity Based on Potential Growth Rate

A series of mathematical models were developed and used to compute the tree height/tree age ratio for the timber producing trees existing in the study area. These models were generated from the data collected in 35 sample sites, preselected based on slope, aspect, geology, and vegetative corer of these sites. The final model for estimating the potential growth rate was based on: 1) potential evapotranspiration; 2) aspect; and 3) soil plant avaiable water. For the detailed description of the potential growth rate models see Colwell et al. (1980).

A brief discussion of the input parameters to the potential growth rate model is as follows:

(1) Potential Evapotranspiration

The procedure for mapping potential evapotranspiration (ETp) was based on the Jensen and Haise (1963) model, but modified as necessary to permit it to be applied to a wildland area. The detailed procedure for potential evapotranspiration mapping is discussed by Khorram and Smith (1979c). The inputs to this model were net radiatian and average daily surface temperature.

The net radiation was estimated from a series of mathematical models which in turn were based on solar constant together with data on elevation slope, aspect, latitude, albedo, cloud cover, and surface temperature. The detailed description of net radiation model is discussed by Khorram (1978).

The surface temperature data was based on Very High Resolution Radiometer data obtained from NOAA-5 satellite. This satellite's daytime pass over the

753

study area occurs approximately at 9:30 AM and its nighttime pass occurs approximately at 9:30 PM. The averaged values of these passes, on pixel by pixel bases, was used as the average daily surface temperature. The detailed procedure for surface temperature mapping is discussed by Khorram and Smith (1979b).

(2) Aspect

Likewise the slope, discussed earlier in this section, the aspect map was computed from the elevation databank of the study area generated from DMA/USGS digital terrain data. The aspect data was determined from the normal vectors representing the elevational gradients between each pixel and the four pixels surrounding it. See Khorram and Smith (1979a) for detailed procedure.

(3) Soil Plant Available Water

The soil plant available water values for each soil type within the study area were determined in the laboratory by analysis of the soil samples collected from the 35 preselected sample sites. As described earlier, these sample sites were selected based on slope, aspect, geology, and vegetative cover.

The soils map of the study area was prepared by compiling all available soils data based on three soils maps generated by Soil Conservation Service, the California Department of Water Resources, and U.S. Forest Service personnel on the Plumas National Forest. Information appearing on these soils maps grouped into specified number of classes, digitized, and transferred to the Landsat-based coordinate system. The digital data on soils were then converted into digital plant available water data using the specific plant available water determined in the laboratory for each soil type. See Colwell et al. (1980) for the detailed procedure.

3. RESULTS

The results included a series of color-coded maps each pertaining to: 1) primary input parameters such as soils type and plant available water, potential timber growth rate, slope, accessibility, and ownership; 2) secondary input parameters such as elevation, aspect, surface temperature, net radiation, and potential evapotranspiration; and 3) the final outputs. The final outputs were defined as a land developability map and a potential residential suitability (assuming that residents would need to be equipped with septic tank systems) map of the study area. All of the color-coded maps were produced in positive transparency form and to the scale of 1:62,500. In this way they can be overlayed onto one another and onto other maps of the same scale for resource management purposes. The originals of these color-coded maps were produced by using an electro-optical film writing device called EGOR (Image Ganged Optical Reproducer) designed and built by personnel of the Remote Sensing Research Program of the University of California at Berkeley. These originals were then photographically enlarged to the desired scale. Because of the high publication cost associated with the colored illustrations, these color-coded maps were converted to the black-and-white forms by the Cartography Section of the School of Geoscience of Louisiana State University at Baton Rouge.

The maps of slope, accessibility, timber producing capacity (potential growth rate), land developability, potential residential suitability, and ownership are shown in Figures 1, 2, 3, 4, 5, and 6, respectively.

Because the slope was one of the criterion for determining the potential residential suitability (according to Table II), it was made of four classes. These classes, expressed in percent, were: Class A = 1 to 10%; Class B = 10 to 20%; Class C = 20 to 30%; and Class D ≥ 30%. The results of slope map were verified, Khorram and Smith (1979a).

The accessibility map was composed of the following four classes: Class 1 = accessible during all times of the year; Class 2 = accessible during the summer time with paved roads; Class 3 = accessible during the summer with dirt roads; and Class 4 = not accessible.

The potential growth rate map expressed in height growth in feet per year, was composed of 6 classes: Class 1 = 0.00 - 0.10; Class 2 = 0.11 - 0.30; Class 3 = 0.31 - 0.40; Class 4 = 0.41 - 0.50; Class 5 = 0.51 - 0.60; and Class 6 = 0.61 - 0.67. The results of potential growth rate map were verified, Colwell et al. (1980).

The land developability map was generated (according to Table I) from the map of timber producing capacity of land (based on the potential growth rate) and accessibility map. This land developability map contained 6 classes ranging from Class I (representing the most developable) to Class VI (representing the least developable) areas. In Figure 3, the Classes V and VI are combined.

The potential residential suitability map was generated (according to Table II) from the land developability map and the slope map. This map contained 8 classes ranging from Class 1 (representing potentially the most suitable land for residential development with individual septic tank systems) to Class 8 (representing potentially the least suitable land for residential development with individual septic tank systems) areas.

The ownership map, originally prepared by the Plumas County Planning Department, was digitized and transferred to the Landsat-based coordinate system. A new version of the ownership map was then produced by IGOR film writing device. In this way, the ownership map was made to the same scale and in the same coordinate system of all other input and output products. This 5-Class ownership map was composed of Forest Service I, Private, TPZ (Timberland Preserve Zone, which restricts the use of land for timber production, established in 1978 as part of the Timber Taxation Reform Act), Williamson Act (restricts the use of land to agricultural production or similar uses, established in 1965), and Forest Service II. The Forest Service I class covers a relatively small area belonging to the Plumas National Forest, but located within the large privately-owned areas.

The final maps (land developability and potential residential suitability) were designed to be visually overlayed onto political and geographic ma s of the same scale and coordinate system (e.g., ownership, zoning, etc.) for selection of urban development sites in this case and generally for large scale land use planning purposes.

4. CONCLUSIONS

Based on our findings in this investigation it was concluded that:

(1) Spatially-referenced databank proved to be very useful in combining the data of various kinds, viz., satellites, aircraft, conventional tabulated and map form, and ground-acquired data to produce more complex resource-related maps such as net radiation, timber-producing capacity, land developability, and potential residential suitability.

(2) Landsat MSS data were very useful in vegetation and resulting albedo mapping.

(3) DMA/USGS digital terrain data provided adequate database for topographic analysis.

(4) NOAA-5 satellite VHRR data provided a good means of mapping surface temperature.

(5) An important consideration in using NOAA-5 satellite data was the 90-day rotating archive. Data greater than 90 days old were systematically over-written with new data due to the limited space available for storage. Advanced planning is recommended.

(6) The intermediate maps (e.g., elevation, slope, aspect, accessibility, etc.) were useful in the assessment of resource conditions and resource management when overlayed or combined with other maps such as net radiation, timber-producing capacity, land developability, etc.

(7) Remote Sensing data when combined with ground-acquired data proved to be very useful in providing the required database for selection or urban development sites and large scale land use planning purposes.

5. ACKNOWLEDGEMENTS

6. REFERENCES

Colwell, R.N., et al., "An Integrated Study of Earth Resources in the State of California Using Remote Sensing Techiniques," Space Sciences Laboratory, University of California, Berkeley, 1980.

Jensen, M.E., and Haise, H.R., "Estimating Evapotranspiration from Solar Radiation." Paper 3737, Proc. ASCE, Jour. Irrigation and Drainage Div. 89, 1963, pp. 15-41.

Khorram, S., "Use of Landsat-1 Multispectral and NOAA-4 Infrared Data in Estimating Solar Radiation Components Over the Middle Fork of Feather River Watershed," Proc. Conference on Climate and Energy: Climatological Aspect and Industrial Operations, American Meteorological Society, Asheville, North Carolina, 1978, pp. 51-56.

Khorram, S., and Smith, H.G., "Topographic Analysis of a Wildland Area Based on Digital Terrain Data," Proc., American Congress on Surveying and Mapping Convention, Washington, D.C., 1979a, 14 pp.

Khorram, S., and Smith, H.G., "Site-Specific Mapping of Surface Temperature Based on NOAA-5 Satellite VHRR Data," Proc., Eighth Annual Remote Sensing of Earth Resources Conference, The University of Tennessee Space Institute, Tullahoma, 1979b, 12 pp.

Khorram, S., and Smith, H.G., "Use of Landsat and Environmental Satellite Data in Evapotranspiration Estimation from a Wildland Area," Proc., Thirteenth International Symposium on Remote Sensing of Environment, Ann Arbor, Michigan, 1979c, pp. 1445-1454.

Remote Sensing Research Program, Electronic Data Processing Unit Information Note 73-4, Revision 2, Space Sciences Laboratory, Series 15, Issue 50, University of California at Berkeley, October, 1974.

United States Department of the Interior, "Digital Terrain Tapes User Guide," Geological Survey, Reston, Virginia, 1978, 12 pp.
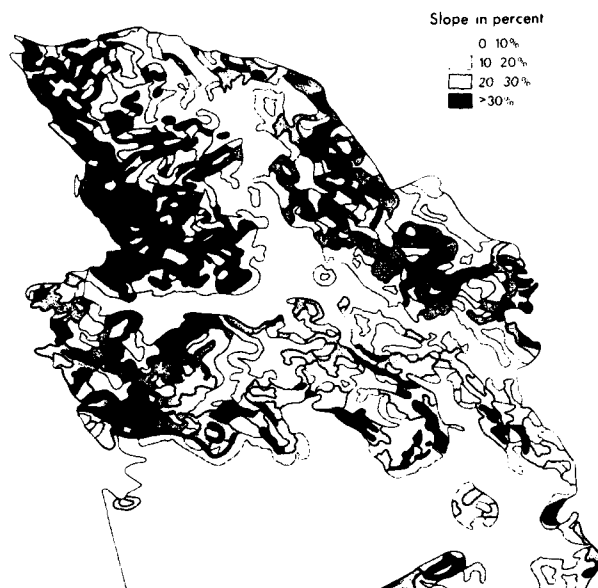
Figure 1. Slope map of the study area.

Table I. Criteria used in producing the land developability map from data appearing on: (a) the accessibility (ACC) map; and (2) the potential growth rate (PGR) map.

PGR \ ACC	Cl. 1	Cl. 2	Cl. 3	Cl. 4
Cl. 1	VI	VI	VI	VI
Cl. 2	VI	VI	VI	VI
Cl. 3	II	IV	V	VI
Cl. 4	I	III	V	VI
Cl. 5	I	III	V	VI
Cl. 6	I	III	V	VI
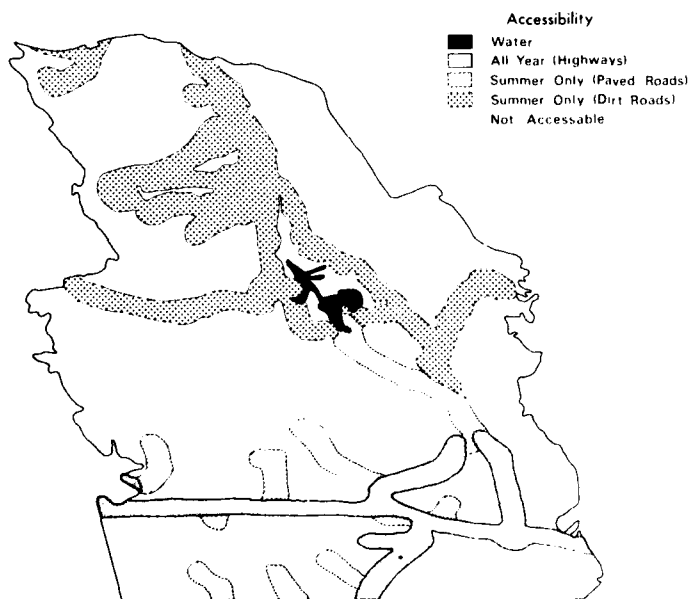
Figure 2. Accessibility map of the study area.

Table II. Criteria used in producing the map of potential residential suitability (with individual Septic tank systems) from slope and developability (DEV) data.

DEV \ Slope	Cl.A	Cl.B	Cl.C	Cl.D
Cl.I	1	1	2	8
Cl.II	2	3	3	8
Cl.III	4	4	5	8
Cl.IV	5	6	6	8
Cl.V	7	7	8	8
Cl.VI	8	8	8	8
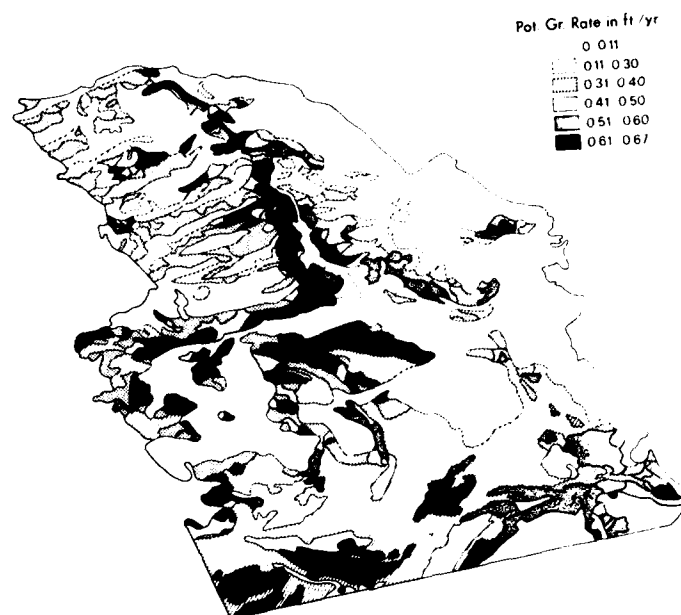
Figure 3. Potential timber growth rate map
of the study area.
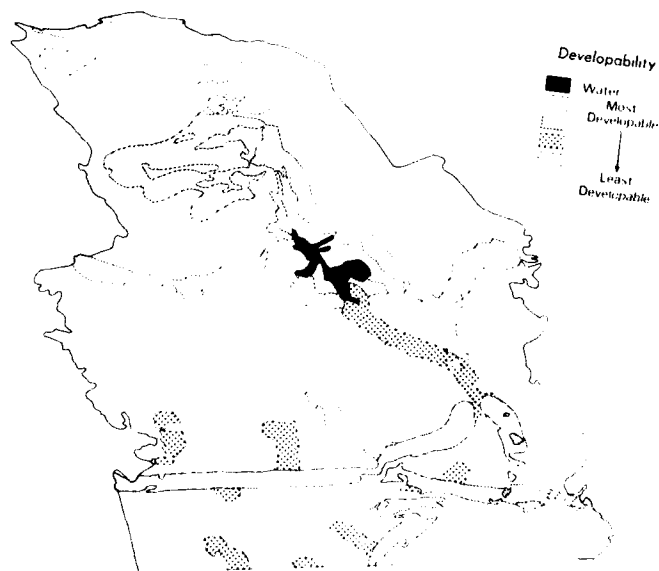
Figure 4. Land developability map of the
study area.
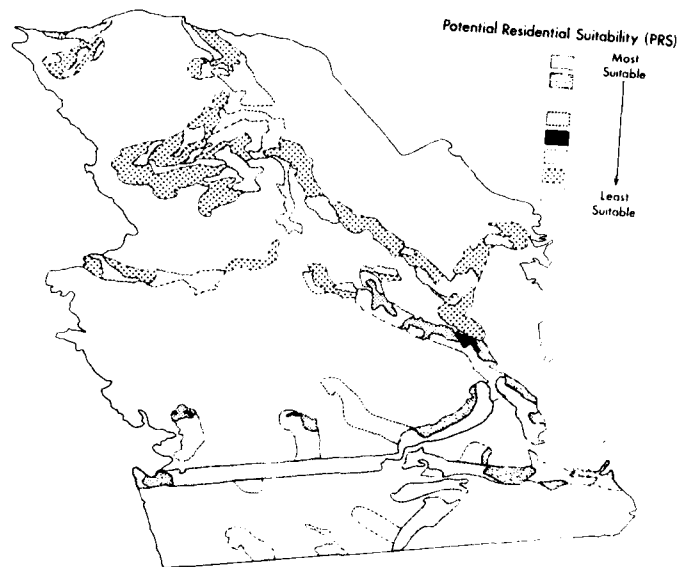
Figure 5. Potential residential suitability
map (assuming that the residents would need
to be equipped with septic tank systems).
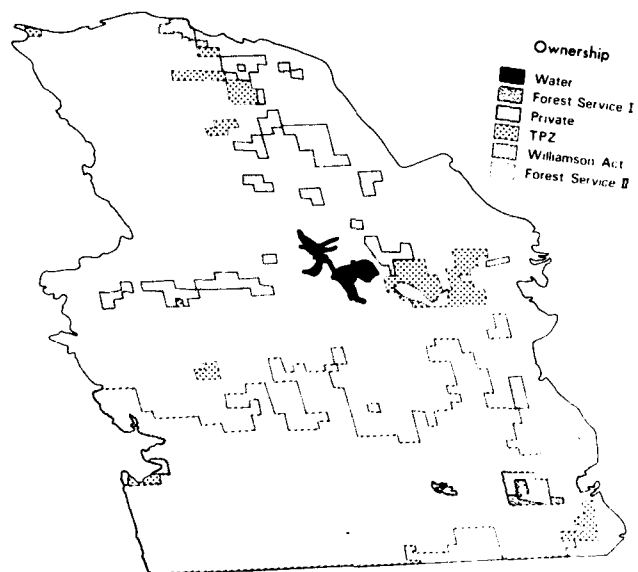
Figure 6. Ownership map of the study area.
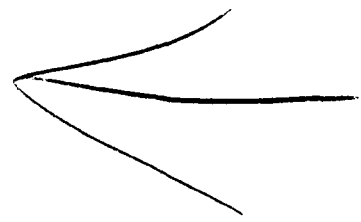
SATELLITE SENSING OF DROUGHTS IN INDIAN ARID AND SEMIARID ZONES

S. THIRUVENGADACHARI

Engineer, National Remote Sensing Agency
Hyderabad, Andhra Pradesh, India

ABSTRACT

In spite of the phenomenal technological advancement during recent years, drought continues to be a major factor of uncertainity in Indian agriculture, which is even today largely dependent on the monsoons. The occurrence of frequent droughts in Indian arid and semiarid zones, covering a sizeable portion of the country, requires special attention to be paid to timely drought monitoring and mitigation measures. Remote Sensing techniques, using space borne sensors, can provide the regional perspective that the problem obviously demands. Landsat monitoring of drought indicators such as depletion in surface water storage, lowering of ground water table and reduction in cropped area seem feasible. Base-line information on drought prone areas in regard to land and water resources can be generated to formulate meaningful drought mitigation measures. Systematic and sustained efforts are called for to transform this potential benefit into operational reality.

1. INTRODUCTION

Studies on the incidence of droughts as well as prediction and undertaking of measures to combat it are extremely vital for India with its predominantly agricultural economy. Indian agriculture, even today, is largely dependent on rainfall, as hardly 25 per cent of the cropped area has assured and adequate irrigation. The dry land farming areas are subject to a number of short spells of droughts during the crop growing season apart from the deficiency of the entire seasonal rainfall itself in some years. Thus in spite of the phenominal technological advancement during recent years by way of introduction of improved crop varieties, higher fertiliser use, better plant protection and better water management practices, etc. drought still continues to be the major factor of uncertainity in Indian agricultural production (Krishnan, 1979).

The incidence of drought conditions is frequent and severe in the semiarid and arid zones covering a sizeable percentage of the geographical area of India

(Fig.1). A study indicated that droughts are more common (60-90 per cent) than good years in arid zone, and constituted 6-20 per cent in semiarid zone, in contrast to 5 per cent in sub humid zone of Rajasthan (Krishnan and Thanvi, 1971). Apart from its obvious impact on agricultural production, the human response to the drought conditions is also important. The relief measures required to be undertaken in these drought prone areas by the Central and State Governments pose a continuous burden of nearly 1500 million rupees annually on the national exchequer.

In spite of the importance of this phenomenon, there is no universally accepted definition of drought. Through some of the initial definitions emphasised the lack of rainfall, it is being increasingly felt that identification and classification of drought by aridity indexes is more rational in that it takes into account the water deficiency in relation to water needs of the area.

In an agricultural country such as India where agriculture is mainly dependent on variable and seasonal rainfall, drought, which is not only periodical but also regional, contributes significantly to unstable agriculture. The regional dimension in drought needs to be explicitly recognised in the identification of drought affected or prone areas as well as in the formulation drought relief measures. It is in this context that remote sensing techniques employing space-borne sensors can play an extremely useful role as a surveying tool.

The large area synoptic coverage of satellite based sensors offer a unique opportunity to view drought indicates in a regional level. The repetitive nature of satellite coverage makes possible comparison of conditions in different seasons of the years as well as between different years. Such comparisions can help indicate drought prone areas as well as areas where drought conditions actually exist.

This paper highlights the results of studies conducted at National Remote Sensing Agency (NRSA) and elsewhere that indicate promise in the use of satellite sensed data over a wide spectrum of applications covering identification of drought prone and affected areas to planning and management of drought mitigation measures.

2. REMOTE SENSING OF DROUGHT

If drought is considered a recurring phenomenon, as in arid and semiarid lands, there is a compelling need for evolving a mechanism for monitoring its onset early so that timely and effective measures can be undertaken to mitigate the sufferings of people. Late sowing of crops, lowered water levels in wells, diminished inflows into tanks, sale of cattle in village fairs and fall of trade in rural towns, the fall in milk collection, increase of labour force in public works, shortage of and increase in price of fodder, fall in collection of institutional loans and migration of labour can indicate drought conditions. Some of these indicators are amenable to remote sensing.

The incidence of drought conditions is immediately reflected by less-than-normal surface water storages in the various tanks (small water impoundments across seasonal streams), lakes and reservoirs. Reduction in streamflow or dried up river beds are a common feature of drought affected areas. Dried up water bodies or those with water not sufficient to raise even a single crop are frequently noticed. There is a strong correlation between incident rainfall and surface water availability at the end of monsoon. This is particularly so in the case of tanks and lakes, which are strongly influenced by the local rainfall in the small watersheds draining into these water bodies. Thus a comparison of surface water storage between a normal year and any other year can indicate the onset and severity of drought conditions.

762

Thus Fig. 2 shows the surface water availability as a function of incident rainfall over a part of Madurai district in Tamil Nadu State. The significantly less than normal rainfall during the northeast monsoon period (Oct-Dec) of 1974 is reflectedby the dried up tanks, amongst which are also tanks fed by Thirumangalam main canal taking off from the Peranai regulator across Vaigai river. In the case of reservoirs and lakes with large watersheds the drought conditions are generally manifested as significant decreases in water availability (Fig. 3). The use of carry over storage can mask the early impact of drought in large water b odies.

Studies in Tamil Nadu and Andhra Pradesh States have shown that surface water bodies can be mapped and monitored (Thiruvengadachari, 1980). Thus the depression storage in a specified region can be mapped at the end of monsoon rainfall period and the total water spread area can be deter ned (Fig.4). It should however be remembered that satellite derived information is constrained by the spatial resolut on of 1.1 acres (0.45ha). Based on an analysis of historic records it thus seems possible to develop an index or threshold value related to surface water availability, for use as an indicator of drought conditions as well as its severity. Since rainfall in India is concentrated during the two periods of southwest monsoon (June-Sept) and northeast monsoon (Oct-Dec) it is essential that such an index be com uted at the end of each rainfall period to determine drought conditions. Surface water monitoring during the monsoon periods may however be hampered by possible cloud cover conditions.

The first effect of drought in agriculture is low soil moisture caused by the below normal rainfall. The additional irrigation required depletes the reserves in both surface and ground water storages. The increased exploitation of gr undwater res rves coupled with the less-than-normal recharge results in noticeable lowering of water levels and well yields. Quite a few wells dry up and may have to be deepened. The dwindling g round water reserves compel a decrease in area irrigated. Under drought relief measures, most of the new wells are for drinking water supply for human beings and cattle.

Though lowering of ground water levels can not be directly detected, a significant reduction in well irrigated area or absence of natural vegetation along streams discernable on satellite imagery are indicators of the drought situation. An investigation in the semiarid districts of Tamil Nadu State showed that the cropland can be mapped with acceptable accuracy (Thiruvengadachari, 1981). Use of suitable single date satellite data resulted in the delineation of irrigated areas. Use of supplementary information helped in differentiating tank, canal and well irrigated croplands (Fig. 5). Multidate data could enable monitoring the change in irrigated cropland status over years. The percentage of ir rigated to cropped area can be an important parameter for defining susceptibility of an area to drought conditions.

The extent of area under rainfed agriculture naturally has a strong dependence on the monsoon rainfall. For instance, the eratic, untimely and less-than-normal rainfall in 1980 caused about 34 per cent of kharif area (South West monsoon crop) and 40 per cent of Rabi area (north east monsoon crop) to remain unsown in Karnataka State. In fourteen out of twenty three districts in Andhra Pradesh State, against a normal sown area of 14.2 million acres in the kharif, crops were not at all sown in some 17 lakh acres. In the rabi, against a normally sown area of 94 lakh acres, crops were not raised in 16 lakh acres. Thus in khariff and rabi seasons put together, against a normal area of 19.6 million acres, crops were not sown in an area of 33 lakh acres while crops were damaged in some 65 lakh acres. Thus r emote sensing of acreage under dryland crops can provide information on the prevalence of d rought situations. However, differentiation of r ainfed cropped areas from those irrigated using

remotely sensed data, may be difficult due to the absence of unique phenological cycle. With the rainfed crop growth periods contained within the southwest and northeast monsoon periods, possibility of cloud cover on days of satellite data acquisition is quite strong and thus may introduce a major limitation to use of satellite data.

The extent of area under rainfed tanks is again a good indicator of drought conditions. There is a direct relationship between the area irrigated and water availability in tanks and hence to rainfall. Monitoring tank irrigated areas can thus help identify drought conditions as well as the degree of severity.

In arid and semiarid zones, the specification of drought cannot be divorced from land utilisation. Rainfall too meagre to produce crops may be adequate for pasture. An amount of rain which would give normal growth of indiginous pasture may prove inadequate for another area. Thus climatic criteria for drought may have to be viewed in the context of type of crop growth, pasture conditions, and the soil type. Hydrologic land use mapping using satellite data in Tamil Nadu, Andhra Pradesh and Karnataka States have shown the feasibility of dividing the area into different land use/cover zones, in which suitab le climatic criteria may be applied for identification of drought conditions. Such a map is prerequisite to controlled land use planning for better management of available land and water resources. Land cover/use zoning will also help in the application of average values for various hydrologic processes such as evapotranspiration, interception and infiltration for use in detailed water balance studies.

3. DROUGHT MITIGATION MEASURES

Drought mitigation measures can involve either short-term or long-term strategies. The long term drought prone area programme launched by the Government of India during the fifth plan aims at reducing the severity of the impact of drought and stabilising the income of the people by mobilising all the available land and water resources in these areas. Remote sensing techniques can be used to aid planning and management of drought prone area programmes taken up all over the country to alleviate the hardships due to droughts.

In the drought prone area the rainfall is scanty and not evenly distributed during the monsoon period. Minor irrigation schemes are needed to harness the availab le water resources for raising irrigated dry crops such as jowar, bajra, ragi, maize, wheat, pulses, ground-nut, gingelly, sunflower, cotton and chillies, requiring minimum water supply and approximating to average monsoon rainfall in the locality. No high water consuming wet crop such as paddy is to be encouraged. A remote sensing survey covering the drought prone districts of Bijapur, Belgaum and Dharwar helped to generate information in the land suitability for irrigated agriculture (Singh, 1980). Based on the soil map and other data on physico-chemical characteristics of soils of the area, a general irrigation suitability classification was made. The irrigation map showed areal units classified according to suitability for irrigation and indicating limitations due to slope, soil or drainage conditions and suggesting natural management needs such as levelling, provision of drainage and intensity of irrigation (Fig. 6). Such a map can help to restrict irrigation to suitable areas where it can supplement natural rainfall for raising irrigated dry crops.

In places where storage work is not feasible and where there is adequate flow in streams lift irrigation schemes from surface flow can be taken up. Since however most of the streams in drought prone areas are seasonal in nature, lift irrigation may be confined to the dominant monsoon season. Interpretation of suitable date imagery can help to establish continuous or intermittent flow conditions, deep water river reaches and suitability of adjoining

cultivable lands by way of elevation of river bank as well as the slope, soil
and drainage limitations. Through only reconnaissance level resources informa-
tion may be provided by satellite data, it can help to narrow down promissing
areas in vast drought prone regions for detailed study from aerial attitude
and ground level.

Scarce availability of surface water resources in arid and semiarid areas
necessitate increased exploitation of ground water. For instance, in the pre-
dominantly semiarid Tamil Nadu State, more than 98 per cent of available sur-
face water has been utilised, necessitating increased attention to use of sub-
surface water. NRSA studies in Tamil Nadu and Uttar Pradesh States have shown
that regional level reconnaissance level information on ground water potential
can be provided by satellite sensing (Kumar and Thiruvengadachari, 1981). Geo-
logical, geomorphological, soil and land use information were generated and in-
tegrated to support regional ground water programmes which can be followed by
detailed aerial and ground level surveys in promising areas. In another drou-
ght mitigation effort, NRSA succeded in the delineation of ground water poten-
tial areas in the Bundelkhand region of Uttar Pradesh State using Landsat data,
which information was supplied to concerned authorities early in the drought
situation so that immediately well drilling programmes can be taken up on a war
footing (NRSA Report, 1980).

Percolation tanks are increasingly being constructed at suitable places to
augment natural recharge from rainfall. The capacity of these tanks may vary
from 5 to 20 mcft and are intended to store the seasonal or flashy floods dur-
ing the monsoon period. No surface irrigation is permitted under percolation
tanks. The essential conditions for a successful percolation tanks are that
it should have sufficient capacity as well as geology suitable for recharge.
Naturally such tanks should be located where the increase in ground water
reserve can be optimally utilised. Landsat data can provide a first-level in-
formation on these aspects to narrow down potential areas for costlier detailed
studies.

Arid and semiarid lands have a major dependence on tank water resources.
A review of available data indicates the urgent need to modernise irrigation
schemes based on the hundreds of tanks dotted all over the landscape. Satel-
lite data can help provide a se line information on location and identification
of tanks, monitor waterspread areas and, through regional regression relation-
ships, monitor charges in storage volumes and area irrigated by various tanks.
Such crop acreage estimates irrigated by tanks coupled with average water appli-
cation rates can aid estimation of ground water recharge in local aquifers.

Rainfed agriculture, occupying a major part of arid and semiarid and arid
zones, can benefit from remote sensing through soil mapping and consequent
proper selection of suitable soil-water-crop management practices. Many NRSA
investigation in Andhra Pradesh, Haryana, Uttar Pradesh and Tamil Nadu States
have demonstrated the feasibility of generating soil association maps from
landsat data as well as to delineate problem soils.

4. CONCLUSIONS

The problem of droughts in the arid and semiarid lands, occupying a signi-
ficant portion of India, need to be viewed with a regional perspective for for-
mulation of effective drought mitigation schemes. Landsat data can provide such
a synoptic view over large areas. It can help to provide information on re-
duction in surface water storages, decrease in cropped area, absence of natural
vegetation along stream, beds, reduction in streamflow or dried up river beds
and a host of other parameters as indicators of drought conditions. The base-
line information needed for development of drought prone areas may be obtained
through satellite surveys. Formulation of minor and lift irrigation schemes
utilising surface flows, rational and systematic exploitation of underground

765

water resources, location of percolation tanks to augment ground water recharge, crash ground water exploitation programmes on water footing during drought periods, optimising agricultural production in drylands and renovation of tank irrigation schemes are some of the aspects that can be benefited by satellite sensing. The Indian experience reviewed in this paper thus indicates the feasibility of utilising remote sensing techniques for drought identification and mitigation. Sustained efforts are however needed to transform some of these potential benefits into operational reality.

ACKNOWLEDGEMENT

REFERENCES

Krishnan, A., and Thanvi, K.P., 1971, "Occurrence of Droughts in Rajasthan during 1941-1960", Proceedings of All India Seminar on Dryland Farming, New Delhi, India.

Krishnan, A., 1979, "Definition of Droughts and Factors Relevant to Specification of Agricultural and Hydrologic Droughts", International Symposium on Hydrologic Aspects of Droughts, New Delhi, India, p 67-102.

Kumar, S., and Thiruvengadachari, S., 1981, "Satellite Sensing for Extraction of Groundwater Resources Information", Fifteenth International Symposium on Remote Sensing of Environment, Environmental Research Institute of Michigan, U.S.A.

NRSA Report, 1980, "Ground water consultancy for Bundelkhand Vikas Nigam, Uttar Pradesh, Using Satellite Imagery", National Remote Sensing Agency, Hyderabad, India.

Singh, A.N., 1980, "Land Irrigability in Parts of Karnataka Using Landsat data" Technical Report 0788, National Remote Sensing Agency, Hyderabad, India, 12 p.

Thiruvengadachari, S., Subba Rao, p., and Rao, K.R., 1980, "Surface Water Inventory through Satellite Sensing", Journal of the Water Resources Planning and Management Division, ASCE, Vol. 106, No.WR2, P 493-502.

Thiruvengadachari, S., 1981, "Satellite Sensing of Irrigation Patterns in Semiarid Areas: An Indian Example", Photogrammetric Engineering and Remote Sensing, Vol. 47, No.10, P 1493-1499.
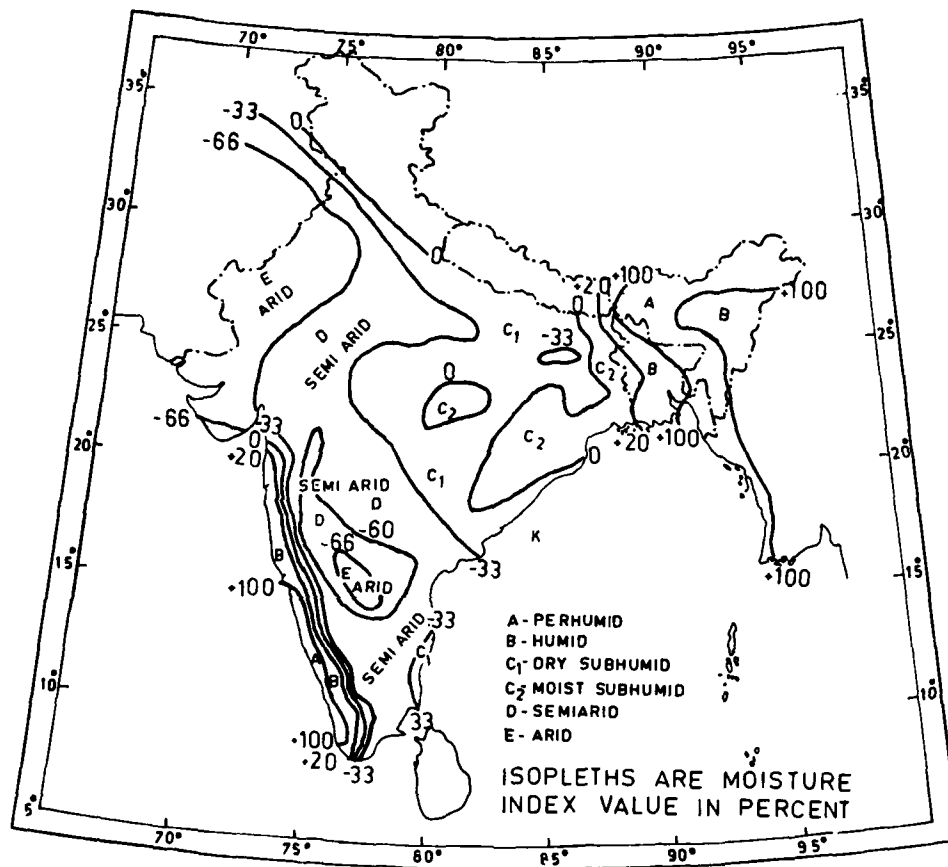
Fig.1. Arid and semi-arid zones of India (Thornthwaite Classification)
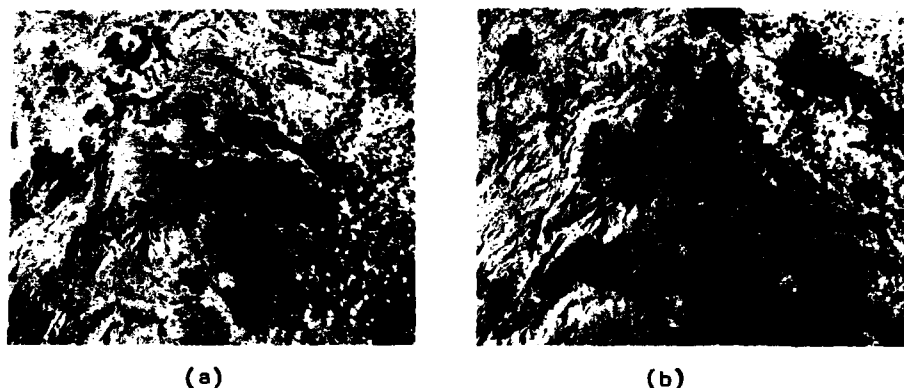
(a)   (b)

Fig.2. Depression storage as a function of northeast monsoon rain-
       fall. The low rainfall during Oct-Dec. 1974 of about 240 mm
       resulted in dried-up tanks (a) in contrast to abundant sur-
       face storage from the high winter monsoon rainfall of about
       740 mm in 1979(b)

METTUR RESERVOIR   BHAVANISAGAR RESERVOIR

NORMAL YEAR
February 1973

DROUGHT YEAR
February 1975
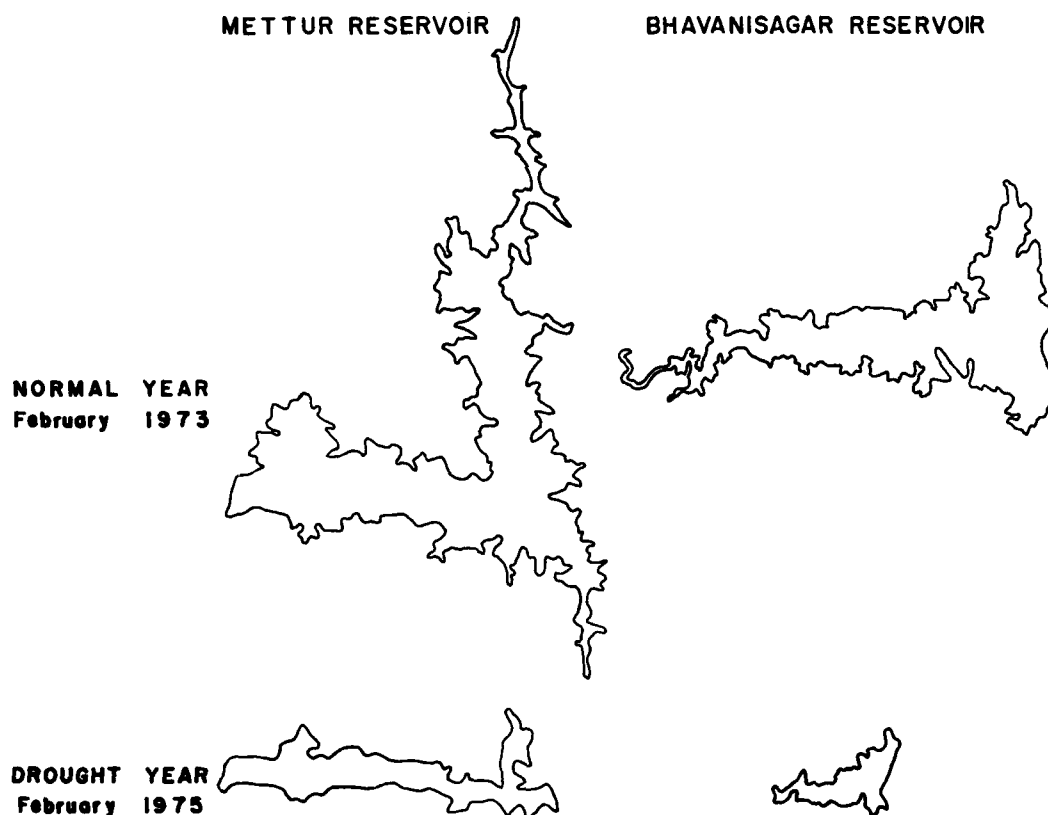
Fig. 3. Post-northeast monsoon reservoir storage in semi-arid
        Tamil Nadu State

768
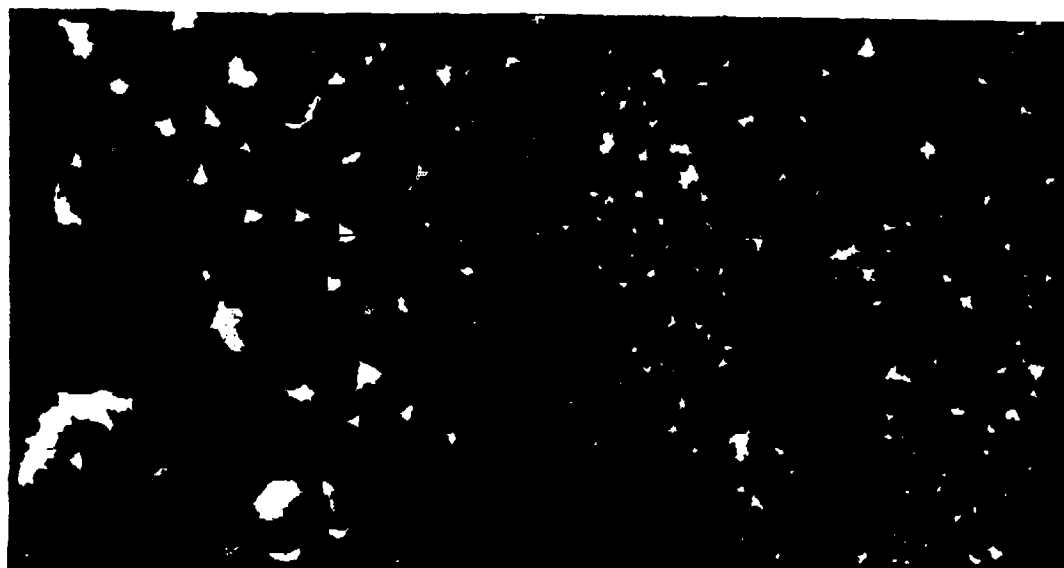
Fig. 4. Landsat derived surface water map of part of Anantapur district in Andhra Pradesh State
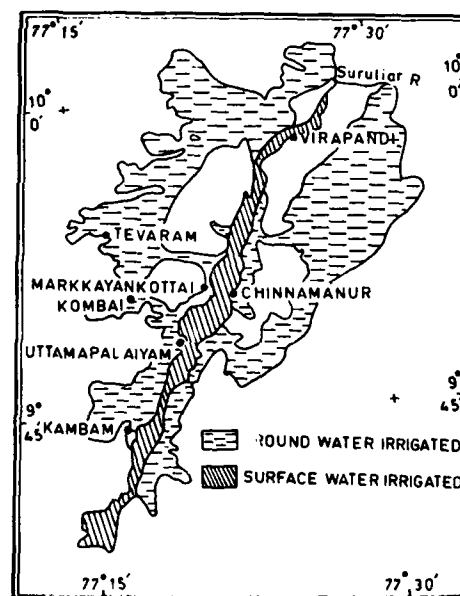
Irrigated cropland thematic map

Interpretation into canal and well irrigated areas

Fig.5.Canal and well irrigated croplands in cumbum valley in Tamil Nadu

MICROCOPY RESOLUTION TEST CHART

NATIONAL BUREAU OF STANDARDS-1963-A

SCALE

District Boundary	—·—·—	I	Highly irrigable
Taluk Boundary	— — —	II,III	Moderately irrigable
Land Irrigability class	III st	IV	Marginally irrigable
		V	Restricted irrigable
		VI	Non-irrigable

s,t,d Limitations due to soil, topography or drainage
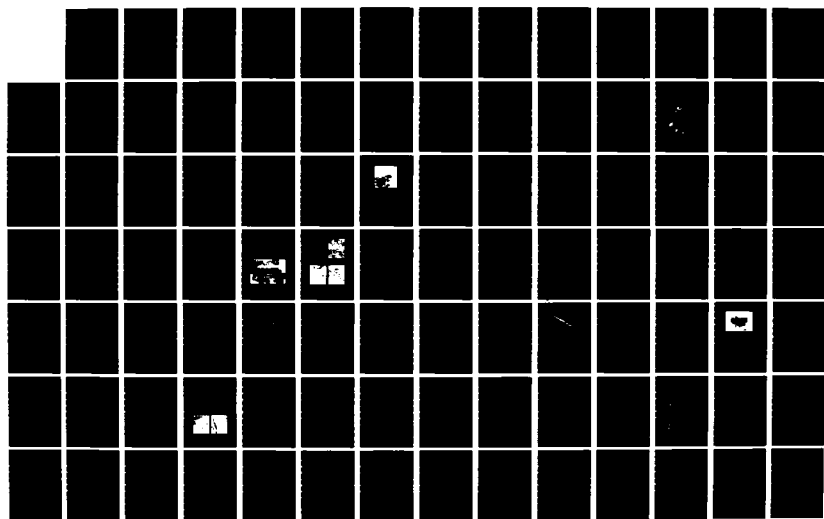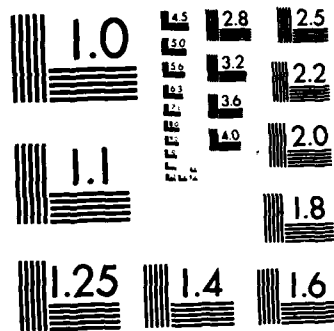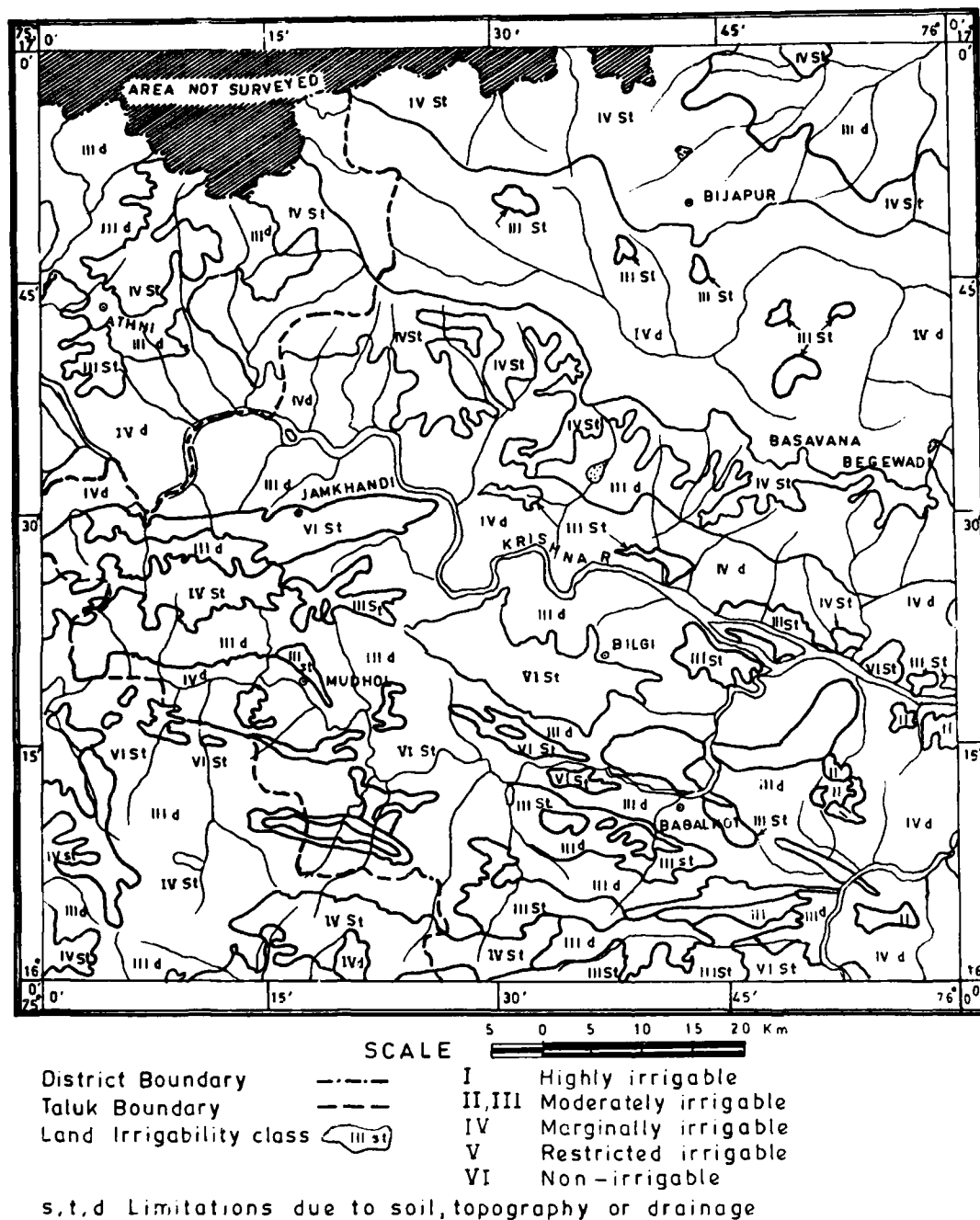
Fig. 6. Land irrigability map of part of Karnataka State (after Singh, 1980)

770

IMPROVED CALIBRATION ALGORITHMS
FOR THERMAL IR MAPPING

Sune R.J.Axelsson

SAAB-SCANIA AB
Linköping, Sweden

ABSTRACT

The thermal inertia and the soil surface
moisture can be estimated from the diurnal
variations of the surface temperature using
thermal IR and albedo measuring imagery. A
main problem at the data analysis is the
local variations of the sensible heat flux,
which degrades the accuracy of the interpre-
tation.

In this paper, an improved interpretation
algorithm is described for prediction of
thermal inertia, surface humidity and
evaporation of the mapped area. The prediction
errors are minimized by estimating the local
sensible heat transfer from dry subsurfaces
in the IR-imagery. Further improvements are
possible if calibration points with known
emissivity, humidity and thermal inertia are
available. The potential accuracy of the
algorithms is investigated and results from
ground-based experiments are described.

1. INTRODUCTION

The basic principles of thermal inertia mapping using thermal infrared and broad-band visible imagery are known since about a decado ago [1] - [3]. The application of the technique and the development of inversion algorithms for the interpretation of the data are still progressing, however.

A main-problem at the data analysis is the strong influence of the atmospheric conditions which degrades the accuracy and makes the data analysis much complex. A further reduction of the accuracy is obtained at the translation of the thermal inertia map into user data like soil-type, porosity and moisture content [9], [11].

Earlier investigations have shown that both thermal inertia and surface evaporation can be estimated using day/night thermal IR and albedo imagery, if uniform weather conditions are assumed over the whole survey area [6], [7]. This is a considerable approximation, since there usually are significant differences in incident sun radiation and the sensible heat flux as a result of varying atmospheric transmittance, surface topography, and atmospheric stability.

Consequently, there is a need for inversion algorithms, which give a denser estimation of the atmospheric influence than is possible using data from widely spaced weather stations.

In this paper, improved calibration algorithms are presented which reduce the effects of local variations in the atmospheric heat transfer. Contrary to earlier methods 10 , the local sensible heat flux is estimated from dry surfaces in the imagery without any prior knowledge of the albedo and the thermal properties of the surface material. If albedo and thermal inertia are well-known for some of the subsurfaces in the survey area, they can be used as calibration points for the estimation of the solar radiation.

2. THERMAL MODELS

2.1 INTRODUCTION

The surface temperature of the ground is controlled by the heat transfer at the surface boundary. If a one-dimensional model is assumed, the temperature $U(x,t)$ and the heat flow $Q(x,t)$ are determined by

$$Q = -\lambda \frac{\partial U}{\partial x} \tag{1a}$$

$$\frac{\partial Q}{\partial x} = -\frac{d}{dt}(CU) \tag{1b}$$

where

t = time
x = depth
λ = thermal conductivity
C = heat capacity per unit volume

The boundary condition at the surface is controlled by the heat balance equation:

$$Q = -\lambda \frac{\partial T}{\partial x} = I(1-A) - \varepsilon\sigma(T^4 - T_{sky}^4) - H - q_e - q_s \tag{2}$$

where

T = $U(0,t)$ = surface temperature
I = short-wave irradiance
A = albedo of the ground surface
ε = long-wave emissivity
σ = Stefan-Bolzmann constant
T_{sky} = long-wave sky-temperature
H = sensible heat flux
q_e = latent heat flux
q_s = geothermal heat flux

The solar irradiance $I(t)$ can be described by $I = \tau_o I^*$, where τ_o is the transmittance compared to a standard atmosphere. The irradiance $I^*(t)$ can be computed when latitude, solar declination, local time, and surface elevation are well-defined [11].

2.2 SENSIBLE AND LATENT HEAT TRANSFER

The atmospheric heat exchange is represented in (2) by H and q_e.

The sensible heat flux H can be described by

$$H = k_o(T - T_a) \tag{3}$$

772

where T_a is the air-temperature.

The factor k_o $\left[W/m^2K\right]$ is highly influenced by the local wind-speed (w) but also the surface roughness, atmospheric stability, and the air-surface temperature variation have significant effects. An approximation which mainly takes into account the wind-speed dependence is [4]

$$k_o = (w+2)\rho_a c_p C_D \qquad (4)$$

where

ρ_a = air density
c_p = specific heat of dry air at constant pressure
C_D = drag coefficient

The drag coefficient is defined by

$$C_D = 0.002+0.006(Z/5000) \qquad (5)$$

where Z is the test site elevation (m).

For z = 200 m, ρ_a = 1.25 kg/m^3 and c_p = 1000 J/kgK

$$k_o = 5.6+2.8w \qquad (6)$$

is obtained with w in m/s.

More general relationships which also include the dependence on surface roughness and atmosphere stability can be found in [12], [13].

The latent heat flux q_e has a very significant influence upon the surface temperature of moisty surfaces. Like the sensible heat transfer it is difficult to model with a good accuracy. A commonly used expression is:

$$q_e = k_o (L/c_p) (X_g - X_a) \qquad (7)$$

where

L = latent heat of vaporization
X_g = mixing ratio of the air at the ground
X_a = mixing ratio of the air at 1.5 m height

If the relative humidity of the air close to the surface (h_s) and at 1.5 m height (h_a) are introduced, Eq. (7) can be rewritten as

$$q_e = k_o (L/c_p) (h_s X_s(T) - h_a X_s(T_a)) \qquad (8)$$

where $X_s(\ )$ is the saturation mixing ratio.

The water losses due to evaporation (mm/hr) is determined by

$$E_h = 3600 q_e/L \qquad (9)$$

In Eq. (8), the factor h_s strongly depends upon surface moisture, but it is also influenced by the relative humidity of air.

A more non-ambiguous measure of the surface moisture is obtained by the following more approximate description of the latent heat flux

$$q_e = M k_0 (L/c_p) (X_s(T) - h_a X_s(T_a)) \qquad (10)$$

where the surface moisture index M represents the ratio of the actual and potential evaporation.

773

By this definition, a dry surface has M << 1, while M ≈ 1 when the soil is saturated by water.

By night, when q_e < 0 and the dew falls, even dry surfaces become moisty. Therefore, M has to be changed to M = 1 when the surface is covered bv dew.

More complex models [6] also take into account the surface moisture dependence of matrix potential, temperature, moisture conductivity and capacity of the upper soil layer. However, these parameters are usually unknown for the survey area, which justifies the use of more simplified models.

2.3 FINITE DIFFERENCE MODEL

The surface temperature can be predicted from Eqs. (1) and (2) under very general conditions using the method of finite differences [4]. The upper ground surface layer is then subdivided into thinn horizontal layers (∆x) to a depth of D. Before the start of the computer processing, the initial temperatures of the layers and all the parameters involved are defined. The temperatures and heat flows at time t = (m+1)∆t are updated from Q and T at time t = m∆t, using (1) expressed in terms of differences and (2) as the boundary condition.

A great advantage of the finite difference model is the fact that it can be used under very general conditions, e.g. in-homogeneous surface layers and time-varying weather parameters.

The ultimate accuracy of the model primarily depends on how accurate start conditions, thermal data and weather conditions can be defined.

2.4 FOURIER MODELS

An improved understanding of how the involved parameters and processes influence the surface temperature is obtained by assuming periodic heat fluxes, which are expressed as Fourier series.

Watson et al [1] - [3] first applied this approach to the interpretation of thermal IR imagery. Their simplified model was further developed by including the atmospheric heat transfer [6] and the time-variations of air and sky temperature [11]. An improved linearization procedure was also introduced [11], which highly reduces the prediction errors of the model.

For dry surfaces and stable wind conditions, the error of the predicted surface temperature is usually less than one degree Kelvin. For moisty surfaces, or significant wind variations during the day, however, the accuracy is reduced as a result of the non-linearity of $q_e(T)$.

When the Fourier model is applied [11], we first develop I(t), $T_a(t)$, $T_{sky}(t)$ of Eq. (2) as Fourier series

$$
\left.
\begin{aligned}
I(t) &= I_0 + \sum_{n=1}^{\infty} I_n \cos(n\omega t - \varepsilon_n) \\
T_a(t) &= T_0 + \sum_{n=1}^{\infty} T_n \cos(n\omega t - \phi_n) \\
T_{sky}^4(t) &= B_0^4 + \Sigma B_n \cos(n\omega t - \beta_n)
\end{aligned}
\right\} \tag{11}
$$

By using a similar linearization technique as in [11], the temperature of dry surfaces (q_e = 0) can be expressed as

$$T(t) = \bar{T} + \tilde{T}(t) \tag{12}$$

774

where the mean surface temperature is defined by

$$\bar{T} = T_o + (I_o(1-A) + \varepsilon\sigma(B_o{}^4 - T_o{}^4))/S \qquad (13)$$

with

$$S = 4\varepsilon\sigma T_o{}^3 + k_o \qquad (14)$$

and the amplitude of the temperature variations by

$$\tilde{T}(t) = \sum_{n=1}^{\infty} H_n \Big[(1-A) I_n \cos(n\omega t - \varepsilon_n - \delta_n)$$

$$+ k_o T_n \cos(n\omega t - \phi_n - \delta_n) + \varepsilon\sigma B_n \cos(n\omega t - \beta_n - \delta_n) \Big] \qquad (15)$$

The attenuation factor H_n and the phase delay δ_n are both related to the thermal inertia of the ground surface

$$P = \sqrt{\lambda C} \qquad (16)$$

and the sensible heat flux factor k_o, according to

$$\left.\begin{aligned} H_n &= \frac{1}{\sqrt{(S+Pr_n)^2 + P^2 r_n{}^2}} \\ \delta_n &= \arctan(Pr_n/(S+Pr_n)) \end{aligned}\right\} \qquad (17)$$

where

$$r_n = \sqrt{n\omega/2} \qquad (18)$$

For evaporating surfaces $(q_e > 0)$, an approximative solution is obtained by linearizing $q_e(t)$ about T_o

$$q_e \approx q_o + k_1(T-T_o) \qquad (19)$$

where

$$\left.\begin{aligned} q_o &= q_e(T_o, M; h_a, T_a) \\ k_1 &= \frac{\partial q_e(x, M; h_a, T_a)}{\partial x}\bigg|_{x=T_o} \end{aligned}\right\} \qquad (20)$$

The factor S in (13) and (17) is then changed to

$$S = k_o + k_1 + 4\varepsilon\sigma T_o{}^3 \qquad (21)$$

and (13) to

$$\bar{T} = T_o + (I_o(1-A) - q_o + \varepsilon\sigma(B_o{}^4 - T_o{}^4))/S \qquad (22)$$

The major limiting assumptions of the Fourier model are (i) the periodicity of I, T_a, T_{sky}, (ii) a near-constant k_o-value, and (iii) the linearization of the evaporation losses (q_e). Therefore, the accuracy is reduced at unstable wind conditions, or evaporating surfaces. The analytical solution, however, gives an improved insight into how the various parameters influence the surface temperature. This knowledge is a useful tool at the definition of efficient interpretation algorithms.

775

3. INVERSION ALGORITHMS

3.1 INTRODUCTION

At the translation of the IR- and albedo imagery into thermal inertia, evaporation and soil surface moisture maps, tables of the day/night temperatures of the surface are first computed as a function of albedo, thermal inertia, surface slope and surface moisture for the weather conditions at the time of acquisition. From the measured albedo and day/night IR-imagery combined with topographic data, the thermal inertia (P) and surface moisture (M) are then determined from the inverted tables. The evaporation is computed from Eqs. (9) and (10).

An alternative approach is to compare simulated day and night temperatures with the monitored ones and adjust the thermal inertia (P) and the surface moisture (M) until a near-optimum match is obtained.

The matching procedure is simplified if the day-night temperature difference

$$\Delta T = T_D - T_N \tag{23}$$

and the mean deviation between the surface and air temperatures

$$T_d = (T_D + T_N)/2 - T_O \tag{24}$$

are used as inputs.

This is obvious from Figure 2, which shows that T_d mainly depends upon M and to a less extent upon P.

Therefore an approximate estimate of the surface moisture index M can be derived directly from T_d (Figure 2a).

The thermal inertia value is then obtained from Figure 2b, showing ΔT versus thermal inertia (P) and surface moisture (M). An improved accuracy is obtained, if the procedure is repeated.

3.2 IMPROVED INVERSION ALGORITHMS

A major disadvantage of the conventional inversion model using weather station data as inputs is the fact that uniform meteorological conditions are required over large regions. Even at clear sky, this is an approximative assumption, since the local topography has a significant influence upon the wind conditions close to the ground.

This draw-back can be relaxed by estimating the local k_o-value from the IR-imagery using dry subsurfaces as calibration points. The local k_o-value and the thermal inertia (P) of non-evaporating surfaces are determined from tables, which show ΔT and T_d versus k_o, P and are calculated for the actual albedo value and weather conditions (Figure 3).

Often the convection loss factor k_o is varying during the day. In that case, k_o should be described in the inversion model by

$$k_o(t) = k_{oo} f(t) \tag{25}$$

where k_{oo} is a local average value and f(t) is a normalized function: $\overline{f(t)} = 1$. The local average value k_{oo} is estimated from the dry surface IR-data as shown above, while the shape of f(t) is based upon wind-speed data from weather stations.

776

For uniform wind conditions all the day, simplified algorithms can be derived from the Fourier solution.

From (22), the following k_o-estimate is obtained ($q_o = 0$)

$$k_o = \left[I_o(1-A) + \varepsilon\sigma(B_o^4 - T_o^4) \right] / (\overline{T} - T_o) - 4\varepsilon\sigma T_o^3 \qquad (26)$$

where $\overline{T}$ is estimated from T_N, T_D. An approximation is: $\overline{T} = 0.5(T_D + T_N)$, but an improved accuracy is obtained by also taking into account the shape of $T(t)$ and the times of acquisition.

The corresponding relationship of ΔT versus P, k_o is given by

$$\Delta T = \widetilde{T}(t_D) - \widetilde{T}(t_N) \qquad (27)$$

where t_D, t_N are the local times of the day and night mapping, respectively, and $\widetilde{T}(\ )$ is substituted from Eq. (15).

An approximative solution is obtained, if we neglect all but the first term of the series, giving

$$\Delta T \approx 2H_1 \left[(1-A)I_1 + k_o T_1 + \varepsilon\sigma B_1 \right] \qquad (28)$$

where

$$H_1 = 1/\sqrt{S^2 + 2P^2 r_1^2 + 2PS r_1}$$
$$S = k_o + 4\varepsilon\sigma T_o^3 \qquad (29)$$
$$r_1 = \sqrt{\omega/2}$$

Surface moisture estimation

Usually, the scene consists of both dry and moisty surfaces. In that case, there are three unknown parameters:

a) Thermal inertia (P)
b) Soil surface moisture (M)
c) Sensible heat loss factor (k_o)

Since there are only two independent temperature values available (T_D and T_N), not more than two unknown variables can be determined at the analysis. For moisty surfaces ($M \neq 0$), we therefore must use the same k_o-value as is determined from dry adjacent subsurfaces.

The surface moisture (M) and the thermal inertia (P) are then estimated by a similar procedure as was discussed in section 3.1. Even for semi-dry and wet surfaces, an improved accuracy is usually obtained compared to the conventional procedure, which uses a fixed k_o-value based upon wind-speed data from weather-stations.

The soil moisture factor M can be derived more easily from Eq. (2), if stationary conditions ($\overline{Q} = 0$) and negligible geo-thermal flow ($q_s = 0$) are assumed. In that case,

$$\overline{q_e} = I_o(1-A) + \varepsilon\sigma(\overline{T_{sky}^4} - \overline{T^4}) - \overline{H} \qquad (30)$$

where the sensible heat flux

$$\overline{H} = k_o(\overline{T} - \overline{T_a}) \approx k_o T_d \qquad (31)$$

is estimated using the k_o-value of adjacent dry surfaces and the measured

777

temperature difference T_d.

The soil-moisture factor M is then estimated from the ratio of the actual and the potential evaporation

$$M = \overline{q_e}/\overline{q_s} \tag{32}$$

where $\overline{q_s}$ is the average latent heat flux from a fully evaporating surface with the same day and night temperatures as the analyzed surface.

3.3 USE OF CALIBRATION POINTS

Further improvements of the accuracy is achieved, if the survey scene contains calibration surfaces with known thermal inertia, albedo and surface humidity.

Pratt et al [10] have earlier discussed this technique for the estimation of k_o of dry surfaces, using ΔT as input to a simplified Fourier model. From the calibrated k_o-value, P and a measure of the atmospheric heat flux were then determined for the other subsurfaces of the imagery.

The calibration procedure suggested in the preceding section does not require any prior knowledge of albedo and thermal inertia at the estimation of k_o. Therefore, this knowledge can instead be used for reducing the uncertainty of some other parameter of the model.

This fact can be further displayed by the Fourier model for dry surfaces. From Eq. (15), the day-night temperature difference, $\Delta T = T_D - T_N$, is given by

$$\Delta T = \sum_{n=1}^{\infty} H_n \{ (1-A) I_n \left[\cos(n\omega t_D - \varepsilon_n - \delta_n) - \cos(n\omega t_N - \varepsilon_n - \delta_n) \right] +$$

$$+ k_o T_n \left[\cos(n\omega t_D - \phi_n - \delta_n) - \cos(n\omega t_N - \phi_n - \delta_n) \right] +$$

$$+ \varepsilon \sigma B_n \left[\cos(n\omega t_D - \beta_n - \delta_n) - \cos(n\omega t - \beta_n - \delta_n) \right] \} \tag{33}$$

where the attenuation factor is defined by Eq. (17).

From (33), the dominating error of ΔT is usually generated by the uncertainty of I_n due to local variations of the atmospheric transmittance of the solar radiation.

Let $I_n = \tau_o I_n^{*}$, where I_n^{*} are the Fourier amplitudes of the solar insolation for a clear standard atmosphere and τ_o is a transmittance factor.

The irradiance function $I^{*}(t)$ and its Fourier components I_n^{*} are well-defined when latitude, longitude and solar declination are specified.

If max/min IR-temperatures are measured over a bare ground surface with known albedo, emissivity and thermal inertia, we can estimate τ_o by adjusting τ_o until measured and computed T_D- and T_N-values agree. If Eq. (33) is used, the two ΔT-values are matched.

From Eq. (33), an approximative calibration algorithm can be deduced, if we neglect all but the first term (n = 1) of the series. In that case, the thermal inertia (P) of a dry subsurface (A, ΔT) is estimated from the calibration point data (P_{*}, A_{*}, T_{*}) using the calibration ratio

$$y = \frac{H_1}{H_1^{*}} = \frac{\Delta T}{\Delta T_{*}} \frac{(1-A_{*}) I_1 + k_o T_1 + \varepsilon \sigma B_1}{(1-A) I_1 + k_o T_1 + \varepsilon \sigma B_1} \tag{34}$$

778

where H_1 and H_1^* are defined by Eq. (29).

From Eqs. (34) and (29), P can be solved, giving

$$P = \frac{S}{\sqrt{2\omega}} (-1 + \sqrt{2Z^2/S^2 - 1}) \tag{35}$$

where

$$Z^2 = (S^2 + P_*^2 \omega + P_* S \sqrt{2\omega})/y^2 \tag{36}$$

and S is defined by (14).

Since Eqs. (33) and (34) also include the time-variations of sky and air-temperature, an improved accuracy is expected compared to earlier suggested algorithms, which are based upon more simplified versions of the Fourier model.

3.4 ERROR ANALYSIS

An important question is how accurate the k_o-estimate is, considering the prediction errors of the parameters involved. From Table I, which shows the results of a sensitivity analysis based upon Eq. (26), it is obvious that the main errors are generated by uncertainties in incident radiation (B_o, I_o), and from the IR-measurements of the day/night surface temperatures (T_d).

The accuracy of the evaporation estimate is analysed from Eq. (30). As shown by Table II, the main errors are generated by the uncertainties in the incident radiation (I_o, B_o).

If calibration sources with well-defined albedo, thermal inertia and surface humidity are available, the uncertainty of both I_o, B_o can be reduced, so that the accuracy of the estimated atmospheric heat flux is further improved.

The accuracy of the thermal inertia estimation (P) is displayed by Table III. As shown, considerable errors can be generated by uncertainties in absorbed radiation, and the atmospheric heat flux. In particular, for semi-dry and moisty surfaces, the main error is often induced by the estimation error of the surface humidity (M).

Table I. Errors introduced at the estimation of
k_o, calculated for $k_o = 10$ W/m^{2}K, $T_o = 290$ K
$B_o = 270$ K, $\varepsilon = 0.9$, A = 0.1, $I_o = 370$ W/m^2

Parameter	Δk_o $\left[\text{W/m}^2\text{K}\right]$
$\Delta A = 0.02$	0.5
$\Delta \varepsilon = 0.04$	0.4
$\Delta T_o = 1$ K	0.4
$\Delta B_o = 3$ K	0.7
$\Delta I_o = 20$ W/m^2	1.1
$\Delta T_d = 1$ K	0.9
$\Delta q_e = 10$ W/m^2	0.6

Table II. Errors introduced at the estimation of
the diurnal evaporation (E), calculated
for k_o = 10 W/m^{2}K, T_o = 290 K, B_o = 270 K,
ε = 0.9, A = 0.1, I_o = 350 W/m^2.

Parameter	$\overline{\Delta q_e}$ W/m^2	ΔE mm/day
ΔA = 0.02	7	0.2
$\Delta\varepsilon$ = 0.04	4	0.1
ΔT_o = 1 K	5	0.2
ΔB_o = 3 K	12	0.4
ΔI_o = 20 W/m^2	18	0.6
ΔT_d = 1 K	10	0.3
Δk_o = 1 W/m^{2}K	15	0.5
Δq_s = 10 W/m^2	10	0.3

Table III. Errors introduced at the estimation of
P, calculated for k_o = 10 W/m^{2}K, A = 0.1,
T_a = 10-25°C, M = 0, T_{dew} = 10°C, ε = 0.9,
T_{sky} = 265-275K, P = 1500 TIU.

Parameter	ΔP [TIU]
ΔA = 0.02	70
$\Delta\varepsilon$ = 0.04	3
ΔT_a = 1 K	30
ΔT_{sky} = 3 K	50
ΔI = 30 W/m^2	100
Δk_o = 1 W/m^{2}K	200
δT_d = 1 K	100
ΔM = 0.1	500

4. APPLICATIONS

The dependence of the IR-temperature upon surface moisture, evaporation
and thermal inertia was investigated at a ground-based experiment, outside
Linköping in July 1981. The test objects were solid rock, sand, clay and peat
soil of varying moisture content and porosity.

From the measured albedo and day/night IR-temperatures, thermal inertia
(P) and the soil-moisture index (M) were computed, using the inversion
algorithm described in sects. 4.2 and 4.3. Air temperature, wind speed, and
air humidity were obtained from weather stations in the region. The local
sensible heat coefficient k_o and the solar transmittance τ_o were estimated
using the rock surface as calibration point (A = 0.13, M = 0, P = 2750 TIU).
The results are described in Figure 4 and 5.

Figure 5 shows the estimated surface moisture from the measurements of the
9th and 11th of July, 1981. As shown by the Figure, the wet clay, which was
close to a water puddle, had high evaporation both the days. The sand surface,

which was watered on the 8th of July and the peat soil also had strong evaporation on the 9th of July. Two days later, a reduced evaporation was measured for both surfaces. This agrees with Table IV, which shows a considerable reduction of the water content of the watered sand surface between the 9th and the 11th of July. As was expected, low M-values were obtained at the data analysis for all the dry test objects.

The estimated thermal inertia values varied between 2750 for the rock (calibration point) to 750 TIU for the porous dry sand. A significant increase of the thermal inertia is obtained when the soil density increases. This is a result of a reduced porosity, or increased soil-moisture. The ambiguity can be relaxed by also using the M-value and the albedo as indicators of the soil-water content.

Table IV.   Estimated water content of the soil-types used as test objects at a ground based field experiment on the 8th - 11th of July, 1981

Soil type		Time	Water content [weight percent]
A.	Dry porous sand	9/7	0.7
B.	Dry dense sand	11/7	0.5
C.	Moisty sand watered on the 8th of July	9/7 11/7	8 1.7
D.	Porous peat soil	11/7	11
E.	Dense peat soil	11/7	18

5.   CONCLUSIONS

In this paper, improved calibration algorithms have been discussed for the estimation of thermal inertia and surface moistness/evaporation of bare soil based upon albedo and day/night thermal IR imagery.

Contrary to conventional interpretations methods, which assume uniform atmospheric conditions between the weather stations, the proposed algorithm permits local variations of the sensible heat flux. Also the effects of varying insolation can be reduced if calibration points with known albedo and thermal inertia are available in the survey scene.

The experimental results confirm the usefulness of the technique for soil-surface moisture and thermal inertia mapping. The best accuracy is obtained at the soil-surface moisture estimation. The thermal inertia estimate is more sensitive to errors in soil-surface moisture and meteorological data inputs.

6. REFERENCES

[1] L.C.Rowan, T.W.Offield, K.Watson, P.J.Cannon and R.D.Watson,
"Thermal infrared investigations, Arbuckle Mountains Oklahoma",
Geol. Soc. Amer. Bull. 81:3549-3562, 1970.

[2] H.A.Pohn, T.W.Offield and K.Watson,
"Thermal inertia mapping from satellite-discrimination of geologic
units in Oman", U.S. Geol. Survey J.Res. 2 (2): 147-158, 1974.

[3] K.Watson,
"Geologic applications of thermal infrared images",
Proc. IEEE, vol. 63 (1): 128-137, 1975.

[4] A.B.Kahle,
"A simple model of the earth's surface for geologic mapping by remote
sensing", J.Geophys. Res. 82 (11): 1673-1680, 1977.

[5] S.H.Miller and K.Watson,
"Evaluation of algorithms for geological thermal-inertia mapping",
Proc. of 11th Int. Symp. Rem. Sens. Env., pp 1147-1160, 1977.

[6] A.Rosema,
"Heat capacity mapping, is it feasible?", Proc. of 10th Int. Symp.
Rem. Sens. Env., pp. 571-584, 1976.

[7] A.Rosema, J.H.Bijleveld, P.Reineger, G.Tassone, K.Blyth and R.J.Gurney,
"TELL-US, A combined surface temperature, soil moisture and evaporation
mapping approach", Proc. of 12th Int. Symp. Rem. Sens. Env.,
pp. 2267-2276, 1978.

[8] J.C.Price,
"Thermal inertia mapping: A new view of the Earth, J.Geophys. Res. 82:
2582-2590, 1977.

[9] D.A.Pratt and C.D.Ellyett,
"The thermal inertia approach to mapping of soil moisture and geology",
Rem. Sens. Env. 8: 151-168, 1979.

[10] D.A.Pratt, S.J.Foster and C.D.Ellyett,
"A calibration procedure for fourier series thermal inertia models",
Photogram. Eng. Rem. Sens. 4b (4): 529-538, 1980.

[11] S.R.J.Axelsson,
"On the accuracy of thermal inertia mapping by infrared imagery",
Proc. of 14th Int. Symp. Rem. Sens. Env., pp 359-378, 1980.

[12] J.A.Businger, J.C.Wyngaard, Y.Zzumi and E.F.Bradley,
"Flux-profile relationships in the atmospheric surface layer",
J.Atm. Sc. (28): 181-189, 1971.

[13] K.Watson,
"Direct computation of the sensible heat flux", Geophys. Res.
Letter 7 (8): 616-618, 1980.
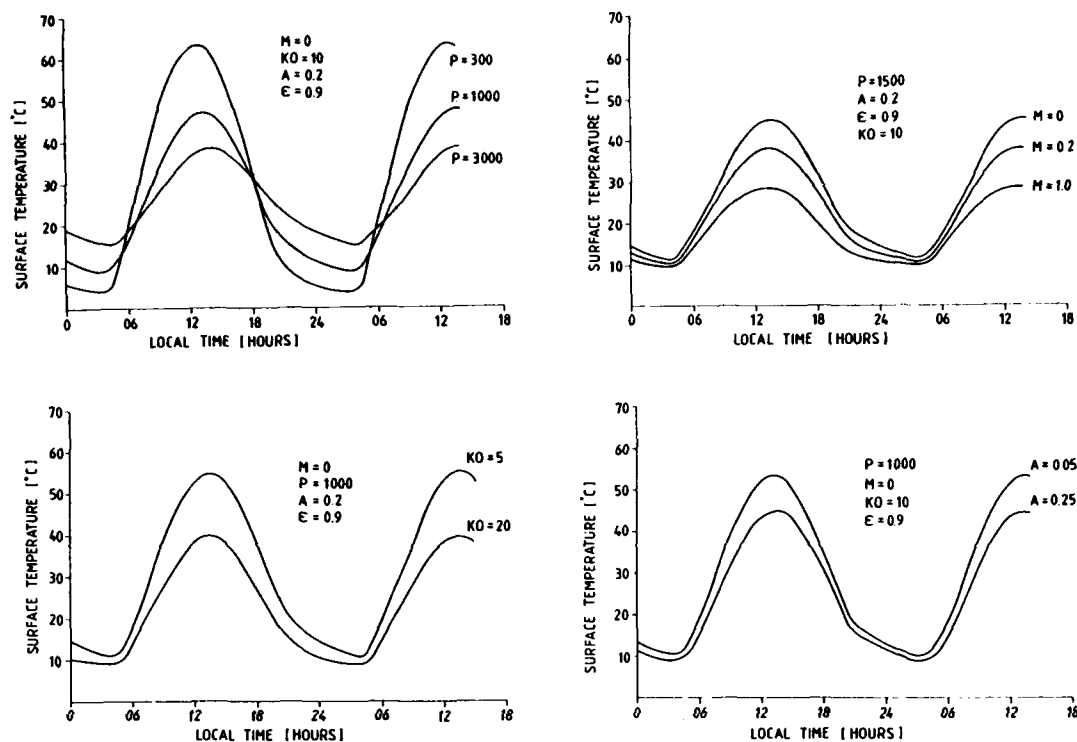
Figure 1. Diurnal ground surface temperature
predictions for clear sky.
Latitude: 58°, solar declination: 20°
and air-temperature: 10-25°C.
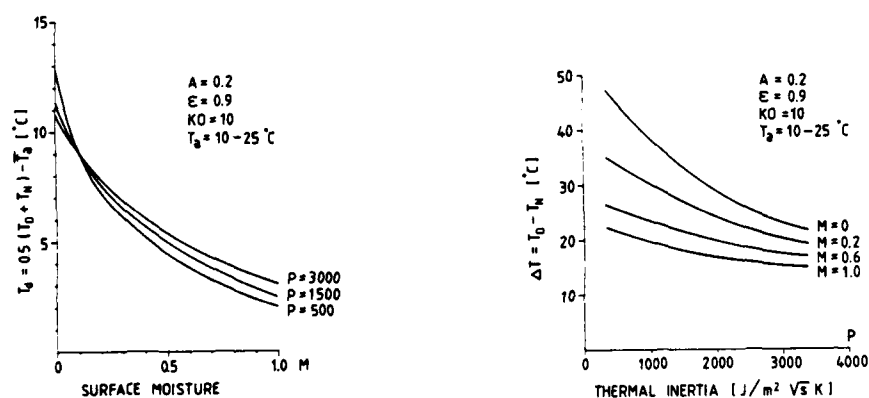
Figure 2. Relationships between T_d, ΔT and M, P.
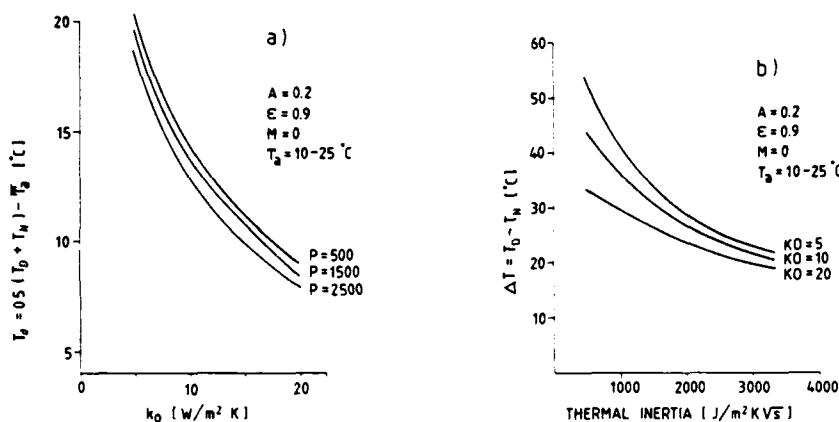
Figure 3. Relationships between T_d, $\wedge T$ and k_o, P for a dry surface.
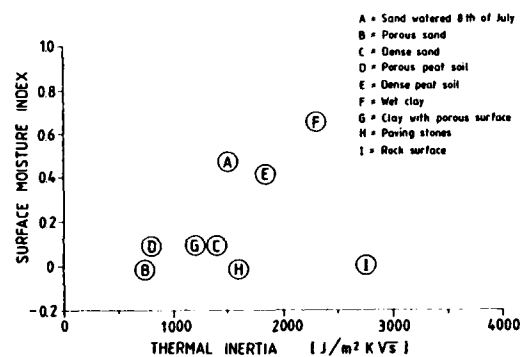
Figure 4. Estimated surface moisture and thermal inertia from measurements on the 9th of July, 1981.
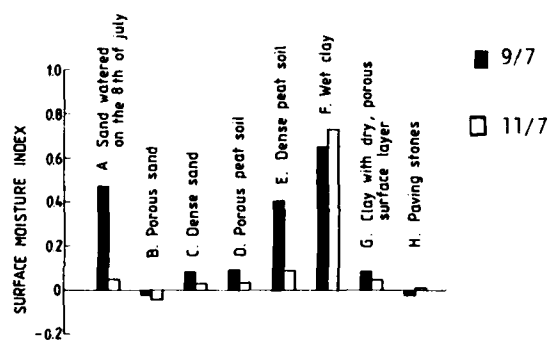
Figure 5. Estimated surface moisture variations between the 9th and 11th of July, 1981.

ECOSYSTEM MAPPING OF INTERPRETATION OF
LANDSCAPES FROM SATELLITE IMAGERY

Donald L. Williams

University of Southern Mississippi
Hattiesburg, Mississippi

SUMMARY

Ecosystem or biogeocoenosis mapping, productivity analysis, and condition monitoring programs are important constituents of agricultural and other resource development planning. Ecosystems are physically expressed on the surface of the Earth by landscapes, which are spatial units composed of recurring patterns of vegetation, soils and landforms which are interactively related in origin and occurrence. Accepted landscape models indicate that the two most visible components of the landscape, vegetation and landforms, are sufficient to identify landscapes. Operational mapping of landscapes as ecosystem surrogates depends upon development of an adequate methodology applicable in any region where such mapping may be required.

This study presents a four-point methodology for preparing landscape maps from satellite imagery. The methodology was initially developed during an experiment to determine feasibility of landscape mapping based on small-scale, low-resolution satellite imagery. Images produced by Landsat-1 were interpreted for five test sites. These sites, located in the United States (Kansas and Tennessee), Uganda, Western Australia, and Papua New Guinea, were selected to include a wide range of vegetation and landform types in areas where either direct surface observations or previously published landscape maps were available. Results of that experiment indicate that landscape boundaries may be delimited from Landsat-type imagery with accuracies of 85 to 95 percent. This accuracy range is the same as the range found on published landscape maps. Based on that result, the hypothesis that satellite imagery may be used as a base for landscape mapping was accepted. The results indicated that vegetation and landform features are the predominant mapping criteria when using satellite imagery. This represents a departure from the traditional emphasis on lithology as a landscape mapping criterion but also improves the connection between landscapes and ecosystems.

Based on the original results and subsequent investigations of a number of other sites, the following methodology has been developed.

1. **Preliminary activities** involves the selection of imagery and acquisition of supporting data. The ideal image set appears to consist of at least two images possessing, among the members of the set, the following characteristics; (1) vegetation at near optimum growth condition, (2) vegetation in dormant or near-dormant growth condition, (3) relatively high (45-55°) solar elevations in high relief areas and relatively low (40-45°) solar elevations in low relief areas, and (4) complete cloud-free coverage among the image set.

Supporting data include both published and field-acquired data covering topics such as climate, vegetation types, soil types, landforms, lithology, tectonics, and human land use practices. Rarely, if ever, will all of these types of data be available for a study area. Nor will the absence of some of them make the interpretation impossible. Nevertheless, they should be obtained and employed if available.

2. _Image interpretation_ consists of boundary delimitation and description of the bounded areas. Delimitation is the essential interpretation function while description may be added during post-interpretation field work if necessary. Image interpretation consists of a three-step sequential process, involving (1) vegetation, land use, and water boundary delimitation, (2) landform type boundary delimitation, and (3) bounded area description. In an actual mapping situation, these three activities can be performed simultaneously and all boundary delimitation might as well be done as a single activity, but description of the units should be reserved as a separate activity.

3. _Field survey_ is designed to refine the image interpretation map and obtain data which cannot be extracted from the imagery. Field investigations are structured to visit the largest possible number of mapping units and mapping unit boundaries to check boundary locations and develop full descriptions of vegetation, landforms, soils, geology, human use, animal communities, and any other appropriate topics. In addition, interactions of these features may be examined.

4. _Final preparation_ of the map and report involves, (1) re-examination of the imagery to refine boundary locations and to determine which mapping units are to be assigned to each landscape as established by the field survey, (2) aggregation of mapping units to a level appropriate to the planning objectives of the project, and (3) publication of the results.

The report illustrates the sequence of steps outlined above with examples appropriate to land resources development, for which this methodology appears quite suitable.

UTILISATION OF LANDSAT DATA FOR DELINEATING,
MAPPING AND MANAGING OF SOIL RESOURCES -
THE PROBLEMS AND PROSPECTS UNDER INDIAN CONDITIONS

A.N. SINGH,   L. VENKATARATNAM,
A.K. SINHA, ** P. VENKATACHALAM,**
K.R. RAO   AND   R.S. DWIVEDI

NATIONAL REMOTE SENSING AGENCY, HYDERABAD, INDIA
**
CENTRE FOR STUDIES IN RESOURCE ENGG., IIT, BOMBAY, INDIA

ABSTRACT

The utility of Landsat data, both digital and
analog, for small scale mapping of soils and their
limitations/hazards has been discussed in this paper.
The areas covered for mapping of soil resources by
using Landsat multispectral data in India are shown.
Both image oriented as well as computer-aided numerical
approaches have been used in this study. Delineation
of areas affected by salinity/alkalinity, erosion, water
logging etc. have been successfully done for some areas
in the country. The problems and prospects in utilisa-
tion of Landsat data for mapping of soils and their
limitations have also been discussed.

1. INTRODUCTION

India, with a total geographical area of 326.8 million hectares, dis-
playing a great diversity of climate, vegetation and soils, is mainly an
agricultural country. It has been estimated that about 81.0 million hectares
of the total cultivable land in India require protection through soil conser-
vation measures. In addition to this, several million hectares of agricultural
land have been affected by salinity/alkalinity, ravines, water logging and
drifting sand. It is very essential to ameliorate the salt-affected land,
stabilise the sand dunes, control sand drifts, check the soil erosion and
reclaim the ravine-infested land. For this purpose, soil maps showing these
problem areas are needed so that corrective measures can be taken up by
appropriate agencies. Soil maps hitherto have been prepared by ground surveys
which are rather tedious and time-consuming. Now, aircraft and satellite
multispectral remote sensing techniques along with computer systems have
provided the soil scientist with a new mapping tool which enables mapping
soils at a faster rate. In this paper, the utility of Landsat multispectral data
for mapping soil resources in India together with the problems encountered
and the prospects are briefly discussed.

---

2. METHODOLOGY

Both the image oriented as well as computer-aided numerical oriented approaches have been followed in NRSA, the premier organisation engaged in using Landsat data for soil mapping in India,and at other centres as well. In the image-oriented approach,soil boundaries are first drawn on an overlay based on the image characteristics, slope, vegetation pattern and erosion conditions. Field visits are made for the collection of ground information regarding the soil composition,magnitude of erosion, slope and vegetation pattern in each image-interpretation unit and to verify its areal extent. Modifications in the boundaries drawn earlier, wherever needed, are made based on the ground observations. The soil boundaries are then transferred to a base map prepared using the Survey of India toposheets. In the computer-aided, numerical oriented approach, the methodology followed is same as reported earlier by Venkataratnam (1980) and Venkataratnam & Rao (1977 a). In short, this involves utilising Landsat computer compatible tapes for supervised classification on the Bendix Mulspectral Data Analysis System (M-DAS) using a maximum likelihood algorithm.

3. REMOTE SENSING FOR SOIL SURVEY AND MAPPING

The establishment of the Indian Photo-interpretation Institute at Dehradun in 1966 gave an impetus to the use of aerial photographs for soil survey and mapping in India. However, Apichandani (1965) had earlier reported the use of aerial photographs for soil mapping in the arid tracts followed by many other workers. Later, Apollo space photo (Krishnamoorthy and Srinivasan, 1973) and Landsat imagery (Mirajkar and Srinivasan, 1975) were used for small scale soil mapping. However, it was only after the establishment of the National Remote Sensing Agency (NRSA) in 1975 that the Landsat data have been extensively used in the field of soil surveying in India.

For the first time in India, NRSA (1976) used the Landsat MSS data together with computer-implemented pattern recognition techniques for small scale soil mapping. Map generated from IBM 370/140 computer was found to be fairly comparable with a soil map prepared by using aerial photographs. In another study,soil map prepared using Multispectral Data Analysis System (M-DAS) and enlarged on printer-plotter system for Ghaspani area of Nagaland was found comparable with the reconnaissance soil map prepared by the soil survey wing of State Agricultural Department (Venkataratnam and Rao,1977 b). Small scale soil maps were later prepared for four canal command areas in Andhra Pradesh, part of Tamilnadu, Nagaland, Upper Barak Watershed area, Drought prone areas of Karnataka, part of West Coast, Haryana, parts of Uttar Pradesh etc. using the Landsat MSS data. The areas covered for soil mapping by NRSA are shown in Fig.1. The soil maps so far prepared are at 1:250,000 scale showing mainly the association of subgroups. But in some cases, if the units are larger and spectrally separable,lower taxonomic categories could also be separated. It was also shown that by interpretation of Landsat imagery along with topographic and geological information, more accurate soil maps as compared to conventional maps in terms of boundary delineation and composition of soil mapping units could be prepared (Singh,1980 a). Apart from NRSA, other organisations, namely All India soil and Land Use Survey, Centre of studies in Resource Engg., Central Arid Zone Research Institute and Haryana Agril. University have also made attempts to use Landsat data for soil studies.

4. MAPPING SOIL ASSOCIATIONS

Soil associations are soil landscapes that occur in repeating patterns. Although soil association maps of small scale are not as precise for interpretations as detailed soil maps of large scale, they are much cheaper and are useful for regional planning. Case studies from two different physiographic regions of India-parts of Karnataka and Kerala in West Coast region and Chandrapur in Deccan Plateau region wherein Landsat data have been used for preparation of soil association maps are presented here. Fig.2 is the soil map of a part of West Coast region prepared by visual interpretation of standard False Colour Composite on 1:250,000 sca . Based on the lithology, four major landscape units have been identified and further sub-divided into various physiographic units based on image characterstics, slope, drainage, land cover and erosion conditions. Table-1 is the legend showing soil composition, land use and erosion hazard in each mapping unit.

Fig. 3 is the soil map of a part of Chandrapur prepared by visual interpretation of black and white and false colour composite Landsat prints. The broad physiographic divisions delineated in the map correspond to three major land systems, namely Fluvial, Sedimentary and Archean. In the sedimentary landscape, map unit 1 represents hilly, forested terrain whereas unit 2 is moderately gullied, gently sloping pediplains under forest. Units 3 and 4 are severely gullied, gently sloping to undulating forested pediplains and gently to undulating cultivated pediplains, respectively. The Archean landscape consists of hilly, forested terrain(map unit 5), gently sloping to undulating, moderately eroded pediplains(unit 6), gently sloping to rolling, severely eroded pediplains (map unit 7) and gently sloping pediplains under cultivation(map unit 8). The alluvial plains(map unit 9) are under cultivation.

A comparison of the map shown in Fig.3 with the soil map prepared earlier by systematic air photo-interpretation technique showed a significant correlation with respect to delineation of soil boundaries which indicates the usefulness of Landsat data for soil association mapping.

5. MAPPING SOIL LIMITATIONS/HAZARDS

The major soil limitations of agricultural lands include salinity/sodicity, erosion, water logging, excessive permeability, rockiness, etc. The salt-affected soils appear white in the Landsat false colour imagery due to salt efflorescence on the surface. Studies carried out at NRSA in the States of Haryana and Uttar Pradesh have shown that two degrees of salinity as well as waterlogged areas could be delineated using Landsat MSS data(NRSA 1979&1981,Venkatratnam 1980, Malleswara Rao et al. 1980) Fig.4 is the M-DAS classified, printer-plotter map of two levels of salinity delineated for a big saline patch seen south of Meerut city in Uttar Pradesh. This is based on the classification of Landsat MSS data (path row No.157-040) dated 8 March 1977. The rest of the soil units in the area which are normal or slightly saline were merged into a single category.

A qualitative estimation of soil erosion can be deduced from landscape and soil characteristics, vegetation intensity and landuse pattern as observed on Landsat imagery. The study carried out in the West Coast region of India(Legend-Fig.2) has shown that six soil erosion classesviz. nil to slight,slight,slight, to moderate, moderate, moderate to severe and severe could be delineated in the area. On this soil erosion class map, watershed boundaries of approx.8,000 to 12,000 ha size, which is easily delineated on the Landsat imagery, can be overlaid. The area under different erosion classes in each watershed can then be estimated and an average erosion index of watersheds prepared. This index will be useful in locating the priority areas for soil conservation measures.

Ravines comprising intricate networks of gullies offer great potential for the development of agriculture and forestry after necessary reclamation.Landsat data have been used by Singh(1977) and Singh(1980 b) in earlier studies for

broad reclamative groupings of these lands into deep, medium and shallow ravines. Shallow and medium ravines can be developed for intensive cultivation by undertaking suitable soil conservation measures whereas deep ravines could be used for forestry.

6. PROBLEMS & PROSPECTS OF UTILISATION OF SATELLITE DATA FOR STUDIES ON SOILS IN INDIA

Soil maps in India have been prepared hitherto by ground surveys although stereoscopic observation of aerial photographs have increased the efficiency of soil surveyors to a great extent. Accuracy in delineation of boundaries of various soil units has increased with the use of aerial photographs. Now, it is established that the remotely sensed data from space platforms could be used for preparing low intensity soil maps which could be used later for more detailed soil mapping. Although a very small scale soil map has been prepared in 1965 for world soil map project by mostly compiling the data available on soils in the country, till now, there is no soil map of India even at 1:1 million scale. Probably satellite data is the only answer for the geographically larger and a developing country like India to prepare an accurate map of soil resources atleast on 1:1 million scale. There is a worldwide thinking to improve the resolution of the satellite data in the future remote sensing satellite programmes in which case the efficiency of soil mapping would further increase.

It was also found possible to delineate and map the soils affected by various soil limitations/hazards like salinity/alkalinity, waterlogging, ravines, erosion, excessive permeability and rockiness/rock outcrops. Of course misclassification might creep in especially when satellite data is processed on computer aided multispectral data analysis systems because of presence of moisture and/or vegetation on the soil surface. However, seasonal changes in the soil cover, salinity in the soils and efficiency of reclamatory efforts on the problem soils could be monitored very effectively by using Landsat multitemporal data.

The soil maps, prepared using the remotely sensed data, would give necessary information needed for the regional planning for effective utilisation of other natural resources like surface and ground water. After suitable annotation and superimposing the drainage pattern and topographic features, these soil maps would be very beneficial for proper landuse planning in various developmental projects.

7. ACKNOWLEDGEMENTS

790

REFERENCES

Abichandani, C.T. 1965. Use of aerial photographs in soil survey of arid zone of Western Rajasthan.Ann. Arid Zone, 4:172-184.

Bali, Y.P. and Karale, R.L. 1977. Reclamability classification of ravines for agriculture. Soil Cons. Digest, 5 (2): 40-47.

Krishnamoorthi, G. and Srinivasan, T.R. 1973. Interpretation of an Apollo Space photo for small scale soil mapping in respect of an area in Bihar. J. Indian Soc. Photo-int.1 (1 and 2) : 75-82.

Mirajkar, M.A. and Srinivasan, T.R. 1975. Landsat photo-interpretation for preparation of small scale soil map through a multistage approach. J. Indian Soc. Photo-int. 3 (2): 87-92.

National Remote Sensing Agency, 1976. Pilot project for satellite remote sensing survey of parts of Punjab and Haryana. NRSA Abstract Report, Secunderabad, India.

National Remote Sensing Agency, 1979. Satellite Remote Sensing Survey of Haryana. NRSA Project Report, Secunderabad, India

National Remote Sensing Agency, 1981. Satellite remote sensing survey of soil and landuse in a part of Uttar Pradesh. NRSA Project Report, Secunderabad, India.

Malleswara Rao, T.Ch.,Venkataratnam, L. and Rao,K.R. 1980. Contrast enhancement of Landsat data on Multispectral Data Analysis System.J. Indian Soc. Photo-int. and Remote Sensing , 8 (2): 27-32.

Singh, A.N. 1980 a. Comparison of reconnaissance soil maps prepared by conventional method and Landsat imagery interpretation. J. Indian Soc. Photo-int. and Remote Sensing. 8 (1): 1-6.

Singh, A.N. 1980b. Delineating ravinous areas on aerial Photographs and satellite imageries-a comparative study. Paper presented at the seminar on Application of Photo-interpretation and Remote Sensing Techniques for Natural Resources surveys and Environmental Analysis, IPI, Dehradun, India.

Singh, B.M. 1977. Interpretation of Satellite imagery for delineation of ravines. J. Indian Soc. Photo-int. 5 (1) : 31-34.

Venkataratnam, L. 1980. Delineation and mapping of agricultural soil limitations/hazards in arid and semi-arid tropics using Landsat MSS data-an Indian example. Proc. Fourteenth Internat. Symp. Remote Sensing Environment. ERIM, Ann Arbor, Michigan, 23-30 April, 1980 pp. 905-914.

Venkataratnam, L. and Rao, K.R. 1977a. Ground truth methodology for soils. NRSA Document 21, Secunderabad, India.

Venkataratnam, L.and Rao, K.R. 1977b. Computer-aided classification and mapping soils and soil limitations using Landsat multispectral data. Proc. Symp. on remote sensing for Hydrology, Agriculture and Mineral Resources, Nov. 15-17, SAC Campus, Ahmedabad, India, pp. 101-104.

Fig. 1

INDIA
STATUS OF SOIL MAPPING
BASED ON LANDSAT MSS DATA IN NRSA
1982

REFERENCES

LANDSAT IMAGE FRAME

SOIL MAPPING COMPLETED

SOIL MAPPING BEING TAKEN-UP

SOIL MAP
PART OF WEST COAST, INDIA

Fig - 2

BASED ON LANDSAT IMAGERY INTERPR-
ETATION

793
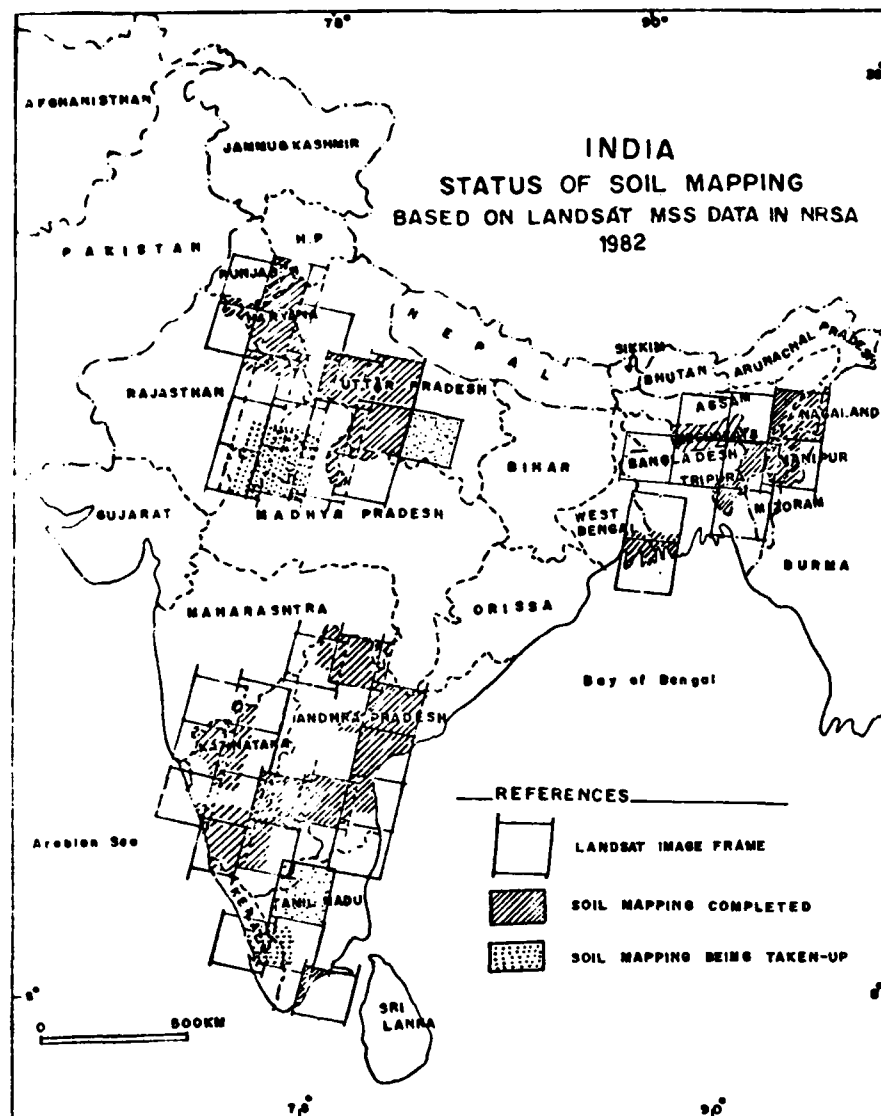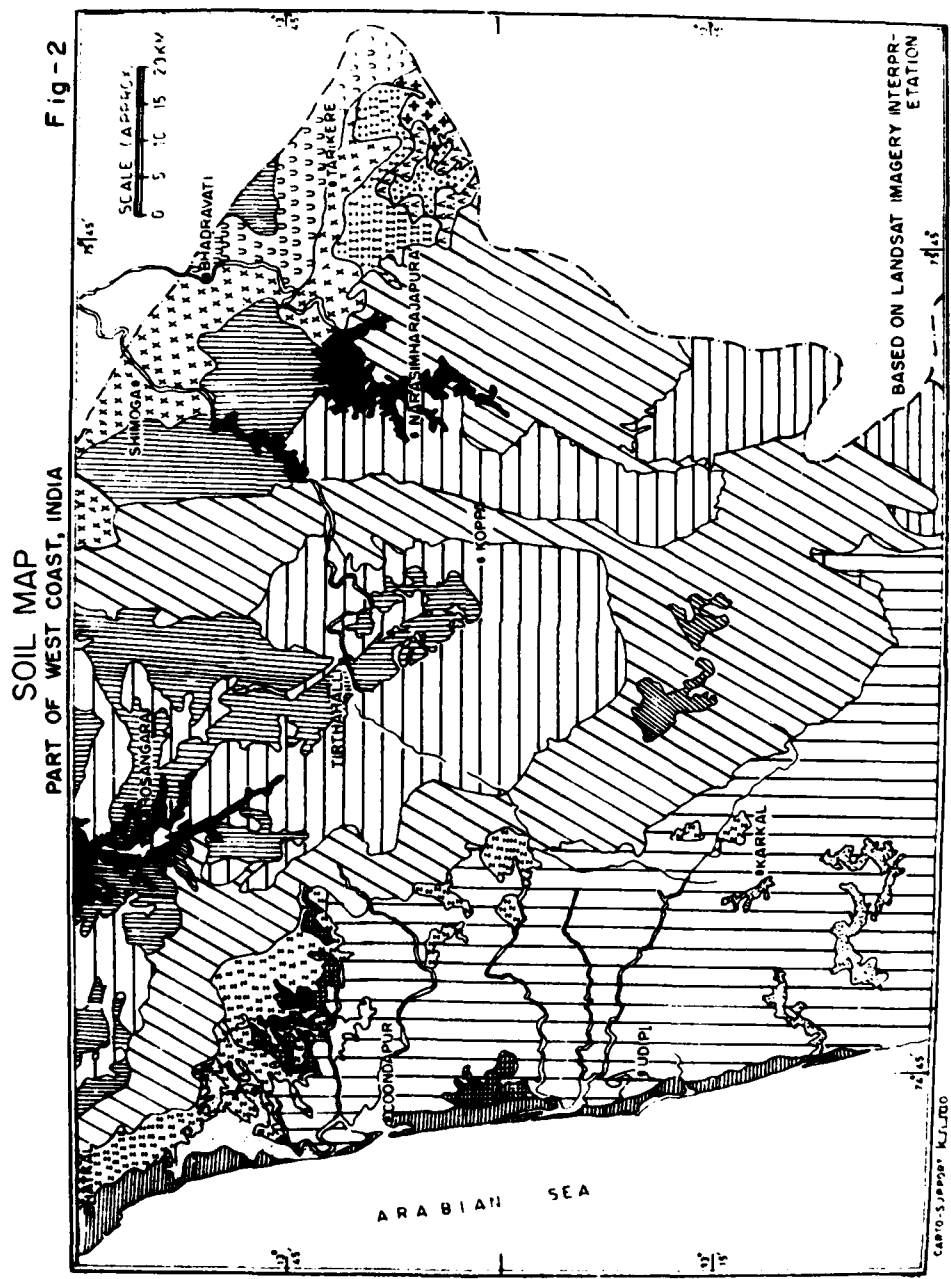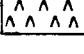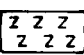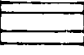
Table-1 LEGEND FOR SOIL MAP OF PART OF WEST COAST (FIG.2)

Symbol	Landform	Soils	Landuse	Erosion

Soils from Dharwar schists

Symbol	Landform	Soils	Landuse	Erosion
/////	Steep sloping hills	Very deep, loamy soils(Ultic Tropudalfs and Ultic Rhodudalfs	Thick forest	Slight
/////	Steep sloping hills	Very deep, gravelly sandy loam to loams (Typic Dystropepts)	Scrubs	Moderate to Severe
I I I	Low hills	Very deep,loamy soils(Udic Rhodustalfs and Udic Haplustalfs)	Thick forest	Moderate
^ ^ ^	Low hills	Moderately deep, gravelly loam, (Typic and Lithic Ustorthents)	Scrubs	Moderate to Severe
· · ·	Narrow infilled valleys	Very deep loams to clay loams, poorly drained soils(Aeric and Typic Tropaquepts)	Cultivation	Nil to slight
· · ·	Broad Valleys	Very deep, dark, cracking clay soils(Typic Chromuderts)associated with very deep poorly drained calyey soils(Aeric Ochraqualfs)	Cultivation	Nil to slight

Soils from Laterites

Symbol	Landform	Soils	Landuse	Erosion
Z Z Z	Hills	Deep gravelly loam soils with low bases(Typic Hapludults and Rhodudults)	Thick forest	Slight to moderate
(dotted)	Hills	Moderately deep gravelly loams (Lithic Troporthents)	Scrubs	Severe
(grid)	Valleys	Very deep loams and clay loams (Tropofluvents)	Cultivation	Slight
(vertical lines)	Uplands	Deep,gravelly loams to clay loams (Typic Rhodudults)	Plantation	Moderate

Soils from Cordierite Gneisses

Symbol	Landform	Soils	Landuse	Erosion
(horizontal lines)	Hills	Deep,loamy soils(Ultic Tropudalfs)	Thick forest	Moderate
(vertical lines)	Hills	Deep, gravelly loams (Typic Dystropepts)	Waste land & grasses	Severe
u u u u	Broad valleys	Deep,dark,cracking clays (Typic Paleuderts)	Cultivation	Nil to slight
x x x	Broad Valleys	Deep,poorly drained loamy soils(Typic Tropaqualfs)	Cultivation	Nil to slight

Soils from coastal alluvium

Symbol	Landform	Soils	Landuse	Erosion
(lines)	Coastal alluvium	Very deep sandy soils(Tropopsamments) associated with heavier,poorly drained,deep soils (Tropaquents)	Cultivation	Moderate erosion

794

SOIL MAP OF A PART OF CHANDRAPUR DISTRICT, MAHARASHTRA   Fig.3

(BASED ON LANDSAT IMAGERY INTERPRETATION & SELECTIVE FIELD CHECK)

795

Fig -4

SALT AFFECTED SOILS
SOUTH OF MEERUT CITY

DELINEATED FROM LANDSAT MSS DATA 27/0/40

HIGHLY SALINE
MODERATELY SALINE
VEGETATION/BUILT UP AREA

MEERUT
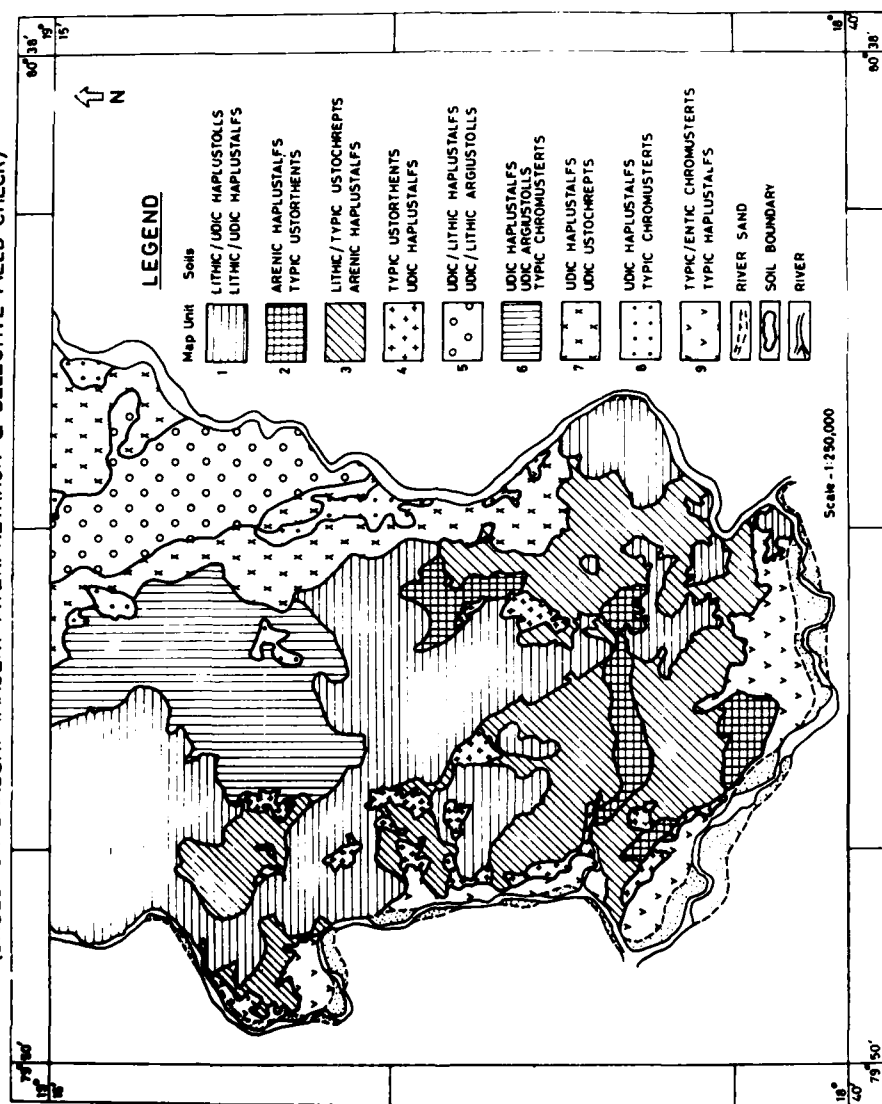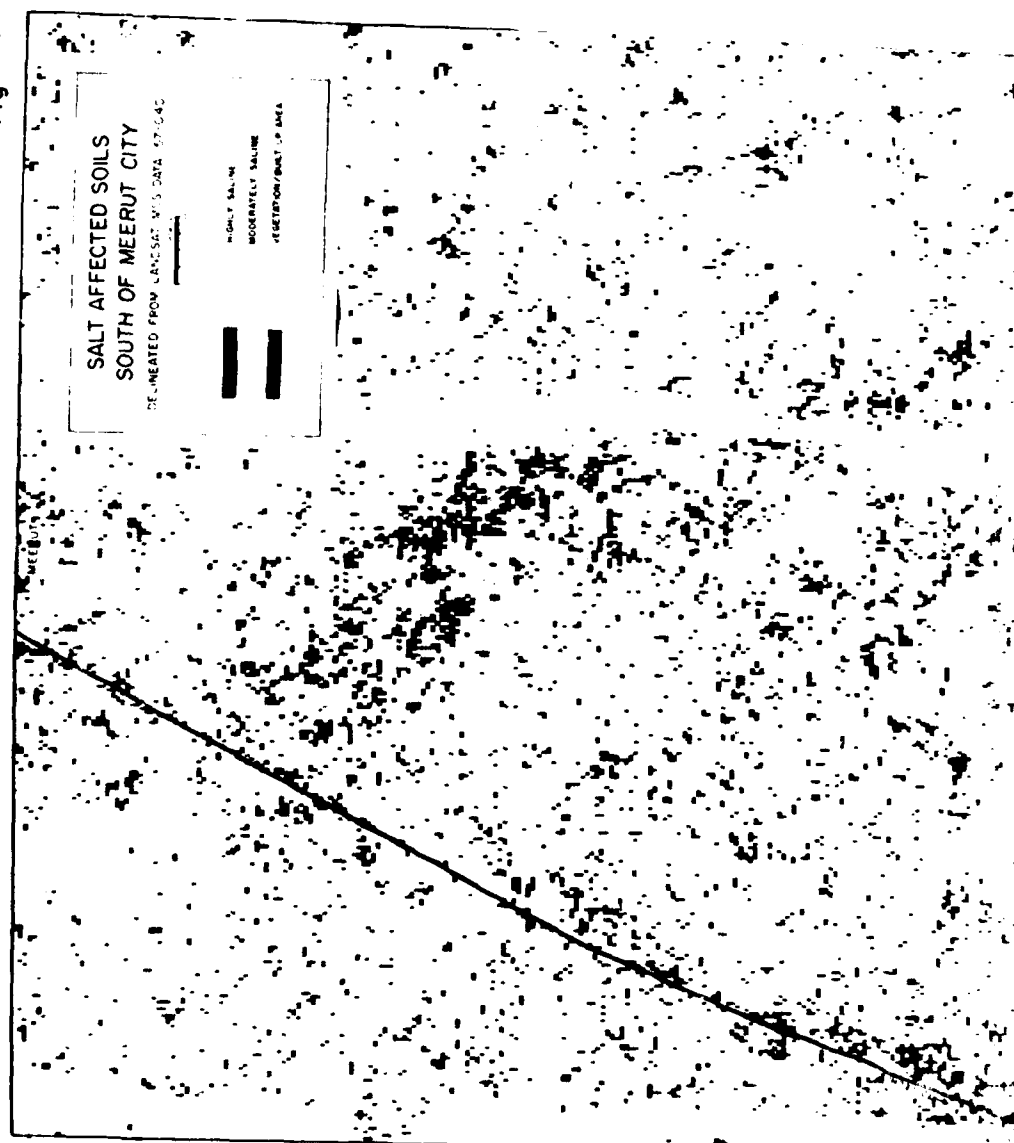
VEGETATION SURVEY IN AMAZONIA USING LANDSAT DATA*

Y. E. Shimabukuro
J. R. dos Santos

Instituto de Pesquisas Espaciais - INPE
Conselho Nacional de Desenvolvimento Científico e Tecnológico - CNPq
C.P. 515 - São José dos Campos - SP - Brasil

L. C. S. de Aquino

Comissão Estadual de Planejamento Agrícola - CEPA
Estrada do Aleixo, Km.2 - Manaus - AM - Brasil

ABSTRACT

The objective of this study is to analyze vegetation of the pilot area selected which is among the various program-areas of the Project for Rural Integrated Development (PRID) for Amazonas State. This study was done using automatic Image-100 analysis of LANDSAT data, through the MAXVER classification algorithm. In the pilot area, four vegetation units were mapped automatically in addition to the areas occupied for agricultural activities. The vegetation units are: upland dense forest; forest in humid areas; secondary vegetation and flood plains. Results from the print-out were verified in the ground observations and good correspondence was noted. The Image-100 classified results together with a soil map and the auxiliary information from RADAR images, permitted the establishment of the final legend with six classes. They are: semi-deciduous tropical forest; lowland evergreen tropical forest, secondary vegetation; tropical forest of humid areas, predominant pasture land and flood plains. In addition, the automatic analysis separated two water types based on their sediments indicating different geological and geomorphological aspects. The physico-chemical conditions of water are associated with the agricultural productivity. When combined, this information facilities the planning for agricultural activities of upland and humid areas, and through these activities the rational utilization of the available resources in the Amazonas State.

1. INTRODUCTION

To advance the socio-economic development of the Amazonas State, the government implanted the Project for Rural Integrated Development (PRID). This program will be sponsored by World Bank and the State Commission of Agricultural Planning consultants. This project proposes the study of various program-areas with the aim of giving an orientation to the occupation and better use of the natural resources. Recognizing the need to efficients survey the resources of that extensive region, the technical group of the PRID project decided to use Remotely Sensed data from the Multispectral Scanner Subsystem (MSS) of LANDSAT.

This work is a part of the PRID and therefore has the objective of surveying the vegetal cover in the pilot area, through the automatic analysis of digitized MSS data. The study of the vegetation is a fundamental step in planning the rational interaction of man and land.

2. STUDY AREA

The pilot area (Figure 1) is located between 2°40' to 3°00'S Latitude and

57°00' to 57°20'W Longitudes in the Barreirinha program-area which is a part of the Project for Rural Integrated Development for Amazonas State. This pilot area was chosen because it is representative of the general area and also has a priority in the developmental plan for that region.

3. METHODS FOR AUTOMATIC ANALYSIS

The interpretation of data recorded on CCT tapes (246 path/62 row on July 15, 1978) was executed by the Image-100 System of the Instituto de Pesquisas Espaciais (INPE). The Image-100 is one of several processors used for the extraction of remotely sensed information with unique spectral characteristics (Schaller and Towles, 1975).

The methodology developed for the Image-100 system to discriminate the types of vegetative cover included: projection of the scene on the image monitor and application of the program "noise" to eliminate defects; delimitation of the pilot area at the scale of 1:100,000, and application of the program "single-cell" to evaluate the spectral responses of the classes which could be mapped; application of the MAXVER algorithm, developed by Velasco et al (1978), to obtain spectral parameters of each class, together with the covariance matrix and the classification matrix which permitted the evaluation of the superposition among all the classes. The classification results were shown in DICOMED format and the print-out at the scale of 1:20,000. The classification results on the image monitor was also enhanced using the program "Theme Uniformization" a 3 x 3-pixel spatial filter (Dutra, 1982).

4. RESULTS AND DISCUSSION

Based on the supervised classification using the "MAXVER" classifier algorithm, it was possible to discriminate the following classes of vegetation: upland dense forest, flood plains, forest of humid areas, secondary vegetation and predominant pastureland. The spectral signatures of these classes can be seen in Table 1.

Due to the different spectral characteristics of the surface water observed in MSS images, it was possible to discriminate two other classes: "white" water and "dark" water according to the typology created by Sioli (1967) during studies of limnology, carried out in the Amazonia region.

Figure 2 shows the spatial distribution of the mapped classes obtained by using the "MAXVER" classifier, while Table 2 shows the areal extent of each class.

It can be verified in Figure 2, that the surface water studies may help the agriculture planning in this region once the higher concentration of agriculture activities is located near the areas of "white" water. According to Junk (1979) rivers with "dark" water have a low capacity of biological production due to the low pH and fertility and high concentration of humus. "White" water is geochemically richer than "dark" water.

The print-out (scale 1:20,000) obtained from the automatic classification was checked with ground observations and a very high correlation was found. The combined information from soil map, radar image and LANDSAT data permitted the defining of the final legend: semideciduous tropical forest, low land evergreen tropical forest, secondary vegetation, tropical forest of humid areas, predominant pastureland and flood plains.

The knowledge of the physiognomy and floristic composition of vegetation obtained by the ground observations are important source of additional information in this kind of work. The forest species like Bertholletia excelsa, Pouteria sp., Diplotropis purpurea, Dipterix odorata and Ocotea sp. were in

798

the upland regions. In areas subjected to flooding the presence of
Montrichardia arborescens is very common and, more specifically in flood plains
the presence of Euchinochlos polystachya, Paspalum rupens, Panicum zizanoides,
Paspalum fasciculatum. In agricultural areas of uplands Hevea brasiliensis and
cassava plantations are found, while in low lands, the major crops being
cultivated are beans, corn,"juta" and "malva".

The study of Hueck (1972) provides information about the forest composition
in the Amazonia region. This information permitted a better understanding of the
typology employed in this study.

The land-use in the humid tropics is discussed by Molion and Bentancurt
(1980). They call attention to the consequences of deforestation and the
destruction of the vegetal surface layer (serrapilheira). This first
planting and pastures causes a transformation of the soil into a nutrient
deficient mass.

5. CONCLUSIONS

The methodology used in the automatic analysis of LANDSAT data permitted
the mapping of the vegetal coverage of the region as well as the characterization
of the crop areas.

The knowledge of the spatial distribution of the vegetation units can
permit the monitoring of the occupation process. It will also be possible to
indicate the best areas for pasture land and cropping.

REFERENCES

DUTRA, L.V. Desenvolvimento de alguns métodos de pós-processamento aplicados
a imagens digitais multiespectrais. (Técnicas de uniformização de temas).
São José dos Campos, INPE, 1982 (No prelo).

JUNK, W.J. Recursos hídricos da Amazônia: utilização e preservação. In:
Simpósio Nacional de Ecologia, 2., Belém, 1979. Anais. Belém, 1980, V.1.
p. 54-70.

MOLION, L. C. B.; BENTANCURT, J.J.V. O clima e o uso da terra nos trópicos
úmidos. Roessléria. 3(2): 165-187, 1980.

SCHALLER, E.S.; TOWLES, R.W. Image-100: the interactive multispectral image
processing system. In: NASA Lyndon B. Johnson Space Center. Nasa Earth
Resources Survey Symposium; proceedings of a Symposium held in Houston, Tx,
june 9-12, 1975. Washington, DC, NASA, 1975, V.1 B, p. 1275-1291.

SIOLI, H. Studies in Amazonian waters. In: Simpósio sobre a Biota Amazônica,
Belém, 1966. Atas. Belém, 1967, V.3, p.9-50.

VELASCO, F.R.D.; PRADO, L.O.C.; SOUZA, R.C.M. Sistema MAXVER: manual do
usuário. São José dos Campos, INPE, jul. 1978 (INPE-1315-NTI/110).

Table 1. Spectral Parameters of Classes Obtained from the MAXVER Program.

C L A S S	MSS CHANNELS			
	4	5	6	7
"DARK" WATER	17.99	9.49	4.37	2.49
"WHITE" WATER	24.79	22.29	11.25	4.16
UPLAND DENSE FOREST	22.67	14.89	54.60	65.56
PREDOMINANT PASTURELAND	25.77	17.50	74.87	85.75
FLOOD PLAINS	30.98	23.55	71.80	76.54
FOREST OF HUMID AREAS	20.25	12.21	19.01	17.92
SECONDARY VEGETATION	28.69	21.71	57.21	59.68

Table II. Area Occupied for Each Class Obtained through Image-100 System.

C L A S S	AREA (HA)	PERCENTAGE
"DARK" WATER	1,996.48	10.19
"WHITE" WATER	770.09	3.93
UPLAND DENSE FOREST	8,359.50	42.55
PREDOMINANT PASTURELAND	2,005.57	10.23
FLOOD PLAINS	1,426.25	7.28
FOREST OF HUMID AREAS	1,518.10	7.74
SECONDARY VEGETATION	3,197.85	16.31
NOT CLASSIFIED	346.56	1.77
STUDY AREA	19,600.00	100.00
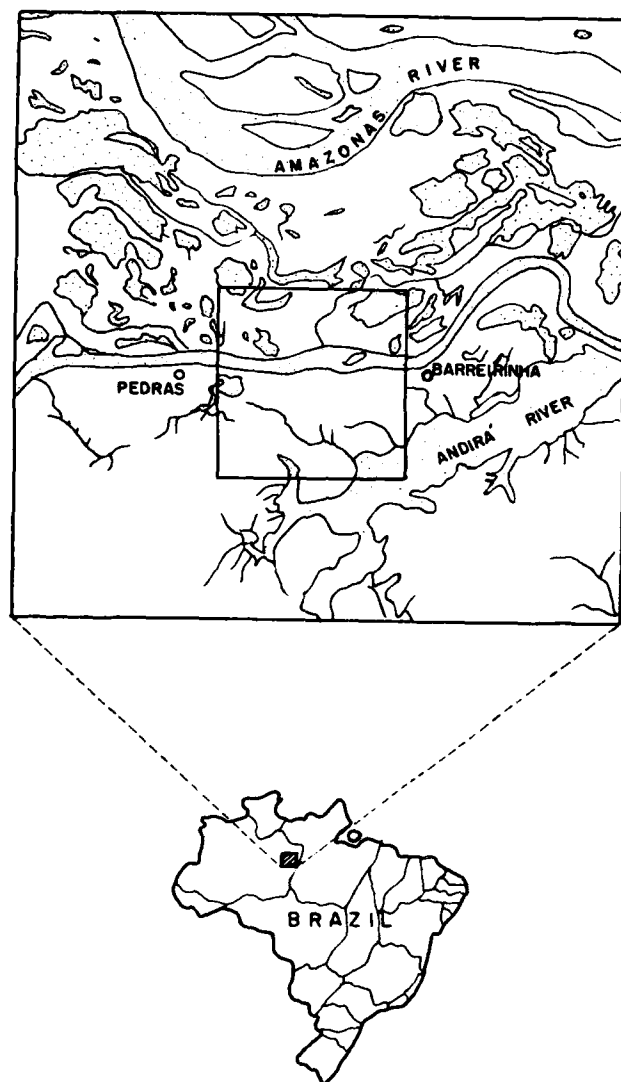
Figure 1. Location of the study area.

801

● "DARK" WATER

"WHITE" WATER

● UPLAND DENSE FOREST

● PREDOMINANT PASTURELAND

● FLOOD PLAINS

● FOREST OF HUMID AREAS

● SECONDARY VEGETATION

Figure 2. Automatic classification obtained from the MAXVER algorithm.
(Original figure in color)

DEVELOPMENT OF A KNOWLEDGE-BASED EXPERT SYSTEM FOR
RICE CROP IDENTIFICATION

Larry R. Tinney
John E. Estes

University of California
Santa Barbara, California

SUMMARY

A basic research effort has been initiated to demonstrate the feasibility
of building a knowledge-based expert system capable of scene inference tasks
associated with renewable resources applications. A fairly well-constrained
problem -- the identification of rice fields using satellite remote sensing and
collatoral data sets -- has been selected for developing the first renewable
resources system using this new approach to pattern recognition. Artificial
intelligence techniques used in expert systems more closely mimic human decision-
making processes than previously used paradigms, exhibiting a number of powerful
characteristics which clearly differentiate them from traditional algorithmic
or numerical approaches. These characteristics include the ability to pursue
and explain decisions in terms of a line of reasoning as opposed to merely
following a sequence of steps in a calculation. These and other useful charac-
teristics offer the potential to improve the performance of remote sensing
systems and hopefully bridge a gap that has in the past existed and to a very
real extent continues to exist today between remote sensing discipline experts
and the eventual user of information derived from them.

In addition to specifically addressing the knowledge base necessary for
rice crop identification, this research effort will systematically examine the
current status and future potential for automated generation and incorporation
of all input feature used in the decision-making procedure. A top-down design
approach is being used for system development; this will allow the system to
be exercised immediately using manually interpreted features. Specific feature
elements will be assessed in terms of how critical to the decision-making
process they are and how amenable their derivation is to automated calculation.
This evaluation should provide a solid foundation for selecting input features
(e.g., is it a field? what is the texture like? etc.) to be automated while
leaving others, at least temporarily, to the analysts interpretation. To
facilitate automation we plan to explore the interfacing requirements necessary
for linking expert systems with data base management systems, including consid-
eration of the unique data structure characteristics found in pictoral data
base systems.

Initial results of applying an expert systems approach will be presented
and compared to conventional manual and digital crop identification procedures.
This new approach appears capable of eventually incorporating both "common sense"
and expert knowledge into pattern recognition procedures, something that has
been largely missing from existing automated systems.

LAND USE MAP FOR THE CHACO PROVINCE OF ARGENTINA
BASED ON VISUAL INTERPRETATION OF LANDSAT IMAGERY

Lino Luis Ledesma

Instituto Nacional de Tecnologia Agropecuaria
Buenos Aires, Argentina

SUMMARY

Through a process of visual interpretation of Landsat images a land use map differentiating five classes was created at scale 1:500,000 for the Chaco province of Argentina. The study utilized information from Landsat 1 and 2 using channel 5 and 7 at scales 1:1,000,000, 1:500,000, and 1:250,000.

A total of 550 soundings taken in 1972 were selected to define the capability and potential of the land. Each sounding was classified using the system developed by the United States Department of Agriculture for soil Taxonomy and Land Use.

The Chaco province is divided in 22 geomorphological areas, in each one of these areas a sounding was selected as a representative sample for the geomorphological environment. The soundings were plotted in black and white photography at 1:35,000 and 1:50,000 scales.

Although the United States Department of Agriculture classification system recognizes eight land use classes for agriculture and forestry, this study utilized only five classes due to limitations imposed by the scale of 1:500,000 selected for the study. The five classes have the following characteristics:

Class 1: (II in Soil Conservation Manual 210 USDA)
- Large crop potential.
- Light hydrological and wind erosion.
- Light salinity and alcalinity.
- Crop yield reduced due to lack of humidity.

Class 2: (III in Soil Conservation Manual 210, USDA).
- Average crop potential.
- Moderate hydrological and wind erosion.
- Crop yield frequently reduced by lack of humidity during normal dry periods.
- Moderate salinity and alcalinity.
- Flooding can destroy crops or prevent the use of soil for a certain number of years.

Class 3: (IV in Soil Conservation Manual 210, USDA).
- Limited crop possibilities.
- Better suited for pasture or hay production.

Class 4: (V in Soil Conservation Manual 210, USDA).
- Permanent pastures.
- Large risk of water erosion.

Class 5: (VII in Soil Conservation Manual 210, USDA).
- Potential use of land for grazing or forestry purposes with moderate limitations.

The assignments of land types to each one of the classes are based on the physical characteristics of the soil, the land cover, and in function of the regional climate. For the present study, the class assignment was based on the knowledge of the taxonomic classification of soil in the Chaco province. The information derived from the Landsat images together with the field information permitted the regional classification of the land according to the taxonomic classification of soil.

The land use map will be used to solve the problems of uncontrolled development, deterioration of environmental quality, loss of prime agricultural lands, destruction of important wetlands, and loss of fish and wildlife habitats.

MONITORING GEOMORPHOLOGICAL PHENOMENA OVER ARID AND SEMI-ARID LANDFORMS IN SOUTHERN TUNISIA UTILIZING IN SITU AND SATELLITE SPECTRAL DATA

T.J. Munday

Imperial College of Science and Technology
London, England

SUMMARY

The Tunisian Pre-Sahara is characterized by a variety of landform types typical of the arid and semi-arid regions in North Africa. In particular the area is dominated by the presence of three large closed depressions similar in form to the playas of the Western United States. Known locally as the Chotts, the largest of the three is the Chott Djerid.

The surficial forms that characterize the Chott and its periphery are varied both in their nature and extent. They include salt clay flats, thin puffy crusts, nebkhas and thick salt pavements among others. All these forms are a direct response to a variety of geomorphic processes, although those found on the Chott proper are largely a function of groundwater discharge. Fluctuations in this discharge are a response to long term hydrologic trends, and also to short term atmospheric pressure changes. These fluctuations manifest themselves in changes in the crustal morphology of the Chott's surface and they may occur in the space of a few days, or several months.

Remote sensing techniques may offer the geomorphologist a unique means for monitoring these fluctuations by identifying alterations in the crustal morphology, thereby providing an insight into the processes active in the Chott's origin and subsequent development.

With this in mind a small study was undertaken to assess the potential offered by these techniques for fulfilling two aims. First, to indicate that geomorphic parameters that were significant in determining reflectance, and second, to determine whether Landsat MSS data was capable of discriminating between different surface types on and within Chott Djerid.

A small sample area on the edge of the Chott was stratified into eleven visually distinct units. In situ spectral data and ground measurements were collatated for each unit. Ground spectra were gathered using a Milton Multiband Radiometer with Landsat bandpass equivalents.

These data were correlated with geomorphic parameters using multiple regression analysis. Those measured parameters most significant in determining reflectance were % iron content, % soluble salts, % soil moisture, % detrital cover (blown sand), and % vegetation cover. Bivariate analysis of the ground spectra indicated a high correlation between bands, and considerable overlap between some sample units. This was substantitated by similar analysis of Landsat MSS data derived for each of the units. Previous work indicated that the discrimination between different surface types in the sampled area was primarily a result of their differing albedos. Differences in albedo are the result of variations in the levels of iron and soluble salt in the surface crusts of the Chott. On its periphery, changes in albedo were largely the result of changes in % vegetation cover and the amount of blown sand lying over the surface.

Discriminant analysis run on Landsat MSS digital data derived for each sample unit, showed a variety of results. Poor discrimination occurred between units located on the Chott proper which exhibited a high % of soluble salts in their crusts relative to the detrital materials present. Moreover discrimination between sites with high %'s of wind blown sand cover was also shown to be poor. Strong discrimination was seen between units that had high levels of iron present in the surface layers, and those with vegetation and blown sand cover.

Landsat MSS data was capable of distinguishing between most of the classes initially selected. It is suggested, however, that because the relative brightness of the sample units assumes so much importance in this discriminatory process, perhaps comparable results might be obtained using RBV data, for example. The use of satellite based data sources shows much potential as a means for monitoring geomorphic processes, and as shown in this study, it affords the geomorphologist the opportunity to record changes in the nature and extent of several cover types. In the case of Chott Djerid this data might provide a means for monitoring, indirectly at least, changes in ground water discharge.

THE INTEGRATION OF IMAGERY, ELEVATION MODELS AND POLYGON COORDINATE FILES

THROUGH A COMMON MAP BASE*

Jerry Clark

Research Scientist
SCIENCE APPLICATIONS, INC.
1001 Knox Street
Torrance, CA 90502

ABSTRACT

The purpose of this study was the integration of remotely-sensed imagery and cartographic data by reprojecting them to match a common map base with a Universal Transverse Mercator projection. The three data types were: aircraft multispectral NS001 scanner imagery simulating the spectral channels of the Landsat-4 Thematic Mapper from visible to thermal infrared; Digital Land Mass Simulator (or Arc-Second) digital terrain models; and, land use polygon coordinate files created by the Environmental Sciences Research Institute. Each of the data types had inherent resolutions and projections that were changed somewhat during the reprojection process. Techniques included control point selection from imagery and reference maps; map base calculations based on the cataloguing and manipulating of control points with the Image Based Information System (IBIS); and spatial and spectral rectifications of the imagery and cartographic data using algorithms of the VICAR (Video Image Communication and Retrieval) image processing system. The resultant data base, with reprojected imagery, elevation models and land use files are available (from the EROS Data Center, USGS, Sioux Falls) as data sets having an areal coverage corresponding to USGS 7½-minute topographic quadrangles in the Los Angeles, California area.

1. INTRODUCTION

The integration of disparate data through a common map base provides a means for making imagery and cartographic data more functional for analytical comparisons. Seven channels of imagery from an aircraft multispectral scanner (MSS) were spatially-registered with a digital elevation model and a series of land use polygon coordinate files by using a Universal Transverse Mercator (UTM) map projection as a reference for reprojecting the data. The purpose was to make disparate data types more compatible, and to make the data sets available to researchers who would show the analytical value of the integrated data for fundamental research or applications. Several studies have already made use of disparate data that were spatially-registered [1-11].

An important difference in approach in this study is the use of a common map base to which all data types were registered through a process that included map base creation, image reprojection, and data integration.

2. DATA TYPES

Three data types were used: Thematic Mapper Simulator (TMS) imagery, Digital Land Mass Simulator (DLMS) digital elevation model and the Environmental Science Research Institute (ESRI) land use polygon coordinate files for Los Angeles. All the imagery and cartographic data sets have inherent resolutions that were changed somewhat during the reprojection process to permit comparisons between data sets. A 15 meter resolution was chosen to maintain the high level of detail available in the MSS imagery and ESRI land use files. The 30 meter resolution was used to more appropriately simulate the 30 meter resolution of the Thematic Mapper sensor on Landsat-4. The cartographic data were integrated with the imagery so they could be used as ancillary data for analysis of the imagery.

The NS001 MSS, functioning as the TMS, had eight channels in the ultraviolet to thermal infrared range. However, only the last seven channels were functioning at the time of data acquisition: channel 2 had a wavelength of .52 to .60 microns; channel 3, .63 to .69 microns; channel 4, .76 to .90 microns; channel 5, 1.00 to 1.30 microns; channel 6, 1.55 to 1.75 microns; channel 7, 2.08 to 2.35 microns; and channel 8, 10.4 to 12.5 microns. Its inherent resolution of about 14 to 16 meters along the flight path was reprojected to 15 and 30 meters. It was flown in a C-130 at 20,000 feet altitude over Los Angeles on July 12, 1980, by Johnson Space Center in Houston. Five flight paths were flown, with two images per flight path.

The DLMS is a type of digital elevation model distributed by the National Cartographic Information Center (NCIC) of the United States Geological Survey (USGS) in Reston, Virginia. They were created by the Defense Mapping Agency (DMA) but were reformatted by the USGS for public distribution. The DMA refers to them as DLMS digital terrain elevation data and the USGS calls them Arc-Second digital elevation model. Each DLMS covers an area one degree square with resolution cells that are measured in arc-seconds, not meters. One cell is a three arc seconds square with an equivalent resolution of about 76 meters along the latitude and 92.5 meters along the longitude. The DLMSs were reprojected to a UTM projection with resolution cells standardized to 15 and 30 meters. Original resolution cells were replicated using a bilinear interpolation. The digital elevation data were reformatted to register terrain data to the TMS imagery at the selected resolutions, 15 meters and 30 meters.

Finally, the ESRI (of Redlands, California) land use polygon files provided coordinate points demarking the land use boundaries within the area of standard USGS 7½-minute topographic quadrangle maps. ESRI mapped land use from high altitude color infrared and conventional quadrangle maps. ESRI mapped land use from high altitude color infrared and conventional 1:24,000 scale low altitude photography flown in November, 1976 and field checked throughout 1977. The polygon coordinate data were converted from State Plane Coordinates to the UTM projection coordinates of the map base and their land use identifiers were made into images with 15 and 30 meter resolution. Eighty-five land use classes were available among eight general groupings: residential, commercial, industrial, transportation/utilities, institutional, open space, agriculture, and vacant[12].

3. COMMON MAP BASE CONCEPT

In their existing forms, the disparate spatial data did not match; however, a commonality was established by rectifying the data to a common map base. A common map base made disparate image and cartographic data types more functional by providing a standard spatial reference that minimized unique projection differences and reformatted data to the same scale. The imagery, digital terrain models and polygon coordinate data were acquired or produced in different, and unregistered forms. The reference used was the UTM map projection, a projection commonly used as the basis for mapping physical and cultural features. UTM mathematical characteristics provided the link between the coordinate system of the data and the map base. The unique projection differences of the disparate data types were minimized by transforming to the common map base. The imagery had an inherent projection which was determined by the movements of the platform as well as the sensor mechanisms [13]. Similarly cartographic data was presented in different projections. However, when the different data types were reprojected to approximate the common map base projection, the data were easier to use in conjunction with each other, especially because the data were reprojected to a similar scale. Finally, imagery and cartographic data integrated to a common map base make available to researchers a layered data base for multispectral, multitemporal, multisensor, and multiscale analysis.

4. MAP BASE CREATION

Therefore, a map base was used to convert a map projection to image coordinates with map coordinates accurately expressed to fractions of picture elements in a line and sample coordinate system. [14,15,16,17]. The process for creating a map base, which is a translation of map projection coordinates to image lines and samples, and reprojecting imagery to match the map base, is summarized in three steps: control point selection, map base calculations, and image reprojection (Figure 1). Common features, such as street intersections, were found to tie the imagery to the map base. Linear features were so prominent in the MSS imagery that an individual street intersection and its line and sample location were easily found. The same intersection was also found on a USGS 1:24,000 scale 7½-minute topographic quadrangle map. Therefore, the line and sample location of the intersection had an equivalent latitude and longitude location. Thus, not only were images and maps related visually through similar features, but with the proper referencing, the coordinates were interchangeable so that the coordinate system of one data type could also define the respective features of other data types [18]. Dissimilar coordinate units were made compatible through calculations setting up the map base that was compatible with the UTM map projection and served as the basis for relating multiple data types to one another. The image, through a process of geometric corrections, would approximate the orientation and systematic distortion of the map projection and would adapt, within the realm of the map projection, to the scaling, or resolution, constraints of picture elements. In other words, all picture elements in an image reprojected to match the projection of the map base, would have a specific resolution, such as 30 meters per picture element.

The map base data set, an Image-Based Information System (IBIS) [19,20] interface file, was formed by merging the reformatted image and map control points, then detection and editing of bad control points. It contained information about each point, indicating where that point was in the original image and where it should be in the reprojected image. Residuals were calculated to show the variation of image control points from a "best fit" surface of the map control points for use in editing bad points. The edited control points were subjected to a surface fit algorithm to establish a smooth surface that described the best use of the points to create a potentially error-free reprojected image.

5. IMAGE REPROJECTION

The images were reprojected using a geometric and radiometric bilinear-resampling program available with the Video Image Communication and Retrieval (VICAR) program package [21,22]. The program approximated the UTM map projection of the map base by a spatial alteration of the images through rotation, expansion/contraction, and local adjustments so that the picture elements matched the calculated parameters controlling resolution, orientation and distortions. The spectral information was preserved by bilinear interpolation.

6. DATA INTEGRATION

The reprojected imagery and the cartographic data were not completely spatially-registered until they were extracted by quadrangle areas, based on USGS 7½-minute quadrangle maps. After the individual aircraft MSS imagery were reprojected they were digitally mosaicked into a composite image (see reference 23 for mosaicking of Landsat data). Each of the ten reprojected images had a position within the larger mosaic map base, as determined by a line and sample offset from the origin, and was digitally-positioned within the mosaic (Figure 2). Quadrangle areas (Figure 3) were extracted from the mosaicked MSS imagery and from the reprojected DLMS image. A binary mask for each quadrangle area was created from boundary coordinates that had been reprojected with the same map base standards that existed for the imagery and cartographic data. Each binary mask was used to isolate its equivalent area in the MSS mosaic and the DLMS image. The resulting extracted areas completed the spatially-registered quadrangle areas for the three data types (Figures 4,5,6).

7. CONCLUSIONS

Several disparate data types were integrated by using control points as the basis for spatially-registering the data to a map base. The data were reprojected to match the coordinates of the reference UTM map projection, as expressed in lines and samples. The most critical aspect of integrating the Thematic Mapper Simulator MSS imagery with the cartographic data was control point selection. Control points chosen from the imagery were subject to error from mislocated points, either points that did not correlate well to the references map or minor pixel offsets because of interactive cursorring errors. Errors also developed in map control points when points were improperly located and digitized, leading to inaccurate latitude and longitude coordinates. Non-systematic aircraft platform variations, such as yawl, pitch, and roll, affected the spatial fidelity of the imagery, when compared with the quadrangles. Features in adjacent flight paths did not always correspond properly because of the systematic panorama effect and alteration of flight line direction, as well as platform variations. The map base creation and image reprojection process was not able to correct all variations, but the TMS data sets provided a good approximation of Thematic Mapper data that will be available from the space platform. Control point selection with the cartographic data was done with relative ease because only the corner coordinates of the quadrangle areas needed to be defined.

The integrated imagery, digital elevation models and digital land use maps are organized by quadrangle areas and are available on magnetic computer tape to researchers by contacting User Services at the U.S. Geological Survey EROS Data Center, Sioux Falls, South Dakota 57198, area code (605) 594-6511, and requesting the Los Angeles Integrated Data Sets.

812

8. ACKNOWLEDGEMENTS

9. REFERENCES

1. Chavez, Jr., P.S., J.T. O'Connor, D.K. McMacken, and E. Eliason, "Digital Image Processing Techniques of Integrated Images and Non-Images Data Sets," Proceedings, Thirteenth International Symposium on Remote Sensing of Environment, Environmental Research Institute of Michigan, Ann Arbor, April, 1979.

2. Clark, J., "Training Site Statistics from Landsat and Seasat Satellite Imagery Registered to a Common Map Base," Proceedings, Fall Technical Meeting, American Society of Photogrammetry, Niagara Falls, New York, October 7-10, 1980, pp. RS-1-F-1 to 9.

3. Clark, J., "Improved Land Use Classification from Landsat and Seasat Satellite Imagery Registered to a Common Map Base," Proceedings, 47th Annual Meeting, American Society of Photogrammetry, Washington, D.C., February 22-27, 1981, pp. 591-599.

4. Davis, J.B. and S.Z. Friedman, "Updating Urbanized Area Maps Through the Integration of Landsat and Conventional Data," Proceedings, 45th Annual Meeting, American Society of Photogrammetry, Washington, D.C., March 19-23, 1979, pp. 776-791.

5. Friedman, S.Z., Image-Based Approach to Mapping, Charting and Geodesy, JPL Internal Document 715-153, Jet Propulsion Laboratory, California Institute of Technology, Pasadena, California, February 1982.

6. Goodenough, D.B., B. Guindon, and D.M. Teillet, "Correction of Synthetic Aperture Radar and Multispectral Scanner Data Sets," Proceedings, Thirteenth International Symposium on Remote Sensing of Environment, Environmental Research Institute of Michigan, Ann Arbor, April, 1979, pp. 259-270.

7. Strahler, A.H., T.L. Logan, and C.E. Woodcock, "Forest Classification and Inventory System Using Landsat, Digital Terrain and Ground Sample Data," Proceedings, Thirteenth International Symposium on Remote Sensing of Environment, Environmental Research Institute of Michigan, Ann Arbor, April, 1979.

8. McLeod, R.G. and H.B. Johnson, "Resource Inventory Techniques Used in the California Desert Conservation Area," Proceedings, Arid Lands Resources Inventories Workshop, La Paz, Mexico, Nov. 30 - Dec. 6, 1980; and, Resource Inventory Techniques Used in the California Desert Conservation Area, JPL Internal Document 715-91, Jet Propulsion Laboratory, California Institute of Technology, Pasadena, California, October 15, 1980.

9. Naraghi, M., W. Stromberg, and M. Daily, "Geometric Rectification of Radar Imagery Using Digital Elevation Models," Photogrammetric Engineering and Remote Sensing, Vol. 49, No. 2, February, 1983, pp. 195-199.

10. Wu, S.T., Analysis of Results Obtained from Integration of Landsat Multispectral Scanner and Seasat Synthetic Aperture Radar Data, Report. No. 189, Earth Resources Laboratory, National Space Technology Laboratories, NSTL Station, Mississippi, February, 1981.

11. Zobrist, A.L., R.J. Blackwell, and W.D. Stromberg, "Integration of Landsat, Seasat, and Other Geo-Data Sources," Proceedings, Thirteenth International Symposium on Remote Sensing of Environment, Environmental Research Institute of Michigan, Ann Arbor, April, 1977, pp. 271-289.

12. ESRI, _Central Division Land Use Study For Southern California Edison Company and Los Angeles County Planning Department Using the Polygon Information Overylay System (PIOS)_, Environmental Systems Research Institute, Redlands, California, April 3, 1978.

13. Ungar, S.G., "Scanner Imaging Systems, Aircraft," _Proceedings_, NASA Workshop on Registration and Rectification, N.A. Bryant, editor, JPL Publication 82-23, Jet Propulsion Laboratory, California Institute of Technology, Pasadena, California, June 1, 1982, pp. 138-152.

14. Moik, J.G., _Digital Processing of Remotely Sensed Images_, NASA Special Publication 431, National Aeronautics and Space Administration, Washington, D.C., 1980

15. U.S. Dept. of Army, _Remote Sensing Applications Guide_, Engineer Pamphlet 70-1-1, Technical Guidance, Part 2 of 3, Dept. of the Army, Office, Chief Engineers, Washington, D.C., October, 1979, pp. 5-32 to 5-44.

16. Zobrist, A.L., "Multiple-frame, Full Resolution Landsat Mosaicking to Standard Map Projections," _Proceedings_, Fall Technical Meeting, American Society of Photogrammetry, Albuquerque, N.M., October, 1978, pp. 608-616.

17. Zobrist, A.L., "Map Characteristics of Landsat Mosaics," _Proceedings_, 45th Annual Meeting, American Society of Photogrammetry, Washington, D.C., March 19-23, 1979, pp. 260-273.

18. Graham, M.H., _Digital Overlaying of the Universal Transverse Mercator with Landsat-Data Derived Products_, NASA Technical Memorandum 58200, Lyndon B. Johnson Space Center, Houston, Texas, September, 1977.

19. Bryant, N.A., and A.L. Zobrist, "IBIS: A geographic Information System Based on Digital Image Processing and Image Raster Data Type," _IEEE Transactions on Geoscience Electronics_, The Institute of Electrical and Electronics, The Institute of Electrical and Electronics Engineers, Inc., Volume GE-15, No. 3, July, 1977, pp. 152-159.

20. Zobrist, A.L., N.A. Bryant, S.Z. Friedman, and G.L. Angelici, _Image-based Information System (IBIS) System Guide_, JPL Internal Document 900-909, Jet Propulsion Laboratory, California Institute of Technology, Pasadena, California.

21. Castleman, K.R., _Digital Image Processing_, Prentice-Hall, Inc., Englewood Cliffs, New York, 1979.

22. Seidman, J.B., and A.Y. Smith, _VICAR Image Processing System_: Guide to System Use, JPL Publication 77-37, Revision 1, Jet Propulsion Laboratory, California Institute of Technology, Pasadena, California, December 1, 1979.

23. Zobrist, A.L., N.A. Bryant, and R.G. McLeod, "Technology for Large Digital Mosaics of Landsat Data," _Photogrammetric Engineering and Remote Sensing_, submitted for publication 1983.
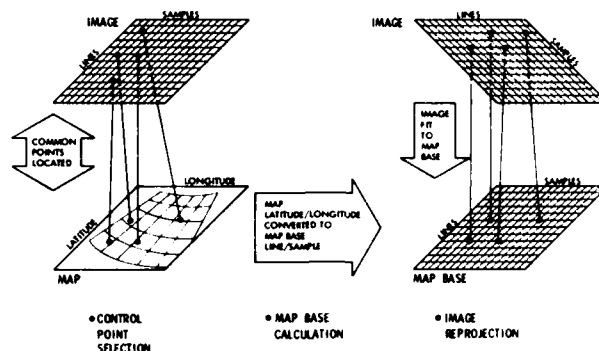
Figure 1. Image to map base transformation: Common ground control points are selected between an image and map; the latitude and longitude coordinates of the map control points are converted to the map base line and sample coordinate system; and, the image is reprojected to fit the line/sample coordinate system of the map base--the image is rectified so it acquires the resolution and map projection characteristics of the map base.
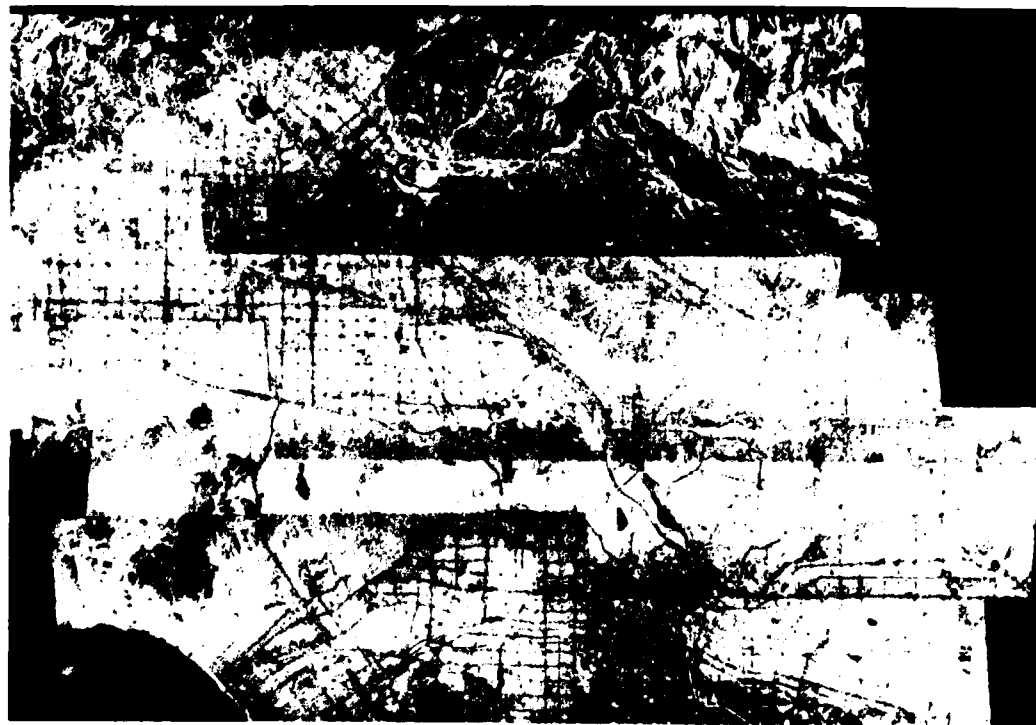
Figure 2. Ten aircraft MSS images (Thematic Mapper simulation of spectral channel 4, in the .76 to .90 micron near infrared range) of the Los Angeles area were reprojected to a UTM map projection and digitally mosaicked at a 15 meter resolution. The imagery were acquired from the NS001 sensor flown at 20,000 feet on July 12, 1980, by the C-130 aircraft from Johnson Space Center.
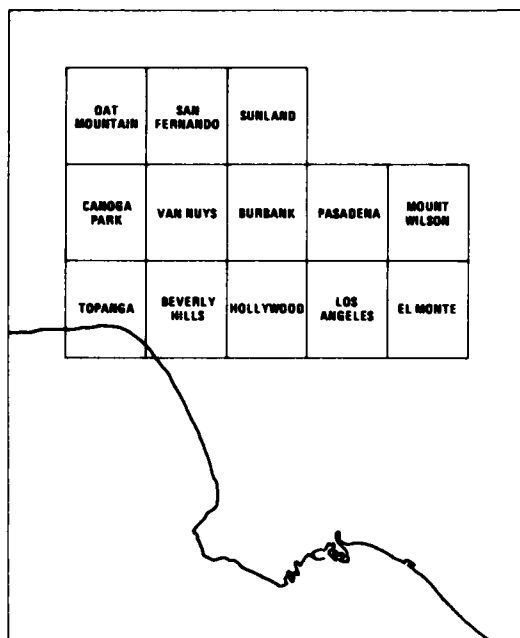
Figure 3. Quadrangle areas in the Los
Angeles Basin that have reprojected
aircraft MSS imagery, digital terrain
files, and land use data sets with
areal coverage corresponding to USGS
7½-minute quadrangle maps.

Figure 4. The reprojected Thematic
Mapper simulation of spectral chan-
nel 3 (.63 to .69 microns; red) for
the Los Angeles quadrangle.
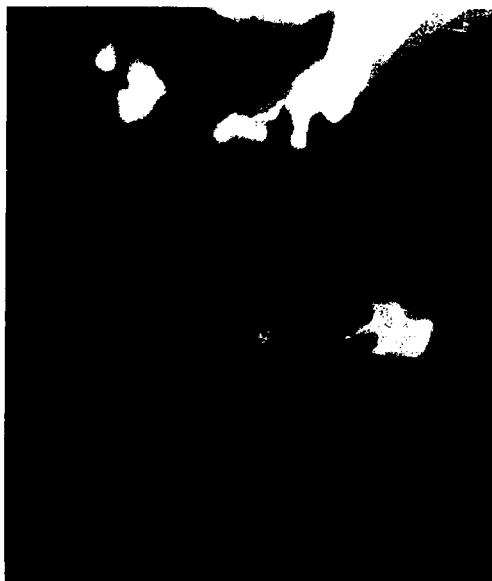
Figure 5. The reprojected DTM for the
Los Angeles quadrangle area. (Each
change in greytone indicates a 9 meter
change in elevation, however, the digi-
tal data retains 1 meter elevational
accuracy).

Figure 6. The reprojected land use
map for the Los Angeles quadrangle
area. A possible 85 different land
use classes are represented in the
digital data.

DESIGN AND DEVELOPMENT OF ACTIVE MICROWAVE INSTRUMENTS
FOR OCEANOGRAPHIC MEASUREMENTS FROM SPACE

Erich H. Velten

Dornier System GMBH
Friedrichshafen, West Germany

SUMMARY

The first European Remote Sensing Satellite (ERS-1) which is to be launched
in 1987 will serve oceanographic data requirements with first priority. Two
payload instruments have been chosen as a core payload, namely a Radar Altimeter
and an Active Microwave Instrumentation (AMI).

The Radar Altimeter will be able to measure significant waveheight in the
range from 0 to 24 m over ocean on a global basis. Furthermore, measurement of
the backscatter coefficient for wind field determination will be performed. In
addition, altitude information will be available at those parts of the orbit,
where accurate position determination of the satellite is being performed.

The present instrument design is based on a Ku-band (13.7 GHz) front end
-sing a direct feed parabolid antenna. The microwave system includes the duplexer,
calibration unit, frequency and chirp generators, receiver and high power ampli-
fier. An instrument dedicated onboard processor, either of the split gate
tracker type or of the maximum likelihood estimator type will be included.

The Active Microwave Instrumentation is a C-band (5.3 GHz) multipurpose
radar which can be used for high resolution imaging over land or over oceans
for wave spectrum measurement and for wind field (wind speed and wind direction)
measurement. The imaging and wave measurement modes apply the synthetic aper-
ture radar (SAR) techniques. The wind observation is based on a close relation-
ship between the wind velocity and the ocean surface roughness due to capillary
waves. The backscatter coefficient is in turn a function of the sea surface
roughness. Thus, the windspeed can be determined from backscatter coefficient
measurement. Wind direction is derived from the assymetry of upwind/downwind
backscattering and the polarization dependency.

Both instruments which have been investigated in detail in feasibility
studies under contracts from the European Space Agency (ESA) require significant
advances of the present state of the art. Therefore, a technology program for
early development of critical elements has been started in 1979. Examples of
activities being performed presently are:

o   The SAR-antenna, which is a 10 m x 1 m unfoldable planar array slotted
    waveguide antenna. Breadboarding activities for manufacturing of metal-
    lized waveguides made from Carbon Fibre Reinforced Plastics have been
    completed successfully. Presently the electrical, mechanical and thermal
    testing of a 1 m antenna panel is underway.

o   The WIND-SCATTEROMETER antennas will most probably use similar technolo-
    gies to achieve a very different radiation pattern in two polarizations.
    Design and Breadboarding has just been started.

o   The High Power Amplifiers for AMI and for the Radar Altimeter consisting
    of Travelling Wave Tubes (or Klystrons), Electronic Power Conditioner
    and associated RF electronics.

o   The onboard processor for the AMI-wind scatterometer mode and the
    processor for altimeter data extraction as well as the ground processor
    for SAR Quick-look image generation from raw data. All these processors
    have to operate at real-time speeds.

   The paper will review the mission requirements for ERS-1 and its payload
instruments in terms of their application potential for oceanographic and
land measurements. The major part will be concentrated on the instrument design
and selected reference solutions. The major achievements of technological
development activities for critical areas of the instruments will be presented.

A METHOD FOR THE RETRIEVAL OF PHYTOPLANKTON AND SEDIMENT CONTENTS FROM
REMOTE MEASUREMENTS OF SEA COLOUR IN THE COASTAL ZONE -
RESULTS OF VALIDATION TESTS

S. Tassan

Commission of the European Communities
Joint Research Centre
Ispra, Italy

SUMMARY

Remote measurements of sea colour, carried out by satellite-borne sensors, are capable to provide information on the substances contained in the upper water layers. The problem of obtaining quantitative results about the main seston components, i.e., phytoplankton and inorganic sediment, is, however, far from being solved for the general case when the above quantities are independent variables (e.g., coastal waters).

The main difficulties encountered are linked to the low value of the water upwelling radiance relative to the measured radiance component due to the presence of the atmosphere, as well as to the particular spectral signatures of chlorophyll-a and sediment, which do not allow a simple discrimination between these substances on the basis of their optical effects.

A method for the retrieval of phytoplankton and inorganic sediment contents in the general case including a procedure for the determination of the atmospheric correction, has been elaborated through a theoretical simulation pattern and tested by sensitivity analysis techniques (ref. 15th ERIM Symposium). This paper presents the results of validation tests of the proposed method versus experimental data collected in a coastal zone of the Adriatic Sea, where high quantities of inorganic sediment (uncorrelated to phytoplankton) are discharged by the Po River. The data considered (CZCS images and sea truth values) were provided by the Joint Research Centre of the European Community, in collaboration with the Istituto per lo Studio delle Grandi Masse of the Italian National Research Council.

REMOTE SENSING OF SNOW AND ICE

USING NIMBUS-7 SMMR DATA OVER FINLAND

Martti T. Hallikainen

Helsinki University of Technology*
Espoo, Finland

ABSTRACT

Nimbus-7 SMMR data at 18 GHz and 37 GHz are applied to studies of snow-covered sea ice and snow-covered terrain in Finland. First the dielectric properties of sea ice, snow, and frozen soils are reviewed. Brightness temperatures are calculated using the radiative transfer model. The theoretical results show that snow-covered sea ice and snow-covered terrain are practically identical systems. The only major difference is the presence of vegetation in the case of terrain. Using horizontally polarized satellite data in five test areas of mixed surface types in Finland, slopes of the change of $T_B(18\text{ GHz}) - T_B(37\text{ GHz})$ vs. water equivalent of dry snow are derived for pure surface types of forests, boglands farmlands and lakes. A new algorithm to mapping the water equivalent of dry snow is suggested. The theoretical model is used to interpret the satellite data on snow-covered sea ice.

1. INTRODUCTION

Brightness temperature measurements of first-year, low-salinity sea ice and snow-covered terrain have been made in Finland for several years. It has been shown that the thickness of sea ice (salinity below 2 $^0/_{00}$ by weight) along the Finnish coast can be determined approximately by using a three-channel UHF radiometer (Hallikainen, 1980). At 5 GHz, only open water and thin ice can be discriminated from thick ice. The brightness temperature of snow-covered terrain was measured in 1978-1979 at 5 GHz and 37 GHz (Tiuri et al., 1978). Since 1980, the ground in the test area has been covered by metal sheets to eliminate emission from ground. A theoretical snow model has been used to explain the experimental results (Tiuri, 1982).

The Nimbus-7 SMMR data over Finland, made available by the NASA Goddard Space Flight Center, have been applied to snow and ice studies recently (Tiuri and Hallikainen, 1981; Tiuri and Sihvola, 1982). The data covers the period from October (no snow or sea ice in Finland) through November 1978 (thin snow and ice cover in northern Finland) and February (50 cm to 80 cm of snow, the Finnish coast covered by sea ice) through March 1979 (warm periods start to occur, making the snow wet). The Nimbus-7 radiometer system operates at frequencies of 5 GHz, 11 GHz, 18 GHz, 21 GHz, and 37 GHz. The system is dual-polarized and the look angle is 50°. The surface resolution varies from 144 x 92 km² (5 GHz) to 26 x 17 km² (37 GHz).

---

*On leave of absence from the Helsinki University of Technology at the University of
 Kansas Center for Research, Inc., Lawrence, Kansas, USA.

In this paper, the 18-GHz and 37-GHz data are applied to snow and first-year ice studies. First the dielectric properties of snow, low-salinity sea ice, and frozen soils are reviewed at the two frequencies. A radiative transfer model is employed to calculate the brightness temperatures of snow-covered terrain and snow-covered sea ice. Finally, satellite data under different circumstances is studied and compared with the theoretical results. The size of the resolution cell in the data employed is 60 x 60 km^2 for both 18 GHz and 37 GHz.

2. DIELECTRIC PROPERTIES OF SNOW, LOW-SALINITY ICE, AND FROZEN SOILS

2.1 SEA ICE

The dielectric properties of low-salinity, first-year sea ice have been measured in the UHF range (Hallikainen, 1980). The data covers temperatures from -18°C to -0.1°C, salinities from 0.1 °/oo to 1.5 °/oo and viewing angles with the electric field at an angle of 0°, 30°, and 90° from horizontal. This data has been used along with experimental values for higher frequencies, obtained at lower temperatures (Vant, 1976; Sackinger and Byrd, 1972), to approximate the dielectric properties of sea ice with a salinity of 0.5 °/oo (Figures 1 and 2).

Air bubbles and brine pockets scatter electromagnetic fields in sea ice. Air bubbles are mostly spherical and their diameter is usually around 1 mm along the Finnish coast. The relative volume of air bubbles is about 0.05 in mid-winter and may be up to 0.15 in spring (Hallikainen, 1980). The brine pockets are vertically oriented, elongated ellipsoids. Their average length in high-salinity sea ice is 2 to 3 mm (Poe et al., 1974) and the average diameter is 0.025 mm (Pounder, 1965). In low-salinity ice, the length appeared to be smaller (Hallikainen, 1980). In the scattering calculations, the brine pockets are assumed to be spherical with a diameter of 0.5 mm. This is not a severe limitation, because scattering by air bubbles is dominant in low-salinity sea ice (Figure 3). Only at temperatures above -2°C can the effect of scattering by brine pockets be noticed. The scattering albedos in Figure 3 were calculated using the model of England (1975). The model assumes independent scatterers embedded in the host medium. Since the scattering albedo of sea ice is above 0.2 at 37 GHz, scattering contributes to the brightness temperature of ice. At 18 GHz, scattering is practically negligible.

The total loss of sea ice includes both the dielectric and scattering loss (Figure 4). A surface temperature of -2°C is usual for sea ice due to the insulating snow cover upon it (Hallikainen, 1977). At the bottom of the ice layer the temperature is -0.1°C. Figure 4 shows that even at 18 GHz the attenuation is above 30 dB/m at temperatures higher than -2°C.

2.2 SNOW

The dielectric properties of snow are primarily determined by its wetness. So far, 12 GHz is the highest frequency for which dielectric measurements have been reported (Linlor, 1980). Hence, preliminary results from measurements between 4 GHz and 18 GHz are used in this report (Hallikainen et al., 1982; to be published). The free-space method was employed in the measurements. No corrections due to scattering have been made. The measured values at 18 GHz are shown in Figures 5 and 6, along with estimates for 37 GHz. The estimates are based on the change in the dielectric properties of water at 0°C from 18 GHz to 37 GHz. The measured snow was fairly new (density of dry snow below 0.25 g/cm^3), which explains the low dielectric constant at low moisture levels. The measured and estimated values in Figures 5 and 6 can be used to calculate the dielectric attenuation constant (Figure 7). The loss is so high that even a few centimeters of wet snow is enough to prevent the radiometer from detecting terrain or sea ice below it.

The dielectric constant of dry snow follows closely Equation (1):

$$\varepsilon_r' = 1 + 2\rho \tag{1}$$

where ρ is the density in g/cm^3. Equation (1) was verified to hold up to 18 GHz in recent measurements (Hallikainen et al., 1982; to be published) and will be assumed to hold at 37 GHz as well in this paper. The loss tangent of dry snow has been measured at 9.4 GHz by Cumming (1952). For a density of 0.3 g/cm^3 the value is about 4 x 10^{-4} at -5°C, which gives a loss factor of 6.4 x 10^{-4}. In this paper, a value of 1 x 10^{-3} will be used both at 18 GHz and 37 GHz.

The scattering albedo of dry snow was calculated using the method of England (1975) (Figure 8). Although the values cannot be accurate due to the assumption of independent scatterers, the results indicate that scattering dominates over absorption at 18 GHz and 37 GHz even for reasonable particle sizes. The total attenuation constant, including both absorption and scattering, shows that at 37 GHz the capability of radiometer for determining the thickness of snow layer is strongly limited by the size of the snow crystals (Figure 9).

2.3 FROZEN SOILS

The dielectric properties of Goodrich clay and Fairbanks silt have been measured below 0° at 10 GHz (Hoekstra and Delaney, 1974) (Figure 10). At water contents below 0.10 their properties are fairly close to those of sea ice. The data is expected to hold at other frequencies as well (Hoekstra and Delaney, 1974).

Scattering by pebbles and liquid water pockets has been shortly discussed (England, 1974a). He assumed 0.2 volume fraction of pebbles 1 cm in diameter and obtained a scattering albedo of 0.25 for 5 GHz. An assumption of 0.05 volume fraction of water pockets 0.5 cm in diameter resulted in the same value at 5 GHz. Obviously scattering may be considerably high at 18 GHz and 37 GHz with these assumptions.

2.4 SUMMARY OF DIELECTRIC PROPERTIES

Both sea ice and snow have been shown to be high-loss materials at 37 GHz. In sea ice and wet snow absorption dominates over scattering, whereas in dry snow scattering is the dominant loss mechanism.

Sea ice and wet snow are high-loss materials at 18 GHz, too. The total loss of dry snow consists of approximately equal contributions from scattering and absorption for a particle size of 1 mm.

The dielectric properties of frozen soils are fairly close to those of sea ice. Consequently, the snow-soil and snow-sea ice-water systems resemble each other and the results can be expected to be similar. However, the presence of vegetation will modify the brightness temperature of snow-covered terrain, as discussed in Chapter 4.2.

3. THEORETICAL BRIGHTNESS TEMPERATURES OF SNOW-COVERED SEA ICE AND SNOW-COVERED TERRAIN

3.1 THE RADIATIVE TRANSFER MODEL AND PROBLEM GEOMETRY

The present model is based on the method of England (1974). It has been applied for snow studies in Finland to calculate the brightness temperature of snow pack consisting of several layers with slightly different properties (Tiuri, 1982). Recently, it has been applied for sea ice studies as well (Hallikainen, 1982).

In snow studies the interface between soil and snow is often so rough that total transmission of power can be assumed. In the case of snow-ice and ice-water interfaces the roughness depends on the age and thermal history of ice and snow. Consequently, calculations have been made using total transmission and that determined by the Fresnel coefficients. Multiple reflections are neglected and hence the method cannot be expected to hold accurately in the case of thin specular snow layer upon newly formed ice.

3.2 SNOW-COVERED SEA ICE

Since the attenuation of sea ice is high at both 18 GHz and 37 GHz, radiometers can in most cases detect only the snow layer and top of the ice layer. Figure 11 shows that the brightness temperature at 37 GHz, using vertical polarization and a look angle of 50°, depends on both the snow particle size and the thickness of snow layer. At 37 GHz it is not important whether total transmission or that determined by the Fresnel coefficients is used at the ice-snow interface. The difference is less than 3 K. At 18 GHz the difference may be up to 20 K, depending on the snow particle size and polarization. The effects of snow thickness and snow particle size at 18 GHz are considerably smaller than at 37 GHz.

The difference in absorption and scattering between 18 GHz and 37 GHz can be employed to detect the thickness of snow cover. The result is not unambiguous, due to the effect of snow particle size (Figure 12). In Finland the diameter of ice crystals in snow usually ranges from 0.3 mm (newly fallen) to 2 mm (refrozen). In the bottom of the snow layer the particle size may be up to 4 mm in spring. The particle size dependence is further complicated by the fact that several tens of particles may freeze together and thus form huge particles.

The dielectric loss factor of wet snow is so high that obviously the effect of scattering decreases drastically. The scattering albedo of wet snow cannot be calculated easily because of its complicated structure. The model used in Finland assumes that spherical ice particles are surrounded by shells of water. Another approach might be that water particles are located between the ice crystals and their shape is elongated. Obviously the geometry depends on the wetness, too.

In this paper scattering in wet snow is not considered. The brightness temperature is hence determined by the surface properties. The difference in the brightness temperature between vertical and horizontal polarizations depends on the surface wetness (Figure 13). In the daytime the surface wetness may be higher than 10% and result in a bigger difference than in Figure 13.

3.3 SNOW-COVERED TERRAIN

The theoretical brightness temperature of snow-covered terrain behaves much in the same way as that of snow-covered ice (Figure 14). This can be expected from the high loss of snow and the similarity in the dielectric properties of sea ice and frozen soils. In practice the surface types modify the brightness temperature of snow-covered terrain. In these calculations scattering in frozen soil is not considered.

4. APPLICATION OF SATELLITE DATA TO ICE STUDIES

4.1 GENERAL

The Institute of Marine Research produces ice maps of the Baltic Sea (Figures 15-17). They are based on visual observations and are published twice a week. The maps include ice type classification and ice thickness data. The Institute also gathers data on the snow cover along the coast line once a week. Far from the coast line the snow thickness may, however, be totally different from that near the coast. The wind often makes gently sloping formations of snow.

4.2 EXTENT OF ICE COVER AND ICE CLASSIFICATION

Nimbus-7 data on ice-free Baltic in February through March 1979 gave the following averages for the brightness temperatures of sea water (look angle 50°):

> 37 GHz, horizontal polarization 139 K
> 37 GHz, vertical polarization 202 K
> 18 GHz, horizontal polarization 103 K
> 18 GHz, vertical polarization 158 K

The contrast between open water and ice is highest for horizontal polarization. Since the size of the resolution cell in the data available was 60 x 60 km^2 at both frequencies, 18 GHz horizontal data was applied to estimating the percentage of ice cover within each resolution cell. The resolution is too low to allow mapping of leads.

Figures 15 to 17 show that satellite data gives percentages that appear to be slightly different from the visual observations. On March 5 and March 15 this may partly be due to the time lapse of two days between satellite data and visual observations. In Figure 17 satellite data (taken March 17) shows an area north of the Aland Archipelago in the southern Gulf of Bothnia to be 100% covered by ice in contrast to 0% by visual observations. However, in an ice map issued on March 19 the area is shown to be covered by new ice. This is due to the very cold weather at the time.

This demonstration shows that satellite data can be applied to map the extent of ice cover. Obviously discrimation of thin ice from thick ice, which would be important to ice breakers operating along the Finnish coast, is difficult due to high loss of ice.

Horizontally polarized satellite data seems to be effected by surface features of snow and ice. So far no method to relate it in a reliable manner to the ice classification has been found.

4.3. SNOW COVER UPON ICE

Three test areas were chosen to compare the theoretical results with satellite data (Figures 15 to 17). On February 15 the air temperature in all areas was below -10° C, on March 3 it was above 0° C and on March 17 it was again below -10° C. The theoretical snow thicknesses and particle sizes could not be derived unambiguously from Figures 11 and 12. It has been assumed that the snow particle size is about the same in all test areas and that it increases in a manner observed in 1980 (Tiuri, 1982). No experimental data on snow was available in the test areas, but the results agree satisfactorily with the snow data reported along the coast.

TABLE I. Brightness Temperatures of Snow-Covered Sea Ice in Three Test Areas (see Figure 15) as Measured by the Nimbus-7 Satellite. Theoretical Snow Thicknesses and Particle Sizes are Derived From Figures 11 and 12.

| Date | Test Site No. | Brightness Temperature (K) as measured by Nimbus-7 | | | | | Theoretically Derived Values | | Comments |
		18 V	18 H	37 V	37 H	18 H-37 H	Snow Particle Size (mm)	Snow Thickness (cm)	
February 15, 1979	1	245	227	246	223	4	~ 0.4	~ 30	Transmission at the ice-snow interface close to that determined by Fresnel coefficients (Figure 11b). Snow thicknesses not reliable due to low values of $T_B(18\ H)$ - T_B (37 H).
	2	244	231	255	230	1	~ 0.3	very small	
	3	241	227	251	224	3	~ 0.4	~ 25	
March 3, 1979	1	242	216	239	204	11	-	-	($T_B(37\ V)$ - $T_B(37\ H)$ > $T_B(18\ V)$ - $T_B(18\ H)$ obviously means that scattering cannot be neglected.
	2	248	227	259	228	-1	-	-	
	3	245	228	253	225	3	-	-	
March 17, 1979	1	230	212	215	188	24	0.8 ~ 0.9	~ 30	$T_B(18\ H)$ values lower than expected from Figure 11b. $T_B(37\ V)$ - $T_B(37\ H)$ high, may indicate a surface layer with high ϵ_r'.
	2	238	207	245	205	2	0.8 ~ 0.9	very small	
	3	227	209	225	198	11	0.8 ~ 0.9	~ 20	

5. APPLICATION OF SATELLITE DATA TO STUDIES OF SNOW-COVERED TERRAIN

5.1 EFFECT OF SURFACE TYPES

In practice the main difference between the snow-covered terrain and snow-covered sea ice is the presence of vegetation and other surface features in the case of terrain. The main sur-

face types in Finland are forests, boglands, lakes and farmlands. The effect of surface types on the brightness temperature has been investigated earlier (Tiuri and Hallikainen, 1981). From the data for mixed surface types in Figure 18 the changes in $T_B(18H) - T_B(37H)$ vs. water equivalent of snow can be found for pure surface types (Figure 19). The change is biggest for lakes and smallest for forests. Data for lakes cannot directly be applied for sea ice, because the water equivalent of snow is measured over land. Also, the brightness temperature of lake ice is different from that of sea ice at 18 GHz (Hallikainen, 1982).

5.2 SUGGESTION FOR A NEW ALGORITHM TO MAP THE WATER EQUIVALENT OF SNOW

In a recent report (Tiuri and Sihvola, 1982) the first computer generated maps of the water equivalent of snow W, based on satellite data, have been published. The algorithm includes four constants, the values of which have to be found by trial and error. Hence a new algorithm is suggested. It relies on the use of satellite data and can be trained to better take into account the special features of each winter. The new algorithm is described by Equation (2):

$$\Delta T_B = L \; \Delta T_{BL}(W) + F_a \; \Delta T_{BFa}(W) + B \; \Delta T_{BB}(W) + F \; \Delta T_{BF}(W) \tag{2}$$

where L, Fa, B and F are the fractions of lakes, farmlands, boglands and forests within each resolution cell, respectively. Changes in $T_B(18H) - T_B(37H)$ are designated by ΔT_{Bi}, where i refers to surface type. They are obtained from Figure 19. The solution to Equation (2) is unambiguous.

Since Figure 19 includes also the effect of snow particle size, the values do not necessarily hold in all weather conditions for dry snow. For example a thick layer of newly fallen snow may change the slopes in Figure 19 considerably. Hence a more detailed investigation on the surface effects would be useful.

6. CONCLUSIONS

The theoretical brightness temperatures of snow-covered sea ice and snow-covered terrain have been investigated, based on the dielectric properties of snow, ice and soils. The results are in most cases practically identical and mainly depend on the properties of snow.

Satellite data at 18 GHz and 37 GHz have been applied to sea ice studies along the Finnish coast. The fraction covered by ice within each resolution cell can be determined but discrimination of ice types and thicknesses is obviously difficult. This is due to the snow cover upon ice.

The microwave response of pure surface types has been derived from the data for mixed surface types in several test areas using satellite data. Finally a new algorithm to map the water equivalent of snow has been suggested. The data on which the algorithm is based, can be trained to take into account the special features of each winter while in operational use.

7. REFERENCES

1. England, A. W., 1974, Thermal microwave emission from a halfspace containing scatterers. Radio Science, Vol. 9, pp. 447-454.

2. England, A. W., 1974a, The effect upon microwave emissivity of volume scattering in snow, in ice and in frozen soil, Proc. URSI Specialist Meeting on Microwave Scattering and Emission from the Earth. p. 273, 23-26 September, Berne, Switzerland.

3. England, A. W., 1975. Thermal microwave emission from a scattering layer. Journal of Geophysical Research, Vol. 80, pp. 4484-4496.

4. Hallikainen, M., 1977, Dielectric properties of sea ice at microwave frequencies, Report S94, Helsinki University of Technolo., Radio Laboratory.

5. Hallikainen, M., 1980, Dielectric properties and passive remote sensing of low-salinity sea ice at UHF frequencies, Acta Polytechnica Scandinavica, El 45.

6. Hallikainen, M., 1982, The brightness temperature of sea ice and fresh-water ice in the fre-
   quency range 500 MHz to 37 GHz, International Geoscience and Remote Sensing Symposium, June
   1-4, Munich, Germany.

7. Hallikainen, M., Ulaby, F. and Abdel-Razik M., 1982, Dielectric measurements of snow be-
   tween 4 GHz and 18 GHz, The University of Kansas Center for Research, Remote Sensing
   Laboratory report, to be published.

8. Hoekstra, P. and Delaney, A., 1974, Dielectric properties of soils at UHF and microwave fre-
   quencies, Journal of Geophysical Research, Vol. 79, pp. 1699-1708.

9. Linlor, W. I., 1980, Permittivity and attenuation measurements of wet snow between 4 GHz and
   12 GHz, Journal of Applied Physics, Vol. 51, pp. 2811-2816.

10. Poe, G. A., Stogryn, A., Edgerton, A. T. and Ramseier, R. O., 1974, Study of microwave emis-
    sion properties of sea ice, Final Report 1804 FR-1, Aerojet Electrosystems Co., Azusa, CA.

11. Pounder, E. R., 1965, The physics of ice, Pergamon Press, New York.

12. Sackinger, W. and Byrd, R., 1972, The dielectric properties of sea ice in the range from
    26-40 GHz , IAEE Report 7203, University of Alaska.

13. Tiuri, M., Hallikainen, M., Jakkula, P. and Schultz, H., 1978, Microwave signatures of snow
    measured in Finland, EARSeL, Proc. 2nd General Assembly, pp. 51-60, Munich, Germany, April.

14. Tiuri, M. and Hallikainen, M., 1981, Microwave emission characteristics of snow covered
    Earth surfaces measured by the Nimbus-7 satellite, Proc. 11th European Microwave Confer-
    ence, pp. 233-238, Amsterdam, 7-11 September.

15. Tiuri, M., 1982, Theoretical and experimental studies of microwave emission signatures of
    snow, IEEE Trans. on Geoscience and Remote Sensing, Vol. GE-20, pp. 51-57.

16. Tiuri, M. and Sihvola, A., 1982, Remote sensing of snow depth by passive microwave satel-
    lite observations, International Geoscience and Remote Sensing Symposium, June 1-4, Munich.

17. Vant, M. R., 1976., A combined empirical and theoretical study of the dielectric properties
    of sea ice over the frequency range 100 MHz to 40 GHz, Technical report, Carleton Univer-
    sity, Ottawa, Canada.
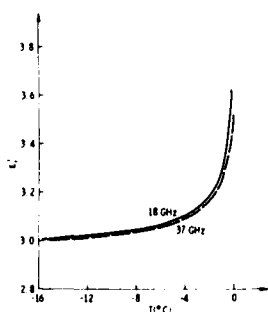
Figure 1. Dielectric con-
stant of sea ice with a
salinity of 0.5 ^{o}/oo.
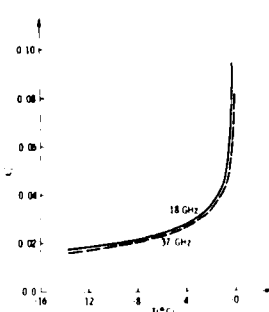
Figure 2. Dielectric loss
factor of sea ice with a
salinity of 0.5 ^{o}/oo.
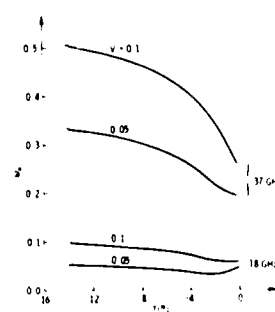
Figure 3. Scattering albedo
of sea ice. Salinity is 0.5
^{o}/oo, diameter of air bubbles
1 mm, diameter of brine pock-
ets 0.5 mm. V is the relative
volume of air bubbles.

827
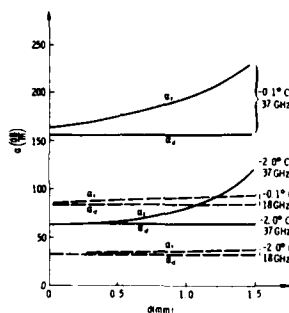
Figure 4. Dielectric attenuation constant α_d and total attenuation constant including scattering α_t for sea ice. Salinity is 0.5 °/oo. Diameter of air bubbles is d.
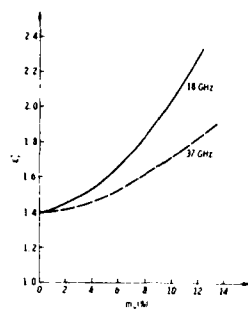
Figure 5. Dielectric constant of snow at 18 GHz (measured) and 37 GHz (estimated) as a function of volumetric wetness.
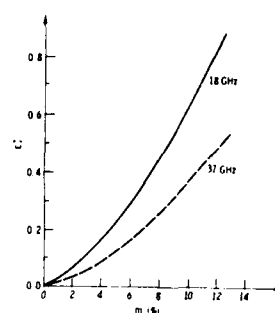
Figure 6. Dielectric loss factor of snow at 18 GHz (measured) and 37 GHz (estimated) as a function of volumetric wetness.
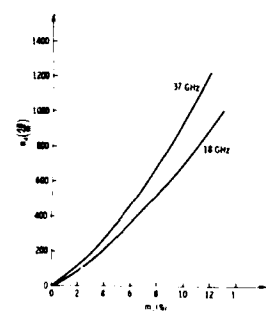
Figure 7. Attenuation constant of snow as a function of volumetric wetness, calculated from Figures 5 and 6.
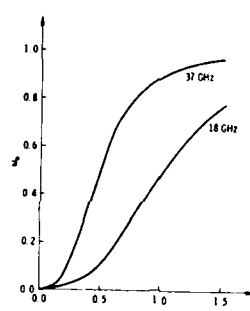
Figure 8. Scattering albedo of snow as a function of particle diameter. $\epsilon_r = 1.5 - j\ 0.001$.
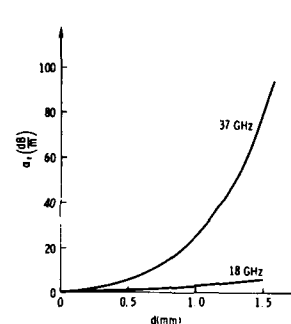
Figure 9. Total attenuation constant of snow including scattering as a function of particle diameter.
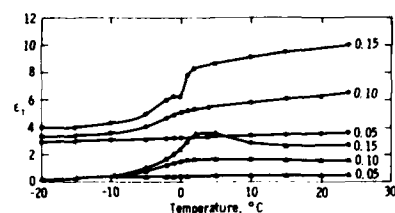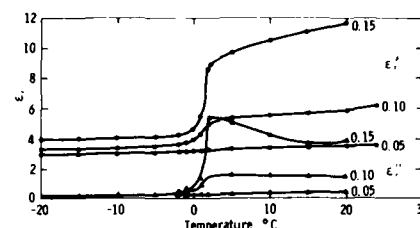
a)   b)

Figure 10. Complex dielectric constant at 10 GHz as a function of temperature at three water contents (g water/g soil) for
a) Goodrich clay
b) Fairbanks silt (Hoekstra and Delaney, 1974).

828

a)   b)
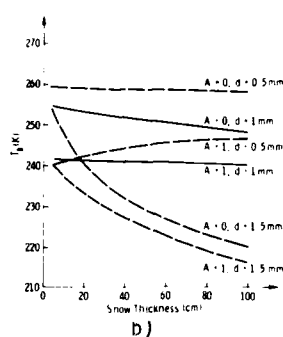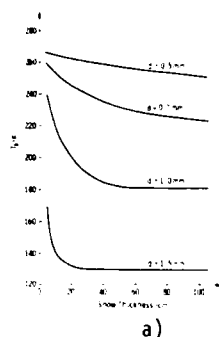
Figure 11. Brightness temperature of an infinitely thick ice layer (salinity 0.5 °/oo) at a look angle of 50 ° for a) 37 GHz, vertical polarization, b) 18 GHz, horizontal polarization. Temperatures: Snow -5°C, ice -2°C. Snow particle size as parameter. 18 GHz: Total transmission at ice-snow interface (A=0), transmission using Fresnel coefficients(A=1).
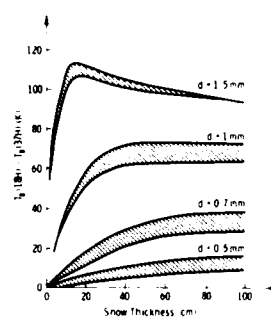
Figure 12. Difference in the brightness temperature between 18 GHz and 37 GHz, horizontal polarization, look angle 50 °, for an infinitely thick ice layer (salinity 0.5 °/oo). Temperatures: Snow -5 °C, ice -2 °C. Snow particle size as parameter.
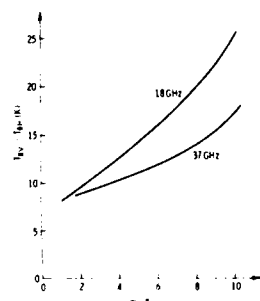
Figure 13. Difference in the brightness temperature between vertical and horizontal polarizations for an infinitely thick snow layer as a function of volumetric wetness. Look angle 50 °, scattering neglected.

February 15, 1979

Open Water

New or Rotten Ice

Level Ice

Open Pack Ice

Compressed Brash Ice

Close Pack Ice

Compact Pack Ice

Rafted Ice

Ridged Ice

Lead
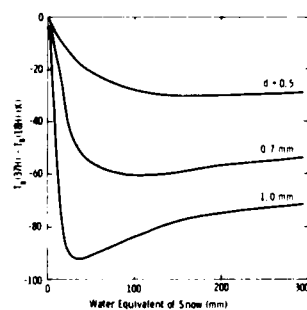
Figure 14. Difference in the brightness temperature between 18 GHz and 37 GHz, horizontal polarization, for snow-covered terrain. Temperatures: Snow -5 °C, ground -3 °C. Look angle 50 °, snow crystal size d.
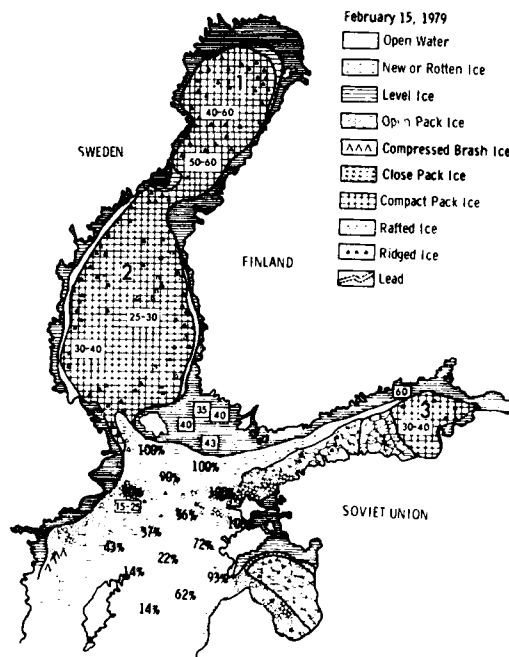
Figure 15. Sea ice map of the Baltic Sea on February 15, 1979 by the Institute of Marine Research. Explanations:

1, 2, 3	Numbers of test areas (Table 1)
25-30	Ice thickness cm
76 %	Percentage of resolution cell covered by ice, based on 18 GHz satellite data, horizontal pol.

Figure 16. Sea ice map of the Baltic Sea on March 5, 1979 *by the Institute of Marine Research.* Explanations:

1, 2, 3	Numbers of test areas (Table 1)
50-60	Ice thickness cm
22 %	Percentage of resolution cell covered by ice, based on 18 GHz satellite data, horizontal polarization, taken March 3.

Figure 17. Sea ice map of the Baltic Sea on March 15, 1979 by the Institute of Marine Research. Explanations:

1, 2, 3	Numbers of test areas (Table 1)
25-35	Ice thickness cm
16 %	Percentage of resolution cell covered by ice, based on 18 GHz satellite data, horizontal polarization, taken March 17.

Figure 18. Observed change in the brightness temperature difference between 18 GHz and 37 GHz, horizontal polarization, using satellite data in five test areas in Finland (Tiuri and Hallikainen, 1981). Surface types:
1) 70 % forests, 30 % boglands (2 areas)
2) 40 % farmlands, 60 % forests
3) 70 % boglands, 30 % forests
4) 30 % lakes, 70 % forests.

Figure 19. Computed change in the brightness temperature difference between 18 GHz and 37 GHz, horizontal polarization, for pure surface types. The results are based on data shown in Figure 18 for mixed surface types.

830

USE OF INFRARED IMAGES IN THE DELIMITATION OF SÃO PAULO'S HEAT ISLAND*

Magda Adelaide Lombardo
Gilberto Câmara
Eduardo Pereira

Instituto de Pesquisas Espaciais - INPE
Conselho Nacional de Desenvolvimento Científico e Tecnológico -
CNPq
Caixa Postal 515
12200 São José dos Campos, SP, Brasil
and

José Roberto Tarifa
Universidade de São Paulo - USP
São Paulo, SP, Brasil

ABSTRACT

The objective of this work is to describe
a way of using remote sensing techniques to delimit
and characterize an urban heat island. The study
was carried out in metropolitan São Paulo.

One can make a thermal maping of an urban heat
island by measuring temperatures *in situ* or by
remote sensing. Since in loco measurements in   a
big city require considerable experimental resources,
remote sensing by satellites maybe   best option when
it is necessary to take extensive and repetitive
measurement.

The technique used in this work is similar to
that used by CHAHINE to derive ocean temperature from
infrared images.

The method was used to analyse a TIROS-N (NOAA 7)
image taken on July 16, 1981, 5:47 PM. On this day the
atmospheric conditions were propitious for the
formation of a heat island in São Paulo.Through this
example, one can conclude that infrared images can be
useful in the definition and characterization of an
urban heat island.

1. INTRODUCTION

A project to delimit and characterize the urban heat island of metropolitan
São Paulo was created about one year ago in INPE. This project involves
geographers and remote sensing specialists from both INPE and USP and its
objectives, besides the characterization of the island, are to find a relation
between the type of urban land use and temperature. In the present paper,
partial results obtained by the workers involved will be presented.

Methods for obtaining temperatures from infrared images have been proposed
by many researchers. The developing of original methods was not tried but
previous works were relied upon. The software to change an image of counts into
an image of temperatures was based in Chahine (CHAHINE, 1980). The first step
in getting temperatures from counts is to construct a look up table of surface
temperature versus counts. This was done in the following way: 1) The

radiance reaching the satellite was calculated for a few known surface temperatures and emissivities. The procedure to do this is straight forward: Planck's law gives the radiance emitted by the surface, which is then corrected for gray-body emissivity, atmospheric effects and for the satellite radiometer calibration curves. 2) Knowing the radiance of the reference temperatures and emissivities and getting the counts from the image, counts can be related to radiance through a polynomial interpolation. 3) A table of surface temperatures versus radiance reaching the satellite is constructed. Again given the table for surface temperature, the radiance can be obtained by using Planck's law corrected for the emissivity. atmospheric effects and for the radiometer calibration curves. 4) Finally the table of counts versus surface temperature is constructed. Given a count, the radiance is found by using the polynomial. The table of radiance versus temperature will give the temperature corresponding to that count to be used in the table of counts versus temperature. This last table will have a temperature for each of the 256 values of counts found in the image. Of course. a table of counts versus temperature is needed for each interval of emissivities found in the urban area.

The procedure used to correct the radiance for the radiometer calibration curves is given by Lauritson et al. (LAURITSON et al., 1979). The way of including the atmospheric effects in the radiance reaching the satellite can be understood by reading one of the many papers about the subject. One of these papers is that of Chahine (CHAHINE, 1980). Note that since surface temperatures are being used as references, there is a slight difference between the present procedure and that described in the introduction of Chahine's paper. In Chahine's procedure, the radiometer internal reference are used to obtain the radiance which is then corrected for the atmospheric effects to obtain the surface radiance. In this work, the tables have been constructed starting from a table of surface radiance and adding atmospheric effects to obtain the radiance reaching the satellite. This slight different procedure was chosen not because it is thought to be a superior one, but because it was found to give almost the same result as the one described by Chahine and, since of ten the internal reference temperature is not obtainable in INPE for technical reasons, the use of an external reference was chosen.

2. THE EMISSIVITY MAPS

One of the authors has constructed maps of estimated emissivities for metropolitan São Paulo. These maps have two uses: The first is to provide the emissivities needed by the software. The second is to provide a tool to find a relation between type land use and temperatures. The last use is possible,since emissivities are estimated partly with the help of maps of land use and partly with the help of "in situ" measurements. The "in situ" measurements are made using aerial photographs. Knowing the type of a land use and its emissivity, the emissivity for a certain area can be estimated. Figures 1, 2 and 3 show one example of these urban land use maps, with emissivity estimates. The aerial photographs used were given to the authors by Emplasa (Empresa Metropolitana de Planejamento da Grande São Paulo S.A.) and were taken in 1973 (scale 1:8000) and in 1981 (scale 1:35000).

3. CORRECTION OF ATMOSPHERIC EFFECTS

As in the paper of Chahine, the atmospheric effects are corrected by using the atmospheric transmittance and path radiance at different frequencies in the channel. To obtain the transmittance and the path radiance, a Lowtran package (SELBY et al., 1978) modified by Alves & Dias (private communication) was used.

Lowtran was used with data from radiosondes collected at Congonhas airport. These data were obtained by IAE.

832

Other researchers have found that the kind of correction proposed, although simple, is quite effective. For example, Bentancurt (BENTANCURT, 1981) has shown that atmospheric correction improves automatic classification effectiviness.

4. A SAMPLE ANALYSIS

To be included in this paper, an analysis of an image of the satellite TIROS N was made. This image was taken on July 16, 1981 at 14:47 local time and was chosen because it was taken in the winter, when the temperature variations due to the heat island is more accentuated. The sky on this day was clear, the atmosphere was stable, there was absence of strong winds, and the local pressure was high. This means that the local climate was predominant and the concentration of pollutants in the center of the city was high.

From figure 4 and from figure 1, it can be seen that the heat island has roughly the same shape as the urban area and is located close to the geometrical center of the city. The difference between temperatures in the heat island and in the skirts of the city is about 5º C.

A rough examination of the temperature images seems to indicate that there is a relation between the type of land use and temperature, as well as between topography and temperatures. Refering to figure 5, it can be seen that the temperatures in regions of high building concentration and in industrial areas are usually higher than in other areas. In area (e) the temperature is low because of the high altitude associated to a tree covering.

The temperatures obtained from satellite data are quite close to the ones measured "in situ" (the difference is smaller than the resolution used in the construction of the temperature images, i.e. 0.5º C). One of the reasons for such good results is, of course, that reference temperature collected "in situ" were used.

5. CONCLUSIONS

Meteorological Satellite infrared images were seen to be an effective tool in the characterization, delimitation, and monitoring of urban heat islands. The method used by the authors, in particular, is useful if extensive ground truth, radiosondes, and reference temperatures are easy to obtain.

In this work the results of analysis of just one image was presented. The analysis of other images, taken at different atmospheric conditions and with improved emissivity estimates is under way. It is hoped that this analysis will lead to more general results.

BIBLIOGRAPHY

BENTANCURT, J.J.V., "Preprocessing of multispectral data from orbital plat-forms" (In Portuguese with an English abstract). Master thesis in Remote Sensing. São José dos Campos, INPE, 1981 (INPE -2181 - TDL/085).

CHAHINE, M.T. "Infrared Remote Sensing of Sea Surface Temperature". In "Remote Sensing of Atmospheres and Oceans". Edited by Adarsh Deepak, Academic Press, 1980.

LAURITSON,L.; NELSON,G.J.; PORTO,F.W. "Data Extraction and Calibration of Tiros - N/NOAA Radiometers". NOAA Technical Memorandum NESS 107, United States Department of Commerce. Washington,D.C., November, 1979.

SELBY,J.E.A.; KNEIZYS,F.X.; CHETWYND,J.H.; McCLATCHEY,R.A. "Atmospheric transmittance/radiance: computer code Lowtran-4". Cambridge,Ma, Air Force Cambridge Research Laboratories, 1978 (AFGL - TR - 78 - 0053).
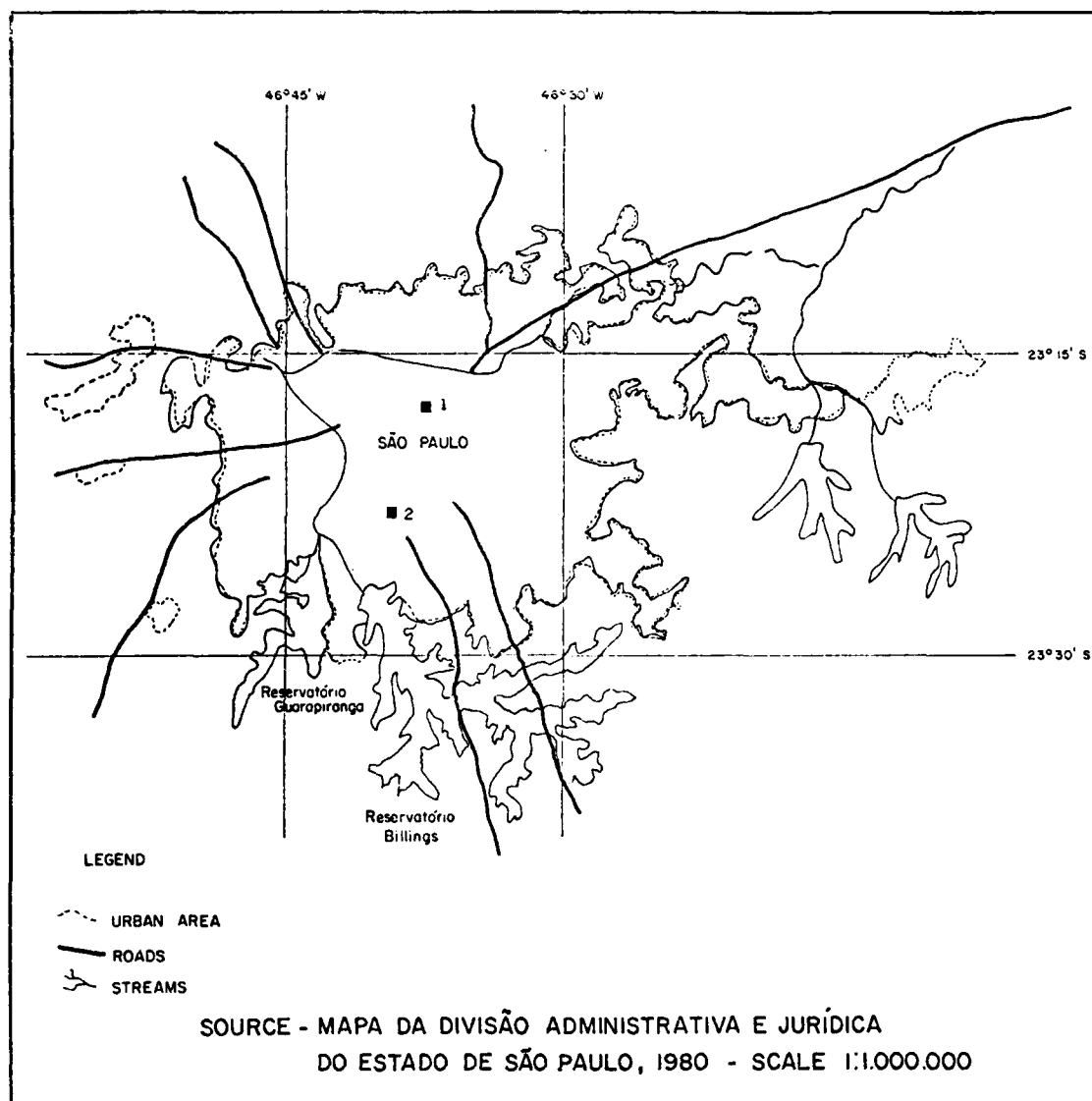
Fig. 1 - Map of São Paulo showing the position of two of the areas used to estimate emissivity.

834

SOURCE: TERRAFOTO S/A-1981   SCALE 1:8.000

LEGEND		% TOTAL AREA	EMISSIVITY
☐	BUILDINGS	78,4	0,97
◤	ASPHALTED AREAS	11,2	0,99
E	PARKING LOTS	5,4	0,98
▩	GRASS	1,9	0,93
Ⓥ	VEGETATION COVER	3,1	0,94

AVERAGE EMISSIVITY: 0,94

Fig. 2 - Map of urban land use in area 1.

835

SOURCE: TERRAFOTO S/A - 1981   SCALE 1:8.000

LEGEND		% TOTAL AREA	EMISSIVITY
🐦	BUILDINGS	0,2	0,92
◣	ASPHALTED AREAS	0,2	0,99
🐚	GRASS	1,1	0,93
V	VEGETATION COVER	97,8	0,94
🐚	WATER		AVERAGE EMISSIVITY: 0,93

Fig. 3 - Map of urban land use in area 2.

836

46°45' W   46°30' W

■ e

23°15' S

■ a

SÃO PAULO

■ b   ■ c

■ d

■ f

23°30' S

Legend

a) Center of the city, characterized by a highter concentration
   of tall buildings. Temperature – 26 – 27°C
b) Great concentration of buildings. Temperature – 26°C
c) Industrial area. Temperature – 25°C
d) State park – high concentration of trees. Temperature – 23,5°C
e) Cantareira park. High concentration of trees. Temperature 21,5°C
f) Water reservoirs. Temperature 20°C.
---- urban area
⌣ roads
⋎ streams

Scale 1:1,000,000

Fig. 4 – Selected areas of different urban land use and equivalent
temperatures.
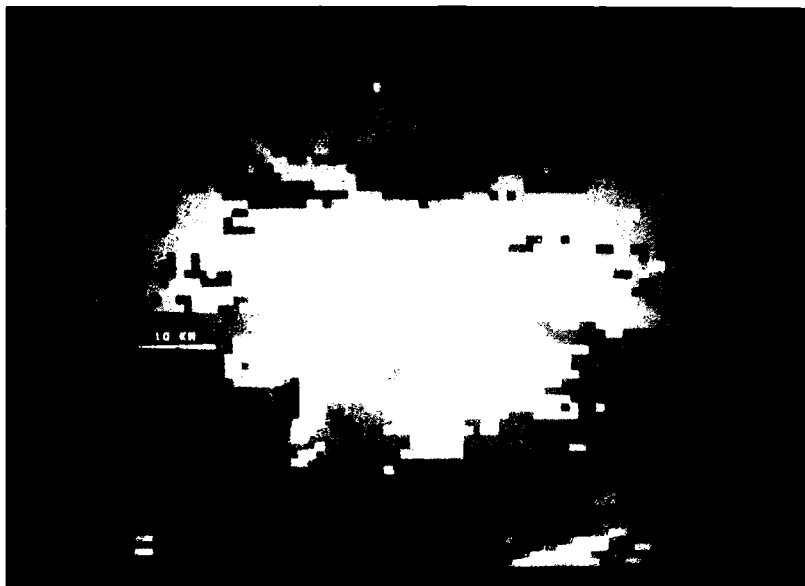
Fig. 5 - São Paulo's urban heat island
July, 16, 1981   17:47 GMT

SAMPLE SURVEYS FROM LIGHT AIRCRAFT COMBINING VISUAL
OBSERVATION AND VERY LARGE SCALE COLOUR PHOTOGRAPHY

M. Norton-Griffiths and T. Hart

EcoSystems Ltd.
Nairobi, Kenya

M. Parton

Office of Arid Lands Studies
University of Arizona
Tucson, Arizona

ABSTRACT

The Systematic Reconnaissance Flight
(SRF) is a sample survey technique
utilising visual observation and small-
format aerial photography taken from low-
flying aircraft. The collection and
assignment of data to a sampling grid
allows for its compilation and integra-
tion with ancillary data, both point-
and grid-referenced. New data variables,
which can be derived from SRF and
ancillary data, are compiled in a highly-
structured database that provides a cost
effective survey technique for developing
countries.

1. TECHNICAL

The Systematic Reconnaissance Flight (SRF) is a sample survey technique
for quantifying the spatial distribution of land use parameters through a
combination of visual observations and vertical photography from low-flying,
high-wing light aircraft. The aircraft flies parallel transects across a
study area at a ground speed of around 160 kilometers per hour and at a height
of some 122 metres above ground level. Visual observations are recorded con-
tinuously along the length of each transect, but are divided into successive
subunits on the basis of elapsed time or distance. One or more vertical
sample photographs are taken within each subunit, and all data recorded during
the survey are cross referenced to an individual transect/subunit.

With the SRF method the aircraft is accurately located along the selected
transects by using a navigation system that tunes into the worldwide network
of OMEGA/VLF radio beacons. Each subunit along each transect, therefore, can
be accurately located in space. The SRF thus yields a set of data points,
each of which is accurately georeferenced.

An SRF survey is always carried out within the framework of a sampling grid, and each data point (subunit) is assigned to an individual grid cell. The Universal Transverse Mercator Grid (UTM) is widely used for such sampling frames since it is a worldwide standard grid system which is projected easily onto aerial photographs or other cartographic/thematic data sources.

1.1 VISUAL OBSERVATIONS

Visual observations supply most of the information on animal numbers and characteristics, both livestock and wildlife, as well as a set of general observations on the land use setting. To conduct systematic visual recording, observers sitting in the rear seats of the aircraft continuously scan a 150m-wide sampling strip that is demarcated by rods attached to the aircraft wing struts. The observers record all their observations onto tape for later transcription, along with time pulses to distinguish between successive subunits. Domestic stock and wildlife species are tallied by subunit; any large herd of animals is photographed (oblique photo through window) for accurate counting at a later date.

Experienced observers also can record a wide range of quantitative and qualitative information on land use characteristics, cultivation methods, settlement types, physiognomic and phenologic characteristics of the vegetation, and erosion phenomena.

1.2 VERTICAL 35MM AERIAL PHOTOGRAPHY

The vertical, 35mm colour diapositives taken along the length of each transect provide most of the data on land use. Typically, one sample photograph is taken in each subunit, although the frequency can be increased over areas of particular interest.

A vertically mounted Olympus OM-2 camera, fitted with an 18mm lens and loaded with high speed Ektachrome film, images approximately 4 hectares at a flying height of 122m above ground level for an image scale of approximately 1:6,700. The actual height above ground level of each photograph is recorded from a radar altimeter at the moment of exposure so that scale and area calculations can be controlled individually for each frame.

The colour diapositives are manually analysed after vertical projection at 10x enlargement onto a 36cm x 24cm dot grid for an interpretation scale of 1:670. Data are obtained from an 18cm x 12cm inner "interpretation area" comprised of 160 cells of 2cm x 2cm, each of which contains four randomly located dots. Each dot has an equivalent ground diameter of approximately 1m, while each grid cell has an equivalent ground area of 183 Km^2.

Three types of data variables are obtained from the 35mm colour diapositives: count, area, and class. Count data are simple enumerations of objects on the colour slides, such as house compounds, buildings with thatched and tin roofs, water tanks, cattle dips, stock compounds, individual trees by species (mango, baobab, coffee, banana), and erosion gullies with associated land use. Area data are estimates of the proportional area of different land use types on the photography. These data can be obtained for land under active cultivation or different crops and crop combinations; areas of fields of different sizes or different methods of cultivation; land taken up by roads, tracks, houses, contour strips and other kinds of on- and off-farm infrastructure; land under fallow or active forest management; canopy cover of woody vegetation; and area affected by gully or sheetwash erosion.

Class data are obtained by classifying the entire frame on some aspect of land use or the environment such as soil colour, method of cultivation (hoe, ox, mechanised), or soil conservation (terraces, contour ploughing, contour bands).

840

1.3 ANCILLARY DATA

Ancillary data can be integrated into the SRF data set from a variety of sources, including maps, ground survey, and additional orbital/suborbital imagery. Map data can include administrative units, local slope angles and/or landform, rainfall and climatic data, soil type, distances to nearest service/veterinary centre/health centre/market centre/major road, and vegetation zone. Ground survey data can include farming systems, population density and structure, crop yields, and measurements of erosion rates and intensities. Satellite/air photo data can include existing land uses, past land uses, and areas of changing land use intensity.

1.4 DATA COMPILATION AND INTEGRATION

Both original and ancillary data collected in the course of an SRF survey are in either "point" or "grid" form. Point data are individual samples or observations collected at precisely determined points in space, while grid data, which are much more coarse, are derived from the classification of individual UTM grid squares by particular attributes such as rainfall, mean slope angle, and elevation. Since every sample point is assigned to a particular grid cell containing a precisely-determined set of sample points, data are freely transferable between points and grids. Thus, a grid cell can be characterised on the basis of some attribute measured at all of the sample points falling within it, while the points assigned to a grid cell can be characterised by any attribute defined for the grid cell as a whole.

Although some data types do not fall naturally into the point/grid classification, they can still be accommodated in the data set. For example, each point can be classified according to an administrative division or Landsat image stratum into which it falls. Similarly, population census data can be accommodated by classifying the points by the census unit in which they appear, and by assigning to them the value provided from the census unit.

Once the data are compiled into point or grid form, new data variables can be created from any combination of original variables. For example, the effective density of livestock can be expressed as a density of livestock on land available for grazing, which is derived from land area less active cropland, forest land, and land taken up by infrastructure. Similarly, the efficiency of land management can be assessed by expressing the area of on- and off-farm infrastructure which is supporting each hectare of acti ely cultivated land. Finally, in those rare cases for which the relevant data are avaialble, crop yields can be calculated from measured crop areas weighted by environmental and management factors.

2. APPLICATIONS

2.1 GENERAL

The lack of systematic land use data in a spatial context is a major constraint to efficient development planning. While orbital level remote sensing techniques are valuable for the compilation of small scale/coarse texture land cover information, the finer details of land husbandry and productivity are very expensive to acquire at a regional scale. The SRF provides a cost-effective solution to this problem through the compilation of a highly structured data base within which development projects can be designed, implemented and monitored, specifically in the context of smallholder rural agricultural systems in the developing countries.

2.2 SEASONAL PATTERNS OF MIGRATION

The seasonal patterns of resource abundance and utilisation can be determined by repeating SRF surveys at critical times of the year. In the

85,000 Km^2 impact area of the Jonglei Canal, Southern Sudan, three SRF
surveys were conducted during the periods of peak and medium flooding at the
height of the dry season. Seasonal movements of domestic stock, of the
people associated with them and of wildlife were monitored and mapped on a
grid of 10Km x 10Km, with other seasonal characteristics of land use and
phenology of the vegetation (Figure 1). The results of the SRF surveys pro-
vided the main source of data for assessing the environmental impact of the
canal, locating crossing points for domestic stock, and designing agricul-
tural and livestock development programmes.
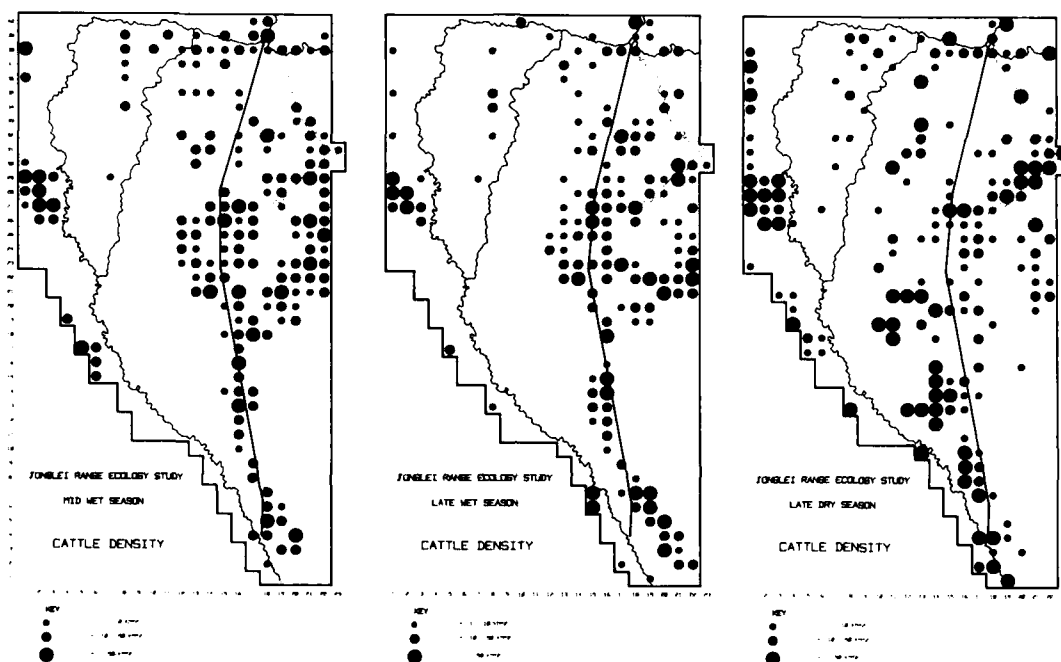
Figure 1. Jonglei Range Cattle Density for A) Mid Wet Season,
B) Late Wet Season, and C) Late Dry Season

2.3 LAND USE INVENTORIES

An intensive SRF survey of Machakos District, Kenya, provided land use
inventories within each division, location, and sublocation of the 14,000 Km^2
study area. Some 86 parameters of land use and erosion were quantified and
mapped from the analysis of 6,500 35mm vertical sample photographs (Figure 2).
In addition to land use inventories within each administrative unit, land use
analyses were made for agro-climatic zones, major soil types, local slope
angles and watersheds (Figure 3). A sediment budget was calculated for the
entire district.
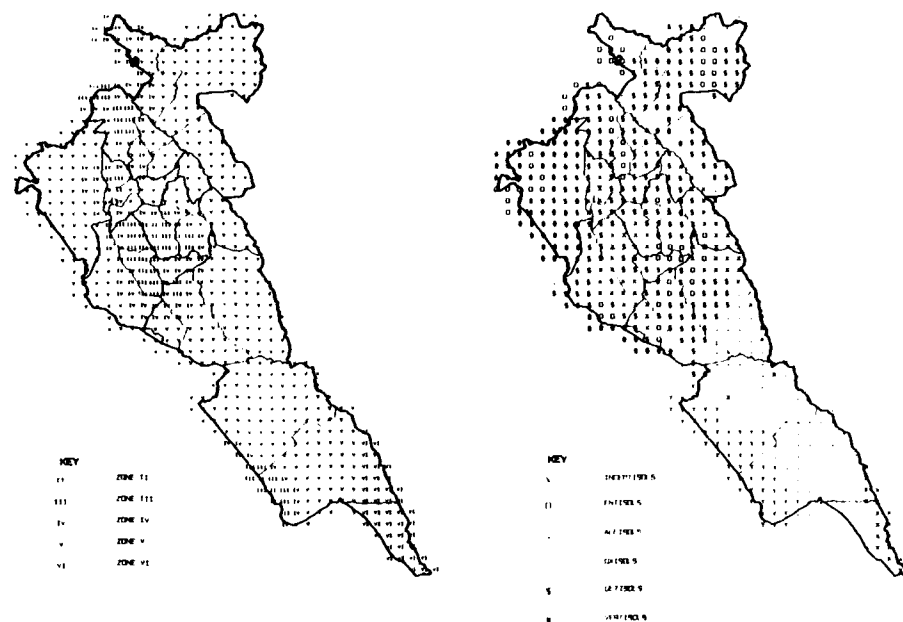
Figure 2. Machakos District Maps of A) Agro-Climatic Zones, B) Major Soil Types
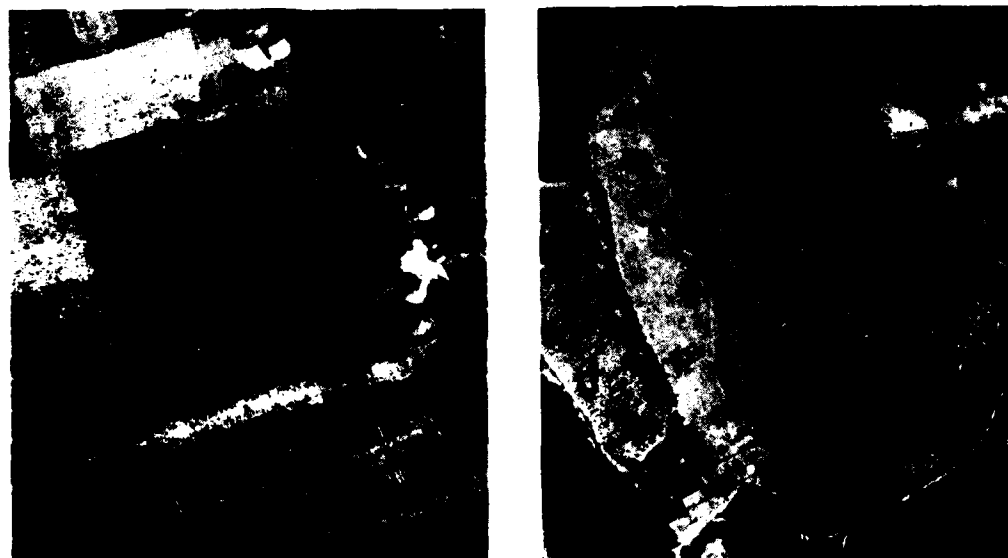
Figure 3. 35mm Aerial Photography, Machakos District

843

2.4 RURAL AGRICULTURAL LAND USE PATTERNS

The characteristics of land use within 2 Km on either side of 52 recently completed rural access roads (RAR) in Kenya were quantified by intensive SRF survey with flight lines spaced 1 Km apart and sample photographs spaced 500m apart. The sample of RARs, which covered the entire environmental spectrum of Kenya, ranged from arid, marginal agricultural land to areas of high agricultural potential. The gradient of land use from shifting agriculture to high intensity commercial farming is clearly demonstrated by ranking the road areas on the percentage of land under active cultivation (Table I).

Table I. Land Use Characteristics of Rural Access Roads

Number of RARs (50 Km^2)	10	11	14	9	8
Resources					
Cultivation/Km^2 (Ha)	6	16	26	36	49
Commercial cultivation %	21	24	32	43	52
Cultivation/Fallow	2	1	3	4	10
Livestock units/Km^2	40	91	101	87	65
Woody Cover/Km^2	37	19	17	11	10
Population/Settlement					
Population/Km^2	52	140	183	264	294
Buildings/Km^2	43	98	109	127	136
Buildings w/tin roof %	21	20	33	34	50
Land Management					
Overhead/Km^2 (Ha)	5.7	8.7	9.4	6.9	11.1
Cultivation/Overhead	1.1	1.8	2.8	5.2	4.4
Per Capita Resources					
Persons/Building	1.2	1.4	1.6	2.0	2.1
Persons/Ha Cultivation	9.0	8.6	7.0	7.3	5.9
Persons/Livestock Unit	1.3	1.5	1.8	4.0	3.3
Persons/Ha Woody Cover	1.3	7.4	10.9	24.2	30.5

Source: Data drawn from 52 rural access roads throughout the Republic of Kenya, each sample area approximately 50 Km^2. Rural Access Roads Impact Study funded by NORAD

2.5 LAND OVERHEAD

The proportion of land that must be set aside for on- and off-farm infrastructure and support can be a major constraint to the absolute level of production. In Machakos District, Kenya, land overhead rises steeply as a function of the area of cultivation per square kilometre. In this hilly and well-terraced area, land is effectively saturated for cultivation at a cultivation intensity of 60 percent. The SRF survey data show that less than 2 percent of the land is cultivated at an intensity greater than 50 percent (Figure 4).

844

LAND OVERHEAD AND INTENSITY OF CULTIVATION

Figure 4. Land Overhead and Intensity of Cultivation

3. REFERENCES

Croze, H., and M.D. Gwynne. 1980. Rangeland Monitoring: Function, Form, and Results. The Global Environment Monitoring System, Selected Works on Ecological Monitoring of Arid Areas (United Nations Environment Programme, GEMS PAC Information Series No. 1, Document 3). vp.

Gwynne, M.D., and J.J. Croze. 1975. The Concept and Practice of Ecological Monitoring Over Large Areas of Land: The Systematic Reconnaissance Flight (SRF). Proceedings of the Ibadan/Garoua International Symposium on Wildlife Management in Savanna Woodland, University of Ibadan, Nigeria.

_____. 1981. Light Aircraft and Resource Monitoring. Low-Level Aerial Survey Techniques (International Workshop, November 1979, Nairobi, Kenya), International Livestock Centre for Africa Monograph 4. pp. 11-25.

Norton-Griffiths, M. 1975. The Numbers and Distribution of Large Mammals in Ruaha National Park, Tanzania. East African Wildlife Journal 13, pp. 121-140.

Norton-Griffiths, M. 1978. Counting animals. Nairobi: African Wildlife Federation, Handbook No. 1 (2nd ed.), P.O. Box 48177, Nairobi, Kenya.

Pennycuick, C.J., J.B. Sale, M. Price, and G.M. Jolly. 1977. Aerial Systematic Sampling Applied to Censuses of Large Mammal Populations in Kenya. East African Wildlife Journal 15, pp. 139-146.

LOCALIZATION OF NEOTECTONIC ACTIVITY WITH THE LANDSAT
IMAGES IN LA LAJA (SAN JUAN   ARGENTINA)

(1) Silvia Lendaro de Gianni

(2,3) Enrique Uliarte

(1) Centro Regional de Agua Subterránea

(2) Universidad Nacional de San Juan

(3) Universidad Nacional de San Luis

Provincia de San Juan

Provincia de San Luis

Argentina

ABSTRACT

The purpose of the present study was the localization of zones with of neotectonic activity in areas with intense asismicity in San Juan province (Central Western Argentina). The locality of La Laja, lying at about 25 km to the North of San Juan city, was choosed as a pilot area.

Landsat images and air photographs wew the main material used for the investigation, the results of which werw checked in the field and with aerial reconnaissance.

It was possible to map separately Quaternary and Pre Quaternary rock units in the images, as well as the alignments present in the former sediments. These linears were checked in the field and with flights done in hours when the sun was close to the horizon. In some cases the neotectonical indicatione could be measured.

Moreover, more than 90% of the alignments detected in the images were confirmed in the field.

The method used permite the quick detection of neotectonical phenomena with low cost, since interesting pointe over a wide area could be localized in images and air photographs, and, thus, time consuming and costly field reconnaissance trips could be spared.

OBJECTIVES

San Juan Province, in the Argentine Republic is one of the regions mostly affected by seismic phenomena. As it is known this province was affected by important earthquakes that practically devastated it. Historically they are: the earthquake that ocurred on October, 27th 1894 of Mercali scale grade 8.2., the earthquake on July 3rd 1941 of Mercali scale grade 6.7., the earthquake on January 15th 1944 of Mercali scale grade 7.8 that destroyed San Juan City and produced a great quantity of fatal victims, the earthquake on June 10th, 1952, whose epicenter was located at the Rinconada, and the last one, on November 23rd, 1977 of Mercali scale grade 7.8 that destroyed Caucete city, whose epicenter was located in the eastern side of "Pie de Palo" hill.

Taking into account these antecedents and not existing an integral study on the neotectonis phenomena in San Juan Province, it was decided to focus on

such a study of wich the actual work takes part. The easter margin of Villicum and Zonda hills were chosen as pilot regions. La Laja is an interesting place because of the historical reactivation of its faults. Tulum valley has a great importance for in it San Juan city and the most important agricultural region in the province (remember that this activity comes to be the principal economic al resource) are located. Besides this region was accessible for field controls.

Region for the study

La Laja is located in the western margin of Tulum valley, having as a limit Villicum hill in the west, that is to say that it is placed at the bottom of the appointed hill.

The climate in Tulum valley where our region of study is located, is continental desertic, with an annual precipitation of 100 mm, with scarce vegetation, something that makes the geological phenomena be more evident.

Under the geomorfological point of view La Laja region is located at the bottom and eastern margin of Villicum hill. Such place (bottom of Villicum hill) is characterized for having certain heights due to fractures that elevate palaeozoic and cenozoic sedimentary layers over sedimentary layers belonging to the quaternary.

Methodology of the work

In order to make the present study structural geology works, geophysical works, general geology works, together with historical information about earthquakes were gathered.

Landsat images 1 and 2 in black and white bands 4-5-6 and 7; and false colour in scale 1:500.000 and in false colour 1:250.000 were obtained.

La Laja region is located in the following images:

```
ERTS E 2238/13435/01    17 Set  75 False colour
ERTS E 2040/13452/02     3 Mar  75 False colour
ERTS E 2040/13445/7/02   3 Mar  75 Black and white
ERTS E 2040/13445/6/02   3 Mar  75 Black and white
ERTS E 2040/13445/5/02   3 Mar  75 Black and white
ERTS E 2040/13445/4/02   3 Mar  75 Black and white
```

These images were covered with an acetate sheet of 0,2 mm and the areas corresponding to quaternary and prequaternary age were marked upon the basis of existing geological information and data obtained from the images. In the latter the contact between the prequaternary rock and the non-consolidated quaternary sedimentary layer is quite noticeable.

In the region under study the unique method of dating neotectonic sedimentary layers taking into account the lack of: pollen, carbonic rests, and volcanic ashes, elements that permitus know their age.

After delimiting the quaternary and prequaternary contacts, they proceeded to observate the alignments in a systematic form and to mark them, giving a greater interest to those that were found in the quaternary area and in the surrounding areas of the hills. Besides they proved the reactivation of old faults when following their strike or dislocation in the quaternary sedimentary layers.

We may define the alignments as all those features of the relief attractively appear in the same line following straight or curved directions that can go through the image or even continue from one image to anather. Its presence is particularly significant when images in little scales are analyzed,

848

and even more when you take into account Landsat images.

Given the scale of work, the alignments of the regional type were given emphasis. The region once marked with alignments in quaternary areas, the aerial photographs of such locality were obtained. In this area the photographs were taken by Spartan in 1965, in an approximate scale of 1:30.000.

Given the scale the alignments could be located in detail, and supporting in the existing information on structural geology, the characteristics of such alignments such as: rejection and the dip of the fault plane.

These alignments once located geographically, the area was observed from a plane and a helicopter. This recognition was done with the sun, in a low angle, in order that the shadows projected by the faulty escarpments be much more noticiable. Various spots to descend were selected to control to prove and design sketch of the faults, to measure the width of the quaternary sedimen tary layers and rejection in the fault planes.

In this way it was proved that practically any of the alignments marked corresponded to faults and the rest were lithological changes in the stratifica tion. Besides, more neotectonic phenomena were located in the aerial photographs, due to the greater detail they let us observe, but the regional faults are much more noticeable in Landsat images taking into account the general vision they provide. Besides the aerial photographs, because of the fact that they are fractioned they make it more difficult their location.

Geology

Stratigraphy the territory in study may be summarized stratigraphically in the following way: limestones and dolomites of marine origin of the Cambric or Inferior Ordovicic; lutites, sandstones, greystones (grauwacka: old sedimentary rocks) and a conglomerite of marine origin of the Middle and Superior Ordovicic, Silurian and Devonian; over them, in great discordance lutites, sandstones and conglometares of Carbonic continental origin are found; over laying the previous sequence, and in soft discordance:claystones, slimestones and conglomerates of Terciary continental origin, and over these,also in great discordance slime, sand, graves and continental conglomerates of the quaternary.

Structure

The area covering Villicum and Zonda chica hills are tipical for the structure of the compressional type that produces inverted faults, regional, with a direction from North to South with dip of the fault plane to the East that elevate the Paleozoic and Mesozoic sediments. In some cases imbrications that make the stratigraphic sequence be repeated one or more times are produced, being this the result of various orogenies that affected the region.

From the beginning of the quaternary the area covering the bottom of the hills presents a tectonic of accomodation of blocks and as a result faults of the inverted type with a shortening of the stratigraphic sequence.

The course of the dislocations is from North to South in general with a fault plane dipping to the East, with a valve of 30° in the proximity of the surface, the collapsed block being to the West of the fault.

Faults of less importance with a direction from North-West to South East and North-East to South-West of the vertical type are also present. They could be the ones conjugated to the principal faults.

The neotectonic produced new faults, but also reactivated old structures, this can be proved analizing the whole group and context of the regional structures. As a result of the neotectonic faults in sediments of the quaternary

849

and also in sediments of the Prequaternary have been produced.

In general this type of faults puts sediments of the Terciary upon sediments of the Quaternary, with a rejection up to 15 m (measured), while in others, a greater rejection is estimated. The length of the faults, as it is observed in the images, goes from a few meters to several kilometers.

RECOMENDATIONS

In studies of this type, it is recommended that the structural map be juxtaposed to the map of seismic activity (map of hipocenters, epicenters, microseism, of seismic isodensity, etc.) to see the relationship between structural geology and seismic phenomena.

It is of great importance to be hold geophisic information, due to the fact that with this infotmation you can verify faults that affect the sode and that they are manifested in a very weak form in the Landsat images and the verification of their field turns to be difficult.

The present work is the beginning of a series of investigations about the theme, and the relationship between it and other disciplines will constitute a second stage.

CONCLUSIONS

1. Low cost in obtaining the images.

2. The images come to be a regional sinthesis.

3. The shorten the time spent in locaticn and in study of the phenomena, consequently it lowers the cost, factors of great importance taking into account our present economic situation.

4. In order to provide a vision from a different angle, the regional alignments are more noticiable, and they are not fractioned as the aerial photographies.

5. The larger structures may be related to the minor ones.

6. The images in band 7 (receive part of the electromagnetic spectre close to the infrared) permits the detection of faults in which loss of heat is produced (thermal zones).

7. The results obtained in a simple way are of a great utility for works of different disciplines like: Seismology, Geomorphology, Hidrology, Hidrogeology and studies of urbane distribution.

ESTUDIO DE
FENOMENOS DE
NEOTECTONICA

REFERENCIAS

CUARTARIO
PRECUARTARIO
FALLA peine indica bloque hundido
LINEAMIENTO
CONTACTO
IMAGEN LANDSAT
E 2040 13452

Silvia ` ndaro de Gianni
Enrique Uliarte

UBICACION DEL
AREA DE ESTUDIO
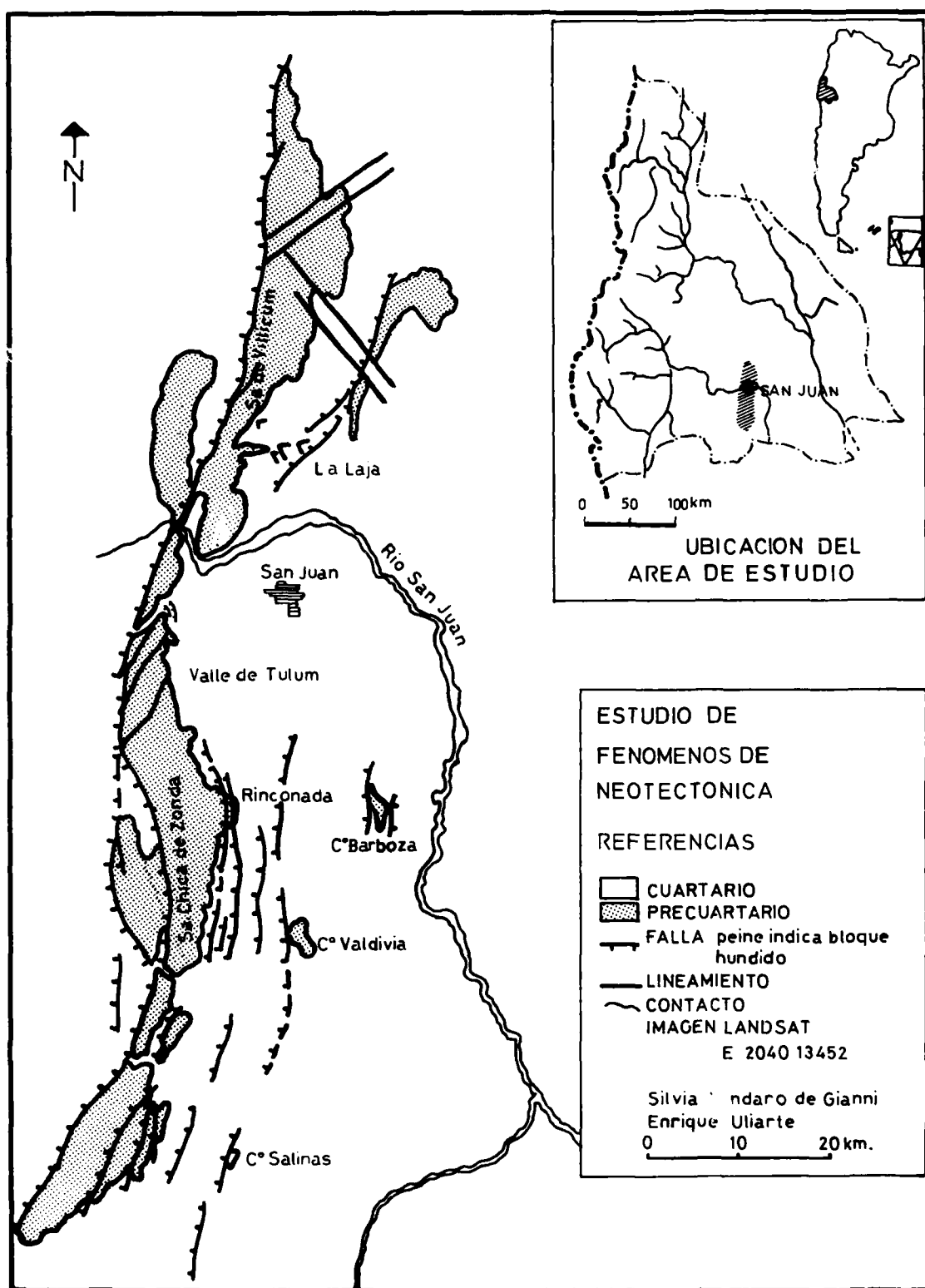
EVALUATION OF FUTURE GEOLOGICAL REMOTE SENSING SYSTEMS FROM SPACE:

THE JOINT GEOSAT/NASA/JPL TEST CASE PROGRAM

Frederick B. Henderson III

The Geosat Committee
San Francisco, California

SUMMARY

The Geosat Committee, supported by 100 exploration and engineering companies, was organized in 1976 to recommend Landsat supplementary sensing systems to optimize geological remote sensing from space to NASA. These recommendations include: rock/soil sensitive spectral bands; worldwide, high resolution film (Large Format Camera), and Landsat compatible digital stereoscopic imaging data (STEREOSAT); and Synthetic Aperture Radar (SAR).

These systems, as well as other potential space remote sensing systems, are currently being evaluated under the joint Geosat-NASA/JPL Test Case Program. The objective of this program is to assess the value of existing and potential satellite remote sensing methods for mineral and petroleum exploration and engineering geology applications over known areas. The study includes an evaluation of sensors, data processing techniques and interpretation methods.

Companies belonging to the Geosat Committee have provided geological, geophysical, and geochemical ground truth data and access to the Test Case sites. These sites include 3 oil/gas, 3 porphyry copper, and 2 uranium deposits. NASA/ JPL is providing data acquisition and processing of over 18 potential sensing systems. The results of this study will be published sometime in 1982.

EVALUATION OF TRADITIONAL AND "GREEN MEASURE"
REMOTE SENSING TECHNIQUES FOR
SHRUB CROP ASSESSMENT IN SRI LANKA

Jacquelyn S. Ott

Environmental Research Institute of Michigan
Ann Arbor, Michigan

ABSTRACT

Remote sensing techniques for agricultural inven-
tories have generally been applied to monocatyledenous
field vegetation in flat terrain. This paper evaluates
the ability to monitor shrub-type vegetation in hilly
terrain with Landsat.

As part of the Tea Rehabilitation Project in Sri
Lanka, the extent and condition of Tea plantations was
mapped from February 1980 Landsat data. The Government
of Sri Lanka was interested in Tea Crop condition, which
was defined as a function of maturity or percent vege-
tative cover. The results were presented to them in
April 1982.

Soil albedo and slope and aspect were quite vari-
able in the Sri Lanka study area. These factors inhi-
bited the utility of standard maximum likelihood
classifiers, particularly for sparse vegetation.
Alternative techniques that are less affected by variable
conditions were evaluated. These include ratios and
linear transformations of MSS bands, that offer a single
continuous measure of vegetative cover. The results from
the various procedures were compared and the best
techniques for monitoring shrubby Tea crops in Sri Lanka
were determined.

1.0

INTRODUCTION

The use of Landsat data for resource inventory projects around the world
has led to a great variety of procedures for processing the data. One
objective of this project is to compare the performance of various processing
algorithms and enhancement techniques. The other purpose is to evaluate the
utility of Landsat data for assessing Tea Crop condition in the rugged
Tatnapura-Hatton region of Sri Lanka. The techniques investigated include
contrast enhancement, supervised classification, generation of hybrid
"indicator" variables, and level slicing. Each of these enhances certain
scene features that aid in mapping Tea conditions. They provide much useful
information when the resulting images are considered collectively. The study

site and data descriptions are presented in Section 2 of this report and the various data processing routines are discussed in Section 3.

2.0

STUDY SITE AND DATA DESCRIPTION

The 100 sq km study area is part of the Kelani Ganga Catchment in south central Sri Lanka (Figure 1). It is free from cloud cover on Landsat scene 8-30703-04704 collected on 06 February 1980. Multitemporal Landsat data would provide additional seasonal information and was requested for this study area. However, only the one cloud-free acquisition was available. Ancillary data was provided by the Sri Lankan Ministry of Plantation Industries to augment the satellite data. Well documented ground truth maps were provided from data collected within several weeks of the satellite overpass (Figure 2). Condition of Tea land and estimates of percent green cover for the fields were included, as was a description of the major tea development stages: newly cleared fields; pruned, immature and mature tea. Black and white aerial photography from 1972 and 1973 contributed information about local agricultural practices. The terrain is extremely hilly and the fields are often small and irregularly shaped, both conditions that need to be considered during data processing.

3.0

PROCEDURE

Initially, false color images and a supervised caregorization were produced for the Sri Lanka data set. Ratio and green measure techniques have recently been investigated to help minimize topographic effects and optimize separability of green vegetation. Several of these were applied to the Landsat data, and the performances in the Sri Lanka Tea situation were evaluated. Signatures for the same training areas were taken for each processed data set and compared for maximum separability of classes. Images were then produced for the best techniques.

3.1 FALSE COLOR COMPOSITE

First, a contrast enhanced false color composite image was produced. The data has been resampled to 50 m pixels and geometrically corrected to the Transverse Mercator Projection. The Maskeliya Oya and Castlereigh Reservoirs and Maskeliya Oya River are good sources for geographic reference. The forested areas are distinct and mark much of the study area boundary. Many types of vegetative cover are apparent within the cultivated areas. Because the image was produced to emphasize the variation within heavy vegetation, some areas that appear newly cleared on the image or bright, actually have some degree of regrowth. This is indicated by an examination of the MSS signal values for these areas.

3.2 SUPERVISED CATEGORIZATION

The ground truth maps were used to identify supervised training sets for the Landsat data for areas of Tea, forest and other vegetation. The

multispectral signatures were extracted on the ERIM/ERDC facility. An MSS7 vs MSS5 plot (Figure 3) was produced to illustrate the arrangement of the signatures in spectral space. An unsupervised clustering was also performed to help define the extent of each category.

The signatures for shrub-tea from the ground truth classes are reasonably separable, but there is some confusion between "new clearings" and other signatures. Apparently, new clearings can vary in vegetative cover from very sparse to very dense and thus are spectrally confused with most of the tea growth stages. Also, the amount of vegetative cover (weeds, grass, etc) on new clearings can apparently change rapidly. For example, some new clearings which ground truth indicates have 80-100% vegetative cover were examined. Based on previous calibration of Landsat data to green vegetation cover (Colwell, et al., 1977), we infer that at the time of Landsat acquisition there was only 50% vegetation cover on these fields.

Categories of tea condition were thus defined from the spectral location and percent green cover of the signatures from the shrub-tea classes. The final map categories are summarized as follows:

Color on Image Map	Name	Ground Truth Labels
dark green	Mature Tea	(VP/OT)
medium green	Moderately Developed Tea	(PT:40-60% cover; NC:80-100% cover)
light green	Sparse Tea	(NT:5-20% cover)
light yellow	Well-Developed Tea	(NT:50-70% cover)
orange	Mana Grass	(NC:60-100% cover)
light red	Other Vegetation	(Homestead, grass, abandoned tea)
medium red	Forest	
tan	Bare	
blue	Water	
black	clouds and unclassified data	

One signature, extracted from a field marked as new clearing with dense green cover (60-100%) is as bright as mature Tea. Because it is spectrally unique from both Tea and other vegetated new clearings it is given a separate category. The description of Tea cultivation practices suggests this might be mana grass.

The categorization emphasizes separability of Tea condition classes, and therefore, less consideration has been given to other classes. Some confusion exists in Other Vegetation classes outside the study area and between cloud shadows and water.

3.3 DATA TRANSFORMATION TECHNIQUES

Many techniques have been investigated to transform multichannel Landsat data into a single channel of information sensitive primarily to a specific

feature. This can minimize the effects of undesirable features and provides a measure of variability that is more easily understood than the original Landsat data. The data handling efficiency is also improved because the amount of data is reduced. Several of these techniques are discussed below.

3.3.1 PRINCIPAL COMPONENT TRANSFORMATION

Agricultural scene characteristics fall in a predictable arrangement in the four Landsat dimensions. Directed Principal Components Analysis can be used to transform this pattern so that most of the variation within the data is described by 2 new axes, one corresponding to Brightness, and the other orthogonal to it, corresponding to Greenness. Similar procedures have been described elsewhere (see e.g., Kauth and Thomas, 1976). Signatures from several training sets were used to determine the most suitable axes for the Sri Lanka data set. The transform coefficients that describe the axes were then applied to the Landsat data. The final equations used are:

For Brightness:

$$[(MSS4*.50385)+(MSS5*.62121)+(MSS6*.49061)+(MSS7*.34613)]*.90+10 \quad (1)$$

For Greenness:

$$[(MSS4*.3538)+(MSS5*.42329)+(MSS6*-.37393)+(MSS7*-.74526)]*-3.0+30 \quad (2)$$

Previously, Greenness measures have sometimes been modified to produce a measure that may more surely separate sparse vegetation and bare soil. For example, Hay (1979) proposed GRABS (G-.1B), and it has been used in the AgRISTARS program. Because of our uncertainty about which features were truly bare in the Sri Lanka data, we adopted the same convention.

Signatures were extracted from the G-.1B transformed data for the previously selected training sets. The data was accordingly level sliced to correspond to several general classes. The final image was color coded as:

dark green	mature tea
medium green	immature and new tea
red	forest and other vegetation
tan	bare soil
blue	water

Although Principal Component Greenness values and GRABS values have been found to be useful in the United States Great Plains, their applicability to other environments is not yet demonstrated. The soils in the Sri Lanka project area are described as lateritic, with "Reddish Brown Colour". (Ground Truth document, 1980). Colwell (1982) has found that reddish soils can be confused with sparse green vegetation in the Principal Component Greenness channel because the transformation is sensitive to visible absorption in MSS4 (such as iron oxide) as well as absorption in MSS5 (chlorophyll). A Green Measure which does not use MSS4, such as (MSS7 - MSS5)/(MSS7 + MSS5), should be largely unaffected by the iron oxide absorption.

858

3.3.2 RATIO TECHNIQUES

Various ratios of Landsat MSS bands have been used to help reduce undesirable effects from soil variability and topography, two problems that may affect interpretability of the Sri Lanka data. A ratio of adjacent spectral bands will normalize many effects that soil variability may have on the scene reflectance (e.g., see Colwell and Suits, 1975; Nalepka, Colwell, and Rice, 1977). The same principle applies for reducing topographic effects and has been well-documented in other studies (e.g., Holben and Justice, 1980).

A ratio transformation masks some vegetation characteristics associated with their overall brightness, so there may be some confusion between vegetation of different types and Brightness but with similar Greenness, such as mature tea and forest. Within the tea cultivation area, because the continuous tone nature of the black and white images is representative of the greenness of the data, the tone can be related to tea condition:

lighter tones	mature tea
medium tones	moderately developed tea
darker tones	sparse tea

The very dark tones are unvegetated, including water and bare soil. It is especially desirable to minimize topographic effects for the tea survey, because the crops are grown in extremely hilly terrain.

Several different ratios were applied to the Sri Lanka data, including MSS7/MSS5; MSS6/MSS5; [(MSS7-14)/(MSS5)]÷B; G/B; (MSS7-14)÷MSS5; (MSS7-MSS5) ÷ (MSS7 + MSS5). Signatures were again calculated for the supervised training sets and the results were evaluated (Table 1). Images were filmed for (MSS7-14)/MSS5 and (MSS7-MSS5)/(MSS7+MSS5). The offset of 14 was chosen for the MSS7/MSS5 transform to optimize the contrast within the vegetation for this particular data set. The MSS7-MSS5/MSS7+MSS5 ratio has been used extensively elsewhere with good results (e.g., Tucker, et al., 1979). For the Sri Lanka data, the (MSS7-MSS5)/(MSS7+MSS5) transformation appears to be more sensitive to variability within the Tea, but produces more confusion between Tea and other vegetation than the MSS7-14/MSS5. Because each ratio emphasizes slightly different features, the images should be considered collectively.

4.0

CONCLUSIONS

Each of the procedures investigated vary in complexity, cost of implementation and the type of information produced. Contrast enhancement emphasizes variability throughout the scene, but may overlook subtle differences in vegetation type. The Green measures are more sensitive to differences in vegetation condition, but not to vegetation type. The Supervised classification is helpful for separating vegetation type, but not as good for separating condition classes. The contrast enhancement and classification procedures are more affected by topography.

Each procedure has advantages and limitations that should be taken into consideration during interpretation. They will provide the most information when used together.

REFERENCES

Colwell, John. Personal Communication. Environmental Research Institute of Michigan, Ann Arbor, Michigan, February 1982.

Colwell, John and G. Suits. Yield prediction by analysis of multispectral scanner data. 109600-17-F, Environmental Research Institute of Michigan, Ann Arbor, Michigan, May 1975.

Ground Truthing-Maskeliya tea Rehabilitation Project Area, Centre for Remote Sensing, Colombo, Sri Lanka, 1980.

Hay, C.M. Development of AI procedures for dealing with the effects of Episodal events on crop temporal spectral response; Annual Progress Report. NASA Contract NAS9-14565, Principal Investigator, R.N. Colwell, University of California, Berkeley, California, November 1979.

Holben, B. and C. Justice. An examination of spectral band ratioing to reduce the topographic effect on remotely sensed data, NASA/Goddard Technical Report. Greenbelt, Maryland, 1980.

Kauth, R.J. and G.S. Thomas. The tasselled cap - a graphic description of the spectral-temporal development of agricultural crops as seen by Landsat. NAS9-14123, Environmental Research Institute of Michigan, Ann Arbor, Michigan, 1976.

Nalepka, R.F., J.E. Colwell, and D.P. Rice. Forecasts of winter wheat yield and production using Landsat data, NAS5-22389, Environmental Research Institute of Michigan, Ann Arbor, Michigan, December 1977.

Tucker, C.J., J.H. Elgin, Jr., and J.E. McMurtrey III. Temporal spectral measurements of corn and soybean crops, Photogrammetric Engineering, Vol. 45, No. 5, May 1979, pp. 643-653.
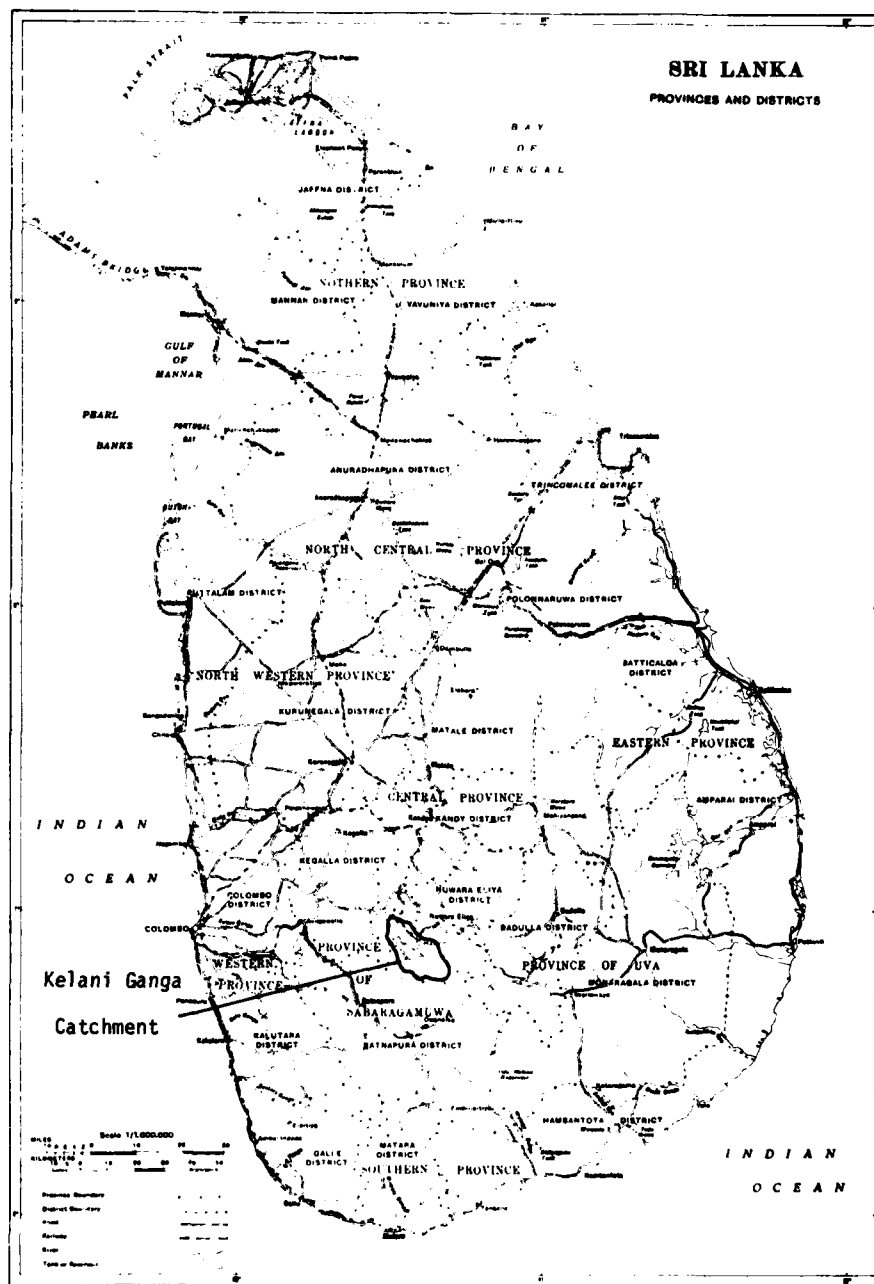
FIGURE 1. LOCATION OF STUDY SITE
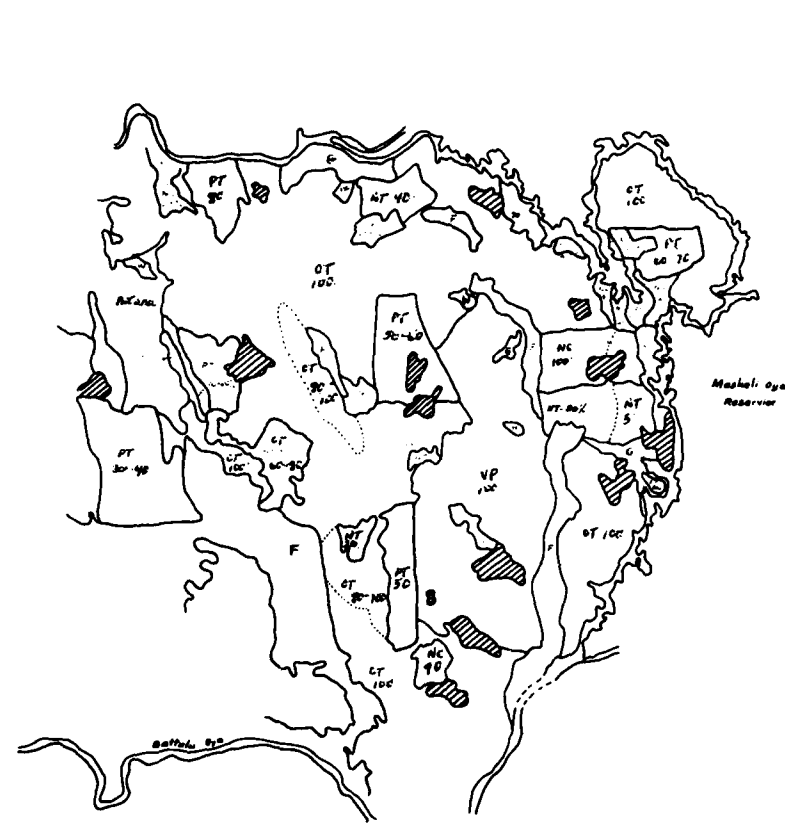
861

FIGURE 2. EXAMPLE GROUND TRUTH MAP FOR ONE OF FOUR ESTATES
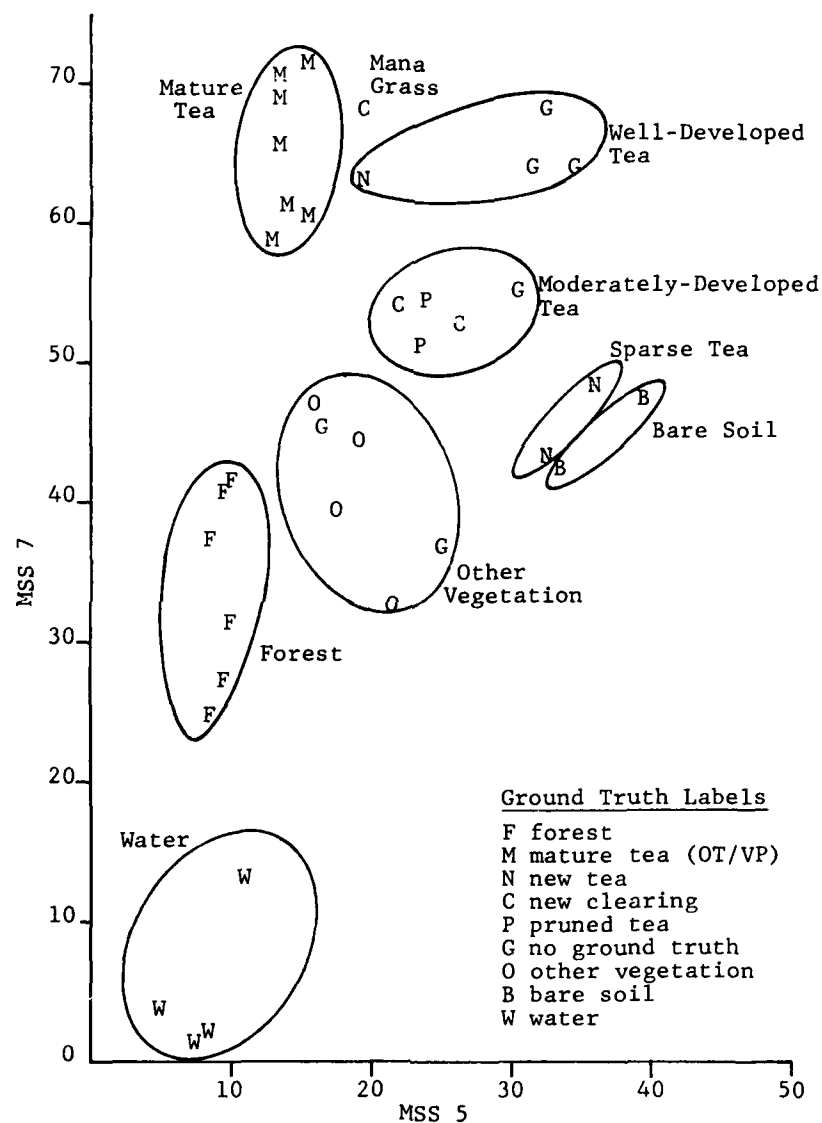
FIGURE 3. PLOT OF SIGNATURES FOR SUPERVISED TRAINING SETS

Table 1. Summary of Signatures for Various Transformations

Category	MSS 7	MSS 5	MSS7-14 / MSS5	7-5 / 7+5	7/5	G/B	G-.1B	Ground Truth Code* % Green Cover
Forest	37.6	8.8	2.6818	.6207	4.2727	135.9	117./	
Forest	41.8	9.8	2.8367	.6202	4.2653	138.5	128.8	
Forest	31.4	9.7	1.7938	.5280	3.2371	123.4	98.4	
Forest	27.0	9.1	1.4286	.4958	2.9670	117.4	86.6	
Forest	40.8	9.3	2.8817	.6287	4.3871	136.3	126.2	
Forest	24.7	8.2	1.3049	.5015	3.0122	115.6	81.8	
Mature Tea (MT)	61.1	13.9	3.3885	.6293	4.3957	142.4	179.4	OT-100%
MT	65.9	13.6	3.8162	.6541	4.8456	145.2	193.1	VP-100%
MT	71.8	15.5	3.7290	.6449	4.6323	146.2	208.8	VP-100%
MT	70.8	13.6	4.1765	.6777	5.2059	149.8	207.3	OT-100%
MT	5b.4	12.5	3.5520	.6474	4.6720	142.8	172.2	OT-100%
MT	69.6	13.4	4.1493	.6771	5.1940	148.5	206.6	VP-100%
MT	60.9	15.1	3.1060	.6026	4.0331	136.5	177.3	VP-100%
Mana Grass	68.1	19.2	2.8177	.5601	3.5469	131.5	191.3	NC-60-80-100%
Well-Dev. Tea(Wd)	63.8	19.4	2.5670	.5337	3.2887	128.5	180.5	NT-50-70%
Wd	64.8	31.7	1.6025	.3430	2.0442	102.9	165.0	
Wd	68.5	32.1	1.6978	.3618	2.1340	106.8	175.0	
Wd	64.0	34.3	1.4577	.3021	1.8659	98.0	160.3	
Mod.-Dev. Tea(Md)	54.5	23.7	1.7089	.3939	2.2995	110.2	146.5	PT-50-60%
Md	54.3	21.9	1.8402	.4252	2.4795	110.9	146.0	NC-80%(Grass)
Md	51.7	23.6	1.5975	.3732	2.1907	105.1	137.2	PT-40-50%
Md	55.2	30.7	1.3420	.2852	1.7980	94.2	138.7	
Md	53.1	26.1	1.4981	.3409	2.0345	103.3	140.1	NC-100%
Sparce Tea	43.8	32.1	.9283	.1542	1.3645	79.8	106.2	NT-10-20%
Sparce Tea	48.7	36.1	.9612	.1486	1.3490	77.1	113.1	NT-5-20%
Other Veg. (OV)	37.1	25.1	.9203	.1929	1.4781			
OV	40.0	17.5	1.4857	.3913	2.2857	106.9	110.5	Grass
OV	47.5	15.9	2.1069	.4984	2.9874	123.2	137.8	Abandoned
OV	45.8	16.1	1.9752	.4798	2.8447	115.7	129.2	
OV	32.7	21.6	.8657	.2044	1.5139	81.0	85.1	Homestead
OV	44.5	18.9	1.6138	.4036	2.3545	108.6	123.3	
B	42.4	33.4	.8503	.1187	1.2695			Homestead
B	47.7	39.2	.8597	.0978	1.2168			
W	1.6	7.1	-1.746	-.659	.208			
W	1.8	7.7	-1.584	-.621	.233			
W	3.6	3.8	-2.737	-.027	.947			
W	13.4	10.9	-11.500	.1029	1.229			

*Ground Truth Codes:
  OT/VP - Mature Tea
  NC   - New Clearing
  NT   - Young/Immature Tea
  PT   - Pruned Tea

LAND COVER MAPPING IN PARTS OF SOUTH GUJARAT AND TAMIL NADU STATES OF INDIA USING BHASKARA-I TV DATA

A.R. Dasgupta, I.C. Matieda, S.D. Naik, K.L. Majumdar,
J.S. Parihar, S.K. Pathan, P.D. Yadav
Space Applications Centre (ISRO),
Ahmedabad-380 053 (India)

ABSTRACT

Bhaskara, India's first experimental remote sensing satellite was launched on June 7, 1979 by an Intercosmos rocket under a collaborative agreement with the USSR. One of the two primary payloads onboard was the two camera TV system operating in the ranges of 0.54 to 0.66 micrometer and 0.75 to 0.85 micrometer. On 16th May, 1980, the TV camera operating in the 0.54 to 0.66 micrometer band was switched on successfully. Since then the satellite has acquired a large number of imagery over the Indian terrain with this camera. The imagery acquired by the Bhaskara offers a synoptic view of the earth covering an area of 340 x 340 km from a satellite nominal altitude of 525 km with the spatial resolution of one kilometer.

Various projects were formulated for the utilisation of the Bhaskara TV data by the user agencies in collaboration with the Indian Space Research Organisation (ISRO). A number of application areas like land use, snow cover, geology, geomorphology etc., were identified to assess the utility of Bhaskara imagery. This presentation briefly reports the analysis of the Bhaskara imagery and the results obtained for two test areas, one covering parts of South Gujarat State and the other around Cuddalore in Tamil Nadu State of India.

Land cover maps have been prepared for both the study areas using bulk processed and digitally enhanced data. An attempt has been made to prepare geomorphological and geological maps of the Cuddalore region in Tamil Nadu State. The Bhaskara imagery yielded significant information regarding land cover, geomorphology and geology of the study area on regional scale i.e. 1:2 M.

Limited digital processing aided the interpretation in
land cover mapping.

1. INTRODUCTION

India's first experimental remote sensing satellite Bhaskara-I (known
before launch as the Satellite for Earth Observations - SEO 1) was put into
the space from a Soviet Cosmodrome by an Intercosmos launcher under an Indo-
Soviet collaborative agreement. The satellite was launched on June 7, 1979.
The principal aim of this Bhaskara-1 project was to gain experience of an end-
to-end remote sensing system but on a reduced scale, which ultimately would
help in learning the techniques involved without the additional burden of
having to handle large volumes of data and operate large systems.

The satellite carried, among their payloads, a two band TV super vidicon
payload system operating in the 0.54 to 0.66 and 0.75 to 0.85 micrometer bands.
One of the cameras in the band 0.54 to 0.66 micrometer was successfully operat-
ed on May 16, 1980 and was used to aquire TV data over the Indian subcontinent
till March, 1981 from a satellite nominal altitude of 525 km. Each imagery
covered an area of 340 by 340 km with a spatial resolution of one kilometer.
The tracking, ranging, telecommand and telemetry data acquisition was the re-
sponsibility of the ISRO Tracking Network (ISTRAC) stations at SHAR Centre,
Sriharikota and Space Applications Centre, Ahmedabad. The TV data aquired
were pre-processed at SHAR. This consisted of reformatting the TV high bit
rate telemetry data into computer compatible tapes (CCTS). Post facto orbit
and attitude parameters of the satellite were also computed and inserted in
the pre-processed CCT. The pre-processed data was transferred to the Data
Products Group at Ahmedabad which converted them to standard user oriented data
products.

With a view to utilize the Bhaskara data, ISRO launched a programme to
approach user agencies and formulate projects as early as in February, 1976.
Projects in different application areas like geology, geomorphology, hydrology,
soils, land use, etc., were identified. The present report primarily deals
with the studies conducted for land cover mapping in parts of South Gujarat
and Tamil Nadu States of India based upon the visual analysis of Bhaskara-1
TV imagery. The studies indicate the capability of the Bhaskara-1 single band
data with a fair degree of completeness for land cover mapping in the study
region.

2. DATA USED

Following are the imagery used for the studies

i)   ID No. 357-14234 dated 29.5.80, Gulf of Cambay, South Gujarat

ii)   ID No. 511-12382 dated 30.10.80, Cuddalore, Tamil Nadu

Standard products consisting of diapositives and paper prints on 1:2 M
scale were used initially for visual interpretation. The corresponding data
on CCT was further studied on an Interactive Digital Image Processing System
(INDIPS), developed by the Space Applications Centre (SAC), Ahmedabad and sub-
scenes containing the test sites were selected which were further processed
on an off line computer, (PDP11/70). Linear and non-linear contrast stretch-
ing and a single band classification and colour coding scheme developed at SAC
were utilized. The analysed products in the form of B&W or colour prints were
again subjected to visual interpretation.

3.   METHOD OF ANALYSIS

3.1   VISUAL INTERPRETATION

The above mentioned standard and digital processed data products were
analysed using visual interpretation techniques. In the B&W imagery, various
grey levels were identified and their boundaries were delineated. The grey
level map was compared with the thematic maps given in the 'Forest Atlas of
India', 'The Irrigation Atlas of India' and the 'Geological Map of India' on
1:2 M scale, which served as the collateral information. From colour coded
imagery, various colour tones were identified and were also correlated with
the collateral information.

3.2   CONTRAST STRETCHING

Quite often the images acquired by the remote sensors are degraded due
to noise, low contrast between the object of interest and the background, etc.
In contrast stretching the grey levels of the original pixels is modified by
a grey level transformation. This transformation changes the grey levels in
a uniform manner for a part of the scene or for the entire scene by increasing/
stretching the contrast.

Two types of transformations, namely linear and non-linear stretching,
were attempted to increase the contrast. In linear contrast stretching if an
image does not occupy the fully grey level range it is possible to linearly
increase the range to the desired limits, upto a maximum of 127 levels. The
concept of linear stretching is presented in the fig. 1. If the original data
has a Gaussian distribution in its grey levels, a non-linear transformation
may be used to increase the grey level range. The effect of stretching is
minimum near the mode and goes on increasing with increase in the distance
from the mode.

3.3   SINGLE BAND CLASSIFICATION AND COLOUR CODING

The basic approach of the single band classification technique is to
identify different grey value clusters such that each cluster represents a

cover type. A frequency distribution of the pixels in various grey levels are used for the selection of grey level clusters. The range of grey values which lie between two stable minima and includes one stable maxima is considered to be a cluster which represents a class of cover type. The concept of this level slicing is shown in fig. 2. In order to obtain a pseudo colour composite similar to a false colour composite imagery, each cluster (cover type) is assigned a unique colour. As every colour is essentially a weighted mixture of three primary colours, red, blue and green, each cluster colour can be composed of these primary colours with suitable weights assigned to them. Thus three pseudo grey values for each cluster can be generated, each representing the weightage for the three primary colours. Wehn the three pseudo grey level imagery are combined with the primary colours in an additive colour viewer, a pseudo colour compsoite is obtained in which each cluster of grey values, representing a cover type, has a unique colour. This methodology in principle is similar to the density slicing technique.

4. LAND COVER MAPPING

As mentioned earlier, two areas, one in Gujarat state, around Gulf of Cambay and the other in Tamil Nadu State, around the town of Cuddalore was taken up for the land cover studies.

4.1 GULF OF CAMBAY, SOUTH GUJARAT

The standard imagery used for the interpretation work is presented in fig. 3. The water-land interface in the Gulf of Cambay region can be easily demarcated. Traces of major rivers like Narmada, Tapti and the upper reaches of Godavari rivers are discernible. Ukai reservoir can be easily picked up due to its light grey tone. Surat city appears in a light grey tone. In all, four classes of cover types were identified on the Bhaskara-1 imagery and are as given below.

i) Forest Area .. Dark grey tone
ii) Agricultural land .. Medium grey tone
iii) Scrub and grass land .. Very light grey tone
iv) Marshy land .. Light tone in the coastal region

A land cover map thus prepared from the standard imagery is given in fig. 4. It was observed that two forest areas with similar species of vegetation were represented by two different tones namely dark and light grey. The confusion was attributed to the difference in vigour of vegetation in the two forests.

Linearly stretched imagery covering the study area is presented in fig. 5. It is noted that in this imagery the contrast of various land cover types is more than is observed in the bulk processed imagery. The river courses of

Tapti, Narmada and Godvari stand out in higher contrast with the surroundings in the linearly stretched imagery. The non-linearly stretched imagery was not found very useful as the grey values were saturated.

The colour coded imagery showed up different land cover categories like agricultural land, irrigated and non-irrigated, scrub land, marshy land and forest in distinct colour tones. A land cover map prepared from the colour coded imagery is presented in fig.6. A close correspondence could be established between the colour tones on the imagery and the existing land cover categories. It can be concluded that the enhancement of the imagery could facilitate the interpretability of the Bhaskara-1 imagery.

4.2 CUDDALORE REGION, TAMIL NADU

Analysis of the standard Bhaskara-1 imagery of the study region (fig.7) led to the delineation of four cover types, namely

i)   Agricultural land irrigated   .. medium grey tone
ii) Agricultural land non-irrigated   .. light grey tone
iii) Tropical dry deciduous forest   .. dark grey tone
iv) Tropical thorn deciduous forest   .. dark grey tone

It can mentioned here that the last two categories show similar grey tone and could be assigned different categories, based upon the collateral information taken from the Forest Atlas of India (fig. 8).

The visual interpretation of linearly stretched imagery offered the same number of categories, however, their boundaries are sharper as can be seen in fig. 9. Colour coded imagery was found helpful in refining the forest boundaries.

5. GEOLOGICAL AND GEOMORPHOLOGICAL STUDIES

An attempt was also made to extract geomorphological and geological information on gross level using Bhaskara-1 imagery covering Cuddalore region, Tamil Nadu. Three prominent categories namely, alluvial plains, denuded pediplains and residual plains could be identified and have been shown in the accompanying geomorphological map (fig. 10). A photogeological map was prepared for the Ponnaiyar river basin area and was confirmed with the ground truth data provided by the Ground Water Board of the Public Works Department, Tamil Nadu (fig. 11). Four main categories namely, alluvium, granite gneiss, charnockites and hybrid gneiss were delineated. The river course of Ponnaiyar river on entering the plains, appears prominenly on the imagery as it becomes more broad while flowing through alluvial plains. There is a very little difference between the grey tone of granite gneiss and charnockites. On careful observation, however, a narrow band of charanockites can be noted bordering the forested hillrocks of hybrid gneiss appearing in dark grey tone.
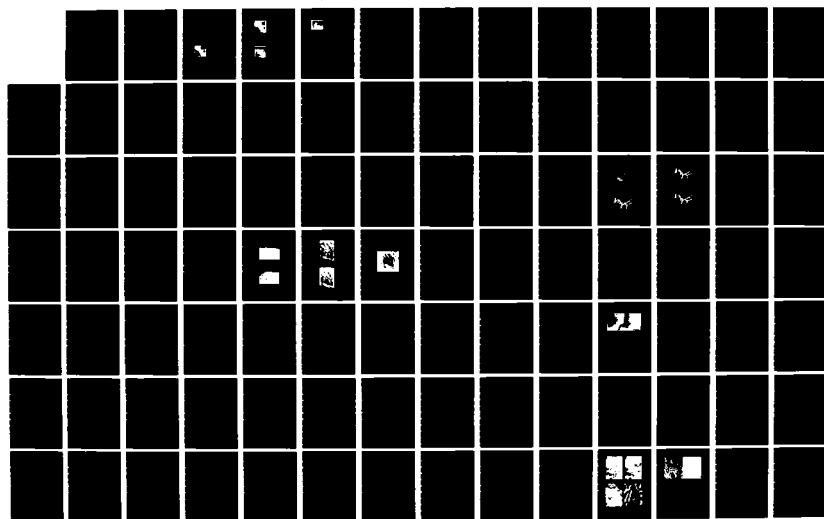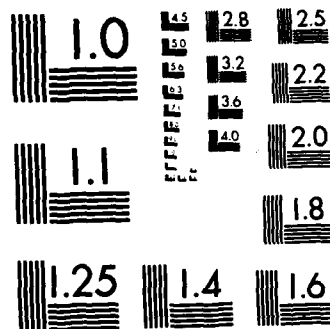
MICROCOPY RESOLUTION TEST CHART
NATIONAL BUREAU OF STANDARDS-1963-A

6. CONCLUSIONS

Bhaskara-1 imagery was found useful in delineating various land cover categories on a gross level. Enhancement of the imagery using linear stretching and single band-classification techniques, could facilitate the interpretation. Broad geomorphological categories and lithological units on a very gross level could be delineated in the imagery covering Cuddalore area of Tamil Nadu.

7. ACKNOWLEDGEMENT

8. REFERENCES

1. Dasgupta A.R., Matieda, I.C., Majumdar, K.L., Naik,S.D. Paihar J.S.,Pathan S.K. and Yadav, P.D. 1981. Bhaskara TV Data Utilisation, Space Applications Centre, Ahmedabad, India, Technical Report No. SAC-RSA-TN-02/06-81.

2. Senchaudhari, P., Patel, A.N., Majumdar, K.L., Gopalan, A.K.S., Kanat, D.S., 1981. An approach to develop interpretation keys for the analysis of single band Bhaskara TV Data, Technical Report No. RS-IP/TN-01/81.
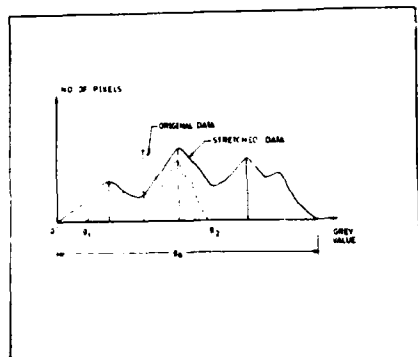
Fig.1. Concept of linear stretching
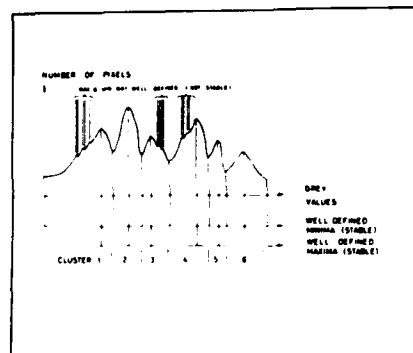
Fig.2. Concept of single band classification
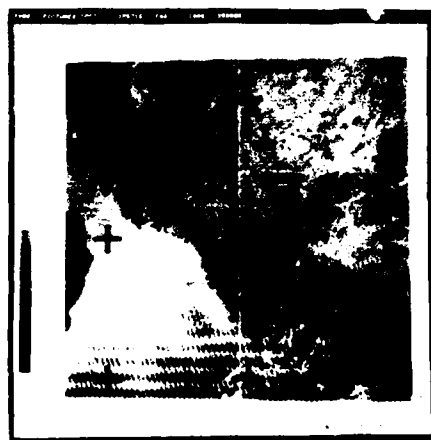
Fig.3. Bulk processed imagery of Cambay area, South Gujarat
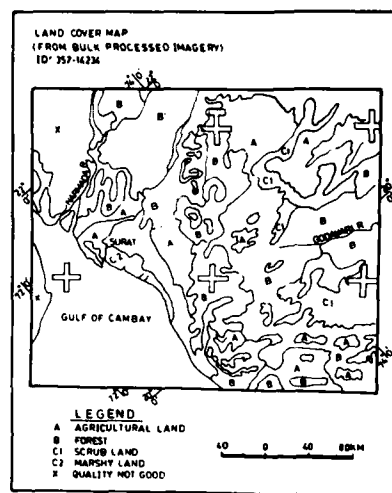
Fig.4. Land cover map from bulk processed imagery of Cambay area, South Gujarat

Fig.5. Linear stretched imagery
of Gulf of Cambay, South
Gujarat
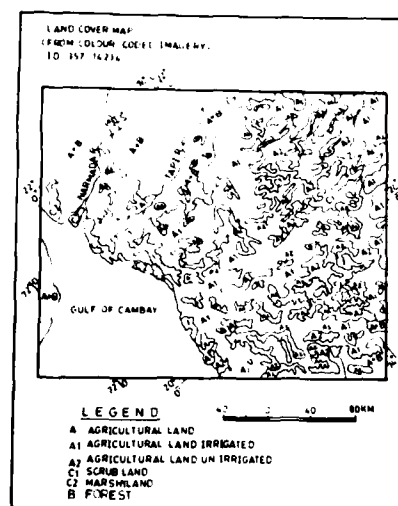
Fig.6. Land cover map from
enhanced imagery of
Gulf of Cambay, South
Gujarat
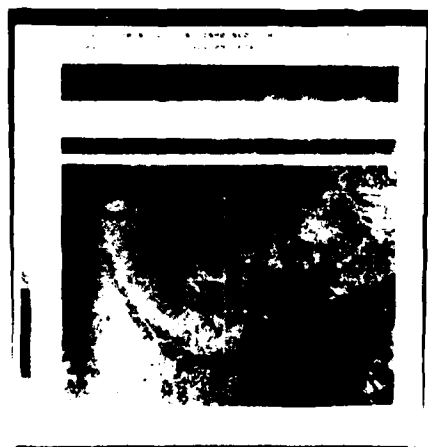
Fig.7. Bulk processed imagery
of Cuddalore area,
Tamil Nadu
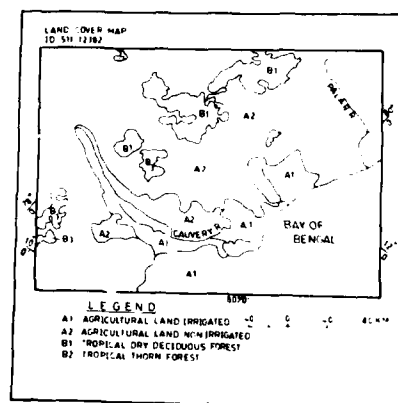
Fig.8. Land cover map of
Cuddalore area,
Tamil Nadu

872

Fig.9. Linear stretched
imagery of Cuddalore
area, Tamil Nadu
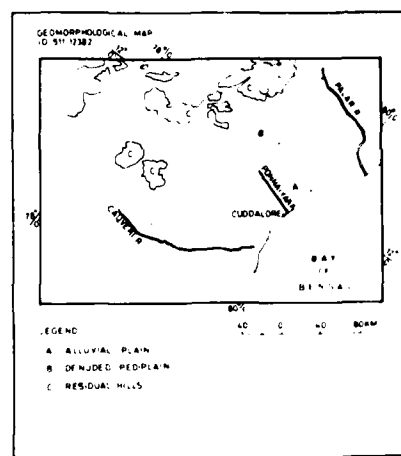
Fig.10. Geomorphological map of
Cuddalore area, Tamil
Nadu
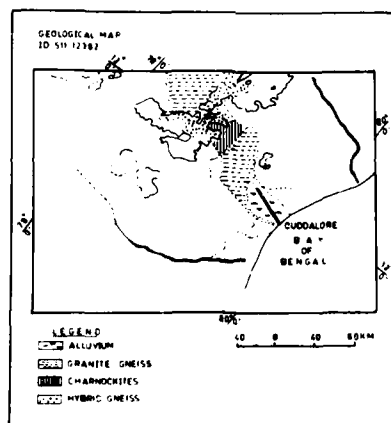
Fig.11. Geological map of
Cuddalore area,
Tamil Nadu

873

COASTAL LAND USE CHANGE MAPPING OF LINGAYEN GULF AREA
USING LANDSAT MSS DATA

Rolando Tomas
Larry Silonga
Rebecca Manuel
Francisco Esporas

Natural Resources Management Center
Quezon City, Philippines

SUMMARY

Proper coastal land use management should be given a special emphasis in the formulation of guidelines in Resource Management and Development Planning, since it involves a wide range of dynamic ecological systems.

At present, we do not have sufficient informations which will enable us to determine the full view of coastal land use dynamics, which led us to misallocation and mismanagement of coastal land areas.

This paper seeks the viability of Landsat MSS data in coastal land use change mapping, using multi-date Landsat imageries in the form of Computer Compatible Tapes (CCT).

CCT's were analyzed in a Multispectral Image Analyzer called Image 100, on lined with the PDP 11 computer system. Spectral signatures of the different land use categories were extracted using special software processing functions built in the system.

Comparative analyses were performed for each imagery to determine spectral variations of each land use category with respect to time. This enables us to maintain spectral signature values of a particular land use category by setting spectral range limit, which would define the classification category.

Land use maps were produced by superimposing base maps in transparencies with the binary theme prints, and assigning theme codes.

Land use change was determined by measuring theme areas of each Landsat based maps.

ESTABLISHING WIND DIRECTIONS FROM DUNE ORIENTATIONS IN
ORBITAL PHOTOGRAPHS OF THE MONTE DESERT, ARGENTINA

Farouk El-Baz
D.M. Warner

Center for Earth and Planetary Studies
National Air and Space Museum
Smithsonian Institution
Washington, DC

SUMMARY

One of the problems encountered in the study of deserts and arid lands is
the scarcity or lack of meteorological data, particularly those relating to
wind direction and velocity. This is caused by the fact that in most desert
regions, particularly in the developing nations, few meteorological stations
exist. Furthermore, the only data available for remote regions is often
collected from stations near towns far from the desert or in depressions that
enclose oases. Data from such locations are usually not representative of the
arid area's wind regime, and their use may be misleading.

Because knowledge of the wind velocity and direction may be essential to
the erection of wind breaks and sand fences, alternative methods should be
found to deduce the direction of high-velocity winds that transport most of
the dust and sand. It is here shown that photogeologic interpretations of
orbital photographs may provide a useful method for establishing wind direc-
tions. The example used is in the Monte Desert in southeastern San Juan,
Argentina.

Good quality photographs of this desert were obtained by the Apollo-
Soyuz mission in 1975. These photographs were used for a reconnaissance
survey of large-scale landforms, and were helpful in distinguishing linea-
ments and probable faults, drainage patterns, rock types, and soil-tonal
variations. The photographs were especially useful in studying the distribu-
tion of sand deposits and large-scale dune morphology.

The physiographic setting of the study area is characterized by mountain-
and-bolsón topography controlled mainly by faulting. Most of the lineaments
detected on the photographs appear to correspond to faults, and some of them
may provide evidence of recent tectonic movement in the area. Typical topo-
graphic features include barren, deeply dissected block mountains bordered
by slopes of alluvial materials that descent to a flat-floored desert basin.

The most prominent features on the desert floor are two dune fields. The
larger field lies south of the town of Vallecito and is approximately 1300
km^2; the smaller dune field is near the town of Marayes and is approximately
160 km^2.

In the southern part of the Vallecito dune field, draa-size complex
ridges display steep western flanks and gently sloping eastern flanks. These
ridges are diagonally crossed by smaller linear dunes. In the central part,
draa-size crescentic dunes with elongated horns abound. The complex array of
transverse, longitudinal, and oblique elements displayed by the Vallecito
dunes cannot easily be explained. Nonetheless, all the dune orientations in
both the Marayes and Vallecito dune fields were plotted and analyzed.

Wind data was collected and analyzed from the closest meteorological station at the city of San Juan, some 60 km to the northwest of the Vallecito dune field. N-Summaries of surface wind and velocity and duration were obtained for the station by velocity categories, and wind roses were made to show the potential movement of sand from 16 compass directions. These diagrams showed that the prevailing sand-moving winds at San Juan are from the south, although strong winds (zonda) from the northwest occur in June through August.

Interpretation of the dune patterns seems to indicate that the prevailing winds are from the south and southeast, with mappable details. In addition, the dominance of right-oblique elements in the western part of the Vallecito dune field suggests the presence of an important crosswind, probably the seasonal zonda, with measurable directions. This interpretation is based on the trend of linear dunes east of the Vallecito field, and the orientation of slip faces on the crescentic dunes.

The study shows that it is possible to establish directions of high-velocity, sand-moving winds by the interpretation of orbital photographs. This information may be critical in desert areas where meteorological stations are few and far between.

MAPPING AND INVENTORY OF CORAL REEF LAGOONS
AS POTENTIAL MARICULTURE SITES
USING LANDSAT DATA

Ricardo T. Biña
Geronimo P. Reyes

Remote Sensing Technology Application Division
Natural Resources Management Center
Quezon City, Republic of the Philippines

SUMMARY

This paper reports on a current project started in June 1982, and being undertaken by the Natural Resources Management Center (NRMC) for the Ministry of Natural Resources, Republic of the Philippines, which involves the use of Landsat data and computerized mapping techniques to map and inventory the coral reef lagoon areas in the Philippine archipelago.

A major aspect of the fisheries development in the Philippines is the expansion of mariculture activities throughout the country such as fish-cage and fish-pen culture, seaweed farming and shellfish culture. This necessitates the mapping and inventory of all potential sites throughout the coastal waters of the country to determine priority areas as well as implementation strategies. Such sites include protected bays, coves, inlet, reef lagoor , and other areas which are protected from heavy wave action.

A major parameter used in site selection aside from wave protection is water depth. Most mariculture practices in the Philippines require water depth of not more than three meters. Such information is available from nautical charts for bays, coves, and inlets, but not for coral reef lagoons which abound in the country. This is to be expected since hydrographic survey ships cannot possibly pass through the shallow reefs surrounding such lagoons. Considering the number and archipelagic distribution of reef lagoons in the country, direct field surveys can be very expensive and time-consuming. Hence, a decision was made to take advantage of the synoptic characteristic of Landsat data.

Using a computer-assisted interactive multispectral image analyzer system, Landsat subscenes at 1:125,000 scale covering all the reef areas in the country were reconstructed from Landsat CCTs and stored in magnetic tapes for subsequent processing and analysis. A software system using the four Landsat MSS bands and based on the water-penetration limit of each Landsat MSS band is currently being used to classify each subscene pixel according to the following bathymetric zones: emergent or exposed areas; very shallow areas (<0.5 m); water areas 1-3m. deep; and water areas deeper than three meters. These water depth categories are expressed in binary theme prints registered into 1:125,000 scale base map. Final output is a color coded map of the reef area showig the four water depth categories emphasizing in particular those areas with water depth range suitable for mariculture activities, together with hectarage measurements.

Preliminary checks with available secondary ground data show a more than 80% classification accuracy, indicating the efficacy and cost-effectiveness of the use of Landsat data for this project.

AUTOMATIC CROP INVENTORY IN ARGENTINA
WITH MULTITEMPORAL LANDSAT DATA

Michael Metzler

Environmental Research Institute of Michigan
Ann Arbor, Michigan

Dr. Robert Cate

Lockheed Engineering and Management Services Corporation, Inc.
Houston, Texas

Julie Odenweller

Space Sciences Laboratory, University of California
Berkeley, California

SUMMARY

The use of Landsat data for crop inventory over large areas has been
explored for nearly a decade. The Large Area Crop Inventory Experiment (LACIE)
conducted by the National Aeronautics and Space Administration (NASA) estab-
lished the feasibility of global inventory of wheat with Landsat, using image
interpretation to establish training data. The joint use of a ground based
inventory procedure with Landsat derived inputs has been investigated by the
U.S. Department of Agriculture. The approaches taken to date rely heavily
upon labor intensive methods (image interpretation or ground survey) to achieve
their respective performance goals. Under the auspices of the AgRISTARS Foreign
Commodity Production Forecasting Project at NASA, the inventory of corn and soy-
beans in Argentina has been pursued with the objective of achieving accpetable
levels of accuracy while eliminating or greatly minimizing the need for labor
intensive techniques. Several approaches have been developed and tested that
are essentially automatic. This paper and the accompanying poster session pre-
sents and compares two approaches to the automatic identification of corn and
soybean crop acreage with Landsat data. The results of tests conducted over the
U.S. Corn Belt sites are presented along with a discussion of the problems and
possible solutions encountered in adapting these procedures to Argentina.

Estimation of crop acreage without the use of ground inventoried training
samples adds a complexity to the problem in requiring techniques to bring prior
knowledge of the spectral appearance of crops and factors that would alter crop
appearance from one location to another. The procedures presented make use of
multitemporal Landsat data and predetermined models of crop spectral patterns
and planting patterns to enable the identification of the crops without ground
data. Along with these predetermined characteristics, the procedures exploit
other predictable or determinable features that are derivable directly from
Landsat, for example, field patterns. One procedure, code named C/S-5, bases
its approach on the premise that multitemporal spectral profiles of crop charac-
teristics derivable from a target like a field in Landsat data can be matched to
pre-established profiles. The other procedure, code named MC-2, establishes
initial estimates of crop acreage by minimizing classification errors of commis-
sion in key crops, and then 'scales-up' estimates according to an empirically
established 'omission' error model.

881

Both techniques have been evaluated using Landsat data over the U.S. Corn Belt. Sample regions, called segments, 5 x 6 nautical miles in dimension, were processed and the bias and variance characteristics of the procedures identified. Each procedure has demonstrated accuracy in the estimation of crop acreage to within 10% of the actual and achieves that level of performance while nearly eliminating the need for intensive image analysis or ground observation.

THE EFFECT OF GROWING SEASON ON THE ANALYSIS OF
LANDSAT MSS DATA FOR INTERIOR ALASKA

Thomas H. George
John M. Miller

Geophysical Institute
University of Alaska, Fairbanks
Fairbanks, Alaska

SUMMARY

Landsat MSS data offers a powerful tool for the inventory of Alaska's vast resources. Computer analysis of Landsat data is growing in popularity as a mechanism to map and inventory large areas. To successfully utilize this tool in interior Alaska, information is required to identify the window in our short growing season which will provide suitable classification results.

In this study, images were selected throughout the growing season, and training sites identified for different vegetation types. Spectral signatures were derived and compared to evaluate the relative information content for each image.

Preliminary results indicate that the optimum window for vegetation discrimination exists in early to mid summer. Later in the season, the separation between certain vegetation types starts to diminish which appears to relate to decreasing sun angle.

In addition, some comparisons have been made between the clustering algorithm ISOCLS and a program called STAT which calculates the mean and covariance matrix for each training set. Considerably different results were derived when starting with the same sample data set. These findings will be presented and their significance discussed in terms of land cover classifications.

EVALUATION OF REFORESTATION USING REMOTE SENSING TECHNIQUES

P. Hernandez Filho
Y. E. Shimabukuro
J. R. dos Santos

Instituto de Pesquisas Espaciais - INPE
Conselho Nacional de Desenvolvimento Científico e Tecnológico - CNPq
C.P. 515 - São José dos Campos - SP - Brasil

ABSTRACT

The objective of this paper is to evaluate the utilization of remotely sensed orbital data for forestry inventory. The study area (approximately 491,100 ha) encompasses the municipalities of Ribeirão Preto, Altinópolis, Cravinhos, Serra Azul, Luis Antonio, São Simão, Santa Rita do Passa Quatro and Santa Rosa do Viterbo (São Paulo State). Materials used were: LANDSAT data of channels 5 and 7, scale 1:250.000 and CCTs. Visual interpretation of the imagery showed that for 1977 a total of 37.766.00 ha and for 1979 , 58.005.75 ha were reforested with Pinus and Eucalyptus within the area under study. The results obtained show that LANDSAT data can be used efficiently in forestry inventory studies.

1. INTRODUCTION

Reforestation prior to 1966 was considered a non-profit economical activity, when the brazilian government, through an appropriate legislation gave tax incentives opportunities to individuals and/or institutions to make investiments in reforestations. Therefore, the reforestation had a strong impetus after 1966, the area reforested within Brazil increasing from 500.000.00 ha up to 3.800.000.00 ha at 1979.

The accelerated rate of reforestation determined the need for more advanced techniques for monitoring of the implanted reforested resources. The first studies on reforestation areas using LANDSAT data, were performed by Hernandez Filho and Shimabukuro (1978) and Hernandez Filho et alii (1978) at the Northeast portion of São Paulo State.

The objective of this study is to show the feasibility of periodic monitoring of the implanted reforested resources through visual and computer--aided interpretation of LANDSAT data.

2. STUDY AREA

The study area is located in the Northeastern part of São Paulo State, Brazil, including the municipalities of Ribeirão Preto, Altinópolis, Cravinhos, Serra Azul, Luis Antonio, São Simão, Santa Rita do Passa Quatro and Santa Rosa do Viterbo. Occupying an area of 4,911 km², this area located between 21°00'S to 22°20'S and 47°00'W to 48°00'W (Figure 1). This study area was selected because it represents various categories of reforestation population density, age groups and cutting rate of Eucalyptus and Pinus plantations.

3. MATHERIAL AND METHODS

3.1 LANDSAT PRODUCTS

LANDSAT CCT and black and white photographic imagery, path 236 and row 75 from 07/01/1977 and 07/27/1979 were used in this study.

3.2 VISUAL ANALYSIS

For visual analysis of LANDSAT imagery, the channels 5 and 7, black and white, at the scale 1:250,000 in the two acquisition dates were used.

The basic photointerpretation techniques such as multitemporal information in tonality and texture pattern together field information were used to define the preliminary reforestation classes.

The preliminary maps of reforestation unities obtained were compared reforestation plans from the area, to check the mapping of the reforestation.

Subsequently, a final map with the discriminations of the reforestation classes including through a legend and an interpretation key, were obtained.

The mapped unities were quantified with a milimeter grid and the results were presented in hectares, per municipality, in the study area.

3.3 COMPUTER-AIDED ANALYSIS

Computer-aided analysis using Image-100 system was carried out in the study area. CCTs relative to the acquisition date 07/01/77 were used. The computer-aided analysis comprehends three steps: data preparation, signature acquisition and study area classification.

Initially, in the data preparation step, the study area was located on the CCT data. Subsequently, the part of the image that encompasses the study area was enlarged to the scale 1:250,000. The study area was divided in four modules.

The signature acquisition was obtained in two training areas at the scale 1:100,000. The choice of sample areas was carried out based on previous existing reforestation map and visual analysis of the LANDSAT imagery.

The classification of the study area was carried out using the program "MAXVER" (Velasco et al ., 1978), and the postprocessing "THEME UNIFORMIZATION". The area was quantified by the program "THEME AREAS".

4. RESULTS AND DISCUSSION

An interpretation key and a legend based on the spectral characteristics of the reforested areas were defined in the visual analysis.

a) Legend

When the reforestation covered completely the soil, the variations due to reforestation spacing, age, species and cutting rate, didn't influence the characterization of the classes. The following classes were defined:

    PA - homogeneous Pinus plantation
    PB - less homogeneous Pinus plantation
    PC - heterogeneous Pinus plantation
    EA - homogeneous Eucalyptus plantation
    EB - less homogeneous Eucalyptus plantation
    EC - heterogeneous Eucalyptus plantation

b) Interpretation Key

The interpretation key presented in Table I, was based on the tonality and photography texture patterns. The tonality was classified in the following classes: CE - dark gray; CE_m - dark gray, with other gray tones; CC_m - light gray, with other gray tones; CM - intermediate gray; CM_m - intermediate gray, with other gray tones and CC - light gray.

The texture was classified in the following classes: L - smooth texture, presented the same gray tone; M - intermediate texture, presented small variation between gray tones; and G - rough texture, presented high variation between gray tones.

The Table II presents the comparison of the results of the reforested areas with Eucalyptus between 1977 and 1979. The increase of reforested areas with Eucalyptus occurred only in the municipalities of Santa Rita do Passa Quatro and Luis Antonio while there was a decrease of reforested area in the municipalities São Simão, Serra Azul and Altinópolis.

The Table III presents the comparison of the results of the reforested areas with Pinus between 1977 and 1979. There was not change of the reforested areas in the municipalities of São Simão, Cravinhos and Altinópolis and in the other municipalities there is no reforestation with Pinus.

In the computer-aided analysis the only genus Eucalyptus was classified; the genus Pinus covered too small areas, hence being insufficient for selection of training samples.

For acquisition of spectral signatures of the reforested classes two training areas were chosen:

The Tables IV and V present the mean of spectral responses of the class Eucalyptus, in the four channels and the covariance matrices of this class, respectively, of the first training area.

In the second training area, two subclasses of Eucaliptus were defined: Eucalyptus 1 and Eucalyptus 2 based on the spectral response of the channels 6 and 7 of LANDSAT.

The Table VI presents the mean of the spectral responses of the subclasses Eucalyptus 1 and Eucalyptus 2, in the four channels; and the Table VII and VIII present the covariance matrices of the subclasses Eucalyptus 1 and Eucalyptus 2, respectively of the second training area.

Based on the spectral parameters obtained in the training areas a classification of the study area was carried out. It was found out that an area of 37,364.50 ha was occupied by the class Eucalyptus.

5. CONCLUSIONS

5.1 VISUAL ANALYSIS

The visual analysis showed that it was possible to map the areas of Pinus and Eucalyptus reforestation and to monitor these areas in each municipality.

5.2 COMPUTER-AIDED ANALYSIS

The computer-aided analysis showed that it was possible to classify the areas of Eucalyptus reforestation.

REFERENCES

HERNANDEZ FILHO,P.; SHIMABUKURO, Y.E. Estabelecimento de metodologia para avaliação de povoamentos florestais artificiais utilizando-se dados do LANDSAT. São José dos Campos, jun., 1978 (INPE-1271-TPT/089).

HERNANDEZ FILHO, P.; SHIMABUKURO, Y.E.; SANTANA, C.C.de. Relatório das ativi dades do projeto IBDF/INPE (Sub-projeto reflorestamento) durante o ano de 1978. São José dos Campos, INPE, dez., 1978 (INPE-1408-NTE/141).

VELASCO, F.R.D.; PRADO, L.O.C.; SOUZA, R.C.M. Sistema MAXVER: manual do usuá rio. São José dos Campos, INPE, jul. 1978 (INPE-1315-NTI/110).

Table I. Interpretation Key

CLASS	TONALITY		TEXTURE	
	CHANNEL 5	CHANNEL 7	CHANNEL 5	CHANNEL 7
PA	CE	CM/CE	L	L
PB	CE_m	CM_m/CE_m	M	M
PC	CC_m	CC/CM	G	G
EA	CE	CC/CM	L	L
EB	CE_m	CM_m	M	M
EC	CC_m	CM_m	G	G

Table II. Reforested areas with Eucalyptus (period 1977 - 1979), in the study area.

MUNICIPALITY	REFORESTATION AREA WITH EUCALYPTUS IN 1977 (Ha)	REFORESTATION AREA WITH EUCALYPTUS IN 1979 (Ha)	DIFFERENCE OF THE REFORESTATION OF EUCALYPTUS; BETWEEN 1977 AND 1979 (Ha)
STA. RITA DO PASSA QUATRO	8,600.00	9,012.50	(+) 412,50
SÃO SIMÃO	9,092.25	9,086.00	(-) 6,25
LUIZ ANTONIO	2,937.50	3,556.25	(+) 618,75
SERRA AZUL	3,150.00	2,575.00	(-) 575,00
CRAVINHOS	543.75	543.75	-
ALTINÓPOLIS	7,256.25	7,043.75	(-) 212,50
RIBEIRÃO PRETO	4,387.50	4,387.50	-
STA. ROSA DO VITERBO	1,387.50	1,387.50	-
TOTAL	37,354.75	37,592.25	(+) 237,50

Table III. Reforested areas with Pinus (period 1977-1979), in
the study area.

MUNICIPALITY	REFORESTATION AREA WITH PINUS IN 1977 (Ha)	REFORESTATION AREA WITH PINUS IN 1979 (Ha)	DIFFERENCE OF THE REFORESTATION WITH PINUS BETWEEN 1977 AND 1979 (Ha)
STA. RITA DO PASSA QUATRO	-	-	-
SÃO SIMÃO	210.00	210.00	-
LUIZ ANTONIO	-	-	-
SERRA AZUL	-	-	-
CRAVINHOS	56.25	56.25	-
ALTINÓPOLIS	145.00	145.00	-
RIBEIRÃO PRETO	-	-	-
STA. ROSA DO VITERBO	-	-	-
TOTAL	411.25	411.25	-

Table IV. Mean of the responses of the class Eucalyptus in
the four channels of the first training area.

CHANNEL CLASS	4	5	6	7
EUCALYPTUS	11.34	12.08	55.23	53.08

Table V. Covariance matrix of the class Eucalyptus of the
first training area.

CHANNEL	4	5	6	7
4	2.73	1.52	1.79	2.57
5	1.52	5.32	-0.16	-0.82
6	1.79	-0.16	34.62	31.90
7	2.57	-0.82	31.90	42.85

Table VI. Mean of the spectral responses of the subclasses Eucalyptus 1
and Eucalyptus 2 in the 4 channels of the second training area.

CHANNEL CLASS	4	5	6	7
EUCALIPT 1	8.54	9.24	48.86	48.97
EUCALIPT 2	8.83	10.02	34.75	31.78

Table VII.   Covariance matrix of the subclass Eucalyptus 1 of the second
training area.

CHANNEL	4	5	6	7
4	2.51	0.54	-0.46	0.15
5	0.54	2.23	0.30	0.33
6	-0.46	0.30	21.40	19.40
7	0.15	-0.33	19.40	27.23

Table VIII.   Covariance matrix of the subclass Eucalyptus 2 of the second
training area.

CHANNEL	4	5	6	7
4	3.03	1.10	-0.30	-0.31
5	1.10	4.22	0.86	0.05
6	-0.30	0.86	19.98	19.81
7	-0.31	0.05	19.81	27.36
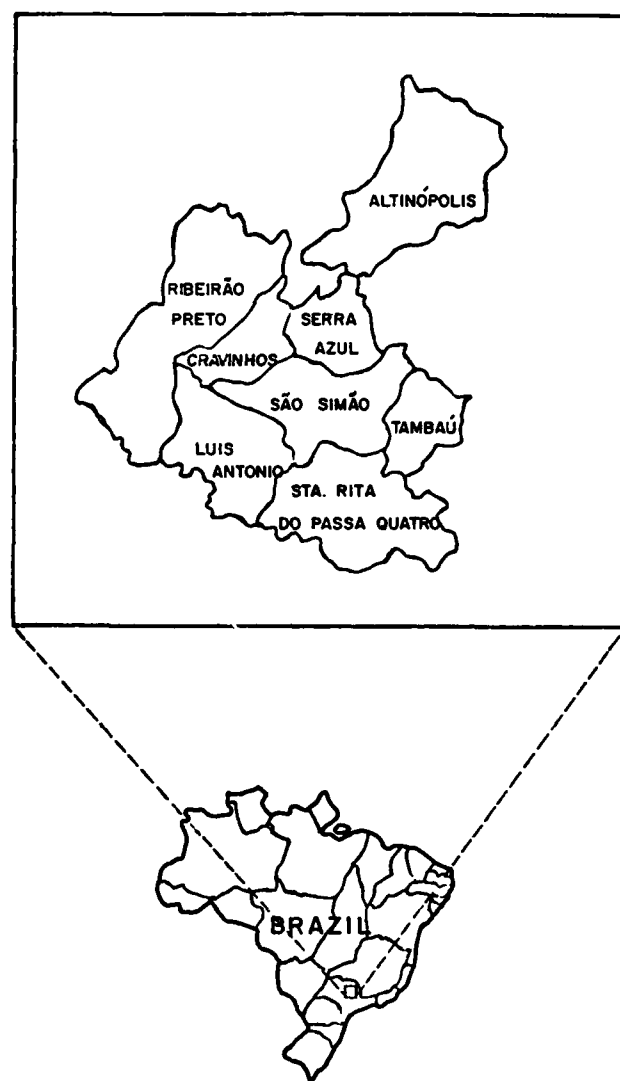
Figure 1. Study area localization.

ON A NEW REFLECTION MODEL FOR THE CORN FIELD

Y. Haba, M. Shikada, K. Miyakita and S. Ueno

Kanazawa Institute of Technology, P.O. Kanazawa-South,Nonoichimachi
Ogigaoka 7-1,Ishikawa 921, Japan

Abstract

It has been generally accepted that the remotely sensed
MSS data are the most efficient way immediately to obtain
the information of a ground surface. It is also an
important fact that they have different count levels in
spite of quite same objects because of the angular effects
caused by the rough surface in the optical sense. There is
no good correction method except by the ground truth data at
present.

A new reflection model (ref.5) for the corn fields,
especially paddy fields,has been proposed on the recognition
that there is a need to develope some approaches in order to
obtain the ground truth data without expensive and time
consuming ground truth observation. The model developed has
an advantage that the situation very close to the real paddy
fields can be simulated by manipulating some parameters and
the data on the ground truth can be gathered under various
conditions.

The simulated results were compared with the actual ground
truth data but they did not coincide. From the results of
model simulation,however,were obtained the important
suggestions that the actual MSS data and the ground truth
data are accompanied with intrinsic and inevitable errors in
themselves when the objects on the ground has the rough
surface like that of a corn or paddy field, and that there
are more difficult problems to be resolved when the MSS data
include the rough surface objects.

1 Introduction

It has been said that there are some difficulties in analyzing the remotely
sensed imageries obtained by the multi-spectral-scanner MSS boarded on a
satellite or an airplane. One of them is that the count level of the imageries
data is different from one solar angle to another and one look angle to another
because the observed objects on the ground have a rough surface in the optical
sence. The effects on the imagery data by the rough surface are more important
than ones by any other factors in point of the distorted levels and areas. The
fields like corn, rice,vegetable and so on are typical examples of the rough
surface.

It is also important to convert the count level of the MSS data into the
precise reflection ratio with the help of the observed ground truth data. But
it is well known that there are two main problems to be settled. One of them
is to apply the ground truth data measured under one condition to the remotely
sensed data observed under another different condition because we do not have
the sufficient knowledges of the correct relationship between the observational
conditions and the observed data. Another is to obtain the accurate and

reliable ground truth data. The space-borne or the air-borne MSS has a very narrow view field angle. And the altitude of their platforms is, of course, very high. On the other hand the view field angle of the spectro-photometer (or the detector) used for the ground truth observation in the real field is generally not small and we can not carry out the measurements from sufficiently high altitude. There are no problems as mentioned above when the ground reflection is governed by Lambert's law. But we are not able to accurately predict what are observed by the spectro-photometer if the ground has a rough surface. We have found all the ground truth data measured from the low altitude and with the large view field angle do not almost have good coincidence or correspondence to the actual MSS data.

To obtain a large amount of the ground truth data, it is necessarily natural and inevitable for many people to consume much time and much money. So it is desired to develop the reflectance model for economically and immidiately obtaining the accurate ground truth data of the paddy fields. Some reflection models for the canopy have been reported. W.A.Allen et al. (ref.2) applied the Kulba-Munk theory to the single layer canopy model in which the canopy is horizontally and vertically uniform, and demonstrated the agreement between the Kulba-Munk theory and experimental reflectance and transmittance data obtained from stacked mature cotton leaves. G.H.Suits et al. (ref.3) extended the single layer canopy model to the multi-layers canopy model. Taking account of the effects caused by the sun-lit and shaded soil, A.J.Richardson proposed the soil,plant and shadow model. There are two important difficulties in their models for obtaining the simulated ground truth data. One is that their models can not explain the important angular effect because only the radiance vertically coming up from the canopy is processed. Another is that the paddy fields can not be represented by their canopy model.

We propose a plant reflection model to give good solutions to these problems in this paper. The model allows us to obtain a series of the reflectance of the paddy fields as a function of the solar angles and the look angles of the detector, provided that we know a set of parameters necessary to demonstrate the circumstance of the actual field like reflection ratio of the leaves, one of the ground, the height of the rice plants and so on.

We will describe the outline and the configuration for the reflection model in the next section. Comparison of the results obtained by the model simulation with ones obtained by the ground truth observation, and their discussion will be described in the fourth section in this paper.

2. The reflection model for the paddy fields

2.1 Theoretical background for the reflection model

Rice plants in Japanese paddy fields are generally arranged in good order at constant spaces between themselves. So we locate stalks of rice plants at each of lattice points in paddy fields as shown in Fig.1(a). A stalk of rice plants is composed of ten to fifty leaves placed on Rmax concentric circles,each of which NLmax leaves are located on. It is desired that the configuration of a leaf is as simple as possible and can approximate the actual leaf very well. Considering that,a leaf consists of LUmax rectangular shaped leaves called "leaf-units" which are connected at the folds. Configuration of a leaf of rice plants is shown in Fig.1(b).

This model has such an advantage that we can easily create various situation of paddy fields by manipulating the parameters like length l_i ,width w ,numbers LUmax,inclination angle θ_i of leaf-units (i=1,2,...,LNmax) and so on. The sun shines upon the paddy field of this model and casts shadows of a leaf on the ground and/or on the other leaves. We here assume that the detector casts shadows on the ground and/or the other leaves as the sun does and we call them the virtual shadows by the detector.

By means of checking to see the sorts of the shadows on the ground and counting up the area of them,we are able to easily obtain the equivalent

894
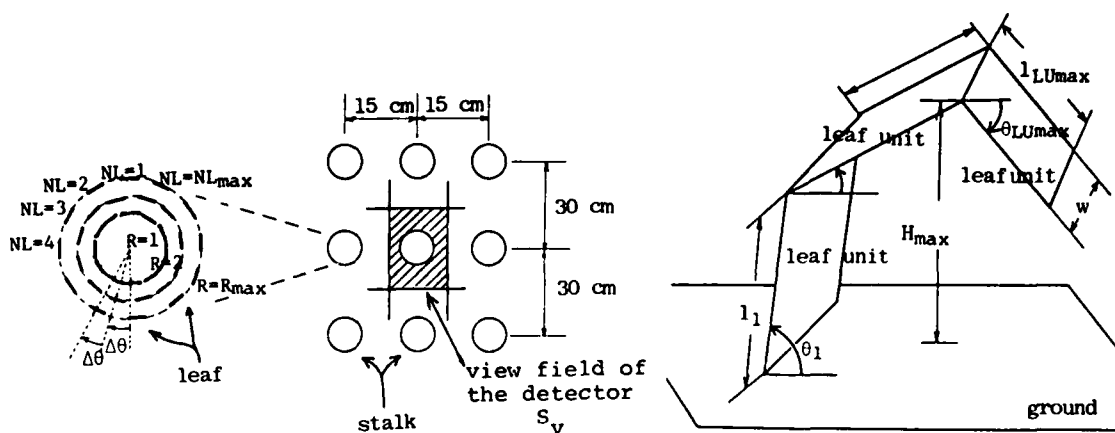
(a) Arrangement for stalks　　　　　(b) Configuration of a leaf

Fig.1　Outline for the paddy field model

reflection ratio as described later in detail. A spectro-photometer detects the radiation coming from the top (or the surface) and the bottom (or the underside) of the sun-lit leaves, the top and the bottom of the shaded ones, the sun-lit ground and the shaded one. Of course, the azimuth and the zenith angle of the sun and the azimuth and the look angle of the detector can be arbitrarily established to create the miscellaneous conditions under which the ground truth measurements are performed. It can be approximately assumed that the leaves and the ground themselves basically have Lambertian surfaces of iso-reflective characteristics.

When the solar incident angle and the detector's look angle onto a leaf are μ_{ls} and μ_{ld}, respectively, the radiation flux $\Delta\phi_l$ coming from the small area ΔS_l on a leaf which is mapped onto the small area ΔS_{gd} on the ground or the small virtual shadow of it by the detector is the followings;

$$\Delta\phi_l = F_l \cdot \Delta S_l \cdot (\frac{S_d}{l^2} \cos\mu_{ld}) \cdot \alpha_{l_0}$$

$$= F_l \cdot \frac{\Delta S_{gd}}{K} \cdot (\frac{S_d}{l^2} \cos\mu_{ld}) \cdot \alpha_{l_0} \tag{1}$$

and

$$F_l = \begin{cases} F_0 \cdot \cos\mu_{ls} & \text{for the top of the sun-lit leaves} \\ \gamma F_0 \cdot \cos\mu_{ls} & \text{for the bottom of the sun-lit leaves} \\ \delta F_0 & \text{for the top and the bottom} \\ & \text{of the shaded leaves} \end{cases} \tag{2}$$

where $F_l, S_d, l, \alpha_{l_0}$ and K mean the incident radiation flux per unit area on a leaf, the area of the detector's lens receiving the radiation, the distance between the detector and a leaf, the intrinsic albedo of the leaf and an area ratio of ΔS_l and ΔS_{gd}, respectively. F_0 in eq.(2) is the solar radiation flux per unit cross section perpendicular to the incident direction. δF_0 means the flux of the diffused and scattered radiation coming to an unit area on a shaded leaf or the shaded ground. γF_0 means the radiation flux penetrated through the sun-lit leaf per unit area. The aspects for these are shown in Fig.2.

The incident radiation flux $\Delta\phi_g$ coming from the small area ΔS_g on the ground is represented by

895

Fig.2 Real shadow and virtual shadow

$$\Delta\phi_g = F_g \cdot \Delta S_{gd} \cdot (\frac{S_d}{l^2} \cos\mu_{gd}) \cdot \alpha_{g_0} \tag{3}$$

and
$$F_g = \begin{cases} F_0 \cdot \cos\mu_{gs} & \text{for the sun-lit ground} \\ \delta \cdot F_0 & \text{for the shaded ground} \end{cases} \tag{4}$$

Total incident radiation flux ϕ_p reaching to the lens of the detector from the paddy field is obtained by accumulating $\Delta\phi_l$ and $\Delta\phi_g$ all over the view field S_v of the detector on the ground. That is

$$\phi_p = \sum_{\Delta S_{gd} \, \epsilon \, S_v} \Delta\phi_l + \sum_{\Delta S_{gs} \, \epsilon \, S_v} \Delta\phi_g \tag{5}$$

where F_g, μ_{gs}, μ_{gd} and α_{g_0} are the incident radiation flux per unit area on the ground, the zenith angle of the sun, the look angle of the detector and the intrinsic albedo of the ground, respectively.

On the other hand, the total flux ϕ_s coming from the standard white reflection board with albedo 1.0 horizontally placed on the ground is represented by

$$\phi_s = F_0 \cdot \cos\mu_{gs} \cdot S_v \cdot (\frac{S_d}{l^2} \cdot \cos\mu_{gd}) \tag{6}$$

From eqs.(5) and (6), the equivalent albedo α_{eq} of the paddy field is obtained by

$$\phi_{eq} = \frac{\phi_p}{\phi_s}$$

$$= (R_{lsunt} \cdot W_{lsunt} + R_{lsunb} \cdot W_{lsunb} + R_{lshdt} \cdot W_{lshdt} + R_{lshdb} \cdot W_{lshdb}$$

$$+ R_{gsun} \cdot W_{gsun} + R_{gshd} \cdot W_{gshd}) / (N \cdot \cos\mu_{gs} \cdot \cos\mu_{gd}) \tag{7}$$

where

$$R_{lsunt} = \alpha_{l_0}, \quad R_{lsunb} = \gamma \cdot \alpha_{l_0}, \quad R_{lshdt} = \delta \cdot \alpha_{l_0}, \quad R_{lshdb} = \delta \cdot \alpha_{l_0}, \tag{8}$$

$$R_{gsun} = \alpha_{g_0}, \quad R_{gshd} = \delta \cdot \alpha_{g_0}$$

896

and
$$W_{lsunt} = \sum_{lsunt} \cos\mu_{ls} \cdot \cos\mu_{ld} /k, \quad W_{lsunb} = \sum_{lsunb} \cos\mu_{ls} \cdot \cos\mu_{ld} /k,$$

$$W_{lshdt} = \sum_{lshdt} \cos\mu_{ls} \cdot \cos\mu_{ld} /k, \quad W_{lshdb} = \sum_{lshdb} \cos\mu_{ls} \cdot \cos\mu_{ld} /k,$$

$$W_{gsun} = \sum_{gsun} \cos\mu_{gs} \cdot \cos\mu_{gd}, \quad W_{gshd} = \sum_{gshd} \cos\mu_{gs} \cdot \cos\mu_{gd} \quad (9)$$

and where N in eq.(7) is the whole number of digitized small areas in the view field S_v.

W_l's and w_g's in eqs.(7) and (9) are the summed up weights contributing to the amount of radiation reaching at the detector in relation to the incident angle, look angle to the leaves or the ground. R_l's and R_g's in eq.(8) called radiance parameters are equivalent albedos for the leaves and the ground. And they vary with the incident flux to the leaves. The symbols beneath $\sum$ in eq.(9), lsunt for an example, means that we have to sum up augend terms over all ΔS_{gd} corresponding to the small area ΔS_l on a sun-lit leaf inside of the view field S_v of the detector. We can obtain the equivalent albedo α_{eq} of the paddy fields by eq.(7).

2.2 The simulation model

As we can understand from eqs.(7)-(9), we have to know the detailed informations about the real shadows and the virtual shadows in order to obtain the equivalent albedo α_{eq} of the paddy fields. We describe the concrete way to obtain the equivalent albedo α_{eq} by using the computer simulation technique as below.

The ground surface is quantumized by the small area dx x dy as already shown in Fig.2. Now consider that a quantumized small area ΔS_{gs} and ΔS_{gd} on the ground are a real shadow of a small area ΔS_l on a leaf and a virtual shadow of it, respectively. We need informations about the virtual shadow ΔS_{gd} which is cast on the ground by a small area ΔS_l on a leaf unit closest to the detector. They are coordinates (x_{ld}, y_{ld}, z_{ld}) of the small area ΔS_l, the leaf number LNO, the leaf unit number LUNO, the top-bottom flag TBF indicating whether the detector sees the top of a leaf or the bottom of it and the weight WT already described before. We call these seven data the virtual shadow informations. The informations about the real shadow ΔS_{gs} of a small area ΔS_l on a leaf unit closest to the sun are also required. In this case, they are only the leaf number LNO, the leaf unit number LUNO and altitude z_{ls} of the small area ΔS_l on a leaf. We call these three data the real shadow informations as before.

The informations are stored into the shadow information table SIT about with 65,000 cells and their cell size 10 words. Only when the virtual shadows are included in the view field S_v, the virtual shadow informations are obtained and stored in the last 7 words in a SIT cell. On the other hand, the real shadow informations are stored in the first three words in a SIT cell either when they are in S_v or when the virtual shadows corresponding to the real ones are contained in S_v even if the real ones are not in S_v. Pointer table PT is also prepared for administrating SIT. The cells of the SIT correspond to each small area ΔS_g on the ground, and PT stores the pointer indicating the address of a SIT cell which the shadow informations are stored in. Provided that a SIT cell to be stored in is already occupied by other shadow informations, old informations are replaced by new ones only when height information out of new ones is higher than old ones'. It means that informations concerning the leaf closest either to the detector or to the sun are stored in a cell.

By the way, it is sufficient and natural that we consider the rectangular area of 15 cm by 30 cm including only one stalk of rice plants at the central point as a view field of the detector Sv as shown in Fig.1 (a). The size of PT is determined to be the minimum rectangular area containing both the real shadows and the virtual shadows made by the view

897
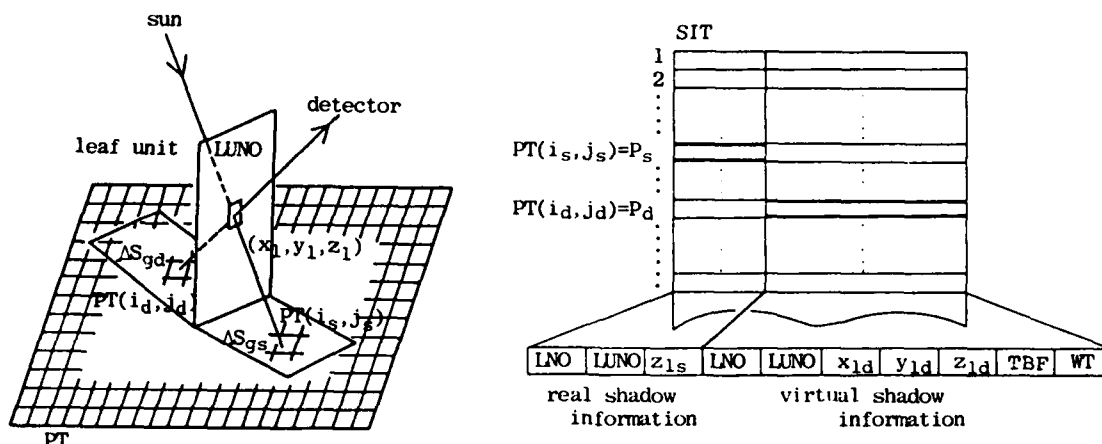
Fig.3 The relation between paddy field and PT and SIT

field at the maximum effective height H_{max} of the rice plants.

Now consider how to obtain the virtual shadow informations by using PT and SIT. We can retrieve the information about the small area ΔS_{ld} on a leaf,which is mapped to the small area ΔS_{gd} on the ground, from the SIT cell pointed to by PT corresponding to ΔS_{gd}.

We can make sure whether the small area ΔS_{ld} on a leaf is sun-lit or shaded by checking sequentially the coordinates of ΔS_{gd},PT,the ones of ΔS_{ld} stored in SIT pointed to by PT,ones of ΔS_{gs} computed by the azimuth and the zenith of the sun,PT and the altitude z_{ls} of ΔS_{ls} in SIT. We can conclude that ΔS_{ld} is sun-lit when z_{ld} is higher than z_{ls} and that ΔS_{ld} is shaded otherwise. We can also obtain the weights and the top-bottom flag of the ΔS_{ld} from the virtual shadow informations in SIT.

The small area ΔS_{g} is considered to be sun-lit ground when the contents in PT corresponding to ΔS_{g} is vacant. On the other hand,the small area ΔS_{g} is considered to be the shaded ground when only informations about the real shadows is included in a SIT cell pointed to by PT.

We can obtain six kinds of weights summed up all over the view field S_v of the detector as related in eq.(9). These are $W_{lsunt}, W_{lsunb}, W_{lshdt}, W_{lshdb}$ W_{gsun} and W_{gshd},respectively. We can compute the value of equivalent albedo α_{eq} by substituting these values and the six kinds of reflection ratios predefined and the other parameters N, μ_{sg}, μ_{dg} into eq.(7).

2.3 The results of the computer simulation

We have to decide the reflectance parameters defined by eq.(8) and the rice parameters demonstrating the aspects of a leaf or a stalk of rice plants preceding the execution of the model simulation. Reflectance parameters described in Tab.3 in section 3.2 were applied to our model. Rice plants parameters were decided by inspection of pictures taken during the ground truth observation on 30 of July and on 17 of Aug. and they are shown in Table 1. The angle parameters in respect to the azimuth and the zenith of the sun and the detector are also described in Tab.1 and they correspond to the parameters for the actual ground truth observation.

The reflectance of the paddy field was computed by our model for variable look angles. The simulation results are shown by the dotted line in Fig.4. These curves can be easily found to be uneven and not smooth. When the detector sees a leaf as illustrated in Fig.5,the effective area S^*_{lsunt} of

898

Table 1
Rice plants
parameters

Table 2 Angle parameters

	7/30	8/17
R_{max}	3	4
NR_{max}	10	12
LU_{max}	10	10
H_{max}	600 mm	800 mm

	7/30			8/17		
	9:30	11:30	14:00	10:00	12:00	14:00
μ_{gs}	58.0	73.0	59.0	55.0	67.0	55.0
ξ_{gs}	-26.0	-90.0	-153.0	-34.0	-90.0	-147.0
μ_{gd}	-	-	-	-	-	-
ξ_{gd}	23.0	23.0	23.0	23.0	23.0	23.0
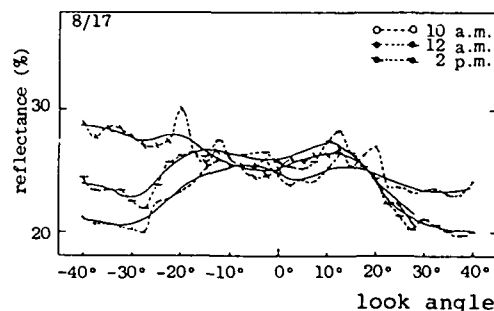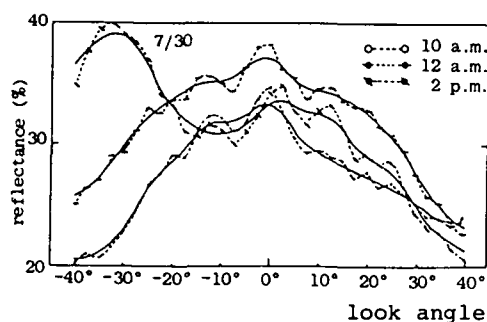
Fig.4 Reflectance of the paddy field for look angles

the top of the sun-lit leaf and the effective area S^{*}_{1sunb} of the bottom of the sun-lit leaf can be easily deduced as represented below.
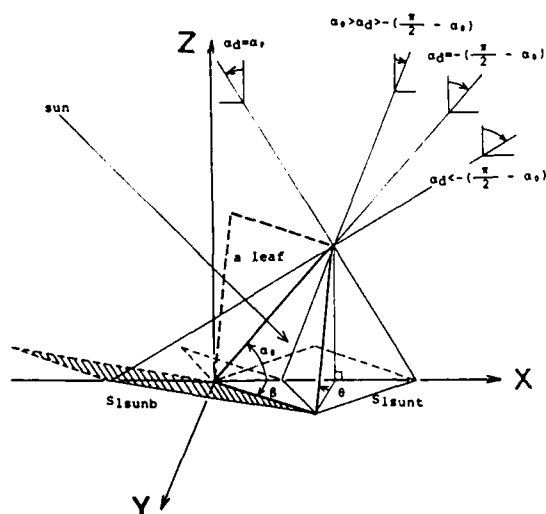
Fig.5 Illustration of leaf unit observation
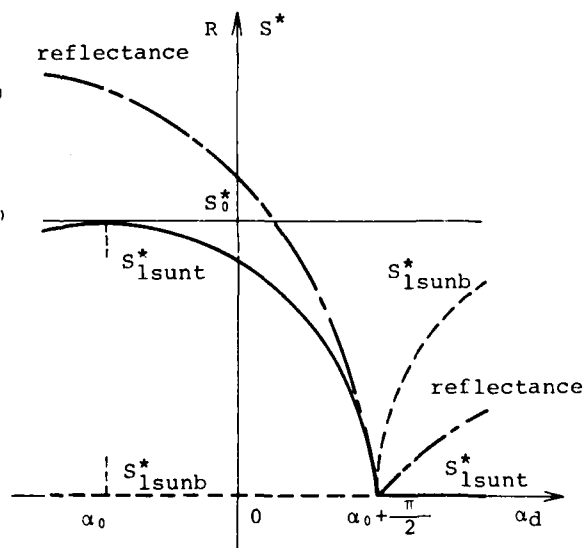
Fig.6 Leaf area and reflectance

899

$$S_{lsunt}^{*}=S_{lsunt}\cdot\cos\alpha_d=\begin{cases} S_0^{*}\cdot\cos(\alpha_d-\alpha_0) & : \alpha_0-\frac{\pi}{2}\geq\alpha_d\geq\alpha_0+\frac{\pi}{2} \\ 0 & :\text{otherwise} \end{cases}$$

$$S_{lsunb}^{*}=S_{lsunb}\cdot\cos\alpha_d=\begin{cases} -S_0^{*}\cdot\cos(\alpha_d-\alpha_0) & : \alpha_d<\alpha_0-\frac{\pi}{2}\text{ or }\alpha_0+\frac{\pi}{2}<\alpha_d \\ 0 & :\text{otherwise} \end{cases} \tag{10}$$

where S_0^{*} is the maximum effective area of the leaf unit when the detector sees it, and

$$\alpha_0=\tan^{-1}(\sin\beta\cdot\tan\theta) \tag{11}$$

S_{lsunt} and S_{lsunb} and total reflectance except the ground contribution are shown in Fig.6 when R_{lsunt} and R_{lsunb} described in the table 3 are used for the simulation. It may be considered that equivalent albedo α_{eq}'s of the paddy fields shown by the dotted line in Fig.4 are approximately summed up such characteristics with sharp discontinuities drawn in Fig.6. That is why α_{eq}'s are uneven and not smooth.

3 The ground truth observation

3.1 Outline of the ground truth observation

It is important to deal with rice plants cultivated in many paddy fields from the view of their significance and effects. That was why we chose the paddy fields for the ground truth. The observation for ground truth was performed at a paddy field nearby our colledge.

The rice plants called "KAGAHIKARI" very popular in our local region was chosen for the object of the ground truth. The matured seedlings were transplanted in the experimental fields at each of rectangular-lattice points with 15 cm by 30 cm in the middle of May. They ripened in the middle of Aug. and harvested in early September. Until the middle of July, the paddy fields were irrigated with river water and depth of water in the field was cyclically changed about from 1 to 10 cm with several days period.

It is desirable that the ground truth observation is carried out from the sufficiently high altitude from the view of accuracy. So a platform was
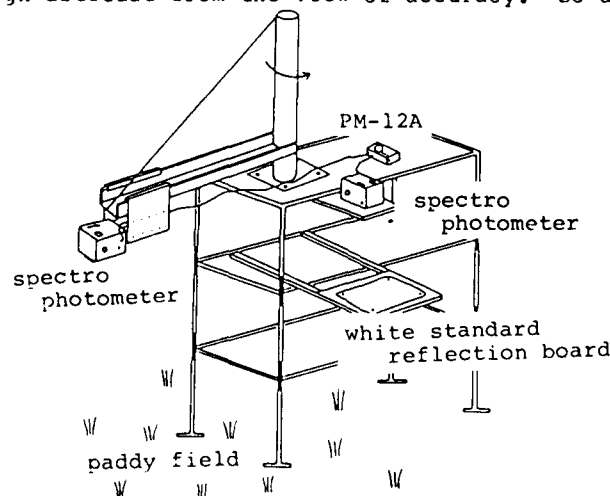
Fig.7 Schematic diagram of the platform
in the experimental paddy field

constructed in the experimental field by using some iron pipes for the building materials easy to obtain. The two spectro-photometers were attached on the top of the 5 meters high platform to observe both the rice plants and a white standard reflection board at the same time. A schematic diagram of the platform is shown in Fig.7.

The portable spectro-photometers called "PM-12A' made by KIMOTO Co. were used for our ground truth measurements. Each of spectro-photometers has two view field angles of 2 and 10 degrees,and we used the latter in our observation because 2 degrees view field angle is too narrow to cover the minimum paddy field unit area 30 cm by 15 cm. The spectro-photometers are equipped with 16 kinds of metal interference filters,their central wavelengths are 400,425,450, 475,500,525,550,575,600,625,650,675,700,750,850 and 1050 nm and their bandwidth are 10 nm. Ga,As,P photocell is used for a sensor in the visible region and Si photocell in the infrared region. The wavelength and the relative radiation flux of the observed data are digitized to three digits,respectively and printed out on a 8-digits printer that brings us the great convenience.

The reflection ratios were calculated at once from both the data of the standard reflection board and the data of the actual rice plants in order to make sure that there are no data handling mistakes. The ground truth observation was performed at intervals of one hour from 10 a.m to 2 p.m,in principle,once a week. The paddy field and the white standard reflection board were observed quite at the same time by two spectro-photometers as mentioned above. It is necessary and important to obtain the reliable data,so the incident radiation flux onto the ground should be nearly constant during a series of the measurements even in the synchronized measurements by using two spectro-photometers. The observation was performed only while a lux-meter was stably indicating about a constant value.

3.2 Observation results

We showed the data on 30 of July in Fig.8 (a) and the data on 17 of Aug. in Fig.8 (b) for some typical examples of angular effects. Their measurement wavelengths were 650 nm. The horizontal axis and vertical axis show the look angle of the detector in degree and the reflection ratio,respectively.

It is very important facts that the reflectance of the vegetation canopies is affected by the amount of shadow in them. It has been empirically found that the reflection ratio when apheliotropically (looking downsun) is most of
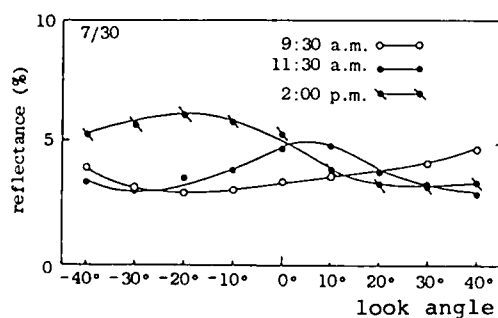
(a) The observational data
    on 30 of July
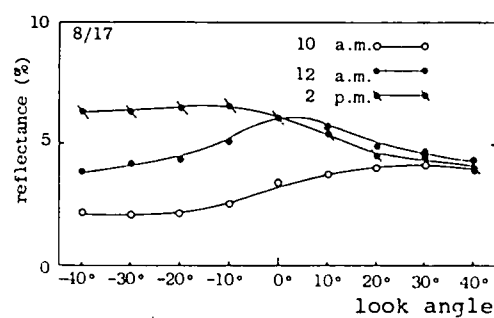
(b) The observational data
    on 17 of Aug.

Fig.8 An angular effects of the paddy field

901

vegetation canopies are observed greater than one when they are observed
heliotropicaly (looking upsun). We call this phenomenon the upsun-downsun
effect in this paper. In our observation of the paddy field,we can easily find
the upsun-downsun effect in all the measured data except ones at noon. The
upsun-downsun effect is clearly found especially in the data observed in the
afternoon because the detector points to the same direction as the sun. On the
other hand,the effect does not remarkably appear in the data measured at 10
a.m. because the angle between the detector and the sun is about 50 degrees.
   The reflectances both on 30 of July and on 17 of Aug. demonstrate the highest
value when the look angle is equal to 0 degree and decrease as the look angle
increases,because the angle between the sun and the detector is almost a right
angle.

Table 3 Reflectance parameters

	albedo		albedo		albedo
R_{lsunt}	0.220	R_{lshdt}	0.040	R_{gsun}	0.150
R_{lsunb}	0.075	R_{lshdb}	0.020	R_{gshd}	0.035

   In order to simulate the reflectance of the paddy fields by our model, we
require the reflectance of the ground or the soil and the leaves when they are
sun-lit or shaded. The soil in the experimental paddy fields was collected and
its reflectance was measured in our laboratory nearly under the same condition
as in the paddy field. On the other hand ,the reflectances of the leaves under
various conditions were occasionally observed in the actual paddy fields.
 Several trials were repeatedly performed to increase the accuracy of the
measurements. These results are shown in Table 3.

                            4. Discussion

   We already knew that the reflectance characteristics of one leaf-unit have
sharp discontinuity. That is why the reflectance curves obtained by our model
simulation were very uneven as illustrated by the dotted lines in Fig.4. We
can understand that the simulated results do not correspond to the measured
ones at a glance.
   The spectro-photometer used for the ground truth observation has a wide view
field angle like 10 degrees for an example,so the detector sees the object on
the ground within range of ±5 degrees to the set look angle. On the other
hand,it is assumed that the detector used for the simulation model has the same
very narrow view field angle as the MSS. This means that the simulated
reflectances $R_n(a_i)$ should be smoothed by a low path filter to compare with the
measured reflectances as below

$$R_w(\alpha_i) = \frac{c \cdot R_n(\alpha_{i-2}) + b \cdot R_n(\alpha_{i-1}) + a \cdot R_n(\alpha_i) + b \cdot R_n(\alpha_{i+1}) + c \cdot R_n(\alpha_{i+2})}{(a+2 \cdot b+2 \cdot c)} \qquad (12)$$

where R_n and R_w are reflectances by the detector with a narrow view field angle
and ones with a wide view field angle,respectively. A,b and c are 0.4940,
0.4245 and 0.1134 computed from relationship between the sampling look angles
and each area in the view field of the detector. A_i's show the i-th look angle
with intervals of 2.5 degrees. The simulated characteristics smoothed by in
eq.(12) are shown by the solid lines in Fig.4.
   The simulation results reasonably show characteristics as followings;

     1. the higher the solar azimuth is,the greater the reflectance is
        (12 a.m. data show the highest reflectance when the view angle is 0
        degree),

                                    902

2. upsun-downsun effect is very remarkably brought out when the detector and the sun are roughly in line (2 p.m. data) and
3. the results show the tendency of upsun-downsun effects even when the detector is neither in parallel with the sun nor orthogonal to each other (10 a.m. data at right hand in horizontal axis are higher than ones at left hand but 2 p.m. data are vice versa).

The similar characteristics can be found in the ground truth data except 10 a.m. data on 30 of July by the careful inspection of Fig.4 and Fig.8.

The simulation results suggest that the wavy dotted curves shown in Fig.4 are intrinsic characteristics and the amplitude of waves in wavy curves implies the accuracy limit for the MSS data or the ground truth data. The ground truth observation without the sufficient comprehension to the waving phenomenon will result in the meaningless data.

5 Conclusion

We proposed a new reflection model for the paddy fields where the ground truth data under different conditions can be immediately obtained by at low costs. This model has such an advantage that we can easily establish various aspects of the paddy fields by manipulating the rice plants parameters ,the reflectance parameters and the angle parameters.

The results told us the fact that the imagery distortion due to the angular effects caused by the rough surfaces is greater and more important than one by the other effects. The ground truth data do not have good coincidence with ones gathered by the MSS because each view field angles is generally quite different. We can not directly utilize the ground truth data for the correction of the angular effects caused by the rough surfaces. The simulation model allows us to obtain the ground truth data directly available for correcting the MSS data. The results also suggest that there is necessarily a intrinsic limitation in the accuracy of the actual MSS data or the ground truth data.

We give additional remarks that our reflection model is very useful for the researchs on the important effects caused by the rough surfaces and helpful for serious attempts to find the best way of observing the ground truth of the plants.

Reference

1) J.E.Colwell, "Vegetation Canopy Reflectance", Remote Sensing of environmental, pp.175-183 (1974)
2) W.A.Allen and A.J.Richardson, "Interaction of Light with a Plant Canopy", Jurnal of the Optical Society of America, pp.1023-1028 (1969)
3) G.H.Suits, "The Calculation of the Directional Reflectance of a Vegetation Canopy", Remote Sensing of Environment, pp.117-125 (1972)
4) A.J.Richardson,C.L.Wiegand,H.W.Galsman,J.A.Cuellar and A.H.Gerbermann, "Plant,Soil and Shadow Reflectance Comporments of Row Crops",Photogrammetric engineering and Remote Sensing, pp. 1401-1407 (1975)
5) M.Shikada,Y.Haba and K.Miyakita, "On the Observational Conditions for the Reflectance of the Plants", Proc.of 7th Symposium on the Remote Sensing, Society of Instrument and Control Engineers, 17 Nov., pp.109-112 (1981)
6) C.M.Tucker, "Spectra Estimation of Grass Canopy", Remote Sensing Environment 6, pp. 11-26 (1977)

THE USE OF LANDSAT DATA TO MONITOR THE URBAN GROWTH OF

SÃO PAULO METROPOLITAN AREA*

M. Niero
C. Foresti

Instituto de Pesquisas Espaciais - INPE
Conselho Nacional de Desenvolvimento Científico e Tecnológico - CNPq
Caixa Postal 515, 12200 - São José dos Campos, SP, Brasil

M.A. Lombardo

Universidade de São Paulo - USP
Caixa Postal 8105, 01000 - São Paulo, SP, Brasil

ABSTRACT

>The urban growth monitoring of São Paulo Metropolitan region has been done by conventional techniques which involve a high cost sistematic control. On the other hand, the orbital remote sensing allows a continuous land use control at lower cost.

For being under governmental control the region located between Billings and Guarapiranga reservoirs was chosen as test site for monitoring urban growth through LANDSAT data.

Mapping the urban growth over the period from 1977 to 1979 and identifying the problematic urban areas with several LANDSAT products constitute the basic aims of this work.

Visual and automatic interpretation techniques were applied to the data. Computer compatible tapes (CCT) of LANDSAT multispectral scanner data were analyzed through the Maximum Likelihood Gaussian algorithm. The results pointed out the feasible monitoring of fast urban growth by remote sensing techniques leading to an efficient urban planning and control.

1. INTRODUCTION

The urban growth monitoring of São Paulo Metropolitan region has been done by conventional techniques which involve a high cost due to the need of a sistematic control. On the other hand the orbital remote sensing leads to a continuous land use control at lower cost.

By selecting as test area the south region of São Paulo Metropolitan area located between the Billings and Guarapiranga reservoirs (Figure 1), one aimed at some specific goals in this study stated as follows:

- to analyse the performance of several LANDSAT products (MSS, RBV and CCT) for monitoring urban growth;
- to derive the spectral response in the rural-urban fringe;
- to map and evaluate the urban growth over the period from 1977 to 1979;
- to identify the problematic areas where a very careful governmental control becomes necessary.

The choice of the study region was based upon several reasons like:

- it presents high rates of urban growth;
- it is already under a governmental control by a specific law called "fountainhead protection act";
- it is bounded by water bodies which are useful as control points for comparison of data obtained from different dates.

2. MATERIAL AND METHOD

2.1 TEST AREA

The test area corresponds to the south of São Paulo Metropolitan area. It is located between the Billings and Guarapiranga reservoirs and extends from the junction of Grande and Guarapiranga rivers to the parallel $25°49'S$.

According to Emplasa (1980) the fastest growth of São Paulo Metropolitan area from 1974 to 1977 was verified in the south area. This area presented 21,65 km^2 of expansion during this period which represented about 45% of the growth in the Metropolitan area. The high rates of urban increase are due to the development of a very attractive industrial concentration. Another reason for this fast growth comes from the influences of its neighbourhood which is also industrialized. In addition, this area does not present any restriction to the urbanization concerning to its physical characteristics.

2.2 MATERIAL

The work was developed using LANDSAT products (row path annotation 164/28) as described in Table I.

Computer compatible tapes were analyzed using Image 100 described on General Electric (1975).

In addition, land use of Great São Paulo at the scale of 1:50.000 (1977) and photo indice (1980) at scale 1:32.000 were also available to assist the analysis of the data.

2.3 METHOD

The development of the work implied the following steps:

2.3.1 VISUAL INTERPRETATION

In the visual interpretation of MSS imagery the urban area was separated from the surrondings using conventional criteria of photointerpretation such as grey level, texture and site aspects. The land use map available and the photo indice from 1980 were used to help the delimitation of rural-urban fringe.

The superposition of the overlays obtained from visual interpretation for different periods permitted a better definition of urbanized area.

With the help of ground observation urban areas that presented difficult spectral separability were identified.

After including the built up area, growing urban area and urban allotment as urban area, it was calculated the total surface of these areas for the different periods of analysis.

2.3.2 AUTOMATIC INTERPRETATION

The automatic interpretation of LANDSAT data was carried out using a Maximum Likelihood algorithm (Velasco et alii, 1978). With the aid of land use map of São Paulo Metropolitan area, training areas were selected, on the display of the Image 100, for the following classes: built up area, urban allotment, dense vegetation, scattered vegetation and water bodies with

different amount of sediments. The samples of each class were selected
carefully so that they could be considered representative of the respective
land use classes.

The computer program "Cálculo de área" available at the library of the
Image-100/INPE was applied to calculate the area of each urban class.

2.3.3 URBAN GROWTH: A COMPARATIVE ANALYSIS

On the urban growth analysis, it was only considered the data obtained
from visual interpretation of MSS imageries.

The automatic analysis data were not taken into consideration since some
difficulties occurred in selecting representative samples of urban areas for
1977.

From the overlays superposition obtained by visual interpretation, it was
possible to identify the areas where a very careful governmental control is
required. The analysis of superposed data allowed the localization of the
largest urban growth areas.

3. RESULTS

3.1 VISUAL INTERPRETATION

With the MSS band 5, it was possible to identify the following classes:
built up area, growing urban area and urban allotment. It was considered as
growing urban area the partial or completely edified regions not agglutinated
to the continuous urban nucleus.

The visual interpretation comparison with previous data pointed out that
several horticulture regions were, in the past, uncorrectly classified as
urban areas. According to Wehrwein (1959) the rural-urban fringe can be
defined as the area of transition between well recognized urban land uses and
the area devoted to agriculture. In many cases the economic and sociological
city (the area within which people live the urban way of life) has extended
far beyond the city limits; in other cases farms on wich people live the rural
way of life are found within the political boundaries of cities.

Due to these aspects, the rural-urban fringe constitutes a very difficult
region to be delimitate.

To make easier the separability between urban area and horticulture
regions, it was tried the spectral analysis of the MSS band 7.

By analysing the data obtained from MSS bands 5 and 7, one can be resumed
the following results:

- the continuous urban areas presented large tonal and texture variations in
  both bands. The reason for that may be related to the co-existance of
  arbored and high demographic neighbourhoods as observed in the field check;
- the urban growth and horticulture areas appeared with similar tonalities in
  both channels. They showed light grey levels in channel 5 while large tonal
  variations were observed in channel 7;
- some horticulture area were showed with light grey levels in channels 5
  and 7 similar to the allotment areas response;
- since the horticulture area did not appear with a regular shape in channel
  5, it was very difficult to separate it from the urban areas. The main
  reason for this irregular behaviour of the analyzed horticulture regions
  comes from their small sizes;
- the localization itself was not so important in the identification of the
  urban and horticulture areas since both land uses are contiguous.

907

Therefore it was not possible to discriminate urban from horticulture areas only by conventional visual interpretation of LANDSAT imageries. So, a temporal analysis was performed through a map comparison from different dates. From the overlays superposition one could make the following conclusions:

- the correctly mapped urban areas showed an increase in area, during the period of 1977 to 1978, without any significant tonality modification, while the horticulture zones mapped as urban, displaied different tonalities and localizations. As a consequence, several light grey levels areas considered as urbans in 1977 did not present the same tonality in 1978;
- from 1978 to 1979, the horticulture areas appeared with different tonalities. However, the actual urban areas showed light grey levels for any analyzed period.

The grey level changes which occurred in the horticulture areas are due to active soil utilization. As implied by Filgueira (1972), the vegetable crop cycle is in general shorter than other cultivations, so the soil is constantly occupied.

The visual interpretation results from the MSS imagery for 1977, 1978 and 1979, are shown in the Figures 2, 3 and 4.

3.2 VISUAL INTERPRETATION OF RBV IMAGERY

The RBV imageries have spectral sensitivity from 0.505 to 0.750 μm and a spatial resolution of about 40 m. The use of RBV imagery did not improve the separation between urban areas and their neighbourhood when compared to MSS imagery (bands 5 and 7).

By the visual interpretation of the RBV imagery one could identify the following classes: built up area, growing urban area and allotment. The spectral signature of the urban area did coincide with that obtained from band 5 of MSS imageries. As occurred for the MSS band 5, some horticulture areas were also uncorrectly classified as urban.

The enlargement to the scale of 1:125.000 and the period of analyzed RBV imagery possibly made more difficult the precise urban class delimitation.

3.3 AUTOMATIC INTERPRETATION

The automatic classification of the data was performed using the Maximum Likelihood algorithm (MAXVER).

By the analysis of the sample matrices it was noted the superposition among the built up area and the allotment for every date analyzed. These classes showed higher spectral responses for the bands 4 and 5 when compared to the other classes.

The built up area presented medium values of grey levels while the allotment areas showed higher levels in channels 6 and 7. Class superposition occurred, therefore, in the visible wavelenght region. The reason for that comes from the fact that some allotment regions were already becoming urban areas.

However, the hard separability between built up area and allotment did not disturb the classification since the embankment and the scattered built up regions were considered as urban areas.

By comparing the results with existing maps it was found that the arbored urban areas were not classified as urbans. In the ground observation, it

908

could be noted that these regions typically present large arbored areas around sparsed residences.

Since some allotment areas were already occupied by scattered vegetation, these classes appeared overlapped in many cases.

Table II shows the obtained surface occupied by every analyzed class using the automatic interpretation.

For 1977, the allotment class was overestimated when compared to the following years as shown in Table II. This comes from the overlapping between the allotment class, the built up areas, scattered vegetation and horticulture areas for 1977.

The data for 1977 corresponde to a dry season period where a very weak spectral differentiation occurs between scattered vegetation and either bare soil or partially built up areas. At this time of the year the biomass is relatively small and so the vegetation spectral response will be modified by the reduced amount of chlorophyll. The class scattered vegetation from 1977 was classified as allotment in 1978.

By comparing the results with the available data, one can conclude that the classification obtained for 1978 is more accurate. (Figure 5).

This can be explained by the rainy period of the imagery which is followed by a strong contrast between vegetation and urban area.

The recreation areas and parks in the building urban area were classified as scattered vegetation. So the built up area was underestimated.

In the 1979 classification, the urban area increased of 12,41 km² when compared to 1978 (Table II). For that period regions close to Guarapiranga reservoir were uncorrectly classified as urbans. In the dry period, as the one analyzed, there is a lowering of the reservoir levels leading to an uncorrect classification of the borders.

3.4 URBAN GROWTH: A COMPARATIVE ANALYSIS

Based upon the urban area data obtained for the different periods, an urban growth analysis was performed in the study region.

By analyzing the Figure 6 one can observe that the urban area presented an almost constant growth in the studied periodes. Table III shows the relative growth of the analyzed urban area which indicates the major expansion rate in the period from 1977 to 1978.

One can also observe the urban growth rate became lower within the last period of analysis. In spite of this declining rate some problems occurred. The first of them is due to the fact that this region is situate at the reservoirs protection areas which are under governmental control. Another problem comes from the random urban growth leading to a chaotic neighbourhoods.

By comparing the Figures 2, 3 and 4 one verifies that the major change occurred close to the Parelheiros road and the Billings reservoir.

According to Emplasa (1980), Parelheiros showed the highest growing rate at the São Paulo Metropolitan Region with 16,28% per year from 1970 to 1979 justified by the industrial poles attraction.

The region close to the Billings reservoir and The Parelheiros road is occupied by the low income class residences with high built up density and

random growth as noticed in the ground observation.

4. CONCLUSIONS

The basic results of this work can be summarized in the following conclusions:

- in the urban growth study it is convenient to collect information on land use at the rural-urban fringe during the imagery selection procedure. This way, the data analysis becomes easier and more precise;
- the multidate approach allowed the discrimination between urban and horticulture areas;
- in the automatic analysis, the omission and commission errors occurred more frequently in the arbored urban and allotment areas respectively;
- the urban area analyzed growed at a rate of 28,7% during the period from 1977 to 1979. This demonstrates the needs of a sistematic land use control for this area by the governmental agencies.

5. REFERENCES

EMPRESA DE PLANEJAMENTO METROPOLITANO S.A. Projeto 4133 - Revisão da Legisla ção referente à Proteção aos Mananciais. Sub-Produto: 3.1. Relatório Pre liminar "Análise das Tendências de Expansão da Metrópole". São Paulo, out. 1980.

FILGUEIRA, F.A.R. *Manual de Olericultura*. São Paulo, "CERES", 1972. 451 p.

GENERAL ELECTRIC COMPANY. Image-100: Interative Multispectral Image Analysis System. User Manual. Daytona, 1975.

SÃO PAULO, SECRETARIA DE ESTADO DOS NEGÓCIOS DO INTERIOR. Divisão Administra tiva e Judiciária do Estado de São Paulo - 1980, São Paulo, 1980. Mapa na escala 1:500.000.

VELASCO, F.R.D.; PRADO, L.O.C.; SOUZA, R.C.M. *Sistema MAXVER*; Manual do Usuá rio. São José dos Campos, INPE, jul. 1978. (INPE-1315-NTI/110).

WEHRWEIN, G.S. The Rural-Urban Fringe. In: Readings in Urban Geography, Chicago, Mayer and Kohn, 1959. Section 16, p. 533-543.

Table I. LANDSAT products (MSS, RBV and CCT) utilized
          on the work

Product	Date	Scale
MSS image	02/24/77 04/05/78 07/04/79	1:250.000 1:250.000 1:250.000
RBV image	08/04/79	1:125.000
CCT	09/10/77 04/05/78 07/08/79	

Table II. Total area (km^2) of analyzed class obtained by automatic
           interpretation for 1977, 1978 and 1979

Class	Area (km^2)		
	1977	1978	1979
Built up area	29.01	32.83	45.24
Urban allotment	40.11	3.74	3.09
Dense vegetation	26.62	29.23	39.31
Scattered vegetation	37.52	64.43	52.49
Guarapiranga reservoir	19.02	21.64	15.27
Billings reservoir	24.44	26.27	22.83

Table III. Analysis of the urban growth for 1977, 1978 and 1979

Period	Total of Urban Area (km^2)	Urban growth (km^2)	Growth rate (%)
1977	30.68	-	-
1978	35.50	4.82	15.70
1979	39.50	4.00	11.20
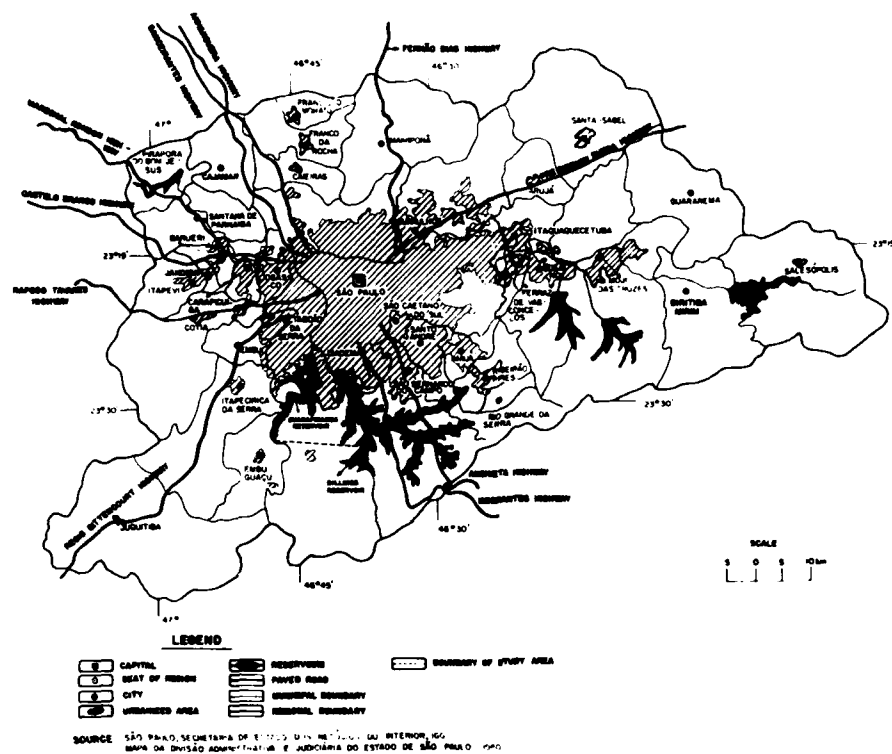
Figure 1. Localization of the Study Area.
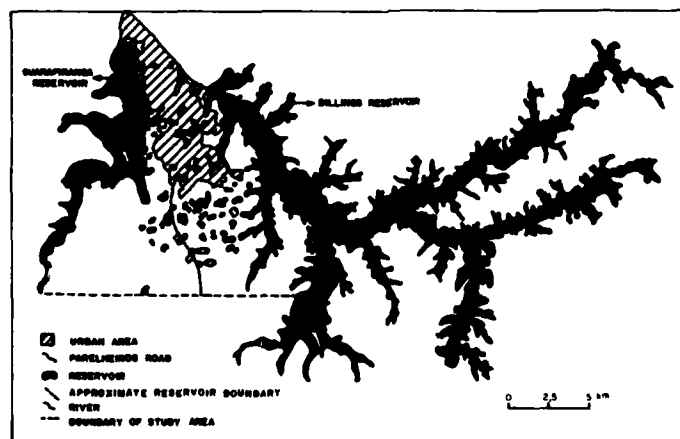
Figure 2. Urban Area Obtained from 1977 MSS Data (visual interpretation).
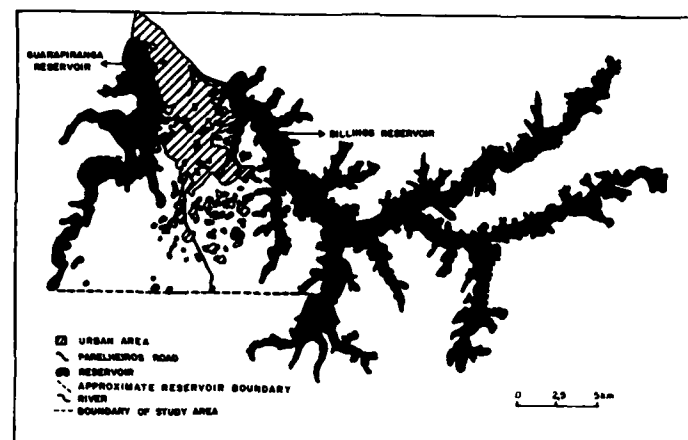
Figure 3. Urban Area Obtained from 1978 MSS Data (visual interpretation).
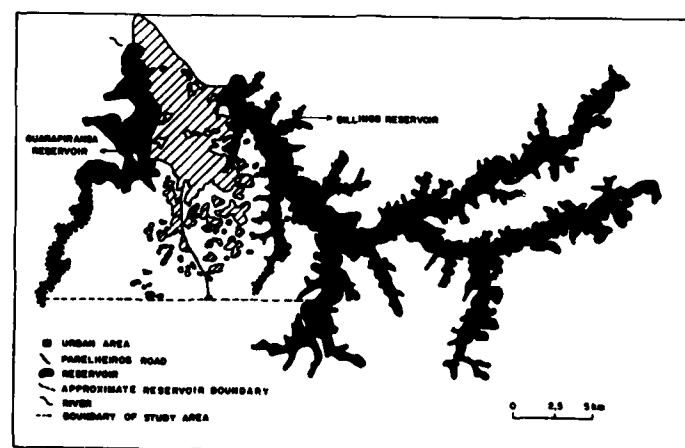
Figure 4. Urban Area Obtained from 1979 MSS Data (visual interpretation).

913
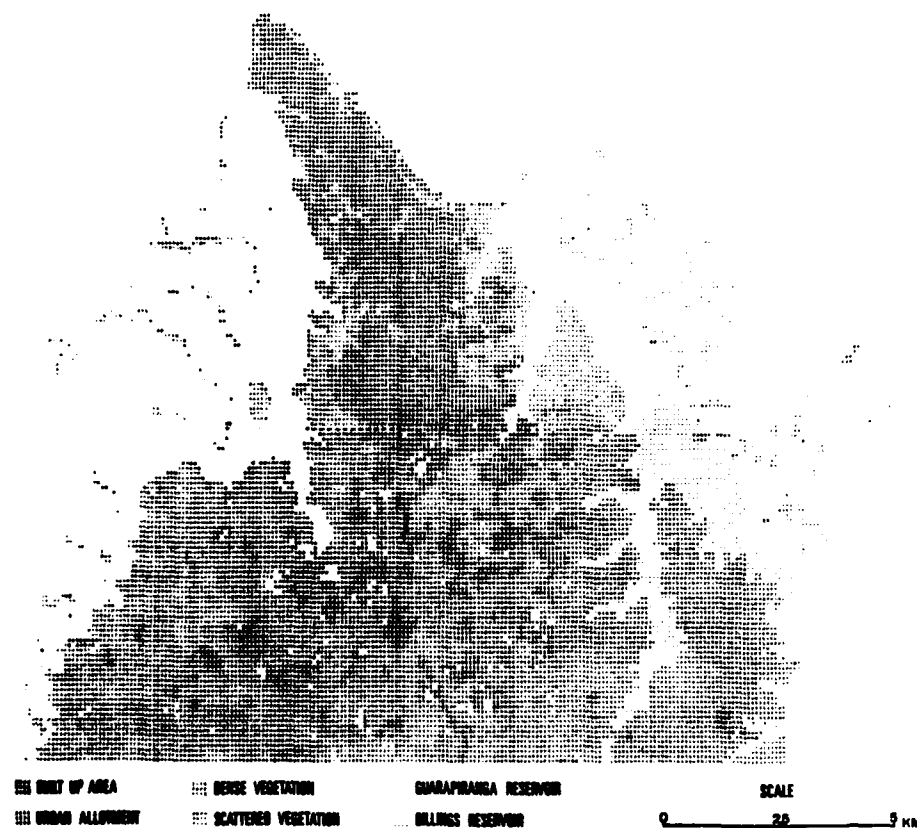
Figure 5. Urban Area Obtained from 1978 MSS Data (automatic interpretation).
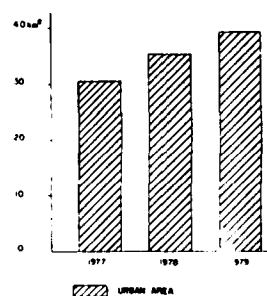
Figure 6. Total Urban Area Obtained from MSS Data
(visual interpretation).

914

MULTITEMPORAL AND GEOBOTANICAL APPROACH IN THE REMOTE DETECTION OF GREISENIZATION AREAS IN THE SERRA DA PEDRA BRANCA GRANITE, GOIÁS STATE, BRAZIL

R. Almeida Filho

Instituto de Pesquisas Espaciais - INPE
Conselho Nacional de Desenvolvimento Científico e Tecnológico - CNPq
C.P. 515 - São José dos Campos - SP - Brazil

ABSTRACT

A multitemporal (multiseasonal) analysis of LANDSAT multispectral images in CCT format permitted the mapping of lithologic facies in the Pedra Branca Granite, using geobotanical associations, which occur in the form of variations in the density of the "cerrado" vegetation, as well as the predominance of certain distinct vegetation species. Dry season images did not show very good results in lithological differentiation due to anomalous illumination conditions related to the low solar elevation and the homogeneity in the vegetation cover, specially the grass that becomes dry during this season. Rainy season images, on the other hand, allowed the separation of the lithological types, a fact that can be attributed to a greater differentiation among the geobotanical associations. As a result of this study, the muscovite-granite facies with greisenization zones within the Serra da Pedra Branca were mapped. This methodology can be sucessfully applied to similar known granite bodies elsewhere in the Tin Province of Goiás.

1. INTRODUCTION

The goal of this work was to test the applicability of LANDSAT multispectral imagery on discrimination of geobotanical associations observed in zones of cassiterite (Tin-bearing ore) rich metasomatic alteration in the granitic body of Serra da Pedra Branca.

The Serra da Pedra Branca Granite is located approximately 400 km north of Brasília, in Central Brazil (Figure 1). The area is dominated by a semi-humid climate with a rainy season (October to April) characterized by an average precipitation of 1500 mm, and a winter dry season (May to September). The mean annual temperature is around 25°C.

The native vegetation is the Savanna ("Cerrado") characterized by sparse small trees with twisted trunks and branches, some shrubs and a continuous grass mat covering the soil. The grass is very sensitive to the soil water content and becomes dry in prolonged dry spell, or luxuriant soon after the first rain.

2. GENERAL CHARACTERISTICS OF THE PEDRA BRANCA GRANITE

2.1 GEOLOGY

The Serra da Pedra Branca Granite is a dome, 12 km long by 9 km wide; with a relief of around 400 meters. The granite is surrounded by gneisses and migmatites of the undivided basement, probably of archean age, and by metasedimentary and metavolcanic rocks of Middle Proterozoic Arai Group. The contacts are generally by faults. Rb/Sr dating for the granite indicates

915

preliminary values around 1600 million years (Hasui et al.. 1981).

The geological characteristics of the granite have been described by Padilha & Laguna (1981) in some detail. The Pedra Branca dome is a biotite--granite varying from gray to rose, and from medium to coarse grained texture, but sometimes the granite is locally porphyritic. The granite body suffered intense post-magmatic transformation processes represented by several granitic facies varying from slightly greisenized (muscovite-granite) to typical greisens, strongly controlled by faults and fractures. These lithological types, derived from late differentiations, are light-colored and are cataclastically foliated, which gives them a gneissic appearance. The main region of greisenized muscovite-granite occurrence is located at the western portion of the body, in a basin like depression locally known as "Bacia", with dimensions of 4 km in the north-south direction, and 2 km wide (Figure 2). Typical greisen rocks (quartz-mica) occur at fracture displacement gaps, as lenses that can reach lengths of 100 meters or more. These metasomatic rocks are rich in cassiterite which constitute important deposits of tin.

The cataclastic processes affecting portions of the granite developed extense mylonite belts very similar in appearance to the true greisen zones, that was also affected by these processes, making it very difficult the visual distinction between greisens and mylonites in the field.

2.2 VEGETATION COVER

The occurrence of geobotanical associations adapted to different lithologies is very clear in the Pedra Branca Granite: they appear as variations in the vegetation density or because of the local predominance of some vegetation species best adapted to the soil characteristics. The "cerrado" is found in the more fertile soil derived from biotite-granites, whereas smaller vegetations and grasses are found in the less fertile soil derived from muscovite-granites (Figure 2). In areas where the metasomatic alteration processes were more intense, the soils are still less fertile and much more acid, allowing only the growth of grasses and of a few other very specialized plants such as "Canela-de-Ema" *(Vellozia flavicans)* and the "Barba-de-Bode" grass *(Aristida pallens)*, shown in Figure 3.

3. ANALYSIS OF LANDSAT IMAGES

Computer compatible magnetic tapes of multispectral imagery of the dry and rainy seasons (E-173177 of June 06, 1973 and E-175077 of March 18, 1975, respectivelly) were used in this study. These LANDSAT images covered the area of interest at a time immediately after the discovery of the cassiterite deposits, and were chosen so that later human activities around the deposits, such as the removal of vegetation cover, could be avoided.

These images were analyzed in a Multispectral Image Analyzer/Image-100 (GE, 1975) with a grey scale of 256 levels between zero (black) and 255 (white). The following steps have been used in this work:

A) Image Enlargement - LANDSAT images in computer compatible tapes for the dry and rainy seasons were analized at video scale of 1:75,000.

B) Corrections - the images were corrected for noise effects and atmospheric scattering.

C) Linear Contrast Stretch - Band 5 images of both dry and rainy season were contrast stretched.

D) Ratioing of Non-Correlated Spectral Bands - Ratioing of band 7 by band 5 of rainy season images with a gain of 30.0 and offset of 80.0.

916

Since most of the information contained in the spectral channels of the visible (Bands 4 and 5) and of the infrared (Bands 6 and 7) are redundant, only bands 5 (0.6 - 0.7 μm) and 7 (0.8 - 1.1 μm) were used.

The products obtained with the use of Contrast Stretch and Band-Ratio Techniques were analysed in conjunction with aerial photographies (at the 1:60.000 scale), topographic charts (at the 1:50,000 scale), light airplane reconnaissance and successive field checking during winter and summer seasons.

3.1 LINEAR CONTRAST STRETCH

The analysis started with Band 5 since the vegetation and bare soil show contrasting spectral behaviour at this interval. The first objective was to characterize areas with varying vegetation cover percentage, representing different geobotanical associations within the Pedra Branca Granite. In this channel the darkest areas (lowest gray levels) would represent regions with more dense vegetation cover, which would correspond to the biotite-granites, whereas the lightest areas (highest grey levels) would represent surface regions with greatest percentage of bare soil and sparse vegetation corresponding to the muscovite-granite zones. Thus, an attempt to increase the contrast between these two areas were made by using a Linear Contrast Stretch of Band 5 of both the dry and rainy season.

Figure 4 shows a contrast stretched enhancement of Band 5 for the dry season (winter) of Serra da Pedra Branca granite. The analysis of the product shows that the tonal variations observed in the enhanced image does not represent, in most of the cases, known regions where different soil-vegetation associations occur within the granite body. Therefore this contrast stretched product contains *little clear-cut geobotanical information.* Even the broad "Bacia" composed of greisenized muscovite-granite was not well defined by this enhanced product. The observed tonal variations are mainly caused by the particular illumination conditions affected by the relationship between topography and the low angle of sun elevation (30⁰). During this time of the year the topographic slopes facing the sun appear as light toned region due to the intense frontal solar irradiation. On the other hand, the other slopes facing away from the sun have dark areas because of topographic shadowing.

Besides the non-favorable conditions of illumination, a weak geobotanical differentiation of lithologies in winter images is attributable to the fact that all the grasses are dry at this time. The water deficient grass leaves do not contain the chlorophyll absorption band at 0.65 μm, which consequently makes less contrasting the different vegetation cover densities, otherwise responsible for the tonal variations observed in Band 5.

The image from the rainy season (summer) shows much better the vegetation cover differentiation, adapted to the biotite-granite and the greisenized muscovite-granite. Figure 5 shows the Pedra Branca Granite in a Band 5 image from the rainy season. It can be noticed at the western portion of the body a lighter area corresponding to the muscovite-granite that form the "Bacia" while the remain of the granite body appears in darker shades. This distinction of the "Bacia" is possible at the summer time because all forms of vegetation, including the grasses, are luxuriant in the zones of biotite-granite, at this time of the year, while in areas of the muscovite-granite the presence of water would not change substantially the vegetation cover, due to the acidity in these areas. At these areas the grasses are less developed and their associated "Canela-de-Ema" and "Barba-de-Bode" plants do not change with the season.

The high sun elevation angle observed in summer images (about 46⁰), is propitious to homogeneous illumination conditions for the whole granitic body, even though there remains a few shadow areas where the relief is accentuated.

917

3.2 BAND-RATIO TECHNIQUES

Band ratioing between non-correlated LANDSAT images are useful since they can show density variations within the vegetation covering the terrain (Raines et al., 1978). The ratio of band 7 by band 5 ($R_{7,5}$) is directly proportional to the vegetation density of the area: regions with more dense vegetation will appear in light shades in the $R_{7,5}$, whereas those with sparse vegetation will show up in darker tones. Furthermore, ratio images have the ability of condensing spectral information of two bands into a single product, which is less dependent on the illumination within the target of interest.

While the enhancement by contrast stretch of band 5 of the rainy season (Figure 5) was able to delineate with relative assurance only the areas of muscovite-granites of the "Bacia", the product of ratio $R_{7,5}$ of the same time indicated new areas of metasomatic alterations in the Pedra Branca Granite. These areas have been found to be within a grey level interval in the ratio images, that varies from 131 to 181. Figure 6 shows the areas enhanced by a "Level Slicer" (GE, 1975) of the $R_{7,5}$ product and inserted as a theme in Band 7 for better geographic localization within the granite body. The use of the standard Band 7 as a background is necessary since the ratio image cancels identifying morphologic features, by minimizing shadowing effects, which difficult visual identification of geographic reference. In figure 6 the area indicated by the number 1 corresponds to the muscovite-granite that form the "Bacia", partially shown in figure 2. The area marked by number 2 corresponds to new greisenized muscovite-granite geologically identical to the area of "Bacia". In the area marked by number 3, field work indicated the presence of metasomatically altered rocks, but with biotite-granite present at the botton of some valleys. At the high-lying land, however, these areas are covered by quartz pebbles and have a very sparse vegetation cover, very alike the vegetation of areas 1 and 2. The target areas indicated by number 4 correspond to mylonites which are very similar to the greisenized granites that have also been cataclasized, and so they are indistinct in appearance from the mylonites. The target 5 indicates colluvium deposits devoid of vegetation cover. The area shown by number 6 is also a colluvium deposit however in this case is rich in cassiterite originated from the weathering of rocks from the "Bacia".

4. CONCLUSIONS

Band-ratioing of non-correlated channels ($R_{7,5}$) of rainy season (summer) images permits to distinguish areas with different vegetation coverage percentage, which corresponds to geobotanical associations in metasomatic altered zones with cassiterite, in the Pedra Branca Granite. On the other hand, the linear contrast stretch of channel 5, specially of dry season (winter) image is very unsatisfactory for this area.

The results of this study show that LANDSAT-MSS images are very powerful tools and of great potentiality to complement and help the traditional mineral prospecting methods.

The utilization of LANDSAT images must be preceded by judicious analysis, that should consider the type of mineral deposit, its controlling factors, the physiographic characteristics of the region, the role of the ambi al variables, the time of the satellite passage and the use of several computer enhancement techniques.

REFERENCES

GENERAL ELECTRIC. Image-100; user manual. Florida, 1975, 119p.

HASUI, Y.; TASSINARI, C.C.G.; SIGA JR.,O; TEIXEIRA, W.; ALMEIDA, F.F.M.;
    KAWASHITA, K. Datações Rb-Sr e K-Ar do Centro-Norte do Brasil e seu signifi
    cado geológico-geotectônico. In: Congresso Brasileiro de Geologia, 31,
    Camboriu, 1980. Anais. Camboriu, SBG, 1980, V.5 p. 2659-2676.

PADILHA, J.L.; LAGUNA, A.M.G. Geologia dos granitos da Pedra Branca, Mocambo,
    Mangabeira e Serra do Mendes. In: Simpósio de Geologia do Centro-Oeste, 1,
    Goiânia, 1981. Atas. Goiânia, SBG, 1981, p. 622-641.

NASA. Earth Resources Technology Satellite; data user handbook. Greenbelt,
    MA, 1976.

RAINES, G.L.; OFFIELD, T.W.; SANTOS, E.S. Remote Sensing and Subsurface
    Definition of Facies and Structure Related to Uranium Deposits, Powder
    River Basin, Wyoming. Economic Geology 73(8): 1706-1723, 1978.

ROWAN, L.C.; WETLAUFER, P.H.; GOETZ, A.F.H.; BILLINGSLEY, F.C.; STEWART, J.H.
    Discrimination of rock types and detection of hydrothermally altered areas
    in South-Central Nevada by the use of computer-enhanced ERTS images.
    Geological Survey Professional Paper. Nº 883, 1976, 35p.
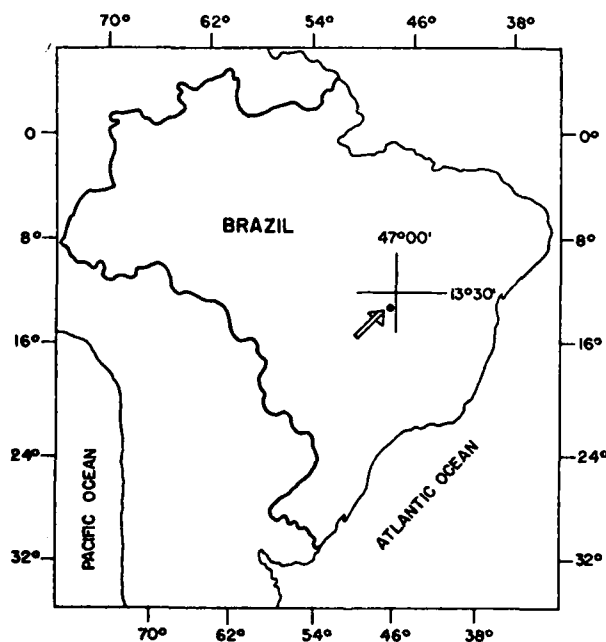
Figure 1. Geographic Localization of the Study Area.

Figure 2. General View of Part of the Top of the
Pedra Branca Granite, Showing the
Contrasting Vegetation Coverage Between
the Biotite-Granite Areas (B-G) and the
Muscovite-Granite (M-G) in the "Bacia"
Region.

Figure 3. Details of the Vegetation in Areas   of
Intense Metasomatic Alteration Characterized
by the Predominance of the "Canela-de-Ema"
and "Barba-de-Bode grass.

Figure 4. Linear Contrast Stretched Band of the Dry Season Image.

Figure 5. Linear Contrast Stretched Band of the Rainy Season.
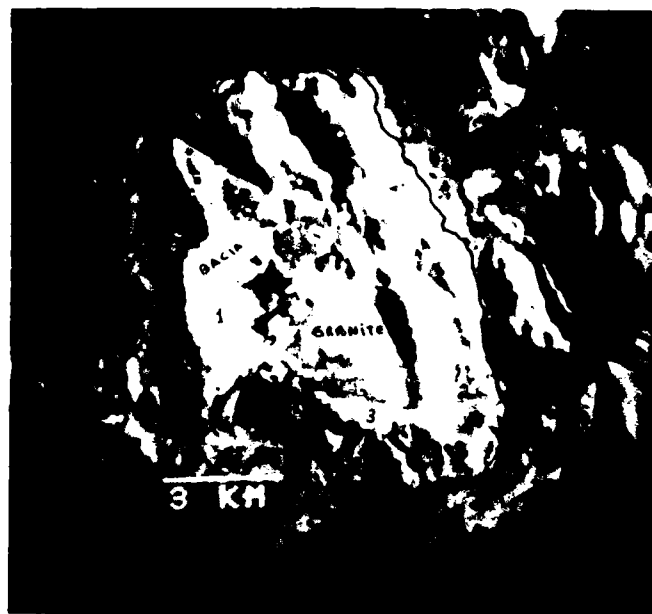
Figure 6. Geobotanical associations indicative of metasomatic and hydrothermal alteration areas within the Serra da Pedra Branca Granite, as shown by band-ratio ($R_{7,5}$). The numbers in the image correspond to target areas described in the text.

AD P002066

AN APPROACH TO OPTICAL AIR-TRUTH

Kei Muneyama & Yasunori Sasaki

Japan Marine Science and Technology Center
Yokosuka, Japan

Yoshiaki Takahashi

Asia Air Survey Co., Ltd.
Tokyo, Japan

ABSTRACT

Remote sensing data was measured over
Tokyo Bay on November 24, 1981, which was a
clear day. An aircraft with an MSS on board
was used to collect the data (at an altitude
of 4,000 m — about 12,000 feet). In addition,
air-truth data was acquired at the seashore,
on the sea's surface and at the altitude of
the aircraft in flight.

From these air-truth data, we evalu-
ated the spectral "path radiance" quantity
and rid the apparent remote sensing data
(MSS data) of atmospheric influences. This
means that the quantity of spectral radiance
at the sea's surface could be measured with-
out the use of data from various altitude,
vertical or sea's surface measurements.

1. INTRODUCTION

When evaluating areas or objects on the earth's surface such as the sea,
it is very important to consider and evaluate atmospheric influences on these
objects because every object has its own spectral character with minute
spectral differences and atmospheric influences can alter the appearance of
the character of the objects on the MSS.

When remote sensing water quality, it is especially important to rid
optical data of atmospheric influences by evaluating and correcting the remote
sensing data. One of the ways of getting rid of these atmospheric influences
was discussed in a previous paper (14th ERIM 1980).

In this report, another way is discussed — namely, using the parameters
of variable atmospheric extinction coefficients and direct-diffuse radiation
components of solar irradiance on the earth's surface. Upward radiance by
scattering in the atmosphere is discussed and the way to obtain the air-truth
parameter experimentally is described. Direct solar radiation and global
solar radiation were measured. From these data, spectral transparency of the
atmosphere and upward radiance (path radiance) were analyzed and the surface
radiance estimated.

These atmospheric parameters of air-truth, which were utilized for each measurement, changed with each measurement, but we were able to standardize all remote sensing data, under any optional condition such as optional altitudes or optional time under any atmospheric condition — except a cloudy condition.

2. CONCEPT

Optical characteristics of the atmosphere.

In general, the upward spectral radiance Ea(λ) from the earth's surface (sea or ground surface) is as follows:

$$Ea(\lambda) = Eo(\lambda) \cdot Tr(\lambda)^m + P(\lambda) \tag{1}$$

where

> Eo(λ): Spectral surface radiance
>
> Tr(λ): Spectral transparency per unit air mass
>
> m : Air mass (from surface to remote sensor)
>
> P(λ) : Additional spectral radiance (Path Radiance)

With formula (1), it has been very difficult in the past to evaluate Tr(λ) and P(λ) for each measurement because actual atmospheric optical conditions are unstable and changeable within short periods of time. For this reason, it seemed unreasonable to apply an average or typical optical parameter to actual remote sensing data.

As will be seen in this paper, we measured and evaluated these two important parameters of the actual atmosphere using MSS-acquired data. The spectral transparency Tr(λ) was obtained from the measurement of direct solar radiation. And the additional spectral radiance P(λ) was obtained by Böere's Method using extinction coefficients. With these parameters and apparent surface radiance Ea(λ) (measured by MSS), the surface radiance Eo(λ) could be estimated.

3. EXPERIMENT

The following instruments were used in experiments for "Air Truth".

1. In the sea surface stage:
   * Spectral upward and downward flux meter (4 channels)

2. In the seashore stage:
   * Spectral pyranometer (4 channels)
   * Spectral radiometer (400 to 1,100 nm)
   * Sun-photo meter (4 channels)

3. In the aircraft flight stage (with an MSS):
   * Spectral upward and downward flux meter (4 channels)

(The 4 channels of all instruments, except the sun-photo meter, have the same wavelength.)

All measurements were made when the sun was in the southern declination, and data was acquired under clear sky conditions.

To evaluate the data of the spectral output of all instruments, except the sun-photo meter, we calibrated the energy of light by using a standard radiant lump (Optronic labo. HTS 212 and 218).

4. THEORY

The following method was used to evalute the spectral transparency $Tr(\lambda)$ and the additional radiance $P(\lambda)$ (Path Radiance).

(1). Spectral transparency $Tr(\lambda)$

Solar irradiance $E(\lambda)$ on horizontal surface is written as follows:

$$E(\lambda) = Id(\lambda) \cdot Sin(h) + D(\lambda) \tag{2}$$

where

$Id(\lambda)$: Direct solar irradiance

$D(\lambda)$: Diffuse solar irradiance

h : Solar elevation

The relation between $E(\lambda)$, $Id(\lambda)$, air mass m and extinction coefficients $Km(\lambda)$, $Kr(\lambda)$ is as follows:

$$E(\lambda) = Id(\lambda) \cdot F(\lambda) \tag{3}$$

$$F(\lambda) = Sin(h) \cdot (1+0.63(Exp(Km(\lambda)\cdot m)-1)+0.5(Exp(Kr(\lambda)\cdot m)-1) +0.07(Exp(Km(\lambda)\cdot m-1))$$

where

$Km(\lambda)$: Mie's extinction coefficient

$Kr(\lambda)$: Rayleigh's extinction coefficient

$Kr(\lambda)$ and m are evaluated as follows:

$$Kr(\lambda) = (P/Po) \cdot (0.00838) \cdot (\lambda)^{-(3.916.0.074(\lambda)+0.050/(\lambda))}$$

λ : in μm

P : Actual pressure of the atmosphere at the sea's surface

Po : Standard pressure of the atmosphere

Total extinction coefficient $K(\lambda)$ is written as follows:

$$K(\lambda) = Kr(\lambda) + Km(\lambda) + Ko(\lambda)$$

where

$Ko(\lambda)$: Extinction coefficient of Ozon

From sun-photo meter measurements, $K(\lambda)$ is shown as follows:

$$K(\lambda) = (1/m) \cdot ln(Co(\lambda)/C(\lambda))$$

where

$Co(\lambda)$: Output value out of the atmosphere (calibration value)

$C(\lambda)$: Measured output value

925

$$m = 1/(Sin(h)+0.15(h+3.885)^{-1.253})$$

h : Solar elevation in degrees

$$h = Sin^{-1}(Sin(f) \cdot Sin(d)+Cos(f) \cdot Cos(d) \cdot Cos(t))$$

where

f : Latitude of observation point

d : Solar declination

t : Hour angle

Thus Mie's extinction coefficient is given, but about 4 channels. Using interporate method, we were able to get a value every 10 nm from a wavelength of 400 to 800 nm. This was based upon the condition that the relation between $Km(\lambda)$ and wavelength 400 to 800 nm was nearly linear.

In another method, $E(\lambda)$ was measured by a spectral pyranometer, but about 4 channels. Using spectral radiometer data from a white diffuse plate, we were able to evaluate the relative spectral value $R(\lambda)$ 400 to 800 nm. Using 4 channel $E(\lambda)$ and $R(\lambda)$, the spectral energy value was given 400 to 800 nm.

Using formula (3), direct radiation $Id(\lambda)$ is as follows:

$$Id(\lambda) = E(\lambda)/F(\lambda)$$

Finally, spectral transparency $Tr(\lambda)$ for unit air mass is as follows:

$$Tr(\lambda)^m = Id(\lambda)/Io(\lambda)$$

where

$Io(\lambda)$: Spectral irradiance in outside the atmosphere

(2). Additional radiance (Path Radiance) $P(\lambda)$

$P(\lambda)$ is shown in the following formula (proposed by Böere).

Upward radiant flux $U(\lambda)$ is given in:

$$U(\lambda) = Id(\lambda) \cdot (0.5(Exp(Kr(\lambda) \cdot dm)-1)+0.1(Exp(Km(\lambda) \cdot dm)-1))$$

where

dm : Air mass between earth's surface and flight altitude

$$dm = (P -P')/P$$

where

P : Surface pressure of the atmosphere during the operation

P': Flight altitude pressure of the atmosphere

And $P(\lambda)$ is shown in the following formula:

$$P(\lambda) = U(\lambda)/\Pi.$$

Finally, using $Tr(\lambda)$, $P(\lambda)$ and formula (1), surface radiance $Eo(\lambda)$ is shown in following formula:

$$Eo(\lambda) = (Ea(\lambda) - P(\lambda))/Tr(\lambda)^{dm}$$

926

5. EXPERIMENTAL RESULTS

o Extinction coefficients of actual atmospheric conditions during the operational time.

Figure (1) shows the Rayleigh extinction coefficient $Kr(\lambda)$ and the Mie extinction coefficient $Km(\lambda)$ as measured by sun-photo meter.

o Solar irradiance and direct-diffuse components at earth's surface during the operational time.

Figure (2) shows solar irradiance and its components measured by a spectral pyranometer and a spectral radiometer.

o Spectral transparency during the operational time.

Figure (3) shows atmospheric spectral transparency evaluated by means of analyzation.

o Additional radiance (Path Radiance) at the flight altitude during the operational time.

Figure (4) shows the spectral additional radiance at the flight altitude (4,000 m) estimated by analyzation.

And figure (5) shows the additional spectral radiance at the optional altitude using an actual optical parameters.

6. SUMMARY

From this study, it was found that atmospheric influences strongly depend upon direct solar irradiance, and this direct solar irradiance strongly depends upon atmospheric optical conditions such as extinction coefficients. A practical method was given for demonstrating this by using atmospheric optical parameter measurements.

It may be said that our experimental method of atmospheric correction of using the atmospheric parameter is one of the air-truth methods. However, we believe that the one proposed is very effective for estimating the radiance of the sea's surface experimentally.

Finally, the data of the spectral upward fluxmeter in the aircraft flight stage (with an MSS) and spectral upward fluxmeter in the sea surface stage were not sufficient for effective analyzation, because the influence of sun-glitter on the sea's surface was an unavoidable problem in the upward radiant flux. This problem needs to be studied in the future. As a consequence, data from the seashore stage was sufficient for analyzing this air-truth. And other data from the sea surface stage and the aircaraft flight stage were available and were used for effective data calibration.

7. ACKNOWLEDGEMENTS

This study was sponsored by The Science and Technology Agency of Japan.

8. REFERENCES

1. Muneyama, K. et al., 1980. Measurement of Spectral Upward Radiance at Several Altitudes over the Sea and Atmospheric Correction of the Radiance by Water Vapour Quantity. 14th ERIM.

2. A. Corrons and A. Pons, 1979. Solar Irradiance Measurements by Means of
   Optical Fibers and Silicon Detectors. Applied Optics Vol. 18, No. 16.

Extinction Coefficient
24 Nov. 1981   11:15

Fig 1

Fig 2

Fig 3

928

24 NOV 1981   Path Radiance   Alt 4000 m   11:15

Fig 4

Atmospheric Condition
80 Oct 3 12:15   Apparent Sea's Surface Radiance
at the optional altitudes

3000 M
2500 M
2000 M
1500 M
1000 M
500 M
0 M

Fig 5

929
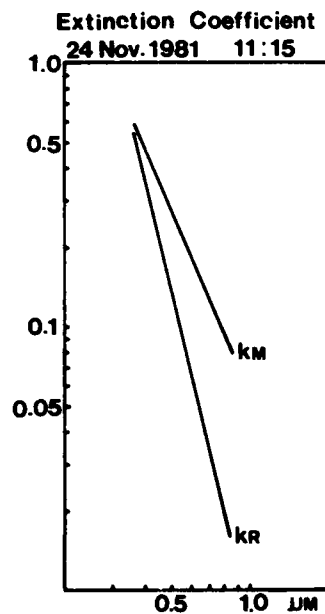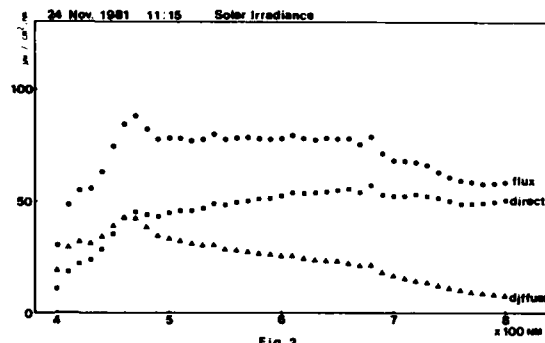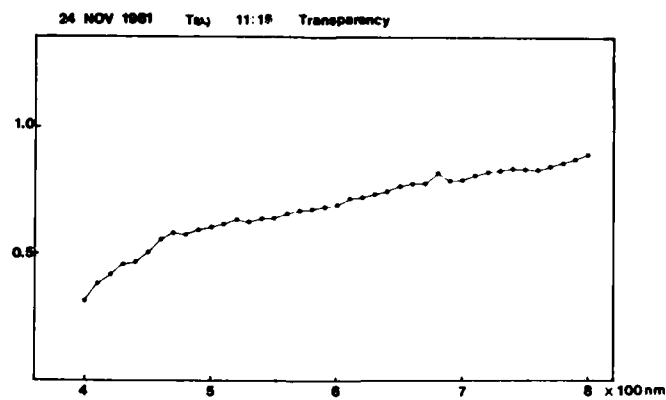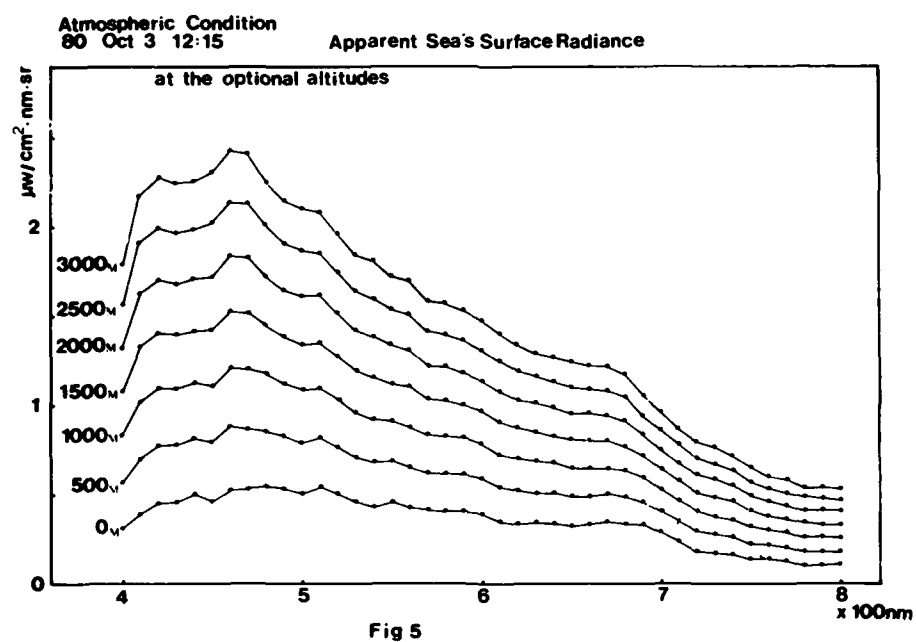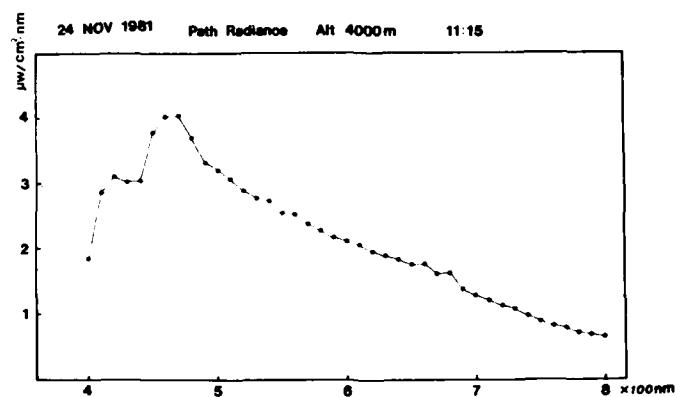
ANALYSIS OF LANDSAT DATA USING THE

INTERACTIVE IMAGE PROCESSING SYSTEM DEVELOPED BY CNIE

Serverino Fernandez
Marcelo Campi

Comision Nacional De Investigaciones Espaciales
Buenos Aires, Argentina

SUMMARY

A digital image processing system has been developed at CNIE to satisfy internal needs and those of external users.

The system was developed on a PDP-11/34 computer with 80 kwords memory, two standard tape drives, one CRT, two 5 Mbyte disks and a 300 Mbyte disk used for image data storage.

The interactivity of the system is provided by a COMTAL VISION ONE/20 image display system connected to the PDP.

The philosophy followed to develop the software system was to provide a tool to users with no knowledge of data processing in the form of a very simple language to specify image and data processing operations as used in Landsat data analysis.

From the user's point of view each algorithm has a specific name and must be fed by the user with parameter values and image names.

Two modes of use exist: for the beginner, where the system asks for interactive input of parameters and image names, and for the experienced user, where several modules can be chained after each other allowing practically to define a sequence of algorithms to be applied to an image.

Application modules have been written to do multispectral supervised and non-supervised classification, interactive training set definition and archival, multidimensional statistics calculation and archival, image enhancement, geometric correction with ground control points and auxiliary image handling and display.

In the future new modules will be implemented oriented by user's needs and the development of new algorithms.

It has been proved that a user can be trained in a relatively short time.

Moreover, new application programs can be easily incorporated to the system allowing fast expansion of system capabilities and flexibility.

Further development is now being carried out to modify and install the system in a VAX-11/780 computer.

This new version will control the COMTAL and a RAMTEK display system, allowing two users to work simultaneously.

ADP002067

ACCURACY OF DIRECT MEASUREMENT OF MEAN SURFACE WATER VELOCITY
OF THE KUROSHIO USING MULTI-TEMPORAL NOAA-6 IMAGERIES*

Sotaro Tanaka
Toshiro Sugimura

Remote Sensing Technology Center of Japan
Uni-Roppongi Bldg., 7-15-17, Roppongi, Minato-ku, Tokyo 106 Japan

Tsukasa Nishimura

Science University of Tokyo
Noda-shi, Chiba-ken, Japan

Yuji Hatakeyama

Asia Air Survey Co., Ltd.
Atsugi-shi, Kanagawa-ken, Japan

ABSTRACT

This paper discusses a method of directly
measuring the mean surface velocity of the Kuroshio
Current using multi-temporal NOAA-6/AVHRR imageries
and investigating the accuracy of the measurements.
The data from Channel 4 of the NOAA-6/AVHRR show the
water temperature of the sea's surface; some special
features such as a vortex, the so called "Sea Mark", can
be clearly recognized along the line formed by the
meeting of different water masses. The NOAA-6 imageries
can be observed about every 12 hours; two successive
imageries can give us the drifting distance during that
period. If distance is divided by time, the result is
corresponding water velocity. The accuracy of current
velocity measurement was found to be 0.05 knots in
standard deviation. The velocity distribution map of
the entire sea zone around Japan's bow-shaped islands
was made by this means, namely, from time serial NOAA
imageries and was then compared with the most recently
published map of oceanic current by the Maritime Safety
Board of Japan.

1. INTRODUCTION

The method of measuring the direction and speed of oceanic currents
using the Geomagnetic Electrokinetograph (GEK) is most prevalent at the
present time[1]. Also, since the ARGOS Service started in 1979, a survey of
trajectories of the surface water masses of the ocean has become possible
using a drifting buoy[2]. However, though the accuracy of current measurement
by GEK is superior, a ship is needed for such a direct measurement of current
vector. In order to obtain instantaneous data in a broad oceanic area, many
ships are needed; but for financial reasons, it is difficult to carry out

the above instantaneous oceanic observation.

The method using a drifting buoy has merit in that the trajectories of the surface water masses can be tracked for a long term. However, with this method as with the GEK method, it is difficult to carry out simultaneous observation of a broad oceanic area.

In this paper, the authors try a new method using NOAA-6/AVHRR Ch.4 imageries to make a simultaneous observation of current vectors in a broad oceanic area, namely, the "Sea mark chase method using NOAA-6/AVHRR imageries". In the next chapter, they review the conventional methods for current measurement, and in the following one, describe the new technology.

2.   CONVENTIONAL METHODS FOR CURRENT MEASUREMENT

2.1 GEK (GEOMAGNETIC ELECTROKINETOGRAPH)

This instrument is one kind of current meter to measure the surface currents of a deep sea zone. This was completed by an American scientist, von Arx in 1950. The principle was completely different from that of any current meter that had been devised up to that time. In sea water moving in the magnetic field of the earth, an electric current is induced in proportion to the current speed. Thus, an electric current is always flowing in sea water. Current speed of sea water can be obtained by measuring the electric potential difference.

Supposing a current speed is v (cm/sec), in the normal direction of the line connecting points A and B, the distance between the two points is 1 (cm), and a vertical component of geomagnetic force is Hz (gauss), then the following electromotive force is induced between A and B.

$$E = Hz \cdot 1 \cdot v \times 10^{-8}$$

Because the value of Hz can be known for a designated area, (ex. 0.2-0.4 off Japan), current velocity v can be computed by measuring the value of E under a known value 1. In case the current direction is not normal to the line connecting two points, the measurement value v can be considered as the normal component of the current velocity.

In general, 60 meters are taken as the value 1 from the allowable length range $40\ m \leq 1 \leq 100\ m$. The longer the distance between two electrodes becomes, the bigger the electric potential difference between them grows. Therefore, the sensitivity of measurement increases with 1, but because of the difficulty of handling and the allowable stress of the wire, it is suitable to take a ratio, 1 mV/knot.

2.2 ARGOS PLATFORM LOCATION SYSTEM

The ARGOS Data Collection and Location System (DCS) provides a means for locating and/or data collecting from fixed free floating buoy and balloon platforms. The ARGOS receiving system is carried by the TIROS-N satellite and by each of its seven operational satellites (designated NOAA-A to G). The quasi-polar orbit provides world coverage with operational service taking place from 1978 until at least 1985.

Principle of platform location: The location information is determined by measuring the platform carrier frequency received by the DCS instrument in the spacecraft at each transmission. When several transmissions are obtained from a platform, different Doppler techniques of computation allow the platform position to be determined.

Errors associated with platform location: The main sources of error

934

regarding platform location are:

- the accuracy with which the platform altitude is known. This is relatively unimportant in the case of drifting buoys, but may be very important in the case of balloons;
- the stability of the PTT (Platform Transmitter Terminal) oscillator, in particular the drift in transmitting frequency during a satellite pass (lasting approximately 10 minutes);
- the availability of information concerning platform speed and variation therein. The speed must be less than 100 m/s and is assumed to be constant between successive satellite passes.

Table I shows the performance of the ARGOS Platform Location System. Figure 1 illustrates a configuration of the drifting buoy of the ARGOS system used for the Kuroshio tracking.[3] A drogue hangs from the buoy by chain. The drogue has a size of 6.5×2.5 meters, therefore the buoy drifts with the movement of sea water at the depth of 4 to 10 meters below the sea's surface. Figure 2 shows an example of the Kuroshio tracking obtained by the

Table I. Performance of ARGOS System

Performance data for 99% of cases	Drifting buoys	Drifting balloons
Location accuracy	3 km	5 km
Accuracy of speed determination	0.5 km	1.5 km

ARGOS system from the western sea area of the Okinawan Islands to the eastern sea area of the Izu and Ogasawara Islands, carried out by the Maritime Safety Board of Japan. For example, a mean velocity of the Kuroshio offshore Shikoku Island can be estimated to be about 1.4 knots from the drifting of Buoy VII from 20th of February to 1st of March.

3. SEA MARK CHASE METHOD ON NOAA-6/AVHRR IMAGERIES FOR CURRENT MEASUREMENT

The "Sea mark" chase method using time serial NOAA-6/AVHRR imageries is a new method to measure ocean current proposed in this paper. With this method (as shown in Figure 4), current velocity can be obtained by comparing two time serial scenes and measuring the drifting distance of the corresponding sea mark.

"Sea mark" means the special point pattern on the sea's surface which can be clearly identified in both scenes. For example, the central point of an oceanic eddy, or the sharp corner of a sea current boundary can be considered as a kind of sea mark. Another kind of sea mark is a front line, that is, a curved boundary of different waters.

Movements of these sea marks show where the current has drifted to. However, in the case of a front line, it is difficult to measure the ocean current in a vector form, because there may occur a parallel current in which a component of the current moves along the front line.

The method to obtain the current vector can be explained as follows. Figure 4a and 4b show the AVHRR imageries taken by NOAA-6 in the morning (at 8:14) and in the evening (at 19:31) on April 23, 1981, respectively from the orbit shown in Figure 3. Therefore, there is a time difference of 11 hours and 17 minutes between these scenes. Both scenes have been orientated rigorously on the earth coordinate system by the method described in a later chapter. Because of temperature differences between the Kuroshio and its environmental waters, clear fronts can be identified on the imageries. Furthermore, oceanic eddies, probably generated on the shallow sea bottom due south of Tanegashima Island, can be recognized as A to E.

Since water drifts as a mass keeping its configuration, tracking the corners of fronts or the centers of eddies identified as above gives a current vector.

935

Figure 4c and 4d show the plotted positions of the fronts or the eddy centers identified in Figure 4a and 4b. Symbols P to U show the front lines, and A to E show the eddy centers. Also, symbols F to K show the ridges of fronts.

In Figure 4e, Figure 4c and 4d are composed on the same plane. Shifted distances of eddy centers A to E show the velocity by each. Also, relative positions of corresponding fronts can be useful for the estimation of current velocity. Shifted distances of front ridges F to K, show the current velocity as well as shifted distances of eddy centers.

Drifted vectors measured at the eddy centers A to E, and at the ridges of fronts F to K are shown in Table II. Listed values show the components of drifted vectors and current velocities, applying time differences. Components of drifted vectors were measured on TV monitor directly using a cursor for positioning. Directions of vector components dx and dy, were chosen — eastward and northward —on the earth coordinate system respectively.

Table II. Current Velocities from Sea Marks (Cf. Figure 4)

	dx	dy	knots
A	26	8	1.30
B	20	18	1.23
C	30	32	2.09
D	26	44	2.44
E	18	38	2.01
F	16	60	2.97
G	6	24	1.13
H	2	2	0.13
I	-6	4	0.34
J	-4	6	0.34
K	-10	12	0.74

4. ACCURACY OF ORIENTATION OF NOAA-6/AVHRR IMAGE USING GCP

As described in the previous chapter, current velocity can be obtained using time serial imageries taken by NOAA-6/AVHRR. A basic item for this object is rigorous orientation of NOAA-6/AVHRR imagery. We can consider two methods, i.e., a method using orbital parameters, and another method using ground control points (GCP).

In this paper, the latter method by which a wide range imagery of about 3000 km × 2000 km can be orientated in as high a precision as possible, was studied for following map projection.

Map projection : Oblique conformal secant conic projection
Applied map : 1:3,000,000 scaled map "Japan"

4.1 PROCEDURE OF NOAA-6/AVHRR IMAGE ORIENTATION

A procedure to orientate NOAA-6/AVHRR data against the earth coordinate system is as follows. First, a tangential transfomation image is obtained by applying Mapping 1 shown in Figure 5 to the raw AVHRR data. On this transformed image, ground control points (GCP) for NOAA image orientation which can be identified clearly, i.e., tip of cape, center of lake or island, or central point of river mouth, are chosen. Ground feature chosen for GCP should be kept at a suitable size, because the pixel size of NOAA-6/AVHRR image is fairly large, about 1 square km. As a special case for NOAA-6/ AVHRR image, the center of a city of suitable size can be chosen as a proper GCP.

Coordinate values (p',l') of the chosen GCP on a tangentially transformed image can be measured using a cursor on a TV monitor (in the authors' case, on that of Image-100). On the other hand, its corresponding geodetic coordinates (B,L) can be measured using digitizing equipment on a geographical map scaled 1:200,000.

Geodetic coordinates (B,L) can be transformed into the oblique equidistant cylindrical coordinates (x,y) by the following Mappings (Also,

936

refer to Figure 5.);

(1) Mapping 5 : Geodetic coordinates (B,L) to Spherical coordinates (ϕ,λ)
(2) Mapping 4 : Spherical coordinates (ϕ,λ) to Oblique spherical coordinates (z,α)
(3) Mapping 3 : Oblique spherical coordinates (z,α) to Oblique equidistant cylindrical coordinates (x,y).

NOAA-6/AVHRR raw image coordinates (p,l) can be transformed into oblique equidistant cylindrical coordinates (x,y) by the following Mappings in Figure 5;

(1) Mapping 1 : Raw image coordinates (p,l) to Tangentially corrected coordinates (p',l')
(2) Mapping 2 : Tangentially corrected coordinates (p',l') to Oblique equidistant cylindrical coordinates (x,y).

Among the above Mappings, the transformation coefficents for Mapping 1, 3, 4 and 5 can be led from the geometric conditions. Other coefficients for Mapping 2 are obtained from GCPs using the least square method.

Table III shows an example of GCP list including geodetic coordinates of GCPs and the residual errors of each GCP after the orientation in a unit 'pixel'. Standard deviations are p=0.7 pixels in the swaying direction, and l=0.8 pixels in the orbital direction, that is, about 800 m and 900 m respectively in terms of actual distance on the ground.

Table III. GCP List with Orientation Accuracy

No	Location	Longitude	Latitude	residual error (pixel)		No	Location	Longitude	Latitude	residual error (pixel)	
1	Shiriya-saki	41°25'37"	141°27'59"	-0.4	-0.6	16	Muroto-misaki	33°14'37"	134°10'47"	0.3	0.0
2	Nyudo-saki	40° 0'13"	139°42'16"	0.6	-0.4	17	Shiono-misaki	33°26'56"	135°46'41"	0.8	-0.3
3	Kinka-san	38°17'33"	141°34'22"	-0.4	0.1	18	Sakura-jima	31°35' 2"	130°39'33"	-0.7	0.3
4	Inawashiro-ko	37°28'34"	140° 5'59"	-1.0	-0.2	19	Kuchinoerabu-shima	30°26'35"	130°13' 8"	-0.4	-0.3
5	Sawazaki	37°49' 8"	138° 2'29"	0.9	0.9	20	Mi-shima	34°46' 5"	131° 8'33"	-1.0	-0.1
6	Kasumigaura	36° 5' 0"	140°13' 8"	-0.6	-0.3	21	Oro-shima	33°51'50"	130° 2'16"	0.0	-0.8
7	Choshi	35°42'33"	140°52'26"	-0.1	1.4	22	Chifuri-jima	36° 1' 2"	133° 1'20"	1.0	-0.3
8	O-shima	34°43'59"	139°24' 4"	-0.5	-0.4	23	Takara-shima	29° 8'35"	129°12'31"	-0.7	0.3
9	Miyake-jima	34° 5' 7"	139°31'45"	-0.7	-0.8	24	Pohang	36° 4'52"	129°33'23"	0.9	0.2
10	Omae-zaki	34°35'40"	138°14' 7"	0.7	-0.1	25	Ullung do	37°29'45"	130°52'37"	0.6	0.8
11	Suwa-ko	36° 2'45"	138°14' 7"	0.7	-0.1	26	Dunay	42°45' 8"	132°21'10"	0.5	1.6
12	Irago-misaki	34°34'30"	137° 1'11"	-0.4	1.6	27	Hsiao-hsing-kai hu	45°24' 8"	132°23'49"	-0.9	-1.0
13	Ashizuri-misaki	32°43'15"	133° 1'25"	1.2	-0.9	28	Yoron-jima	27° 2'32"	128°26' 8"	0.1	1.3
14	Iwai-shima	33°46'54"	131°58'40"	0.5	-0.8	29	Kasari-shima	28°31'38"	129°41'33"	0.4	-1.3
15	Toyo-shima	33°14'37"	134°10'47"	0.6	-0.5	30	Minamidaito-jima	25°50'33"	131°14'23"	-0.2	0.3

In general, the developed accuracy of the map is considered to be 0.2 mm regardless of the mapping scale. Therefore, because the developed accuracy for a 1:3,000,000 scaled map leads to 600 m in horizontal distance, the residual errors of Table III can be considered enough for NOAA-6/AVHRR image mapping at a scale of 1:3,000,000.

4.2 OUTPUT PROCEDURE OF NOAA-6/AVHRR IMAGE TO 1:3,000,000 SCALED MAP

The procedure to generate the output imagery of NOAA-6/AVHRR data orientated into the 1:3,000,000 scaled map, can be described as follows;

937

First, the geodetic coordinates (Bi,Li) (i=1~4) of four corners, namely, of four points A1 to A4 shown in Figure 6 are measured. These coordinates are transformed into NOAA map plane coordinates (Xi,Yi) (i=1~4) by means of the next procedure, where the authors call the final NOAA imagery (orientated to the oblique conformal secant conic projection map scaled 1:3,000,000) the "NOAA map".

(1) Mapping 5 : Ellipsoid coordinates (B,L) to Spherical coordinates (ϕ,λ)
(2) Mapping 4 : Spherical coordinates (ϕ,λ) to Oblique spherical coordinates (z,α)
(3) Mapping 6 : Oblique spherical coordinates (z,α) to Oblique conical coordinates (r,θ)
(4) Mapping 7 : Oblique conical coordinates (r,θ) to NOAA map plane coordinates (X,Y)

Next, film coordinates (I,J) are defined so that a corner A1, a vector A1A4 and a vector A1A2 will lead to the origin, X axis and Y axis respectively. In these film coordinates, an image output mask, i.e., a square $a_1\, a_2\, a_3\, a_4$ which consists of 50 output pixels divided from the origin by equidistance of 50 pixels, can be extracted. Where, the size of output pixel has been decided to be 1 km×1 km on the bow circle with a scale factor 1.0.

Four corners (p_i', l_i') (i=1~4) on the tangentially corrected coordinate system corresponding to the four corners of each film output mask a_i (i=1~4) can be computed through the following procedures;

(1) Inverse mapping 3 : Film coordinates (I, J) to NOAA map plane coordinates (X,Y)
(2) Inverse mapping 7 : NOAA map plane coordinates (X,Y) to Oblique conical coordinates (r,θ)
(3) Inverse mapping 6 : Oblique conical coordinates (r,θ) to Oblique spherical coordinates (z,α)
(4) Mapping 3 : Oblique spherical coordinates (z,α) to Oblique equidistant sylindrical coordinates (x,y)
(5) Inverse mapping 2 : Oblique equidistant sylindrical coordinates (x,y) to Tangentially corrected coordinates (p',l')

Coordinates of image output mask on the tangentially corrected map being obtained, the output image for a mask can be linearly resampled. This output image being enlarged to the size of an actual map, and superimposed on it, thus, NOAA map can be produced. This enlargement process in Figure 5 is called Mapping 9.

4.3 CONTENTS OF MAPPING USED FOR NOAA MAP COMPILATION

Mappings shown in Figure 5 used for compiling the 1:3,000,000 scaled NOAA map of "Japan" projected by Oblique conformal secant conic projection are explained as follows;

Mapping 1 : $p'=f1(p)$
         where,
         f1: To rearrange the pixel position collected in equiangle
             around the scanner to an equidistant position on the earth
             surface
         p : pixel number of scanned image
         p': pixel number of corrected scanner image
Mapping 2 : $(x,y)=f2(p',l)$
         where,   pixel
         f2: transformation from coordinates to Oblique equidistant
             cylindrical coordinates
         p': same as p' in Mapping 1
         l : line number of scanned image

938

(x,y): Oblique equidistant cylindrical coordinates
Mapping 3 : (x,y)=f3(z,α)
                    where,
                    (x,y): same as (x,y) in Mapping 2
                    (z,α): co-latitude and londitude defined on the Oblique spherical
                          coordinate system
Mapping 4 : (z,α)=f4(φ,λ)
                    where,
                    f4: Transformation from Spherical coordinates to Oblique spherical
                        coordinates, hereby, the pole position of Oblique sphere should
                        be defined previously in the Spherical coordinate system
                        as (φ₀,λ₀)
                    (z,α): same as (z,α) in Mapping 3
                    (φ,λ): latitude and longitude defined on Spherical coordinate
                          system
Mapping 5 : (φ,λ)=f5(B,L)
                    where,
                    f5: Transformation from ELLipsoid coordinates to Spherical
                        coordinates, because of the difficulty of direct transformation
                        from Ellipsoid coordinates to Oblique spherical coordinates,
                        the Ellipsoid coordinates are transformed to Spherical
                        coordinates temporarily.
                    (φ,λ): same as (φ,λ) in Mapping 4
                    (B,L): latitude and longitude on the Ellipsoid coordinate system
Mapping 6 : (r,θ)=f6(z,α)
                    where,
                    f6: Transformation from Spherical coordinates to Oblique conical
                        coordinates
                    (r,θ): Oblique conical coordinates
                    (z,α): same as (z,α) in Mapping 3
Mapping 7 : (X,Y):f7(r,θ)
                    where,
                    f7: Trasformation from Oblique conical coordinates to Plane
                        orthogonal coordinates
                    (X,Y): Plane orthogonal coordinates
                    (r,θ): same as (r,θ) in Mapping 6
Mapping 8 : (I,J)=f8(X,Y)
                    where,
                    f8: Transformation from Plane orthogonal coordinates to Film
                        coordinates
                    (I,J): Film coordinates
                    (X,Y): same as (X,Y) in Mapping 7
Mapping 9 : (U,V)=f9(I,J)
                    where,
                    f9: transformation from Film coordinates to Enlarged coordinates
                    (U,V): Enlarged coordinates
                    (I,J): same as (I,J) in Mapping 8

5. CONCLUSIONS AND PROSPECTS

     Technical points of directly measuring the mean surface velocity of an
oceanic current like the Kuroshio, can be summarized in the following two
items:

(1) To obtain the timely adjacent data of NOAA-6/AVHRR containing "sea marks",
    i.e., some special points floating with the current which can be
    recognized clearly on both scenes.
(2) To have a procedure to orientate the NOAA-6/AVHRR imageries into the
    earth coordinate system with highly geometrical accuracy.

     Developing a method of orientating the NOAA-6/AVHRR data into the oblique
conformal secant conic projection map "Japan" scaled 1:3,000,000, the authors

checked the mapping accuracy at ground control points. The mapping area covers a fairly big range about 2,100 km wide east to west, and about 3,000 km long south to north. 23 ground control points were chosen as uniformly as possible, and their orientation accuracy was found to be 1.4 pixels in standard deviation, namely, about 1.5 km in actual distance on the ground.

Sea marks are rather more difficult to recognize than land marks are. In order to recognize them as clearly as possible, a method in which one can adjust the image contrast, i.e., an interactive watching method on TV monitor, was adopted.

Sea current phenomena vary regularly in an interval of 12 hours. Observation periods of 12 hours, or 24 hours, in this case, are reasonable. Measurement accuracy of mean surface water can be considerd as about 0.1 knots on an assumption of a "Sea mark" orientation accuracy of "2.0 pixels".

The authors think that this method may by useful in some limited fields such as a study of current dynamics, while on the other hand, it will be difficult to use it in ordinary observation services, because it is a rare occasion when data containing no cloud cover can be obtained. In a very fortunate case, current velocities of an entire area may be observed simultaneously. The ocean current chart for Japan and neighbouring areas strengthened with data obtained by this method is shown in Figure 7.

6. REFERENCES

1) WADACHI, K. (1960): Encyclopedia of Oceans (Kaiyo no Jiten in Japanese). Tokyodo.
2) CNES (1976): Pamphlet for Argos System.
3) ISHII, H. (1981): Tracking of Kuroshio Current by Argos Buoy. Marine Sciences Monthly, vol.13, No.5.
4) MORIMOTO, H. (1976): Compilation of Map. Survey Association of Japan.
5) GEOMETRICAL SURVEY INSTITUTE (1977): Jiho. No.44.
6) PERSON, F. (1977): Map Projection Equations. Naval Surface Weapons Center.
7) LAURITSON,L., G.J.NELSON AND F.W.PORTO (1979): Data Extraction and Calibration of TIROS-N/NOAA Radiometers. NOAA Technical Memorandam NESS 107
8) THE MARITIME SAFETY BOARD OF JAPAN (1981): The Most Recently Published Map of Ocean Current (published twice a month).
9) GEOMETRICAL SURVEY INSTITUTE: 1:3,000,000 scaled map "Japan".
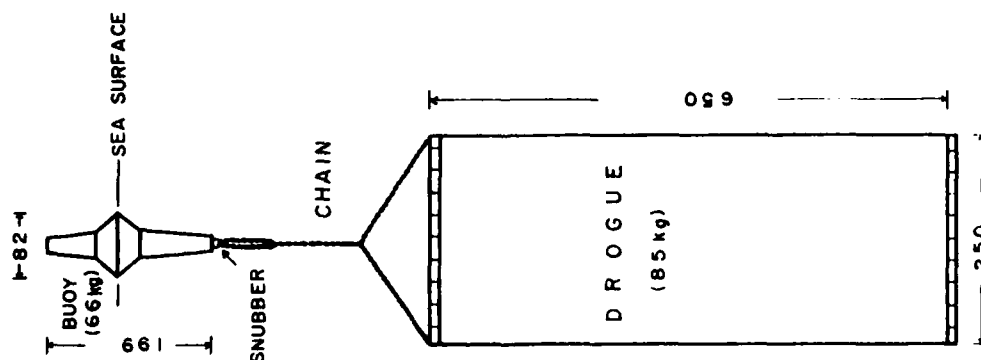
Figure 1. Configuration of Drifting Buoy[3]
(unit : cm)
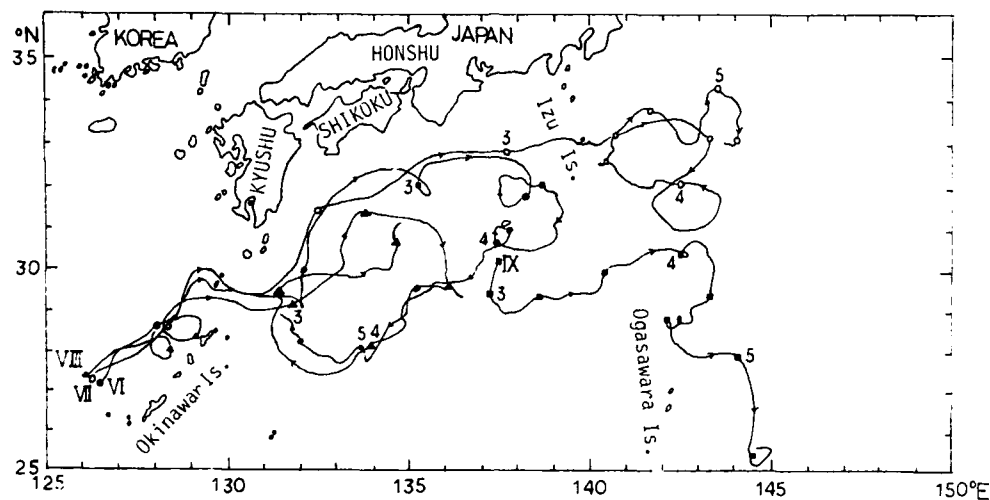
Figure 2. Tracks of Buoys VI – IV (Feb. 2, 1981 – May 15, 1981. Digit shows the Position of each Buoy on the First Day of the Month. Symbols show the Positions of each Buoy on the 1st, 10th and 20th Day of the Month.)[3]
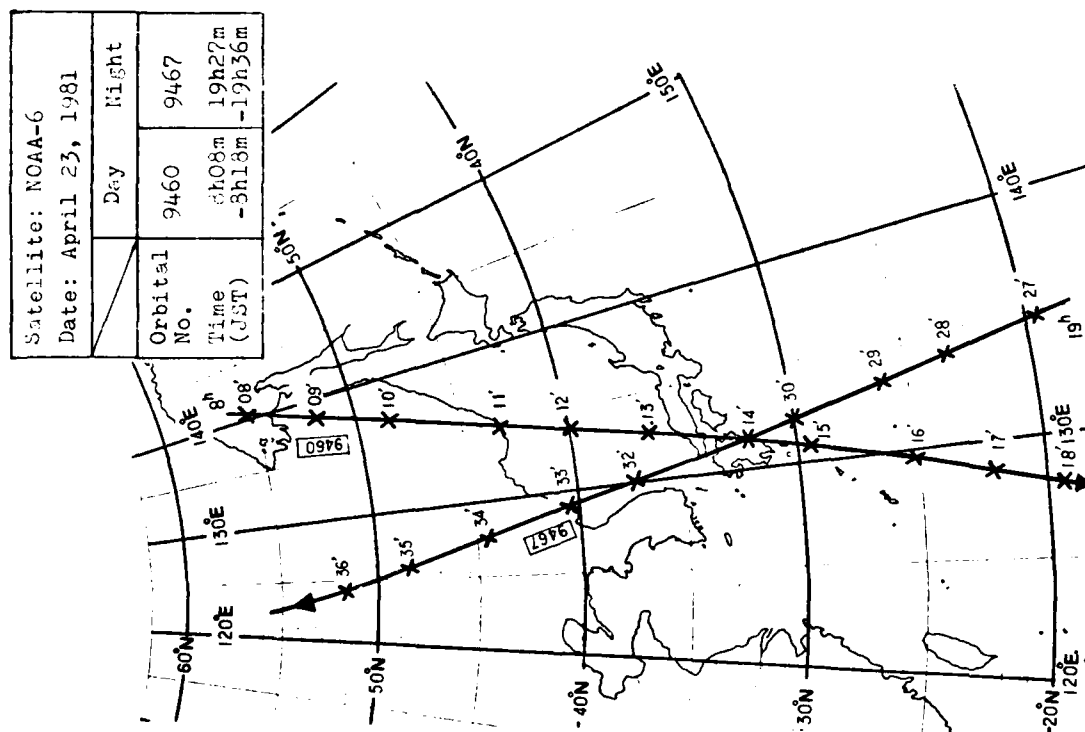
Figure 3. Time Diagram of NOAA-6 Orbits within a 12 Hour Period.

Figure 4. Sea Mark Chase Method for
           Current Vector Measurement.

a,b : Time Serial Imageries of
      NOAA-6/AVHRR Channel 4
      a—April 23, 1981, 8:14 JST
      b—April 23, 1981, 19:31 JST
c,d : Sea Mark Positions and Fronts,
      Corresponding to a and b
      Respectively
e : Current Vectors and Front
    Movements

(Current vectors can be measured
as shown in Table III.)

942
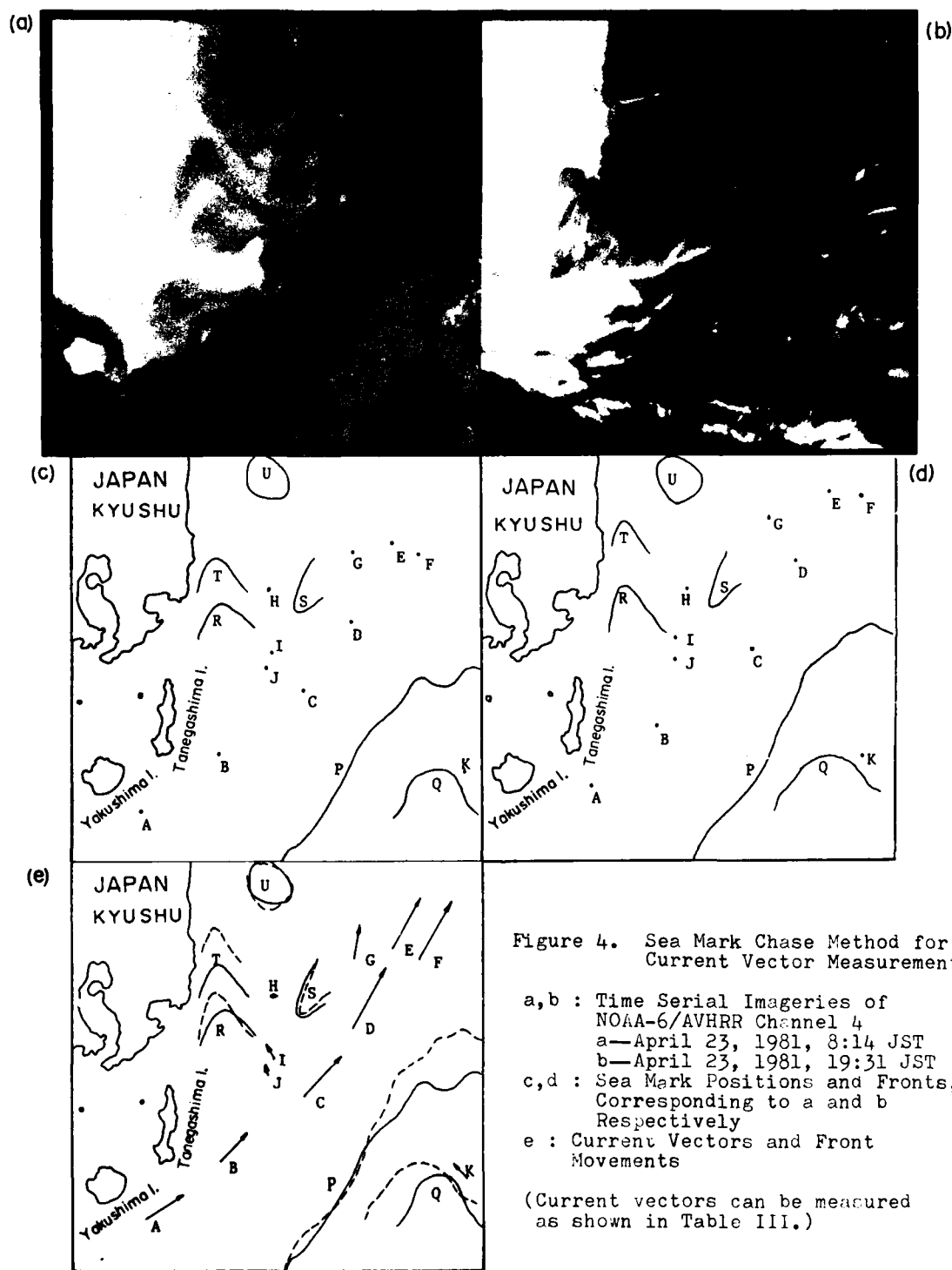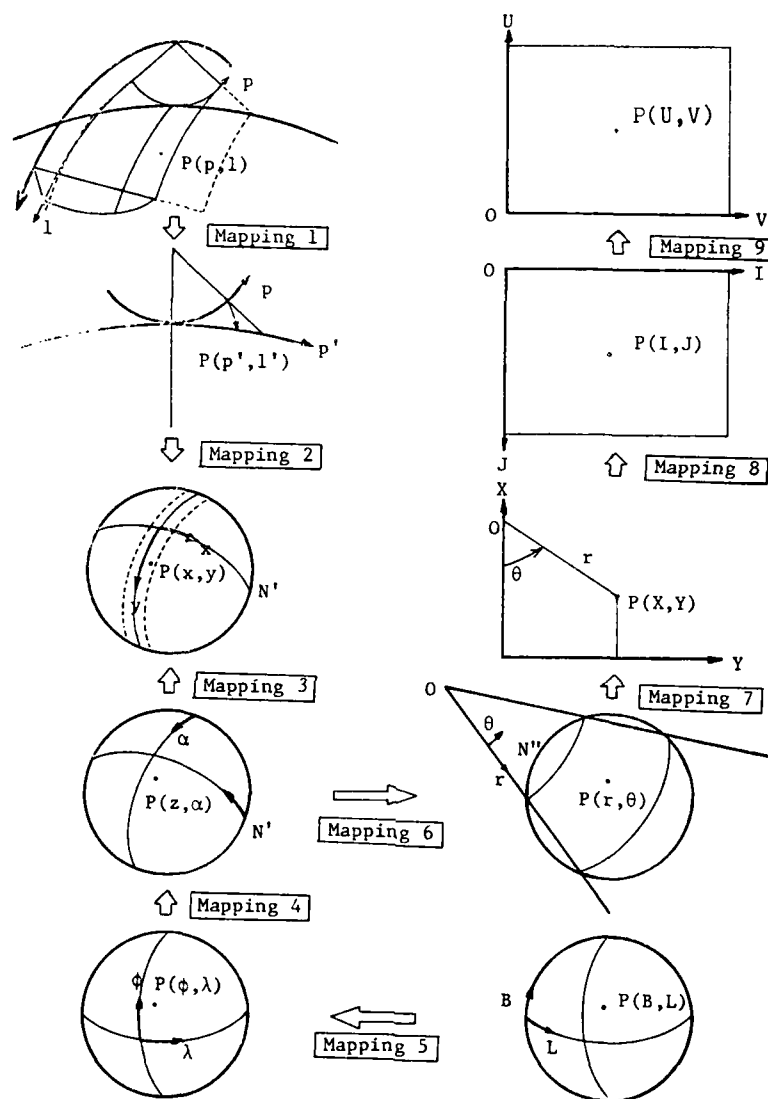
Figure 5.   Mappings used for NOAA Map Compilation.

Map Projection : Oblique Conformal Secant Conic
Projection
Applied Map : 1 : 3,000,000 Scaled Map "Japan"

Figure 7. Ocean Current Chart strengthened by NOAA Data. (Base Map: Current Chart Provided by M.S.B. from April 15 to April 29, 1981)
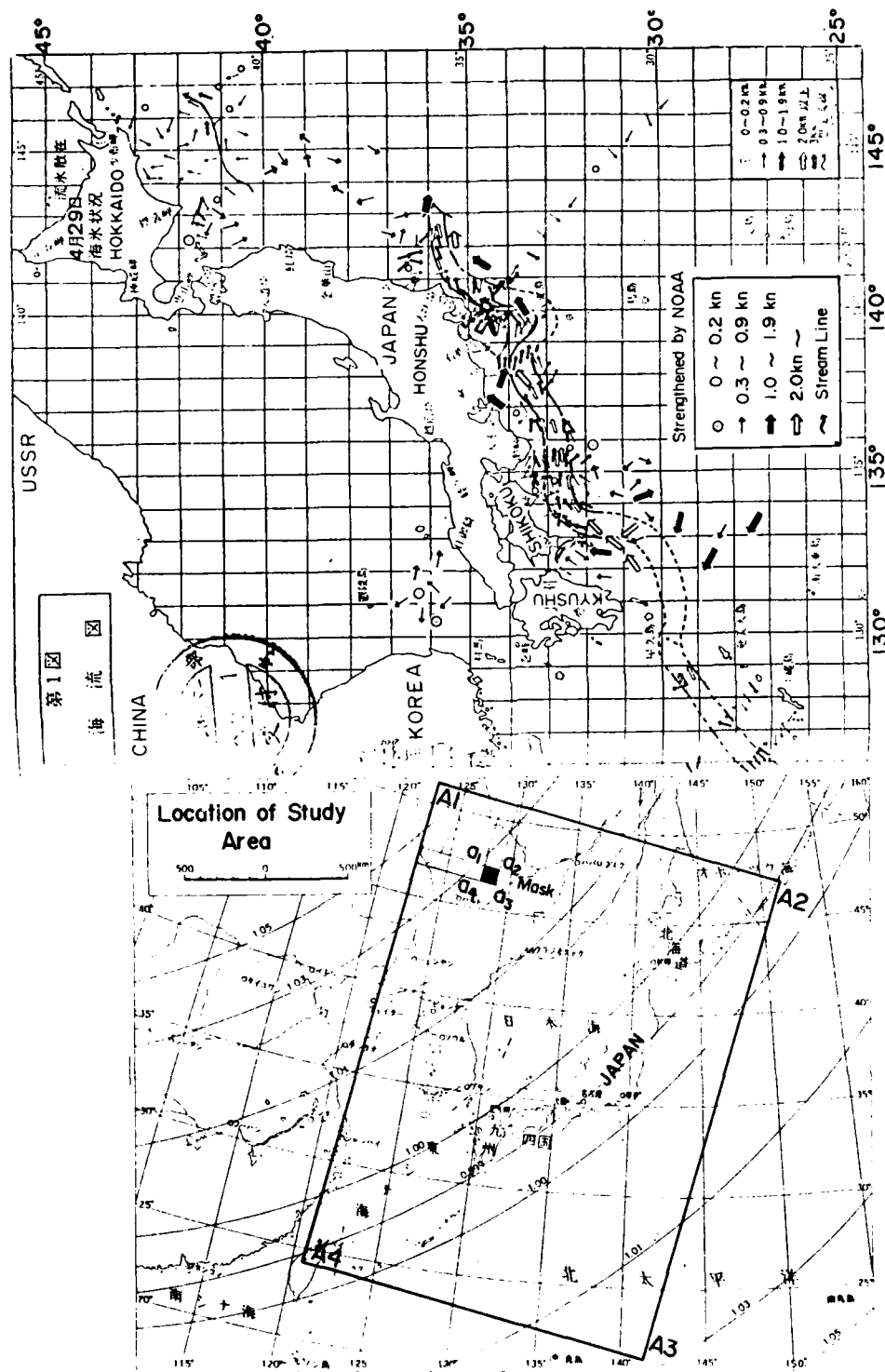
Figure 6. Applied Range of NOAA Map and Image Output Mask.

A CONCEPTUAL METHOD OF SNOWMELT
RUNOFF FORECAST

A.K. Bagchi
Civil Engineering Department, University of Roorkee
Roorkee (U.P.) 247672, INDIA
Currently on deputation to Kwara State College of Technology,
Land Surveying Department, Ilorin, PMB 1375, NIGERIA

ABSTRACT

The paper presents a method of calculating
Snow depth by using Landsat imagery and such
hydrometeorological data as may be available in a
mountainous basin. Only one point data has been
used.

It is thus possible to get an estimate of
snowmelt portion of runoff, that would be available.
This forecast can be done on the day the snowmelt
season starts and can be corrected and updated on
subsequent days.

INTRODUCTION

Hydrologists and managers of water resources have always been
interested in the forecast of runoff. The methods could be conceptual,
statistical or based on indexes. For forecast of runoff in snowfed
mountainous rivers the usually adopted method is based on indexes. Index
method is simple and in many situations is the only one practically
applicable. California which has one of the longest tradition of water
resource management uses largely the index methods.

Index methods however are possibly not the ones that one would like
to adopt. They are black box techniques, do not admit continuous
improvement and further, knowledge gained in one basin is not applicable
in another. If index methods have been widely used it is because of
practical difficulty in collecting data that are needed for a conceptual
model.

The present paper describes a conceptual method of forecast of
runoff in a mountainous snowfed river. A self imposed constraint is that
the method should not call for any data that are not normally available
in an average mountainous basin.

EXPERIMENTAL BASIN

Beas basin (Fig.1) above Manali situated in Western Himalayas has
been chosen for this study. The basin ranges from 1900 m to 5900 m and
covers an area of 345 Sq.Km. During winter almost the entire basin
becomes covered with snow and by summer end the transient snowline

recedes to around 5000 m elevation. Beyond 5000 m it is perennial snow. The following hydrometeorological data are routinly collected at Manali the lowest point of the basin:

Maximum daily temperature T_{max}

Minimum daily temperature T_{min}

Rainfall (total of 24 hours)

Snowfall (total of 24 hours, water equivalent)

Discharge in river Beas at Manali.

Snowfall is collected on a horizontal board and the depth of the collected snow is measured hourly by a rod. The sum of the measured depths over 24 hours is multiplied by 0.1 to obtain water equivalent of daily snowfall. Discharge is measured once a day at 1100 hours. The basin was divided into 20 elevation zones (j) each 200 m high. Area of each zone (ΔAj) was planimetered from 1:50000 scale topographical map with contour interval 40 m. $\sum_{j=1}^{20} \Delta A_j$ = 345 Sq.Km. Only a small percentage of area lies above 5000 m elevation. Glaciation is therefore insignificant.

THE CONCEPT

The total amount of runoff that would generate from the snow that stands on a particular day can be calculated if it is possible to calculate the water equivalent of the standing snow in the basin on that particular day. For this let us assume that

(i) precipitation in any altitude zone (j) is uniform and there is no internal variation,

(ii) similarly temperature in zone j is uniform,

(iii) temperature at higher altitudes can be calculated by adopting a suitable lapse rate. The temperature calculated at the mid-altitude of the zone is the temperature of the zone throughout.

Depth of standing snow can be calculated if one can estimate daily snowfall and snowmelt in different zones. The difference between the two is the net accretion or depletion of the standing snow. By keeping an account of the daily accretion/depletion it is possible to estimate the depth of standing snow.

This is to be done from the record of precipitation and temperature data recorded at one point (Manali) of the basin as there is no second data recording station. It is therefore necessary to develop a method of estimating the orographic increase/decrease of precipitation. Further requirements are (i) development of a method of estimating the percentage of snowfall in the total precipitation and (ii) a method of estimation of snowmelt.

SNOWFALL

Form of precipitation can be predicted from a record of ambient temperature at the time of precipitation. A continuous record of temperature is however not available. It has been found that the following equation can be used for predicting the percentage of snowfall:

946

$$x = 9(3.5 - T_{min}) - - - - - - - - (1)$$

(Bagchi 1981)

where x is the percentage of snowfall in the day's precipitation

This equation is perhaps not quite as good for predicting snowfall percentage on a day to day basis. However over a reasonably long period the equation works well.

Temperature can be transferred vertically up via lapse rate and hence the percentage of snowfall in any altitude zone.

OROGRAPHIC INCREASE IN PRECIPITATION

Hydrologists have found it difficult to transfer precipitation quantity vertically. Many have therefore been forced to ignore this factor (Hawley et al 1980). A comparison of annual precipitation recorded at Manali and runoff shows clearly that the orographic increase in precipitation is considerable making areal precipitation 2.5 times the point precipitation at Manali. Thus orographic increase must be taken into consideration.

Determination of orographic precipitation increase/decrease factor by ground measurements in different basins is impractical, at least in the Himalayas where no such studies have been reported. Further this orographic variation of precipitation may depend upon topography and thus transfer of data from one basin to another is not justified. A method has been proposed (Bagchi 1981) to find out orographic precipitation variation factor β using Landsat imagery.

If an elevation zone j remains under snow for n days then the following equation is valid

$$a \sum_{i=1}^{n} (T_{max})_{ij} = \frac{\beta_j}{100} \sum_{i=1}^{n} P_{i1} \cdot x_{ij} - - - - - - - -(2)$$

where, $(T_{max})_{ij} = T_{max}$ on i^{th} day in j^{th} zone.

P_{i1} = Precipitation on i^{th} day at Manali (j = 1)

β_j = Orographic precipitation variation factor

= $\dfrac{\text{precipitation in } j^{th} \text{ zone}}{\text{precipitation at the base station}}$

x_{ij} = $\dfrac{\text{snowfall x 100}}{\text{total precipitation}}$ on i^{th} day in j^{th} zone

a = degree day factor, areal value, taken as constant over time and space

Thus $\beta_j = \dfrac{a \sum_{i=1}^{n} (T_{max})_{ij}}{\frac{1}{100} \cdot \sum_{i=1}^{n} P_{i1} \; x_{ij}}$ - - - - (3)

The areal value of 'a' has been calculated using Landsat snow

947

cover data and hydrometeorological data and has been found to be 2.1 mm
per °C day (Bagchi 1981). All other terms on the right hand side of
Equation 3 can be calculated from daily records of T_{max} and T_{min}
recorded at the base station and applying a suitable lapse rate which
has been taken as 0.65°C per 100 m.

The summation extends over n days, the period during which the
zone remained under snow and this was found by analysing Landsat data.

TRANSIENT SNOWLINE ALTITUDE

Transient snowline altitude was determined by projecting Landsat
imagery on scale 1:1,000,000 onto a map of the basin which is on scale
1:100,000 with 40 m contour interval. A precision stereoplotting
instrument A8 was used for this projection. Discrete points on the snow-
line were transferred onto the map by placing the floating mark of A8 on
the snowline. Heights of these points were read from the map. Mean
height was taken as the transient snowline altitude on the day the image
was acquired.

Such heights were determined for all the days for which Landsat
imageries were available and were plotted against time; snowline elevation
on any intermediate date was obtained by linear interpolation (Fig.2).

The number of days (n) during which a particular altitude zone
remained under snow can now be read from Fig.2. Thus the elevation zone
number 10 (between 3700 and 3900 m) remained under snow during the
period 9 December 1978 to 16 June in the year 1979.

VALUES OF β_j

β_j values were calculated for different zones using 1978-79
Landsat imageries (Fig.3). That the calculation of β_j values is basica-
lly correct is proved by examples show elsewhere (Bagchi 1981, 1982).
These β_j values are taken to be invariable over time.

SNOWMELT

Snowmelt (M_{ij}) in any zone (j) on any day (i) is given by

$$M_{ij} = a\,(T_{max})_{ij} \quad - - - - - - - - - (4)$$

SNOW DEPTH

Snow depth ξ_{nj} in zone j on the nth day starting from the first
day (i=1) of snow cover is given by,

$$\xi_{nj} = \frac{\beta_j}{100} \sum_{i=1}^{n} P_{i1}\, x_{ij} - a \sum_{i=1}^{n} (T_{max})_{ij} \quad - - - - (5)$$

Snow depth figures, calculated by the above formula, in a few
selected elevation zones on different days are shown in Fig.4. The
formula does not work in the perennial snow cover zone.

FORECAST OF SNOWMELT RUNOFF

The total amount of snow (water equivalent) that would be available subsequent to any particular day after the snow accumulation season is given by the expression

$$\sum_{j=j'}^{J} \xi_j \cdot \Delta A_j \quad - - - - - - - \quad (6)$$

Where j' is the lowest snow covered zone, ξ_j is depth of snow in zone j on that day and J is the zone just below the permanent snow covered area. In deriving the above expression, contribution from permanent snow cover area has been ignored.

It is however not possible to verify the result as much of the snowmelts in the rainy season (July to September) and is thus mixed with rain water. The result can be verified for the summer season by calculating runoff by using a suitable streamflow model (which accounts for snowmelt and rainwater input). This will need forecast of T_{max}.

Analysis of mean T_{max} recorded at Manali shows that the monthly mean T_{max} can be modelled empirically and thus affords forecast. Comparison of mass curves forecast on 1 April with that observed during April, May, June of 1978 and 1979 are shown in Fig.5 (Bagchi 1981a).

CONCLUSION

A method has been presented in this paper for calculation of snow depth on any day, at any elevation zone below permanent snow line. This has been done by using Landsat imagery and such hydrometeorological data as may be available in an average Himalayan basin. Only one point data has been used.

On any day, in the snow melt season, it is now possible to calculate the total volume of standing snow in the basin, thus giving a method of estimating the amount of assured water supply in the basin.

Time distribution (monthly) of the snowmelt portion of runoff can be done by forecasting monthly mean T_{max}. This is a meaningful exercise for the summer season (before the onset of rainy season).

The paper breaks a new ground in snow survey and snow hydrology.

ACKNOWLEDGEMENT

REFERENCES

Bagchi A.K., Snow Survey from Landsat imagery, Final Report submitted to Indian Space Research Organisation, September 1981.

a. Bagchi A.K., Snowmelt runoff in Beas basin using satellite
imageries, Ph.D. thesis submitted to the University of Roorkee,
1981.

Bagchi, A.K., Orographic Variation of Precipitation in a high rise
Himalayan basin, Proceedings of Symposium 5, IAHS Conference,
Exeter, July 1982.

Hawley, M.E., R.H.McCuen and A.Rango, Comparison of models for
forecasting snowmelt runoff volumes, Water Resources Bulletin,
Vol 16 No.5, October 1980, pp 914-920.

Martinec J., Snowmelt runoff model for streamflow forecast,
Nordic Hydrology, Vol.6, 1975, pp.145-154.

Murray R., Rain and snow in relation to the 1000-700 mb and
1000-500 mb thickness and the freezing level, The Meteorological
Magazine, No.955, January 1952.
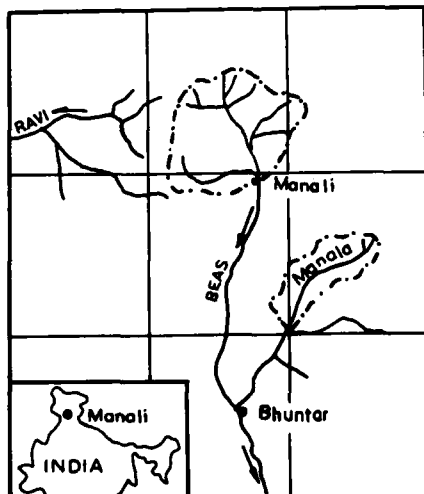
Fig.1 - Beas Basin
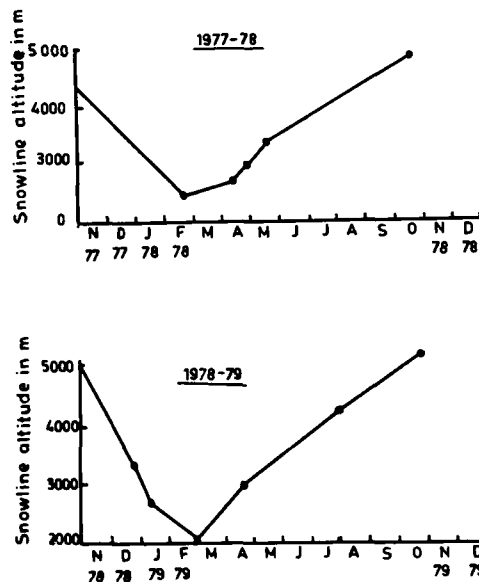
Fig. 2 - Snow altitude in beas basin

Fig.3 - Variation of β with altitude

Note: Snowmelt portion only
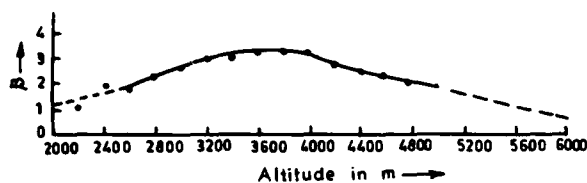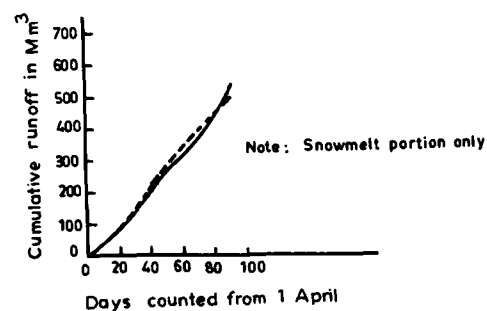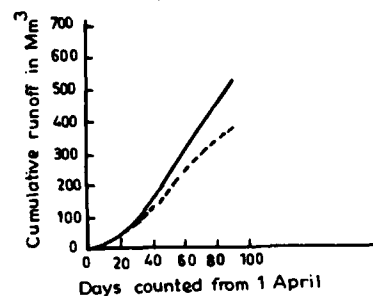
Fig. 5 -Comparison of observed mass curve with that predicted on 1 April
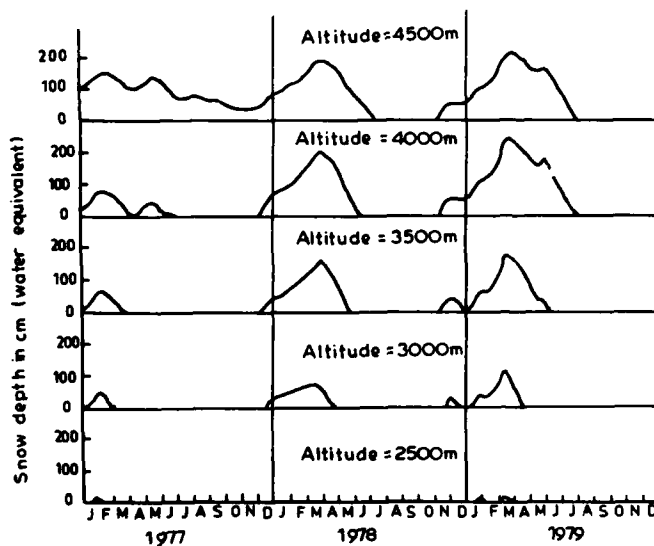
Fig. 4 -Standing snow at differet altitude

951

PROJECT "PERCEP"
CANADA/PERU CURRENT REMOTE SENSING TECHNOLOGY TRANSFER ACTIVITIES

B. Bruce

Canada Centre for Remote Sensing
Ottawa, Canada

F. DuBois

Oficina Nacional de Evaluacion de Recursos Naturales
Lima, Peru

SUMMARY

In January 1977 work began on a remote sensing technology transfer project between Canada and Peru. Project "PERCEP" embodied certain innovative concepts of project management and technology transfer which have attracted international interest. Early progress in this project was reported in Manilla at the Twelfth International Symposium on Remote Sensing of Environment (1978).

This paper reviews the "PERCEP" philosophy and summarizes acrivities and milestone achievements from 1978 to the Project's conclusion in 1982. Contributions in the areas of management, research, training, equipment and infrastructure are outlined. The current status of remote sensing activities in Peru is assessed.

In 1980, activities were initiated to assess the contributions of this experimental project and to identify any needs for continued Canadian support of remote sensing development in Peru. The recommendations of a formal project evaluation mission which visited Peru in 1981 are outlined. It now appears likely that an expanded Project "PERCEP" Phase II will be established this year. The paper outlines probable areas of emphasis for Phase II. Particular priority would be placed on consolidating resource satellite applications activities and on expanding Peruvian capabilities in the meteorologic satellite and airborne remote sensing sectors.

MAPPING TAILINGS-AFFECTED FARMLANDS
USING LANDSAT TEMPORAL DATA

Jose Bernardo R. Lim
Daniel R. Guerrero

Natural Resources Management Center
Quezon City, Philippines

SUMMARY

Among the most pressing environmental concerns in the Baguio Mining District is the problem of mine tailings damage and disposal. Approximately 54,000 tons of mill tailings result daily from operations of six mining companies.

Farmers downstream of the mines have constantly complained that tailings-laden irrigation and flood waters have reduced crop productivity and consequently their income. As a result, an investigation was carried out to determine the areal extent of tailings-related riceland damage for possible compensation of affected farmers.

One of the faster methods used in determining damage extent was digital analysis of Landsat data. This was done specifically for the Bued River (one of the rivers draining the district) along which two mining companies operate. Total tailings produced by the 2 mines total approximately 3000 tons per day which is relatively small when compared to other operations. However, the inefficiency of their tailings impounding systems is such that the tailings are released into the river during times of heavy rain.

The Bued River has a narrow, ravine-like channel as it works its way through the Southern Cordillera Mountains. Upon reaching the plains of Central Luzon, it assumes a braided drainage pattern, upon which thousands of hectares of farmlands depend on for irrigation.

Field investigations of farmlands along the floodplains of Bued River definitely show some areas to be affected by mine tailings. The areal extent of damage had never been studied and this is the first attempt to use the temporal capabilities of Landsat for monitoring and assessing tailings-damaged agricultural lands.

Six Landsat overviews, taken at different times, were analyzed through a multispectral imager analyzer. Various packaged digital programs and hardware ratio functions were applied and tested for applicability. In addition, temporal band ratioing of the different scenes were also undertaken. Incorporated in the digital analysis were rainfall and stream gauge data. Land use features and patterns were also taken into account during analysis.

Results obtained from the study showed that some standard algorithms can delineate tailings-laden farmlands with a high degree of confidence. This is not due directly to the spectral response of the tailings, but rather a combination of the land use and the area's proneness to flooding. It was found that simultaneous analysis of an after-flood and non-flooded imagery, coupled with field data provides the best results in delineating tailings-affected farmlands.

Ground verifications of the test area, which involved field survey and low-oblique aerial photography, whoed the high credibility of temporal Landsat scenes in monitoring tailings-affected agricultural lands.

USING KNOWLEDGE OF AGRICULTURAL PRACTICES TO ENHANCE
THROUGH-THE-SEASON INTERPRETATION OF LANDSAT DATA*+

Christian R. Pestre** and William A. Malila
Environmental Research Institute of Michigan
Ann Arbor, Michigan 48107

ABSTRACT

Landsat data contain features that can be
interpreted to produce information about crops,
in support of crop estimation procedures. This
paper considers ways in which detailed knowledge
of agricultural practices and events might
increase and improve the utilization of Landsat
data in both the predictive and observational or
measurement components of such procedures.
Landsat observables related to agricultural
practices and events throughout the cropping
season are listed. Agricultural fields are
identified as the preferred observational units
for incorporating refined agricultural
understanding, such as crop rotation patterns,
into machine procedures. Uses of Landsat data
from both prior seasons and the current season
are considered, as is use of predictive models
of crop appearance. The investigation of
knowledge engineering systems tailored to
through-the-season estimation problems is
recommended for long range development.

1. INTRODUCTION

A continuing need exists for estimates throughout the growing season of
the current status and eventual production of crops. Traditional methods exist
for producing these estimates, but Landsat provides a new source of
observational data about the crops. Landsat provides us with features,
features that need to be interpreted in order to give us the information we
need.

The paper considers ways to increase and improve the utilization of
Landsat data in procedures for estimating crop status and production throughout
the growing season, through the incorporation of detailed knowledge of
agricultural practices into interpretative procedures. Our context is one of
highly automated crop area estimation over large areas without support of
direct ground observations. For this problem, the main body of technology
currently available relies on crop recognition using temporal-spectral
signatures of crops. Accurate differentiation of crops usually requires
advanced stages of phenological development [1-5] and these approaches become

957

much less accurate early in the season when crops exhibit little spectral uniqueness. However, a visual examination of early season Landsat data reveals marked differences between fields and crops in the scenes, giving an idea of the potential information content of these data for an agricultural analyst. Therefore, it appears reasonable that use of specific knowledge of cropping practices and events in a given locality should improve one's ability to extract information from such Landsat data.

2. THE CROP ESTIMATION PROCESS

The process of crop estimation appears to us to be a combination of prediction and measurement components. Measurement takes precedence when available, but prediction is needed (especially in early season) to fill gaps in available knowledge and to anticipate future events [3, Section 2.2].

The nature of estimation is primarily prediction very early in the season and changes gradually to observation or measurement by the end of the season. Table 1 lists various elements that may be included in the predictive and observational components of a crop estimation procedure.

In our understanding, the two major aspects of prediction are (a) predicting what the farmers' actions will be and (b) predicting their outcome. Both aspects are affected by a number of factors (as listed in Table 1) whose relative importance varies , depending on both what has happened up to the current time in the growing season and the current conditions.

Similarly, the measurable quantities change during the course of the growing season, increasing in number and/or accuracy as the farmer's decisions are implemented and the crops emerge and develop. The quantities of interest depend on the goal of the estimation process.

3. LANDSAT OBSERVABLES RELATED TO AGRICULTURAL PRACTICES AND EVENTS

Agricultural Practices and Events. From a prediction standpoint, the growing season starts long before the crops are actually planted. The farmer usually makes plans for allocating his lands to various crops (including pasture and fallow) soon after the previous season's harvest and may begin to prepare the fields for planting well in advance of the actual planting date. The planning decisions and crop selections made by the farmer result from his interest in making a profit while avoiding too much risk, compounded by constraints that may exist on his farm. Up to the time of planting, plans may be modified.

Field preparation usually consists of several passes over the field. Practices depend on the location and field conditions. One may even observe a no-till practice for soil conservation. In the spring in the U.S. Corn Belt, planting takes place when the soil is dry enough to be worked and warm enough for the seeds to germinate and the crop to grow. A delayed planting season, for example due to cold or wet weather, may cause a farmer to change his plan and may switch from one crop to another with a shorter growing season, such as from corn to soybeans. The farmer also may replant crops seriously damaged in early stages of development.

Crop management in early season includes varied practices to insure adequate moisture supply to the crop and prevent proliferation of weeds, disease, or pests. Late season management of crops is reduced as it becomes impossible to drive a machine over the field without damaging the crop. A farmer may cut green or turn to grazing a crop initially intended for grain harvest, due to changed needs from his livestock or diminished value of the crop in the marketplace.

958

Landsat Observables. Described in simple terms, the first level of information conveyed by Landsat data is the absence or presence of vegetation. At the next level of detail, one can see differences due to the condition and vigor of vegetation, or to the color and moisture level of the soil. That information alone does not allow one to infer crop types or crop conditions, unless it is interpreted in conjunction with expected crop phenology at the time of observation. With a sequence of observations one has greater support for drawing inferences as to which crops are present and their condition. This sequence need not be restricted to the period when crops are growing and may include pre-season appearance of fields or prior-years' land use.

The features extracted from Landsat observables need to be interpreted in order to produce the desired information, i.e., crop acreage and condition. This interpretation should be made within the context of the observation (location, time of year, and local conditions), which could be enhanced through use of interpretive models [e.g., 6-9]. Explicit models are necessary for machine processing. One important type of model would be of crop growth, such as predictive models of crop spectral appearance, which take into account local weather and other local conditions [10]. Others could model farmers' decisions during the season.

The agricultural practices, features, and events that may be observed in, or inferred from, Landsat have various spatial associations, applying to different strata such as pixels, fields, districts, soil groups, regions and even countries. For most purposes, our judgment is that fields are the preferred observational units for incorporating refined agricultural understanding into machine processing of Landsat data. This is in large part due to the fact that fields are the primary unit of land use management. Algorithms do exist which can find fields or quasi-fields in Landsat data [e.g., 11 and 12].

The following are potentially observable by Landsat:

(a) Pre-Season Conditions and Planning: Observations continued over several years can be used to determine cropping practices for the individual fields and regions. Crop rotations, for example, can be tabulated. In general, an extensive history of each field may be obtained and related to factors affecting subsequent use.

(b) Preplanting and Planting: Pre-season preparations may be observed in one or more acquisitions. Irrigation preparations or practice, flooding and abnormal conditions, and indications of changed usage may be observed.

(c) Early Growth and Season:; Substantial emergence may be detected and used to infer planting dates. With continued observations during the season, the duration and general timing of plant cycles may be observed and plant development stages estimated, and condition of assessed, all subject to having adequate acquisition histories [13,14].

(d) Harvest: Time of harvest and progression of harvest may be monitored. Unusual timing can be noted when crops are cut early for silage or are left unharvested for long periods.

4. APPROACHES FOR USING LANDSAT OBSERVABLES

Use of Data from Prior Seasons. Stratified area estimation procedures are often used with Landsat data. The availability of direct observations of land use from prior-season Landsat data should provide information to improve the stratification employed by these procedures. Furthermore, such data could provide expectation on the responses that will be observed from specific sample

segments. These expectations can be relative to other sample segments in their strata which can be of substantial help when there are segments without coverage. They can also be relative to the temporal-spectral responses of the various crops, which is useful for crop recognition and for cases with missing acquisitions.

Usually farmers will manage their land employing rotation patterns that are consistent and predictable. Based on the crops that have been on the field during preceding years, one can develop a priori expectations as to which crop will be planted in the current year.

The stratifications discussed above for estimation purposes, of necessity, are developed at macro levels, that is they generalize agrophysical characteristics over substantial geographic areas. However, for accurate crop recognition in a segment, there may be a need for refined stratifications that take into account the local variations in topography, soil types, natural drainage, irrigation and other similar factors. In other words, one would like to come to know the "personalities" of individual fields.

Use of Data from Current Season. With the availability of Landsat data from the current season, the crop estimation process can benefit from the opportunity to directly observe the crops of interest as they develop.

Early in the season one might not be able to identify the specific crop types, but might be able to recognize a crop group, such as summer crops. However, as the season progresses and more acquisitions become available, one should be able to produce increasingly specific levels of class identification, estimate growth stages and perhaps assess the condition of the identified crop classes.

Since the objective of the estimation process is to draw inferences regarding the farmers' actions and their results, one can use the extracted information at various levels of specificity for estimation purposes. For example, crop group information derivable from Landsat has been used to augment conventional crop acreage response models [3,15] for specific summer crops.

Another aspect of predicting farmers' actions has to do with their responses to in-season events that can modify or change the crops that will grow. Examples are replanting, crop switch, double cropping and green cutting. These types of actions are amenable to modeling through an understanding of the factors that act upon them, such as optimum yield, length of remaining season, livestock requirements, and market conditions.

We also note that improved estimates of total production can be made through definition of crop subclasses with different yield potential. For example, double-cropped soybeans have smaller yields than single-cropped soybeans.

5. SUMMARY AND RECOMMENDATIONS

The crop estimation process was characterized as being a time-varying combination of prediction and measurement (observation) processes through the season (TTS), with the balance swinging from prediction to measurement as time progresses through the growing season. Potential Landsat contributions to both processes were discussed.

Reference was made to procedures merging traditional prediction variables (prices, government policy, etc.) with early season Landsat observation of the farmers' actions (gross crop group acreages) to produce improved early estimates of specific summer crop acreages.

960

Field-by-field Landsat observations were suggested as the appropriate and preferred basis for use in TTS estimation, and agricultural practices were identified which are observable by Landsat and could be of high interpretive value in TTS estimation. Predictive models of crop spectral appearance, which take into account local weather and other factors, were suggested for enhancing interpretation of Landsat observations.

For long-range development, we recommend the investigation of knowledge engineering systems tailored to the TTS estimation problem. They seem well suited to handling the varied information sources available and have a potentially large payoff.

REFERENCES

1. The LACIE Symposium: Proc. of Plenary Session, JSC-14551, October 1978 and Proc. of Technical Sessions, JSC-16015, NASA Johnson Space Center, Houston, TX, July 1979.

2. FY 1982 AgRISTARS Research Report. NASA Johnson Space Center, Houston, TX, January 1983.

3. Horvath, R., R.C. Cicone and W.A. Malila. Research and Development of Landsat-Based Crop Inventory Techniques. AgRISTARS Report MU-E2-04226, ERIM Report 152400-21-F, Environmental Research Institute of Michigan (ERIM), Ann Arbor, MI, January 1982.

4. Cicone, R., E. Crist, R.Kauth, P. Lambeck, W. Malila and W.Richardson. Development of Procedure M for Multicrop Inventory, With Tests of a Spring Wheat Configuration. Report 132400-16-F, ERIM, Ann Arbor, MI, March 1979.

5. Badhwar, G.D. A Semi-Automatic Technique for Multitemporal Classification of a Given Crop. AgRISTARS Report SR-J0-00481, NASA/Johnson Space Center, Houston, TX, July 1979.

6. Suits, G.H. The Calculation of the Directional Reflectance of a Vegetation Canopy, Remote Sensing of Environment, 2, p.117, 1972.

7. Suits, G.H. The Calculation of the Directional Reflectance of a Vegetative Canopy and the Cause of Azimuth Variations in Directional Reflectance of the Vegetative Canopies, Remote Sensing of Environment, 2, (p.117 and p.175), 1972.

8. Malila, W., J. Gleason and R. Cicone. Multispectral System Analysis Through Modeling and Simulation. Proc. of the 11th International Symposium on Remote Sensing of Environment, ERIM, Ann Arbor, MI, April 1977.

9. Malila, W., J. Gleason, F. Sadowski, R. Cicone and E. Crist. Applications of Modeling to Analysis and Processing of Landsat Data. Proc. of the 12th International Symposium on Remote Sensing of Environment, ERIM, Ann Arbor, MI, April 1978.

10. Holmes, Q.A., R. Horvath, R.C. Cicone, R.J. Kauth and W.A. Malila. Development of Landsat-Based Technology for Crop Inventories, Volumes 1, Section 4.5.2: Modeling of Crop Spectral Phenology (Seed-to-Satellite Model). Report 132400-29-F, ERIM, Ann Arbor, MI, December 1979.

11. Kauth, R.J., A.P. Pentland and G.S. Thomas. BLOB, An Unsupervised Clustering Approach to Spatial Preprocessing of MSS Imagery. Proc. of the 11th International Symposium on Remote Sensing of Environment, ERIM, Ann Arbor, MI, Vc'. 2, pp.1309-1317, 1977.

12. Bryant, J. Applications of Clustering in Multi-Image Data Analysis. NAS9-14689-89S, Texas A&M University, College Station, TX, August 1978.

13. Badhwar, G.D. and D.R. Thompson. Estimating Emergence Date of Spring Small Grains Using Landsat Spectral Data. Agron.J. 75:75-78, 1983.

14. Crist, E.P. and W.A. Malila. An Algorithm for Estimating Crop Calendar Shifts of Spring Small Grains Using Landsat Spectral Data. AgRISTARS Report SR-EO-00459, ERIM Report 132400-41-T, ERIM, Ann Arbor, MI, June 1980.

15. Thelen, B. and D. Mitchell. Remote Sensing Augmentation of Conventional Crop Acreage Response Models for Estimation of Corn, Soybeans, and Sorghum Acreages, ERIM Report 152400-16-T, ERIM, Ann Arbor, MI (to be submitted for publication)

BIBLIOGRAPHY

USDA Weekly Crop and Weather Reports for Illinois, Indiana, Iowa and Missouri, 1979-1981.

U.S. Agricultural Attache Reports from Argentina and Brazil, 1980 and 1981.

Various other periodic reports by the U.S. Department of Agriculture in 1980 and 1981.

S.R. Chapman and L.P. Carter, Crop Production, W.H. Freeman and Co., San Francisco, CA, 1976.

Table 1. Potential Information Sources and
Variables for Crop Estimation

Prediction	Observation
Market variables	Enumerative surveys
Government policy	Ag expert observations
Prior weather	Ag expert judgments
Prior experience	Market surveys
Trends in technology	Production reports
Mail surveys	Current-year weather
Remotely sensed data	Remotely sensed data

IMPROVEMENTS IN FOREST CLASSIFICATION AND INVENTORY

USING REMOTELY SENSED DATA

Curtis E. Woodcock
Janet Franklin
Alan H. Strahler*

Geography Remote Sensing Unit
University of California
Santa Barbara, California, USA

Thomas L. Logan

Jet Propulsion Laboratory
California Institute of Technology
Pasadena, California, USA

ABSTRACT

For the past four years, a Forest Classification
and Inventory System (FOCIS) has been under develop-
ment at the University of California, Santa Barbara,
and the Jet Propulsion Laboratory at Pasadena.
Originally devised and tested in the Klamath National
Forest, FOCIS is currently being used for a timber
inventory of the Eldorado National Forest in Cali-
fornia's Sierra Nevada Mountains. This new trial has
led to some operational improvements, including the
use of an effective simplification algorithm to pro-
duce classification maps exhibiting raster polygons
that conform to a minimum size. An interface has
also been developed to allow conversion of the raster
image to a vector format polygon image compatible
with Forest Service geobased information systems. In
addition, some experiments using variables measuring
illumination geometry for each pixel (as calculated
from registered digital terrain data) showed that
small but significant increments in accuracy can be
achieved by including channels of irradiance angle,
reflectance angle, and angle of azimuth of reflec-
tance relative to irradiation, along with Landsat
data in unsupervised clustering and classification
procedures.

1. INTRODUCTION

A Forest Classification and Inventory System (FOCIS) has been under develop-
ment for three years at the University of California at Santa Barbara and the Jet
Propulsion Laboratory at Pasadena, California. FOCIS is designed for large area
forest inventory and uses registered Landsat and digital terrain data. The po-
tential advantage of FOCIS is that it can provide timely inventories at a reduced

---

*Present address: Dept. of Geology and Geography, Hunter College, 695 Park
Avenue, New York, NY, 10021.

cost that are easily updated. The test area used for the initial development of FOCIS was the Klamath National Forest in Northern California. In that Forest, FOCIS produced accuracies commensurate with a concurrent inventory conducted by Region 5 of the U.S. Forest Service using conventional techniques (Strahler et. al., 1981). Currently, FOCIS is being applied in an inventory of the Eldorado National Forest, located on the west slope of California's Sierra Nevada Mountains.

While FOCIS can be considered operational, it is constantly being changed and improved. Two recent additions to the inventory system are a spatial filtering algorithm that improves the spatial coherence in the final classified image, and a modification to the classification procedure designed to reduce the adverse effects of local topography on classification accuracy. The spatial filtering algorithm has been incorporated as part of the current Eldorado inventory, but the modifications to the classification procedure are still in the testing and evaluation phase. The purpose of this paper is to report on the findings of research in these two areas. A brief overview of FOCIS will be provided, but for greater detail see Woodcock et. al. (1980), and Strahler et. al. (1981).

2. FOCIS OVERVIEW

FOCIS is designed to produce classes that resemble the strata used by the U.S. Forest Service in their conventional inventory techniques. Thus, the final classes in FOCIS have a three-component label consisting of regional type, size, and stocking. Regional type is a nominal variable that reflects the general species composition of the canopy: R, red fir; M, mixed conifer; and A, alpine conifer. Tree size is an ordinal variable that indicates crown diameter: 1, 1-6 ft. (.3-1.8 m); 2, 6-12 ft. (1.8-3.7 m); 3, 12-24 ft. (3.7-7.3 m); 4, 24-40 ft. (7.3-12.2 m). Stocking, or stand density, measures areal crown closure, and for forest inventory purposes is divided into two categories: P, 10-40% cover; and G, 41-100% cover. In areas where conifers do not have an areal coverage of at least 10%, only the regional type component of the label is used. The regional type label is assigned through the use of ecological models operating on digital terrain data that predict regional type for each pixel given elevation and slope aspect. The size and stocking labels are derived by manually assigning them to clusters derived from an unsupervised Landsat-based classification procedure. The final class labels, then, combine the labels from these two independent steps.

The individual steps that constitute the FOCIS procedure are not executed on an entire forest at a single time. Instead the forest is divided into smaller, more manageable units, termed "natural regions," which are expected to have consistent ecological and spectral characteristics. The concept of natural regions is closely aligned with the modeling of regional types. In FOCIS, the regional type component of the class label is derived from terrain-based ecological models. These models are based on graphs that have elevation and a transformed aspect variable as axes; the symbols on the graph record the regional type for numerous locations visited on the ground. Figures 1A and 1B are the regional type graphs used in the Eldorado National Forest. Lines are fit by eye to partition the elevation-aspect measurement plane into areas used to characterize each regional type. Subsequently, each pixel in the natural region is assigned a regional type label by identifying the area of the graph into which its elevation and aspect fall. Natural regions are also defined on the basis of these graphs. When regional types begin to occur in locations of terrain measurement space that were previously characterized by a different regional type, then a natural region boundary has been crossed. Three natural regions were identified in the Eldorado: northern and southern regions in the western portion of the forest at lower and middle elevations, and a high elevation Alpine Region in the eastern portion. In the FOCIS procedure, each natural region was classified and processed separately.

The regional type modeling used in FOCIS proved only partially transportable from the Klamath to the Eldorado. Regional type modeling worked well in the two lower (western) natural regions, where tree growth is influenced primarily by climatic variables. However, the regional type modeling concept broke down at high elevations, where the forest degenerates from very good site quality to timberline. In the intermediate stages between these two extremes, site quality is

964

related to glacial history and local factors such as soil drainage and local tem-
perature extremes. These factors can not be modeled directly using such general
techniques as the elevation/aspect graphs used in the lower natural regions.
Thus, the boundary between the alpine natural region and the two lower natural
regions was manually delineated through ground reconnaissance, and the regional
type label in the Alpine Region was uniformly set to A. This failure of eleva-
tion and aspect to separate the Alpine type from the others does not serve to
either substantiate or undermine the validity of the regional type modeling con-
cept. Instead, the lesson to be learned is that flexibility in approach must be
maintained. It is unrealistic to expect that forest types can be modeled on the
basis of terrain variables in all environments, and alternative strategies may
be required in other situations. However, where terrain-based models are appro-
priate, they can be used to exploit species/terrain relationships with success.

Landsat spectral and texture data are used in an unsupervised classification
procedure to produce clusters labeled according to size and stocking. The tex-
ture data are derived from Landsat Band 5 and are included as an additional data
channel throughout the classification process. To create the texture channel, a
3-by-3 window is passed over the Band 5 image, and the standard deviation of the
nine values within the window is computed, scaled, and placed in the location of
the center pixel in an output image. This channel gives a quantitative measure
of local tonal variation and enhances timber type discrimination.

The classification procedure consists of five main steps: unsupervised
clustering, cluster editing, image classification, illumination masking, and
class labeling. In the unsupervised clustering step, a dataset of statistics
characterizing clusters of commonly occurring spectral measurements is created.
Typically a large number of clusters are preserved from this step so that the
full range of variance in the data will be retained while clusters are kept
tightly defined in measurement space. More clusters are created in the unsuper-
vised clustering step than can be used in image classification. Thus, a cluster
editing step is required to reduce the number of clusters to a more manageable
set. This editing is accomplished manually with the aid of a dendrogram that
illustrates the degree of similarity of all clusters. A hybrid parallelepiped-
maximum likelihood classifier is used to assign pixels to clusters in the image
classification step. Typically, 100 separate classes are maintained through this
step in the classification.

The underlying assumption of the entire classification procedure is that the
pixels in any single cluster or class represent only one timber type. This
assumption proved unreliable under some circumstances in the Klamath project.
The problem was that, due to varying slope angle and aspect, poorly-stocked open
stands of conifers under low angles of illumination exhibited spectral signatures
which were very similar to those of dense, well-stocked stands under more direct
illumination. Thus, an image was created from the digital terrain data that ex-
pressed the cosine of the illumination angle of each pixel during the Landsat
overpass. This image was divided into two categories (poorly illuminated and
well illuminated) and overlain on the classified image. The resulting image
split all classes that were spectrally homogeneous but differently illuminated
so that each portion could be labeled separately. Labeling of size and stocking
for each class was accomplished by displaying the classes on a background Band 5
Landsat image. The analyst, with the help of air photos, then located the classes
and, through photointerpretation, determined the appropriate labels. Following
completion of the Landsat-based classification, the size and density labels were
merged with the modeled regional types to produce the final strata with three-
part labels.

The Landsat-based classification portion of FOCIS was modified somewhat for
the Eldorado inventory. One change relates to the use of the illumination mask.
In the Eldorado National Forest, the terrain is much less steep than in the
Klamath, and the effects associated with variable illumination were considerably
less severe. Thus, illumination masking was used only in the Northern Region of
the Eldorado, where the steep north-and west-facing walls of the Rubicon River
Canyon produced low illumination angles. Another change involved the use of an
iterative clustering, classifying, and labeling procedure. In this procedure,
classes that appeared heterogenous or hard to label were pooled, reclustered

965

using a smaller cluster size parameter, and reclassified. Up to three such iterations were performed. Although these changes altered the processing flow somewhat, the main features of FOCIS as developed in the Klamath also worked well for the Eldorado National Forest to suggest that FOCIS is highly transportable.

3. SPATIAL FILTERING

Conventional timber inventories are usually obtained by sampling from stand maps that have been produced by photointerpretation. These stand maps are also used for other resource management objectives, such as timber site planning, wildlife habitat assessment, etc. Traditionally, a minimum size, such as 5 or 10 acres, has been required for individual stands on such maps. However, the final classification maps produced by FOCIS have a minimum resolution of one acre, the area corresponding to a pixel after resampling. Since there are no spatial constraints imposed in classification, the final classification often exhibits a complex spatial pattern. While this classification may serve as a reasonable substitute for the conventional stand map as a sampling base, the units in the classified image are individual pixels and are therefore too small to be managed individually. Thus, the FOCIS procedure was modified to output regions (groups of connected pixels) no smaller than a prespecified minimum size.

There are two fundamental directions from which the problem of improving the spatial coherence in classified imagery can be approached. The first approach involves segmenting the image into multipixel units prior to, or as part of, the classification process. This approach relies on the assumption that multipixel units exist in the image that are more uniform with respect to some property within their boundaries than outside their boundaries. Typically, spectral uniformity has been the criterion used in image segmentation procedures. The validity of the use of spectral homogeneity for image segmentation depends on the characteristics of the scene being processed. For agricultural scenes the assumption of spectral uniformity is valid because the multipixel units are fields. However, in forested environments the desired units are stands, and many forest stands are characterized by spectral variability, reflecting the discontinuous and irregular nature of the canopy. The photointerpreter is adept at distinguishing among patterns of variability that differentiate stands, but automated detection and delineation of such patterns has not been accomplished. While it is our feeling that this approach will provide the eventual solution to the problem of improving the spatial coherence in classified images, it is not a feasible solution at the present time.

The alternative method to improve spatial coherence is to classify the image using conventional nonspatial techniques and simplify the resulting pattern via a spatial filtering algorithm. This approach has been adopted for use in FOCIS until acceptable automated image segmentation procedures are developed. It is easily implemented because the image classification procedure remains intact, with the spatial filtering algorithm being a single added step. The spatial filtering algorithm adopted for FOCIS is a modified form of the one developed by Peet and Davis (1976). This algorithm has the advantage of removing all groups of pixels below a user-specified minimum size for each class in the image. Central to this algorithm is the concept of a region, which is a group of pixels of the same class that are spatially connected. In the currently implemented version of the program, diagonal connections satisfy the spatial connectivity criteria.

The first step in spatial filtering is the removal of all single pixel regions. This step is accomplished by passing a 3-by-3 moving window over the image and checking for the situation in which none of the eight neighboring pixels is the same class as the center pixel. When this situation is encountered, the class of the center pixel is changed. The criterion used to determine the class of the center pixel has been changed from the original algorithm of Peet and Davis. In the original algorithm, the classes are assumed to be nominal and a simple majority (or plurality) rule is used for class conversion. In the version implemented for FOCIS, the classes are assumed to be at least weakly ordinal and a priori class conversion weights are used (Table 1). In this approach, the counts of pixels in each class in the surrounding window are multiplied by the class conversion weights and the class with the largest value of

966

the resulting products "wins" the center pixel.

Creation of the region table is the second step in the spatial filtering process. An entry is made in the region table for each region in the image that stores, among other things, the number of pixels in the region, their class, and the prequency of occurrence of each class in the perimeter pixels bordering on the region. Diagonal pixels are considered to be bordering on regions and are thus part of the perimeter. The entries in the region table are sorted by size and row number before use in region conversion, the third step. In region conversion, each region is evaluated in turn. If the region is larger than the minimum size specified by the user for that class, then the region is not changed. If the region is below the minimum size, then the entire region is converted to another class depending on the class composition of the surrounding pixels. The class conversion weights are used in this step in the same manner as before. The pixel counts for each class in the perimeter are multiplied by the class conversion weights, and as before the largest value determines the new class. Following class conversion, a region table entry is created for the new region that includes the current region, and all entries of other regions that are subsets of the new region are removed. If the new region does not meet the minimum size requirement, then it is converted to a new class in the same manner as before. In this way each region is evaluated until all regions in the image meet the minimum size requirement for their respective classes.

One result of the spatial filtering of the classified image is that pixels change classes. Because the larger classes will tend to be more frequently represented on the perimeter of a region, large classes tend to grow while small classes shrink. However, class conversion weights can be used to reduce the magnitude of the effect. For the Eldorado inventory, the final class conversion weights are shown in Table I. These weights were determined a priori, based on the experience of the investigators. The weights were chosen to minimize the conversion of pixels between forest and nonforest types. Within timber strata, weight reduction increments of 0.3 and 0.2 were used for differences in stocking and size, respectively.

If the original classification is accurate, the spatial filtering algorithm will degrade accuracies by adding pixels to classes they do not represent. This added variance is an undesirable by-product of producing a stand map with improved spatial coherence. However, the Forest Service has the same problem with manually delineated timber stands required to conform to a 5 or 10 acre minimum. In this situation, the photointerpreter is required to add to an adjacent stand all areas too small to exist as separate polygons. The resulting effect will increase the standard errors of the estimates of timber volumes for individual strata, but for the Forest Service the cost in accuracy is worth the trade-off to obtain a more usable map product.

For the Eldorado inventory, a ten-acre minimum was used to produce some trial images of selected areas. Figure 2 shows a classification both before and after simplification; it also includes a Landsat Band 5 image for orientation. In the classification images, each geometric symbol represents a different class. The original classification exhibits a high degree of spatial variability, whereas the spatially filtered image is much more generalized. USFS Region 5 personnel inspected these and other images produced with differing minimum sizes and selected a six-acre minimum as most appropriate to their needs.

4. INTERFACE WITH FOREST SERVICE
GEOGRAPHIC INFORMATION SYSTEM

Conventional USFS procedures for the inventory of a National Forest begin with the manual interpretation of low altitude aerial photographs. Timber stand polygons that are delineated by this process are transfered to 7/12 minute quadrangle base maps and drafted on stable-base mylar material. The stand maps are then photographed and digitized by scanner (or optionally, by coordinate digitizer) to convert them into electronic computer format for entry into the Forest Service's Wildland Resource Information System (WRIS), (Russell et. al., 1975a, 1975b).

967

WRIS is a vector- (polygon-) based geographic information system primarily designed for timber management use. It "provides a means of collecting, processing, storing, retrieving, updating, and displaying geographic data, and makes possible the performance of logical operations on these data", such as merging, overlaying, and area measurements (Russell et. al., 1975a). WRIS is coordinated with other USFS software that processes field sample data to yield timber inventory statistics. The system operates on a UNIVAC computer, although an IBM-based version called RID*POLY has been developed. The acronyms WRIS and RID*POLY are often used interchangeably.

For the FOCIS inventory of the Eldorado National Forest to be usable by the USFS, the timber stratum map and data must assume a format acceptable for entry into WRIS. Unfortunately, the stratum map is in raster image format, which is not directly compatible with the vector polygon format required by WRIS, so a raster-to-vector conversion program was written to facilitate this process. The basic algorithm was developed by David A. Nichols of JPL and consists of three separate tasks. (1) The first task involves identifying all raster polygons in the image. A raster polygon is defined as any number of horizontally or vertically contiguous pixels of common label. The pixels in each raster polygon are assigned a new common label which is unique to each polygon, and the image is output with an accompanying directory for relating class labels to the new unique label system. (2) The second task involves creating the line segments that define the polygon boundaries. Nodes are labeled and the two adjacent polygons identified. (3) The final task traverses the polygon boundary file to connect appropriate adjacent line segments and produce a vector file. The Nichols algorithm codes polygons in a clockwise manner. Islands coded twice: first in a counter-clockwise manner and stored at the end of the host polygon's coordinate string, and then again as a separate regular polygon. Lollipops (i.e., islands connected by one node to the host polygon) are treated as regular polygons. The raster-to-vector conversion algorithm was coded into the VICAR system and named RASTOVEC. An algorithm for reliably determining centroid coordinates was also developed and incorporated into RASTOVEC.

The Eldorado timber stratum map produced by FOCIS was processed using the spatial filtering algorithm described above and subdivided into 7-1/2 minute quadrangles (each 234 lines by 189 samples with one acre pixels). Each quadrangle was then individually processed by RASTOVEC. A final program called WRISOUT was developed to convert the vector data produced by RASTOVEC into a form directly acceptable by WRIS. The WRIS system has a special, highly structured card-image-based format referred to as the "Universal Data Exchange Format" (XCH6) for transferring data between different computers. The WRISOUT program converts the RASTOVEC output into this format. At the same time, it allows numerical class labels to be replaced with alphanumeric labels, and performs some minor processing of the vector data to suit the specific requirements of the WRIS system. A final step before FOCIS-produced forest stratum data can be used by the USFS involves modification of the WRIS system. As the system is presently implemented, polygons islands are not permitted. This capability will soon be added to the WRIS system (Russell, 1982).

5. REDUCING THE INFLUENCE OF TOPOGRAPHY

Another topic that has received recent attention is a classification procedure designed to reduce the adverse effects of local topography. While this research is still evolving, it should eventually provide a more reasonable approach than the ad hoc illumination masking procedure presently used in FOCIS. Problems associated with local topography are attributed to the topographic effect, which is defined here as the difference in radiance received at a sensor from the same cover type due to variation in local topography. Two principal components of the topographic effect are: (1) variation in incident irradiance due to varying illumination angles; and (2) the bidirectional reflectance distribution function (BRDF) of surface cover types. Past approaches to reduce the topographic effect in Landsat imagery have been dominated by correction for variation in illumination angle (Struve et. al., 1972; Hoffer and Staff, 1975) and by band ratioing (Kriegler et. al., 1969). Justice et. al. (1981) tested these approaches and found them to be of little help. Smith et. al. (1980) proposed a method of correcting the spectral data that requires empirical calibration; while this

approach shows promise, it may require separate calibration for individual cover types due to variation in BRDF's. This situation would require knowing the cover type of each pixel in the image prior to preprocessing the data. However, since a cover type classification is often the desired product, knowing cover type a priori may obviate the need for the image correction procedure.

Although past attempts to correct the Landsat values by dividing by the cosine of the illumination angle have been unsuccessful in reducing the topographic effect (Struve et. al., 1972; Hoffer et. al., 1975; Justice et. al., 1981), the including of a channel derived from the cosine of the illumination angle in the classification has been shown to improve classification accuracy. This apparent contradiction may arise because dividing by the cosine factor requires the Lambertian assumption, namely that the reflectance is proportional to the cosine of the illumination angle; this assumption is known not to hold well for natural vegetation types in areas of diverse topography. Including the illumination angle channel in the classification allows for explanation of variance in the spectral data without specifying the Lambertian model. This situation is similar to the results found by both Cicone et. al. (1977) and Justice et. al. (1981) that a modified form of the cosine factor produced better results than the approach restricted to the Lambertian assumption.

A new classification approach intended to reduce the influence of the topographic effect is to include illumination and reflection variables along with the spectral data in conventional unsupervised clustering and classification procedures. Full details of this procedure and the results of tests of its effectiveness are given in Woodcock (1982). The illumination and reflection variables to be used in the unsupervised classification are the cosine of the angle of illumination (θ_0), cosine of the angle of reflection (θ_r), and the azimuth of reflectance (ϕ_r) measured with respect to the azimuth of the sun. These variables cover all possible combinations of sun/surface/sensor geometry and completely specify the BRDF. By including illumination and reflection variables as channels in clustering and classification procedures, the resulting classes are constrained to be similar spectrally, while at the same time including only picture elements having similar illumination and reflection geometry at the time of the sensor overpass. Note that the illumination and reflection variables should be independent of the surface cover types but correlated with the spectral data, and should be of value in discriminating cover types only when used in combination with spectral data.

An advantage of this approach is that the nature of the bidirectional reflectance distribution function does not need to be specified. Instead, a new assumption that the BRDF does not change sharply over small ranges in the angles of illumination and reflection and azimuth of reflection is necessary. Essentially, the new assumption is that the BRDF's are smooth, gradually changing functions, as opposed to spiked, or stepped functions. This assumption is supported by the measurements made by Coulson (1966) and Kriebel (1978).

Images of θ_0, θ_r, and ϕ_r were calculated for a small test area in the Klamath (Figure 3). A stepwise discriminant analysis using the three illumination and reflection variables as channels in addition to the four Landsat MSS spectral bands evaluated the relative contribution of each to differentiating a set of forest cover types. The order that the spectral, illumination, and reflection variables entered the stepwise discriminant analysis was used to test the increment of improved classification accuracy achieved by including the various channels. Two methods for weighting the variables in the classification trials were also tested. One set of classifications was performed in which input channels were standardized to a mean of 128 and a standard deviation of 32. The second set of classifications used the raw Landsat bands and empirically scaled illumination and reflection variables. In addition to performing classifications using combinations of spectral and illumination and reflection variables in their order of entry in the stepwise discriminant analysis, classifications were performed using only the four spectral channels. These classifications serve as controls for the experiment, providing a standard to which the other classification trials can be compared.

The back-classification accuracies for all combinations of input channels

969

and weighting factors are plotted as a function of the channels used in the particular classification trial in Figure 4. Classification trials using the same channel weighting strategy are connected by line segments to highlight trends in accuracy. The accuracies of the classifications using only the four spectral channels for both weighting strategies are plotted as horizontal lines to form a standard baseline of comparison. The highest classification accuracies were achieved in both sets of trials when only Band 5, Band 6, and the cosine of the angle of illumination image were used. There was a general decline in accuracy as additional channels were added to the classification. This finding does not necessarily indicate that these channels do not contain any additional information for discriminating cover types, but may be the result of the nature of the unsupervised clustering algorithm used in the analysis, which assumes equal weight for variance in all channels. In this case, adding an additional, equally weighted channel reduces the discriminating power of preceeding channels proportionately; the discriminating power lost may be sufficiently great to overcome the additional power gained by adding the new channel.

Although the improvements in accuracy were limited, the idea of using the angle and azimuth of reflection in the classification process should not be abandoned on the basis of the results of this study. The Landsat MSS is essentially a nadir pointing sensor; however, the Thematic Mapper aboard Landsat D will have viewing angles much wider than the multispectral scanner. Because of the position of the Klamath study area, the angle of reflection from a horizontal surface was only 2 degrees from vertical in this dataset. As the sensor is further from nadir, the value of the angle and azimuth of reflection should become more important.

6. CONCLUSION

In automated processing of natural vegetation imagery, two critical problems arise -- first, variation in spectral signatures due to differential illumination caused by rugged terrain; and second, high pixel-to-pixel variability arising from normal variation in the size, spacing, and form of the plants that constitute natural plant communities. The illumination masking method originally developed for FOCIS is a satisfactory solution to the first problem, but it is somewhat unsatisfactory because it requires another empirically calibrated step. Hopefully, the direct use of data channels derived from illumination geometry will, when operational, automatically compensate for the differential illumination effect and increase classification accuracies. For the second problem, the simplifying algorithm of Peet and Davis appears to work well as a postprocessor; however, this technique is but one approach to the area of image segmentation. Hopefully other alternatives that can exploit the inherent characteristics of natural vegetation signatures in a functional or deterministic manner will arise as research continues.

Although the Eldorado timber inventory is not yet complete, the application of FOCIS to this new area in California has validated the major principles upon which FOCIS is based -- the use of a standard deviation texture image as an additional channel to aid in discrimination of forest types with open canopies, ecological modeling of species composition labels using registered digital terrain data, illumination masking through calculation of the illumination angle of each pixel, and the independent labeling of large numbers of small, tightly-defined clusters. Early indications are that classification accuracy, as measured by a ground-checked independent stratified random sample will probably exceed ninety percent. In addition, samples of timber strata drawn from the FOCIS classification appear to exhibit good within-stratum homogeneity. Thus, FOCIS presents an operational, if not fully mature, technology to use Landsat and digital terrain data for mapping timber stands and stratifying stands for timber volume sampling and inventory.

7. REFERENCES

Cicone, R.C., W.A. Malila, and E.P. Crist, 1977. Investigation of Techniques for Inventorying Forested Regions. Final Report: Vol II Forestry Information System Requirements and Joint Use of Remotely Sensed and Ancillary Data. NAS-CR-ERIM 122700-35-F2, 146 p.

Coulson, K.L., 1966. Effects of reflection properties on natural surfaces in aerial reconnaissance. Applied Optics, Vol. 5, No. 6, p. 905-917.

Davis, W.A. and F.G. Peet, 1976. The Identification and Reclassification of Small Regions on Digital Thematic Maps. Forest Management Institute, Ottawa, Ontario. Information report FMR-X-90.

Goldberg, M. and D.G. Goodenough, 1978. Analysis of a spatial filter for Landsat imagery. Journal of Applied Photographic Engineering, Vol. 4, No. 1, p. 25-27.

Guptill, S., 1978. An 'optimal' filter for maps showing nominal data. Journal of Research U.S. Geologic Survey, Vol. 6, No. 2, p. 161-167.

Justice, C.O., S.W. Wharton and B.N. Holben, 1981. Application of digital terrain data to quantify and reduce the topographic effect on Landsat. International Journal of Remote Sensing, Vol. 2, No. 3, p. 213-230.

Kriebel, K.T., 1978. Measured spectral bidirectional reflection properties of four vegetated surfaces. Applied Optics, Vol. 17, No. 2, p. 253-258.

Kriegler, F.J., W.A. Malila, R.F. Nalepka and W. Richardson, 1969. Preprocessing transformations and their effects on multispectral recognition. Proceedings of the 3rd International Symposium on Remote Sensing of the Environment, Ann Arbor Michigan, p. 97-106.

Hoffer, R.M. and Staff, 1975. Natural Resource Mapping in Mountainous Terrain by Computer Analysis of ERTS-I Satellite Data. LARS Information Note 061575, Laboratory for Applications of Remote Sensing, West Lafayette Indiana.

Russell, R.M., D.A. Sharpnack and E.L. Amidon, 1975a. WRIS: A Resource Information System For Wildland Management. Pacific Southwest Forest and Range Experiment Station, Berkeley, California, USDA Forest Service Research Paper PSW-107, 12 p.

Russell, R.M., D.A. Sharpnack and E.L. Amidon, 1975b. Wildland Resource Information System User's Guide. Pacific Southwest Forest and Range Experiment Station, Berkeley, California, US Dept. of Commerce NTIS PB-288-048, 36 p.

Russell, R.M., 1982. Letter to J. Levitan, #6610, May 11, 1982.

Smith, J.A., T.L. Lin and K.J. Ranson, 1980. The Lambertian assumption and Landsat data. Photogrammetric Engineering and Remote Sensing, Vol. 46, No. 9, p. 1183-1189.

Struve, H., W. Graham and H. West, 1972. Acquisition of Terrain Information Using Landsat Multispectral Data. Report I of series, Technical Report M-77-2, Engineering Waterways Experiment Station, Vicksburg, Ms, 50 p.

Strahler, A.H., J. Franklin, C.E. Woodcock and T.L. Logan, 1981. FOCIS: A Forest Classification and Inventory System Using Landsat and Digital Terrain. Final Report, NASA contract NAS 9-15509, 60 p.

Woodcock, C.E., 1982. Reducing the Influence of Topography on the Classification of Remotely Sensed Data. Master's Thesis, University of California, Santa Barbara, 69 p.

Woodcock, C.E., A.H. Strahler and T.L. Logan, 1980. Stratification of forest vegetation for timber inventory using Landsat and collateral data, Proceedings of the 14th International Symposium on Remote Sensing of the Environment, San Jose, Costa Rica, p. 1769-1787.

TABLE I. CLASS CONVERSION WEIGHTS

CLASS NUMBER	STRATUM LABEL	0	1	2	3	4	5	6	7	8	9	10	11	12	13	14	15	16
0	Unclassified	1.00																
1	Water	0.01	1.00															
2	Bare	0.01	0.05	1.00														
3	Very sparse vegetation	0.01	0.05	0.80	1.00													
4	Brush with hardwood	0.01	0.05	0.70	0.80	1.00												
5	Hardwood with brush	0.01	0.05	0.60	0.60	0.80	1.00											
6	M4G	0.01	0.05	0.10	0.10	0.10	0.10	1.00										
7	M4P	0.01	0.05	0.30	0.30	0.30	0.30	0.70	1.00									
8	M3G	0.01	0.05	0.10	0.10	0.10	0.10	0.80	0.70	1.00								
9	M3P	0.01	0.05	0.40	0.40	0.40	0.40	0.50	0.80	0.70	1.00							
10	Plantation	0.01	0.05	0.20	0.20	0.20	0.30	0.40	0.40	0.40	0.50	1.00						
11	R4G	0.01	0.05	0.10	0.10	0.10	0.10	0.10	0.70	0.30	0.50	0.30	1.00					
12	R4P	0.01	0.05	0.10	0.30	0.30	0.30	0.70	1.00	0.70	0.80	0.50	0.70	1.00				
13	R3G	0.01	0.05	0.10	0.10	0.10	0.10	0.80	0.70	1.00	0.70	0.30	0.80	0.70	1.00			
14	R3P	0.01	0.05	0.40	0.40	0.40	0.40	0.50	0.80	0.70	1.00	0.60	0.50	0.80	0.70	1.00		
15	A3G	0.01	0.05	0.10	0.10	0.10	0.10	0.80	0.70	1.00	0.70	0.30	0.80	0.70	1.00	0.70	1.00	
16	A3P	0.01	0.05	0.50	0.50	0.70	0.10	0.10	0.10	0.70	1.00	0.60	0.10	0.10	0.70	1.00	0.70	1.00

Table 1. Class conversion weights used in spatial filtering algorithm.
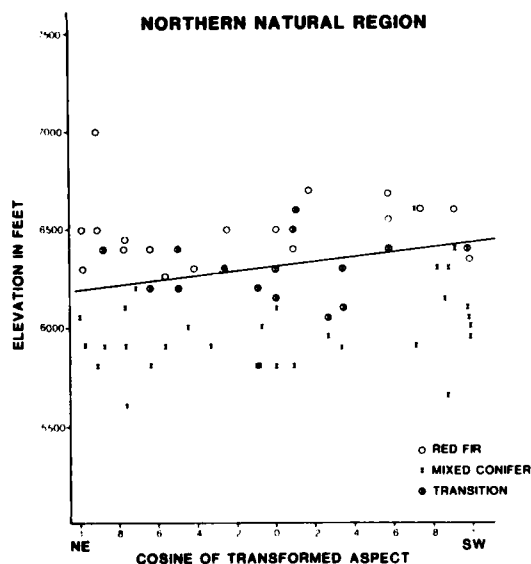
Figure 1A. Regional type graph for the Northern Natural region, Eldorado National Forest. This graph was used for regional type labeling and definition of the natural region boundary.
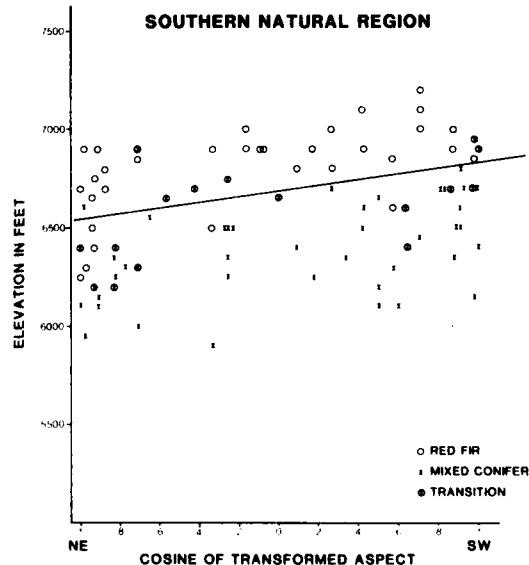
Figure 1B. Regional type graph for the Southern Natural region, Eldorado National Forest.

972

Figure 2A. Original classified image of a test area in the Eldorado National Forest. Each geometric symbol represents a different cover type.

Figure 2B. Spatially filtered image of the area shown in Figure 2A with a 10-acre minimum area for cover types.

Figure 2C. Landsat Band 5 image for the test area, shown for orientation.

Figure 3A. Image of the angle of illumination ( ) for a test area in the Klamath National Forest.

Figure 3B. Image of the angle of re-
flection (O_r) for the Klamath test area.
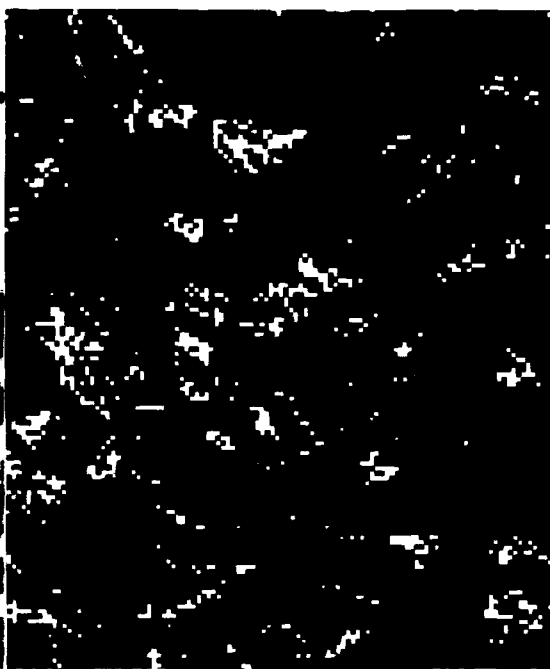
Figure 3C. Image of the azimuth of
reflectance (ϕ_r) for the Klamath test
area.

CLASSIFICATION NUMBER AND VARIABLE ADDED
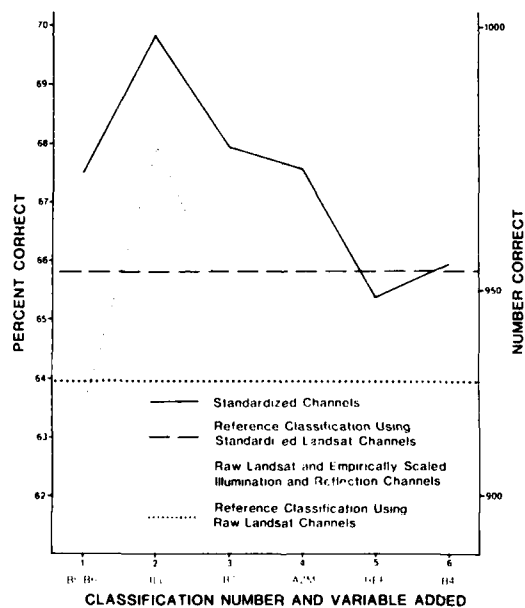
Figure 4. Graph of classification
accuracies for all combinations of in-
put channels and weighting factors
plotted as a function of the channels
used in the particular classification
trial.

974

A NEW VERSATILE REFLECTANCE SPECTROMETER AND
THE MEASUREMENT OF SPECTRAL SIGNATURES OF OBJECTS
IN REMOTE SENSING RESEARCH

R.A. Buckwald
D. Cabib
T. Florentin
E. Sapir

C.I. Ltd.
Ramat Yishai, Israel

SUMMARY

The ever growing applications of infrared remote sensing for research in geology, botany, and natural resource studies have been spurred by the recognition that the reflectance spectra of many materials and plants in the visible, near infrared and infrared regions of the spectrum can give very indicative character signatures. One of the most interesting and promising effects today is the shift of the chlorophyll absorption edge due to stresses, maturation, etc. In other cases the relative reflectance between different spectral bands can be shown to yield useful information.

We describe in this paper a new instrument especially designed for field measurements of spectral reflectance signatures of rocks and plants, an instrument which will fill a specific need of the market and will contribute appreciably to the advancement of remote sensing radiometric research. The main characteristics of the instrument are:

1. Spectral range from 0.4 to 2.5 μm, and farther infrared as an option.

2. Instantaneous ratio out with respect to a diffuse reference, sky or other, with continuous scanning of the wavelength.

3. Large parabolic collecting optice (5") for high sensitivity and dynamic range.

4. Rugged for field use.

5. Microprocessor data handling with spectral signal averaging, differencing, ratioing, and standard interfacing with recorders and with large computers.

Examples of outdoor measurements will be given, with a block diagram of the functions and more of operation of the instrument, including data processing options and calibration procedures.

INTERPRETABILITY OF LANDSAT IMAGES FOR PHYSIOGRAPHY AND SOIL MAPPING
IN THE SUB-HUMID REGION OF THE NORTHEAST OF ARGENTINA

J.M. Sayago

Faculty of Natural Sciences
National University of Tucumán
San Miguel de Tucumán, Argentina

ABSTRACT

The full incorporation of the extensive sub-humid Chaco region to the farmingcattle activity demands, as a previous condition, the systematic and integrated inventory of its natural resources, through which land capability and priority areas of development are defined. LANDSAT images, shown up in recent years, could further the fulfilment of such objetives since this information is inexpensive, of acceptable planimetric accuracy, and periodically available.

The present paper deals with the possibilities and limitations of using such information in mapping on small scales the physiography and soils in a region representative of the environmental conditions of the "sub-humid Chaco". First, the morphogenetic characteristics and the relief-soil relations of the units in the studied area are described, and methodological cryteria and technical recommendations for mapping on small scales are included. Finally, interpretability of images as to distribution, characterization, dynamics and soil aptitude is evaluated.

INTRODUCTION

In a world threatened by a food crisis, our country should find a priority objective in increasing its primary production. To achieve this objective implies, among others, such aspects as the yield increase in the now existing productive areas and or the incorporation of still under-developed or not productive large spaces.

The development of border lands demands careful planning, one of whose essential pre-requisites is the systematic inventory of its natural resources. In this sense, greater importance is being as signed day by day by planners to thematic mapping on small scale in geological, geomorphologica¹, etc. aspects, which, integratedly analyzed, permit defining land capability choosing areas of priority development, or establishing the type and intensity of more detailed studies.

In recent years, the use of satellite images due to the large surface range, acceptable planimetric accuracy and posibility of repetitions, has contributed to transform schematic or surveymapping in to a technical-scientific document which is accurate, speedy and cheap. Unfortunately, there is a notorious lack of information about the technical features, interpretation possibilities and practical limitations of such images for our enviromental conditions. And there is also a lack of methodological cryteria about its use on small scale.

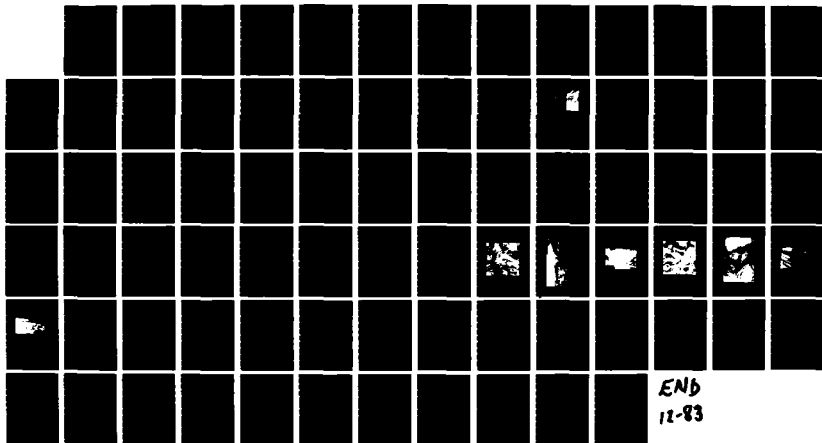This paper is a contribution to the knowledge of physiography and soils in
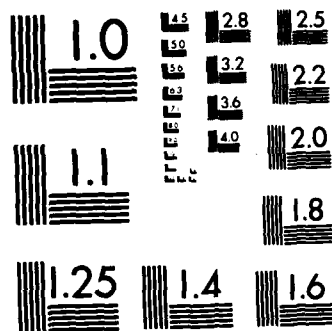
977

MICROCOPY RESOLUTION TEST CHART

NATIONAL BUREAU OF STANDARDS-1963-A

an area which typifies the conditions of the extensive semiarid and sub-humid
Chaco region and, at the same time, it presents methodological cryteria for
regional studies with LANDSAT images, evaluating their interpretability, advan-
tages and mapping limitations.

I . DESCRIPTION OF THE AREA UNDER STUDY

Situated in the transition between the pampean and Chaco regions, this
area includes five large physiographic units*, the denomination of which indi-
cates a distinctive morphogenetic character added to its traditional name. The
map included in this paper is a schematic synthesis of survey mapping on a
1: 500,000 scals.

The Aeolic Pampean Plain

As a northern extension of the pampean plain, this unit has geomorphic
elements characteristic of the same, coexisting sporadically with forms belon-
ging to the Chaco environment.

The genesis and evolution of the unit is dominated by the influence of a
sub-recent period of loess erosion-sedimentation, whose paleofeatures, although
masked by farming occupation, characterize today's landscape.

The loess materials which cover with marked homogeneousness the whole unit
would indicate formational arid to semi-arid conditions whose age, since TRI-
CART'S investigations (1971), should be attributed to the last glacial period**.
Nevertheless, evidence of the existence of an arid Holocene happening - after
a humid post-glacial period GROEBBER (1958), BRADBURY and MARKGRAF (1981),
appears when comparing in the Chaco plain the lesser pedogenesis of loess soils
in relation to those developed on paleoforms attributed to the mentioned plu-
vial period.

The aeolic pattern is shown fundamentally by a dynamics of deflation,
expressed in ondulated planes, depressions and parabolic dunes, masked in great
part by natural or cultivated vegetation. The deflation depressions seem trans-
formed into hydroaeolic depressions due to a humid post-depositional period,
also shown in edaphic characteristics.

The present morphodynamic processes are represented by sheet erosion and
removal of slow mass spiding, brought about by deforestation and overgrazing,
a reiterated situation in the whole studied area.

In the regional distribution of soils a close relationship between rainfall
gradient and soil development is shown. With the increase of rainfall, soils
acquire greater development in a northwest-southeast direction, changing from
typic and aridic Haplustolls in the northwestern part, to typic and udic Argius
tolls in the southeast.

The old alluvial migratory plain of the Salado-Juramento

The area under study is the southern extension of the western Chaco plain,

---

* The term "physiography" is used as synonym to "geomorphology" indicating the
  part of natural landscape that fits into a characteristic soil pattern.

**Tricart featured the environmental conditions of the quaternary glacial pe-
  riods in the pampean plain as being cold and dry, alternanting with warm and
  humid interglacial periods.

whose distinctive geomorphological features are the relict forms of an ancient fluvial system of the Salado-Juramento, which migrated over a great part of the territory of the Santiago del Estero and Chaco provinces.

Practically overimposed on the aeolic pampean region, the morphology of this region shows coexistence of a typically aeolic relief together with buried or non-active paleofluvial forms.

The development of this system is related to a humid period of the Holocene, characterized by a fluvial dynamics of great competence, succeptible of moving materials to long distances, favored by the existence of an older loess cover which, by making the soil water-tight, facilitated runof. The morphologic pattern is that of river beds or channels, partly buried or invaded by natural vegetation which alternate with interfluvial planes affected by aeolic action. The pattern of old runoff is irregular, sometimes straight, other times meandering or trellis, which shows a constructional dynamics of currents which are relatively strong but ephemeral for lacking depositional recurrence.

Two characteristic paleoforms are distinguished: the typical paleochannels and the overflow splays. The paleochannels present a leves of variable height, with a bed that still maintains the primitive features of the primitive covex profile. The overflow splays developed as a consequence of local changes of topographic gradient, look like an alluvial fan as much for their morphographic as for their sedimentological characters.

In this unit there is a close relationship, at a regional level, between pedogenetic development and rainfall gradient. In this sense, the typic Hapwstolls of the northern limit of the pampean plain give way to aridic Haplustolls and Salortids in the western part of the unit. At a local level there is evidence of the influence of the paleochannels on greater pedogenetic development shown by the presence of entic Haplustolls in an area of predominant aridic soils.

The alluvial overflow Salado plain

The low river basin of the Salado in the southeastern part of Santiago del Estero shows the typical conditions of rivers which flow through the flat Chaco plain: recurrence of seasonal floods, periodically increased to a disastrous degree by the influence of land occupation along and across its basin.

The epigenesis of the present Salado course is a still unclear point. One hypothesis says that it settled in a very recent pariod of the Holocene as culmination of its migration to the southeast, integrating the paleofluvial system of the Salado-Juramento. Another possibility is that it has coexisted contemporarily with the development of that system, forming part of the low basin of the Dulce River, to occupy later the present cutline by transfluence or capture.

Whatever its origin may be, in the morphogenetic evolution of the present river bed, two priods are set off clearly shown in their internal geomorphic elements. The first, previous to human occupation, is characterized by the development of the meander band, the levees and depressions of back swamps, which are signs of a typical constructional regime of overflow. The second period starts with the falling of extensive forest masses situated in the river influence area, which brought about soil degradation and transportation of the denudated materials, beginning a process of infilling, which was accelerated when farming occupation started.

The progressive infilling of the alluvial plain, added to the increase in runoff by deterioration of soil infiltration, intensified the normal or extra-

979

ordinary floods covering extensive areas formaly not soaked, with their harmful effects on soils, vegetation and underground water.

As a consequence of the process described, the morphogenesis not only has conditioned the original pedogenesis, but is also quickly transforming the endoge nous characters of many soils. In the interfluvial not soaked planes there still subsist well drained soils without hydromorphic problems(Haplustolls), which have given way to hydromorphic and alkaline soils (uftalphic Argiustolls and Natracualfs).

The western dorsum (Sachayoj-Pozo del Toba)

Disturbing the extreme uniformity of the western Chaco plain, in the centereast of the province of Santiago del Estero, there appears a set of smooth hills and shallow valleys, which extend from southwest to northeast decreasing in width, over an extension of approximately 150 kilometers.

It is called dorsal for the evident structural influence of its geomorphological style, manifest in the highest regional position, in the meridian course of the eastern adge that separates it from the "Bajos Sub-meridionales" and in the recurrence of internal geomorphic elements.

The development of this unit-posterior to the primitive tectogenesis is dominated by an erosive dynamics, clearly displayed in U-shaped and V-shaped vales. The slight esplanades that concur in shallow talwegs without concentrated runoff, indicate an evolution under arid to semi-arid climate in which the sheet flow flattened the relief and transported fine materials toward the talwegs.

A more recent arid period (Holocene?), preceded by a humid event that did not affect the previous geomorphic style, covered the area with a relatively mighty loess layer that "fossilized" the relief and obstructed the drainage net, whose reordainment in present environmental conditions is difficultly done.

A sub-present period of intense hydric erosion, produced by the dissappearance of the forest masses that covered the region, acquires particular importance in the geomorphological evolution of this area. Favored by extended slopes and high erosionability of loessic materials, rills and even in gullies, reached a severe degree. The regeneration of natural vegetation after felling facilitated stabilizing erosive forms, although the farming stage already begun, will probably contribute to start the process again, unless adequate conservationist practices be applied.

The concept that "every soil is a landscape" is evident in this unit with great clearness. In the vales, the slope conditions the runoff and the consequent edaphic development, with udic Argiustolls in the talwegs and typical Haplustolls in the mid and high slopes. The interfluvial aeolic, planes covered with slightly modified loessic materials, present soils with less genetic development (aridic Haplustolls). Altohough dependent on the influence of local or regional relief, there is also noticeable in the edaphic development a lessening of rainfall to the West, evident in the growing presence of aridic soils

Western depressions of the Bajos Sub-meridionales

To the South of the dorsal Sachayoj-Pozo del Toba, contrasting with its morhostructural style, there appears a set of depressions of saline concentration that extend to the East of the Santa Fé Bajos Sub-meridionales.

The most conspicuous internal geomorphic elements are the salt lagoons, the periodically flooded lowlands and the hilly margin. The first constitute the principal collectors of runoff from the surrounding areas. Subject to the seasonal and multi-annual fluctuations, hydric dynamics has an irregular charac ter that shows in the variability of the area occupied by lentic bodies. Today

they have lost their primitive pattern by infilling and increase of the perio-
dically flooded area, mixing up with the extensive soaked lowland that extends
to the east into the Bajos Submeridionales and to the Southeast into the aeo-
lic pampean flatland.

A set of flat hills looking like levees border the depressions by the
South and Southwest. The saline character of its materials would indicate
that they were formed during an arid period in which the lagoons - turned into
actual salines transformed fine materials into micropolyhedrons, which the
wind deposited in peripheric areas. When these hills become lower, paleochannel
of the early Salado system appear isolatedly, which carries within morphocro-
nological implications of great interest.

*Despite having been affected by paleoclimatic fluctuations already cited
for the other units, the present morphodynamic processes are the ones most
relevat to the shaping of relief.* Degradation of the higher areas produced the
increase of normal runoff by lessening infiltration of soils and, at the same
time, transporting denudated materials toward depressions. The most direct
effect of its infillling was shown in the extraordinary increase of the pe-
riodically flooded areas and its incidence on soils and vegetations, formerly
not subject to soaking. Furthermore, affecting a still larger area, the ground
water layer nearby has produced salination and saturation of the soils and de-
gradation of the non-saline communities.

In this unit the development of soils is not only conditioned by relief,
but the pedogenetic characters confirm the described stages of geomorphologi-
cal evolution. Thus we can see in the permanent soaked planes the predominan-
ce of halohydromorphic soils (Natracualfs), while on the sporadically soaked
plain and on the border, early prairie soils (Haplustolls) appear today affec-
ted by hydromorphic (acuic Haplustolls) or halomorphic (salortidic Haplustolls)
conditions.

II . THEMATIC MAPPING ON SMALL SCALES

Despite their usefulness in several aspects of regional development, only
in recent years have surveys of exploratory or reconaissance type been paid
attention to in our country. The cause of this was certainly not lack of know-
ledge about their applied possibilities; limitations regarding their poor pla-
nimetric reliability and excessive generalization of information contributed
to diminisch the practical usefulness of them.

The lack of a reliable planimetric base has been an important difficulty
to get trustworthy maps. The reduction of aerial mosaics on greater scale,
carried distrrsions of the original aerial photographs over to the final map.
On the other hand, the regular planialtimetry on small scale, usually made by
compilation, did not offer an acceptable fidelity. In sum, "the realization of
this kind of survey was considered difficult and extremely expensive except in
those regions where making them was possible through compilation of already
existing maps of greater detail"(VAN BARNEWELD, 1971).

The use of satellite images(LANDSAT) opened favorable perspectives to
eliminate such obstacles, since the uniform covering, planimetric reliability
and the possibility of reproduction on several scales increased their planime-
tric accuracy, while greater resolution and multispectral character benefited
their interpretability.

Types of surveys

The exploratory and reconaissance surveys of physiography and soils can
be grouped as follows: 1) those based exclusively on soil properties, where

981

mapped units are defined in conventional terms of morphology and taxonomic classification; and 2) those multidisciplinary or "integrated surveys" defined in terms of landscape-soil relations.

The demands of economic development justify the need of multidisciplina ry survey of natural resources with its advantages of speed, integrality and economy. "A careful integrated work, with good information on soils and their relation with physiography - achieved with adequate field study, good taxono- mic correlation and determination of use limitations - may result in as much as or more application than any other conventional method" (ETCHEVHERE, 1976).

Methodological aspects

A reconaissance mapping on a 1:500,000 scale of the southeast of the pro- vince of Santiago del Estero by means of the intense use of LANDSAT images, led to the definition od some cryteria which permit adequating the known con- cept aspects to the use of satellite images.

The proposed methodology has been divided into three main stages, each one equally important, and on whose fulfilment will depend the quality of the fi- nal product.

a) Planning

In the beginning stage, the purpose of the survey must be defined and the objectives to be reached to get the desired result should be establiched. This calls for decisions about scales and other characteristics of the final map which, in turn, requires a careful election of satellite images, base map and reference material.

Particular attention should be paid to the election of the characteris- tics that the images should have. In farming areas, it will be important to know the calendar of predominant crops, to select the most favorable period to establish the physiographic soil units through satellite images. In natural vegetation areas, it will be important to know its response to seasonal clima- tic variations and, particularly, the spectral characteristics of the diverse physiognomies in relation to such changes.

b) Preparation

The importance of this stage appears from the close relationship among the steps which make it up. The preliminar interpretation permits defining the methodology and classification type, which in turn conditions the techni- ques for interpretation.

The preliminar interpretation rests on three essential aspects: experien- ce in interpreting LANDSAT images, knowledge of the subject under study and of the surveyed region. Considering the nototious lack of basic information in large regions of the country, interpretation will be more efficient if it is done by some one who has a good knowledge of the area under study.

Choosing the system of classification in physiography and soils is based on such diverse aspects as the final map scale, the type and intensity of land occupation, availability of human and financial resources, access possibilities etc. In the study of the southeast of Santiago del Estero, GOOSEN'S (1967) "physiographic analysis" was used, based on interdependence between physiogra- phy and external and internal soil conditions, since it adapted perfectly to the use of LANDSAT images. Regarding the satellite material for surveys on small scale in the semi-arid and sub-humid Chaco, we recommend the following: diapositives on a 1:1,000,000 scale (bands 4,5 and 7) to make "diazo" images in false colors, black and white copies on a 1:500,000 scale (bands 5 and 7) of the dry and humid periods within the normal annual cycle and, eventually, a black and white copy on a 1:250,000 scale (band 5) to be used as planimetric base and field control.

The techniques of optical improvement of images offer a wide range, adequate to all economic possibilities, so as to be able to choose, among others, monocular enlargement, binocular enlargement, stereoscopy, image mixture, colour additive viewer, etc.

c) Operation

With the materials and optical improvement techniques selected in the previous stage, there begins detailed interpretation by means of traditional cryteria for detection, recognition, delineation and classification (VAN GENDEREN, et al, 1978) to produce the legend and the preliminar map. To get this preliminar information implies defining the type of material to include, the colours and symbols of the different categories, the integration of mapping units,etc.

The ground controls also depend on the chosen method, topographic characteristics, complexity of the physiographical pattern, accesses, etc. In this paper, taking advantage of the good existing road system, transections were made that permitted efficient sampling end expedient control over accurate interpretation.

III . INTERPRETABILITY OF LANDSAT IMAGES

The lack of objective cryteria regarding interpretation of physiographic and/or edaphic aspects thorugh satellite images in the environmental condition of our country, led us to make an evaluation of several interpretation possibilities which would permit us to define ghide lines applicable to the extensive region known as the semi-arid and sub-humid Chaco.

Planimetric, seasonal and spectral characteristics of images were taken into consideration.

Planimetric characteristics: black and white copies on 1:1,000,000 ; 1:500.000 and 1:250,000 scales were used, which are the most common size in this type of material.

Seasonal characteristics: images taken during the wettest, the driest and transition seasons were used, considering the marked seasonal climatic contrasts and their influence on image interpretability.

Spectral characteristics: the following images were used:

- band 5 (0,6 to 0,7 micrometers)

- band 7 (0,8 to 1,1 micrometers)

- in false colors ("diazo" system)

Character of attainable information

Considering the wide range of satellite information attainable on physiography and soils, increased with the different planimetric, seasonal and spectral combinations, it was decided to evaluate separately the image aptitude of reflecting physiographic and edaphic aspects as to distribution internal characteristic, morphodynamic and aptitude.

DISTRIBUTION: (location, areal extension, homogeneity, heterogeneity, distinctive patterns, etc.)

In soils distribution, it was verified regarding planimetric characteristics, that the 1:500,000 and 1:250,000 scales offered greater advantages, being the first more useful as topographic base and the second for field control. In the seasonal aspects, greater definition was found in summer images, because spectral contrast diminish during the dry season. In this sense, good results were obtained comparing summer and winter interpretations.

Greater interpretability from the spectral perspective was found in the band 5 and 7 combination in black and white, which, because of less tonal

variation, homogenizes patterns and facilitates definition of units, while for a detailed interpretation the tonal richness of the false color image permits noticing any anomalous or interesting element for mapping purposes.

INTERNAL CHARACTERISTICS: (texture, fertility, drainage, permeability, etc.)

The endogenous characteristics of soils were poorly shown. The different scales did not offer any significant difference except the greater limitation of the 1:1,000,000 scale.

The multiseasonal observations and especially those made on summer images gave a better definition of internal drainage conditions, due to the increase of spectral contrasts derived from differences in edaphic humidity.

The combination of bands 5 and 7 and the false color images gave more information about texture and drainage, particularly through indirect signs of vegetation, but with a notable limitation in interpretability of these aspects.

MORPHODYNAMICS: (flooding capability, erosion, water-logged, human action, etc).

The variability of spectral reflection and particularly the possibility of obtaining sequential images in short periods, give the greatest possibilities of interpretation through satellite images to the aspects of environmental dynamics.

In the planimetric characteristics, the 1:500,000 scale appears to be more convenient because it permites set analysis, fairly diminished on greater scales.

The multiseasonal sequence contributed the best combination in response to spectral variability of the area under study, derived from its considerable climatic irregularity.

A combination of bands 5 and 7 favored analysis of the dynamic aspects of landscape, due to its spectral sensitiveness to the changes in vegetation and to the hydric conditions of the land respectively.

APTITUDE: (farming, pasturage, forestal, present land use).

The land capability "sensu stricto" is a factor of difficult valuation through LANDSAT imagery. Only the aspects of present land occupation offer greater possibilities of determination.

CONCLUSIONS

Interpretability of edaphic aspects through LANDSAT images is detailed in the included table, of which we can draw the following conclusions:

1 - The aspects related to environmental dynamics (overflow, erosion, evolution of natural or cultivated vegetation) present the greatest interpretability.

2 - Planimetric distribution (placement, extension, homogeneity, etc.)of the edaphic and physiographic units admits acceptable definition.

3 - The endogenous characters of soils (texture, structure, drainage, development degree, etc.) and land capability are very poorly manifested.

4 - The use of multiseasonal images, by enhancing the spectral contrasts, increases the given information considerably.

5 - The combination of images bands 5 and 7 and/or in false colors, on 1:500,000 and 1:250,000 scales, offers the best interpretation conditions.

REFERENCES

ETCHEVEHRE P. 1976. Normas de reconocimiento de suelos. 2da. Edición actualiza-
da - Unidad reconocimiento de suelos INTA - Castelar.

GOOSEN D. 1967. Aerial photo interpretation in soil survey - soil Bull n°6
F.A.O. Pub.

HILWIG F.W. 1976. Visual interpretation of Landsat imagery for a reconnaissance
soil survey of the Ganges river fan, south west of Hardwar, India, ITC
Journal 1.

MARKGRAF V. and BRADBURY J. 1981. "Climatic History of South America" BOREAS.

NATIONAL ACADEMY OF SCIENCES. 1977. Resource Sensing from space.Washington.

GROEBER P. 1958. Bosquejo geológico y climatológico de Formosa, Boln.Acad.Nac.
Cienc. 40.

SAYAGO J.M. 1976. Utilidad de las imágenes orbitales (LANDSAT) en el inventario
de los recursos naturales, IDIA. INTA n°337-342.

TRICART J. 1971. Geomorfología de la pampa deprimida. Publicación del Instituto
Nacional de Tecnología Agropecuaria - Buenos Aires.

VAN BARNEWELD G.W. 1971. Levantamientos de suelo de reconocimiento. Estación
Experimental INTA. Paraná (Inédito).

VAN GENDEREN J.L., VASS P., FLOCK J. 1978. Guidelines for using LANDSAT data for
rural land use surveys in developing countries. ITC Journal 1.

INFORMATION AVAILABLE (soils)	(Landsat characteristic)									
	PLANIMETRIC			SEASONAL			SPECTRAL (Photograph)			
	1:1.000.000	1:500.000	1:250.000	summer	winter	multi-seas.	band 5	band 7	band 5-7	color compos.
DISTRIBUTION (location, area, pattern)	□	+	+	+	□	+++	+	+	+++	+++
INTERNAL CHARACT. (texture, drainage, etc.)	−	□	□	+	□	+	+	□	+	+
MORPHODYNAMIC (erosion, flood, sedimentat.)	□	+++	+	+	+	+++	+	+	+++	+++
APTITUDE (farm, pasture, forestal)	□	+	+++	□	□	+	□	+	+	+++

QUALIFICATION	
+++ good	□ fairly
+ fairly good	− bad

Table I. Interpretability of soil aspects

985
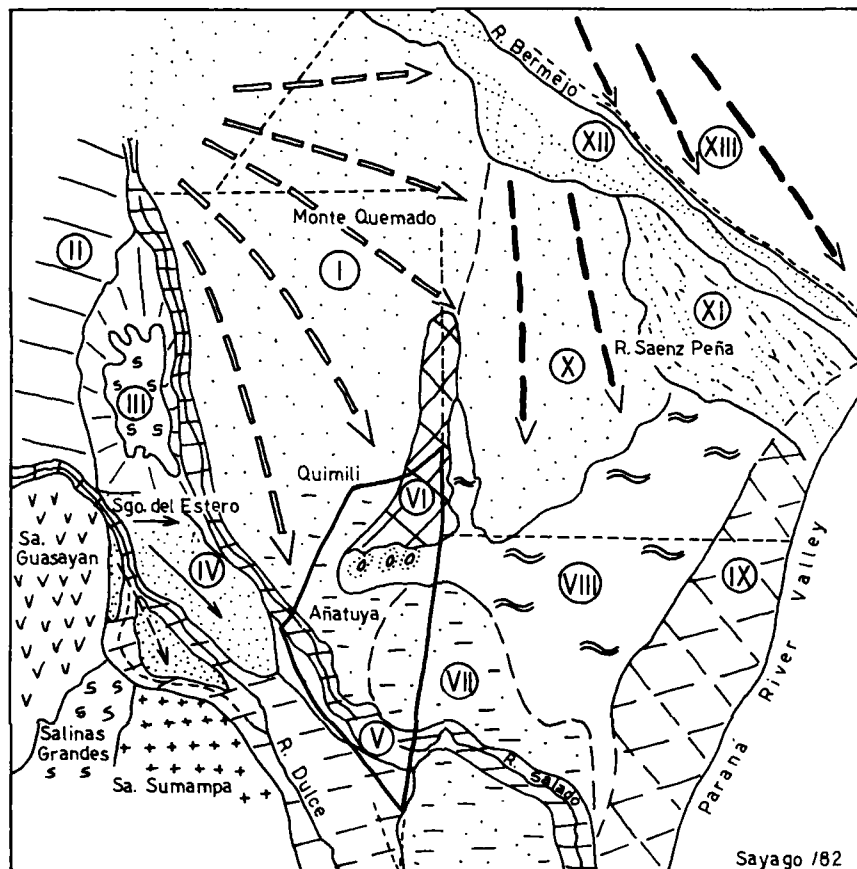
I - Old alluvial migratory plain of Salado R.

II - Eastern tucumán plain

III - Uyamampa salty flats

IV - Alluvial overflow plain of Dulce R.

V - Actual alluvial plain of Salado R.

VI - Western dorsum (Sachayoj-Pozo del Toba)

VII - Pampean aeolian plain

VIII - Lowlands periodically flooded (Bajos Sub-merid.)

IX - Eastern dorsum (Cuña boscosa)

X - Old alluvial overflow plain of Bermejo R.

XI - Sub-recent alluvial plain of Bermejo R.

XII - Actual flood plain of Bermejo R.
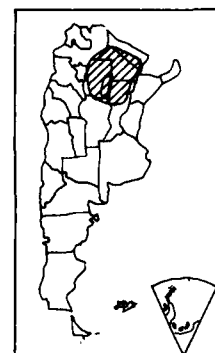
XIII - Old alluvial overflow plain of Pilcomayo R.
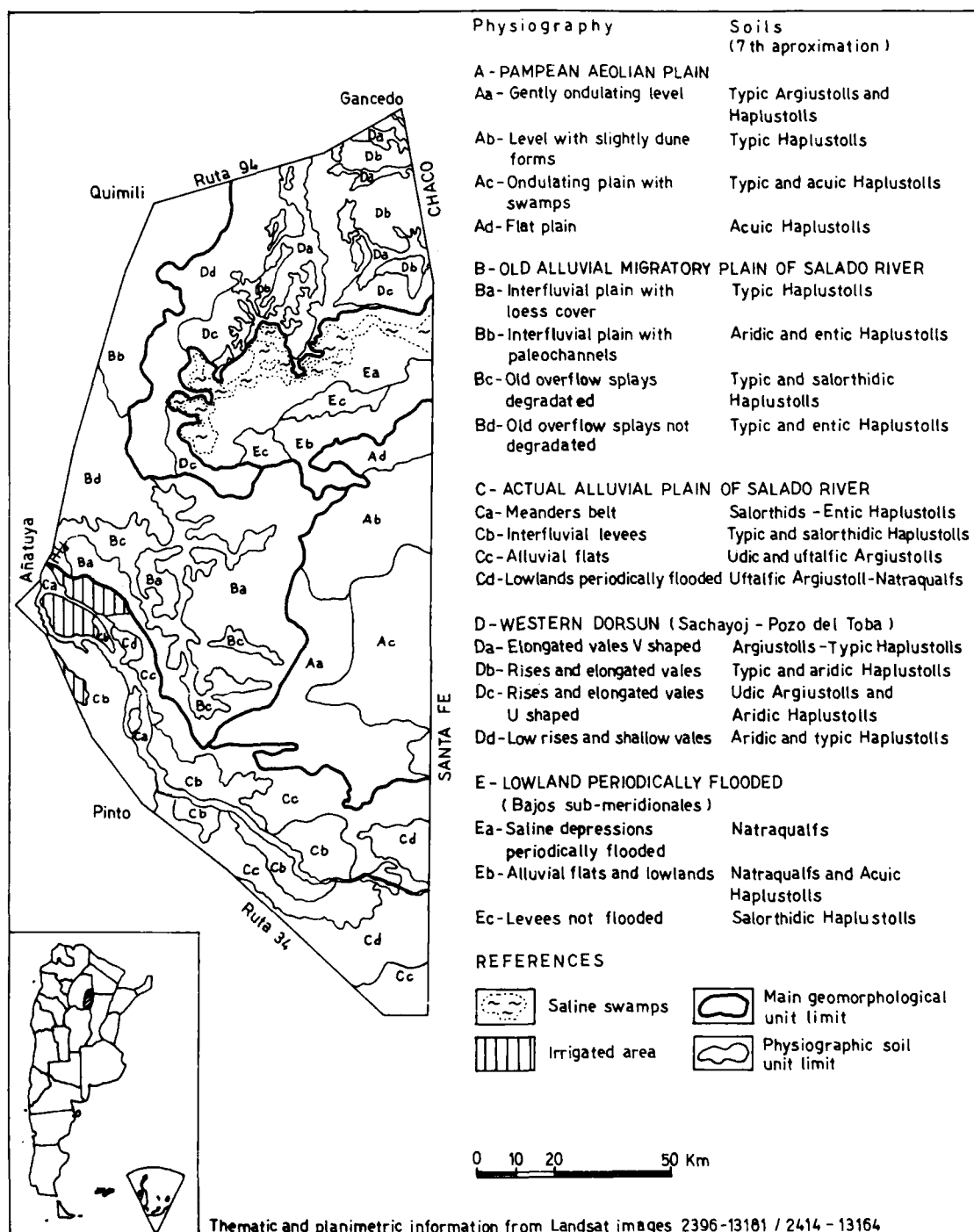
Figure 1. Main geomorphological units of Chaco region

Physiography / **Soils** (7 th aproximation)

A - PAMPEAN AEOLIAN PLAIN
Aa - Gently ondulating level — Typic Argiustolls and Haplustolls
Ab - Level with slightly dune forms — Typic Haplustolls
Ac - Ondulating plain with swamps — Typic and acuic Haplustolls
Ad - Flat plain — Acuic Haplustolls

B - OLD ALLUVIAL MIGRATORY PLAIN OF SALADO RIVER
Ba - Interfluvial plain with loess cover — Typic Haplustolls
Bb - Interfluvial plain with paleochannels — Aridic and entic Haplustolls
Bc - Old overflow splays degradated — Typic and salorthidic Haplustolls
Bd - Old overflow splays not degradated — Typic and entic Haplustolls

C - ACTUAL ALLUVIAL PLAIN OF SALADO RIVER
Ca - Meanders belt — Salorthids - Entic Haplustolls
Cb - Interfluvial levees — Typic and salorthidic Haplustolls
Cc - Alluvial flats — Udic and uftalfic Argiustolls
Cd - Lowlands periodically flooded — Uftalfic Argiustoll - Natraqualfs

D - WESTERN DORSUN (Sachayoj - Pozo del Toba)
Da - Elongated vales V shaped — Argiustolls - Typic Haplustolls
Db - Rises and elongated vales — Typic and aridic Haplustolls
Dc - Rises and elongated vales U shaped — Udic Argiustolls and Aridic Haplustolls
Dd - Low rises and shallow vales — Aridic and typic Haplustolls

E - LOWLAND PERIODICALLY FLOODED (Bajos sub-meridionales)
Ea - Saline depressions periodically flooded — Natraqualfs
Eb - Alluvial flats and lowlands — Natraqualfs and Acuic Haplustolls
Ec - Levees not flooded — Salorthidic Haplustolls

REFERENCES
~ Saline swamps
||||| Irrigated area
Main geomorphological unit limit
Physiographic soil unit limit

0 10 20   50 Km

Thematic and planimetric information from Landsat images 2396-13181 / 2414 - 13164

Figure 2. Phisiographic soil map

987

CROP CLASSIFICATION ACCURACY THROUGH REMOTE SENSING

Norberto Scquizzato

Comisión Nacional de Investigaciones Espaciales
Centro de Sensores Remotos
Buenos Aires, Argentina

SUMMARY

This paper deals with the accuracy in computer aided Landsat MSS data classification and its comparison with the airborne MSS scanner data, having a compatible resolution element, in specific crop applications.

Several aerophotographic flights were carried out together with the multispectral SAMPOI sensor with the subsequent field sample acquisition, over a selected agricultural area of the Province of Buenos Aires for the Argentine Crop Estimation Program (UNDP ARG 78/016).

High density tapes obtained from the flight were converted into computer compatible tapes. The Landsat magnetic tapes and imagery from the above mentioned areas were requested from the CNIE Processing Station.

With these magnetic tapes computer aided classification on the different availability systems are being carried out in the Comision Nacional de Investigaciones Espaciales, aiming to determine the accuracy degree in classification through several methods.

In this way the percentages for the classified areas with the correspondent errors are expected to be obtained.

In the final paper images belonging to the classified and unclassified areas, with copies of the corresponding listings for their processing are going to be presented.

In brief, the paper will be divided in four main parts. These are as follows:

(1) Description of the equipments used;
(2) Description of the classification methods used;
(3) Description of the sample used; and
(4) Results and conclusions.

MODELING SOYBEAN DEVELOPMENT FROM DAYLENGTH AND

TEMPERATURE DATA

Andres C. Ravelo[1], Antonio J. Pascale[2], y Ana M. Planchuelo Ravelo[3]

ABSTRACT

A crop calendar model which tracks the development of a crop is of particular importance to satellite imagery analysts. A soybean growth stage model was developed using an iterative regression analysis (IRA) technique. The IRA relates span of days for soybean growth stages to daylength and daily air temperatures and evaluates the simple and interacting contribution to soybean development of these environmental variables. The effects of daylength and temperature on soybean development were studied in date of planting experiments. Dates for significant crop growth stages such as beginning of flowering, beginning of pod development, end of pod development, beginning of leaf senescence and leaf falling were recorded for three soybean cultivars from maturity group IV (Clark, Bethel and Scott). A total of 16 planting dates at about three-week intervals during seven growing seasons (1962/63 to 1969/70) provided a number of temperature and daylength treatments. In order to test the model, three planting dates selected at random were withheld from the iterative regression analysis. Comparisons of the estimated phenological dates and those observed from the test data provided encouraging results. These suggested that the proposed model can be a useful tool for soybean growth stage prediction.

I. INTRODUCTION

Interpretation of crop development and condition from Landsat imagery can be enhanced by field reports or accurate estimates of the crop growth stages. Unfortunately, such field reports are not always available. Therefore, crop growth stages can also be predicted from weather information. (Robertson, 1968; Phinney and Trenchard, 1977).

---

[1]/University of Missouri, Atmospheric Science Department
701 Hitt St., Columbia, Missouri 65211 U.S.A.
[2]/Facultad de Agronomia de Buenos Aires
Av. San Martin 4453, Buenos Aires, Argentina
[3]/University of Missouri, Division of Biological Sciences,
106 Tucker Hall, Columbia, Missouri 65211 U.S.A.

Temperature summation has proven to be an adequate method of predicting development of field crops, such as corn (Cross and Zuber, 1972), which show only small local variability in daylength response. However, development of soybeans is strongly influenced by photoperiod (Johnson et al., 1960; Pascale and Escales, 1971) and cannot be adequately predicted using temperature summation methods alone (Major et al., 1975).

Robertson (1968) developed mathematical expressions to relate stages of development of wheat to both air temperature and daylength. Robertson's work provided the basis for this study in relating air temperature and photoperiod to soybean growth stages.

The objectives of this study were to develop a soybean growth stage model using readily available meteorological information, to evaluate this model for accuracy in predicting soybean development and to provide useful information to the Landsat imagery analyst on soybean stages of development.

II. DATA

Data maximum and minimum air temperature data for Buenos Aires were obtained for 1962 through 1970.

Estimates of daylength were calculated using the following equation:

$$DL = 7.6432 * ARCOS(-TAN(ALAT*0.01746)*TAN(-23.45* \qquad (1)$$

$$(-COS((JLN+10.5)*0.01746)))*0.01746$$

where: DL is the daylength in hours and decimals,

JLN is the Julian day of the year, and

ALAT is the latitude of the experiment plots.

Three commercial soybean cultivars (Clark, Bethel and Scott), from maturity group IV, were grown in a date of planting experiment at the Facultad de Agronomia, Buenos Aires, Argentina. A total of 16 planting dates at about three-week intervals during seven growing seasons (1962/63 to 1969/70) provided a number of temperature and daylength treatments. Three planting dates selected at random were withheld for model testing. The cultivars selected were part of a larger field experiment (Pascale et al., 1963).

The stages of development recorded were: beginning of flowering (about 10 percent of the plants with at least one flower), beginning of pod development (about 10 percent of the plants had at least one pod of one centimeter length), end of pod development (last pods of one centimeter length have appeared and there are no more flowers), beginning of leaf senescence (about 10 percent of the plants showed yellowish leaves), and leaf falling (more than 50 percent of the leaves have fallen).

The dates of beginning and ending of the growth stages for each cultivar were averaged and these mean dates were used in the analysis.

III. BIOMETEOROLOGICAL MODEL

A mathematical model consists of an equation or a set of equations and represents quantitatively the assumptions or hypotheses that have been made about the real system. The proposed biometeorological model for soybean development has a mathematical expression which relates maximum and minimum air temperatures and daylength to the stochastic value of 1 for each growth stage as follows:

$$1 = \sum_{S3}^{S2} (a_1 (DL-a_0) + a_2 (DL-a_0)^2 * (b_1 (T_m-b_0) + b_2(T_m-b_0)^2 +$$

$$b_3 (T_n-b_0) + b_4 (Tn-b_0)^2) \tag{2}$$

where the a's and b's are regression coefficients,

> DL is the daylength,
>
> Tm is the maximum air temperature,
>
> Tn is the minimum air temperature,
>
> S1 is the date of beginning of any growth stage, and
>
> S2 is the date of ending of the growth stage.

The regresison coefficients were evaluated and tested by an iterative multiple regression technique adapted from Robertson (1968).

IV. MODEL OUTPUT

The biometeorological model for soybean development has been designed to provide the following output after each iteration:

> o A set of regression coefficients for the quadratic and linear form of equation (2) for maximum and minimum air temperature and daylength (Table 1). These coefficients are used to compute the daily effect of air temperatures and daylength on soybean progression towards maturity.
>
> o The estimated dates for the growth stage calculated from the daily input data.
>
> o The difference between observed and estimated growth stage dates, the standard error of estimates and the coefficient of determination for estimated and observed dates.

The iterative regression analysis is continued until the coefficient of determination becomes stable at its highest value or when the standard error of estimates becomes stable at its lowest value.

The regression coefficients developed for each growth stage were used to estimate the number of days for each period. Figure 1 shows the close relation between observed and estimated number of days for the 62 soybean growth periods. In addition, the regression coefficients were tested with an independent set of three planting dates. The results are shown in Figure 2. Most data points fall relatively close to the 1:1 line.

In two cases a solution containing all of the coefficients of equation (2) were not possible (Table 1). The situations which resutled in incomplete solutions were discussed at length by Robertson (1968).

The mean of predicted versus actual development gives the average number of days by which the prediction differed from the actual and the standard deviation gives the standard error of the estimates. Therefore it is desireable that both the mean and the standard error of the estimate be close to zero. Table 2 shows the absolute error of the estimate, the mean and the standard error of the estimate. In addition, the coefficients of determination between observed and estimated dates are presented.

V. SUMMARY AND CONCLUSIONS

The effects of seasonal temperature and daylength patterns on development of three field grown soybean cultivars were studied in date of planting experiments at Buenos Aires, Argentina.

A biometeorological model for soybean growth stages was developed and tested using an iterative multiple regression technique. The model produced an estimate of the soybean growth stages which was compared with the observed growth stages. The model error for the developmental and for the test data were not significantly different from zero.

The model proved to be a useful tool for soybean growth stages prediction. This should be providing valuable information in Landsat imagery analysis.

VI. REFERENCES

Cross, H.Z. and M.S. Zuber, 1972. Prediction of flowering dates of maize based on different methods of estimating thermal units. Agron. J. 64: 351-355.

Johnson, H.W., H.A. Borthwick and R.C. Leffel, 1960. Effects of Photoperiod and time of planting on rates of development of the soybean in various stages of the life cycle. Bot. Gaz. 122: 77-95.

Major, D., D.R. Johnson, J.W. Tanner and I.C. Anderson, 1975. Effect of daylengths and temperature on soybean development. Crop Sci., 15 (2): 174-179.

Pascale, A.J., y A. Escales, 1971. Requerimientos bioclimaticos de los grupos de cultivares de soja. II. Subperiodo siembrafloracion. Rta. Fac. Agron. Vet. Univ. Buenos Aires, 19 (1-2): 15-24.

Pascale, A.J., C. Remussi y L. Marzo, 1963. Reaccion de distintas variedades de soja a los factores bioclimaticos en Buenos Aires. Rvta. Fac. Agron. Vet. Univ. Buenos Aires, 16 (3): 28-54.

Phinney, D.E. and M.H. Trenchard, 1977. Rederivation of the winter wheat adjustable crop calendar based on crop reporting district data. Tech. Memo. LEC-10692. 16 pages.

Robertson, G.W., 1968. A biometeorological time scale for a cereal crop involving day and night temperatures and photoperiod. Int. J. Biomet. 12 (3): 191-223.

Table 1. Iterative Regression coefficients relating daylength (a_0, a_1, and a_2), maximum temperature (b_0, b_1, and b_2) and minimum temperature (b_0, b_3, b_4) to number of days for indicated periods.

Regression Coefficients	P E R I O D[1]				
	P – BF	BF – BPD	BPD – EPD	EPD – BS	BS – LF
a_0	0.273×10^{-4}	0.722×10^{-2}	-0.314×10^{-3}	0.0	0.0
a_1	0.112×10^{-1}	0.194×10^{-1}	0.172×10^{1}	0.183×10^{1}	0.216×10^{1}
a_2	-0.683×10^{-1}	0.390×10^{-1}	0.105×10^{0}	-0.123×10^{0}	-0.138×10^{0}
b_0	0.131×10^{2}	0.132×10^{2}	0.133×10^{2}	0.133×10^{2}	0.122×10^{2}
b_1	0.906×10^{-3}	0.873×10^{-3}	0.798×10^{-3}	0.866×10^{-3}	0.106×10^{-2}
b_2	-0.127×10^{-4}	0.116×10^{-4}	-0.114×10^{-4}	-0.856×10^{-5}	-0.135×10^{-4}
b_3	0.319×10^{-3}	0.294×10^{-3}	0.291×10^{-3}	0.219×10^{-3}	0.317×10^{-3}
b_4	-0.331×10^{-4}	0.329×10^{-4}	-0.359×10^{-4}	-0.296×10^{-4}	0.382×10^{-4}

[1]
P - BF = Planting to beginning of flowering
BF - BPD = Beginning of flowering to beginning of pod development.
BPD - EPD = Beginning of pod development to end of pod development.
EPD - BS = End of pod development to beginning of senescence.
BS - LF = Beginning of senescence to leaves falling.

Table 2. Correlation statistics for observed versus estimated number of days for indicated periods.

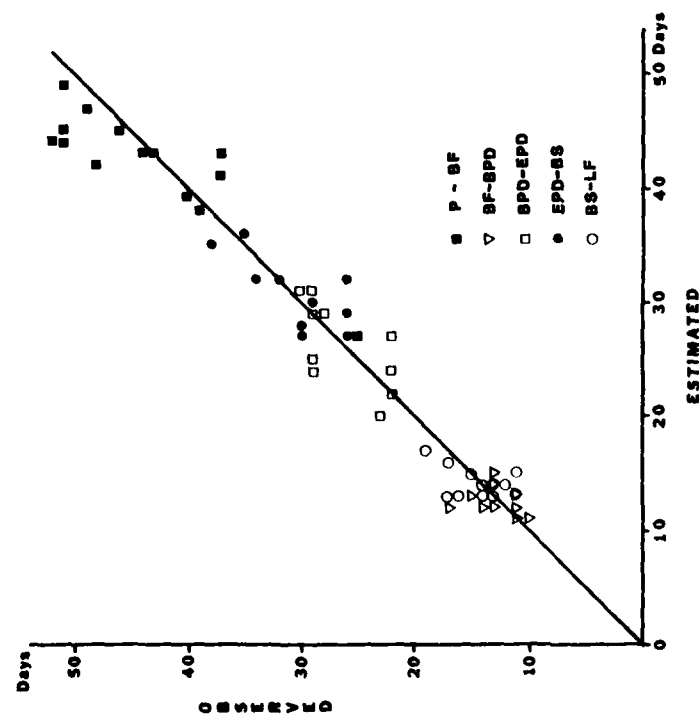|	P E R I O D[1]				
	P – BF	BF – BPD	BPD – EPD	EPD – BS	BS – LF
Average number of days	44.4	12.8	26.5	30.4	14.2
Mean error of estimates	-1.9	-0.46	0.0	0.27	-0.25
Standard error of estimates	4.25	1.98	2.74	2.75	2.18
Coefficients of Determination (R^2)	0.60	0.80	0.46	0.65	0.24

[1] Same as Table 1.

995

Figure 1. Scatter diagram of observed versus estimated number of days for all soybean growth periods used in developing the iterative regression coefficients. The 1:1 regression line is also shown. Periods : P-BF= planting to beginning of flowering; BF-BPD= beginning of pod development to end of pod development; EPD-BS= end of pod development to beginning of senescence; BS-LF= beginning of senescence to leaves falling.
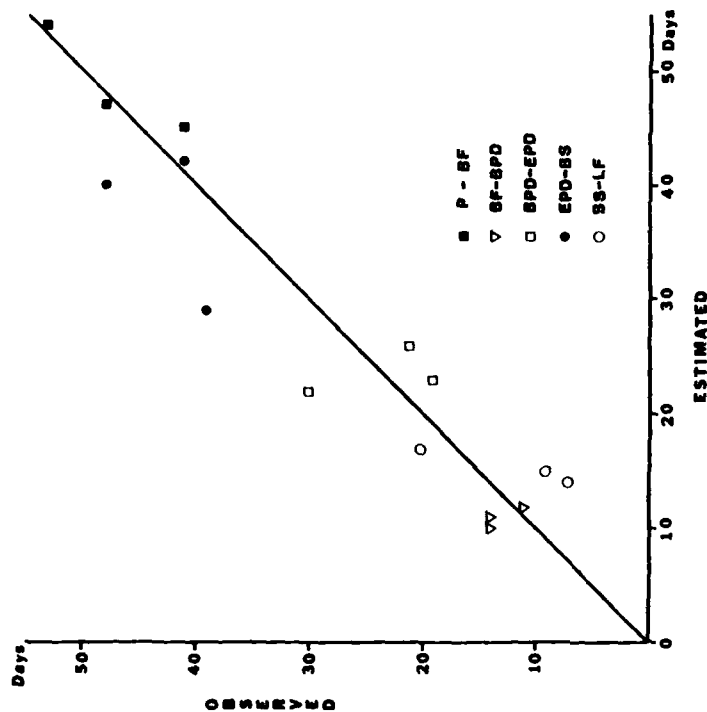
Figure 2. Scatter diagram of observed versus estimated number of days for all soybean growth periods used in testing the iterative regression coefficients. The 1:1 regression line is also shown. Periods : same as Figure 1.

THE APPLICATION OF REMOTE SENSING TECHNIQUE
TO THE SURVEY OF GEOLOGICAL STRUCTURES IN
LUSHAN GEOTHERMAL AREA, TAIWAN, R. O. C.

Wen-Jung Yuan and Wen-Tse Cheng

Assisstant Research Scientist and Senior
Research Scientist
Taipei, Taiwan, Rep. of China

ABSTRACT

Landsat images and B/W aerial photographs
were used to study the geologic and structural
features of the Lushan Geothermal Area. This
800 Km area is covered by the Miocene-
Paleogene submetamorphosed rocks of slates,
phyllites and quartzites. Some lineaments were
recognized and most of hot-spring localities
are found to scatter at the vicinity of the
intersection of major lineaments. Two
interlinked circular patterns with radial
drainage pattern inside the circle and
bounded by faults and major lineaments. Hot-
springs are mostly located at the intersections
of the circular rim and major lineaments.
Further studies on the circular patterns are
recommended.

1. INTRODUCTION

The Lushan Geothermal Area, the most important Geothermal area in
Taiwan, is situated at the central part of the Central Mountain Range of
Taiwan (Fig, 1). According to the date investigated by Mining Research And
Service Organization (MRSO), the potential of geothermal power in this
survey area is about 60 NW or more and the mechanism of it is mainly
fracture controlled.

Under the sponsorship of the Ministry of Economic Affairs, R. O. C.,
the purposes of this study are to investigate the geological information
under the scope of remotely-sensed data and to examine the applicability of
remote sensing technique (MRSO, 1966 and 1967).

2. DRAINAGE ANALYSIS AND INTERPRETATION

There are four main streams in this area, namely: Ta-Chia Hsi, Pei-Kang Hsi, Mei Hsi, and Cho-Shoi Hsi. The major direction is running from east to west except the upstreams of Mei Hsi and Pei-Kang Hsi. All fo them are consequent streams. The tributaries of them are mostly subsequent streams, parallel to the bedding and running southward (Thornbury, 1954).

A drainage pattern analysis was carried on basis of Landsat images and panchromatic aerial Photographs of various scales ranging from 1:18,000 to 1:250,000 (Liu, 1982). In broad sense, most of the drainage patterns are angular, although there are modified patterns such as: sub-dentritic, feather-like or rectangular patterns (Fig. 2). The intersection angles between main streams and their tributaries change along with the change of lithology. Generally, the intersection angle in the sandstone area is smaller than that in the slate area. And, the drainage in sandstone area is better developed. The control factors of the drainages in the whole survery area include relief, lithology and geological structures.

3. LINEAMENT ANALYSIS

Totally, 989 lineaments were interpreted from the Landsat imagery. Their azimuths were measured to the nearest degree and their lengths caculated in kilometers. Then, a rose diagram with three-degree interval and a histogram were constructed which depict the distribution of lineaments interpreted in Lushan Area (Fig. 3a3b&4) (Liu, 1982).

In general, there are two major groups of lineaments with central tendency points at N27'20'E and N79'48'W, respectively. These lineament trends confirm the general direction of fold axex and faults (Ho,1975; Chen, 1977).

4. GEOLOGIC INTERPRETATION

The following is a discussion of the stratigraphy together with a description of greytones and lineaments in these units as seen on Landsat imagery. (Fig, 5)

TA-CHI_N Sandstone

The TA-CHIEN Sandstone is a thick-bedded, medium- to coarse-grained, lignt-gray to white-gray quartzitic sandstone. (Chen, 1977). Somtimes it is arkosic to subarkosic with increasing amount of feldspars in coarser varieties. The total thickness of the Sandstone varies from 400 to 2400 m on Landsat imagery. The Sandstone appears as a massive, light-toned resistant ridge-forming unit and usually associated with anticlinal structures. There are several lineaments trending to NW-BS and NE-SW in this unit. The one of NW-SE trend was interpreted as Hsuehsan Fault and the

998

others as the result of facies change. Three lineaments of NE-SW trend were interpreted as faults situated at the left-upper part of the imagery.

CHIA-YANG Formation

The CHIA-YANG Formation is a massive dark-gray slate, intercalated thin sandstone. (Chen 1977) It is hard to see the bedding except the slate-intercalated sandstone area. On the imagery the CHIA-YANG Formation appears lighter-toned than the TA-CHIEN Sandstone. The resistant ridge-forming unit is also associated with anticline structures. Two NNE lineaments at the upper-right part of the imagery were inperpreted as faults and two NNE lineaments at the lower-left part of imagery were interpreted as faults, too.

MEI-HSI(MS) Sandstone

The MS sandstone is situated at the middle part of the imagery. It is a massive, light quartzitic sandstone. (Chen, 1977) It looks like TA-CHIEN Sandstone on the imagery. The differences between MS Sandstone and TA-CHIEN Sandstone are that the sorting of MS Sandstone is better and that the cementing matrix of MS Sandstone is calcite but the TA-CHIEN Sandstone is cemented by clay. On the imagery the MS Sandstone appears as massive ridge trending to NW-ES with monoclinic structures.

KAN-KOU   Formation

The KAN-KOU   Formation is predominately black- to darkgray argillite or slate or Phyllitic slate. (Ho, 1975) These beds are also abundant in interbedded sandstone and siltstone. The expression of the KAN-KOU Formation on the imagery is very similar to that of Lushan Formation. The most important criterion for interpreting the Formation is its stratigraphic position above the MS Sandstone. Between KAN-KOU   Formation and Lushan Formation there is a major lineament trending to NW-SE. It is Lushan Fault, one of the most important fault in Taiwan Island.

Lushan Formation

The Lushan Formation of lower to Lower-middle Miocene age is composed of argillite and slate. (Ho, 1975) The type locality of this Formation is the Lushan hot spring, to the east of Wushe (Jenai) in Nantou-Hsien. The Lushan Formation was originally a time stratigraphic unit soley defined by its faunal content and was recently described as lithostratigraphic unit. Essentially the Lushan Formation consists of black- and dark-gray argillite, slate and Phyllite with local interbeds of dark-gray compact sandstone and disseminated marly nodules. One the imagery the Lushan Formation is a resistant ridge-forming unit which has a medium to light tone. There is also apparent pseudo-bedding which is parallel with the Lishan

999

Fault. The drainage texture is medium to coarse which suggests a high sand content. Two interlinked radial drainage pattern, located between Mei Shi and Pei Kang Hsi and bounded by faults and lineaments, were found. Hot spring areas in the vicinity are mostly located at the intersection of major lineaments. At the right-lower part of the imagery, there are some lineaments trending to NNW and one lineament of ns trend passes through them. Lushan hot spring is situated at the intersection. The NS trend lineament was thus interpreted as a fault and the sandstone interbedded with slate forms the NNW lineaments which is parallel to the bedding.

5. CONCLUSIONS

In this study, the drainage analysis, lineament analysis and stereoscopic Photogeological interpretation were carried out by using the Landsat images and B/W aerial photographs and accompanied with field checks.

Two interlinked radial drainage patterns, situated at the upstreams of Mei-Hsi and Pei-Kan-Hsi and bounded by faults and major lineaments, were found to have good relationship with hot-spring occurrences. Further-more, several places with high concentration of lineaments were identified and the geothermal prospect of these areas could be higher than the other places due to the structure-controlled characteristics of geothermal mechanism (Figure 6).

The result of this study proves that the remote sensing techniques are useful in executing geological investigation in Lushan Geothermal Area of low accessibility. Consequently, these techniques can be applied efficiently in the study of other geothermal areas in Taiwan where they are mostly distributed in hilly or mountainous lands.

6. REFERENCES

1. Chen, C. H. (1977) Some stratigraphic problems of the Hsuehshan Range of Taiwan: Proceedings of Geological Society of China, No. 20, PP. 61-72.
2. Ho, C. S. (1975) An Introduction to the Geology of Taiwan, Explanatory Text of the Geologic Map of Taiwan, 153 pages. The Ministry of Economic Affairs, Rep. of China.
3. Liu, J. K. (1982) Drainage Analysis, Chapter 1, Photo-Geologic Interpretation Techniques Series: to be publicshed in Journal of Mining Technology, MRSO.
4. Liu, J. K. (1982) Lineament Analysis, Chapter 2, Photo-geologic Interpretation Techniques Series: to be published in Journal of Mining Technology, MRSO.
5. MRSO (1977) Investigation of the Geothermal Resources in Taiwan, Part II, MRSO Report-163: Mining Research & Service Organization (MRSO).
6. Thornbury, W. D. (1954) Principles of Geomorphology. New York: Wiley. 618 Pages.
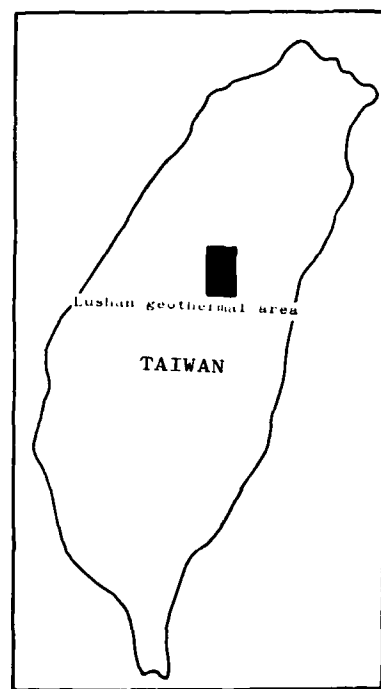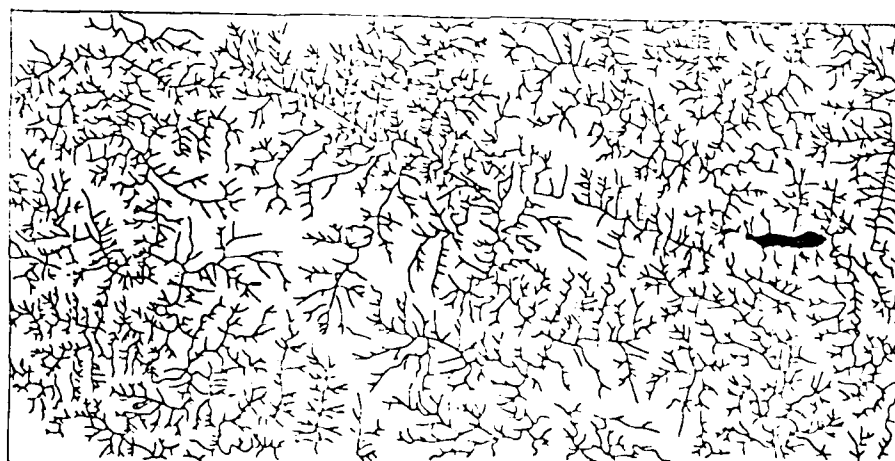
Figure 1: The index map & the LANDSAT IMAGE of Lushan geothermal area.

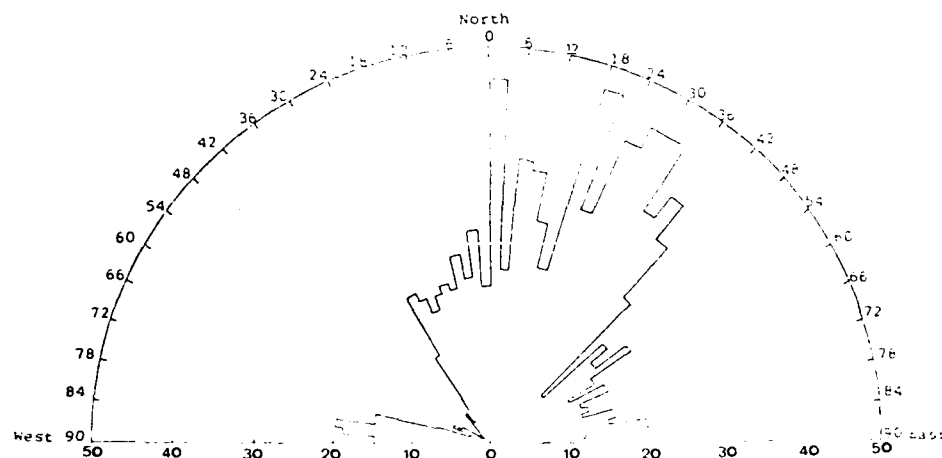Figure 2:The Drainage map of Lushan geothermal area.

0 2 4 6km

Figure 3a:The rose diagram of interpeted lineaments
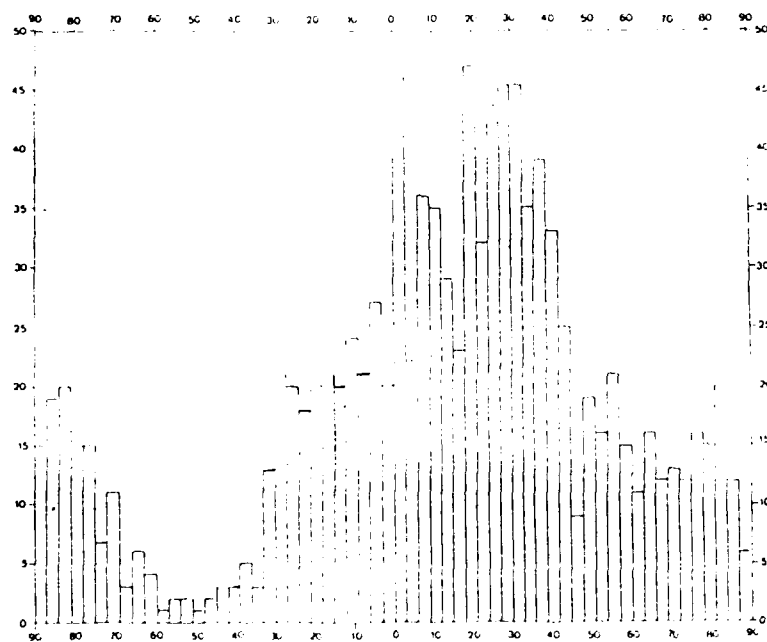per three degree azimuth cell.

Figure 3b:The histogram of interpreted lineaments
per three azimuth cell.

1002

Figure 4:The lineaments interpreted map of
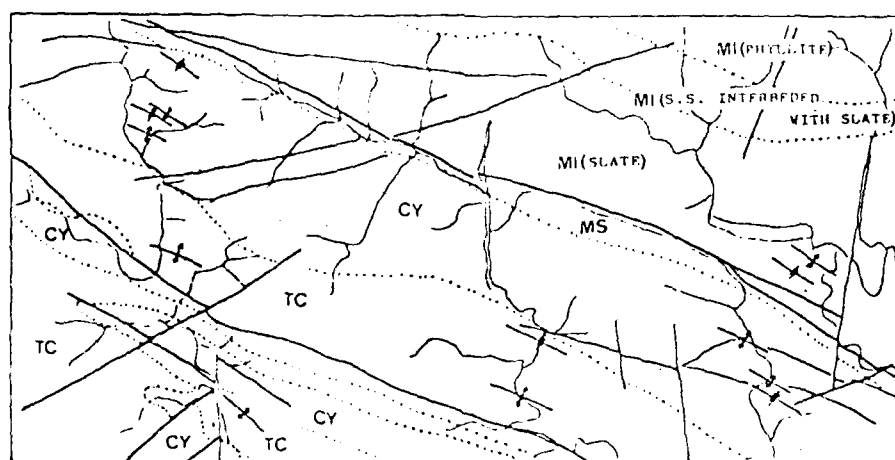Lushan geothermal area.

0 2 4 6km

Figure 5:The geological interpretation map
of Lushan geothermal area.

0 2 4 6km

LEGEND

⋰ LITHOLOGY BOUNDARY	MS:MEI-HSI SANDSTONE
╱ FAULT	MI :LUSHAN FORMATION
TC:TA-CHIEN SANDSTONE	✗ ANTICLINE AXES
CY:CHIA-YANG FORMATION	✗ SYNCLINE AXES
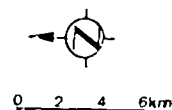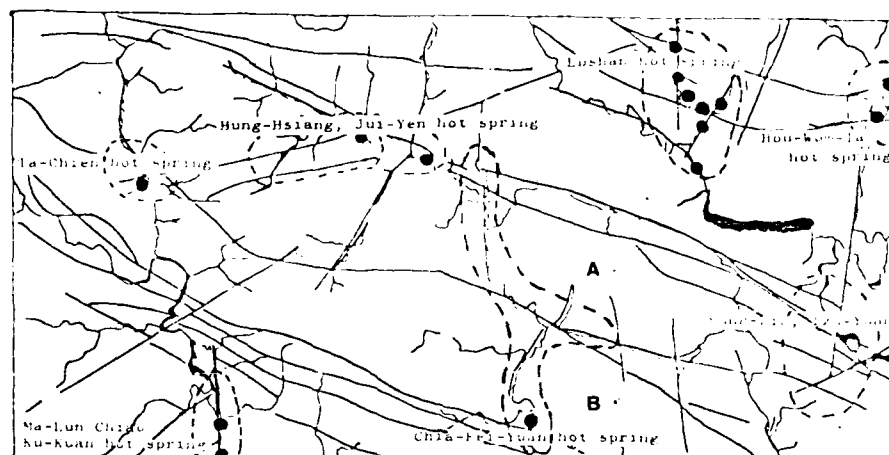
Figure 6: The distribution of hot-springs major Lineaments and circular patters.

0 2 4 6km

LEGEND

⊙ POTENTIAL GEOTHERMAL AREA

● HOT SPRING

╱ MAJOR LINEAMENT

A,B TWO INTERLINKED RADIAL DRAINAGE

REMOTE SENSING TECHNIQUES IN MORPHOSTRUCTURAL INTERPRETATION
FOR HYDROCARBON PROSPECTION IN BRAZIL

Juércio Tavares de Mattos
Milton Garcia Balieiro
Paulo Roberto Meneses

Instituto de Pesquisas Espaciais
Conselho Nacional de Desenvolvimento Científico e Tecnológico
São José dos Campos, SP, Brazil

SUMMARY

The utilization of Landsat and SLAR imagery is believed to be of fundamental
importance for regional geological reconnaissance in the characterization of
structures and tectonics of areas potentiality favorable to hydrocarbon
accumulation. In Brazil, increasing demands for secure petroleum supply deter-
mine that the possibility of locating new oil traps be thoroughly investigated.
Interpretation of remote sensing data is a prime tool to optimize the gathering
and analyzing of geological information in large or poorly explored areas. In
recent years, geological prospection for petroleum in intracratonic Phanerozoic
sedimentary basins of Brazil was resumed. The great extension of these basins in
Brazil (more than 1,000,000 km^2) and the lack of studies in structural geology
provide an ideal setting for remote sensing exploration efforts. The develop-
ment of methods and their systematic application to sedimentary basins consist
of visual interpretation of Landsat and SLAR images at the 1:250,000 scale.
The interpretative process consists, initially, of analysis of drainage and
relief features determined by their radial and annular patterns and asymmetry
of the drainage system, which are considered to represent anomalous structural
features within a regional context. The combined occurrence of such anomalous
features (radial, annular and assymetric) makes it possible to define and
characterize the morphostructural anomalies of interest to the petroleum explor-
ation. In this way, it is possible to qualify, within a structural interpreta-
tion, the anomalies as superficial reflections of highs and lows in the basement.
Such interpretation is dependent on how intense is the degree of structural
control over the anomaly, as compared to the geomorphological control. Further-
more, lineaments associated with drainage and relief were analyzed in association
with rigid deformations that were tectonically produced. The geometric and
genetic relationship between lineaments and high and low structural features
has also been sought with a compressional model. The geological content obtained
in each morphostructural anomaly was evaluated and qualified, so that information
of highly interpretation content could be deduced, which allowed the confirmation
of remote sensing potentiality in the exploration for petroleum.

ADAPTATION OF THE SPOT SPECTRAL BANDS
TO SPECTRAL SIGNATURES OF OBJECTS

G. Bégni

Centre National d'Etudes Spatiales
(CNES)
Toulouse - France

ABSTRACT

The aim of this paper is to present how the SPOT spectral bands have been adapted to the spectral properties of the observed ground objects.

The text starts with generalities : brief description of the SPOT system and of the simulations we are making so as to prepare future users of SPOT data, precise description of measured radiances and reflectances, review of atmospheric effects.

We show how the profiles of the 3 spectral bands have been optimized with respect to thematic objectives : minimization of atmospheric perturbations, spectral properties of some objects such as vegetation.

We show how the choice between two types of panchromatic bands (0.50 - 0.70 μm) and (0.50 - 0.90 μm) was made by studying contrast between objects thematically characterized, taking into account the most interesting features to be observed by a scanner with the SPOT resolution.

The expected spectral profile for both spectral and panchromatic SPOT bands is presented.

1. GENERAL : THE SPOT SYSTEM

1.1. THE SPOT SYSTEM

The SPOT system comprises two identical and independant instruments called HRV (high resolution visible). They provide three "spectral bands", the expected detailed profiles of which are given in Figure 1, normalized with respect to their maximum values ; the bands are described by the wavelengths corresponding to the values at half the maximum values :

These are : B1 : 0.50 - 0.59 μm
B2 : 0.61 - 0.68 μm
B3 : 0.79 - 0.89 μm

The "ground resolution" is 20m. This means that the instrument, at any instant, measures the radiance spatially integrated over a given surface (this surface is the impulse response of the system, which is the convolution of optical diffraction, detector suface, smearing effect and electronic interaction between detectors, and is roughly 20 x 30m for the three spectral bands) and samples this data at 20 m intervals in two orthogonal directions. The HRV instruments also have a so-called "panchromatic band", the profile of which is also shown in figure 1 ; the wavelengths correspondint to the values at half maximum are :

P : 0.51 - 0.73 μm

The ground resolution is 10 m.

Besides higher resolution, the major innovation of the SPOT system is the possibility of pointing the optical axis of the system perpendicularly to the velocity vector, out to an angle of 27°. The effective range corresponding to the ground look angle θ_v is increased slightly due to the effect of earth curvature. The major interest in "off-nadir viewing" is in applications such as : repetitive coverage, rapid accessibility, stereoscopy, but we can also foresee radiometric applications such as stereoradiometry.

1.2. THE SPOT SIMULATION PROGRAM

So as to prepare SPOT users as fully as possible, we have set up a SPOT data simulation program. Because complete simulation of SPOT image has been shown to be impossible, two types of simulations have been implemented : a geometrical section and a radiometric section. They are elaborated thanks to the image delivered by a 10 channel airborne DAEDALUS scanner. The SPOT channels are generated by a linear weighted combination of the original channels, which is designed so as to insure a maximal similarity over some determined themes.

An operational procedure allows us to deliver standard products to users. However, some particular operations have been made for study purpose ; an example is developed in Section III.

1.3. PRECISE DEFINITION OF MEASURED RADIANCES AND REFLECTANCES

Consider an object on the ground having a certain reflectance (Lambertian or not) $\rho(\lambda)$, where λ is wavelength. In the absence of the atmosphere, the radiance L_λ of this object in the direction of observation will, by definition, be given by :

$$L_\lambda = \frac{E_{s_\lambda} \rho(\lambda) \cos \theta_s}{\pi}$$

and where E_{s_λ} is the solar irradiance and θ_s is the angle between the sun's direction $_{s_\lambda}$ and the surface normal. The atmosphere modifies this radiance as described in paragraph I.2. ; the satellite then sees a modified radiance $\hat{L}_\lambda$, to which we can associate an apparent reflectance $\hat{\rho}(\lambda)$ defined by

$$\hat{\rho}(\lambda) = \frac{\pi \hat{L}_\lambda}{E_{s_\lambda} \cos \theta_s}$$

Observation systems provide a spectral analysis in a certain number of bands, and the spectral sensitivities of these bands wary with wavelength. We describe these sensitivities as S_k (λ), where k is the characteristic index of a particular band. The quantity measured is of the normalized form :

$$\hat{L}_k = \frac{\int_0^\infty S_k(\lambda)\, \hat{L}_\lambda\, d\lambda}{\int_0^\infty S_k(\lambda)\, d\lambda}$$

where $\hat{L}_k$ is a quantity equivalent to spectral radiance ; it represents the weighted average of $\hat{L}_\lambda$ in the band. Note that if $\hat{L}_\lambda$ equals L_0 (a radiance independent of λ), then $\hat{L}_k = L_0$. We can express this by saying L_k is the spectral radiance of an object whose radiance does not change with , giving the same signal as the object being considered (and therefore indiscernible from it). In this paper, L_k will be called the "equivalent radiance". Similarly we can define an "equivalent solar irradiance" E_k and an "equivalent reflectance ρ_k. We can easily show that

$$\hat{\rho}_k = \frac{\int_0^\infty \tilde{E}_{s_\lambda}\, S_k(\lambda)\, \hat{\rho}(\lambda)\, d\lambda}{\int_0^\infty E_{s_\lambda}\, S_k(\lambda)}$$

The k numbers $\hat{\rho}_k$ constitute the spectral signature of the object as produced by the observation system under consideration. It provides a set of outputs :

$$x_k = B_k\, \hat{\rho}_k\, E_k\, \cos\theta_s$$

where B_k is the absolute calibration coefficient of the spectral band. So, the precise disign of spectral bands for thematic use involves a study of :

- the manner how atmosphere transforms L_λ to $\hat{L}_\lambda$ (and $\rho(\lambda)$ to $\hat{\rho}(\lambda)$)

- the correlation which can exist between thematic parameters and the form of $\rho(\lambda)$ for determined wavelengths ;

- the manner how atmosphere transforms $\rho(\lambda)$ to $\hat{\rho}(\lambda)$

- the manner how the weighting by $S_k(\lambda)$ interacts with the detailed form of $\hat{\rho}(\lambda)$.

1.4. REVIEW OF ATMOSPHERIC EFFECTS

We shall review the atmospheric modification of object radiance, giving a range of $\hat{L}_\lambda$ values (that can be referred to $\hat{\rho}_k$ values) different from L_λ (the polarization is also changed).

Atmospheric effects are due to two phenomena, absorption and scattering, that attenuate a light beam when it encounters atmospheric "particles" (gas molecules, aerosols). The radiance observed by a satellite sensor viewing a point on the earth's surface comprises several components as shown in figure 2.

1.4.1. the most important component of irradiance of the point of interest is that due to direct, partly attenuated solar flux.

1.4.2. a second source of irradiance of the point of interest is due to atmospherically scattered flux that has not been reflected from the ground.

1.4.3. a third source of irradiance is reflected flux, from points other than the point under consideration, that is redirected by atmospheric scattering to be incident on the point of interest.

1.4.4. these three components of irradiance are reflected from the ground, and a part of this reflected flux is directed toward the sensor. It is further attenuated by scattering and absorption before reaching the sensor.

1.4.5. the radiance at the sensor includes flux reflected from points on the ground, other than the point under consideration, that is redirected by atmospheric scattering into the sensor.

1.4.6. "intrinsic atmospheric reflectance" is the main component of so-called "atmospheric path radiance" and refers to the radiant flux that, after single (6) or multiple (6 bis) scattering, reaches the sensor without encoutering the ground.

These different components are sensitive to different parameters. Thus the atmospheric scattering due to gaseous molecules decreases rapidly with wavelength (proportionnaly to λ^{-4} : Rayleigh scattering explaining the blue color of the sky) ; the decrease is less rapid for aerosols (the color is whiter). The absorption by certain molecules (O_3, H_2O) is important at certain wavelengths ; it is related to the total quantity of gas contained in the atmosphere, which is quite variable. The most important parameters in the visible and the near infrared (0.45 to 1.1 μm) are :

1- the geometry : the angle θ_s between the solar direction and the local normal, the angle θ_v between the look direction and the surface normal, and the angle θ_N between the solar and the look direction.

2- the wavelength of interest,

3- the concentration of aerosols, generally measured in terms of visibility (V = 23 km and V = 5 km are two cases typically studied).

4- the ozone concentration (values fall between 0.25 and 0.45 cm atm.) ; ozone presents a weak absorption in the visible part of the spectrum (transmittance 0,90 at λ = 0,60μ for $[O_3]$ = 0,35 cm.atm, θ_s = 41°, θ_v = 0)

5- the water vapor concentration (values fall between 0.3 and 3 cm precipitable) water vapor present a first weak absorption in the band (0,69 - 0,74μ), a second weak absorption in the band (0,78 - 0,84μ) and a third strong absorption in the band (0,89 - 0,99μ) (transmittance = 0.85 at λ = 0.72μ , 0.82 at λ = 0.81μ and 0.22 at λ = 0.93μ , for $[H_2O]$ = 2 cm precip. ; θ_s = 41° , θ_v = 0°).

The influence of atmosphere is greater in side-looking images than in nadir-looking ones because the atmospheric effective thickness is larger.

2. STUDY OF SPECTRAL BANDS

2.1. GENERAL CONSIDERATIONS

The choice of the three SPOT spectral bands was based on the most recently available spectral signatures of ground objects and on our ability to minimize the effect of the atmosphere upon them.

The definition of $\hat{L}_k$ can be interpreted as a weighted mean of $\hat{L}_\lambda$ in the spectral band ; it can be shown that the result depends very weakly on the precise form of $S_k(\lambda)$, except if L_λ presents important variations within the band.

Most objects observed and readily studied by remote sensing techniques in the visible range do not show large changes in spectral reflectance within narrow spectral bands. The most noticeable exception is vegetation. A typical spectrum for vigorous vegetation shows a first local maximum at about 0.55 μm and a

1010

minimum at about $0.67 \mu m$, followed by a rapid increase up to a plateau in the region of $0.75 \mu m$ (the amplitude of this plateau being much larger than that of the first maximum). It is possible to establish correlations between changes in vegetation and its spectral signature in these three spectral regions, which correspond to the three SPOT bands.

In fact, a detailed study can show that the two first bands are strongly correlated. So, for a first order purpose (such as vegetation discrimination), one may only use the two last spectral bands. However, since the second spectral band has a thematic meaning (absorption by chlorophyll), the subtle difference between spectral bands 1 and 2 may be used for thematic advanced studies such as vegetation disease.

A specific interest of the first spectral band is water penetration by its shorter wavelengths ; this allows a detailed study of water in streams, lakes and coastal zones.

The atmospheric perturbations described in 1.4. must be taken into account, so as to minimize their influence on the measured spectral signatures.

The most important atmospheric effects are :

1- the rapid decrease of Rayleigh scattering ($1/\lambda^4$) as the wavelength increases, and the much less rapid change corresponding to scattering by aerosols.

2- absorption due to water vapor ; the first absorption peak is located at the limit of SPOT second spectral band ; the second and third peak are located at the two limits of the third SPOT spectral band.

We also must note that solar irradiance, which has a maximum at about $0.48 \mu m$, decreases at longer wavelengths, so the irradiance at $0.82 \mu m$ is only about half that at $0.48 \mu m$.

2.2. DETAILED STUDY OF THE CHOICE AND PROFILES OF SPOT SPECTRAL BANDS

In band B1, it is not possible to eliminate the influence of ozone absorption. Numerical studies show that absolute variations in apparent reflectance can be in the order of 0.03 for high reflectances. It is interesting to lower, as much as possible, the response to short wavelengths in order to minimize the influence of Rayleigh scattering. Aerosols have a large influence (absolute variations in apparent reflectance can be in the order of 0.05) ; $\hat{\rho}$ is greater than the actual ρ at low reflectances, and lower at high reflectances because of compensation between aerosols absorption and scattering. This is a problem for precise assessment of water quality in band B1, which correspond to rather low reflectances. For vegetation observation, it is interesting to center the point of maximum sensitivity on the vegetation local maximum, which is at $0,55 \mu m$.

In band B2, it is also not possible to eliminate the influence of ozone absorption; however, this effect is weaker than in B1 (maximum variations in ρ_2 in the order of 0.01). Influence of aerosols is also important, but the effect is also weaker than in B1 (maximum variations in the order of 0.03).

Water vapor influence is not negligible (maximum variations in the order of 0.03). For vegetation assessment in chlorophyll absorption domain, we are measuring reflectance in a low reflectance region between two regions where it is high, so it is essential to block the band efficiently, in other words, to reduce, to the maximum extent possible, the residual transmission below $0.55 \mu m$ and above $0.69 \mu m$. The former is easy but the latter is more difficult, for technological reasons, which is aggravating because of the high reflectance of vegetation as we approach the near infrared ; thus a residual very weak sensitivity can produce a significant increase in the signal. A relative error

1011

of 10 % in the measurement of the reflectance of vegetation in this band can result.

In band B3, the influence of aerosols is still important (mainly for low reflectances) ; maximum variations in ρ_3 can be in the order of 0.03. It is possible to reduce the influence of water vapor absorption by limiting the response of the bands to wavelengths less than $0.89 \mu m$. This cutoff is not sharp (again for technological reasons), but the residual effects are minimized. Variations in ρ_3 due to this phenomenon can be in the order of 0.05 for high reflectances.

The detailed profiles of the three SPOT spectral bands is shown in figure 1.

3. STUDY OF THE PANCHROMATIC BAND

The width of the panchromatic band makes it of little interest for spectral signature studies because spectral changes in ground features are averaged out across its width. Its value lies more in photointerpretation, cartography, etc.. This is, of course, a general idea which can be denied in some particular cases.

The study of spectral reflectances provides us a way to determine how the integration over a wide band can enhance or reduce the contrast between objects having different characteristics. Two kinds of panchromatic bands are commonly used : $0.5 - 0.7 \mu m$ (visible) and $0.5 - 0.9 \mu m$ (visible and near ir). The latter is used for meteorological satellites because it provides good discrimination among water, damp soil, and vegetation. This is valuable for satellites having resolutions of several kilometers.

A satellite system having a resolution of 10 m poses a different problem On the one hand, instrumental considerations (optimization of signal level, improvement of the transfer function - and therefore the effective resolution-) tend to impose the former solution ; on the other hand, a thematic study must be intertaken.

We considered the problem as follows :

We selected a certain number of spectral distribution $\rho(\lambda)$ corresponding to gray granite, red clay, dry soil, vigorous sugar beet (strong ir reflectance) fallow ground, trees, and grass (moderate ir reflectance). We assumed the radiance outside the atmosphere, L_λ to be given by the model described above. Then we chose a realistic model for the spectral sensitivity $S(\lambda)$ as a function of two parameters, λ_1, λ_2, in such a way as to simulate a panchromatic band λ_1 to λ_2. We then determined the calibrated response of the instrument to several different targets as a function of λ_1 and λ_2 (for an instrument with a specific calibration, a reference distribution $\rho(\lambda)$ gives a specific output).

We studied the response as a function of different cutoff wavelengths : first, by varying λ_2 with λ_1 fixed at $0.5 \mu m$, and then, varying λ_1 with λ_2 at $0.9 \mu m$.

The effect of varying λ_1 was inconsequential ; it simply reduced the output signal from the instrument and was therefore not considered further. We proceeded to examine the effect on the response of the system of a change in λ_2.

If we consider vigorous vegetation, there is more or less rapid increase in the signal when λ_2 changes from $0.7 \mu m$ to $0.9 \mu m$. For sugar beet this corresponds to an increase in signal by a factor of 1.7, and for trees by a factor of about 1.8. This is because of the rapid increase in reflectance of this type of feature at about $0.7 \mu m$ (considered earlier in detail with reference to band B2). These increases are partially offset by the decrease of solar irradiance, the absorption of water vapor, and the artificial increase of the signal in the blue due to Rayleigh scattering.

On the other hand, vegetation that is not in vigourous growth, rocks, and targets consisting of asphalt or concrete don't vary much.

We can distinguish two tendencies :

1- the choice of a band between 0.5 and 0.9 μm provides contrast between different types of vegetation, which is related to the degree of vigor of vegetation. However, the high value of the signal of crops like sugar beet approaches that of bare soil, and there is therefore the possibility of confusion between the two different signatures. The choice of a band between 0.5 and 0.9 μm can help identify thematic details within the vegetation class, but also creates the risk of confusing it with another. Certain types of rock (schists) have low reflectance and are often confused with vegetation ; the same applies to asphalt, but experience shows that roads are easily recognized because of their context (long straight lines crossing varied thematic areas).

2- the use of a band from 0.5 to 0.7 μm reduces the signal due to vegetation. It makes the contrast between different types of vegetation less perceptible (this contrast can be studied in the third spectral band since the 10 meters resolution is not critical) but on the other hand, improves the differenciation between vegetation and bare soils, rocks or artefacts.

We have not evaluated the situation for water. Calm, pure water (not close to the condition of specular reflection) shows very low reflectance, decreasing with wavelength, and is very easily distinguished on panchromatic images.

A more difficult situation is damp soil, for which the reflectance is between that of dry soil and of water ; it is lower than that for dry soil, decreasing with wavelength. There is therefore a tendency to confuse damp soil with vegetation, and this is more noticeable for a band from 0.5 to 0.9 μm than one from 0.5 to 0.7 μm because of the increase in the signal provided by vegetation and the slow drop in signal due to soil. Therefore : (1) for satellites with low resolution (SMS, Meteosat) it is desirable to have a high contrast between dry and damp regions on a scale compatible with the resolution of the satellite, we prefer the band between 0.5 and 0.9 μm , which accentuates contrast, the distinction between vegetation and damp soil being less important. We can say, a posteriori, that the panchromatic Meteosat (0.5 to 0.9 μm) is of more value than the panchromatic SMS (0.5 to 0.7 μm) for this goal. (2) for a satellite with high resolution, the contrast between dry and damp regions is at far too large a scale, and we want to be able to observe much finer detail. We have therefore chosen a band from 0.5 to 0.7 μm , which reduces the confusion caused by moisture on the contrast between bare soil and vegetation. (This band is the usual IGN (Institut Géographique National) choice for photography in the panchromatic mode).

Since the transfer function of CCD is better for shorter wavelengths, this choice tends to improve the geometric resolution, as we previously said.

Detailed studies show that the λ_2 limit may be raised up to $\lambda_2 = 0,73 \mu$; this is the SPOT choice.

These theoretical studies have been validated by a specific SPOT simulation (see 1.2). Original DAEDALUS channels have been combined so as to fit to panchromatic channels in the form $[0,5 \mu m - \lambda_2]$, λ_2 ranging from 0,7 to 0,9 μm . The two kinds of panchromatic channels can easily be separated. The transition can be observed for $\lambda = 0.75 \mu m$ approximately.

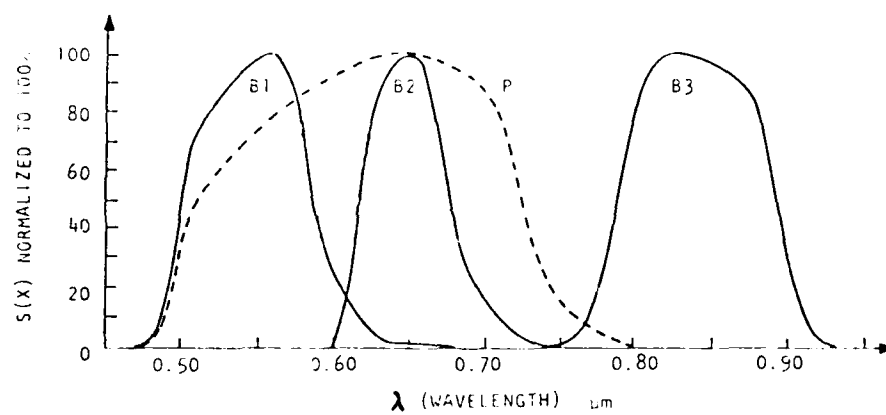Figure 1 shows the panchromatic band profile, superimposed to the spectral bands.

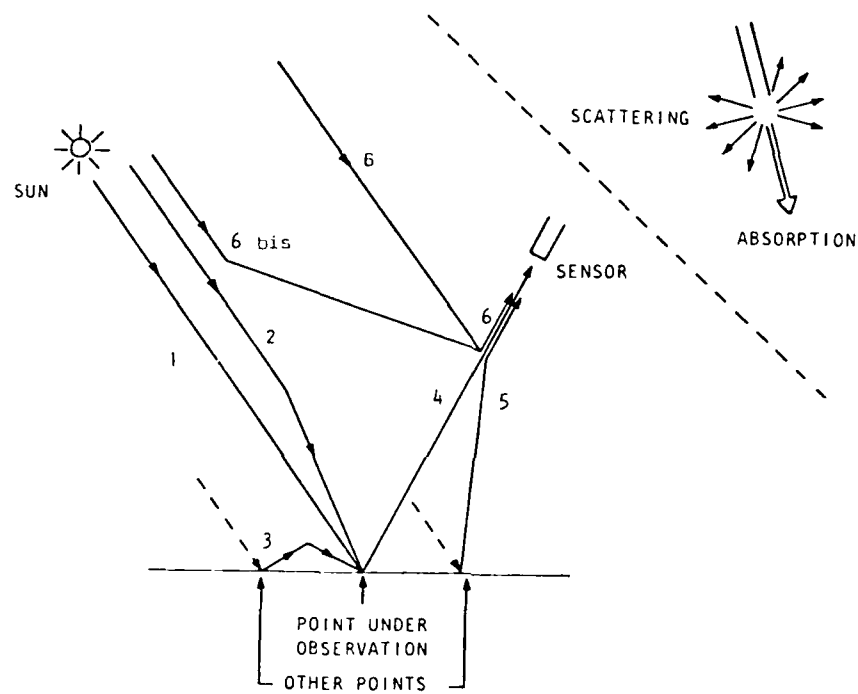Figure 1. Spectral response of the SPOT bands

Figure 2. Atmospheric effects

AN INTERACTIVE MODEL FOR ATMOSPHERIC CORRECTION IN SATELLITE IMAGES*

L.A.V. Dias, N.L. Vijaykumar and A.E.C. Pereira

Instituto de Pesquisas Espaciais - INPE
Conselho Nacional de Desenvolvimento Científico e Tecn. - CNPq
12200 São José dos Campos, São Paulo, Brazil

ABSTRACT

The presence of the terrestrial atmosphere is a constant problem in satellite image classification. This paper describes a procedure to test quantitatively the performance of an atmospheric correction algorithm. This specific algorithm was developed at INPE, based on O'Neil's model. It is difficult to obtain a reasonable atmospheric model for Brazilian conditions, due to lack of aerosol data. The procedure consists of correcting two images of the desired scene, for different days, changing the aerosol optical depth, and comparing at selected areas, the contrast and the correlation between the images. For a better correction, the contrast improves, as well as the correlation. Based on the previous information, it is possible to select the proper aerosol optical depth. Care should be taken, however, since an exaggerated contrast improvement by itself or a good correlation alone are not sufficient. Using both criteria, a better judgement can be made. Scenes that have undergone considerable temporal changes, as those at different stages of a given crop, should be avoided. In order to make the interactive model practical, it was necessary to calculate quickly and interactively the atmospheric transmittance. This was done by means of a modified LOWTRAN program. The modifications were introduced in order to make LOWTRAN more user-friendly, by allowing direct user interaction via video terminals, including graphic of the input model and the output profiles.

1. INTRODUCTION

A problem in satellite image classification is the presence of the terrestrial atmosphere: it tends to blur the original scene, making the satellite sensor acquire a different spectral signature depending on the atmospheric conditions.

One of the ways to tackle the problem is to simulate the atmosphere, and compensate for the image the effect that would be produced by this synthetic atmosphere. The problems involved in modelling the atmosphere are enormous (Turner and Spencer, 1972), due to lack of data and to the simplifying assumptions one is forced to make. Fortunately, even a simple model may produce good results, as the algorithm implemented at INPE (Dias et al., 1981) has shown.

Another problem then arises: how to test the correction quality? A direct approach is to check a posteriori, using ground truth. However, this is a slow and expensive procedure. This work suggests an unsupervised procedure to evaluate approximately the quality of an atmospheric correction if the aerosol optical depth is not known.

2. DESCRIPTION OF THE PROCEDURE

The atmospheric correction algorithm used at INPE is rather simple. It uses a LOWTRAN-4 program (Selby et al., 1978) to compute the atmospheric transmittance and O'Neil's tables to determine the path radiance (O'Neil et al., 1978). It was developed for LANDSAT use.

The LOWTRAN-4 program was modifed to allow plotting of the input atmospheric model, and the total absorption output profiles, molecular absorption, and aerosol absorption versus wavelength. Figure 1 is an example of the inputs, and Figure 2, of the outputs. Besides that, the program has been made interactive. Figures 3 and 4 present "menus" for the choice of models, the possible changes into the parameter cards, or the program termination, respectively. All the input parameters are entered in an interactive way. A B-6800 computer with video terminals has been used as input and video, and a Calcomp plotter, or line printer, as output medium.

For the correction itself an Image-100 coupled to a PDP-11/45 is used. The input data are: a) the LANDSAT channel; b) aerosol optical depth; c) ground albedo; d) solar zenith angle; e) transmittance (from LOWTRAN); f) full image (T) or only inside a cursor (C); g) another training area (T) or repeat for another channel (C).

The LOWTRAN program input data is fairly well known, especially if radiosonde data is used for an atmospheric model (which is generally the case). The standard models are not well suited for Brazilian conditions.

There is quite a number of parameters to estimate, as can easily be seen. The proposed procedure keeps the measured or estimated parameters constant, except for the aerosol optical depth, that is an important unknown, especially for Brazilian condition due to lack of reliable data. The correction is made by changing the aerosol optical depth from 0.12 to 0.48 at 0.12 intervals for the desired image, I1, and another image, I2, of the same scene taken at a different time.

Initially, a correlation operation (correlation coefficient) is obtained between I1 and I2 for selected areas that do not have changed in time. The best correlation should indicate a minimum of atmospheric effect. Unfortunately, this is not a strong indication of a "correct" correction, for false interpretations are possible. The size of the area to be correlated is important. If it is too large (a whole image, for instance), part of it can compensate for another part. If it is too small, the result can be meaningless, especially if a good geometric correction was not done, as in our case. A reasonable value is 32 x 32 or 64 x 64 pixels, or areas that are not supposed to change with time.

In order to confirm the better correction, the contrast of selected points is examined. Generally, the better the contrast the better the correction. If the atmosphere were to be removed, the contrast would improve. For contrast the following expression is assumed

$$C = (Ia - Ir) / (Ir + Lp/T), \tag{1}$$

where Ia is the target pixel brightness and Ir, its neighbour's brightness such that $|Ia - Ir|$ is maximum, Lp is the path radiance and T the atmospheric transmittance.

3. PRELIMINARY RESULTS

Extensive tests of this proposed algorithms were not done yet. However, for a preliminary study, two images of Vale do Paraíba, Brazil, on July 11th, 1973 and January 31st, 1978 of LANDSAT-1, channel 4 were used.

The atmospheric correction was made for aerosol optical depths of 0.12, 0.24, 0.48 for November 7th, 1973 and of 0.12, 0.24 for January 31st, 1978. The correlation results (only to 0.12 and 0.24) are presented on Table 1. The albedo was estimated at 0.2.

Point $\neq$ 1 corresponds to a 64 x 64 pixel window on a highway near the city of Taubaté, SP, Brazil; point $\neq$ 2, also 64 x 64, corresponds to the city of Cruzeiro, SP, Brazil; point $\neq$ 3, 64 x 64 pixel, is a hilly region known as Serra do Mar, covered by a tropical forest; point $\neq$ 4 is the whole 512 x 512 subimage. If the averages (64 x 64) are taken, the best correlated pairs are the images 0.12 giving 0.288, followed by 0.12 (January 31st), and 0.24 (July 11th) giving 0.281. The worst correlated pairs are the 0.24 images with 0.265. The other pair's correlation was 0.273.

The contrast is presented on Table 2, for selected pixels inside the windows above, plus a pixel on an improved aircraft runaway at Inpe's airport at Cachoeira Paulista (point $\neq$ 5). Since the images are not geometrically corrected, it is possible that the pixels' number do not correspond, but visually they correspond to the same landmarks.

4. CONCLUSIONS

At this point, a large series of tests with a large number of images has to be done, under different conditions. This work is under way, and not reported yet in this paper. However, based on the preliminary tests, a few conclusions can be drawn in support of the ideas here presented. For this, first test images taken on different seasons and four and a half years apart were chosen.

From Table 1, point $\neq$ 3 (Serra do Mar) was the worst correlated, as expected, since the vegetation should have changed from Winter (73) to Summer (78). Point $\neq$ 2 (city of Cruzeiro) was the best correlated, since the intrinsic reflection of a stable urban area should not change much with time. Point $\neq$ 4 (512 x 512 pixel) was better correlated, because of the larger number of points. The best candidates for aerosol optical depths are January 31st with 0.12 and July 11th with 0.12 or 0.24.

Based on Table 2, it is seen that point $\neq$ 3 did not change much its contrast on July 11th (Winter); but did on January 31st (Summer), again as expected. On the other hand, point $\neq$ 5 had a large variation in 1973, since the runaway was under construction with a considerable amount of particles in the air. In 1978, it was already built and no large variation of contrast occurred for different aerosol optical depths. Taking the averages, the candidates for aerosol optical depth are 0.24 for July 11th, 1973, and 0.12 for January 31st, 1978. This conclusion is in accordance with Table 1, if it is noted that the aerosols are not uniformly spread but with different concentrations over different areas. If point $\neq$ 3 is not included, the best average correlation is 0.12 (January 31st) and 0.24 (July 11th), The exclusion of point $\neq$ 3 can be justified on the basis that it changed with time.

Finally it should be remarked that, if selected windows and points are carefully chosen, this method has a potential to indirectly estimate the aerosol optical depth and determine its proper value for a better atmospheric correction, thus checking its quality.

ACKNOWLEDGEMENTS

REFERENCES

Dias, L.A.V.; Pereira, A.E.C.; Camara Neto, G.; Bentancourt, J.J.V. Correção de efeitos atmosfericos em imagens de satelite. São José dos Campos, SP, INPE, outubro, 1981. (INPE-2281-PRE/059).

O'Neil, N.; Miller, J.R.; Ahern, F.J. Radiative transfer calculation for
    remote sensing applications. In: CANADIAN SYMPOSIUM ON REMOTE SENSING, 5.
    Victoria, Canada, 1978. Proceedings. Ottawa, Canadian Remote Sensing
    Society, 1978, pg 572-578.

Selby, J.E.A.; Kneizys, F.X.; Chetwynd Jr., J.H.; McClatchey, R.A.
    Atmospheric transmittance/radiance: computer code LOWTRAN 4. Air Force
    Geophysics Laboratory, Hanscon AFB, MS, 1978. (AFGL-TR-78-0053).

Turner, R.; Spencer, M. Atmospheric model for correction of spacecraft data.
    In: INTERNATIONAL SYMPOSIUM ON REMOTE SENSING OF ENVIRONMENT, 8. Ann
    Arbor, MI, 1972. Proceedings. Ann Arbor, MI, ERIM, 1972, pg 845-947.

TABLE I. CORRELATION COEFFICIENTS

		July 11th, 1973							
		Point ≠ 1		Point ≠ 2		Point ≠ 3		Point ≠ 4	
		0.12	0.24	0.12	0.24	0.12	0.24	0.12	0.24
Jan. 31st, 1978	0.12	0.269	0.269	0.365	0.366	0.231	0.208	0.408	0.392
	0.24	0.246	0.245	0.343	0.344	0.230	0.208	0.409	0.384

TABLE II. CONTRAST

July 11th, 1973	Original	0.12	0.24	0.48
Point ≠ 1	9.52E-2	8.32E-2	9.42E-2	6.66E-2
Point ≠ 2	1.88E 0	3.20E 0	2.81E 0	2.69E 0
Point ≠ 3	1.00E 0	1.10E 0	1.19E 0	1.26E 0
Point ≠ 5	1.45E 0	1.17E-1	2.39E 0	1.61E 0
AVERAGE	1.106E 0	1.388E 0	1.621E 0	1.406E 0

January 31st, 1978	Original	0.12	0.24
Point ≠ 1	5.55E-1	5.29E-1	5.12E-1
Point ≠ 2	1.91E-1	2.05E-1	1.45E-1
Point ≠ 3	2.66E-1	3.10E-1	2.72E-1
Point ≠ 5	4.47E-1	4.35E-1	4.23E-1
AVERAGE	3.650E-1	3.697E-1	3.382E-1
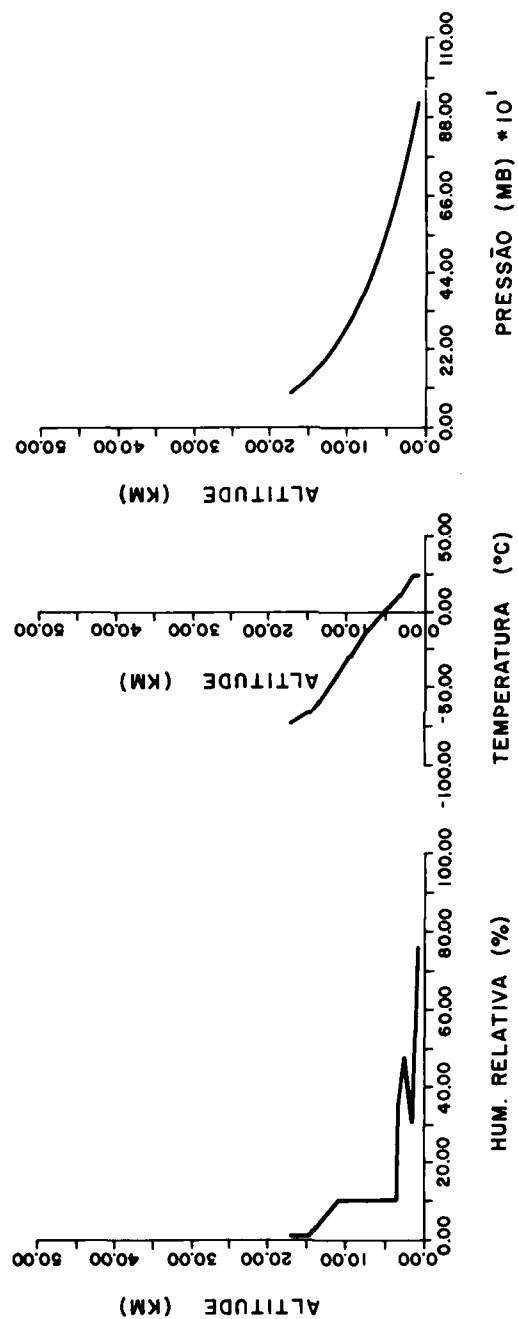
Figure 1 - Input.
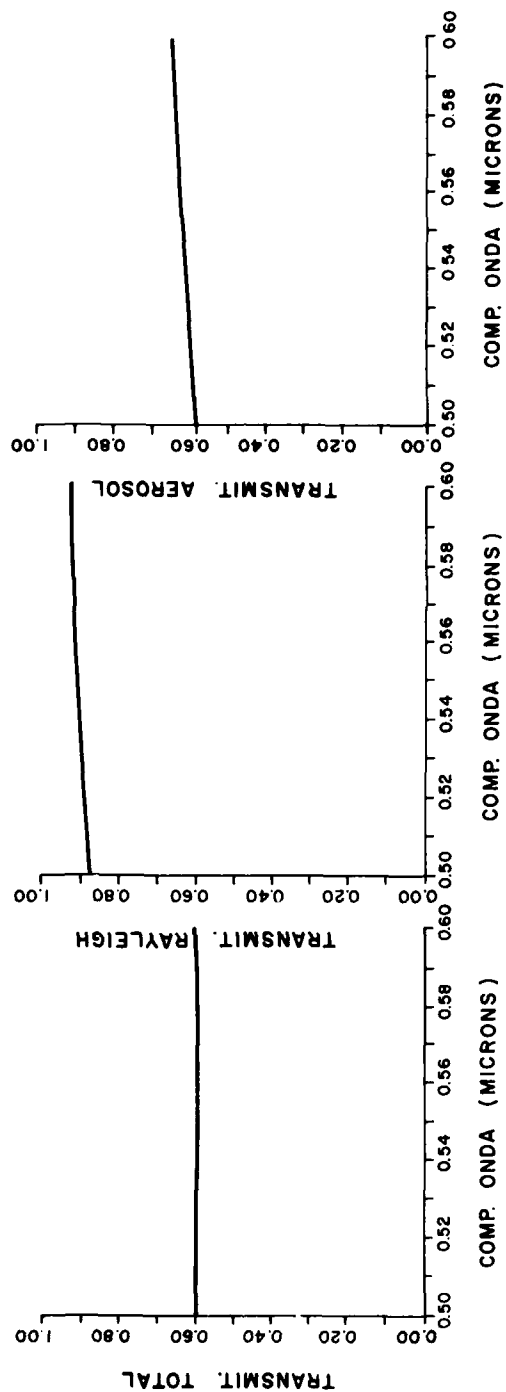
Figure 2 – Output.

ARGENTINE RECEIVING AND PROCESSING FACILITIES

Luis Socolovsky

Comision Nacional de Investigaciones Espaciales
Buenos Aires, Argentina

SUMMARY

Receiving Facility:

The Receiving Facility is located at Mar Chiquita, approximately 400 km from Buenos Aires. The antenna coverage area has a radius of 3,200 km at 3° elevation. It receives MSS and USB data. The reception subsystems are:

(a) Antenna Subsystem: The antenna motions are azimuth and elevation with the possibility of manual and automatic tracking. Antenna diameter is 10 m.

(b) Reception and Control Subsystem: It receives the RF signal emitted by the satellite, uses the satellite ephemeris for pointing purposes and runs the tracking programs. Outputs of this subsystem are data to be recorded on the high density digital tapes and data to be recorded on paper Quick-Look images, 70 mm format.

(c) Recording Subsystem: Recording is performed simultaneously on two Martin Marietta/Honeywell serial-in serial-out high density recorders.

(d) Control Images Generation Subsystem: Images transmitted by the satellite are displayed in real time on a video unit and, by means of a Quick-Look image recorder, 70 mm B&W paper images are obtained.

(e) Time Code Generation Subsystem: A time code is recorded on the high density tapes to enable the correct interpretation of image data at the Processing Facility.

The system is controlled by a PDP 11/34 computer. The receiving link is duplicated in order to improve its reliability. In case of emergency power is supplied by an Uninterrupted Power System.

Processing Facility:

The Processing Facility is located in Buenos Aires, and consists of two subsystems: Electronic Processing and Photographic Processing.

In this facility the information recorded on the High Density Digital Tapes is processed to obtain films and computer compatible tapes (CCTO as final products upon user request.

HDDT's are read and processed in order to build a 70 mm image archive for image availability control and image selection by users.

This archive supplies information such as mission, track, frame, date, time, cloud cover, etc., in order that user may know the characteristics of each image.

Operating Modes

Mode 1: Data read from the HDDT is used to make up the satellite image which is displayed on a CRT, frame by frame. In this mode the necessary information for image retrieval is input, that is: track, acquisition date, mission number and HDDT number. Cloud cover and visibility assignments are also performed here, either by the operator or automatically. This operation is used to generate and update the image archive.

At the end of this phase, the second phase is automatically initiated in order to produce images on 70/240 mm film (selectable) in band 7 which is used to check the general quality of the image.

Mode 2: This mode produces first generation images in four bands on 70/240 mm film (selectable) and computer compatible tapes. Images are corrected according to NASA bulk standard. Image resampling methods are either nearest neighbour or cubic convolution. To complete 18 consecutive scenes (4 bands) on 240 mm film, about 3 hrs 20 min are required (nearest neighbour resampling). Uncorrected CCTs are produced in about 15 min.

Mode 3: This mode is used to produce special products such as digital enlargement and CCT copies in BIL & BSQ formats.

Mode 4: Utilities and test programs.

Mode 5: Archieve management and updating. Mode 1 data is stored as described above. This data is used by mode 5 to search for available images.

The system is controlled with a PDP 11/34 A, 128 KW memory. Products available for users are:

* Black and White 1:1,000,000 positive transparency; 1:1,000,000 paper; 1:500,000 paper; 1:250,000 paper.

* Colour Composite 1:1,000,000 positive transparency; 1:1,000,000 paper; 1:500,000 paper; 1:250,000 paper.

* Computer Compatible Tape (CCT): 9 tracks, 1600 BPI, BIL and BSQ format.

AD P002076

ANDEAN GEOCRYOGENIC FEATURES IN SATELLITE IMAGERY AND ACCIDENTS WARNING

A.E. Corte
D. Trombotto

Instituto Argentino de Nivología y Glaciología
CONICET

Mendoza City, Province of Mendoza, Argentina

ABSTRACT

Four types of andean cryogenic featu-
res are compared based on ground experien-
ces, aereal photographs and satellite image
ry: 1) uncovered glaciers; 2) debris-
covered glaciers; 3) rock glaciers; 4) a
soligelifluction contact.

Satellite imagery can be very useful
in isolated areas for warning on glaciolo-
gical accidents, because the uncovered ice
shows very clearly when located on a dark
background of water, vegetation or rocks.
The other three features are not clearly
distinguished in satellite imagery without
ground experience. Fortunatelly, they are
not related to cryogenic accidents.

INTRODUCTION

In Argentina Andes chain, the solid precipitations are important sources
of water; they are feeding glaciers, debris covered glaciers, rock glaciers,
and a large debris area; through them the water may be kept frozen o re-
tarded in its flow. The diagnosis of such cryogenic bodies is important for
general cryogenic inormation, or for the assessment on possible glacier war-
ning on accidents.

The field experience gained by the author (Corte, 1978; Corte et al.,
1981) in the dry central Andes and other places, will be used in order to
confront ground knowledge with aerophotos information and satellite imagery.

GENERAL APPROACH

Areas in which the authors have a reliable ground experience will be used
as test areas. In general, three types of data will be compared: 1) ground in
formation; 2)aereal photo surveys; 3) satellite images. Such information will
be analysed for four types of cryogenic features: a) debris covered glaciers;
b) rock glaciers; c) soligelifluction contact; d) uncovered glaciers (Table I).

RESULTS

A. Debris covered glaciers (N° 1; 2; 3)

The Horcones, Tupungato, and Tres Dedos are well depicted in aereal photos (photo 1), and in satellite 1:250,000 (249/83). The satellite image (249/83) shows the debris covered glaciers which are in thermokarst and structural debris facies in their development (Corte, 1978; Corte et al., 1981), reveal a series of elevations and depressions (photos 2; 3). Due to the fact that there are no contrasts between the debris covering the ice and the surrounding rocks, it is not possible to forecast covered ice with certainty based only on satellite images, besides, it is difficult to differenciate a debris covered glacier from recent moraines.

B. Rock glaciers "sensu stricto" (N° 4; 5)

Rock glaciers which are not related to cirque or glaciers activity, which are formed by avalanches of snow and debris, located on the southern (cold) face of the mountains, are called rock glaciers or primary origin (Corte, 1978). When such rock glaciers are coalescing, they are very clearly depicted in aereal photos (photo 4), and also show in the satellite images 1:250,000 (249/83).

Single rock glaciers like El Salto (photo N° 5) show well in aereal photos; El Salto is clearly distinguished in the satellite image 1:250,000 (249/83). The ground inspection of this rock glacier reveals that its 100 m high front nose (photo N° 6) is clearly observed in both satellite (249/83) and aereal photos (photos N° 5 and 6).

These permafrost bodies are better defined in satellite images than the debris covered glaciers. However, they cannot be determined with certainty only by satellite images.

C. Gelisolifluction contact (N° 6)

A soligelifluction contact line of 1250 m long (249/83), in a flat mountain terrain at 4000 m high, is clearly identifiable because the solifluction brings two rock types into contact: a black metamorphic one, and a white granitoide (this feature is observed in aereal photos and in satellite image; the ground inspection shows the sharp boundary) (photo N° 7).

D. Uncovered glaciers (N° 7; 8; 9)

Uncovered glaciers are clearly shown in satellite imagery as indicated by several examples (example N° 9 of Table I); images 246/95 and 246/96 show the 1000 m wide tongue wall of the Moreno Glacier ponding the water of the Roca Lake. The Plomo and Laguna Glaciers (249/83; 249/84; examples N° 7 and 8 of Table I) are clearly depicted because of the contrast of the ice and the black rock. This gives hopes for future warnings on glaciological accidents in such areas.

Satellite images 246/95 and 246/96 can be a good case history: satellite image 246/95, of January 2, 1969, shows the Moreno glacier against the rock wall starting the ponding of water in the southern branch of Argentino Lake: the Roca Lake. Image 246/96, taken on May 4, 1979, shows the lake enlarged. The lake kept on expanding until the afternoon of February 15, 1980, when a series of noises like thunder storm began to break the ice wall and the lake started to drop. I was camping close to the lake and the dam, and could observe this nature wonder; unfortunatelly the darkness did not permit photographs.

1028

CONCLUSIONS

Based on ground experience we can observe that debris covered glaciers from 8000 to 12,000 m long, show in satellite images with a corrugated pattern. Without ground experience it is not possible to differenciate debris covered glaciers and recent moraines (Holocene) only by means of satellite imagery.

Coalescing rock glaciers, located along the southern cold face of the mountains show very well in satellite images 1:250,000 if they are larger than 1000 m. Single rock glaciers cannot be identified in satellite images without ground experience.

A gelifluction contact 1250 m long indicated by a contact zone of two rock types is very clearly shown in satellite images 1:250,000; such features require ground experience in order to locate them in satellite images.

Uncovered glaciers are the feature more easily to be determined from satellite images provided they are against a dark background of rock, water or vegetation. In remote inaccesible areas, satellite images at 1:1,000,000 and smaller scale, can be used to a good advantage for warning on glacier accidents.

REFFRENCES

Corte, A.E., 1978, "Glaciers and glaciolithic systems of the Central Andes". World Glaciers Inventory, Proc. of the Riederalp Workshop, Sept. 1978, IASH-AISH Publ. N° 126, 1980.

Corte, A.E., y Espizúa, L.E., 1981, "Inventario de glaciares de la cuenca del Río Mendoza." Parte I (texto) 64 p. Parte II, 24 mapas. Mendoza, CONI-CET.

Polanski, J., 1965, "The maximum glaciation in the Argentine Cordillera." Geological Soc. America, Special Paper N° 84, VII INQUA Congress, Boulder, Colorado, p. 453-472.

TABLE I – Types of Andean cryogenic features considered

		CRYOGENIC FEATURES	TYPE OF INFORMATION			PLACE	S.L.	Size of features m
			Ground	Aereal photo	Satellite Date Row/Path			
A	1	Debris covered glacier (Horcones)	1949	1963 1973	15/3 249/83 1976	Mendoza River (Mendoza)	32.30	8,000
	2	Debris covered and uncovered glacier (Tupungato) Polanski (1965)	1963	1963 1973	15/3 249/83 1976	Tunuyán River (Mendoza)	32.30	12,000
	3	Debris covered glacier (Tres Dedos)	1976	1963 1973	15/3 249/83 1976	Cordillera Central (Mendoza)	32.30	2,500
B	4	Coalescing – Rock glacier	1975	1963 1973	15/3 249/83 1976	Cordillera del Tigre (Mendoza)	32.30	6,000
	5	El Salto – Rock glacier	1976 1979 1981	1963 1978	15/3 249/83 1976	Cordón del Plata (Mendoza)	33	5,700
C	6	Gelisolifluction contact	1982	1963	15/3 249/83 1976	Cordón del Plata (Mendoza)	33	1,250
	7	El Plomo glacier (Mendoza)	1977	1963 1973	15/3 249/83 1976	Cordillera Central – Límite (Mendoza)	33	5,500
D	8	Uncovered glacier La Laguna, Río Atuel	Jan. 1979 Feb 1980	1963	3/3 249/84 1975	Cordillera – Límite Río Atuel (Mendoza)	34.30	3,900
	9	Uncovered glacier Moreno	Feb 1980		4/5 246/95 1978 2/1 246/96 1979	SE Hielo Continental (Sta. Cruz)	50	1,000 m wide ice tongue against a rock wall

Photo N° 1. Rock glacier Tres Dedos. Aerophoto by IFTA for IANIGLA. Cordillera Central, Mendoza, February 1973.

Photo N° 2. The debris cover of the Tres Dedos form the ground.
Photo by Arturo Corte, 1976.

1032
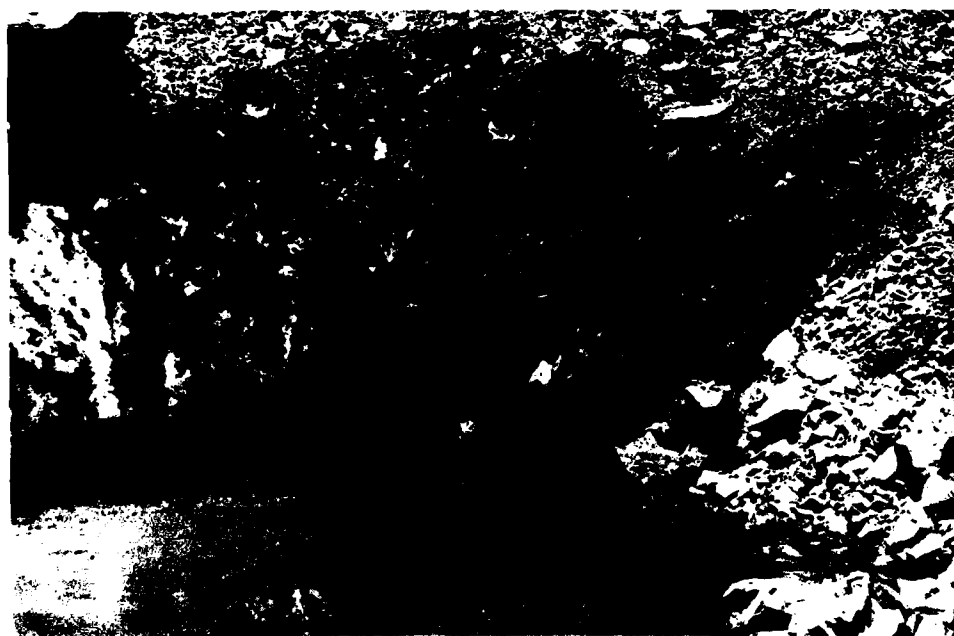
Photo N° 3. Close-up picture of a thermokarst hole in the Tres Dedos
rock glacier. Photo by A. Corte, 1976.
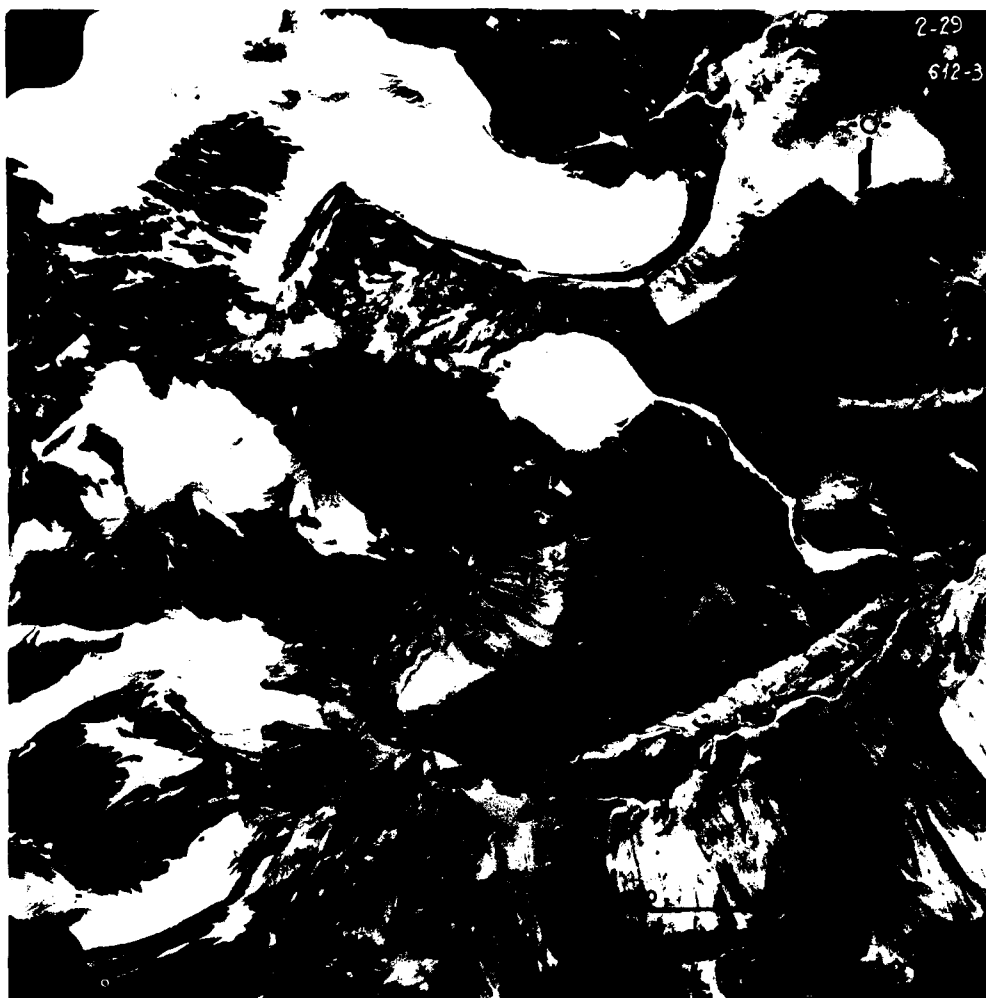
Photo N° 4. Coalescing rock glaciers in the southern cold faces of the valleys (lower right). Aerophoto by IFTA for IANIGLA. Cordille ra del Tigre, February 1973.

Photo N° 5. Primary type of rock glacier "El Salto" taken from a Piper plane. Photo by A. Corte, April 1978.

1035

Photo N° 6. Front view of El Salto rock glacier. Photo by Darío Trombotto, February 1981.

Photo N° 7. A soligelifluction contact at 4000 m between a black meta-morphic rock and a white granitic. Lagunita del Plata. Photo by D. Trombotto, February 1982.

OCEAN WAVE DETECTION WITH SHUTTLE IMAGING RADAR-A SIR-A

David E. Lichy
Michael G. Mattie

U.S. Army Corps of Engineers
Fort Belvoir, Virginia

SUMMARY

During the second mission of the United States Space Shuttle, the remote sensing payload contained the Shuttle Imaging Radar (SIR-A). SIR-A was a Synthetic Aperture Radar (SAR) similar to the Seasat-1 SAR. The shuttle SAR flew at a lower altitude and larger inclination angle than the Seasat SAR.

Two orbits (#17 and #20) crossed the east coast of the United States near Cape Hatteras, North Carolina. During orbit #17 and #20, time coincident ocean wave data was collected and for orbit #17 coincident X-band Side Looking Airborne Radar (SLAR) data was acquired. Preliminary review of the data suggests ocean waves were detected on both SIR-A, and SLAR.

The SIR-A and SLAR imagery will be analyzed for ocean waves and this data will be compared with ground truth measurements.

Since SIR-A orbits #17 and #20 were at different look directions, the effect on wave detection of the SAR look angle relative to the wave crests will be examined. From this evaluation, some general comments on SIR-A wave detection capability will be made.

USE OF LANDSAT IMAGERY FOR GEOLOGICAL AND HYDROLOGICAL MAPPING.

JAVIER ULIBARRENA: Professor of Remote Sensing. Facultad de Ciencias Naturales, U.N.L.P. La Plata. ARGENTINA. ADOLFO ROJO: Professional de Apoyo a la Investigación C.I.C. Cáthedra of Hydrogeology. La Plata. ARGENTINA. CARLOS SCHROEDER: President. Instituto de Ciencia y Técnica Hídrica. La Plata. ARGENTINA.

RESUM

In this work, examples of different application of Landsat imagery are displayed, for different themes. We've worked in a visual form, using for that the conventional methodology of photo-interpretation.

The object of the present work is to choose the form of putting on point a manual operational technic, whose last product will be to a low price, of a great application and which is suitable with the systems of handling information at present.

We show the information about two test areas, situated on the south extreme of Argentine Republic, which present very different characteristics se geological as climatic ones.

INTRODUCTION

The laboratory of Remote Sensing of the Facultad of Ciencias Naturales, has prepared a serie of works which were thought with the last object of checking the goodness and limits of the Landsat information, in different disciplines.

In all the cases, we worked in base to the conventional methodology of photo-interpretation, using the identification of all those evident characteristics on the imagery. For that, the following steps are respected: detection, identification, classification, analysis and measuring of different features, with the object of projecting or defining photomorphologic units which express similar ecologic conditions or surfaces of photographic aspects very identical.

The images were interpreted in a visual form through the traditional elements of analysis, such as drainage system, differential erosion, relative tone or reflecting, lineament of different types, vegetation and use of the ground, trying, when it's possible, to remark specially the different anomalies.

We've worked on Landsat imagery, transparences in white and black at scale 1:1.000.000 and enlarging at scale 1:250.000 in white and black and coleur composite. We used images of different times of the year. For some specific places and/or of a difficult interpretation, we practice a system of simultaneous analysis, parallel, using for that a second covering of air panchromatic photographs conventional, of different scales, which change between 1:40.000 and 1:60.000; with those photographs we made a double control in laboratory, in points considered critical for the interpretation.

OBJECTS

The scientific objects of this work is to know the possibilities of using the Landsat imagery, in the geological and hydrological studies. Specially in countries that, as our own one, are in need of a great roadbed of computation and adequate at the effect.

We try to display a manual or visual technic of interpretation on the Landsat imagery, which will be operational and at a low price; it's to say, to put an point technics based in theoretical concepts well-known and instru-

mental means accessible, which permits to any investigator to obtain a last economic product, that has a great application and that is compatible with the known systems of information and analysis at present. It's destined to be used in those laboratories which are in need of instruments for the automatic interpretation, and which have to work in zones where we can't use a basic cartography adequate to the physical medium.

The main technical objects are more specific and concrete; they're:

a) Preparation of a hydrogeological base map and to search additional useful information which can help a posterior hydric evaluation of the zone.

b) Preparation of a geological sketch and forestal mapping of an economic interest.

The application of the Landsat imagery, for the mapping on geological characteristics, lithological discrimination, vegetal covering and vegetation indicatory of underground waters, have been evaluated for us in different geographic areas of our country, being in all the cases the successful results. Among them, using the technical objects enunciated, we've chosen two areas at proof, which were adequated to this end. For that, we looked for those zones which hadn't the previous information sufficient to that physical medium.

A.- Deseado Port, Province of Santa Cruz.

B.- Grande Island of Tierra del Fuego.

TEST AREA A: DESEADO PORT.

SITUATION: The zone is situated on the northeast extreme of the Province of Santa Cruz. It's the area situated in the Deseado Port's environs. It occupies a surface of 4.000 km2, being defined in geographic situation for the coordinates 47º 20' and 47º 50' of south latitude and 65º 41' and 66º 42' of west longitude from Greenwich meridian.

OBJECTS: a) Extraction of basical information, fundamentally related with the differentiation or separation of hydrolithological units.

b) Delimitation and searching of vegetation, indicator of the existence of underground water, specially for being a semidesert area.

In a large program of hydrogeological investigations which's at present in a full evolution for intermediate of the Cathedra of Hydrogeology of our Faculty, the laboratory of Remote Sensing was asked the preparation of a base planimetry, a geological/hydrogeological map and consequently all type of additional information that could be extracted from the Landsat imagery and which could do a favor or help in the search of a solution at the problem in study.

For that, the present work includes only the preliminary period of the mentioned program, which has the last object of provisioning the potable water in the city of Deseado Port and its zone of influence.

USED MATERIAL: For this first test area, different photographic products were used, at scale 1:1.000.000 in positive transparence, in white and black and colour composite. Copies in white and black and colour composite of an excellent quality, all them at scale 1:500.000, 1:250.000. We've images of different times of the year, what helped enormously in the investigation.

We worked on transparent table, preferably on the following images, colour composite, at scale 1:250.000. One from January, 15th. in 1976 and other from December, 1st. in 1980. Comparing the two images a very marked difference appears in the chromatic aspect; in the second of them the levels of the tonal variations is more pronounced; it's probably because the same one was examined in an epoch with pluvial precipitation abnormal, in that moment that reached the double of the annual mean.

In spite of it, the same one presents an excellent quality and a good chromatic discrimination, what permited to adjust and to complete the photogeological units.

The zone hadn't a basical adequate cartography and we only had the regional sketches. In spite of that and for the relative geological homogeneity, the structural disposition horizontal of the lithological units; the environment of desert type and the easy accessibility of the area, the commended mapping and analysis was relatively easy.

CLIMA: Climaticly, it presents two environments well-defined; one's constituted by the zone of table-land and the other, the coast band. The zone of landing participates neatly of the continental rigorous clime, where the temperature, precipitation and winds present situations more extreme, low temperature and humidity, associated with hard wind and limited precipitation.

In general words or for the principal part of the test area, the precipitation presents an annual mean of 200 mm. with a temperature of 10º C and here the landing obtains a great importance, the hard and persistent wind, that influences notably in the evapotranspiration. The speed of the wind waves between 15 and 19 km/h.

The other one, of a shorter extension, is constituted by a band of parallel terrain to the coast, where the maritime humid clime's influence is felt, with evident influence which moderates the same, because the climatic conditions aren't so extreme.

GEOLOGY AND MORPHOLOGY: The zone is characterized by a serie of terraces (landscape and stairs), of which the included between the quota 100 and 180 m. of altitude, is of a greater areal extension; it's only interrupted exceptionally by island hills or mounds, that are the superficial manifestation of the porphyry rocks present in subsurface. Other morphologic characteristics which interrupt this terrace landscape, are those ones of concave relief, constituted by the depressions or banks without superficial drainage and the radial ravines.

These last, change the exterior contour of the terrace only in part, which is dissected by the advancing headward erosion of the longitudinal valleys, giving as result a very sinuous border, almost digitate, what gives to them a characteristic aspect on the image.

From the geological point, in general lines, the zone is composed by three big rocky complexes, of very different age and varied lithological composition.

a) Volcanic complex Bahia Laura (known also as porphyritic complex) of an age half-jurassic and that lithologically is represented by vulcanites, quartzite porphyries and sedimentites.

b) Marine sedimentites of the Patagonian, constitued by transgressive deposits of marine origin, composed by psammites and pelites with calcareous levels (coquina) inter-stratified, of oligocene-miocene age (tertiary). Lying in erosive discordance about the volcanic complex Bahia Laura.

c) Patagonic or Tehuelches formation, constituted by cobbles, pebbles and granules, in a sandy base, are deposits which aren't consolidated of superior tertiary age - inferior quaternary or concretely Plio-Pleistocene.

This unit lies in discordance on the marine sedimentites of the Patagonian, cover almost all the region in form of continuous stratum with a variable density, although with a shorter areal expression, we can mention:

d) Littoral cordons, of marine origin, of composition-gravel in a sandy base. These cordons dispose parallelly at the actual beach and parallel among themselves, lying discordantly on the Patagonian.

e) Modern sediments or materials, redeposited, specially prosecuted deposits of a fluvial origin and other ones situated in the closed depressions and ravines, preferably of an aeolic and gravitational origin.

VEGETATION: The arid windy clime and the lithological covering's nature, constitute not life-producing and severe features, which include a xerophyte and semidesert vegetation, constituted by the Patagonian steppe, which represents the dominant formation of the regional ecosystem.

Many are the limitary factors that act in the zone; besides the short precipitation, about 200 mm. in a year, inconsolidated soils, fundamentally

rocky ones, predominate in the zone, of a considerable permeability; added to it there's an elevated value of the evapotranspiration, on account of the persistent arid wind from the south-west.

The vegetation is composed fundamentally by shrubs and grass, which occupy topomorphologic positions very well-defined, due to the mentioned limitations. In the valleys, ravines and depressions with a greater hydric availability than in all the area, stains of contracted plants and hydrophilic vegetation appear, these last ones preferably in the swampy ground.

The shrubby formation, predominates specially in the banks and depressions and it's changed by hard grass in the hillsides' superior part.

The xerophyte vegetation is what predominates in all the area, specially in these zones, level-elevated known as "pampas". It's a vegetation with a scatter distribution which develops adjusted to the greater or less possibility for using the soil or subsoil's waters, that exist there, in some epochs during the year.

In some sectors of the terrace, this distribution changes itself, and the presence of the contracted vegetation's bands is very evident, with a greater density of covering, which dispose regionally in a coarsely dendritic form.

This disposition and the change of the vegetation's density that occurs in the "pampas" is because there's a localized improvement of the humidity's conditions. In these zones a greater retention of humidity predominates, what could be indicating a textual change in the soil or the presence of a channel-belt, of an old drainage system.

DRAINAGE SYSTEM: The drainage's model, which corresponds to a system of intermittent drainage, without doubt, presents a model that we could call radial centrifugal, if we look at it in a regional form; with dendritic subsystems of an coarse texture for each ravine, or course, if we look at it in an individual form.

The principal direction of the drainage's system is going on the Atlantic, specially on the east and northeast.

Watching the depressing in a punctual form, in some cases we can see a radial centripetal model, although really, this sub-system, which's enough frequent, is confined to the depressions' borders specially in those ones situated on the high terrace or "pampa".

The most important ravines which flow to the Atlantic, sometimes have in their terminations, frontal lagoons, on account of the antraped, that the litoral marine cordons cause.

The drainage's system is very well checked, due to the subsurface complex's fracturation, known as Bahia Laura, that imposes its preferential fracturation's direction in surface.

In the sectors situated near the Deseado River, the control by fracturation is more evident, what is indicating the presence few close in surface of the mentioned complex.

Almost all the superficial currents are ephemeral in general and half-torrential, being the Deseado River an exception, which's of intermittent regime.

HYDROLOGICAL MECHANISM: The cape of gravel situated stratigraphicly in the sedimental pile's top, conform the sedimental packet where the few precipitations that are produced normally in the zone are kept as concentrated waters.

The passage or transit of these waters toward the greatest profundities is retarded by the presence of a unit which isn't so permeable, composed by the marine sedimentites of the Patagonian, that perform as base rock.

But in account of this vertical retardation, the water will displace in the horizontal sense, from the infiltration place till the terrace's periphery, using the preexistent paleorelief, elaborated on the Patagonian unit and of this manner it finds its exit in the contact between the two formations, generating the sources.

Consequently, the vegetation's presence in big stains, specially situated on the walls near the ravines' head-waters, indicate the punctual dischar-

ge of the subterranean waters which are accumulated transitorily in the te-
rrace's subsoil.

PRELIMINARY RESULTS: In the two images we were very astonished because we saw
the presence od small reddish stains, which are indefectibly in the ravines'
head-waters, situating in the half-part of the ravine or walls of these cha-
racteristics; only in exceptional cases they were found on the floor of the
same ones. Without doubt it was a vegetation in a good state of evolution
and of course, they presented a hard infrared reflectivity.

After this first observation a selected inspection was made, about the
images, in the high terrace and there we could watch also the presence of
banded and alineation of similar reddish colour, although they were smaller.

The same ones seem to follow a certain alineation coarsely dendritic not
being easy, in many cases, to watch the continuity of these lines individua-
lly, it's principally because the small dimensions of the stains and the
chesnut reddish colour of the terrace's cover, that masks them. In general
it's possible to see a zone finely dotted instead of a line, that follows pa-
rallelly at the principal ravines and that keeps this disposition upstreaam,
interning itself in the high terrace, farther away the initial graves of the-
se ravines.

On account of the geological characteristics of the zone, we imagined
that they were, in the first case, it's to say the stains on the ravines'
walls, sources or zones where the lithological unit of surface drained their
waters, known as tehuelches or patagonian gravel, it's to say that specifica-
lly it was the geological contact, between this first sedimentary cape or
parcel, receiver and keeper of water and the subsurface cape of less permea-
bility, known with the name of Patagonian formation and which is used as hy-
drosupport.

These stains represent, for their geological and topographical position
defined, zones of sources situated in the contact of the two lithological u-
nits, more modern, of different relative permeability.

This information was confirmed then, when it contrasted with a map of
sources, which facilitated Sanitary Works of the Nation Regional District De-
seado Port. In the aligned vegetation's case which is situated on the high
terrace or "pampa", it was easily reinterpreted with the air photos helping
at scale 1:60.000, which showed that was contracted vegetation, that is si-
tuated near and parallelly at the ravines head-waters relatively important
and this disposition keeps toward upstreaam, farther away the initial graves
of the same ones, in concordance with the possibility of putting out water,
for its subsistence.

Without doubt, they were zones of a greater biological activity than
their environs for a greater humidity, what translates itself in a vegetation
in a better state of evolution and, of course, presenting a high infrared re-
flectivity.

It's to say that we can use the vegetation as an element indicator of
water in subsurface.

In other way, the greater or minor chromatic intensity of these stains,
with the chemical analysis facilitated by the Municipality of Deseado Port,
with the object of associating these variations of colour with the quality of
the waters. The experience seems to be positive because a narrow coincidence
was observed between the good quality of the waters and reddish colours of
the vegetation: meanwhile the water's quality declines, a greater salinity
makes more and more yellow the stains colour.

In resum, we've obtained information related with the:
- Planialtimetrical situation of the sources.
- Expeditive evaluation of the waters quality.

TEST AREA B: GRANDE ISLAND OF TIERRA DEL FUEGO.

SITUATION: It's a zone very distant, situated on the south extreme of the Ar-
gentine territory, separated by about 2.500 km. from Buenos Aires city. The
central geographic coordenates of the studied water are the parallel 54º

south latitude and 67º west longitude from Greenwich meridian. The surface of Grande Island is of about 21.000 km2.

OBJECTS: The Austral Center of Scientific Investigations asked at the Remote Sensing laboratory, the preparation of a serie of thematic maps, in relation with the following themes.

a) Differentiation and mapping of the lithological units.

b) Identification and mapping of the forest areas, specially those ones with an economic interest.

c) Delineation of the fluvial system.

d) Detection and mapping of the different morphostructural units.

e) Means of communication's map and human establishment.

For concreting the first of these objects the areas free of vegetation were analyzed fundamentally we based in the characteristics originated by selective erosion, differences of microrelief, and-so-on.

For those areas of hard or consolidated rock, of strong topographic expression, and which were affected by the glacial processes, we took into account the glacial cirques geometric form, and in all the cases we gave importance to the resultant mesostructures and the mesolineament, observable on the images.

For the analysis of the morphostructural units, not only we have to analyze the macrorelief's differences, also we took into account those structures such as the fracture's systems and very specially the photolineaments of all type, including tonal stains, areas or bands without vegetation, depressions, crests, rivers ravines and lagoons borders.

USED MATERIAL: We worked fundamentally on images registered on March 20th. in 1979, copies in white and black at scale 1:250.000. We had other serie of images from February 26th., 27th. and 28th. in 1981.

The strong snowfall and the dense covering of clouds, which's permanent in this area, don't permit to use images of a good quality for a normal interpretation in many cases; for that it was indispensable to use scenes from different times of the year, and besides different years, canning cover the area under study totally.

This zone has a few basical and general information adequate, specially referring to geology, topography, vegetation, and-so-on. Equally the mountainous area next to Fagnano lagoon is of difficult access. If we join to it the exiguous quantity of roads and/or tracks, the presence of long impassable peat-bogs, make the terrestrial check very difficult and it only can be made with a helocopter.

CLIME: The clime, in general, is severe, cold and humid, changing in an imperceptible form from south to north in the Island; becoming a little dry when we go on the north.

In the south zone, the absolute maximum and minimum temperatures are 25º and 13 º C in Ushuaia station, and 29º and 14º C in Rio Gallegos, station situated in the south part of the continent. The annual half-precipitation is of 548 mm. in the south, it's to say Ushuaia and 222 in Rio Gallegos, in the north.

The cloudiness with a covering of about 6/8, is present in the area approximately the 75% of the time.

GEOLOGY AND MORPHOLOGY: The studied zone can be divided into four physiographic or morphostructural units, relying on the most important characteristics printed on the surface's materials. We called them, Cordillerean South Unit, Unit of crests and valleys of west center, Wavy Unit of east center and Plain Unit of northeast.

The Cordillerean South Unit has a rough topography and it's strongly sloped, its half-altitude fluctuates between 800 and 1.000 m., getting its maximum altitude about 1.500 snm. in the hills situated in the north of Ushuaia city. In general words, it's the sector most elevated in the Island, it's in the south of Fagnano lagoon and from it till the Beagle Canal, losing

1046

altitude in the east. It represents between 30 and 35% of all the island's surface.

This positive relief was remodeled by an intense glacial action in the Pleistocene epoch. Geologically it's composed by consolidated rocks and in it the oldest units appear.

Really different types of sedimentites predominate, and many of them are affected in different grade by metamorphism of a low rank; they are followed in order by the volcanic rocks of diverse composition, being represented in a bigger percentage those of acid composition chemical. In the west-northwest sector of Ushuaia outcroppings of diverse metamorphites appear and at last, a reduced superficial expression of plutonites of an acid composition to me-sosilicic, among which the granodiorites and granites presominate. These granites are situated a few kilometers on the south of Kaiken.

All this sector is covered in part by glacial deposits; the outcroppings only can be observed in the glacial cirques and/or the rivers'cuts.

Unit of crests and valleys of west center, is characterized by high hills or extended crests, separated by valley with plain botton, occupied by intermittent rivers and/or peat-bogs.

This morphology has a tectonic origin because it'a a zone of folded se-dimentites and then a glacial and fluvioglacial process acts on it.

Its morphologic expression changes progressively on the south, where it gets a great predominance and the resistent rocks'crests, a greater altitude.

Equally, these crests lose altitude on the east and disappear in the surface, near Kaiken.

These crests and valleys are oriented in the direction west-northwest - east-southeast, what originates a characteristic morphology and very diffe-rent of the other zone, because they form an environment predominantly waved with crests and parallel valley among them.

Geologically, they're sedimentites of cretaceous age, are plunged units, folded in some places. They present themselves as big crests of rock, more resistent than those ones which surround them.

This region has been profoundly affected by the quaternary's clime, be-cause the stratum of ice left in retrocession its materials'load of different sizes, giving a potent covering of inconsolidated sediments, of glacial and fluvioglacial origin, that in a good part masks the old preexistent relief.

Wavy Unit of East Center. This unit is limited in the west by a line that would join the locality of Kaiken and the confluence of the rivers Gran-de and Moveta. This unit is constituted by horizontal sedimentites, which lies discordantly on the materials of the previous unit that supplant hori-zontally; it extends from this zone till the Argentine Sea's coasts. This u-nits, as the previous ones, is covered with glacial and fluvioglacial sedi-ments, what gives us a waved morphology definitively.

In resum, it's an extended waved plain with a regional pendant towards the Atlantic, composed by marine sedimentites, such as marls and sandstone of terciary age (inferior and medium) disposed discordantly on the rocks of cre-taceous age.

Plain Unit of northeast is the zone of a softly waved model to plain. In general it's a waved plain with soft pendant towards the Atlantic. In punc-tual form, they're hillock more or less isolated, with a big quantity of de-pressions intercalated among the first ones, we can see many lakes and lago-ons which identify their fluvioglacial or periglacial origin.

A less altitude characterizes the zone; the presence of the mentioned lakes and lagoons, and the drainage main, altough also dendritic, is very co-arse, indicating the more pervious materials'presence.

The inconsolidated sediments predominate, specially fluvioglacial depo-sits, fluvial conducted, peat-bogs and littoral deposits of marine origin.

All them are changed in a greater or smaller grade by the aeolic action and in a smaller proportion by the biotic action.

STRUCTURES AND PHOTOLINEAMENTS: The structural characteristics more conspi-cuous are the mentioned structural lineaments, with an orientation west, northwest - east, southeast which constitute plunging folds of many kilome-

ters of longitude and wave of folding, that expresses in hundreds of meters.

The photolineaments are represented in the fiels by tonal stains clear and/or dark, of humidity and erosion, outcroppings'crests, fluvial river bed's ravines, change in the direction of the rivers and rivulets, lagoons'borders, the vegetation's alineation, and-so-on. The most marked differences in the photolineaments are represented by changes in the direction of the same ones, specially in the units of the Island's center, because in the west they orient northwest - southeast and in the east they orient southwest - northeast; these last ones have a marked influence on the coast border, giving to it a characteristic sinuosity.

In the north sector we can see a marked orientation north-northwest - south-southeast, in the lagoons, although in this case, the orientation is preferently given by faulting.

VEGETATION: The arboreal vegetation cover about 40% of the Island. In the south part we can see a dense wood, whose members have a considerable portage and in a good sanitary state. The altitudinal limit of the vegetation is about 700 meters snm.

In the mountainous sector of the south, we have the Subantartic Province composed fundamentally by Lenga and Ñire, caducous vegetation, which is against the bands always green of perennial vegetation of the rainy wood, formed by Cinnamon trees, Maitenes and Cohiue-trees.

In the north of the Island, the Ñire is predominant, and the Lenga's presence is subordinate. This gradual variation of the vegetation has to be looked for in a climatic and altimetric conditions in the north sector of the Island; although it could not be strange the existence of a limitative factor such as the argillaceous material's presence in subsurface, that is mapped in the zone of Los Hermanos and Ruby Stay. There the forestal mass presents a great change of density and a less portage in the members, and in general we can find more degraded than in other sector. Here the Ñire predominates notoriously.

Lollowing towards the north the arboreal vegetation disappears gradually which is changed by the graminaceous steppe.

CONCLUSIONS.

The utilization of this type of image, specially in zones as the studied with marked seasonal changes and with climatic adverse conditions limitative, has given very satifactory results in the following points:
a) The discrimination of the different types of rock.
b) Structural map.
c) Mapping of vegetation.
d) Searching of water (sources).

The experience shows that is very convenient to use Landsat images for the generation of basical and adequate information, in those zones which not being studied previously, haven't information.

It's convenient and sometimes it's recommended, the simultaneous use of air conventional photographs conjunct and parallelly with the images of satellite, for resolving specific problem in conflictive areas.

It's indispensable for the regional hydrological studies, which conjunctly with the lithology is recognized and studied the associated vegetation, that could be indicator of the water's presence.

With respect to the relieved sources in the test area A Deseado River, the results are really encouraging because in a zone where the subterranean water is very limited, the presence of these sources permit us to glimpse the possibility of trying to propose an hypothesis of working, about the existence, ubication, quality and relative quantity of potable water, for this semi-desert zone. These observations in the future can be extrapolated at different zones of the Patagonian which present a similar ecosystem.

Although for that it'll be necessary new investigations, with a greater profundity of treatment, with the contribution of hydrochemical, phytogeogra-

phic and phenological criterions.

In the test area B, of Grande Island of Tierra del Fuego, where there's a bigger rank of variations, so the physical covering as the geological one, the mapping of surface's units was relatively more easy, canning differentiate four morphostructural units, and also the presence of arboreal vegetation and their differences in the sanitary state.

BIBLIOGRAPHY:
- Cátedra de Hidrogeología (1980) "Investigaciones Hidrológicas Aplicadas en el Area de Puerto Deseado, Provincia de Santa Cruz". Informe correspondiente a la primera etapa. Inédito.
- Obras Sanitarias de la Nación (1974) "Estudio Hidrogeológico para refuerzo de la provisión de agua" a Puerto Deseado. Inédito.
- Pezzuchi, Hugo Daniel (1978) "Estudio Geológico de la zona de Estancia Dos Hermanos - Estancia 25 de Marzo y Adyacencias, Departamento Deseado, Provincia de Santa Cruz". Tesis Doctoral, Facultad de Ciencias Naturales, UNLP.
- Caminos, R. "Cordillera Fueguina". Geología Regional Argentina.
- Caminos, R. et al. (1981). "Reconocimiento Geológico de los Andes Fueguinos. Territorio Nacional de Tierra del Fuego". VIII Congreso Geológico Argentino. (1981) Actas III.
- Codignoto, J. and Malumian, N. (1981). "Geología de la Región del Norte del Paralelo 54º s. de la Isla Grande de Tierra del Fuego". Asociación Geológica Argentina. Rev. XXXVI (1).

DIAGNOSTIC TECHNIQUES FOR METEOROLOGICAL SYSTEM
DEVELOPMENT BY MEANS OF REMOTE SENSING

Helvecia A. Enriquez de Albamonte
Gustavo R. Talamoni
Alicia L. Tejerina Puch de Massaccesi

Servicio Meteorologico Nacional
Buenos Aires, Argentina

SUMMARY

The highly maritime character of the southern zone of the Southern Hemisphere is the principal reason that causes the lack of customary meteorological data, due to the impossibility for developing a direct observation net with a station net fit for a better coverage for weather forecasting and meteorological research. It should be pointed out, especially, the location of countries such as Argentina and Chile.

Due to the aforesaid, it is extremely necessary to rely on means of remote observation, or unconventional observation, from the different meteorological parameters that, being appropriately collected and analyzed in real time, they could foresee the weather system development.

For that purpose, since 1968, satellite images are received at the Argentine Republic, in an operative way. And, from the beginning of the 70' decade, the National Meteorological Service (SMN) receives the relative heights field data of the different standard isobaric surfaces and wind direction and speed at different levels inferred from Geostationary Satellite data through the Washington-Buenos Aires Communications System.

This paper attempts to compare the different data of remote observation, qualitative (images) and quantitative (thickness and winds) with the available conventional data for a better utilization during operative tasks.

Bearing in mind this purpose the analysis of the interrelation and reliability of the mentioned information has been tried in order to determine:

(1) The field of relative heights that it is more representative for the associated meteorological phenomenon; its development.

(2) The field of relative heights that it is more representative for the displacement of systems.

On the basis of the analysis of the same it is wanted to obtain:

(1) To carry out forecasting techniques by means of combined observation methods (remote and local).

(2) Diagnosis of displacment, and development of the different weather systems through the satellite image observation and thickness field analysis.

(3) Influence of surface topography on the displacement of weather systems.

(4) Correlation of weather system analysis carried out on the basis of conventional data and remote sensor information through theoretical methods for evaluating the displacement of the systems considered.

INUNDATION STUDIES BY AUTOMATIC ANALYSIS OF LANDSAT DATA

Sigfredo Pagel
Maria Isabel Spreafichi
Aurora Quinteros
Natalia Marlenko

Comision Nacional de Investigaciones Espaciales
Buenos Aires, Argentina

SUMMARY

The object of this work is to study the efficiency of Landsat data automatic analysis applied to inundations.

A pilot area located in the Province of Santa Fe which was damaged by the last 1981 floods was taken as study area.

The chosen material was a Landsat image dated April 7, 1981, obtained through CNIE's Buenos Aires Processing Station of which a portion was selected for study.

Some ground truth was available and applied in order to accomplish the classification.

Mainly the work was carried out by two independent systems of automatic analysis. On the other hand, the ERMAN II software with a RAMTEK terminal on an IBM/370 computer and the second a system installed on a PDP 11/34 computer with an interactive COMTAL terminal and a software package developed by CNIE (PIDARG).

Two different methods were applied for the Computer aided analysis and a sample autocontrol was intended to achieve. By Clustering a non-supervised classification was carried out in 3 and 4 differentiable categories. Also, a supervised study was done using some test areas.

Reflectance studies were done by displaying line reflectance in different parts of the image taking into account the special properties of reflectances in band 6 and band 7.

Finally, studies in order to differentiate several areas were carried out establishing the different inundation degrees based upon the quotients between band 6 and band 7. Interpretation of these results was not direct, but through a gray level table obtained for the CCT-CNIE through a shoftware program meant for this purpose. This allowed to reach the conclusion that those reflectance quotients over 1.4 of value between band 6 and band 7 corresponded directly to inundated areas.

ESTIMATION OF THE SUGAR CANE CULTIVATED AREA FROM LANDSAT IMAGES USING THE TWO PHASE SAMPLING METHOD

Carlos Alberto Cappelletti
Francisco José Mendonça
David Chung Liang Lee
Yosio Edemir Shimabukuro

Instituto de Pesquisas Espaciais - INPE
Conselho Nacional de Desenvolvimento Científico e Tecnológico - CNPq
Caixa Postal 515, 12200 - São José dos Campos, SP, Brasil

ABSTRACT

A two phase sampling method and the optimal sampling segment dimensions are developed for the estimation of the sugar cane cultivated area. This technique employs visual interpretations of LANDSAT images and panchromatic aerial photographs considered as the ground truth. The estimates, as a mean value of 100 simulated samples, represent 99.3% of the true value with a CV of approximately 1%; the relative efficiency of the two phase design was 157% when compared with a one phase aerial photographs sample.

1. INTRODUCTION

In this paper a statistical system to estimate the sugar cane (Saccharum spp.) cultivated area in a subregion of São Paulo State, Brazil, is presented. The region under study is known as the Great Region of Jaú, located in the central part of the state, within the parallels 22°00' and 23°00' South, and meridian 48°00' and 49°00' West, covering 5046 km².

For this region, the sugar cane acreage was determined by two different approaches. In the first approach, Koffler at al., (1980) made interpretations of panchromatic aerial photographs in the scale of 1:35000 and 1:45000, complemented with a rigorous field control. This information is considered as the ground truth.

In the second approach, Mendonça et al. (1981) used LANDSAT images in the scale of 1:250000 and visual interpretation, associating the spectral variations of the crop with temporal variations in different satellite pass. Channels 5 and 7 were used.

With this basic information, a sampling experiment was designed to estimate the sugar cane acreage and measure the error rate in relation to the ground truth. The applied sampling method was a two phase sampling with regression estimates.

2. STUDY OBJECTIVES

a) To determine segments size in order to have the maximum correlation between LANDSAT data and ground truth.

b) To estimate the sugar cane acreage with a sampling design using LANDSAT data and ground truth and considering the cost of each source of data.

3. SEGMENTS SIZE AND SAMPLING METHOD

a) Determination of segments size

With a grid of size 1 cm by 1 cm (corresponding to 2.5 km by 2.5 km) applied on a composition of LANDSAT images and on a mosaic of aerial photographs, the number of points with sugar cane in each unitary segment was determined.

From that information, a subarea of 60 km x 37.5 km was selected and a uniformity trial (Federer, 1967) was designed. The response variable was the number of hectares cultivated with sugar cane by segment of 6.25 km².

Ten different types of segments were considered:

Type	Size							No. of Segments
1 x 1	2.5	x	2.5	=	6.25	km²		360
1 x 2	2.5	x	5.0	=	12.50	km²		168
1 x 3	2.5	x	7.5	=	18.75	km²		120
1 x 4	2.5	x	10.0	=	25.00	km²		72
2 x 2	5.0	x	5.0	=	25.00	km²		84
2 x 3	5.0	x	7.5	=	37.50	km²		36
2 x 4	5.0	x	10.0	=	50.00	km²		36
3 x 3	7.5	x	7.5	=	56.25	km²		40
3 x 4	7.5	x	10.0	=	75.00	km²		24
4 x 4	10.0	x	10.0	=	100.00	km²		18

The criterion of selection was the maximum correlation between the variables "response to the LANDSAT images interpretation", X, and "ground truth", Y.

b) Sampling design

A two phase sampling design with regression estimates was applied combining the two sources of information.

This design takes advantage of the correlation between X and Y and the cost ratio for collecting the data in each variable. The sample selection was done in two steps. In the first step, a relatively large sample in the less expensive variable, X in this case, was selected, and in the second step a small sample in the other variable that is more expensive to be observed, Y, was selected. This bivariate information permits the calibration of the information from X.

When the correlation between X and Y is sufficiently large, a reduction in the estimator variance and in the sample size is significant in comparison with a single phase sampling design on Y alone.

Before applying the sampling design, the region of study was redefined in order to eliminate parts of it where sugar cane is not cultivated, and also to eliminate some geographical accident as well as some incomplete marginal segments.

The theoretical considerations of the sampling method applied in this study are developed in Cochran (1963), Loestsch and Haller (1973) and Jessen (1978), among other authors.

4. ANALYSIS AND ESTIMATION

The sample size in the two phases was set to achieve a sugar cane acreage estimate within 5% of the corresponding complete acreage evaluation with a 95% confidence level at a minimum cost.

To calculate k and n, the number of segments in the first and second phase, respectively, it was used σy and ρ calculated from the complete enumeration of available ground truth data. When this information is not available, it is necessary to select a pilot sample.

With the obtained values of k and n, it was simulated a sequence of one hundred samples in two phases by means of a simple random selection in each phase, being the second phase sample a simple random subsample from the first one.

The simulation produced a sequence of values of the random variables $\hat{Y}_R$, estimate of the sugar cane acreage; $\hat{V}(\hat{Y}_R)$, variance of the estimate; and of $D = \hat{Y}_R - \alpha$, where $\alpha = 133888$ Ha is the total number of hectares cultivated with sugar cane from the ground truth complete enumeration. This value is assumed without error.

Finally, the simulated data were analysed statistically.

5. RESULTS

a) The selected segment size in the uniformity trial was the one with dimension 2 x 3, corresponding to 5.0 km x 7.5 km = 37.50 km² or 3750 ha. The maximum correlation coefficient between X and Y was r = .82 for this size, being r = .66 and .73 for segments of size 6.25 km² and 100.00 km² respectively.

b) The sampling frame, after being redefined (3 b), had 86 segments with an area of 3082 km², 16% of them incomplete, but with an area greater than one half of the complete one.

c) The standard deviation of Y was σy = 777.46 ha and the correlation coefficient ρxy = .82. The cost ratio considered $c_1:c_2$ was 1:13, where c_1 and c_2 are the unit cost of observing one X_i (in phase one) and one Y_i (in phase two), respectively. The sample sizes were k = 58 and n = 11 for a relative variance of 5% with a confidence level of 95% and a minimum cost of C = 201 monetary units. The regression equation of ground truth and LANDSAT data was Y = 442 + .69X.

d) The results from the analysis of the simulated data were M $(\hat{Y}_R)$ = = 132889 ha (99.3% of the ground truth value). SD $(\hat{Y}_R)$ = 1013 ha (SD% = 1%). Range $(\hat{Y}_R)$ = max $\hat{Y}$ – min $\hat{Y}$ = 29393 ha. $\bar{D}$ = M $(\hat{Y}_R)$ – α = = -999 ha. The confidence interval for the sugar cane acreage at the 95% level was (130963; 134915) = (.97.7%; 100.1%), and for the mean difference μ_D at the 95% level was (-3025; 1027).

1057

MONITORING EVAPOTRANSPIRATION OF THE TAWURGA SALT-FLAT OF LIBYA

Mohamed Al Bakhbakhi
Ahmad Obah

Agricultural Ministry
Sidi Mesri, Libya

J.S. Latham

FAO/UN
Rome, Italy

J.E. Colwell
R. Reinhold

Environmental Research Institute of Michigan
Ann Arbor, Michigan

SUMMARY

Because of its scarcity, water is a very valuable commodity in arid and semi-arid lands. Therefore, accurate information on sources and sinks of water are important for optimal water use management. For large areas, such information cannot be easily obtained by ground observations alone. Satellite data has previously been shown to be helpful in monitoring water resources of large areas. This study is an investigation of the utility of satellite data, when combined with ancillary sources of data, to monitor water resources in an arid environment.

The study site for this investigation is the Tawurga salt-flat in Libya. The quantification of evapotranspiration for this area could have significant impact on its agricultural development. If water loss by evapotranspiration is found to be significant, a program to intercept the water prior to its entry into the salt flat might be warranted. Such a program could allow the water presently lost through evapotranspiration to be utilized for development of additional irrigated agriculture.

The study involves integrating NOAA and Landsat satellite data with ground station meteorological data and field measurements. The study area is initially stratified into zones (strata) excepted to have similar evapotranspiration regimes. A limited number of ground meteorological stations are then established in each zone. The ground stations collect information on air temperature, relative humidity, incoming solar radiation, net radiation, precipitation, and wind speed.

Additional information is obtained for joint utilization of satellite data and field measurements. NOAA thermal data will be used to stratify the open water into relative temperature zones. Limited measurement of actual water temperature within these zones provides absolute temperature calibration. Day/night thermal differences for land above the water line will allow stratification on the basis of relative soil moisture, which will be calibrated to actual soil moisture by limited field measurements within each zone. Landsat indicators of water depth and salinity will similarly be calibrated by field measurements, as will Landsat indicators of vegetation density (% cover, leaf area index).

1059

All of the above data will be used to calculate evapotranspiration of the study area. Satellite monitoring of terrain conditions will allow for updating stratifications and measures of water surface area and condition, as well as soil and vegetation parameters that vary with time. The result is expected to be a considerable improvement in the knowledge of the dynamics of water flux in the region, so that better-informed decisions can produce more effective management of water and agricultural resources.

GEOTECTONIC MAP OF CUYO PROVINCES IN CENTRAL-WESTERN ARGENTINA

Juan Carlos Perucca
Maria Candida Puertas
Enrique Roque Uliarte
Juvenal Jorge Zambrano

Universidad Nacional de San Juan
San Juan, Argentina

SUMMARY

This paper is the result of the first step in a long-range project dedicated to understand what kind of forces have actuated in the area, and how they are still influencing on the tectonics hazards that give to the central-western part of Argentina its most important geologic feature.

The work began by the inventory of all the information available in order to prepare a fracture-lineaments map: conventional geologic surveys, air photo interpretation, geophysical data from oil prospecting companies, inferred fractures from isopach diagrams, and the authors' own analysis of Landsat imagery in bands 5 and 7.

The most significant features in the area are five geologic provinces with important positive forms (structural heights): (1) Sierras Pampeanas, (2) Precordillera, (3) Cordillera Frontal, (4) Cordillera Principal, and (5) Bloque de San Rafael. There exists also topographically negatives forms: Valle del Tulum, Valle del Bermejo, valles precordilleranos, Llanura del NE mendocino, cuencas triasicas, valle extenso de Uspallata-Iglesia, etc.

From conventional geologic surveys it has been evident that in Cuyo Region almost any fracture parallel to mountain ranges is an inverse dip-slip fault, and has always been considered as high-angle. The general trend of these high-angle dips (eastward or westward) is the most important criterion to get geological provinces subdivisions.

However, in the Cuyo Region also exists an important set of normal faults, which are almost generally oriented perpendicular (some times little oblique) to mountain ranges.

In reference to folding in the area covered by Landsat imagery interpretation it is possible to differentiate several styles or trends, in coincidence with the ideas suggested by Mattauer (basement tectonics and sedimentary cover tectonics). In the system of folds that affects the sedimentary cover in Cuyo Region, there exists at the same time significant differences between those observed in cambric-devonian terrains and those that appear in post devonian formations.

Meanwhile, the authors have detected in Landsat imagery a number of markedly concentric, circular to oval shaped lineaments, which were interpreted as the surface expression of a system of faults surrounding a plutonic body. There is an interesting round shaped anomaly that was recognized in the NNE corner of the Pie de Palo range (San Juan), that has not been yet described in the literature. As the area actually is geologically poorly known there are not references about igneous outcrops, taking into account that those hills are considered up-to-date as precambrian metamorphic formations. The presence of such an anomaly is considered a good reason to run a systematic mining prospect.

REVIEW OF NATIONAL PROGRAM TO TRANSFER LANDSAT AND GEOGRAPHIC
INFORMATION SYSTEM (GIS) TECHNOLOGY TO THE PRIVATE AND PUBLIC SECTOR
THROUGH SMALL COLLEGES AND OTHER LOCALLY AVAILABLE INSTITUTIONS

Robert H. Rogers

Environmental Research Institute of Michigan
Ann Arbor, Michigan

Eugene Jaworski

Department of Geography and Geology
Eastern Michigan University
Ypsilanti, Michigan

SUMMARY

This paper reviews the materials and procedures used to conduct a very
successful Landsat technology transfer program during the period from 20 December
1979 to 6 March 1982. To achieve the desired objective, the transfer of Landsat
technology, the program applied a network where the basic partners included
NASA, the sponsor, the Environmental Research Institute of Michigan (ERIM), six
Michigan colleges, and several hundred trainees from local-private and public
organizations. The methodology employed by the program gave local users an
opportunity to obtain "hands-on" training in Landsat data analysis and Geographic
Information System (GIS) techniques using the desk-top, interactive "Remote
Analysis Station" (RAS). The RAS communicates with ERIM's computing facility
via telephone line, and provides for generation of land use and land suitability
maps and other dataproducts via remote command.

The role of ERIM in this program was to train staff from the six partici-
pating colleges, provide host computer services for the RAS terminals, develop
training packages and programs (i.e., users manuals, exercises), and to support
seminars, minicourses and workshops staged by the colleges. For their part,
the colleges classify and organize business and industry in their regions in
accordance with technical or information needs, organize and host seminars for
potential users and suppliers of Landsat and GIS data products, and serve as
local contact points for technical assistance. During the period from
22 September 1980 to 6 March 1981, 15 workshops and other training activities
were successfully conducted in Michigan by the participating organizations.

Since the colleges sponsored the training program through the usual
registration-fee method (which paid for the instructor), the training and demon-
stration activities were almost self-supporting. NASA provided the use of the
two RAS terminals, with host computer support, and training materials.

NASA and other federal agencies have a continuing interest in transferring
new technologies, e.g., Landsat and Geographic Information System (GIS) tech-
niques, to potential users in the public and private sectors. Universities and
colleges (particularly the small colleges), who have a primary role in transfer-
ring these new technologies, generally do not have sufficient funds for acquiring
the facilities (i.e., hardware and software) needed to provide adequate training
and demonstration programs. This support is needed to create demand for Landsat
technology in architectural and engineering firms, major public utilities, as
well as local, regional, and county planning agencies. Greater involvement by

these potential users ᴖan enhance the growth of Landsat and particularly GIS technologies.

This method by which public and private organizations can join in cooperative efforts to share resources, seems to be a sound method of satisfying both training and demonstration requirements and the transfer of Landsat technology to the largest number of professionals at the entry level. Approximately 200 people were provided hands-on training on the RAS terminals. Many others had the opportunity to attend brief demonstrations and one-day workshops.

Future transfer will focus on user-specific applications with participant academic institutions acting as training and demonstration liaison between private industry and ERIM. Research and development firms, such as ERIM, must necessarily continue to provide both hardware and software development to the training consortium and to private industry.

AUTHOR INDEX